JPL Publication 93-16

Proceedings of the Third Spaceborne Imaging Radar Symposium

Held at the Jet Propulsion Laboratory, Pasadena, California, January 18–21, 1993

May 28, 1993

NASA
National Aeronautics and Space Administration

Jet Propulsion Laboratory
California Institute of Technology
Pasadena, California

JPL Publication 93-16

Proceedings of the Third Spaceborne Imaging Radar Symposium

Held at the Jet Propulsion Laboratory, Pasadena, California, January 18–21, 1993

May 28, 1993

NASA
National Aeronautics and
Space Administration

Jet Propulsion Laboratory
California Institute of Technology
Pasadena, California

Prepared by the Jet Propulsion Laboratory, California Institute of Technology, for the U.S. Department of Energy through an agreement with the National Aeronautics and Space Administration.

ABSTRACT

This publication contains summaries of the papers presented at the Third Spaceborne Imaging Radar Symposium held at the Jet Propulsion Laboratory (JPL), California Institute of Technology, in Pasadena, California, on January 18–21, 1993. The purpose of the symposium was to present an overview of recent developments in the different scientific and technological fields related to spaceborne imaging radars and to present future international plans.

This symposium is the third in a series of "Spaceborne Imaging Radar" symposia held at JPL. The first symposium was held in January 1983 and the second in 1986.

CONTENTS

CONTENTS (continued)

CONTENTS (continued)

omit

INTRODUCTION

This publication contains summaries of the papers presented at the Third Spaceborne Imaging Radar Symposium held at the Jet Propulsion Laboratory (JPL), California Institute of Technology, Pasadena, California, in January 1993. The purpose of the symposium was to present an overview of recent developments in the different scientific and technological fields related to spaceborne imaging radar and to present future international plans.

The last five years have seen major advances in the development and utilization of spaceborne imaging radar for Earth and planetary studies. The National Aeronautics and Space Administration/JPL Magellan spacecraft radar mapped the totality of the surface of Venus, which is hidden by the dense global cloud cover, giving us a detailed view of a very dynamic (historically) surface covered with volcanic, tectonic, eolian, and impact features. The European Space Agency (ESA) and Japan launched semioperational Earth-orbiting systems that are providing a wealth of data for ocean study, geologic mapping, and environmental monitoring.

The next five years are expected to be equally exciting, opening a new frontier in the utilization of spaceborne radar systems. The joint U.S./Germany/Italy SIR-C/X-SAR will provide the first multispectral ("color"), multipolarization spaceborne capability using active arrays. ESA will launch the Earth Resource Satellite 2 (ERS-2) (then followed by Envisat), which will ensure long-term continuity of the ERS-1 data. This continuity is crucial for long-term monitoring of environmental changes. Canada will launch RADARSAT-1 (followed by RADARSAT-2), which will allow wide-scale repeat coverage of the world's polar regions. Japan and the U.S. will be launching the first rain-mapping radar, and the U.S. will launch the Titan radar on the Cassini spacecraft, which will orbit Saturn and map the cloud-covered world of Titan.

The next five years also hold the potential for major new exciting missions. Radar interferometry is maturing as the preferred technique for global digital topography mapping, and the U.S. and Italy are planning a TOPSAT Mission. SIR-C/X-SAR could be transformed into a free flyer. Japan, France, and the U.S. each are considering advanced spaceborne systems, and the U.S. and United Kingdom are studying cloud-mapping radar systems.

Collectively these missions, if coordinated, could provide a very powerful element of the Mission to Planet Earth to understand and monitor the global and local changes on our planet.

We all look forward to these exciting developments and to the Fourth Spaceborne Imaging Radar Symposium, which will be held in Spring 1998, the twentieth anniversary of Seasat.

Charles Elachi
Assistant Laboratory Director
Office of Space Science and
Instruments

RECENT AND ONGOING

FLIGHT MISSIONS

Magellan: Principal Venus Science Findings

R. Stephen Saunders
Jet Propulsion Laboratory
California Institute of Technology
Pasadena, California 91109

This is a brief summary of the science findings of the Magellan mission, principally based on data from the radar system. Future plans for Magellan include acquisition of high resolution gravity data from a nearly circular orbit and atmospheric drag and occultation experiments. The Magellan science results represent the combined effort of more than 100 Magellan investigators and their students and colleagues. More extensive discussions can be found in the August and October, 1992 issues of the Journal of Geophysical Research, Planets [1]. The Magellan mission's scientific objectives were (1) to provide a global characterization of landforms and tectonic features; (2) to distinguish and understand impact processes; (3) to define and explain erosion, deposition, and chemical processes; (4) to model the interior density distribution. All but the last objective, which requires new global gravity data, have been accomplished, or we have acquired the data that are required to accomplish them.

Synthetic aperture radar imaging and altimetry were acquired over nearly 99% of the planet with resolution between 120 m and 300 m and at least four looks. Several image geometries were obtained in order to provide the best interpretation of the landforms. For the first 243 day cycle, one Venus rotation, an incidence-angle, or look-angle, profile was used that maximized the image resolution and overall quality everywhere along the orbit. This profile caused the incidence angle to vary from about 15° over the north pole to 45° at the equator. In the first cycle we mapped 83% of Venus, more than meeting the primary mission objectives. In the second mapping cycle, mapping was restricted in order to control spacecraft temperature. Image data were obtained at a constant incidence angle, and looking to the right (toward the west) in the opposite direction from cycle 1. Also, in cycle 2, some of the major gaps were filled with the same incidence angle profile as used in cycle 1. In cycle 2, we also conducted a successful test of a stereo mode in which we imaged at a slightly different angle than in cycle 1. The stereo was so useful that it was decided to devote much of the third mapping cycle to acquiring stereo images. All of the radar image data were processed at JPL in a complex flow that begins at the DSN stations at Goldstone, Madrid, and Canberra. In addition to images and altimetry, Magellan also acquired radiometer data whenever images were obtained [2]. The radiometry samples the radio emission of the surface at the radar wavelength. Emissivity varies from place to place because of variations in surface properties.

Imaging was terminated at the end of the third cycle and gravity data are being acquired during cycle 4. This is accomplished by pointing the 3.8 m high-gain antenna toward Earth during the periapsis part of the orbit and recording the returned radio signal

at the DSN. From this signal we extract the slight accelerations of the spacecraft as it orbits Venus and convert these accelerations into gravity maps that tell us about density variations in the interior.

Magellan image data have provided several improvements in knowledge of the fundamental planetary constants for Venus. The rotation period of Venus was refined to 243.0185 ±0.0001 days and the north pole direction, in J2000 coordinates, has been refined to right ascension 272.76° ±0.02° and declination 67.16° ±0.01°. The mean radius was refined to 6051.84 km, with the lowest point 6048.0 km and the highest point 6062.57 km [3].

Magellan has established volcanism as the dominant surface process on Venus [4]. Volcanism is broadly distributed, not completely random, but does not form linear patterns as on Earth where major volcanic activity tends to occur along plate boundaries. Image analysis reveals thus far 556 shield fields, 274 volcanoes 20-100 km, 156 volcanoes 100 km, 86 calderas (not on shields), 259 arachnoids, 53 lava flow fields, 200 sinuous lava channels, 145 steep-sided domes (pancakes) [4]. Over 360 coronae and corona-like features have been identified [5].

Tectonics is a major process [6], with evidence for extension and compression. Steep slopes (20°-30°), up to tens of km in extent, provide evidence of active tectonics. Deformation is more distributed than on Earth. Shear zones are seen in complex ridged terrain. Trench topography resembles terrestrial subduction. An extensive equatorial zone of fractures is among the most recent tectonic features.

More than 900 impact craters 1.5 km to 280 km have been identified [7,8]. There appears to be a globally random distribution yielding an average surface age of about 500 Myr. Both bright and dark splotches appear to be shock signatures. Most craters are unmodified. Bright and dark E-W oriented parabolic halos are associated with about 20% of craters [9].

Surface processes and surface properties [10,11,12] investigations yield more than 8000 mapped wind streaks with directions consistent with Hadley circulation. Possible dune fields have been identified and there is widespread evidence of landslides [13]. Anomalous left-right reflectivity behavior indicates unusual surface reflectivity behavior, possibly caused by asymmetric shapes. Anomalous low emissivity in elevated regions has been confirmed [2].

Major questions about Venus remain unresolved, pending acquisition of new data and further analysis of existing data. Interpretation of the impact crater population suggests a major secular change in the rate or style of resurfacing [7], but the details or even the reality of this change, whether catastrophic, cyclical, local or global scale is unknown. High-resolution global gravity data will help address some of the unresolved issues concerning the

generation, support, and relaxation of topography.

References: [1] R.S. Saunders et al., J. Geophys. Res., 97, E8, 13,067, 1992; [2] G.H. Pettengill et al., J. Geophys Res., 97, E8, 13,091, 1992; [3] M.E. Davies et al., J. Geophys. Res., 97 ,E8, 13,141, 1992; [4] J. W. Head et al., J. Geophys. Res., 97, E8, 13,153, 1992; [5] E.R. Stofan et al., J. Geophys. Res., 97, E8, 13,347, 1992; [6] S. C. Solomon et al., J. Geophys. Res., 97, E8, 13,199, 1992; [7] G.G. Schaber et al. J. Geophys. Res., 97, E8, 13,257, 1992; [8] R.J. Phillips et al., J. Geophys. Res., 97, E10, 15,923, 1992; [9] D.B. Campbell et al., J. Geophys. Res. [10] G.L. Tyler et al., J. Geophys. Res., 97, E8, 13,115, 1992; [11] R.E. Arvidson et al., J. Geophys. Res., 97, E8, 13,303, 1992; [12] R. Greeley et al., J. Geophys. Res., 97, E8, 13,319, 1992; [13] M.C. Malin, J. Geophys. Res., 97, E10, 16,337, 1992.

Acknowledgement: This work was performed, in part, at the Jet Propulsion Laboratory, California Institute of Technology, under contract with NASA.

ERS 1

18 MONTHS IN ORBIT

J. Louet

European Space Laboratory
The Netherlands

INITIAL OBJECTIVES OF THE ERS-1 MISSION (1)

- TO SERVE BOTH THE SCIENTIFIC RESEARCH COMMUNITY AND THE APPLICATION RESEARCH COMMUNITY
- TO PROVIDE THESE USERS WITH A VARIETY OF SERVICES:

  REGIONAL SERVICE WITH SAR

  GLOBAL SERVICE WITH LBR

  FD SERVICE FOR NEAR REAL TIME USERS

  OFF-LINE SERVICE TO OTHER USERS

INITIAL OBJECTIVES OF THE ERS-1 MISSION (2)

- TO DEVELOP ADVANCED INSTRUMENTS FOR EARTH OBSERVATION (IN PARTICULAR IN THE MICROWAVE DOMAIN)
- TO DEVELOP AND PROMOTE EUROPEAN INDUSTRIAL CAPABILITIES FOR ADVANCED MICROWAVE TECHNOLOGIES
- TO ENSURE AN ACCURATE CALIBRATION OF THE INSTRUMENTS IN ORDER TO ALLOW A QUANTITATIVE USE OF THE DERIVED DATA PRODUCTS

INITIAL OBJECTIVES OF THE ERS-1 MISSION (3)

- TO DEVELOP EUROPEAN EXPERTISE AT SEVERAL LEVELS, IN PARTICULAR BY ENSURING INVOLVEMENT OF NATIONAL CENTRES AND FACILITIES IN THE DEVELOPMENT AND EXPLOITATION PHASE

- TO PREPARE THE USER COMMUNITY TO ANALYZE, ASSIMILATE AND, WHEN APPLICABLE, MAKE OPERATIONAL USE OF ERS-1 DATA

- TO PROMOTE THE INTERNATIONAL COOPERATION IN THE USE OF REMOTE SENSING DATA FOR PEACEFUL PURPOSES AND CONTRIBUTE TO LARGE INTERNATIONAL RESEARCH PROGRAMMES (WCRP, IGBP, TREES..)

ORBIT CONFIGURATION

ORBIT SCENARIO IMPLEMENTED AS PLANNED FAST TRANSITION FROM 3 TO 35 DAY CYCLE)

VERY STABLE ORBIT CONFIGURATION :

- GROUND TRACK STABILITY MAINTAINED WITHIN ± 1 KM THROUGH ORBIT CORRECTION PERFORMED 1/WEEK AT THE BEGINNING OF THE MISSION AND 1/MONTH SINCE APRIL 1992 (REDUCED SOLAR ACTIVITY)

ORBIT CONTROL

ORBIT MAINTAINED WITHIN ±1 Km DEADBAND AT ALL LATITUDES, ALONG TRACK MANŒUVERS REQUIRED AT 4 TO 5 WEEKS INTERVAL END 1992

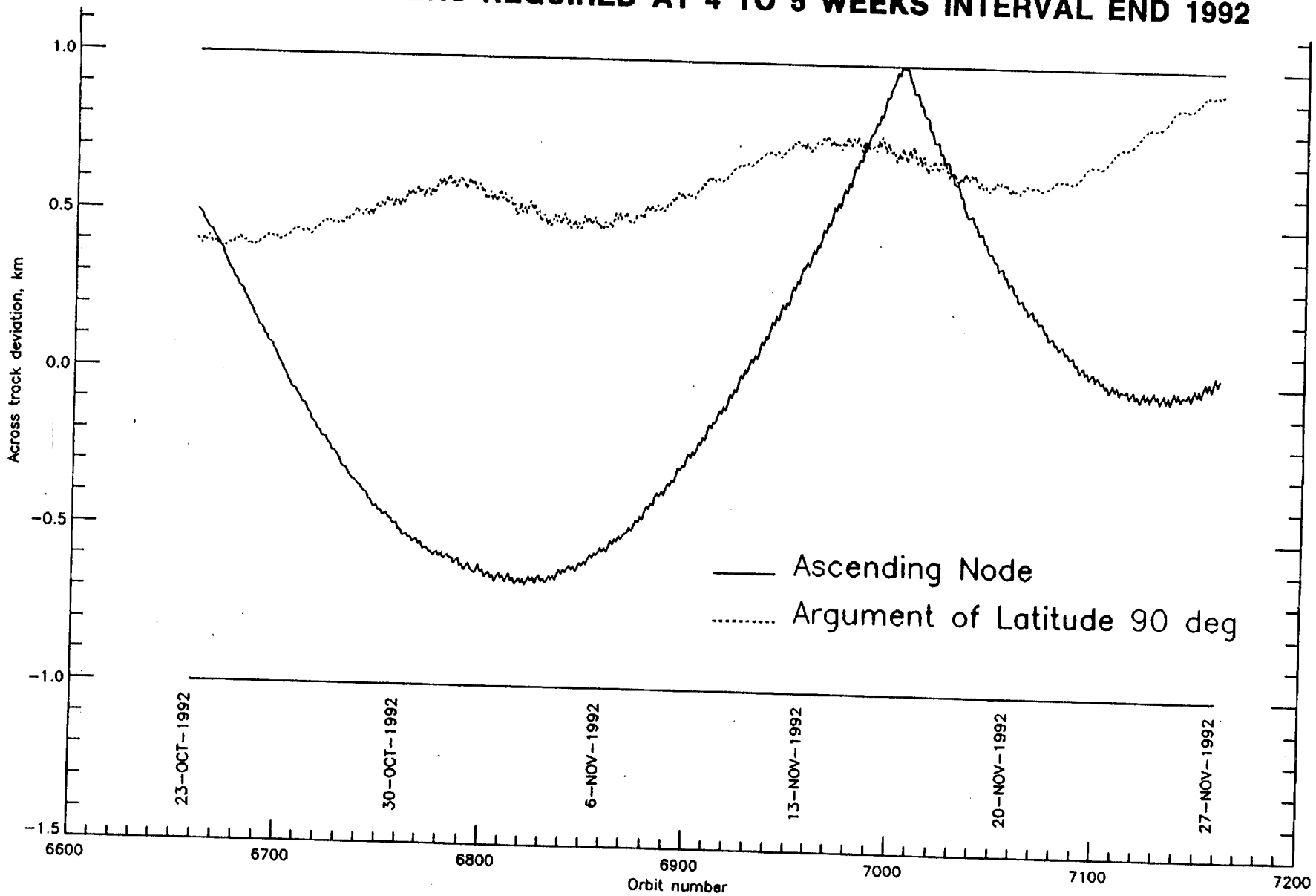

INCLINATION CORRECTION

INCLINATION CORRECTION PERFORMED 16 DECEMBER 1992,
satellite brought back from +1 Km to -1 Km boarder at argument of latitude 90º

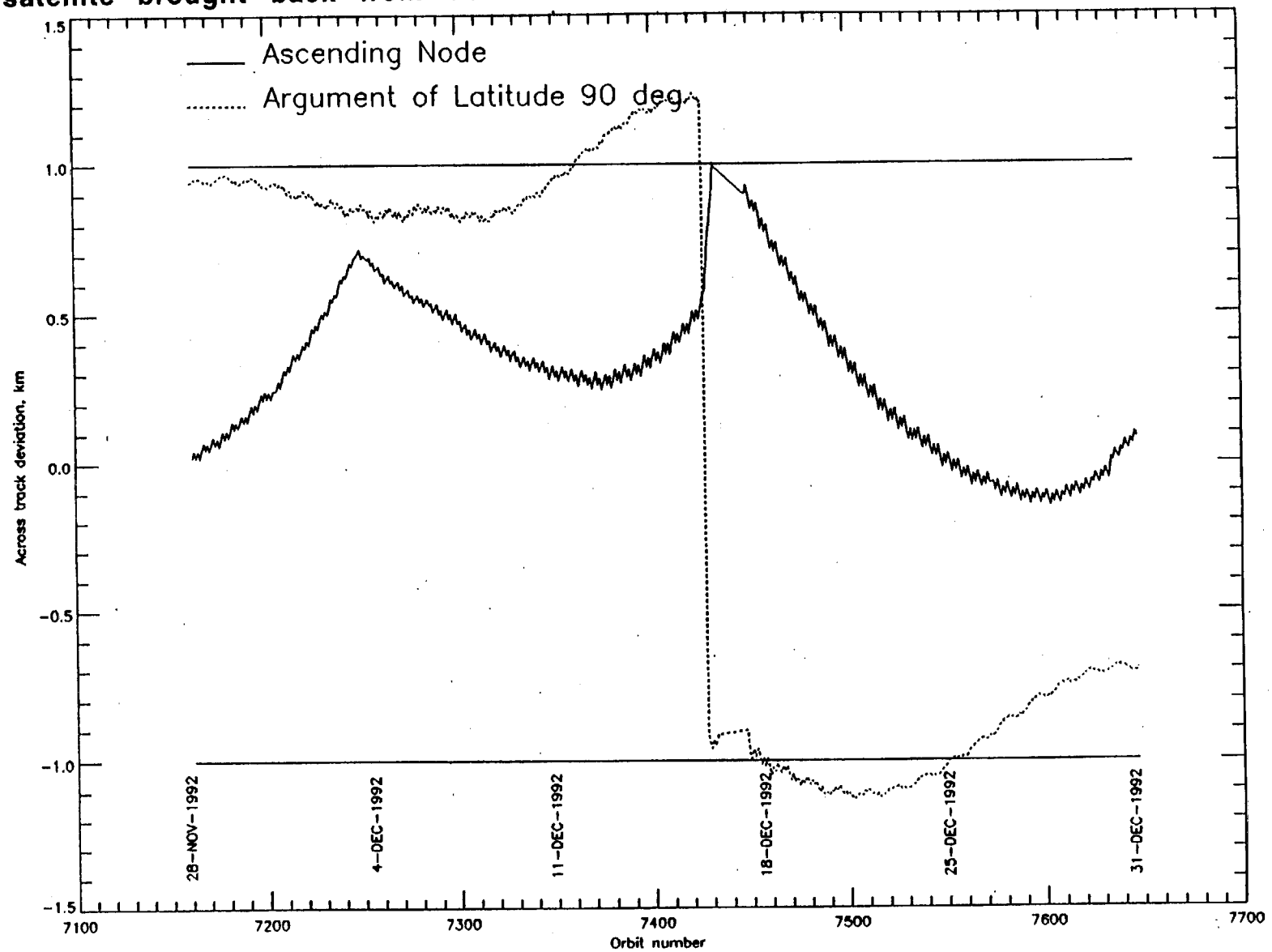

PLATFORM

ENERGY :	**VERY GOOD MARGIN**
THERMAL :	**GOOD STABILITY**
OPERABILITY :	**EXCELLENT**
AOCS :	**NUMEROUS SMALL PROBLEMS AT SENSOR LEVEL : ALL CIRCUMVENTED**

ERS-1 SOLAR ARRAY

MEASURED POWER VERSUS SPECIFIED PERFORMANCES

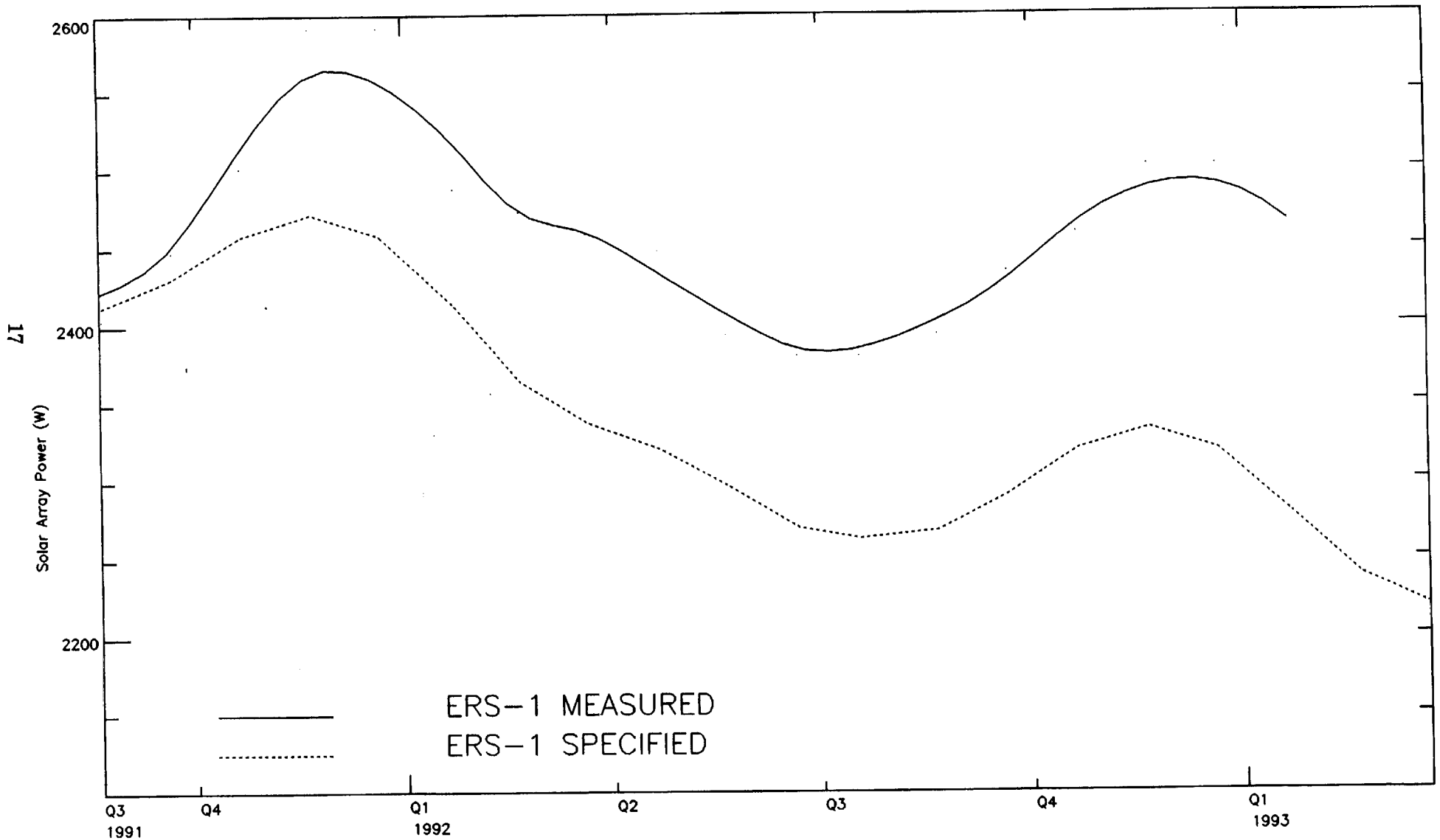

SATELLITE TIME STABILITY

PERIOD 14 SEPT 91 TO 28 JUNE 92

MEAN CLOCK PERIOD: 3906249.470 ns STABILITY OVER THE PERIOD± 9. 10-8

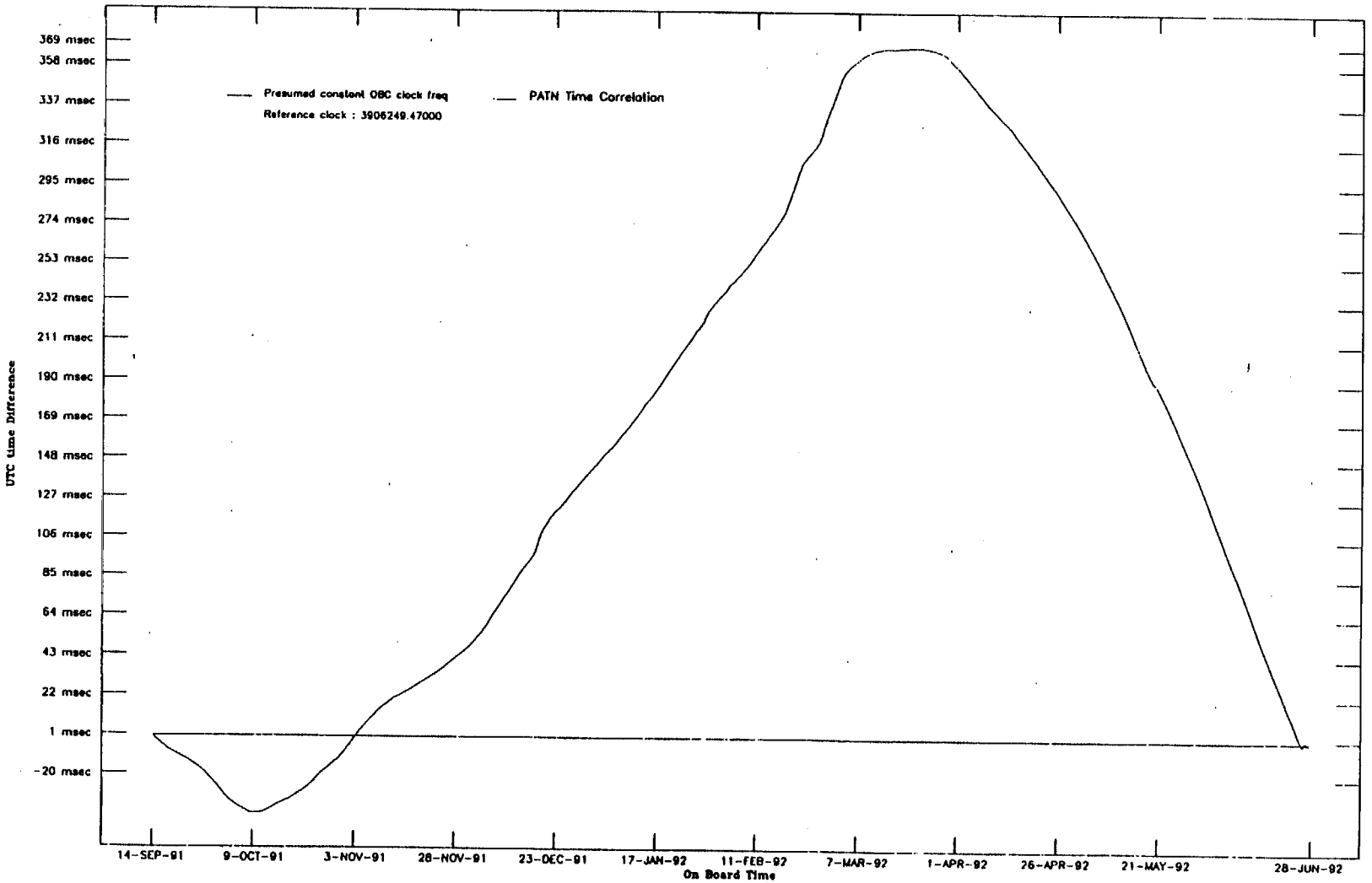

ATTITUDE CONTROL CHARACTERISATION AND STABILITY

* ACCURATE CHARACTERISATION PERFORMED VIA SAR & WAVE MODE DOPPLER CENTROID ESTIMATES

*COMBINED PITCH/YAW HAS SEEN IN SAR ANTENNA PLANE:

- STATIC BIAS: 20 millidegrees
- HARMONIC ERROR: ± 30 millidegrees

ABOVE PARAMETERS HAVE PROVED TO BE STABLE SINCE LAUNCH AND CAN THEREFORE BE REMOVED

- RESIDUAL NOISE ERROR: 20 millidegrees

ERS-1 FUEL CONSUMPTION
&
CENTRE OF MASS EVOLUTION SINCE LAUNCH

FUEL CONSUMED: **33.7 Kg**
(317.6 Kg AVAILABLE AT LAUNCH)

CENTRE OF MASS CHANGE: **5mm ALONG THE Xs AXIS**

INSTRUMENTATION (1)

GENERAL :

- EXCELLENT STABILITY OF BOTH AMI AND RA
- MOST AMI AND RA PERFORMANCES ARE BETTER THAN SPECIFIED
- ATSR HAD VERY SMOOTH OPERATIONS TILL 27 MAY 1992, WHEN THE 3.7 MICRON CHANNEL FAILED. NO RECOVERY WAS POSSIBLE BUT THE IMPACT ON THE MISSION IS LIMITED

INSTRUMENTATION (2)

- PRARE HAD A FATAL FAILURE AT THE END OF JULY 1991, AFTER A FEW DAYS OF SUCCESSFUL OPERATIONS. NO RECOVERY WAS POSSIBLE.
  THE LOSS IS PARTIALLY COMPENSATED THROUGH INTENSIVE LASER TRACKING ACTIVITIES

INSTRUMENTATION (3)

AMI :

- VERY GOOD OPERABILITY AND STABILITY
- ARCING : AUTOMATIC RESTART ACTIVATED WITHIN 15 SEC. EXCEPT MANUAL RESTART ONCE PER MONTH
- NO OBSERVABLE CHANGES SINCE LAUNCH IN INSTRUMENT CHARACTERISTICS
- ALL ENGINEERING CALIBRATION OBJECTIVES MET BEFORE THE END OF COMMISSIONING

AMI PERFORMANCE VERIFICATION

* SAR CHIRP STABILITY: NO VISIBLE VARIATION SINCE LAUNCH

* OVERALL SAR SYSTEM STABILITY AS VERIFIED BY FLEVOLAND ESA TRANSPONDERS :*No variation of mean gain, standard deviation of 0.41dB*

* WIND SCATTEROMETER STABILITY

Brazilian rain forest test area confirms constant corregistration of the three beams within .3dB and no drift since the last calibration correction early March 92

* SAR ANTENNA PATTERN VERIFICATION

The sar antenna pattern can be verified on any single SAR image over selected zones of the Brazilian rain forest known to exhibit constant gamma properties

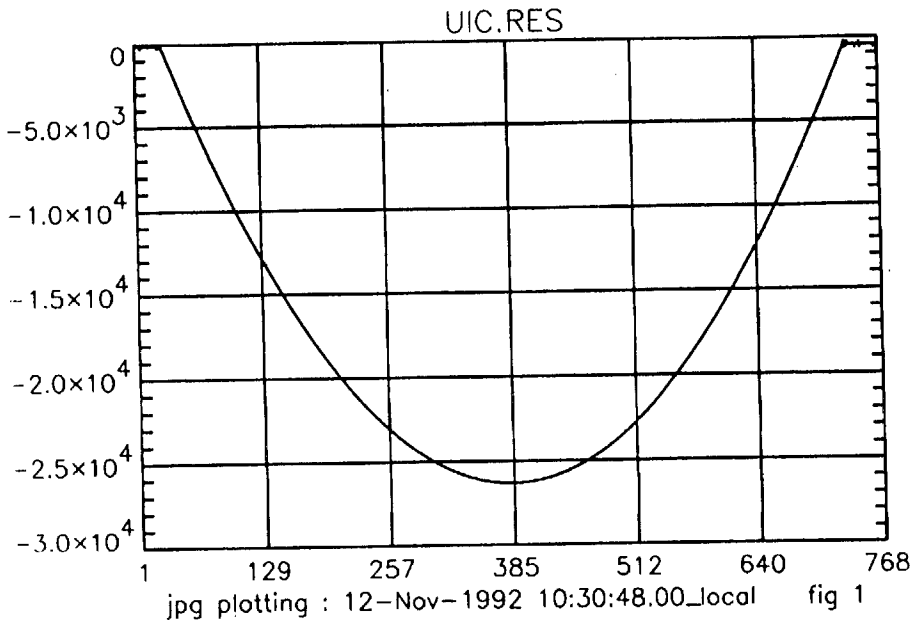
UIC.RES
0
-5.0×10^3
-1.0×10^4
-1.5×10^4
-2.0×10^4
-2.5×10^4
-3.0×10^4
1
129
257
385
512
640
768
jpg plotting : 12-Nov-1992 10:30:48.00_local fig 1

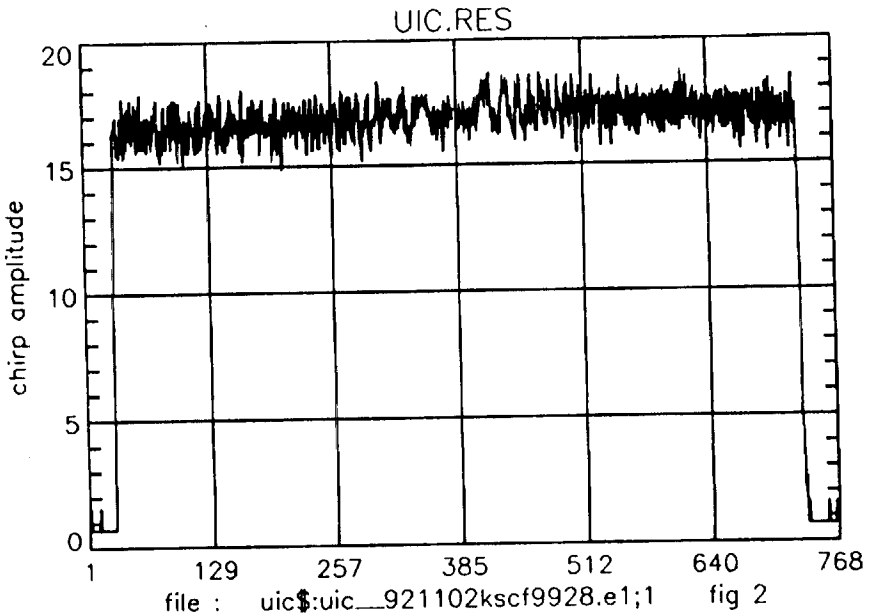
UIC.RES
chirp amplitude
20
15
10
5
0
1
129
257
385
512
640
768
file : uic$:uic__921102kscf9928.e1;1 fig 2

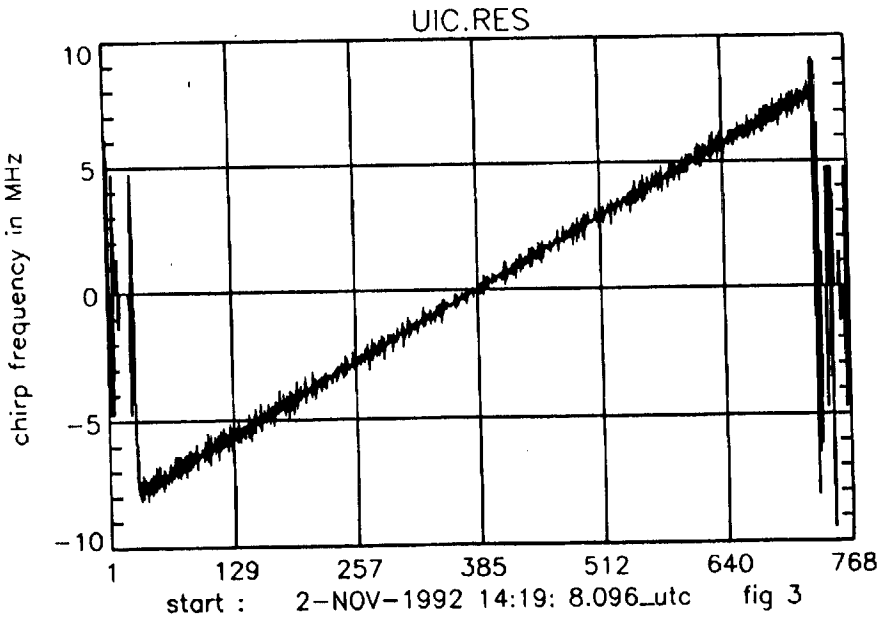
UIC.RES
chirp frequency in MHz
10
5
0
-5
-10
1
129
257
385
512
640
768
start : 2-NOV-1992 14:19: 8.096_utc fig 3

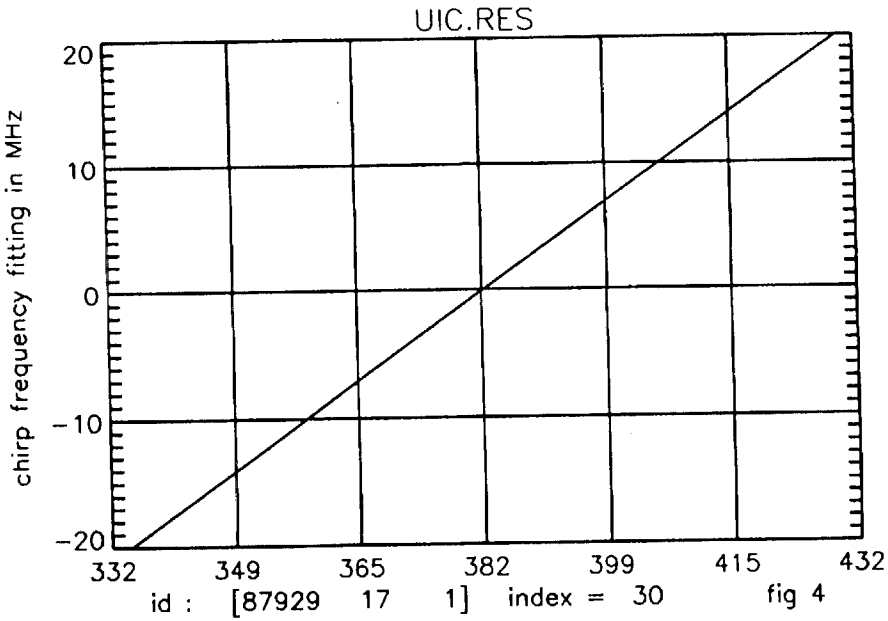
UIC.RES
chirp frequency fitting in MHz
20
10
0
-10
-20
332
349
365
382
399
415
432
id : [87929 17 1] index = 30 fig 4

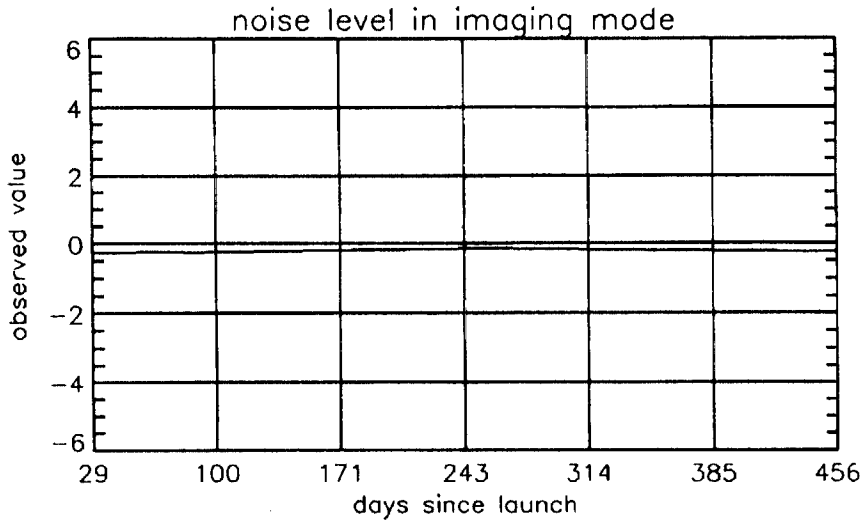
noise level in imaging mode
observed value
6
4
2
0
−2
−4
−6
29
100
171
243
314
385
456
days since launch

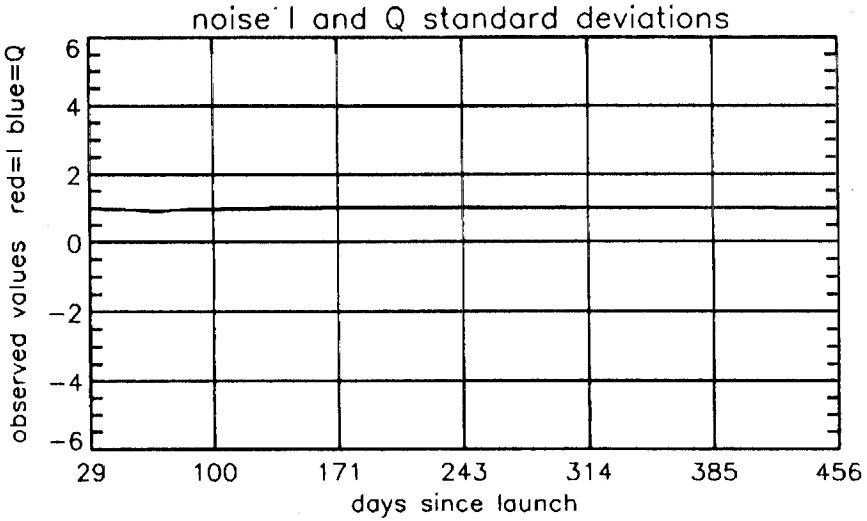
noise I and Q standard deviations
observed values red=I blue=Q
6
4
2
0
−2
−4
−6
29
100
171
243
314
385
456
days since launch

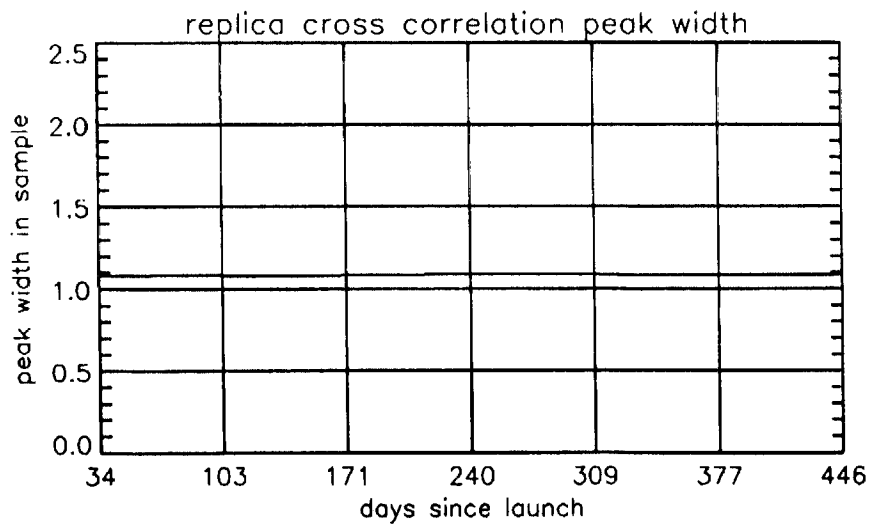
replica cross correlation peak width
peak width in sample
2.5
2.0
1.5
1.0
0.5
0.0
34
103
171
240
309
377
446
days since launch

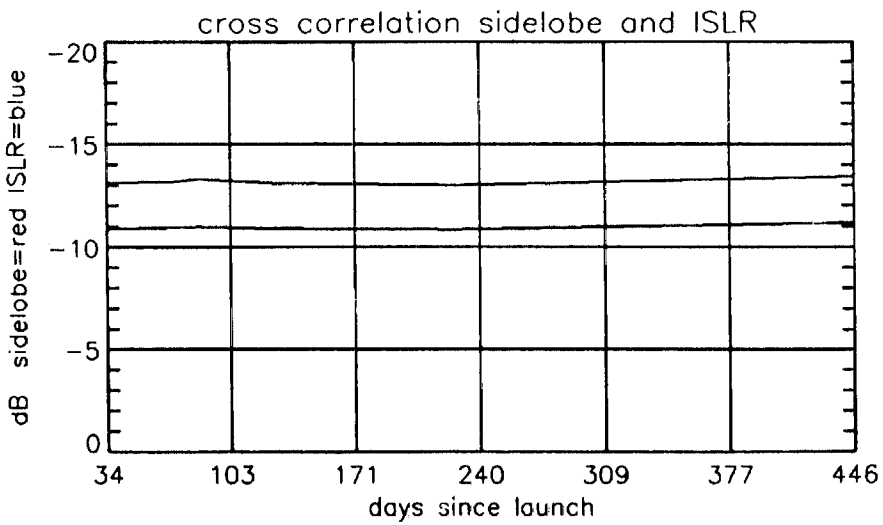
cross correlation sidelobe and ISLR
dB sidelobe=red ISLR=blue
−20
−15
−10
−5
0
34
103
171
240
309
377
446
days since launch

ERS-1 SAR RADIOMETRIC STABILITY
VARIATION AROUND THE REF. VALUE FOR
TRANSPONDER 2 (dB)
0.80
0.60
0.40
0.20
0.00
-0.20
-0.40
-0.60
-0.80
7-Sep-91
19-Sep-91
25-Sep-91
1-Oct-91
7-Oct-91
13-Oct-91
19-Oct-91
25-Oct-91
31-Oct-91
6-Nov-91
12-Nov-91
18-Nov-91
24-Nov-91
30-Nov-91
6-Dec-91
11-Jan-92
17-Jan-92
23-Jan-92
29-Jan-92
1-Feb-92
10-Feb-92
16-Feb-92
22-Feb-92
28-Feb-92
5-Mar-92
8-Mar-92
11-Mar-92
3-May-92
7-Jun-92
16-Jun-92
12-Jul-92
16-Aug-92
25-Aug-92
20-Sep-92
29-Sep-92

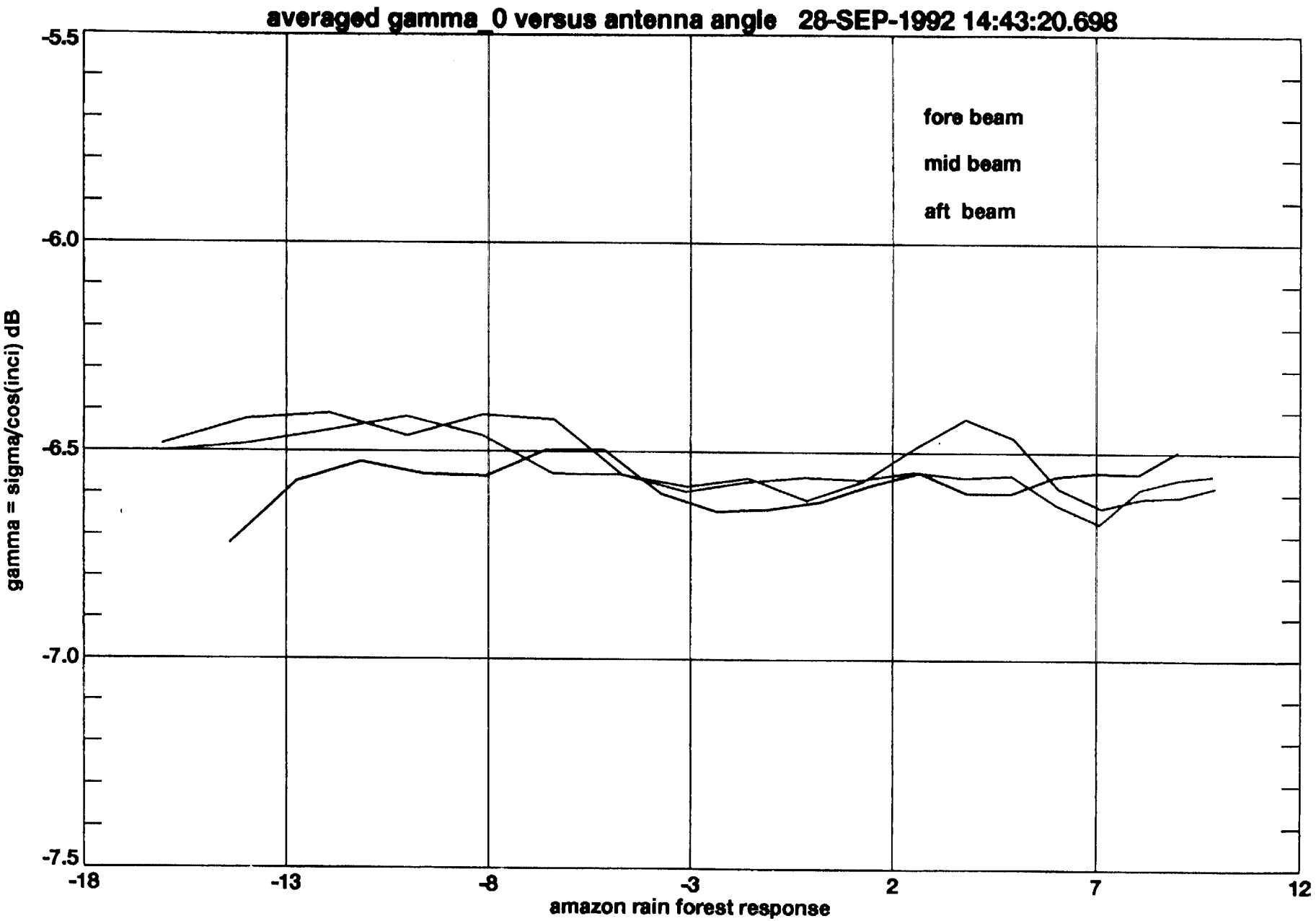
averaged gamma_0 versus antenna angle 28-SEP-1992 14:43:20.698
fore beam
mid beam
aft beam
gamma = sigma/cos(inci) dB
-5.5
-6.0
-6.5
-7.0
-7.5
-18
-13
-8
-3
2
7
12
amazon rain forest response

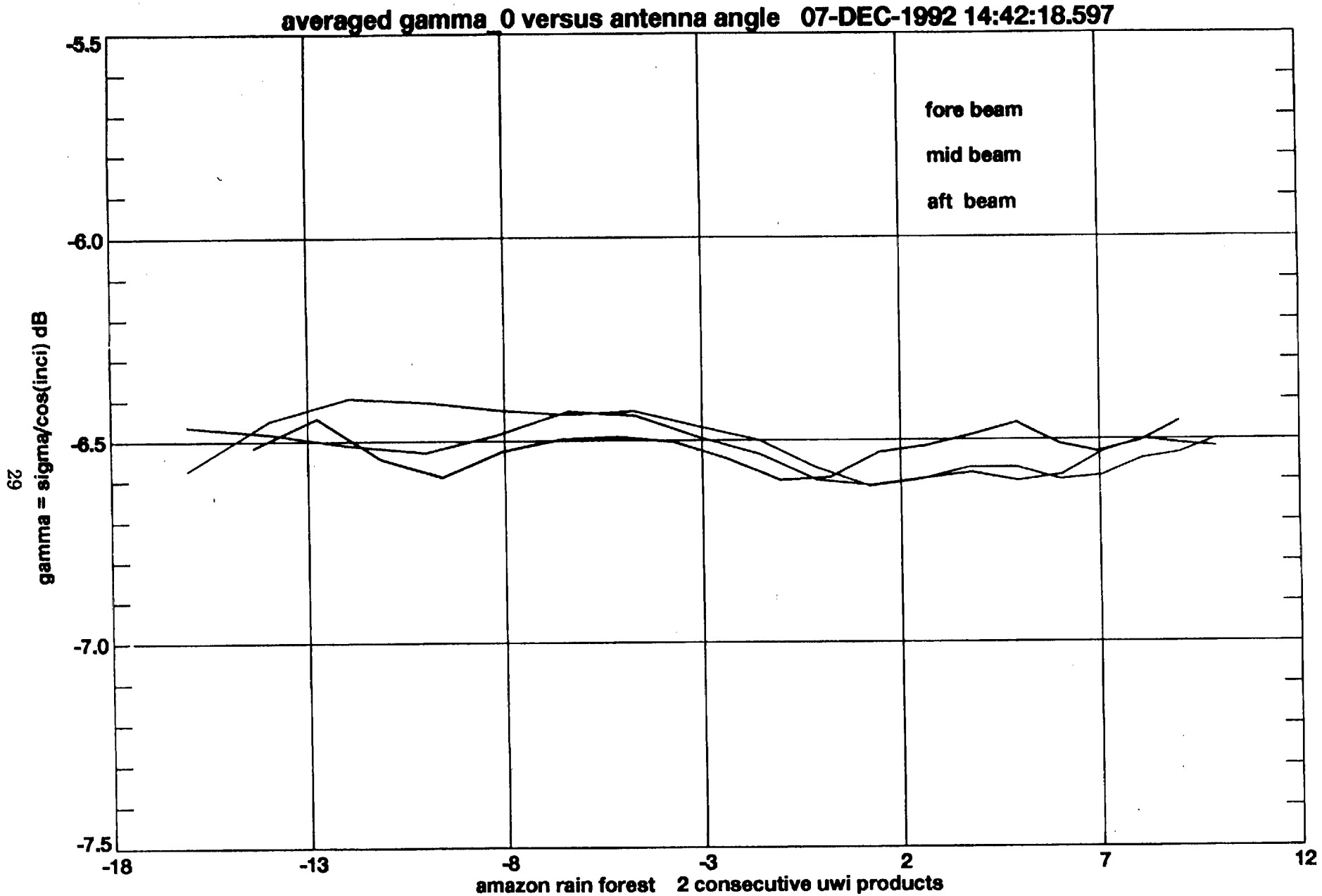
averaged gamma_0 versus antenna angle 07-DEC-1992 14:42:18.597
fore beam
mid beam
aft beam
-5.5
-6.0
-6.5
-7.0
-7.5
gamma = sigma/cos(inci) dB
-18
-13
-8
-3
2
7
12
amazon rain forest 2 consecutive uwi products

INSTRUMENTATION (4)

RA :

- VERY GOOD AND STABLE PERFORMANCES
- NO OBSERVABLE CHANGES SINCE LAUNCH
- CALIBRATION OBJECTIVES MET (VENEZIA CAMPAIGN)
- VERY GOOD ACQUISITION AND TRACKING OVER OCEAN AND ICE
- SEA ICE TRACKING ROBUSTNESS BEING IMPROVED
- THE SW TRACKER INTERRUPTS ABOUT ONCE EVERY 6 WEEKS AND REQUIRES MANUAL RESTART

RA PERFORMANCE STABILITY MONITORING

* ULTRA STABLE OSCILLATOR STABILITY MONITORING

From august 91 until december 92, total peak to peak variation equivalent to 1 cm.

* INTERNAL DELAY MEASUREMENT

Nominal value around 31μs,variation of 1ns in first months (15cm),permanently monitored and used in FD & offline processing

* INTERNAL GAIN LOOP MEASUREMENT

Increase of 0.3 dB in first months, since then stable within 0.15 dB round orbit variation,permanently monitored and used in FD & offline processing

* SYSTEM NOISE MEASUREMENT

Confirms that receiver gain has increased by 0.3 dB in first months

* HEIGHT CALIBRATION CONSTANT

Confirmed to be 41.5 cm, following processing of Venice campaign data

ERS-1

ESOC Mission Management and Planning Office – Pleval

Reference Measurement System

16: Long term stability rest. bit clock link 2 PB (USO)

Nominal Frequency: 15000000.000
ln (freq-nom) : Mean = 0.181 Hz, Sigma = 0.031 Hz
ln (freq-nom)/nom: Mean = 1.206e-08, Sigma = 2.068e-09

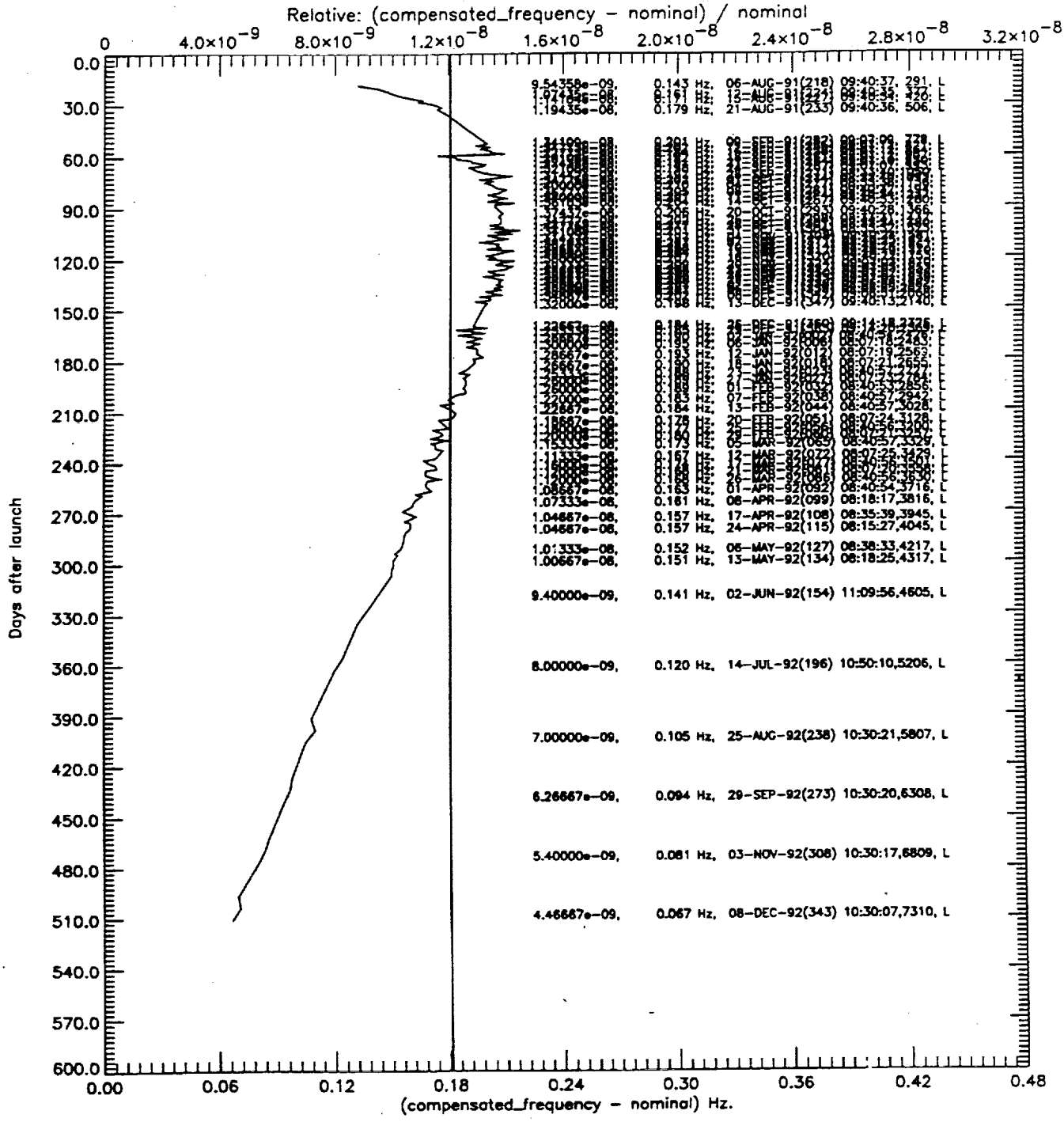

Legenda: relative, freq-nom, date, year_day, hh:mm:ss, orbit, flag
Flag V: Valid measurement
Flag L: Valid measurement: Limits exceeded

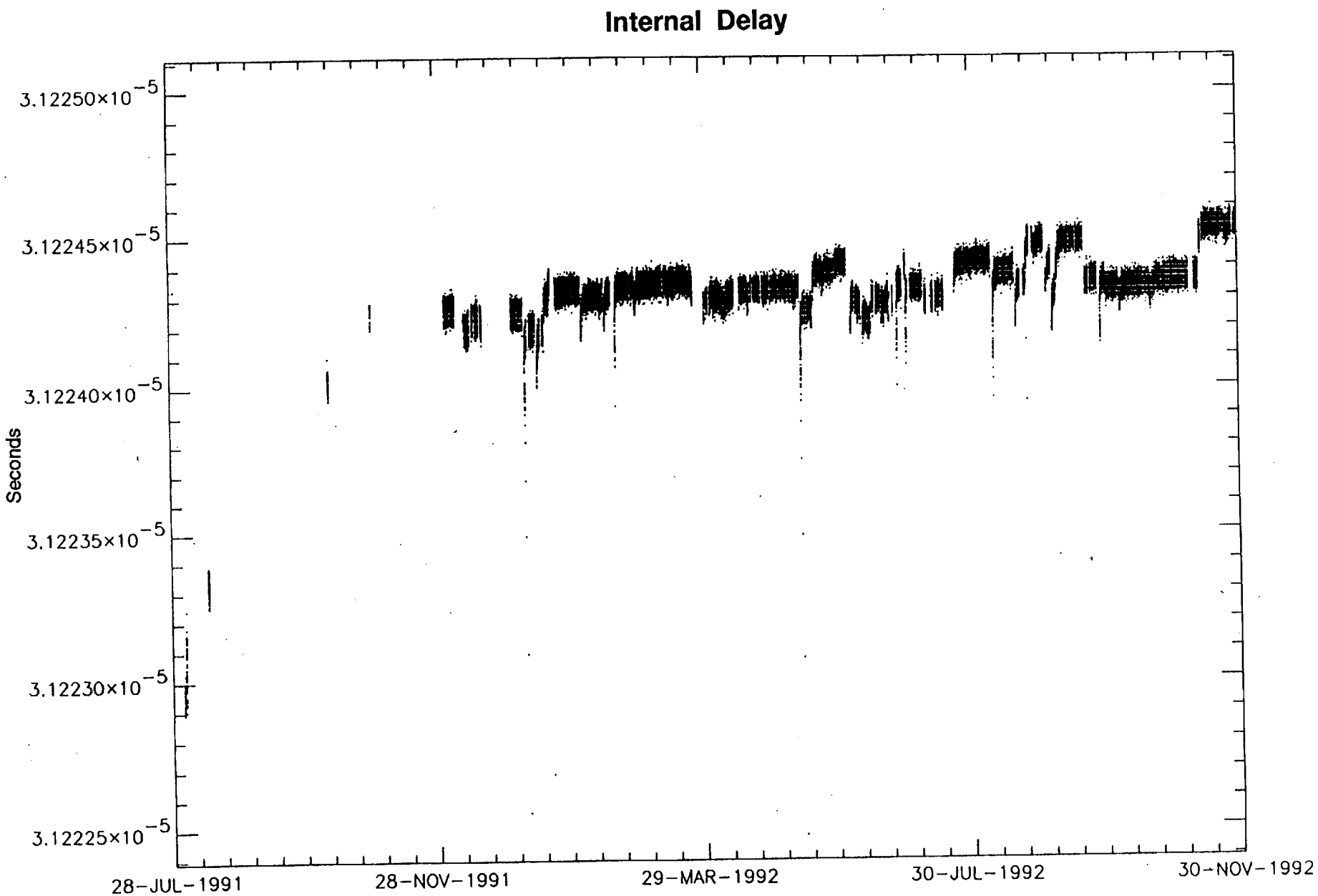
Internal Delay
3.12250×10^-5
3.12245×10^-5
3.12240×10^-5
3.12235×10^-5
3.12230×10^-5
3.12225×10^-5
Seconds
28-JUL-1991
28-NOV-1991
29-MAR-1992
30-JUL-1992
30-NOV-1992

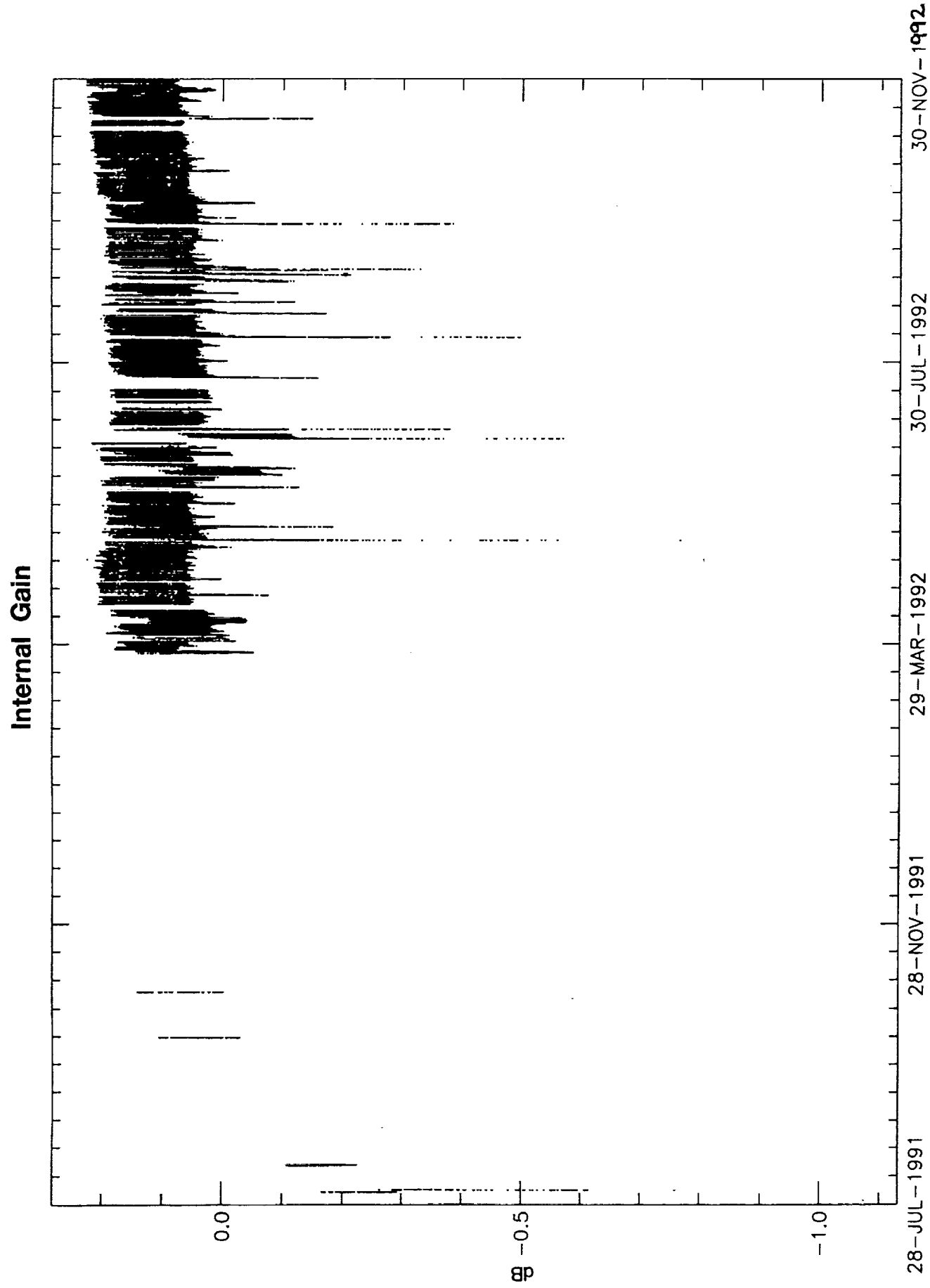
Internal Gain
0.0
−0.5
−1.0
dB
28−JUL−1991
28−NOV−1991
29−MAR−1992
30−JUL−1992
30−NOV−1992

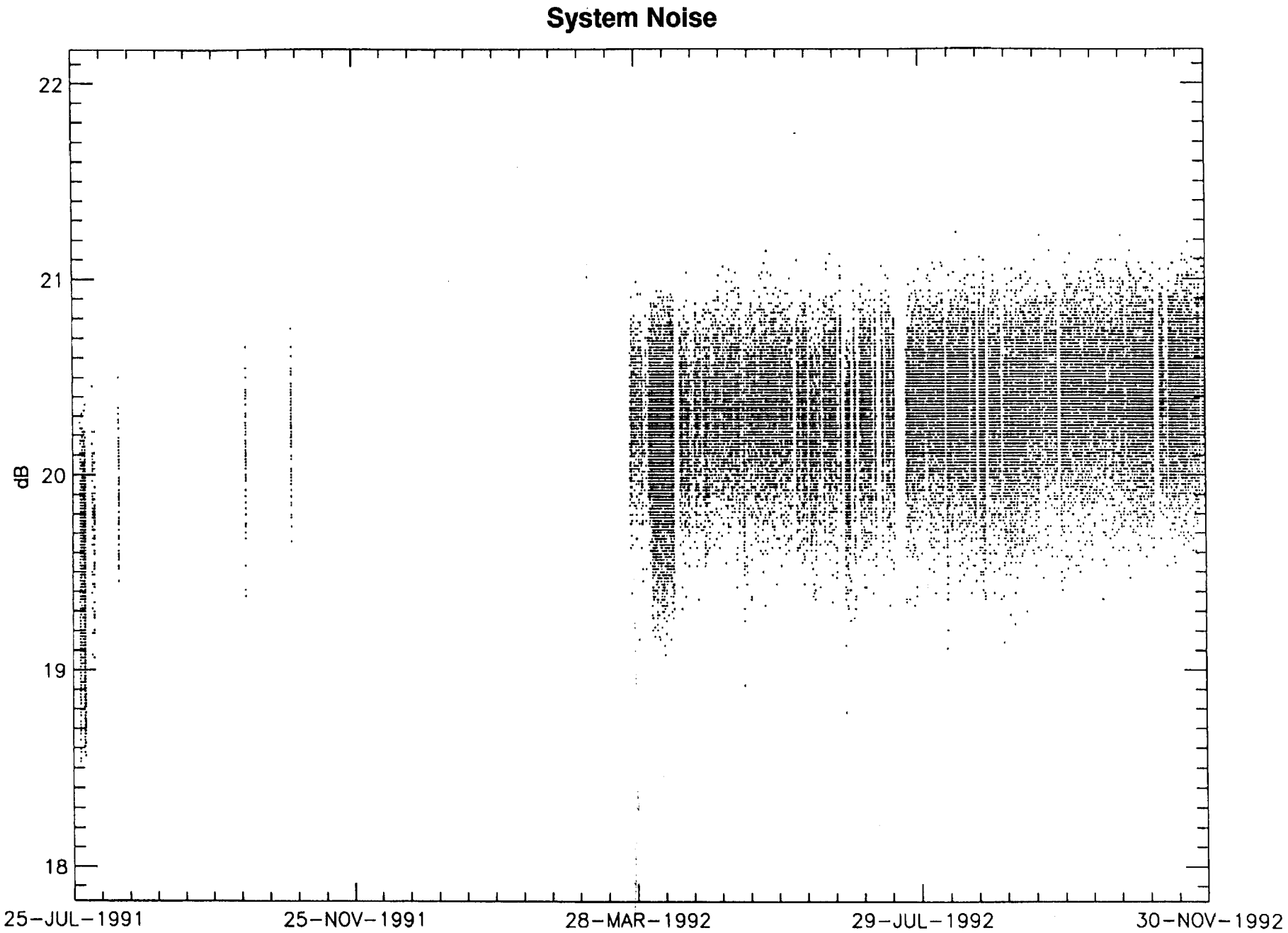
System Noise
22
21
20
19
18
dB
25-JUL-1991
25-NOV-1991
28-MAR-1992
29-JUL-1992
30-NOV-1992

INSTRUMENTATION (5)

IDHT :

- **BOTH TAPE RECORDERS ARE NOMINAL AND ARE USED ALTERNATIVELY EVERY 3 MONTHS**
- **THE TWO X-BAND LINKS ARE NOMINAL AND STABLE**
- **THIRD TUBE NOT USED**

INSTRUMENT OPERATIONS

RA :	**SYSTEMATIC GLOBAL OPERATIONS**
ATSR :	**SYSTEMATIC GLOBAL OPERATIONS**
AMI WIND/WAVE :	**SYSTEMATIC GLOBAL OPERATIONS OVER OCEANS, EXCEPT WHEN SAR IS OPERATED. WAVE MODE IS OPERATED AT 200 KM INTERVALS**
AMI SAR :	**UP TO 12 MINUTES PER ORBIT, INCLUDING UP TO 4 MINUTES IN ECLIPSE**

NOTE : ALL INSTRUMENTS ARE OPERATING ON THE "A" CHAINS SINCE LAUNCH.

PLATFORM AND INSTRUMENT AVAILABILITY

- SINCE LAUNCH : 99 % AVAILABILITY FOR THE PLATFORM. EXCEPT DURING THE PERIOD MID JULY- EARLY SEPTEMBER 1992, WHEN THE AVAILABILITY WAS REDUCED TO ABOUT 85%

- FOR THE INSTRUMENTATION : 97/98% AVAILABILITY. EXCEPT FOR THE PERIOD MID JULY- EARLY SEPTEMBER 1992 BECAUSE OF THE PLATFORM PROBLEMS

ERS-1 OVERALL GROUND SEGMENT

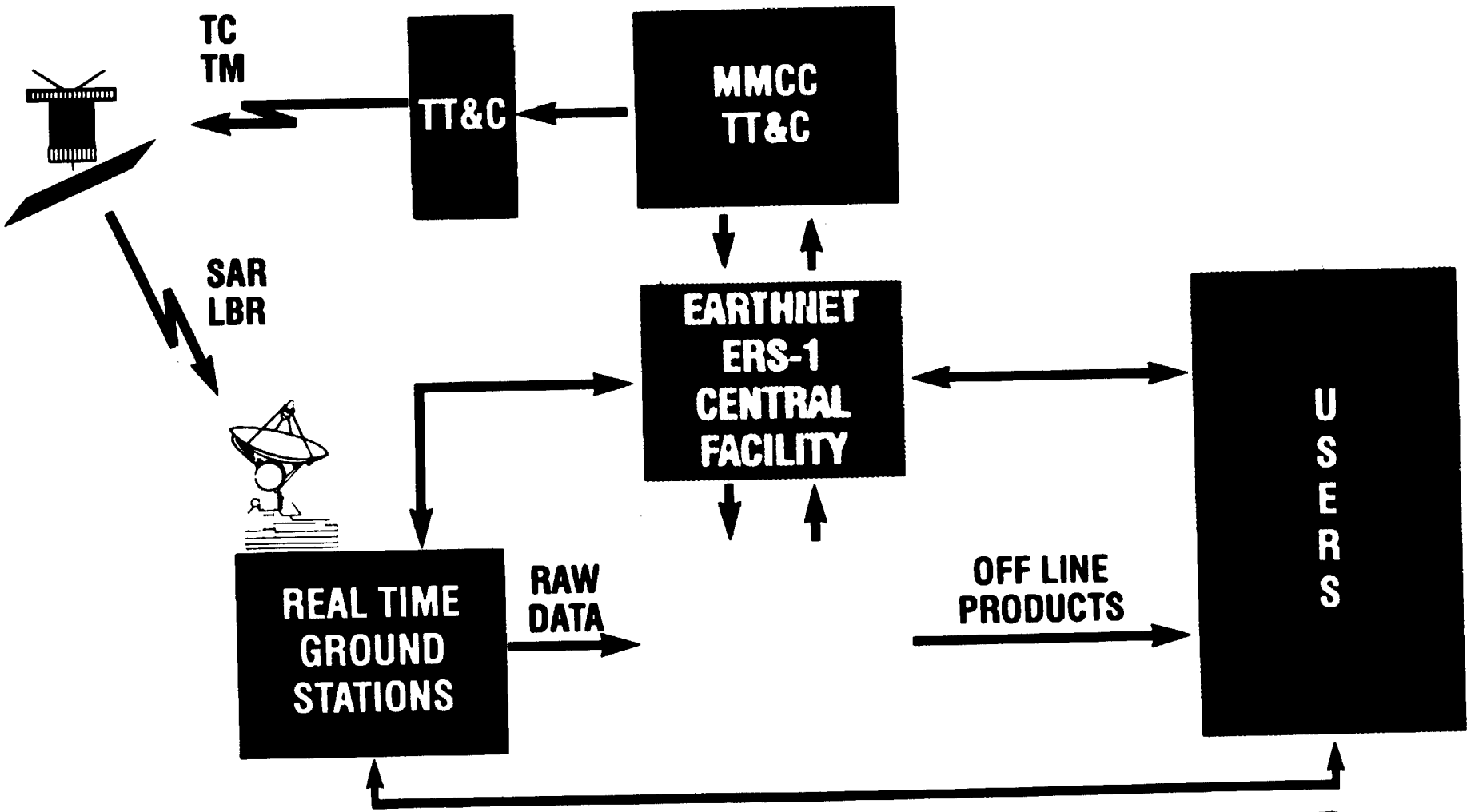

esa

LBR DATA ACQUISITION

- THE ACQUISITION OF LBR TAPE DUMPS IS PERFORMED AS FOLLOWS:

KIRUNA	10 ORBITS/DAY
MASPALOMAS	2 ORBITS/DAY
GATINEAU	1 ORBIT/DAY
PRINCE ALBERT (*)	1 ORBIT/DAY

(*) LBR DATA ACQUIRED AT PRINCE ALBERT ARE PROCESSED AT FD LEVEL AT GATINEAU TO COMPLETE THE GLOBAL LBR FD DATA SET, TO BE THEN ARCHIVED AT F-PAF.

LBR FD PRODUCTS

- WIND SCATTEROMETER (UWI): SIGMA NOUGHT TRIPLETS AND WIND FIELD (SPEED AND DIRECTION)
- RADAR ALTIMETER (URA): SIGNIFICANT WAVE HEIGHT WIND SPEED AT NADIR ALTITUDE
- SAR WAVE MODE (UWA): WAVE IMAGE SPECTRUM (WAVELENGTH AND DIRECTION)

GENERATED IN NEAR REAL-TIME ONLY AT THE FOLLOWING ESA STATIONS :

- KIRUNA
- MASPALOMAS
- GATINEAU

LBR FD DISSEMINATION

- LBR FD PRODUCTS ARE ROUTINELY DISTRIBUTED TO METEOROLOGICAL OFFICES OF PARTICIPATING STATES (AND NOAA) VIA THE GLOBAL TELECOMMUNICATION SYSTEM (GTS) IN WMO BUFR FORMAT

- AVERAGE DELAY FROM SENSING : 2 H 40 MINS.

SAR FAST DELIVERY PROCESSING AND DISSEMINATION

- SAR FD PRODUCT GENERATION SERVICE IS PROVIDED AT THE FOLLOWING ESA STATIONS :

  - KIRUNA
  - FUCINO
  - MASPALOMAS

esa

NEAR REAL-TIME DISSEMINATION OF ERS-1 SAR IMAGES OVER EUROPE

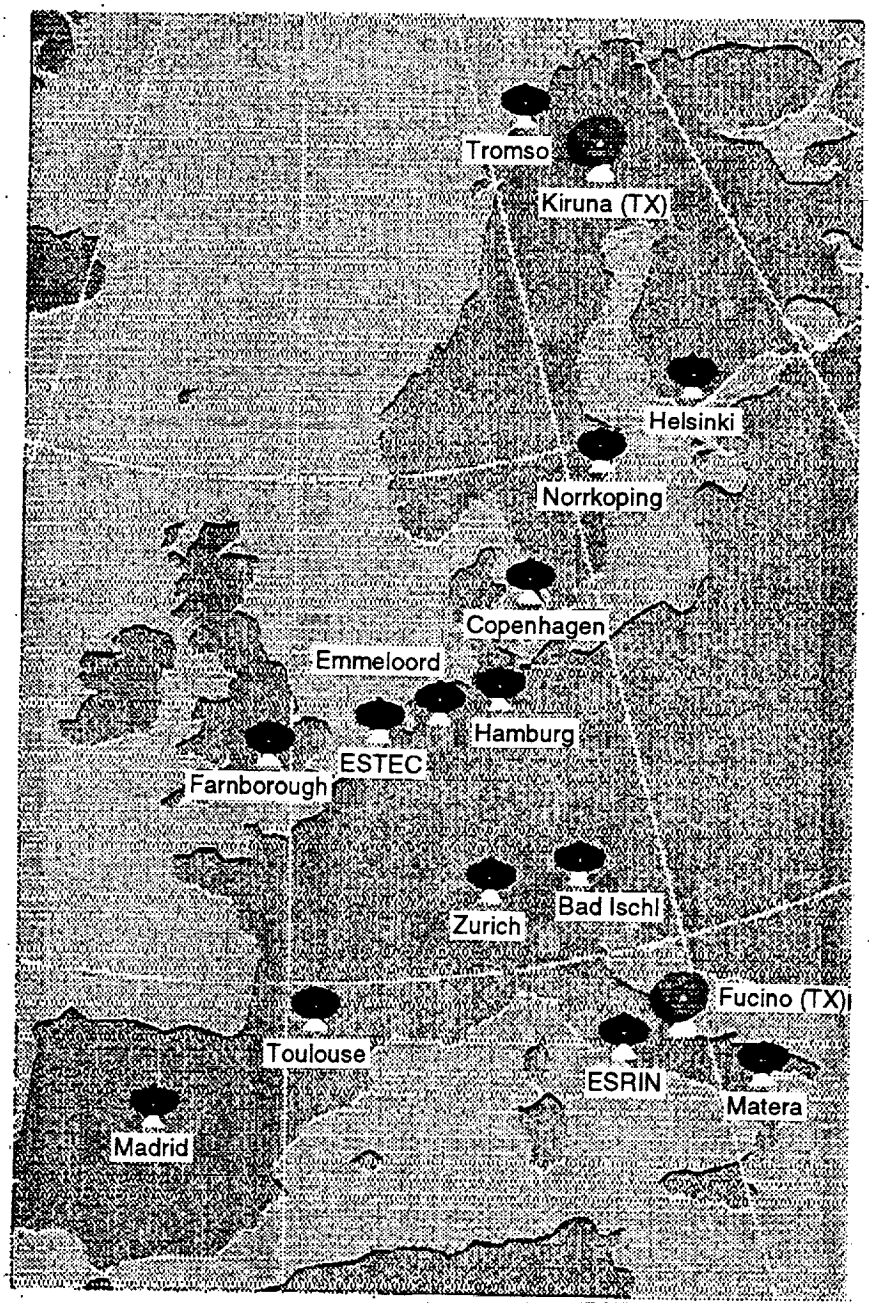

esa
Hobart
Alice Springs
Islamabad
Cuiaba
Syowa
O'Higgins

ACQUIRED SAR FRAMES FROM BEGINNING OF MISSION

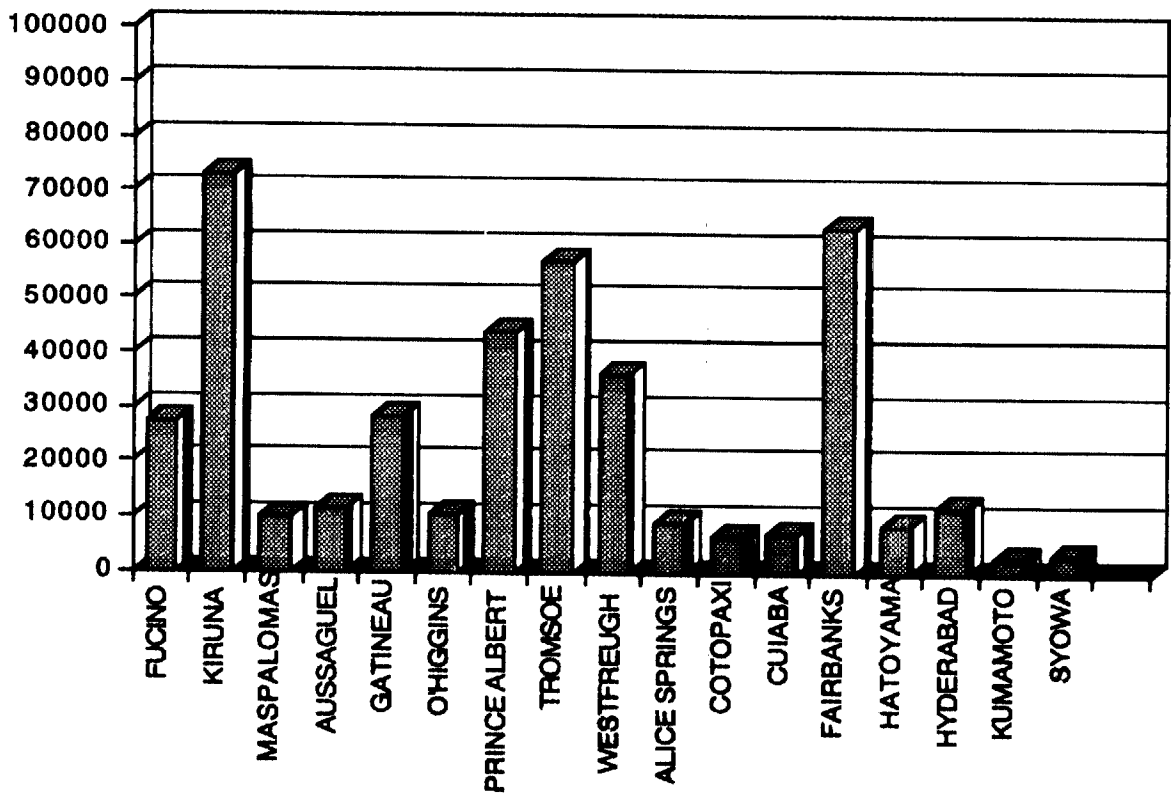

esa

SAR FRAMES PLANNED FOR ACQUISITION

(STATUS AS OF 30 OCT. 92, PLANNING UP TO 28 FEB.93)

	PHASE A	PHASE B	RTM	PHASE C	TOTALS
FUCINO	8594	3545	669	14607	27415
KIRUNA	23876	19634	910	28358	72778
MASPALOMAS	3714	670	174	5562	10120
TOTAL ESA	36184	23849	1753	48527	110313
AUSSAGUEL	3912			7386	11298
GATINEAU	6668	6222	560	14704	28154
O'HIGGINS	514	4742		5309	10565
PRINCE ALBERT	11408	8290	357	23698	43753
TROMSOE	18558	16675		21871	57104
WEST FREUGH	10139	8567		17266	35972
TOTAL NATIONALS	51199	44496	917	98234	186846
ALICE SPRINGS	2027	607		6485	9119
COTOPAXI	108	290	68	6142	6608
CUIABA	311	269	153	6461	7194
FAIRBANKS	13947	16696	136	32714	63493
HATOYAMA	2181	489		5663	8333
HYDERABAD	2048	878		9009	11935
KUMAMOTO	2737	145			2882
SYOWA	1291	889		848	3028
TOTAL FOREIGN	24650	20263	357	67322	112592
WORLDWIDE TOTALS	112033	88608	3027	206083	409751

esa

AN EXPANDING USER COMMUNITY

- THE PARTICIPATION TO THE CALIBRATION AND VALIDATION PROCESS
- THE SCIENTIFIC COMMUNITY AND THE ANNOUNCEMENT OF OPPORTUNITY
- THE (PRE-) OPERATIONAL COMMUNITY AND THE PILOT PROJECTS
- THE COMMERCIAL DISTRIBUTOR AND THE FIRST APPLICATIONS
- LARGE INSTITUTIONAL USERS

INTERNATIONAL COOPERATION

- THE INTERNATIONAL PARTNERS: NOAA, NASA, NASDA, ISRO, INPE ETC.
- THE FOREIGN STATIONS AND THE AGREEMENTS
- THE PARTICIPATION TO THE ANNOUNCEMENT OF OPPORTUNITY AND TO THE PILOT PROJECTS
- THE CEE/JRC COOPERATION
- THE CONTRIBUTIONS OF PARTICIPATING COUNTRIES TO THE DATA ANALYSIS AND EXPLOITATION EFFORT

IMPROVEMENTS TO SYSTEM AND SERVICES

- IMPROVE THE TIME RESPONSE OF THE MISSION PLANNING SYSTEM
- INTRODUCE SAR QUICK-LOOK PRODUCTS
- FUNCTIONALITIES OF THE USER INTERFACE
- IN COOPERATION WITH ERS-C DISTRIBUTOR IDENTIFY NEW PRODUCTS AND SERVICES

OBJECTIVES STILL TO BE ACHIEVED

- WIDEN THE COMMUNITY EXPLOITING THE SAR FD PRODUCTS IN REAL TIME (VIA BBDN) OR OFF-LINE (AS COPY FROM FD)
- IMPROVE DRASTICALLY THE CAPABILITY TO RECOVER DATA FROM SOME NON-ESA STATIONS
- COMPLETE THE FULL VALIDATION OF SOME OFF-LINE PRODUCTS E.G. SAR PRODUCTS FROM SOME FOREIGN STATIONS AND RA PRODUCTS
- IMPROVE THROUGHPUT FOR GENERATION OF OFF-LINE RA PRODUCTS (LEV. 2 AND WAVEFORM). CORRECTIVE MEASURES ARE BEING IMPLEMENTED
- PROCESS LBR BACKLOG AND MORE GENERALLY DEFINE STRATEGY FOR RE-PROCESSING OF ERS-1 LBR DATA

ALMAZ

V. Viter
NPO Machinostroyenia
33, Gagarin Street
Reutov, Moscow District 143952
Russia

BASIC DATA OF THE AUTOMATIC SPACE STATION "ALMAZ-1B"

Launch vehicle	Proton
Operational orbit parameters:	
• Altitude	350-400 km
• Inclination	73 grad
On-orbit mass	18,550 kg
On-board scientific equipment mass	up to 4,500 kg
Active operation time	up to 3 years
Orientation & stabilization accuracy:	
• Orientation	15-30 min. of arc
• Stabilization	4-6 min. of arc
Power-generating system characteristics:	
• Available average power per turn	2,300-3,300 W
• Maximum power (at peak load up to 15-20 min.)	8,600 W

ALMAZ-1B AUTOMATIC SPACE STATION

1. SAR - 70
   SAR - 10 r
2. SAR - 10 l
3. Multizonal Scanner MSU-SK
4. Spectroradiometer
5. Multizonal Scanner MSU-E
6. Side-looking Radar
7. Optoelectronic Equipment

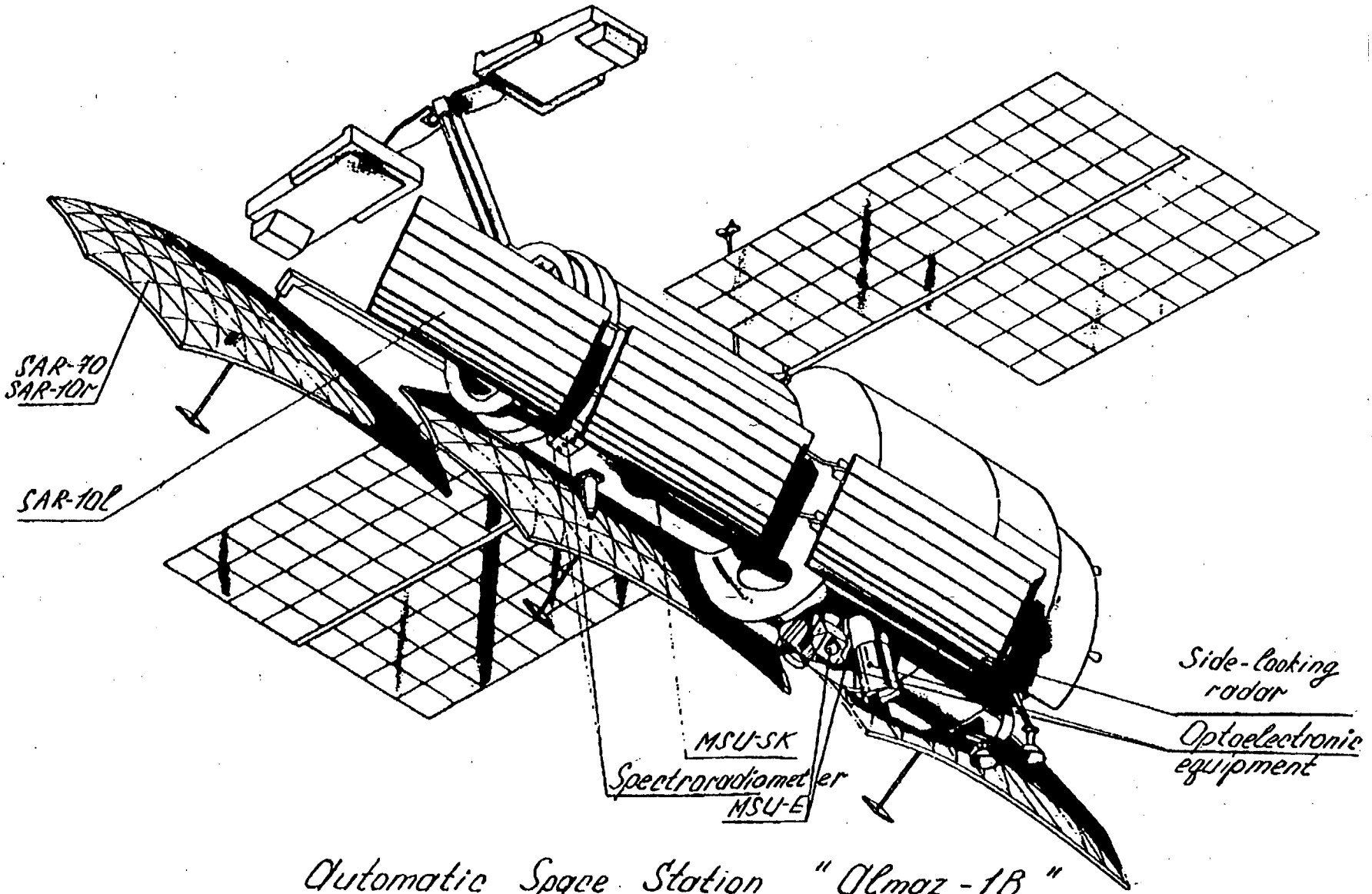

Automatic Space Station "Almaz-1B"

PRINCIPAL TECHNICAL CHARACTERISTICS OF REMOTE SENSING EQUIPMENT ON THE ALMAZ-1B SPACE STATION

A Set of Variant 1

1. Principal technical characteristics of radar equipment

1.1. Synthetic aperture radar — SAR-10

Operating wavelength range		9, 6 cm
Polarization		- horizontal (port) - horizontal or vertical (starboard)
Scanning direction		port or starboard at will
Angle of sight from nadir while turning		25 - 50 grad
Scanning field for re-shooting while turning		320 km
Time of continuous survey		up to 1,200 s
Mode of operation	detailed	general view
scanning field	25 - 50 km	100 - 150 km
resolution	5 - 7 m	15 m

1.2. Synthetic aperture radar — SAR-70

Operating wavelength range	70 cm
Polarization	horizontal or vertical
Scanning direction	starboard
Angle of sight from nadir	25 - 50 grad
Scanning field for re-shooting while turning	320 km
Time of continuous survey scanning	up to 1,200 s
Scanning field	100 - 150 km
Resolution	15 - 25 m

1.3. Side-looking radar

Angle of sight from nadir while turning	25 - 55 grad
Operating wavelength	3, 6 cm
Swath width	450 km
Resolution	400 - 1,200 m

2. Optoelectronic equipment for stereophotography

Number of operating ranges	5
Resolution on the ground	2 - 4 m
Swath width	70 km

3. Characteristics of multizone high-resolution electronic scanner MSU-E

Number of operating ranges	3
Resolution on the ground	10 m
Swath width	2 x 24 km
Potential angles of view	32 grad
Number of on-board sets	2

4. Characteristics of multizone middle-resolution optomechanical scanner MSU-SK

Number of operating ranges	5
Resolution on the ground	
- in visual range	80
- in IR range	300 m
Swath width	300 km

5. Characteristics of spectroradiometer for ocean satellite monitoring

Scanning field	2 x 1,100 km
Number of spectral zones	11
Boundaries of spectral zones	0.4 - 12.5 mkm
Linear resolution at nadir	0.6 km
Temperature resolution	0.1 K

6. Information transmission

Direct transmission to available receiving stations located on the Russian territory and abroad

Data collection on board and transmission to these stations when flown over

Data collection on board and transmission via relay-satellite to central receiving station

7. Effectiveness of information reception

Directly to receiving stations	no more 12 h
via relay-satellite	no more 2.5 h

8. Rate of information transmission

Directly to receiving stations	122.8 Mbit/s
Via relay-satellite	10 Mbit/s
Direct transmission to mobile and small receiving stations	3 Mbit/s or 960 Kbit/s

MAIN FIELDS AND DIRECTIONS OF ALMAZ-1B SPACE INFORMATION APPLICATION

CARTOGRAPHY

- Updating and completing topographic and thematic maps
- Cities development planning
- Transport networks planning
- Mapping of shelf shallow sections

LAND MONITORING

- Information supply of earth catastrophe, lands, forests, pastures and water resources
- Compiling soil maps and determining humus content
- Taking inventory and forecasting harvest yield
- Determining soil temperature and moisture content
- Detecting underground water sources

GEOLOGY

- Revealing perspective areas for mineral prospecting
- Geologic mapping
- Planning and controlling mineral/raw-mineral base
- Specifying data of mining and oil-bearing regions
- Monitoring large open-cast mining development

ECOLOGICAL MONITORING

- Controlling chemical compounds content in soil
- Controlling technogenic actions
- Controlling soil salinization and desertness
- Controlling soil erosion
- Controlling pollution of water surfaces with petroleum products
- Revealing underground unpermitted burials of industrial waste

OCEANOLOGY, PILOTAGE, FISHERY

- Evaluating ice conditions for pilotage
- Controlling chlorophyll content, evaluating bio-productivity of the world's ocean regions
- Studying the world's oceans and seas
- Compiling ocean temperature maps, pollution recording, studying fronts, currents, water, wind, etc.

INFORMATION SUPPLY DURING EMERGENCY

- Controlling situation in geologically dangerous regions (earthquakes, mudslides, avalanches, volcanic eruptions)
- Detecting forest and peat fires
- Controlling situation during accidents at industrial sites (fires, explosions, construction crashing down)

- Controlling situation in large transport accident regions including underground product tubes
- Controlling situation in hydrodynamic accident regions (dams, locks, sewage works)

APPROVED FLIGHT MISSIONS

SPACEBORNE IMAGING RADAR-C INSTRUMENT

BRYAN L. HUNEYCUTT
Jet Propulsion Laboratory
California Institute of Technology
4800 Oak Grove Drive, Pasadena, California 91109

Abstract - The Spaceborne Imaging Radar-C is the next radar in the series of spaceborne radar experiments, which began with Seasat and continued with SIR-A and SIR-B. [1-4] The SIR-C instrument has been designed to obtain simultaneous multifrequency and simultaneous multipolarization radar images from a low earth orbit. [5] It is a multiparameter imaging radar that will be flown during at least two different seasons. The instrument operates in the squint alignment mode, the extended aperture mode, the scansar mode, and the interferometry mode. The instrument uses engineering techniques such as beam nulling for echo tracking, pulse repetition frequency hopping for Doppler centroid tracking, generating the frequency step chirp for radar parameter flexibility, block floating-point quantizing for data rate compression, and elevation beamwidth broadening for increasing the swath illumination.

I. INTRODUCTION

The Spaceborne Imaging Radar-C (SIR-C) is a dual-frequency, quad-polarization imaging radar, designed to fly on the Space Shuttle in a low Earth orbit, and to operate from a stable platform located in the Orbiter payload bay. [6] Several flights are currently planned for SIR-C beginning in 1994. SIR-C has been designed to operate simultaneously at both L-band and C-band frequencies, and to utilize quad-polarization returns at each frequency. [6] SIR-C effectively has four separate radars: L-band horizontal L_H, L-band vertical L_V, C-band horizontal C_H, and C-band vertical C_V. In the nominal mode, SIR-C operates each of its four radars by radiating at broadside, utilizing a fully focused antenna aperture, much like the previous experiments, except that now there are really four radars operating simultaneously. The important SIR-C instrument parameters related to the operating modes and techniques are given in Table 1.

Fully instrumented testing of these various modes and techniques will occur at the experiment developer's facility, and not at the Shuttle launch site. Transmission from the full aperture and reception at far range is not planned even at the experiment developer's facility, due to the complicated and costly logistics of erecting such a large structure in an environmentally protected range. The SIR-C antenna is presently planned to be delivered into the integration flow at the launch site in its ready-to-launch configuration.

TABLE 1
SIR-C INSTRUMENT CHARACTERISTICS

Parameter	L-Band	C-Band
Azimuth Coalignment (arc min)	±8	±2
Azimuth beam steering (degrees)	±2	±1
Extended aperture beams	127	127
Extended aperture dwell time (ms)	20	20
Scansar beams	4	4
Scansar dwell time (ms)	30	30
Interferometry phase center offset (m)	N/A	4
Beam null ratio	1/PRF	1/PRF
PRF hopping dwell time (s)	1	1
Number of selectable PRF's	16	16
Elevation beamwidths	5-18°	5-18°
Number of selectable beamwidths	8	8
Digital chirp pulsewidth (μs)	8.4, 16.9, 33.8	8.4, 16.9, 33.8
Digital chirp bandwidth (MHz)	10,20	10,20
Quantization (bit)	8	8
BFPQ subset (bit)	4	4
BFPQ block length (samples)	128	128
PRF (Hz)	1240-2160	1240-2160
Stalo frequency (MHz)	89.994240	89.994240
Data steering	offset video	offset video
Number of high rate record channels	4	4

Functional tests of the SIR-C instrument will occur during integration with the Shuttle.

II. ANTENNA OPERATION AND TECHNIQUES

SIR-C will operate in modes, which were previously not possible, without electronic beam steering. Figure 1 illustrates the target illumination geometry corresponding to these operating modes.

A. Squint Alignment

Electronic beam steering in azimuth may be needed to align the H and V polarization swath illuminations, even though the antenna design calls for an azimuth electrical-to-mechanical boresight error of less than 4 arc minutes. Azimuth steering allows SIR-C to take data at a given squint angle, whereby the azimuth angle is fixed to one side or the other with respect to broadside. The H-polarization and V-polarization illuminations can be unintentionally

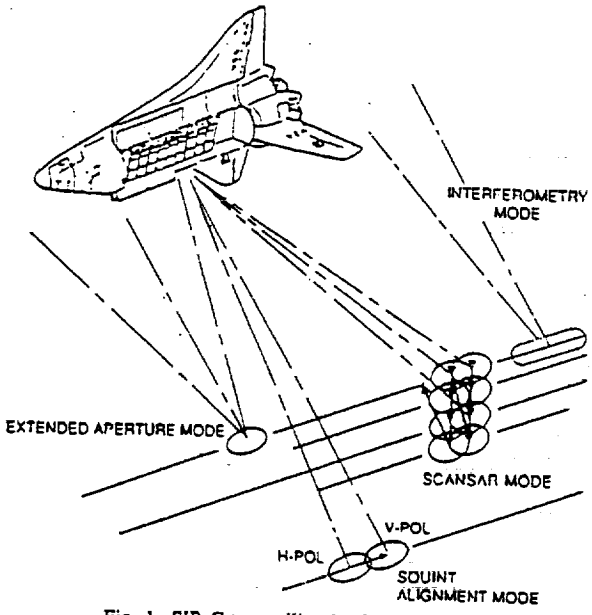

Fig. 1. SIR-C target illumination by modes.

offset due to mechanical tolerances in manufacturing and environmental effects in space such as uneven thermal distribution and zero gravity unloading. The beams can then be commanded to different azimuth squint angles until they are coaligned to within 4 arc minutes. The shape of the azimuth spectrum of the cross-polarization return can be used to verify proper co-alignment. Azimuth steering also allows experimenters to collect synthetic-aperture radar (SAR) data at selected fixed squint angles.

Because of the limited area for locating the electronics on each panel, a single transmit/receive (T/R) module and phase shifter pair feeds a subarray, and not individual elements. The stick-like subarray contains 6 radiating elements for L-band and 18 radiating elements for C-band. This restricts the azimuth steering to only a few degrees. Electronic beam steering can be accomplished for only ± 1 deg in azimuth for C-band, and ± 2 deg in azimuth for L-band; beyond these limits, the side lobes increase, the main lobe broadens, and grating lobes occur at unacceptable levels. [6]

B. Extended Aperture

Azimuth steering allows SIR-C to take data in the extended aperture mode, or "spotlight" mode, whereby the same scene on the ground is illuminated as the Shuttle passes the scene, and the effective aperture is thereby extended. This technique increases the effective azimuth Doppler bandwidth to improve the image quality. This increased bandwidth permits: (1) finer spatial resolution by utilizing the full bandwidth and (2) reduced speckle by incoherently adding more azimuth looks. To implement this extended aperture mode, as an example, the antenna beam is first squinted ahead at the full range positive squint angle, and then decremented in small uniform steps of squint angle at uniform time increments, until the antenna beam is looking behind at the full range negative angle.

C. Scansar

Electronic beam steering in elevation allows SIR-C to image in a scansar mode, whereby the antenna beam is steered to as many as four previously selected elevation angles during each synthetic aperture interval. This dramatically increases the width of the swath which can be imaged during a data take. The beam is electronically steered in elevation as in azimuth by varying the phase-front across the aperture via the microprocessor-controlled phase shifters. The SAR processor must treat the data from each elevation angle as burst data. The azimuth resolution of the processed bursts of data is degraded by a factor of 4; however, the swath width illumination is increased by about the same factor. Since the synthetic aperture interval increases with the look angle off nadir, the dwell time at each of the four elevation angles increases with the look angle.

D. Antenna Beamwidth Broadening

For a uniformly illuminated aperture, the aperture dimension and RF wavelength determine the antenna beamwidth. SIR-C uses a technique of tapering the power in elevation, which provides lower side lobes (approximately -18 dB side lobes) than for the uniform illumination case. This configuration uses less T/R modules, and thus less power. Lower side lobes are achieved in elevation. The resultant antenna pattern is lower in amplitude and has a wider beamwidth.

Within the constraints of the Shuttle payload bay volume, the aperture sizes were optimized to have sufficient aperture gain, yet sufficiently low azimuth and range ambiguities over the pulse repetition frequencies (PRFs) selected. The sizes of the full apertures

are 12.1 m x 2.95 m for L-band and 12.1 m x 0.75 m for C-band, which yield a fully focused elevation beamwidth of 4.7 deg for each frequency. Variable beamwidths in elevation can be accommodated by selecting a pre-programmed phase function across the array. One of eight selectable beamwidths from 4.7 deg to 18.0 deg is selected by an uplink command. The amplitude decreases and the side-lobe levels increase slightly with increasing beamwidths. The beamwidth is optimized for swath illumination at the various look angles.

E. Beam Nulling

The phase shifters in one half the array will be periodically shifted 180 deg in elevation, thereby nulling the elevation beam pattern. This is an echo-tracking technique to determine the roll angle, and thereby accounts for the elevation antenna pattern in the raw SAR data during amplitude calibration. Results from simulations indicate that beam nulling during one receive interval in each one-second interval is sufficient to determine the roll angle and yet not degrade the image significantly. The roll angle can be determined with an accuracy of a few tenths of a degree.

III. RF ELECTRONICS

The RF electronics subsystem is located on the pallet in the cargo bay. The RF electronics subsystem accommodates several new techniques not previously used in the SIR series.

A. Digital Chirp

To attain fine resolution in range, SIR-C encodes each transmitted pulse, such that each pulse of duration T can resolve targets as if a much shorter pulse of duration T/TBW, where TBW is the time-bandwidth product, had been transmitted. SEASAT, SIR-A, and SIR-B used the passive dispersive delay line (DDL) approach; however, for SIR-C a different DDL would be required for every TBW required. SIR-C attains this large time-bandwidth product by distributing the energy of each pulse over the frequency bandwidth, stepwise linearly with time. The SIR-C chirp signal is approximated digitally, in that a tone is successively stepped across the bandwidth within the pulse duration, approximating a linear FM (LFM), or chirp, signal. The number of frequency steps varies with the bandwidth, pulse-width, and frequency-step size combination. The 10-MHz, full pulse-width case requires 76 steps; whereas, the 20-MHz, full pulse-width case requires 152 steps. The number of steps for SIR-C trades off the integrated side-lobe ratio with realistic switching rates. The integrated side-lobe ratio has been measured to be approximately -9.5 dB and the measured impulse response width agrees closely with that of an ideal chirp.

The frequency-step chirp technique provides flexibility in the selection of certain radar parameters: (1) pulse width, (2) calibration tone frequency, and (3) bandwidth. The transmitted pulse width can be decreased by a factor of 2 or 4 to lower the average dc power usage. Fixed frequency calibration tones can be generated from the same digital chirp device, and the frequency of the calibration tone can be selected. The RF bandwidth can be increased from 10 MHz to 20 MHz to improve the range resolution.

B. Interferometry Mode

The L-band and C-band apertures are subdivided into 3 equal area sections called leaves. The two outer leaves are unfolded after attaining orbit in order to transmit. The received echo signals from the two extreme C-Band leaves can be coupled into two separate receiver channels in order to accommodate a special interferometry mode. This requires couplers in the C-Band RF feed system at the initial 3-way power combiner, such that the inputs from the two extreme leaves can be routed to two separate receiver channels. The technique provides returns from the two existing extreme leaf apertures, whose phase centers are separated by the distance of one leaf in the azimuthal direction. Processing of the interferometry data from ocean returns, for example, can provide ocean current direction. [7]

IV. DIGITAL ELECTRONICS TECHNIQUES

The Digital Electronics Subsystem uses engineering techniques required by SIR-C in order to obtain calibrated data and to be much more flexible in radar parameter selection than in previous imaging radar experiments in this series. These techniques are utilized during the normal operation of the radar.

A. Alternating Pulse Mode

The SIR-C exciter operates in an alternating pulse scheme such that the oppositely polarized pulse is delayed by half an inter-

pulse period. The radar effectively operates at twice the nominal PRF. For quad- polarization operation, both like- and cross-polarization echoes are received in the same channel.

B. Block Floating-Point Quantizing

The offset video output from each of the four receivers is digitized to 8 bits per sample with uniform quantization at a constant rate of 45 MHz. A SIR-C feature allows formatting the raw samples as 4 bits, 8 bits, or an (8,4) floating-point block. The block floating-point quantizer (BFPQ) derives its name from "blocks" of data being uniformly quantized and subsets of the available bits being selected by a predetermined algorithm, equivalent to moving the "floating point" marker in binary data. If the data transmission rate to the onboard recorders is held constant, then doubling the number of bits per sample approximately halves the swath width, therefore trading off dynamic range for swath width.

The (8,4) BFPQ is a data rate compression technique. The (8,4) BFPQ method provides an output rate similar to a 4-bit uniform scheme but with the dynamic range of an 8-bit system. For each block of data, a series of bits are transmitted, including the sign bit, followed by the optimally selected 3 contiguous bits per sample, followed by a common exponent for the block. The block size is 128 samples of raw data. The formatted data are transmitted as 8-bit parallel words. The distortion noise for the (8,4) BFPQ is about 24 dB higher than for the 8-bit uniform quantizer (UQ); however, the range of return signal level for which the distortion noise is almost constant is about 24 dB wider than that for the 8-bit UQ. [6] Therefore, the performance of the (8,4) BFPQ is less sensitive to the typically widely varying level of the return echo.

C. Digital Data Steering

In normal data takes, each receiver output is directed to a previously selected, separate digital data handling assembly (DDHA) for digitizing, buffering, and formatting. This steering occurs at offset video. Once the individual offset video signals have been digitized, formatted, and serialized, there is flexibility in steering to a redundant on-board Payload High Rate Recorder (PHRR). This data steering allows for recovery in case one or more of the DDHAs or the PHRRs should fail.

In extended swath data takes, one receiver output is directed to two DDHA's, such that the resulting data represent an image swath twice that of a single DDHA. The SAR processor will have all four channels combined on one tape cassette.

D. Integer PRFs

SIR-C has incorporated integer PRFs, whereby there are an exact integer number of PRF pulses in one second. SEASAT, SIR-A, and SIR-B used a countdown scheme to derive PRFs from the STALO, a stable local oscillator, without regard for whether the PRFs were integral. The SIR-C integer PRF facilitates timing for the radar since the PRF and timing circuitry provides basic control of the radar for PRF changes, receiver gain, exciter timing, digital window position, and data channel switching, all of which change state synchronously on one-second time ticks (OSTTs). Also, SIR-C chose the PRFs such that there are an integer number of 8-bit bytes in a range line. This feature facilitates ground processing. Since the PRFs are derived from a very stable STALO, the requirement of integer PRFs affects the choice of the STALO frequency. By analysis, it was determined that by using a STALO with frequency 89.994240 MHz, there were at least 16 integer PRFs in the range from 1240 Hz to 2160 Hz, which were compatible with the altitude and look-angle range of SIR-C.

E. PRF Hopping

SIR-C uses a PRF hopping technique, or multiple PRF technique, whereby the azimuth Doppler spectrum can be located unambiguously. For the PRF hopping technique, if the azimuth spectrum is offset in frequency because of pointing errors, for example, the centroid of the spectrum falls into different portions of the azimuth processing bandwidth when sampled at various PRF rates. By knowing the ambiguous location of the centroid for three different PRFs, the location of the unambiguous location, and thereby the yaw angle, can be calculated. The PRF hopping will occur at the beginning and end of each data take. There will be a one-second dwell at each of the three PRFs.

V. Summary

Several operating modes and engineering techniques used in the SIR-C instrument have been described: squint alignment, extended aperture, scansar, interferometry, beam nulling, PRF

hopping, antenna beamwidth broadening, generating frequency-step chirp signals, block floating-point quantizing, integer PRF's, and digital data steering.

Acknowledgments

The author thanks C. Elachi, M. Sander, N. Herman, E. Caro, and F. Stuhr of the Jet Propulsion Laboratory; G. Salisbury of Ball Communication Systems Division, Ball Corporation; R. Monson of NASA Headquarters; and the many individuals whose contributions made possible the design of the SIR-C hardware. The work on the instrument as described in this paper was carried out by the Jet Propulsion Laboratory, California Institute of Technology, under contract with the National Aeronautics and Space Administration.

References

[1] R. L. Jordan, "The SEASAT - A Synthetic Aperture Radar System," IEEE Journal of Oceanic Engineering, Vol. OE-5, pp 154-164, April 1980.

[2] J. B. Cimino and C. Elachi, Eds., Shuttle Imaging Radar A (SIR-A) Experiment, JPL Pub. 82-77, Jet Propulsion Laboratory, Pasadena, California, December 15, 1982.

[3] J. L. Granger, "Shuttle Imaging - A/B Sensors," Spaceborne Imaging Radar Symposium, JPL Pub. 83-11, Jet Propulsion Laboratory, Pasadena, California, July 1, 1983.

[4] IEEE Transactions on Geoscience and Remote Sensing, Special Issue on the Shuttle Imaging Radar, Vol. GE-24, No. 4, July 1986.

[5] Shuttle Imaging Radar - C Science Plan, JPL Pub. 86-29, Jet Propulsion Laboratory, Pasadena, California, September 1, 1986.

[6] B. L. Huneycutt, "Spaceborne Imaging Radar-C Instrument," IEEE Transactions on Geoscience and Remote Sensing, Vol. 27, No. 2, pp 164-169, March 1989.

[7] R. Goldstein, et al., "Remote Sensing of Ocean Currents," Science, Vol. 2-16, pp. 1282-1285, December 8, 1989.

[8] C. Y. Chang and J. C. Curlander, "Doppler Centroid Estimation Ambiguity for Synthetic Aperture Radars," Proceedings of IGARSS'89, pp. 2567-2571, July 1989.

X-SAR

THE X-BAND SYNTHETIC APERTURE RADAR ON BOARD THE SPACE SHUTTLE

Marian U. Werner
DLR German Aerospace Research Establishment
Institut für Hochfrequenztechnik
8031 Oberpfaffenhofen, Germany
Tel.08153-28397,Fax.08153-281449

Introduction

X-SAR is the German/Italian contribution to the NASA/JPL Shuttle Radar Lab missions as part of the preparation for the Earth Observation System (EOS) program. The Shuttle Radar Lab is a combination of several radars: an L-band (1.2 GHz)and a C-band (5.3 GHz) multipolarisation SAR known as SIR-C (Shuttle Imaging Radar) and an X-band (9.6 GHz) vertical polarised SAR which will be operated synchronously over the same target areas to deliver for the first time calibrated multifrequency and multipolarisation SAR data at multiple incidence angles from space.

A joint German/Italian project office at DARA (German Space Agency) is responsible for the management of the X-SAR project. The space hardware has been developed and manufactured under industrial contract by Dornier and Alenia Spazio. Besides supporting all the technical and scientific tasks, DLR, in cooperation with ASI (Agenzia Spaziale Italiano) is responsible for mission operation, calibration and high precission SAR processing. In addition, DLR developed an airborne X-band SAR to support the experimenters with campaigns to prepare for the missions.

The main advantage of adding a shorter wavelength (3 cm) radar to the SIR-C radars is the X-band radar's weaker penetration into vegetation and soil and its high sensitivity to surface roughness and associated phenomena. The performance of each of the three radars is comparable with respect to radiometric and geometric resolution.

Instrument development

As of about one year before the first mission, the flight hardware has been manufactured, and the integrated X-SAR instrument is undergoing a phase of thorough testing and characterization of its performance. Following to these tests, the X-SAR has been delivered to the U.S.A. and will be integrated in the SIR-C radars and subsystems at JPL (Jet Propulsion Laboratories in Pasadena). After the three X-SAR slotted waveguide array antenna panels are mounted on to the common mechanical antenna structure the antenna will become for the first time a full 12 m in length. The X-band antenna will be mechanically pointed to its targets while the SIR-C antennas have the capability to point electronically to the same target area on ground. The passive X-SAR antenna is connected to its high power transmitter and its low noise receiver via a quite long waveguide running from the electronic boxes down in the pallet bay up to the top of the antenna structure. The three panels are fed via a rotary joint and a three-way power devider. The predicted mechanical loads and stresses, up to 15 g during launch and landing, are a challenge to the design of this waveguide, which has to be built out of special rigid and flexible pieces to take care of the dynamic and static deflections between the pallet-mounted equipment and the antenna as well as between the movable X-SAR structure and the core structure.

X-SAR/SIR-C Blockdiagram

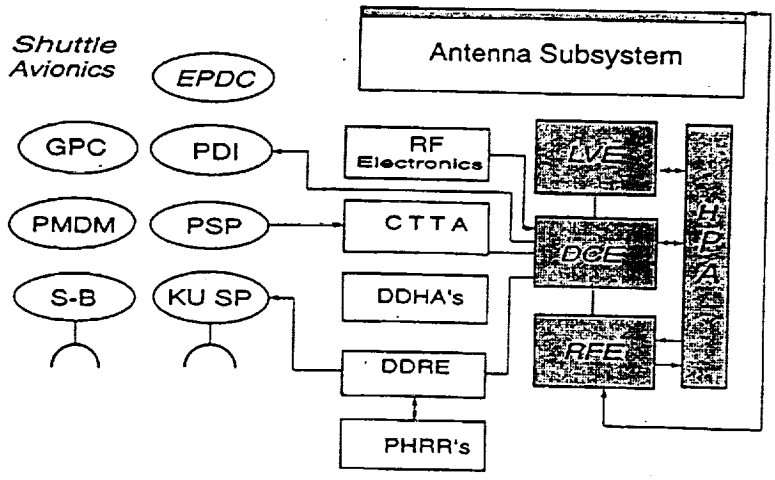

Although it is planned to operate X-SAR and SIR-C synchronously, each radar is also capable of autonomous operation. To insure proper synchronism SIR-C acts as the master for all timing signals as well as for the local oscillator, which is the basis for the common frequency generation. Also part of the telemetry and command subsystems and the high rate data handling, recording and switching is under SIR-C control. Therefore, in addition to the testing of the subsystems itself, careful testing of this interfaces and the compatibility of both systems running, has to be verified before delivery to the Kennedy SpaceFlight Center for integration with the orbiter. The antenna will cover about 60 % of the whole cargo bay and is mounted with a fixed tilt of 14 degrees. All electronic boxes are installed on coldplates under the antenna structure on a spacelab pallet. Inside the shuttle cabin one of the three high rate data cassette recorders will be dedicated to record X-SAR data.

Mission operations

The three radars will be operated during the ten day missions synchronously over selected target areas based on the mission plan, worked out by the SIR-C/X-SAR science team in collaboration with the principal investigators.Highest priority is given to the so-called super test sites in which ground calibration and insitu measurements are made. In total, about 50 hours of X-SAR raw data are expected which will be recorded on board. A part of this data can in addition be transmitted to the ground in real time. The orbit altitude is planned to be 220 km and the inclination will be 57°. The orbiter will fly in a 26° roll and a 180° pitch angle which makes the radars looking 40° off nadar when no beam pointing is commanded.

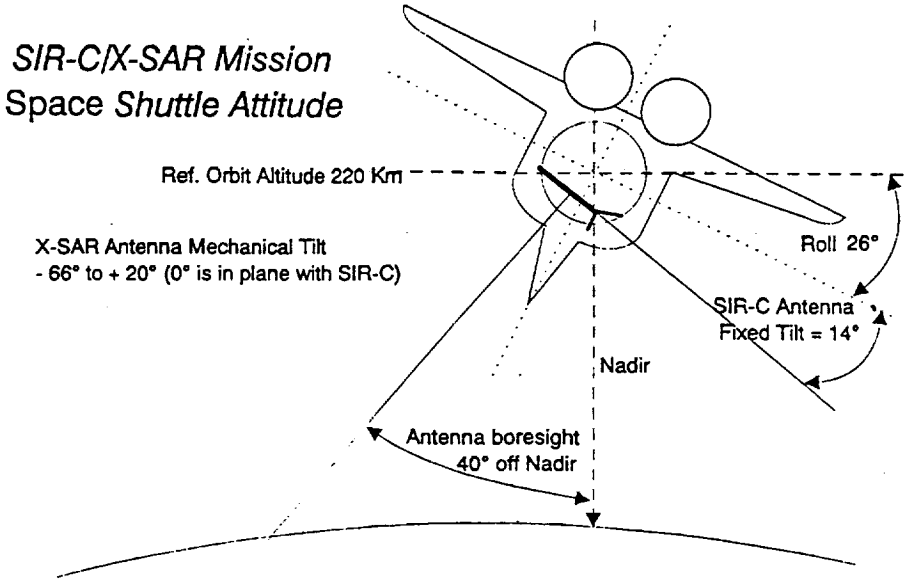

To carry out the ambitious mission plans, a powerful and flexible mission operations and planning tool is being developed which is capable of performing joint, coordinated operations with SIR-C.

The main elements of the MPOS (mission planning and operations system) are the mission planning and analysis system, the telemetry system, the command system and the SAR real time quicklook processing system. While the mission planning software tools such as the mission timeline planning, the data-take selection, the performance estimator and the command plan generator are also necessary for pre-mission preparation, these and the hardware elements mentioned above will all be integrated into the JSC POCC (payload operation and control center at the Johnson Space Flight Center) in Houston.

The flow of the mission planning is normally the following: Input data provide latest information about the sites, the attitude timeline and the orbit state vectors. The mission planning software then calculates and displays the data take opportunities, which are then checked against the requirements and mission rules by the data-take selection software. To determine the optimum and jointly coordinated radar parameter settings, a performance estimator calculates radar parameters and the predicted image performance using known instrument characteristics for each target or data-take. These radar settings are then transformed by the command plan generator into commands which are tagged with the appropriate times for execution in the instrument. Up to 256 command blocks may be sent to the onboard instrument sequencer memory, enough for a whole day of automatic operation if no updates would be necessary.

Real time commanding is possible and might be necessary during the mission when the performance analyser system shows the operator improper radar parameters, or if the parameters are no longer optimum. This might happen because the Space Shuttle is not a very stable platform for a SAR and the attitude and orbit data avaiable during mission are not very accurate. The monitoring of the on-board instrument is performed with the telemetry system which shows the status and health of the X-SAR instrument as well as with the SAR processing system when realtime data transmission is scheduled for X-SAR. The real time data will be recorded on ground and in parallel routed to the deformatter and quicklook SAR processor, which show the processed image of the scene in a waterfall display. This will permit the monitoring of the performance of the instrument, the proper timing of the receive window and the pointing of the antenna to support the control of the test-site coverage.

After the mission an as-run timeline and a mission operations report evaluating the instrument functional performance will be supplied, together with a duplicate of all recorded data for the off-line processing systems.

Performance critical areas

A key instrument parameter for the performance is the in flight antenna pattern, but its prediction has a high uncertainty. Each of the three 4 m long antenna panels had to be measured seperately on a far-field test range. An ideal reconstruction of the full 12 m antenna performed using software tools showed excellent performance.

The inflight antenna pattern will be more or less degraded by the mechanical performance of the antenna truss with its static deflections and temperature effects but also due to the presence of the SIR-C antenna and the orbiter elements. A further problem area is the knowledge of the pointing of the antenna to the target which is depending on the attitude measurement accuracy and the alignement accuracy of the antennas with respect to the orbiter coordinate system. Main regions of concern are the 1. sidelobe levels (up to -8.3 dB in a worst case) of the azimuth pattern which impacts on the ambiguity ratio and the peak gain variation (up to 0.9 dB in worst case) which impacts on the gain stability and calibration accuracy. A verification of the inflight antenna pattern and its pointing will be measured with ground receivers distributed over the swath at least over the calibration test site.

Gain variation of the transmitter and receiver chain over the temperature range is an other critical area which directly impacts on the radiometric accuracy or at least complicates the calibration. X-SAR was not successfull in implementing an automatic compensation of the gain variation over the temperature range of about 40 degrees Celsius. But for the postmission data processing a careful characterisation of the gain versus temperature under thermal vaccum conditions has been done resulting in a set of curves which have to be used together witch the temperature housekeeping recorded during the mission. The measured gain variation is about 0.2 dB per degree Celsius which should not be too bad taking into account the excellent temperature stability of the coldplates in earlier missions.

Performance prediction

Based on jointly agreed upon definitions, X-SAR and SIR-C calculate their predicted performance with validated system perfomance software tools. The performance models use algorithms which transform the instrument parameters and assumptions about the platform, the processor and the target into image performance parameters. The instrument parameters used were taken from the latest measurements of the flight hardware. The performance is calculated for point targets, providing geometric resolutions. For distributed targets radiometric resolution, ambiguity levels, signal-to-noise ratios and the performance swath width are calculated. The following table shows the performance for four typical incidence angles.

Requirement	for point targets				distributed targets			
Incidence angle	20°	30°	40°	50°	20°	30°	40°	50°
Range resolution								
fine < 10 m	9.6	9.8						
coarse < 20 m			17.7	18.0				
Range ISLR >11 dB	12.1	12.1	12.2	12.2				
Range PSLR >20 dB	21.9	21.9	21.9	21.9				
Azimuth resol. 30	27.5	27.5	27.4	27.4				
Azimuth ISLR >11dB	15.47	15.45	15.51	15.51				
Azimuth PSLR >20dB	21.9	21.9	21.9	21.9				
Ambiguity Azimuth					19.4	19.4	20.0	19.4
Ambiguity Range					>40	>40	>40	>40
Total > 18 dB					19.4	19.4	20.0	20.0
Radiom. Res.<2.75					<2.1	<2.8	<2.0	<2.1
Image SNR					>8.7	>8.4	>10.2	>7.7
Dynamic > 20 dB					32.9	34.7	36.7	36.8
Swath width>15 km					30.4	20.7	36.6	32.0

SAR Data Processing

The processing of the X-SAR raw radar data will be performed in two processing and archiving centers one at ASI in Matera Italy (I-PAF) and one at DLR in Oberpfaffenhofen Germany (D-PAF). ASI will be responsible for processing the survey products of all X-SAR data within three months after the mission for the selection of the test sites for which high precision calibrated products will be

processed. The processing of the high precision products will be shared between ASI and DLR. The calibration testsites will be processed first, so that the calibration team can determin the calibration factors to be used from both PAF's for the precision processing. Several data products like single look, multilook, geocoded and several product media can be selected by the data users which place their orders via the science team to the PAF's. All three processing centers JPL, ASI and DLR have jointly agreed on the data products, quality and the formats. The main challenge for the X-SAR data processing is the relative unstable Shuttle plattform and the low precision of the orbit and attitude data. To find the correct doppler and dopplerband a new algorithm to solve the doppler ambiguity problem in the X-SAR data has been developed and will be applied during the screening process of the data. The processor hardware and software development is in good progress and converted ERS-1 and simulated test data have been processed successfully.

As an example for the SAR processing the D-PAF block diagram is shown.

PAF Environment

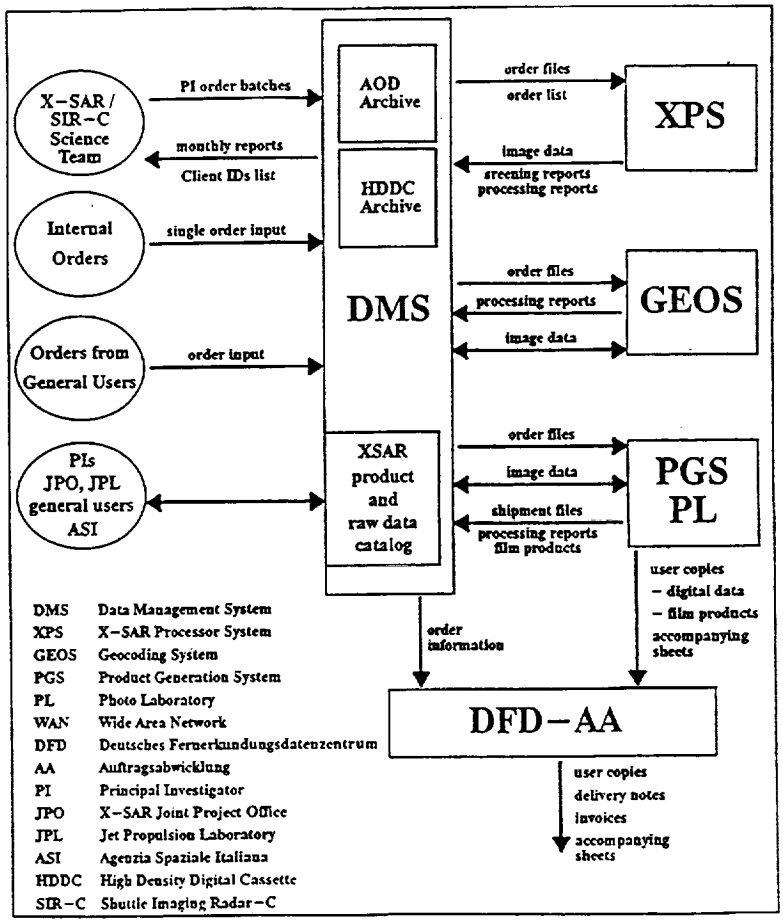

56-18

182846

P. 22

N94-15892

ENVISAT ASAR

J. Louet

European Space Laboratory
The Netherlands

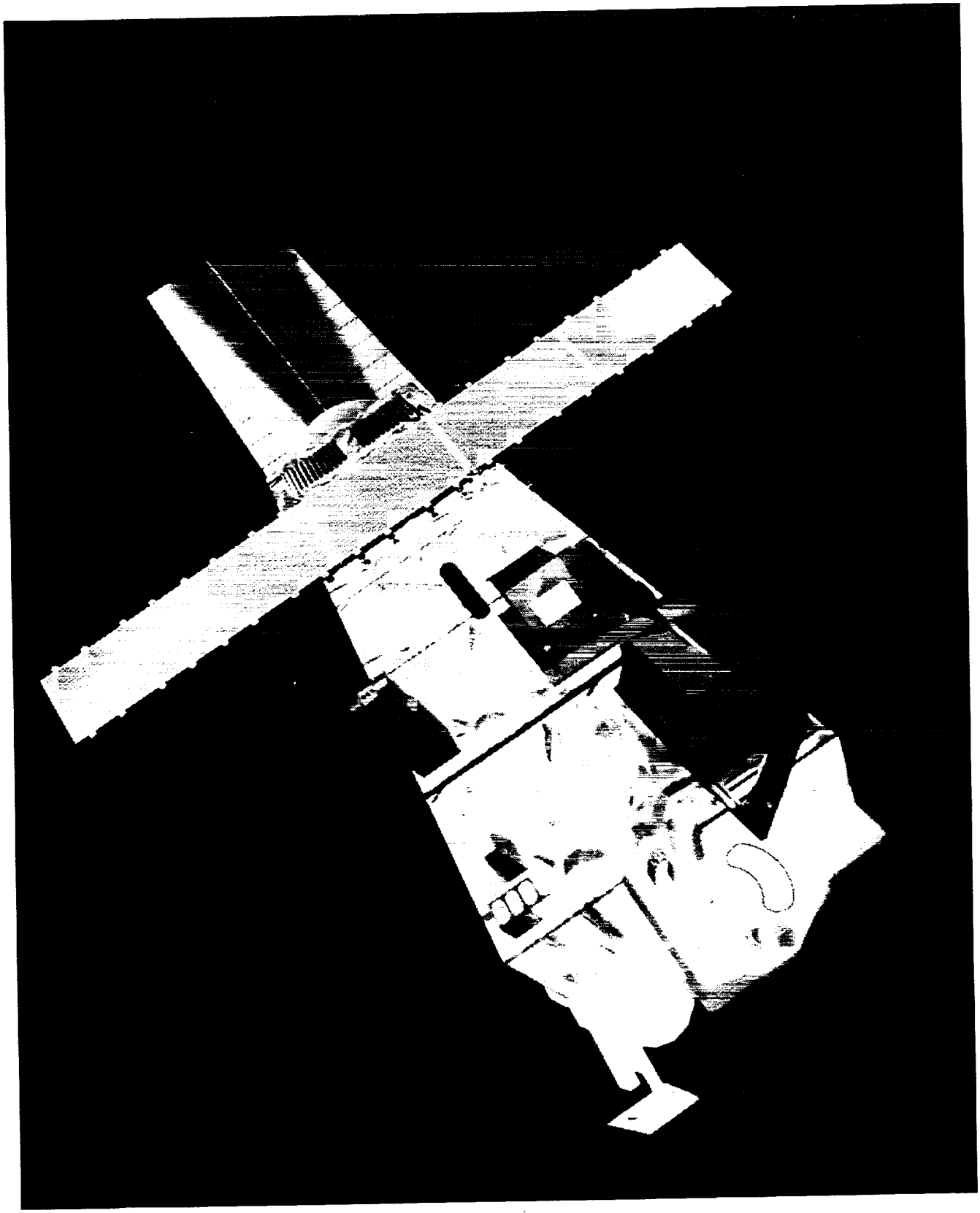

Objectives

The Objectives of ASAR are to measure:

- Sea ice extent, character and motion
- Snow and ice extent and character
- Vegetation, Land use
- Surface topography
- Ocean waves and circulation

Independence of cloud cover/day or night

With respect to ERS-1: extended coverage and dual polarisation

Modes of operation

Image	"ERS" type image mode, high resolution, selectable swath position, two polarisations
Wide Swath	Wide swath with medium resolution, two polarisations
Alternating Polarisation	Alternating VV and HH operation in image mode swaths, using n samples of each polarisation
Wave	Sampled image mode. low data rate, selectable swath positions
Global Monitoring	Wide swath, low spatial resolution, low data rate, HH and VV polarisations

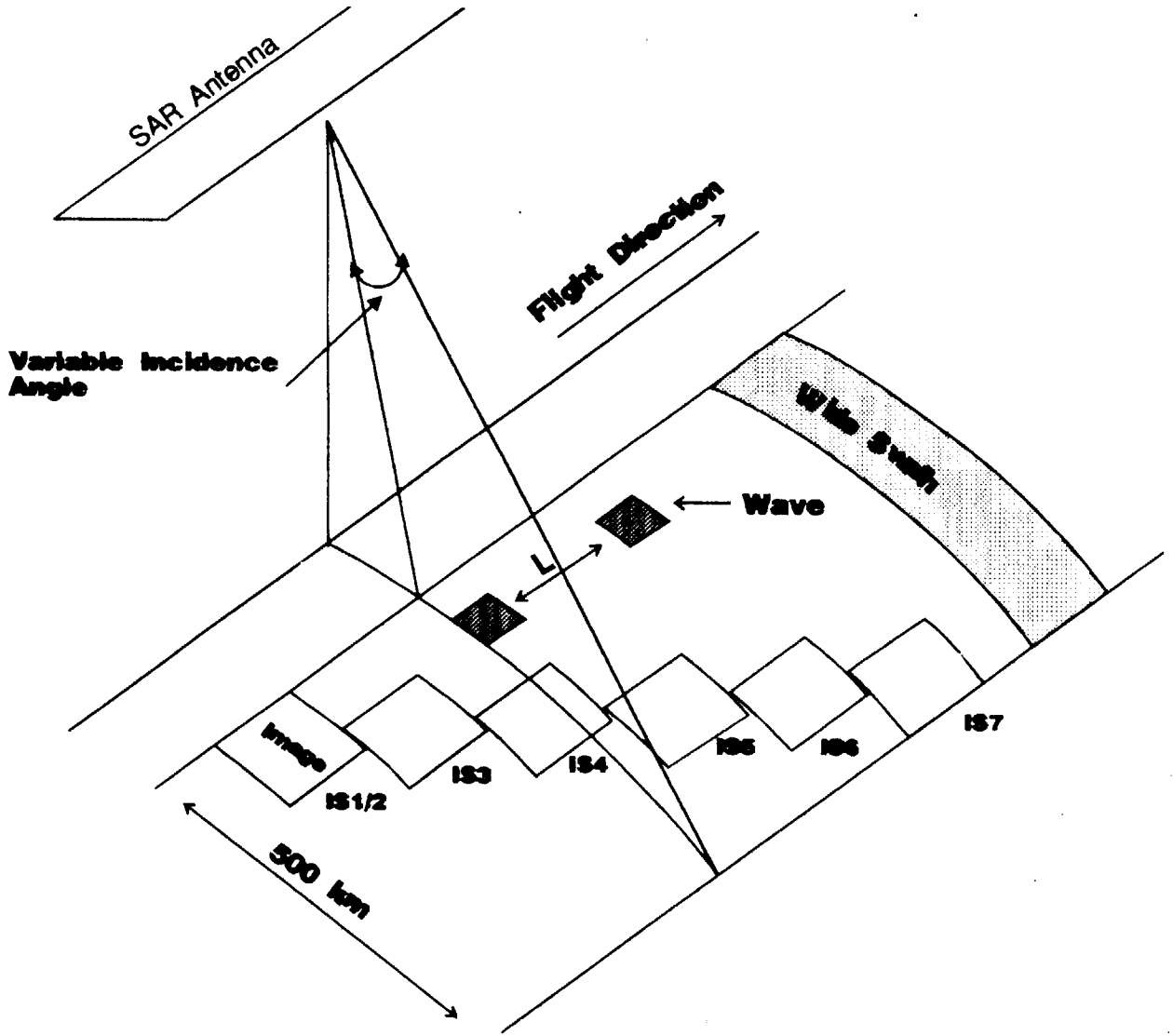
SAR Antenna
Flight Direction
Variable Incidence Angle
Wave
L
Image
IS1/2
IS3
IS4
IS5
IS6
IS7
500 km

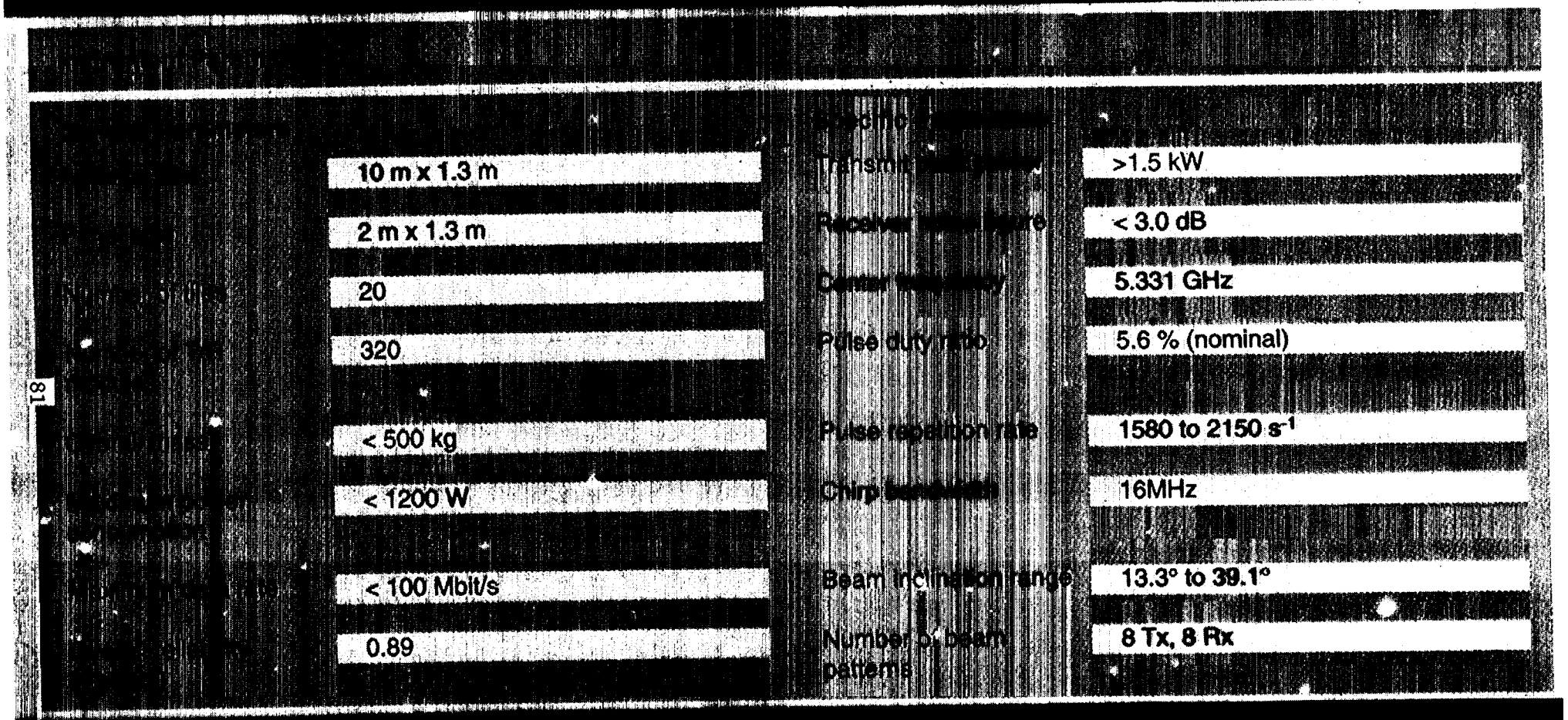
10 m x 1.3 m
2 m x 1.3 m
20
320
< 500 kg
< 1200 W
< 100 Mbit/s
0.89
>1.5 kW
< 3.0 dB
5.331 GHz
5.6 % (nominal)
1580 to 2150 s-1
16MHz
13.3° to 39.1°
8 Tx, 8 Rx

ASAR PARAMETERS

PARAMETER	*UNIT*	*IMAGE (H, V or H/V)*	*WIDE SWATH*	*GLOBAL SAR MONITORING*	*WAVE*
SPATIAL RESOLUTION	m	30	90	900	30
SWATH WIDTH	km	100 to 56 (7 swaths)	405 to 420 (5 swaths)	405 to 420 (5 swaths)	5 x 5 (any swath)
INCIDENCE ANGLE	deg.	15-45	17-43	17-43	15-45
DC POWER CONSUMPTION	W	1200	1200	750	520
DATA RATE	Mbps	96.5	97	1.1	0.9

MISSION LIFETIME 4 YEARS

RELIABILITY .89

Parameter	IMAGE	WIDE SWATH	[illegible]	ALTERNATIVE POLARIZATION	GLOBAL MONITORING
Spatial Resolution along track across track	≤ 30 m ≤ 30 m	≤ 100 m ≤ 100 m	≤ 30 m ≤ 30 m	≤ 30 m ≤ 30 m	≤ 1000 m ≤ 1000 m
Ambiguity Ratio (Point) along track across track	≥ 25 dB ≥ 31 dB	≥ 25 dB ≥ 31 dB	≥ 25 dB ≥ 31 dB	≥ 25 dB ≥ 31 dB	≥ 25 dB ≥ 31 dB
Ambiguity Ratio (Distrib.) along track across track	≥ 22 dB 13 dB below σo min.	≥ 22 dB 13 dB below σo min.	≥ 22 dB 13 dB below σo min.	≥ 22 dB 13 dB below σo min.	≥ 22 dB 13 dB below σo min.
Radiometric Resolution	≤ 2.5 dB	≤ 2 dB	≤ 2 dB	≤ 3.5 dB	≤ 1.5 dB
Radiometric Accuracy	≤ 0.65 dB	≤ 0.65 dB	≤ 0.65 dB	≤ 0.65 dB	≤ 0.65 dB
Swath Width	up to 100 km	400 km	5 km	up to 100 km	400 km

BACKSCATTER MODEL

Incidence Angle (degrees)	*Sigma Naught value (dB)*
10	-10
20	-14
30	-17
40	-20
45	-22
50	-24.4
55	-26.2
60	-27.6

COMPARISON ASAR-AMI

			A S A R						
	ERS-1 AMI	ASAR AMI SWATH	Swath 1	Swath 2	Swath 3	Swath 4	Swath 5	Swath 6	Swath 7
Incidence Angle mid swath	23°	23°	18.8°	22.8°	28.7°	33.7°	37.7°	41,1°	44.0°
Swath Width	80 km	80 km	100 km	100 km	80 km	85 km	65 km	70 km	55 km
Nominal Spatial Resolution	30 m	30 m	30 m	30 m	30 m	30 m	30 m	30 m	30 m
Achievable Spatial Resolution (range)	30 m	30 m	30 m	24 m	19.5 m	17 m	15 m	15 m	13.5 m
Signal to Noise Ratio (worst case) (σ0-18dB, nom.res.)	7.0	5.0 dB(1)	5.5 dB	4.8 dB	5.5 dB	4.8 dB	4.2 dB	7.47 dB	8.65 dB
Polarisation	VV	HH,VV	HH,VV	HH,VV	HH,VV	HH,VV	HH,VV	HH,VV	HH,VV

Instrument Design and Technology

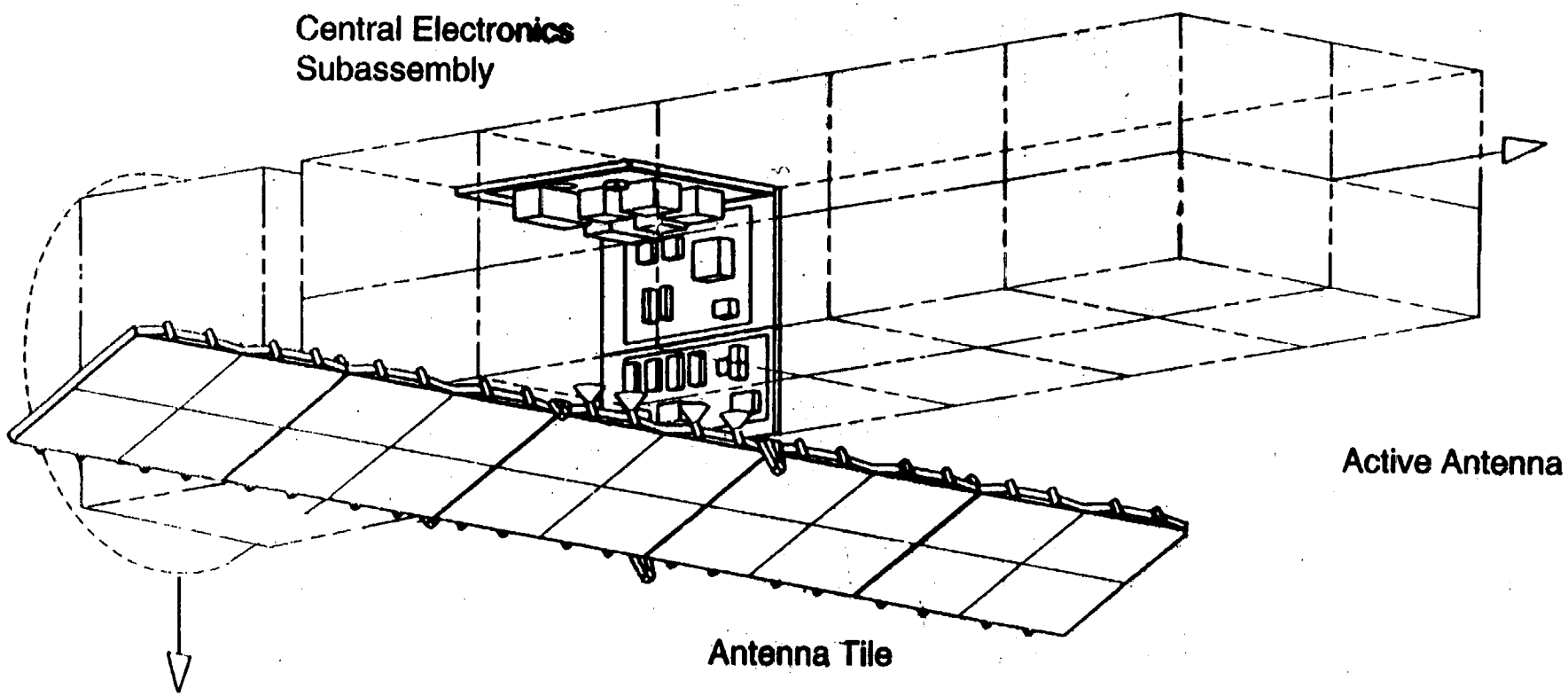

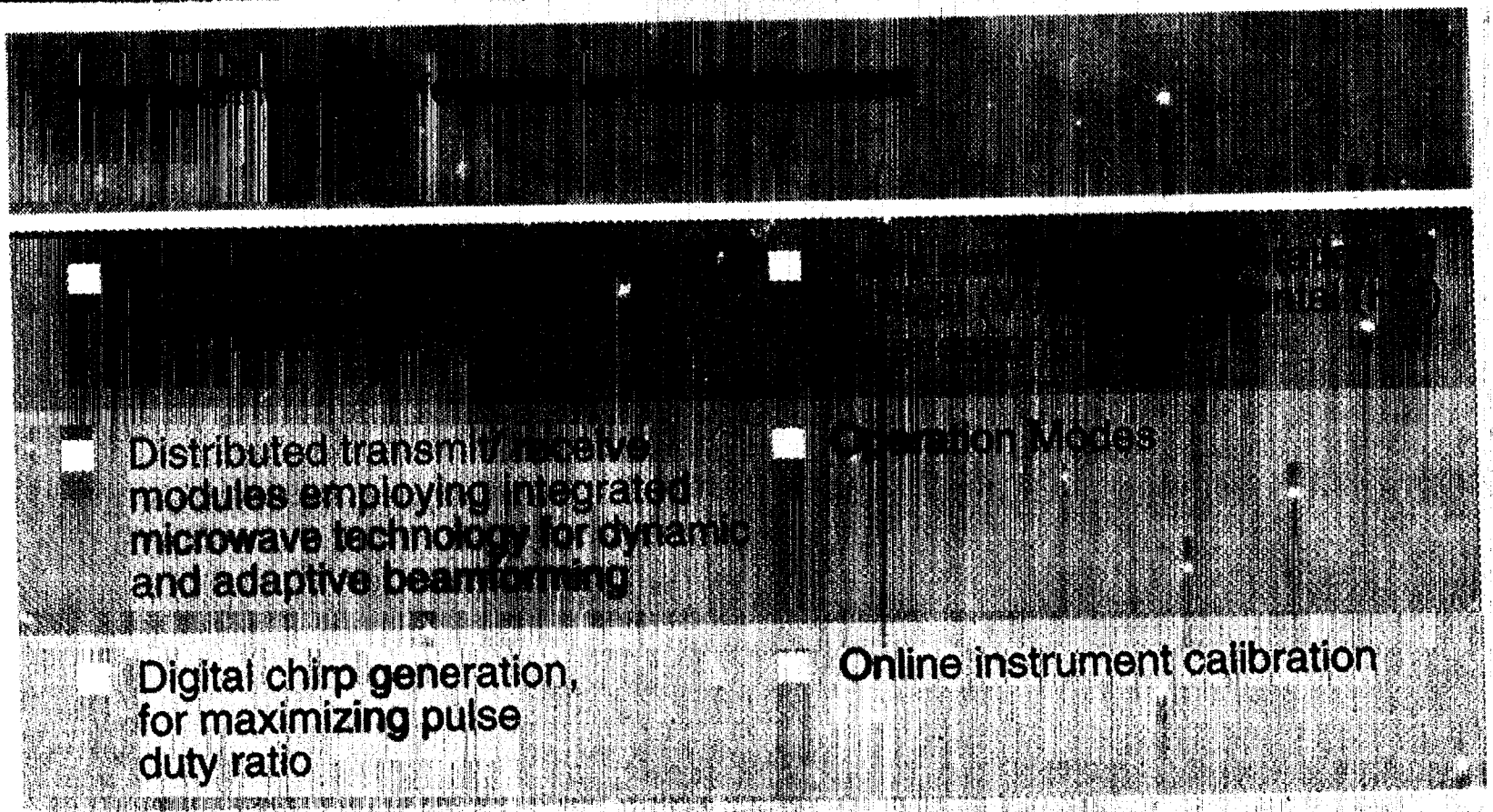
Distributed transmit/receive modules employing integrated microwave technology for dynamic and adaptive beamforming
Digital chirp generation, for maximizing pulse duty ratio
Online instrument calibration
Tx and Rx beams independently controllable to achieve flexible swath coverage

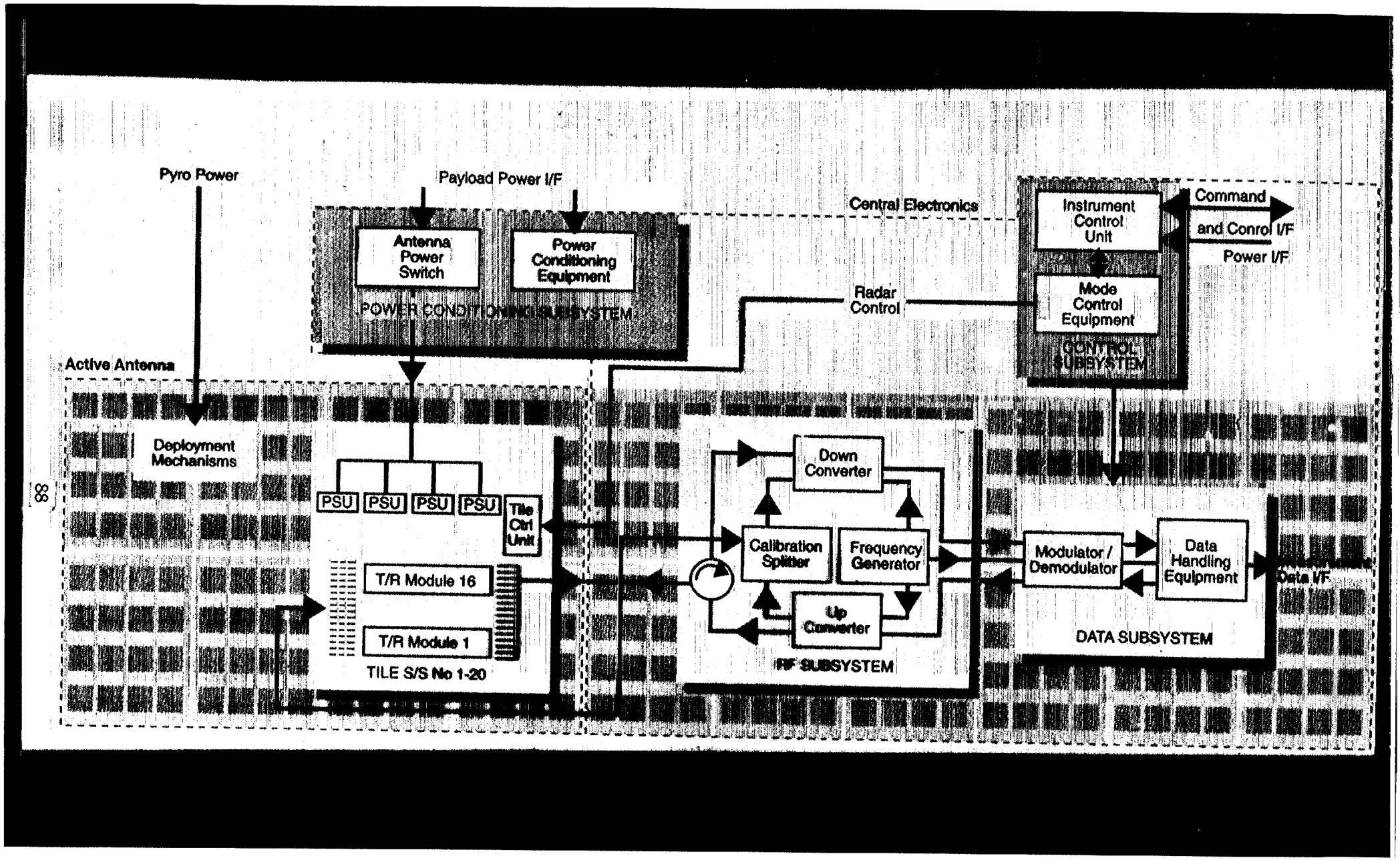
Pyro Power
Payload Power I/F
Central Electronics
Instrument Control Unit
Command and Conrol I/F
Power I/F
Antenna Power Switch
Power Conditioning Equipment
POWER CONDITIONING SUBSYSTEM
Radar Control
Mode Control Equipment
CONTROL SUBSYSTEM
Active Antenna
Deployment Mechanisms
PSU
PSU
PSU
PSU
Tile Ctrl Unit
T/R Module 16
T/R Module 1
TILE S/S No 1-20
Down Converter
Calibration Splitter
Frequency Generator
Up Converter
RF SUBSYSTEM
Modulator / Demodulator
Data Handling Equipment
Data I/F
DATA SUBSYSTEM

TILE

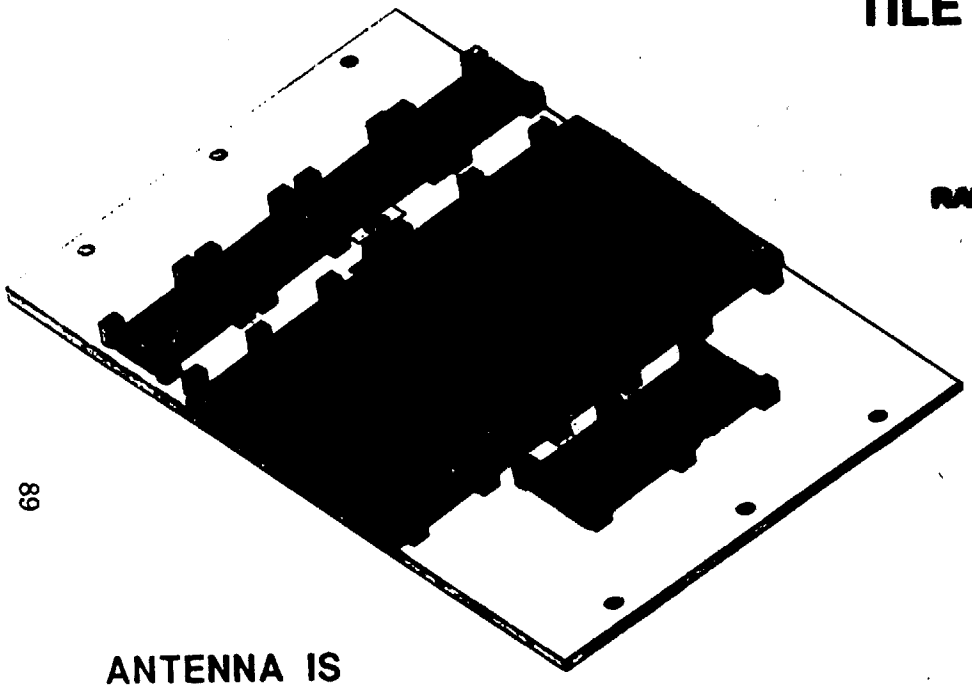

68

ANTENNA IS

COMPOSED OF 20 TILES

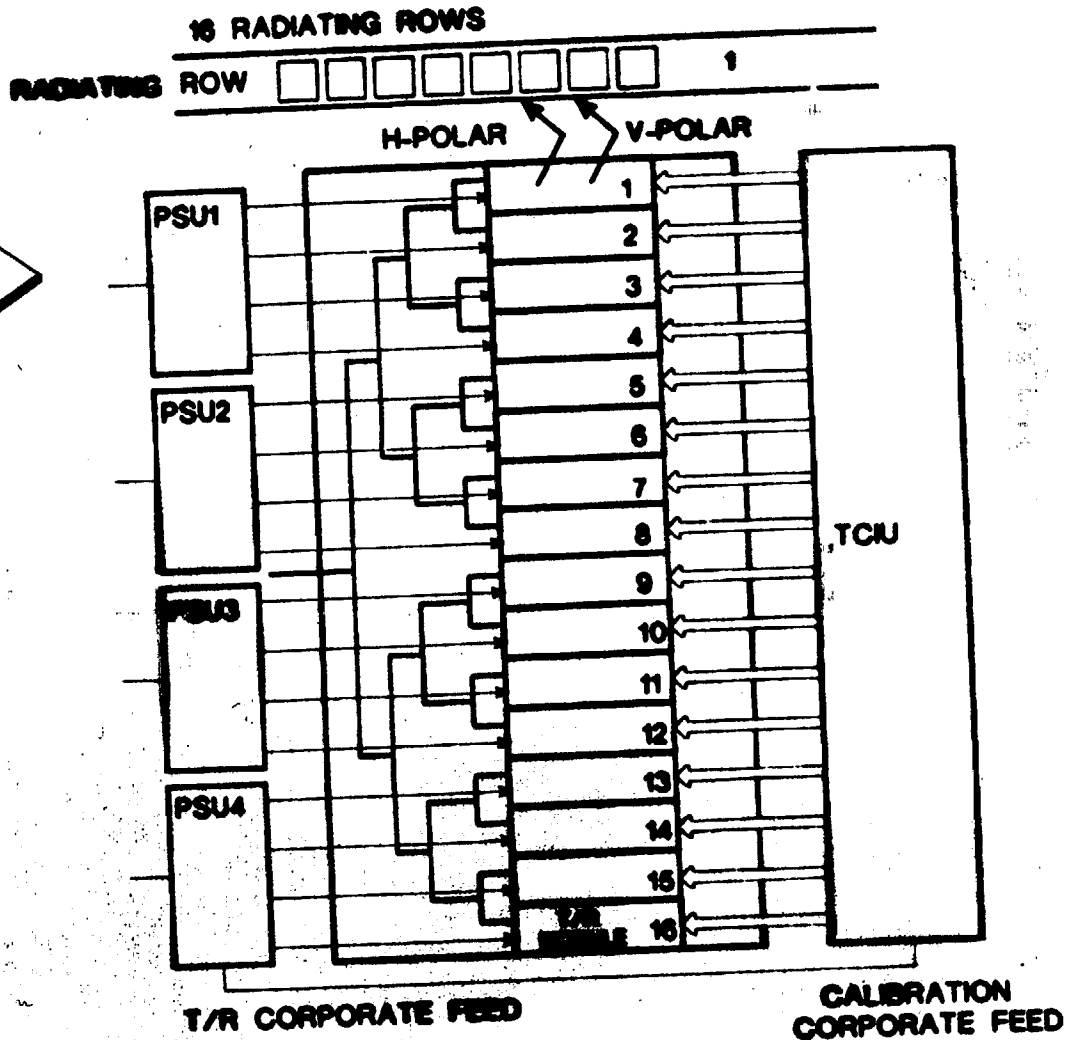

EACH TILE IS COMPOSED OF :

- 1 RADIATING PANEL
- 16 T/R MODULES
- 4 POWER SUPPLY UNITS
- 1 TILE CONTROLLER INTERFACE UNIT
- 1 RX/TX CORPORATE FEED
- 1 CALIBRATION CORPORATE FEED

TRANSMIT / RECEIVE MODULE

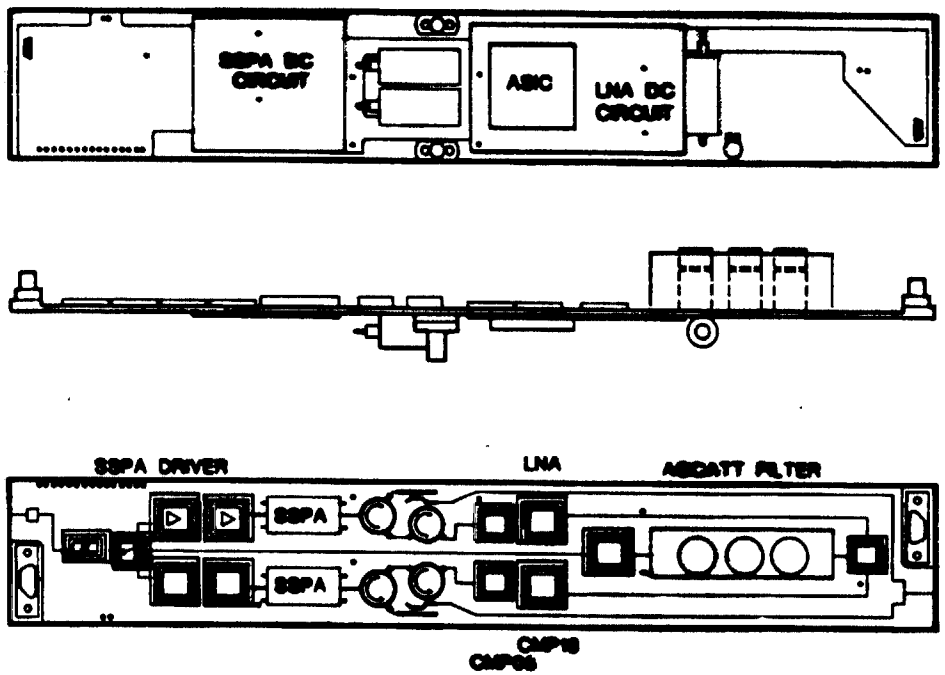

320 modules on the antenna, each of which can provide :

In Transmit :

- Output of 8W
- Phase control on 360° by 5-6 steps

On Receive :

- Noise figure of 3dB
- 20dB dynamic range by 0.5dB step.
- Phase control on 360° by 5-6 steps

Dimensions :

266x38.8x31.4mm3 (l x w x h)

Mass :

170g

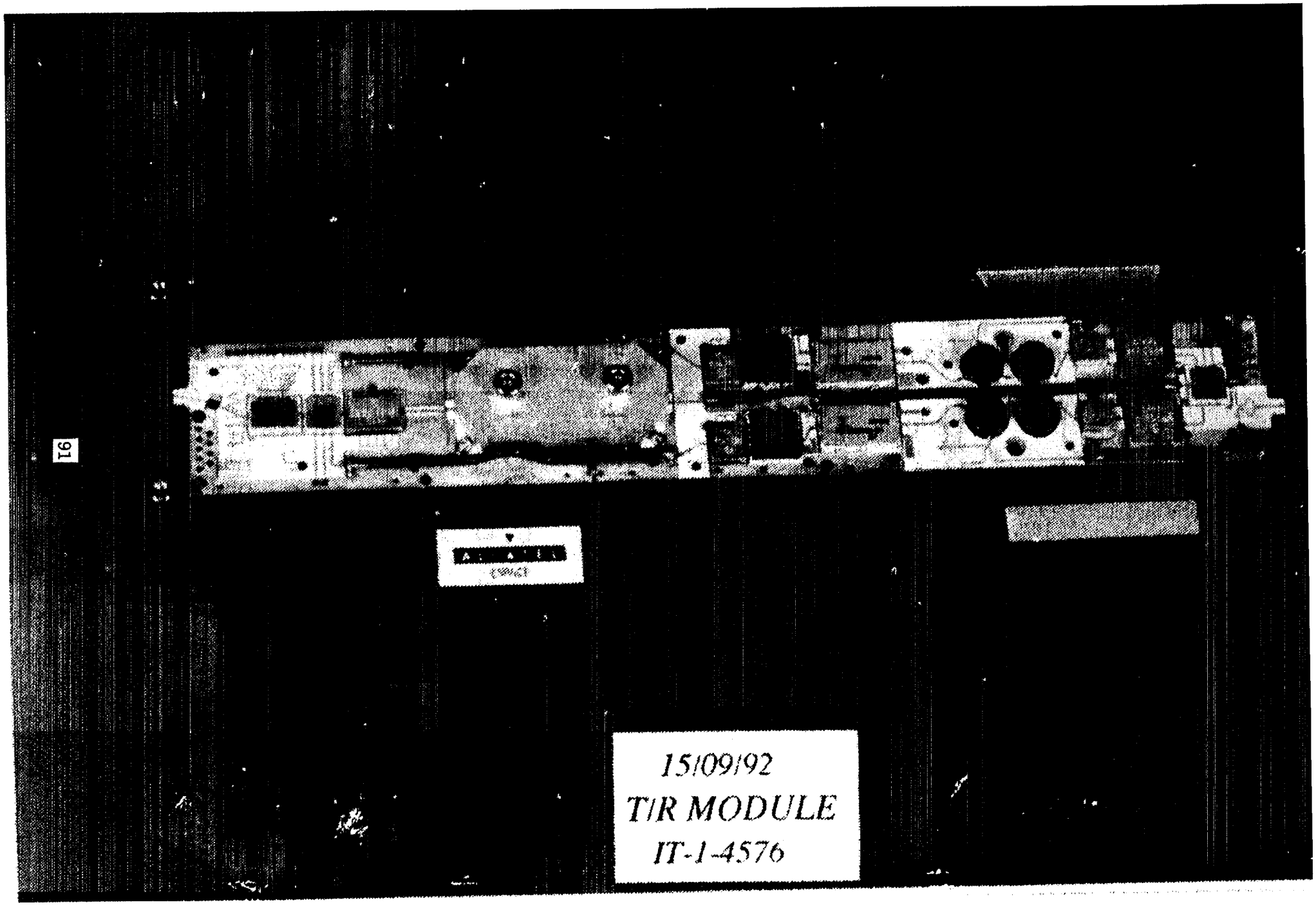
15/09/92
T/R MODULE
IT-1-4576

ASAR C-band Microstrip Patch Antenna Design

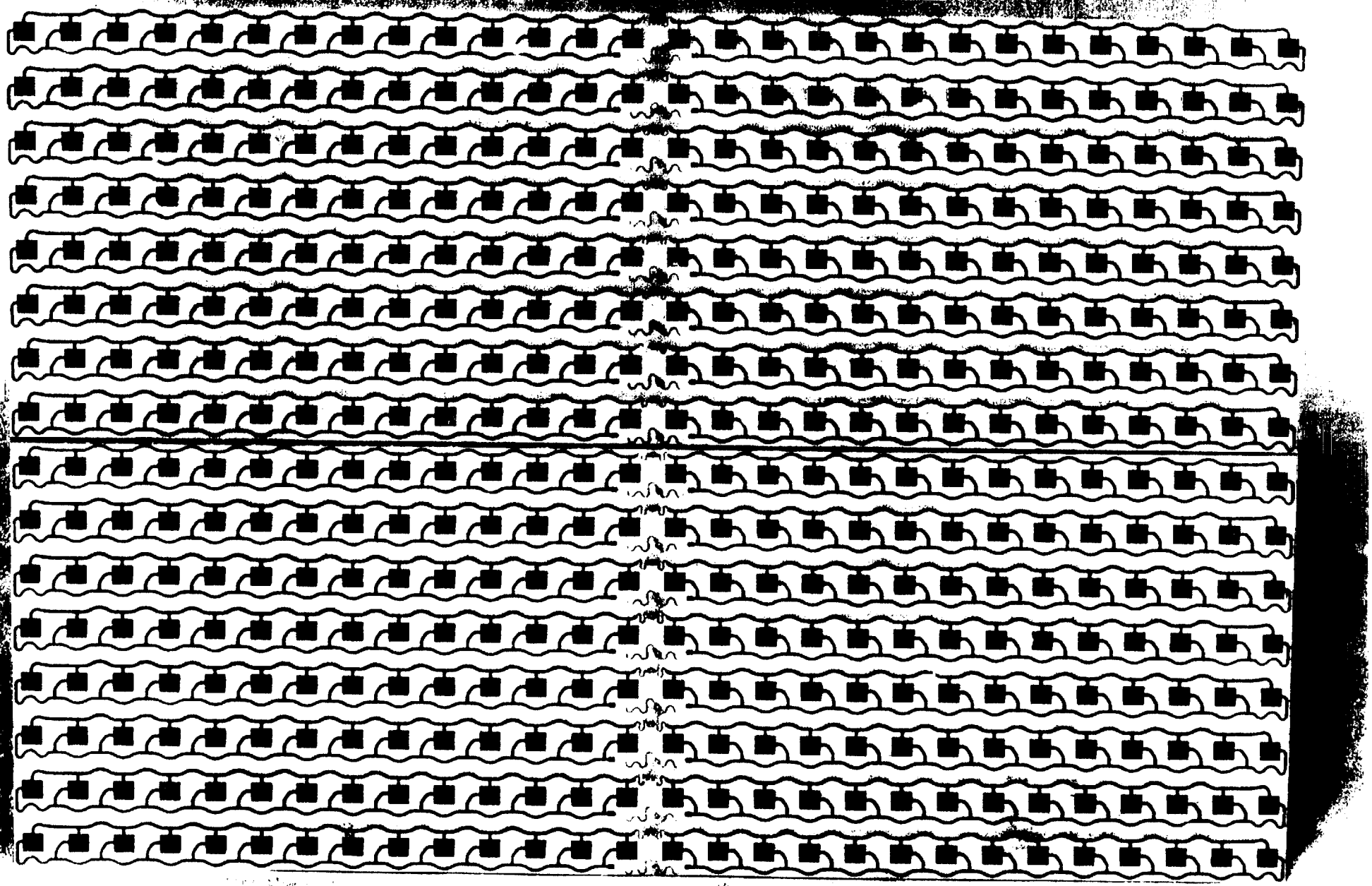

DATA RATES

IMAGE SINGLE SWATH (H, V or ALTERNATE H&V)	< 100 Mbps
WIDE SWATH (>400Km)	< 100 Mbps
WAVE MODE	900 Kbps
GLOBAL SAR MODE	1100 Kbps

WAVE & GLOBAL SAR MODE ARE ON BOARD RECORDED, FOR ALL OTHER ASAR MODES DIRECT TRANSMISSION X BAND AND/OR KA BAND VIA EUROPEAN DRS SYSTEM.

ASAR WIDE SWATH COVERAGE WITHIN 1 DAY

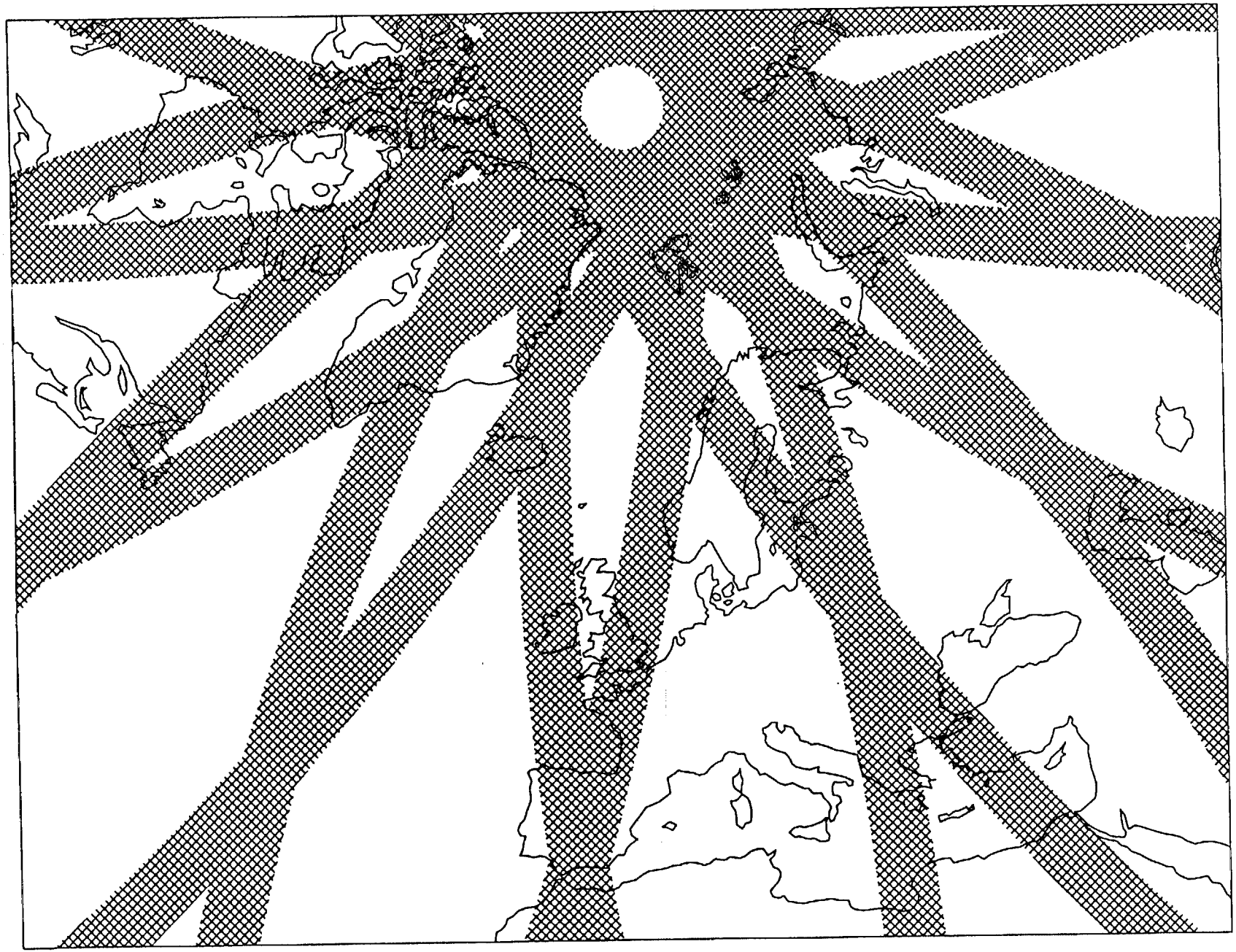

ASAR WIDE SWATH COVERAGE WITHIN 2 DAYS

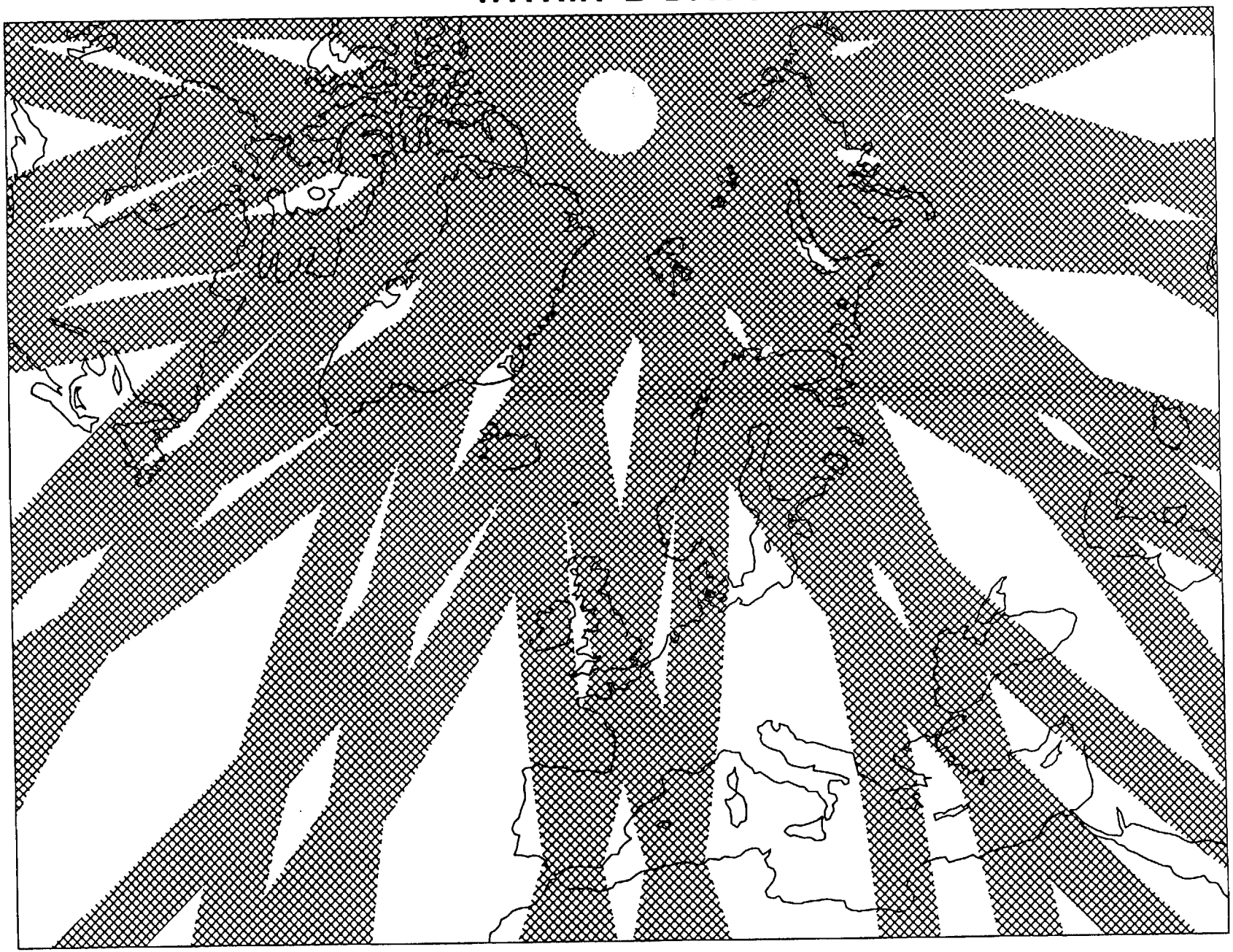

ASAR WIDE SWATH COVERAGE
WITHIN 3 DAYS

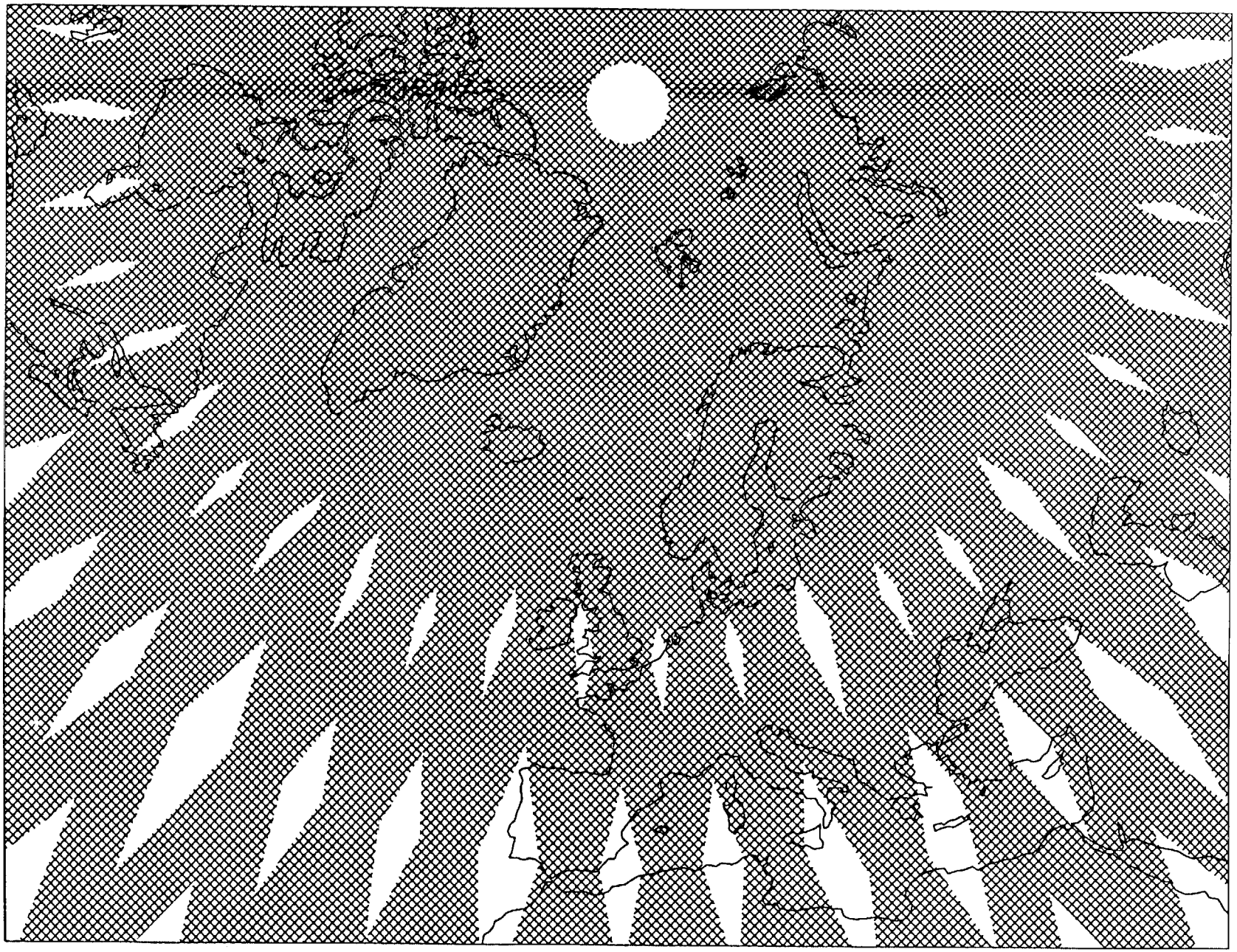

ASAR Programme

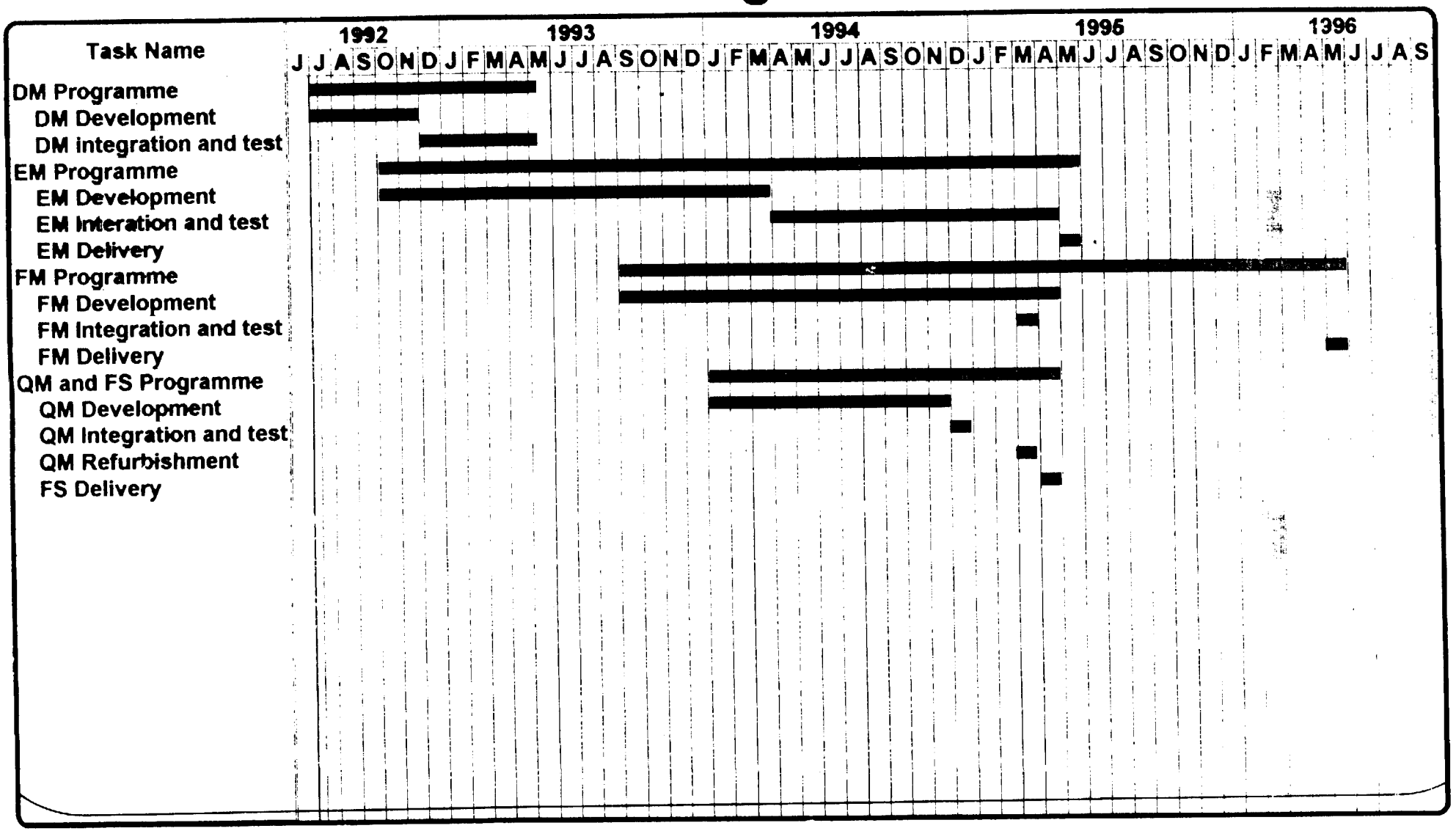

RADARSAT Program

J. McNally and S. Parashar
Canadian Space Agency/Agence spatiale canadienne
110 Rue O'Connor St, suite 200/pièce 200
Ottawa, Ontario K1A 1A1
Canada

ABSTRACT

Work on the RADARSAT system is progressing well to meet the currently scheduled launch date of early 1995. The spacecraft bus and the Synthetic Aperture Radar (SAR) payload are at various stages of development. Requirements for the ground segment have been mostly established. The design of the ground elements such as mission control facility and SAR data processor is underway. The SAR applications development work is continuing and the chosen distributor, RADARSAT International Inc. (RSI) is making preparations to market RADARSAT data internationally. A plan for the follow-on to RADARSAT I is being finalized to ensure continuity of SAR data under the Radarsat program.

INTRODUCTION

RADARSAT is a major Earth Observation (EO) program of the Canadian Space Agency (CSA). The program as presently approved includes construction, launch and operation of Canada's first remote sensing satellite - RADARSAT I, and establishment and operation of associated ground facilities. RADARSAT I will carry one instrument or sensor, a Synthetic Aperture Radar (SAR) operating at C-band (5.3 GH_z frequency) with horizontal transmit and horizontal receive (HH) polarizations. RADARSAT I is being designed to provide global SAR data operationally for five years after launch currently scheduled in early 1995.

RADARSAT I will be launched into a dawn-dusk, sun-synchronous polar orbit by NASA using a Delta II rocket from the Western Test Range. In return for this contribution of the launch and related services, the USA government will receive for its use a pro-rata share of the SAR on-time available during the RADARSAT I mission. CSA will also be splitting the available SAR on-time with the private sector. A Canadian company, Radarsat International Inc. (RSI) has been assigned the worldwide distribution rights for the RADARSAT I SAR data. These rights are in return for financial contributions to the program such as for the ground SAR processing facility in Canada. RSI will develop the commercial data sales worldwide and pay revenues to the Canadian government to offset the cost of the RADARSAT I mission.

One of the purposes of the RADARSAT program is to contribute to the creation of a viable international market for remote sensing data. This is to be accomplished by providing SAR data operationally through RSI to the worldwide remote sensing user community. Development of an international market by RSI, especially for operational applications, requires a continuing supply of SAR data. This need for SAR data continuity is now recognized and CSA accordingly is currently developing plans for follow-on RADARSAT missions. These plans should be finalized during 1993.

RADARSAT I MISSION

The RADARSAT mission is to supply and distribute global SAR data to the worldwide user community for such applications as ice mapping, ocean surveillance, agriculture and forestry monitoring, geological resource mapping and environmental studies. The development of applications and end users to utilize these applications and expand the economic benefits is an integral part of the mission. The Canada Centre for Remote Sensing (CCRS) has been managing a Radar Data Development Program (RDDP) for the last five years. This development work based on SAR data from the Canadian CV-580 aircraft and European ERS-1 satellite will be continuing so as to ensure users are capable and ready to utilize RADARSAT data.

To meet users needs the RADARSAT I SAR is to normally look right of the satellite track. This north looking configuration will provide essentially complete coverage of the Arctic but will leave a gap over the Antarctica. The spacecraft will be capable of undertaking manoeuvres so that the SAR can look to the left (south) for essentially a complete mapping of the Antarctic. This capability is being provided to meet the NASA requirement of mapping the Antarctic, once during a winter season and once during a summer season corresponding normally to the maximum and minimum formation of ice, respectively.

The RADARSAT I SAR is designed to provide options to users in selecting swath-width, spatial resolution, and angle of incidence. As illustrated in Figure 1, these options will be provided through various SAR modes of operation selectable by the ground control. Within the accessability ground swath of 500km it will be possible to select individual beams or SCANSAR with the associated swath width and resolutions as given in Figure 1. Experimental coverage will be possible outside this range. The 500km SCANSAR swath will provide daily coverage of the Arctic, almost complete coverage of Canada and the USA each 3 days period, and global coverage over approximately 5 days. A 24 day exact repeat orbit has been selected for the RADARSAT I mission.

In addition to the SCANSAR and multi-incidence beam observations, RADARSAT I is pioneering the dawn dusk orbit, i.e. the equator orbit crossing at approximately 6:00am or 6:00pm. This orbit offers advantages in solar power generation and associated design. It will avoid conflict in data reception on the ground with the other remote sensing satellites.

SAR data will normally be acquired when RADARSAT is within view of one of the ground data receiving stations (Canadian Prince Albert and Gatineau stations, the USA Fairbank station, and stations as licensed by RSI). Two on-board tape recorders are being provided, however, to acquire SAR data for any part of the globe and dump the recorded data when the satellite is within the Canadian station mask. RADARSAT I will be controlled and programmed by Mission Control System (MCS) in Canada. The MCS will accept user requests from order desks in Canada, USA, and other regions for filling either from the archived data or newly acquired data. The SAR data will be processed using the processing facility being set up in Canada by RSI. The USA Fairbanks station is expected to have its own processing facility. The stations licensed by RSI to receive RADARSAT data will likely have their own processing facilities as well. The quality of the SAR data delivered from this RADARSAT system will be monitored and controlled by the MCS. To facilitate maintenance of SAR data quality a ground calibration site consisting of transporters and passive targets is being established in Canada.

RADARSAT I SYSTEM DEVELOPMENT STATUS

The design and manufacture of flight hardware is well advanced at the prime contractor Spar Aerospace in Quebec and its major sub-contractors, COMDEV, CAL Corporation, MacDonald Dettwiler and Associates (MDA), SED Ltd., Fleet Aerospace and others across Canada. Ball Aerospace of Boulder, USA, the contractor for the spacecraft bus is in the final stages of assembling the flight hardware for the bus module. The other major sub-contractor is Dornier who is producing the High Powered Microwave Circuit which is similar in design to the one used on the ERS-1. The on-board tape recorders being procured from Odetics Inc. are presently under test.

Integration of the payload module (SAR sensor, tape recorders, and data handling system) is scheduled to begin mid 1993 at Spar. The final integration of the payload and bus modules plus the SAR antenna and the solar array will start early 1994 at CSA's David Florida Laboratory in Ottawa.

The existing Canadian receiving stations at Prince Albert and Gatineau, already operational for ERS-1, are being equipped to receive RADARSAT data. The existing Canadian facility for processing ERS-1 SAR data operationally is being upgraded for RADARSAT. The preliminary design review for this upgrade was held in 1992. The preliminary design reviews of mission control facility and telemetry, tracking and command stations of the MCS will be held soon. The requirement review for the mission planning and scheduling component of the MCS is planned for early 1993. The ERS-1 transponder design will be used for the development of the ground calibration transponder for RADARSAT. The concept for order desks has been finalized. The work on operations planning, training, and utilizing development has been started.

BEYOND RADARSAT I

RADARSAT I should supply SAR data till the year 2000. The development of applications and associated utilization technology and the development of market for future sales of RADARSAT data are underway. To strengthen this development and commitment of users to invest in SAR data utilization, the users need to be assured of the continuity of RADARSAT SAR data. Accordingly, it has been realized that continuation of the RADARSAT program beyond RADARSAT I is vital. The Canadian Space Agency is presently developing the Long Term Space Plan (LTSP) for Canada. A plan for the continuation of the RADARSAT program is being developed as part of the LTSP. This plan is proposing that a second RADARSAT satellite be built as early as possible after the launch of RADARSAT I. This will provide a backup should there be a premature failure of RADARSAT I. If RADARSAT I operates for five years as anticipated, then the backup satellite will be launched as RADARSAT II around the year 2000.

In parallel with RADARSAT II, it is proposed that work on enabling technologies for RADARSAT II begins soon. This would entail advanced system and technology development for the SAR and key ground segment elements such as the data processor. It is also planned to support development of new SAR applications and value-added products. RADARSAT III is proposed to be ready for launch around the year 2004 so as to ensure continuity of the supply of SAR data under the RADARSAT program. As these SAR missions are costly and serve global user communities, mutually beneficial cooperation with interested countries or organizations will be explored as part of this plan for RADARSAT II and III.

Figure 1. RADARSAT SAR Modes

Mode		Width (km)	Resolution R x A_z(m)	Looks	Incidence Angle (deg)
Standard		100	25 x 28	4	20 - 49
Wide Swath	(1)	165	48 - 30 x 28	4	20 - 31
	(2)	150	32 - 25 x 28	4	31 - 39
Fine Resolution		45	11 - 9 x 9	1	37 - 48
SCANSAR	(Narrow)	305	50 x 50	2 - 4	20 - 40
	(Wide)	510	100 x100	4 - 8	20 - 49
Extended	(High)	75	22 - 19 x 28	4	50 - 60
	(Low)	170	63-28 x 28	4	10 - 23

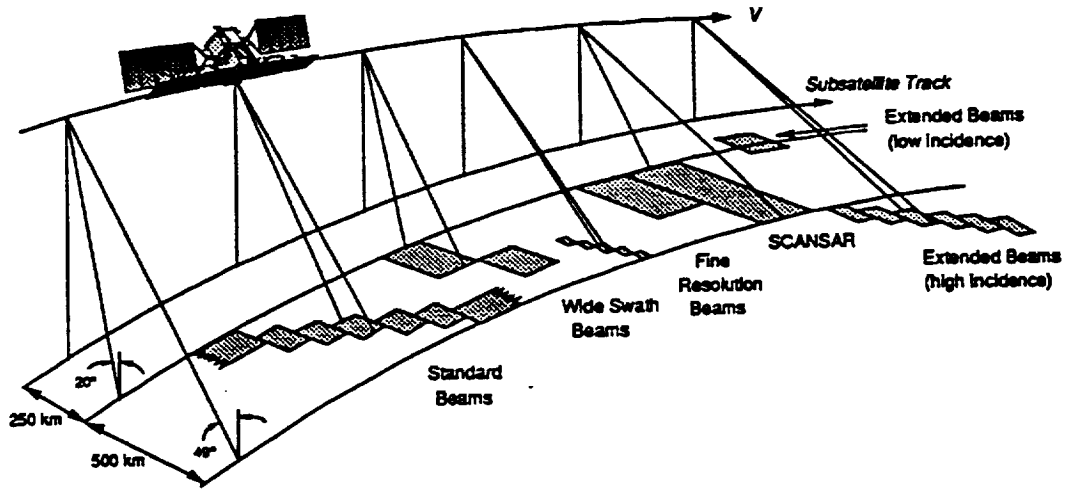

SAR Operating Modes

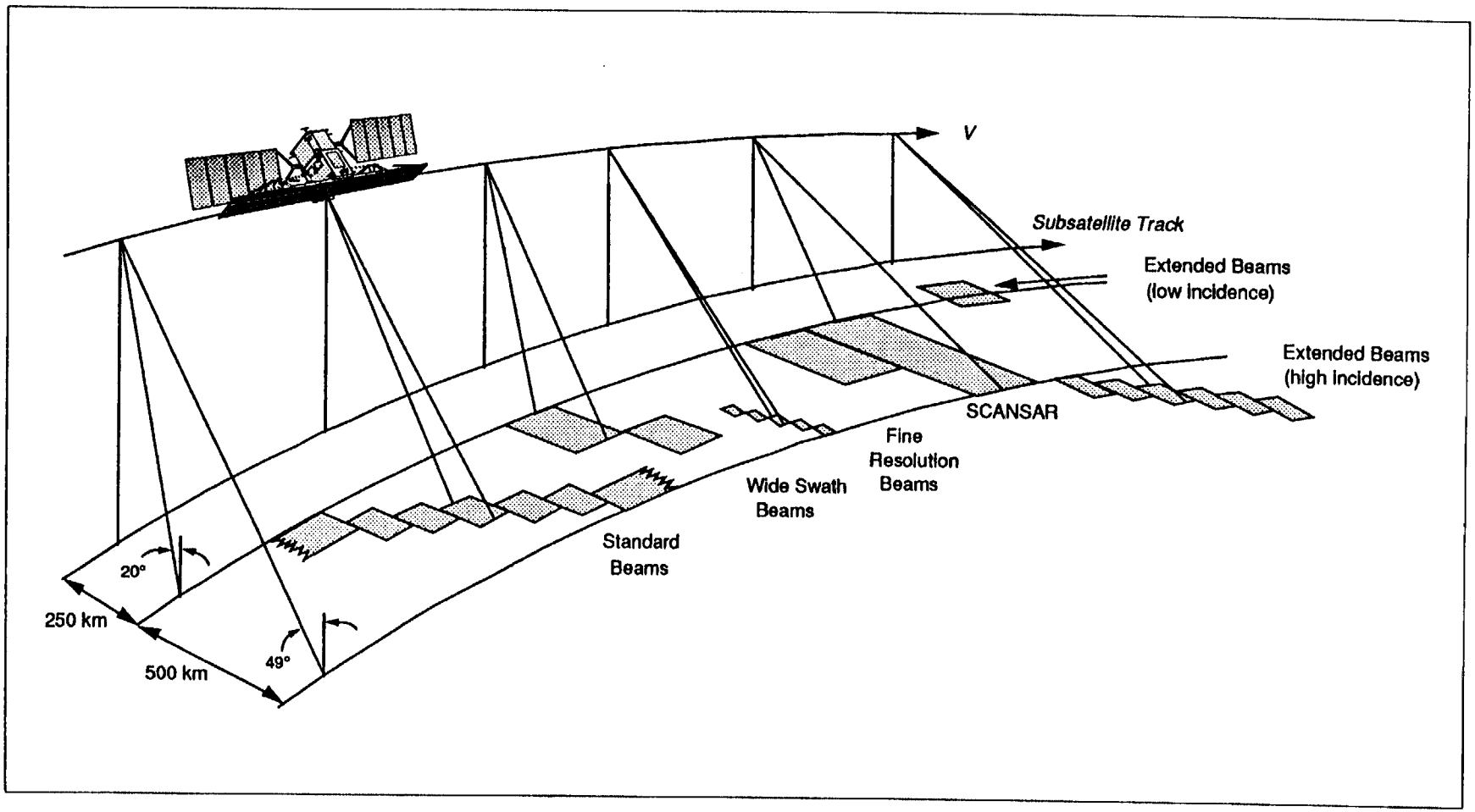

SAR Modes

Mode		Width (km)	Resolution R x A_Z(m)	Looks	Incidence Angle (deg)
Standard		100	25 x 28	4	20 - 49
Wide Swath	(1)	165	48 - 30 x 28	4	20 - 31
	(2)	150	32 - 25 x 28	4	31 - 39
Fine Resolution		45	11 - 9 x 9	1	37 - 48
SCANSAR	(Narrow)	305	50 x 50	2 - 4	20 - 40
	(Wide)	510	100 x100	4 - 8	20 - 49
Extended	(High)	75	22 - 19 x 28	4	50 - 60
	(Low)	170	63 - 28 x 28	4	10 - 23

RADARSAT Mission Concept

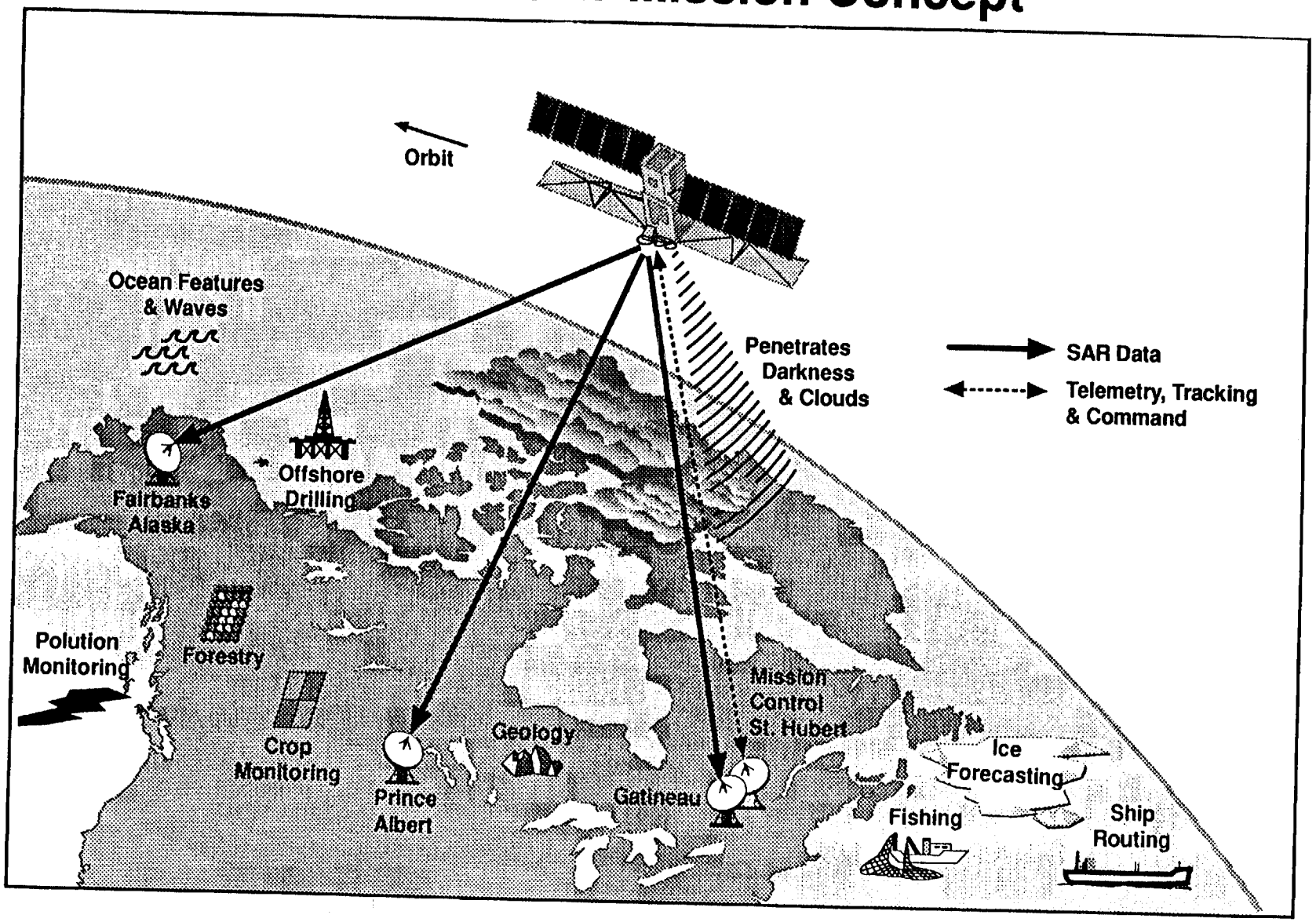

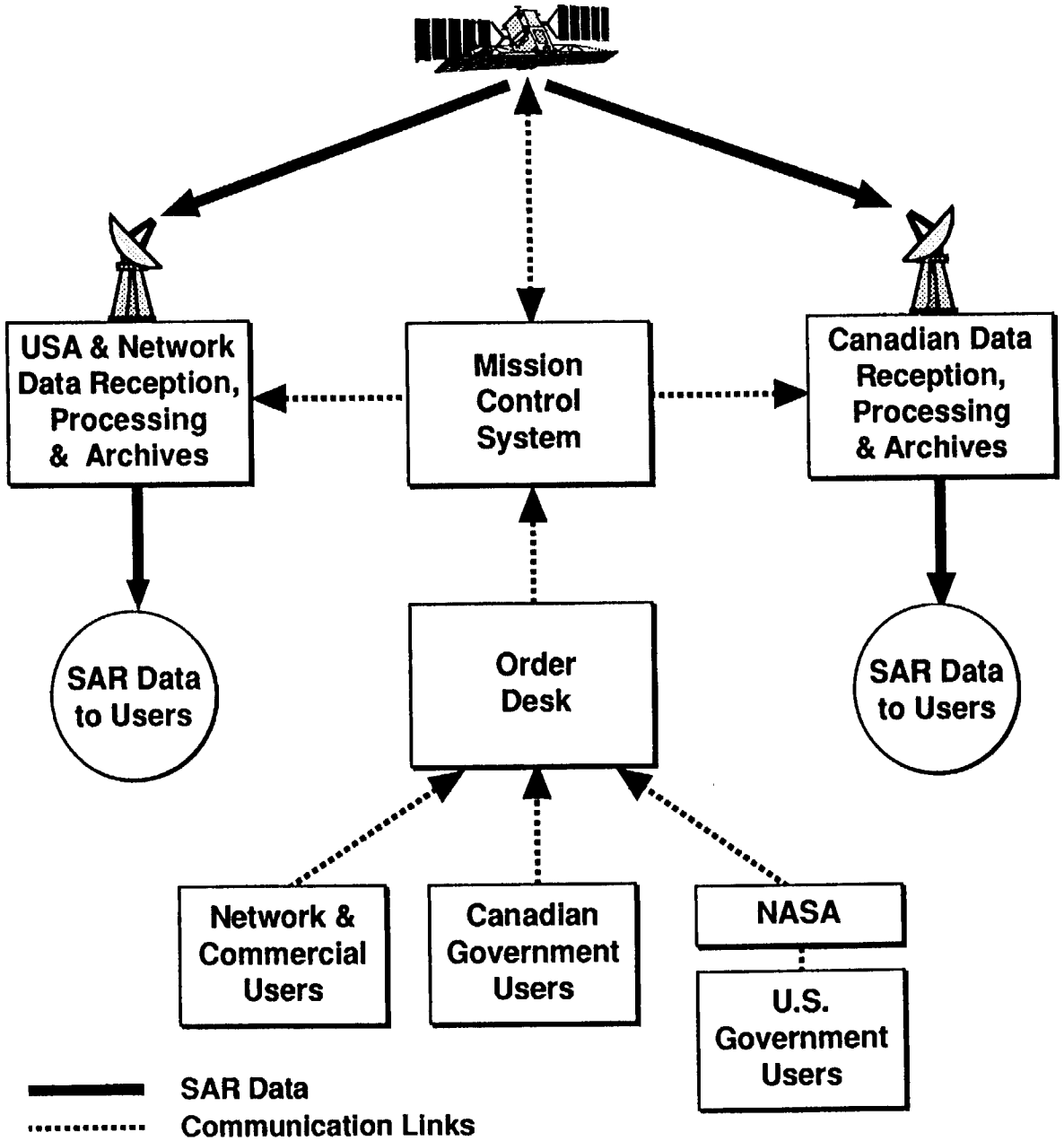
USA & Network Data Reception, Processing & Archives
Mission Control System
Canadian Data Reception, Processing & Archives
SAR Data to Users
Order Desk
SAR Data to Users
Network & Commercial Users
Canadian Government Users
NASA
U.S. Government Users
SAR Data
Communication Links

DAWN-DUSK ORBIT
SUN SYNCHRONOUS

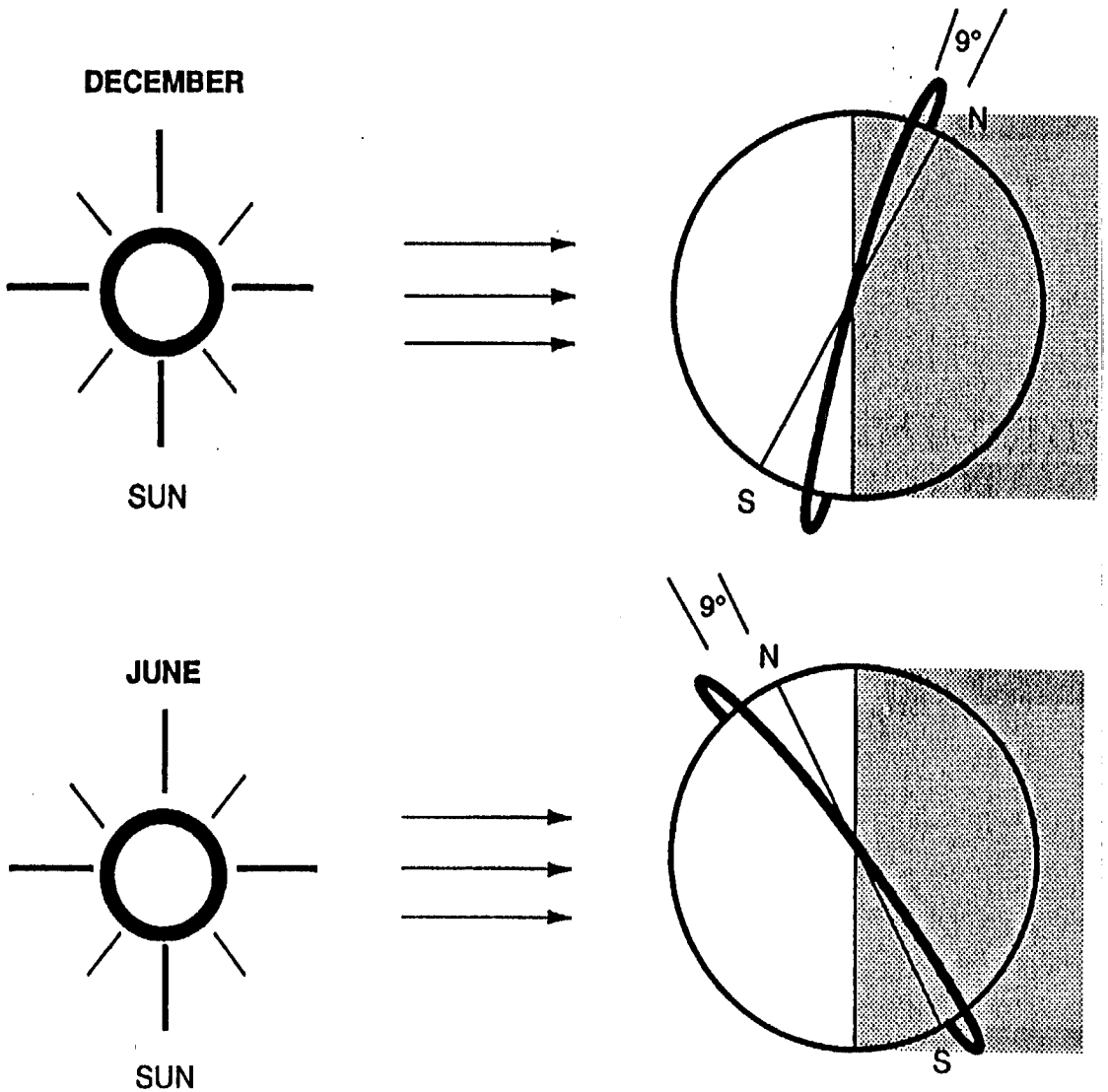

RADARSAT 1 Day Coverage

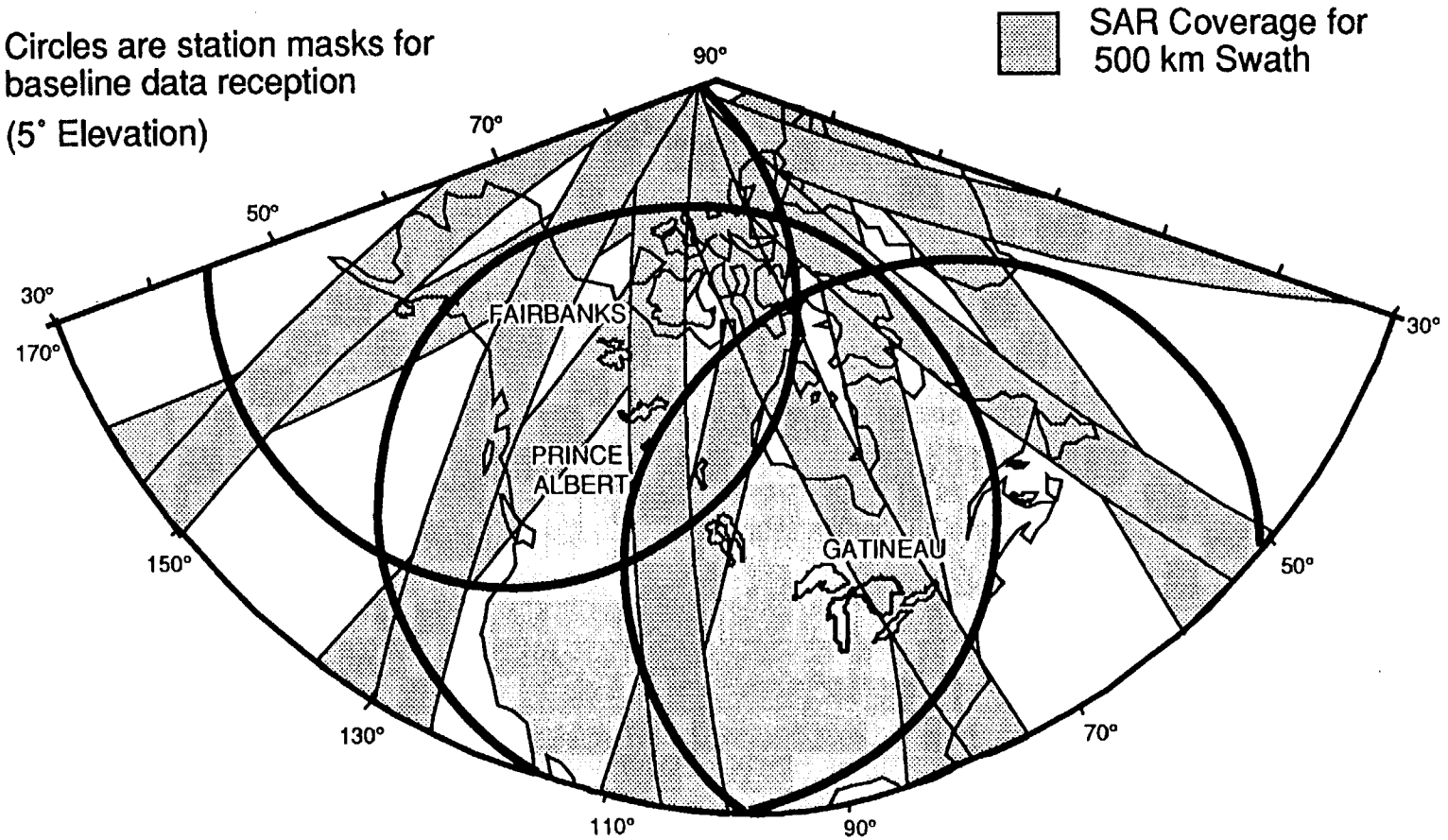

RADARSAT 3 Day Coverage

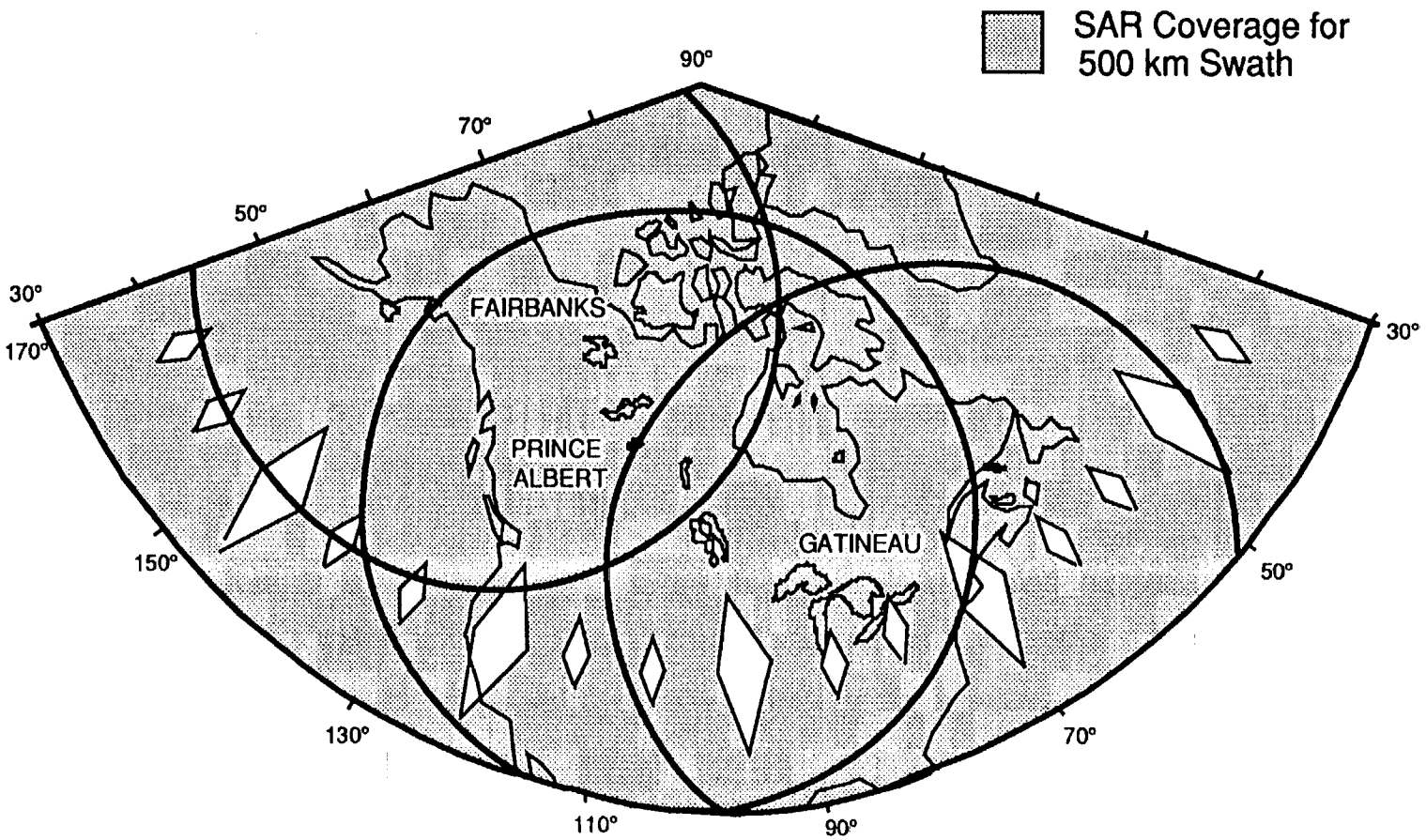

RADARSAT 1 Day Antarctica Coverage

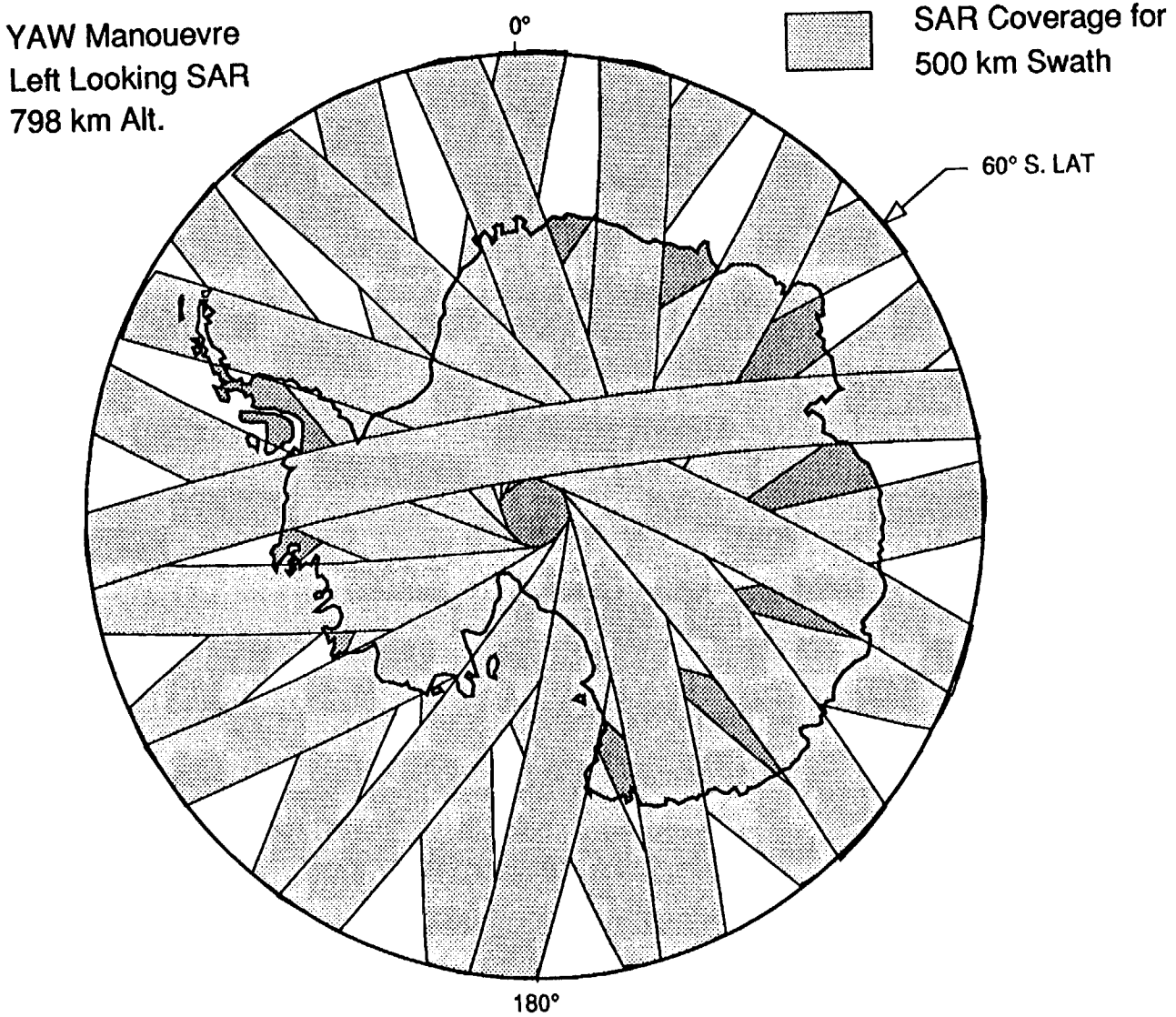

RADARSAT 1 Day Antarctica Coverage

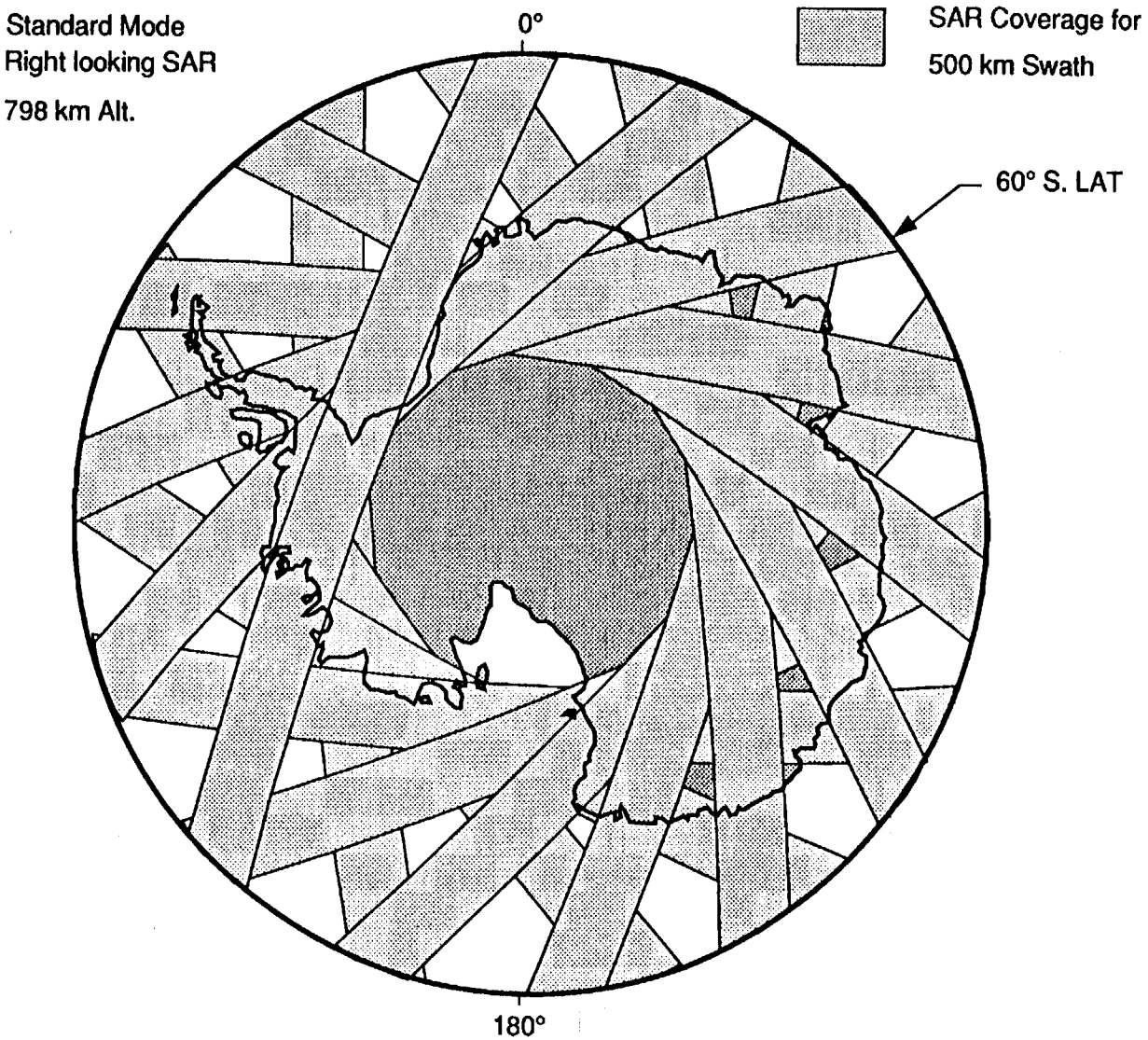

RADARSAT - General Layout

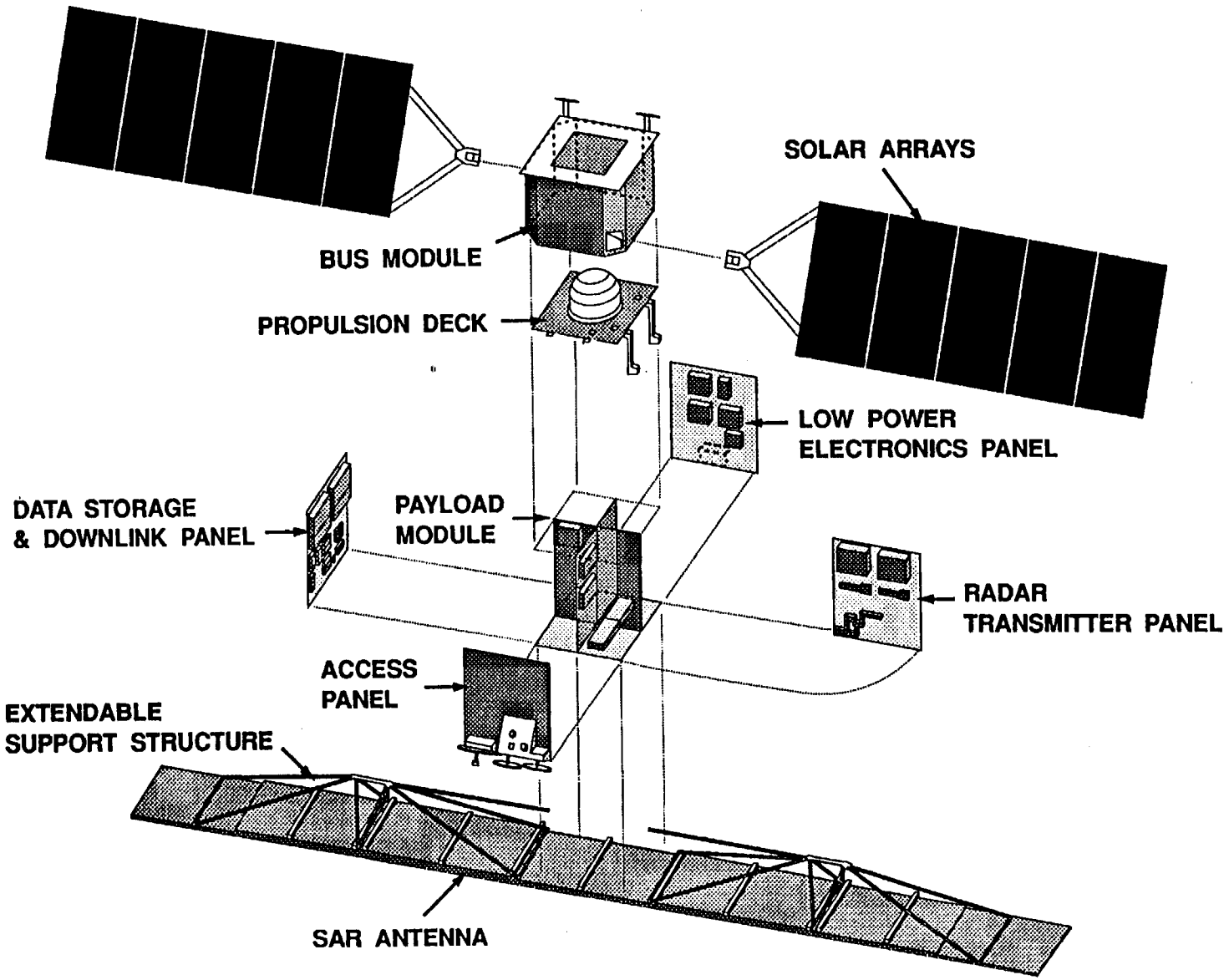

LAUNCH CONFIGURATION

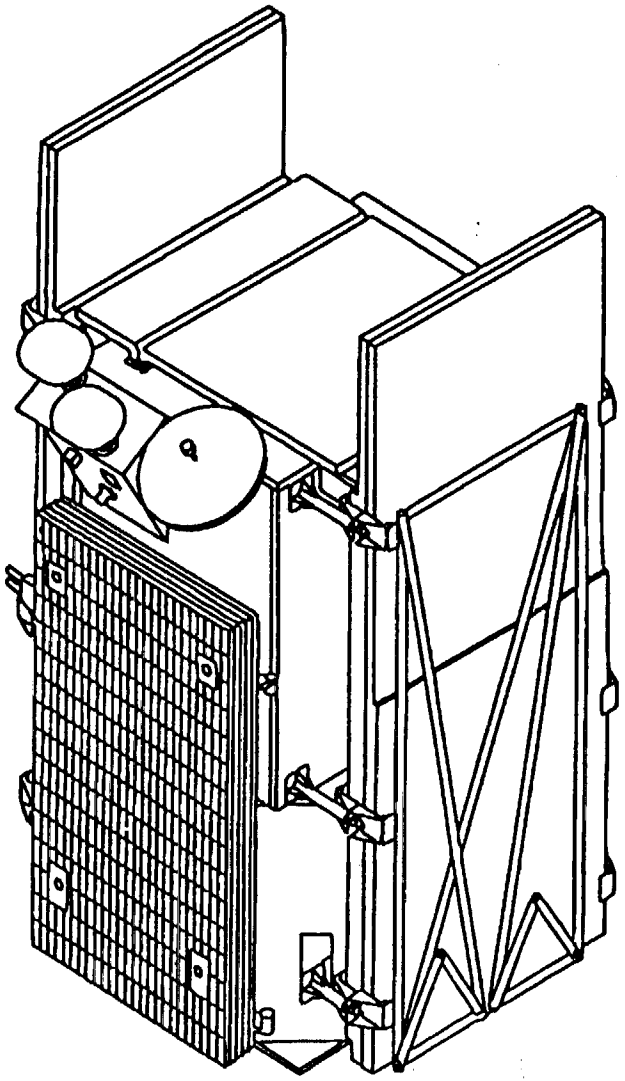

SPACECRAFT CONFIGURATION

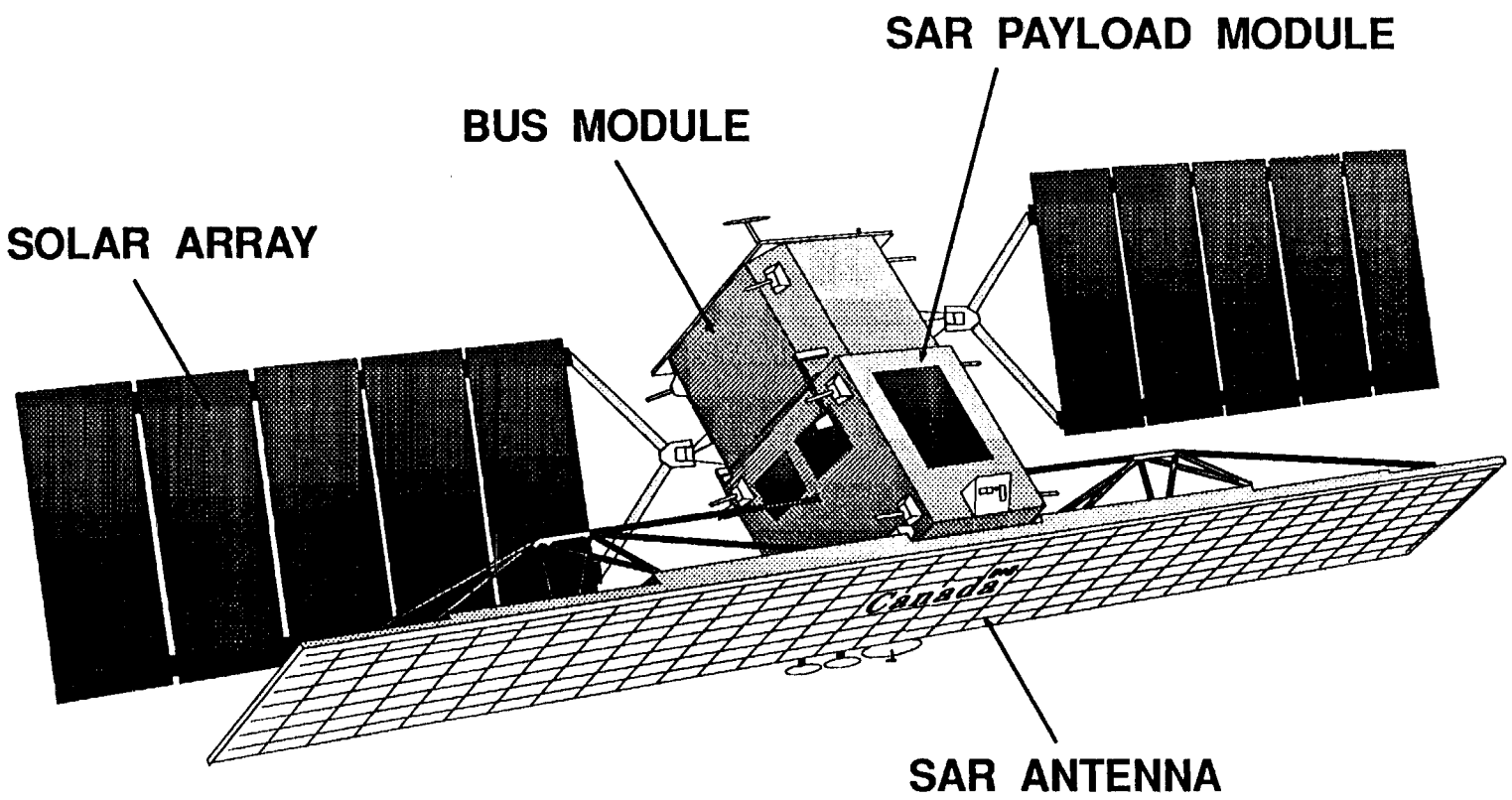

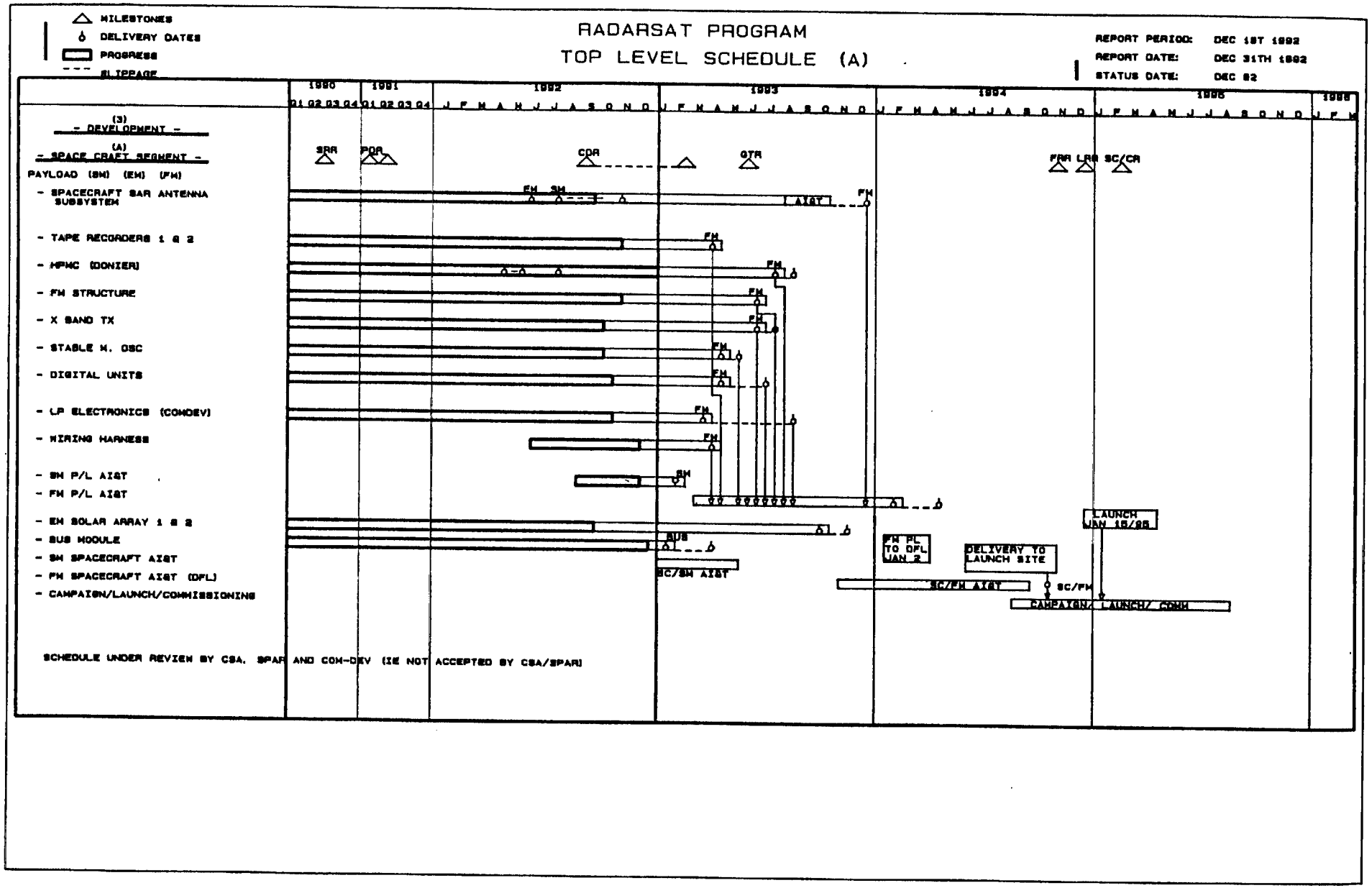
MILESTONES
DELIVERY DATES
PROGRESS
SLIPPAGE
RADARSAT PROGRAM
TOP LEVEL SCHEDULE (A)
REPORT PERIOD: DEC 1ST 1992
REPORT DATE: DEC 31TH 1992
STATUS DATE: DEC 92
1990
1991
1992
1993
1994
1995
1996
(3)
- DEVELOPMENT -
(A)
- SPACE CRAFT SEGMENT -
PAYLOAD (SM) (EM) (FM)
- SPACECRAFT SAR ANTENNA SUBSYSTEM
- TAPE RECORDERS 1 & 2
- MPMC (DONIER)
- FM STRUCTURE
- X BAND TX
- STABLE M. OSC
- DIGITAL UNITS
- LP ELECTRONICS (COMDEV)
- WIRING HARNESS
- SM P/L AIST
- FM P/L AIST
- EM SOLAR ARRAY 1 & 2
- BUS MODULE
- SM SPACECRAFT AIST
- FM SPACECRAFT AIST (DFL)
- CAMPAIGN/LAUNCH/COMMISSIONING
SRR
PDR
CDR
QTR
FRR
LRR
SC/CR
FM
SM
AIST
BUS
SC/SM AIST
FM PL TO DFL JAN 2
DELIVERY TO LAUNCH SITE
SC/FM AIST
SC/FM
LAUNCH JAN 15/96
CAMPAIGN/ LAUNCH/ COMM
SCHEDULE UNDER REVIEW BY CSA, SPAR AND COM-DEV (IE NOT ACCEPTED BY CSA/SPAR)

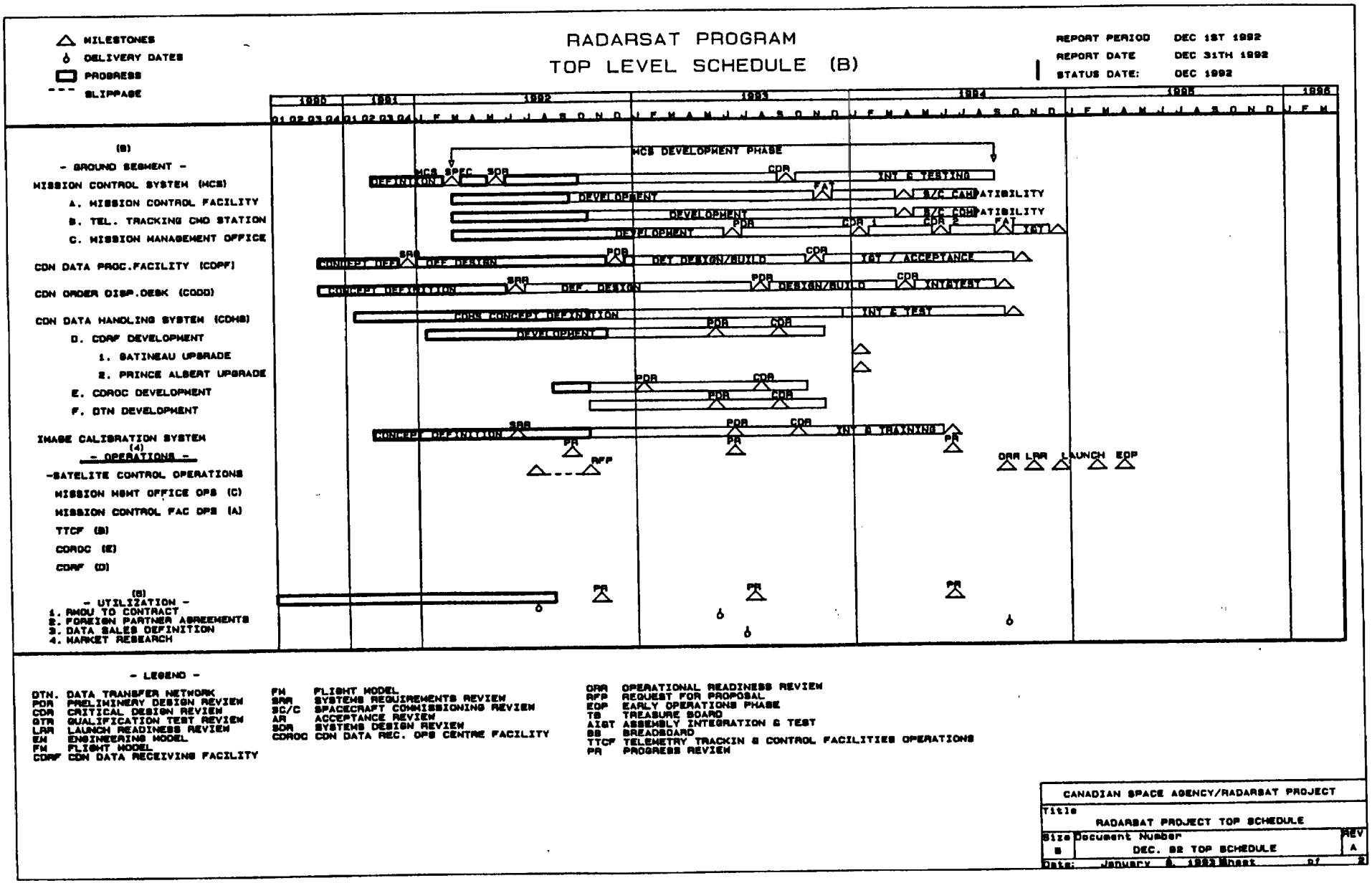

- LEGEND -

DTN. DATA TRANSFER NETWORK
PDR PRELIMINERY DESIGN REVIEW
CDR CRITICAL DESIGN REVIEW
QTR QUALIFICATION TEST REVIEW
LRR LAUNCH READINESS REVIEW
EM ENGINEERING MODEL
FM FLIGHT MODEL
CDRF CDN DATA RECEIVING FACILITY

FM FLIGHT MODEL
SRR SYSTEMS REQUIREMENTS REVIEW
SC/C SPACECRAFT COMMISSIONING REVIEW
AR ACCEPTANCE REVIEW
SDR SYSTEMS DESIGN REVIEW
CDROC CDN DATA REC. OPS CENTRE FACILITY

ORR OPERATIONAL READINESS REVIEW
RFP REQUEST FOR PROPOSAL
EOP EARLY OPERATIONS PHASE
TB TREASURE BOARD
AIGT ASSEMBLY INTEGRATION & TEST
BB BREADBOARD
TTCF TELEMETRY TRACKIN & CONTROL FACILITIES OPERATIONS
PR PROGRESS REVIEW

CANADIAN SPACE AGENCY/RADARSAT PROJECT

Title
RADARSAT PROJECT TOP SCHEDULE

Size	Document Number	REV
B	DEC. 92 TOP SCHEDULE	A

Date: January 8, 1993 Sheet of 2

TRMM Radar

Ken'ichi OKAMOTO
Communications Research Laboratory, 2-1, Nukui-kitamachi 4-chome,
Koganei-shi, Tokyo, 184, Japan

Abstract

Results of conceptual design study and performances of developed key devices of BBM of the TRMM radar are presented. The radar , operating at 13.8 GHz and designed to meet TRMM mission objectives, has the minimum measurable rain rate of 0.5 mm/h with a range resolution of 250 m, a horizontal resolution of about 4 km, and a swath width of 220 km. A 128-element active phased array system is adopted to achieve a contiguous scanning within the swath. The basic characteristics of BBM were confirmed by experiments. The development of EM has started with the cooperation of NASDA and CRL.

1. Introduction

TRMM(Tropical Rainfall Measuring Mission) is a joint space program of the USA and Japan(Ref. 1) to measure rainfall of tropics where about 60% of the global rainfall is concentrated. The feasibility study(Phase A) of TRMM was performed successfully under the joint efforts of the USA and Japan from January 1987 to March 1988 and TRMM project was evaluated to be feasible. Phase B activities of TRMM were completed both in USA and Japan, and both countries are doing Phase C/D activities now. TRMM will adopt a circular orbit with the altitude of 350 km and the inclination of 35° . TRMM will be launched in August 1997 by the Japanese H-II rocket.

The goals of TRMM are, (1)to advance the understanding of the global energy and water cycle by means of providing distributions of tropical rainfall, (2)to understand the mechanism through which the tropical rainfall affects the global circulation, and to improve the global circulation model, and (3)to evaluate satellite system for rainfall measurement. The primary mission product of TRMM is the monthly averaged rainfall over 5° × 5° grid boxes between the latitude of 37° N and 37° S with an accuracy of about 10% over three years. TRMM is required to understand tropical rain processes that play a key role in climate changes, particularly El Nino and Southern Oscillation. TRMM will contribute to international global change programs such as GEWEX.

2. Conceptual Design Study of TRMM Precipitation Radar

TRMM is the first space mission dedicated to measurements of tropical rainfall with the first precipitation radar in space. Communications Research Laboratory (CRL)performed a conceptual design study of TRMM precipitation radar in the feasibility study of TRMM in cooperation with NASA/GSFC (Ref. 2,3). The mission requirements for the TRMM precipitation radar basically specified by NASA are

summarized in Table 1. These requirements were used as the guideline for the design of TRMM precipitation radar.

In the precipitation model, the rain is assumed to be uniform and extends to a height of 5 km. The thickness of the bright band or the melting layer is 0.5 km and the attenuation coefficient in the melting layer is assumed to be twice as large as that of rain below the melting layer. The following relations between the effective Z-factor Ze(mm^6/m^3), attenuation coefficient A(dB/km) and rain rate R(mm/h) for 13.8 GHz are assumed: $Ze = 372.4\ R^{1.54}$ (Ref. 4) and $A = 0.032R^{1.124}$ (Ref. 5).

In the TRMM precipitation radar, radar antenna beam is required to scan a swath width of 220 km in the cross track direction every 0.6 seconds in order to observe a raining area without any gaps between scanning lines which are perpendicular to the moving direction of the satellite. Therefore, high speed electric scanning becomes essential.

Figure 1 shows the block diagram of the TRMM radar(Ref. 6). Active array radar is selected as a reliable candidate for the TRMM precipitation radar after trade off studies in the feasibility study. The system is reliable because it is still operational even if some parts of transmitters or receivers are damaged. The total system loss becomes small because transmission lines between the antenna and transmitter/receiver are short and loss of phase shifter can be compensated by the SSPA(Solid State Power Amplifiers) and LNA(Low Noise Amplifier).

Main system parameters estimated in the feasibility study are shown in Table 2. The attained horizontal resolution is 4.3 km at nadir and the range resolution is 250 m. The swath width is 220 km. The required number of independent samples of 64 is achieved by the frequency agility technique which uses dual frequency separated 6 MHz. Dual frequency pulse will be transmitted mutually in the same pulse repetition period keeping a pulse repetition period long enough to insure the sufficient time for the data acquisition., The minimum detectable rain rate at the rain top is 0.5 mm/h and the measurable rain rate at the rain bottom is between 0.5 mm/h and 52 mm/h, with a signal to noise ratio of 0 dB for a single echo. If we use the attenuation data of the sea surface echo by rain, we can observe the average rain rate as large as 80 mm/h with a signal to noise ratio of 0 dB for a single echo.

3. Development of Key Devices of the Bread Board Model of the TRMM Precipitation Radar

CRL has developed key devices of the Bread Board Model of the TRMM precipitation radar since 1988(Ref. 7). These key devices are (1) slotted waveguide antenna elements, (2) 5-bit PIN diode phase shifters, (3) SSPAs and (4) LNAs. Integration of these components to form an 8-element Bread Board Model of the TRMM precipitation radar was also made. We developed 8-element slotted waveguide array antenna. Major required characteristics of the antenna are (1) the low sidelobe level to suppress the surface clutter, (2) the wide band width for the frequency agility, and (3)the high speed electric scanning with scan angle of ±17 degrees. We adopted the non-resonance type(wide band width)slotted wave guide antenna. The separation between slots cut on the narrow wall of the rectangular waveguide is 13.65 mm. Slot conductance is designed to attain the Taylor amplitude distribution(sidelobe = -35 dB, parameter n = 6) along the waveguide axis. Figure 2 shows outside appearance of the developed 8-element slotted waveguide array antenna part of the Bread Board Model of TRMM precipitation radar. The antenna length is 2.2 m. Measured antenna

Table 1. Mission Requirements

Frequency	13.8 GHz
Satellite altitude	350 km
Scan angle	±17.0 degrees
Swath width	220 km
Range resolution	250 m
Horizontal resolution	around 4 km at nadir
Minimum measurable rainfall rate	0.5 mm/h at storm top
Observation range	
Nadir	15 km + 5 km
Scan angle: θ	15 km/cosθ
Number of independent samples	64
Antenna sidelobe level	around -30 dB

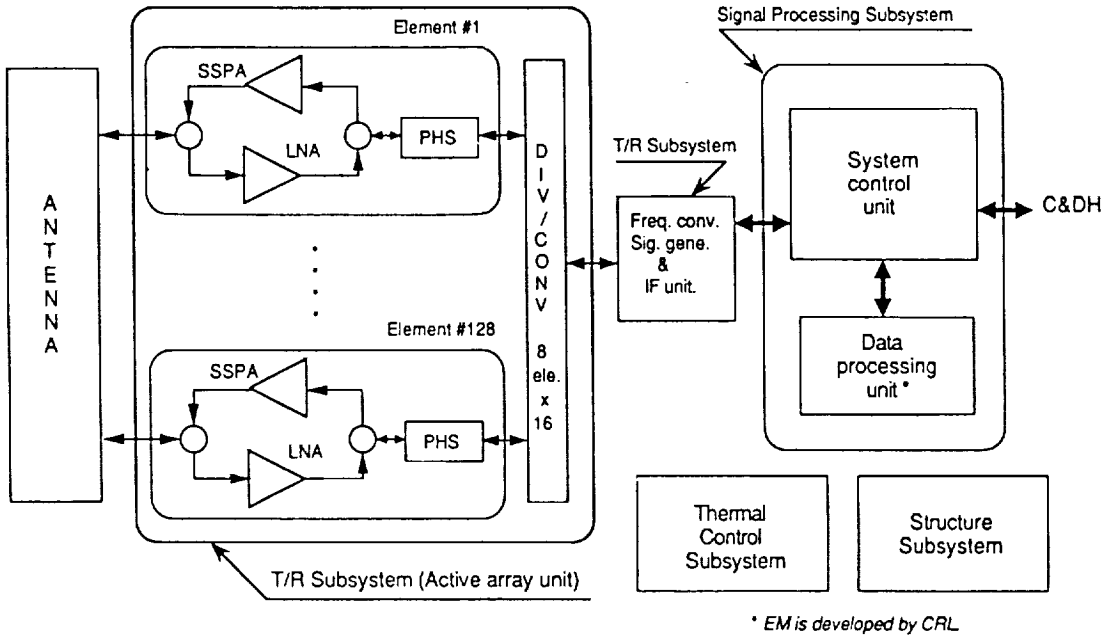

Fig. 1 Block diagram of TRMM radar

Fig. 2 Outside appearance of the 8-element slotted wave guide antenna part of the Bread Board Model of TRMM precipitation radar

radiation pattern in the plane of the wave guide axis of an 8-element slotted wave guide array antenna at 13.8 GHz is shown in Fig. 3 The half power beam width of 0.7° is attained. The peak sidelobe level about -30 dB is attained except for the shoulder level of -28 dB. The wide angle sidelobe level less than -35 dB is also attained. The antenna beam tilts about 4° from the direction normal to the slotted waveguide wall.

We developed PIN diode 5 bit phase shifter at 13.8 GHz. In the PIN diode 5 bit phase shifter, 11.25°, 22.5°, 45° and 90° bits are of loaded line type and 180° bit is of hybrid coupler type. We attained at the worst case between -10°C and +40°C, insertion loss values of 4-5 dB for the variation of the phase values. Phase errors about - 5°~ + 2° and amplitude errors less than 0.9 dB_{p-p} are attained. As the phase and amplitude errors and variation of the insertion loss are directly related to the characteristics of phased array antenna, more detailed examination and evaluation of the phase shifter will be performed for the Engineering Model. Although values of the insertion loss are larger than those of the ferrite phase shifter, these loss values can be compensated by the SSPA and LNA. The mass of the developed phase shifter is about 150 g.

In order to satisfy the peak transmitted power shown in Table 2, the output power of 10 W around the central part of the array is required. By using multi-stage GaAs FET amplifiers, output power of 10 W and an efficiency of more than 15 % is developed. In order to reduce the power consumption, the efficiency of SSPA itself, of the power supply and of the guard time margin for the pulsed operation must be considered. The output power variation is 0.2 dB_{p-p} and the phase variation of the each SSPA is as large as 30° for the temperature variation between -10° C and +40° C. However, variation of the phase difference of 2 SSPAs whose phase difference is set to be equal at room temperature is less than 6° $_{p-p}$ for the temperature variation between -10° C and +40° C, because the temperature dependence of the phase variation of 2 SSPAs is almost equal. The efficiency of the SSPA itself will be improved as large as 25% in the development phase of the Engineering Model. The mass of the developed SSPA is about 400 g.

LNA is composed of the multi-stage MIC amplifiers using the HEMT(High Electron Mobility Transistor). Good characteristics with gain of 30 dB and noise figure of 1.8 dB are attained. Variation of the phase difference of 2 LNAs whose phase difference is set to be equal at room temperature is less than $3°_{p-p}$ for the temperature variation between -10° C and +40° C, because the temperature dependence of the phase variation of 2 LNAs is almost equal. It is important to attain the temperature stability of the phase of each SSPA and LNA, and also to keep uniform the temperature of the whole radar system in order to attain the stable antenna radiation pattern.

Integration of PIN diode phase shifters, LNAs, phase adjusters and a divider/combiner is made to compose the 8-element transmitter and receiver part of the Bread Board Model of TRMM precipitation radar and the appearance is shown in Fig.4. The basic electric antenna beam scanning function by the switching of the 5-bit digital phase shifter was confirmed. The preliminary measurements of both the transmitting and receiving pattern of the 8-element active array antenna were also made to show good electric performances.

4. CONCLUDING REMARKS

Development of the Engineering Model of the radar has started with the cooperation of National Space Development Agency of Japan(NASDA) and the CRL. The Proto-Flight Model of the radar will be developed by NASDA, aiming at the launch of TRMM in August 1997 through joint efforts of USA and Japan. TRMM is

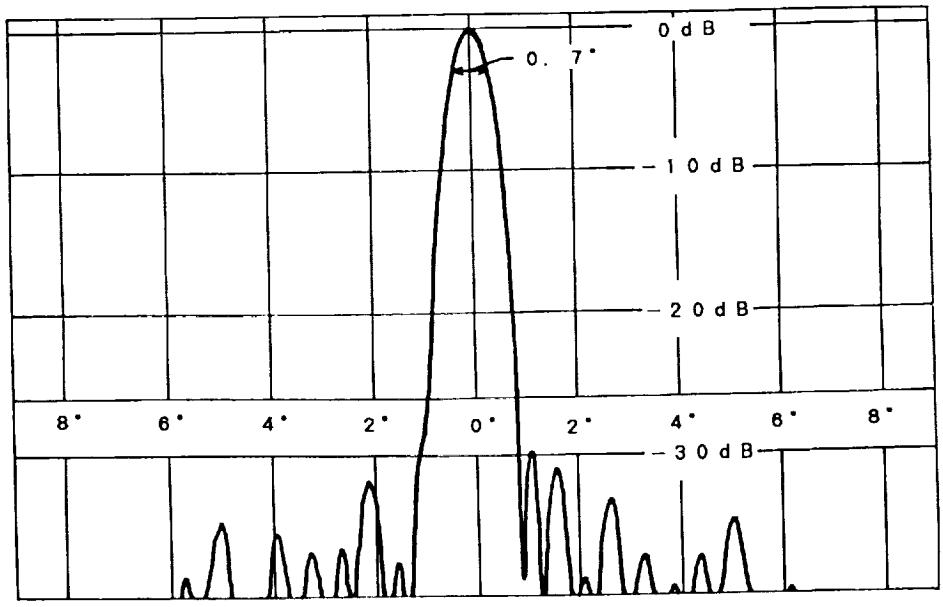

Fig. 3 Radiation pattern of a slotted waveguide array antenna element

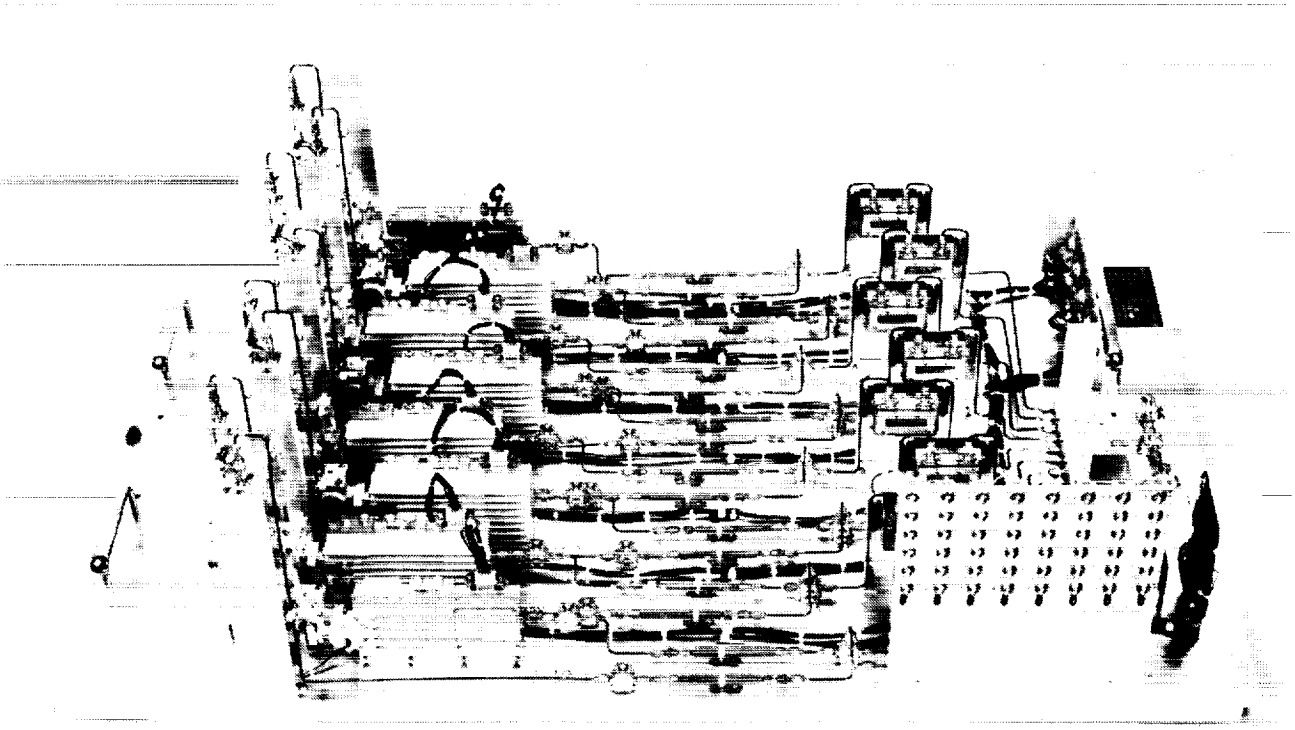

Fig. 4 Outside appearance of the 8-element transmitter and receiver part of the Bread Board Model of TRMM

Table 2. Main System Parameters of TRMM Precipitation Radar (estimated in the feasibility study)

Frequency	13.8 GHz
Antenna	
Type	Slotted waveguide array(128 elements)
Gain	47.7 dB
Beam width	0.71 × 0.71 degrees
Aperture	2.2 m × 2.2 m
Sidelobe level	around -30 dB
Scan angle	±17.0 degrees
Transmitter	
Type	SSPA(× 128)
Peak power	577.8 W
Pulse width	1.67μs × 2ch
PRF(#1)	2778 Hz
Receiver	
Noise figure	2.3 dB
IF frequency	156 MHz, 162MHz
Band width	0.78 MHz × 2ch
Characteristics	logarithmic
Dynamic range	more than 70 dB
Linearity	less than ± 0.5 dB
S_{min}	-112.8 dBm
Others	
Required S/N(#2)	0 dB for single echo
Total system loss	2.0 dB
Filter weighting loss	1.5 dB
Number of independent samples(#3)	64(32 × 2)
Data rate	85 kbps
Power consumption	224 W
Mass(#4)	347 kg

(#1) Fixed PRF; Frequency agility technique (e.g. 13.796 GHz and 13.802 GHz) is applied.
(#2) 0.5 mm/h at storm top.
(#3) Frequency agility technique is applied.
(#4) Without margin

expected to improve the understanding of global atmospheric mechanism and water cycle, which is essential for human life.

References

1. Simpson, J., R.E.Adler and G.R.North, "A proposed tropical rainfall measuring mission(TRMM) satellite", Bull.Amer.Meteor.Soc., 69, 278-295 (1988)

2. Okamoto, K. et al., "A feasibility study of rain radar for the Tropical Rainfall Measuring Mission", J. Commun. Res. Lab. Vol.35, No.145, 109-183(1988)

3. Nakamura, K. et al., "Conceptual design of rain radar for the tropical rainfall measuring mission", Int.J. of Satellite Communications.,Vol.8. 257-268(1990)

4. Ulbrich,C.W., Private communication, based on the empirical fits on the experimental data by Joss. (1987)

5. Olsen, R.L., D.V.Rogers and D.B.Hodge, "The aR^b relationship in the calculation of rain attenuation", IEEE Trans. Antenna Propagat., AP-26, 318-329(1978)

6. Kozu, T. et al., "Development status of rain radar for Tropical Rainfall Measuring Mission" Proc. of IGARSS'92, pp.1722-1724, 1992

7. Okamoto. K. et al. "Development of Bread Board Model of TRMM Precipitation Radar", Proc. of the 18th International Symposium on Space Technology and Science, pp. 1919-1924, 1992

RECENT

SCIENTIFIC ADVANCES

RECENT SCIENTIFIC ADVANCES IN THE USE OF RADAR IN SCIENTIFIC HYDROLOGY

Edwin T. Engman
Head, Hydrological Sciences Branch
Laboratory for Hydrospheric Processes
NASA/Goddard Space Flight Center
Greenbelt, MD 20771 USA

ABSTRACT

The data needs in scientific hydrology involve measurements of system states and fluxes. The microwave region is particularly well suited for measuring the system states of soil moisture and snow and the major flux into the earth as rainfall. This paper discusses the unique data needs for hydrology and presents some recent examples from AIRSAR experiments.

INTRODUCTION

Historically hydrology has developed as an engineering discipline to solve water resources problems such as flood protection and water supply. Evidence of the success of engineering hydrology can be found throughout well developed societies by their relatively high standards of living. Although there are still many water related problems to be solved worldwide, the realizations that water problems are no longer constrained to local drainage basins and the recent concern about climate change have asked completely new questions about hydrology; questions that traditional engineering hydrology is not equipped to answer.

SCIENTIFIC HYDROLOGY

According to Chahine (1992), the hydrologic cycle within the framework of climate change encompasses much more than the classical surface hydrologic framework (precipitation, evaporation, runoff, etc.). In addition to these land surface processes, scientific hydrology must focus on the interactive processes of clouds and radiation, precipitation, oceans, and atmospheric moisture. This conception of the hydrologic cycle not only addresses the transport

and storage of water in the global system, but also the energy needed and released through the phase changes.

If we attempted to phrase these new concerns in the form of a single statement it would most likely be: "The major problem facing scientific hydrology is the tremendous spatial and temporal variability of hydrologic processes across the globe" (National Research Council, 1991). Thus it is primarily a scale effect that separates engineering hydrology from todays needs in scientific hydrology. However it is more than just a scale effect. We are now being asked more detailed questions about the intermediate stages of the hydrologic cycle in contrast to the engineering questions that have been frequently answered empirically. Thus in scientific hydrology we literally are asked where each drop of water resides and for how long and how this drop moves through the Earth's system. That is, we need to quantify fluxes and storages of both water and energy.

ROLL OF SARS

One of the more revolutionary aspects of SAR (Synthetic Aperture Radar) for hydrologists is the potential for measuring and monitoring various states of the hydrologic system. The major state variables that appear to be useful are the soil moisture, snow water content, snowpack condition, frozen soils. For the most part, hydrologists have modeled the hydrologic system pretty much as a "black box," using only input data (usually rainfall and maybe potential evaporation) and the output hydrograph. The unit hydrograph is a good example of a hydrologic "black box." Even though the development of the comprehensive hydrologic models exposed the interior of the black box and subdivided the rainfall-runoff process into a number of so called physical processes, this type of model was still pretty much a black box because there were no provisions for monitoring or measuring any system states or internal processes.

Soil moisture is a system state that can be measured with microwave remote sensing. Techniques for measuring soil moisture include both the passive and active microwave approaches with each having distinct advantages. The theoretical basis for measuring soil moisture by microwave techniques is based on the large contrast between the dielectric properties of liquid water and dry soil. Future applications of soil moisture to hydrologic questions and applications are bound to become more common. Temporally

frequent spatial measurement of soil moisture will some day be available on a routine basis. Hydrologists are going to have to learn how to use these new data. In general, existing models have represented soil moisture in a way to make the model work but have not considered the possibility of independent determination of soil moisture or of soil parameters. For the most part, this approach has been justified because soil moisture data would not be available and hydrologists have not been able to deal with the spatial variability of soil moisture and soil properties. This may change with new microwave measurements.

Snow, the amount and its condition, are important inputs to models the amount of snow in storage and its phase change to snowmelt runoff. Like soil moisture, microwave data appear very promising to the snow hydrologist. Not only can a microwave sensor be an all-weather instrument because it penetrates cloud cover, it can also penetrate the snow pack, which presents one with the opportunity of inferring many of the properties of the snow pack and the under-lying soil. These include depth and water content as well as the degree of ripeness, crystal size, and the presence of liquid water in a melting snow pack. As with soil moisture, the microwave measurement reflects several characteristics at once.

A great deal of progress has been made in demonstrating our capability to measure these storage terms. All measurement approaches, from the laboratory, to truck, aircraft and satellite and shuttle platforms have been successful to some degree In addition there has been a great deal of increased understanding in the areas of theory, radar target interaction and algorithm development

FUTURE SARS FOR HYDROLOGY

The previous sections have discussed the basis of microwave remote sensing for soil moisture and snow and discussed their implications with respect to scientific hydrology. As promising as these new data seem, the future for using microwave data for scientific use is somewhat uncertain. For the next few years, researchers will be limited by the lack of suitable data. Only intensive and science-driven aircraft experiments will be available for collecting soil moisture and snow that hydrologists will find useful. Fortunately, there are a few experiments and satellites with SARs (ERS-1 and JERS-1) that should be invaluable for providing

sample data for developing and testing application models as well as answering some of the target-sensor questions.

Looking ahead to when there may be microwave sensors on orbiting platforms, one confronts the basic differences between passive and active instruments and the intended use of the data. Comparing the instruments simplistically, the active sensors have the capability to provide high spatial resolution data (on the order of tens of meters) but their sensitivity to soil moisture may be confused more by roughness, topographic features, and vegetation than the passive systems. On the other hand, the passive systems, although less sensitive to target features, can provide spatial resolutions only on the order of tens of kilometers from a space platform. However, before the various potential microwave instruments can provide a stream of valuable data for scientific hydrology a number of questions must be addressed.

RESEARCH NEEDED

Although it appears that there will be more and more microwave measurements available in the future, there are a number of research questions that must be addressed before these data are available on a routine basis. The research questions can be split up into two categories for the purpose of discussion, one focusing on the microwave response and the other on hydrologic modeling.

Microwave response: There are a number of unanswered questions regarding the microwave-target interactions that need to be answered before soil moisture and snow can be routinely determined with microwave instrumentation. There is a need to develop algorithms to abstract volumetric soil moisture directly from the microwave measurement (backscatter coefficient) . To do this, the other target characteristics of vegetation and surface roughness will have to be parameterized although recent work by Oh et al, (1992) indicate that polarimetric radar may provide a means for handling the roughness question. Connected directly to this need is a need to better understand the effects of surface roughness on the measured microwave response with respect to incidence angle, azimuth angle, wavelength, and polarization. Also, there is a need to understand the effect of the vegetation canopy on the microwave response. Vegetation variables include the geometry for the individual plant as well as the canopy as a whole, the water content (and perhaps the biochemical makeup) of the plant, and its stage of

growth. Microwave variables would include the incidence angle, the azimuth angle, wavelength, and polarization.

There is a need to investigate the use of change detection algorithms for determining the relative soil moisture of an area and whether or not this information can be useful for hydrologists. Change detection should minimize the influence of target variables such as roughness and vegetation, at least over short time intervals. There is also a reasonable basis for expecting change detection methods to provide adequate data for hydrologic applications if the data are collected from a long term orbiting platform. Long term (multi-season or year) data will establish the upper (wet) and lower (dry) limits for the change algorithm.

There is a need to develop software procedures for correcting the effects of terrain on the microwave response. Active microwave (SAR) is especially sensitive to this. This includes foreshortening, layover, and local incidence angle effects. Also, a potential issue is the relative accuracy of the DEM data with respect to the spatial resolution of the microwave data and the potential effect of subpixel variability on the measured signal.

There is also a need to further investigate the potential for polarimetric SAR and its potential for abstracting target information such as the surface roughness and vegetation characteristics. Studies of this technique need to be carried out with carefully conceived ground data collection programs.

HYDROLOGIC MODELING

Because soil moisture has not been used as measured data in hydrologic modeling, there are a number of issues that hydrologists must address and solve in anticipation of actually working with spatial and temporal soil moisture. Existing hydrologic models and engineering techniques have been developed to solve specific water resource problems (i.e., water supply, flood protection, etc.). As such, many of these are lumped models that have been developed from point measurements. Models with this structure are not capable of using the spatial nature of remote sensing data. Before soil moisture data of this nature can be used in hydrology, there is a need to modify existing models or develop new models that reflect soil moisture in a way that is more physically realistic and so that soil moisture data can be used as input or to verify output. Also,

there is a need to develop procedures for modeling or estimating profile soil moisture from time series near surface measurements and/or using multifrequency data.

Equally important to the research associated with modeling is a necessity to make the remote sensing data easily accessible and usable to the hydrologist. There is a need to develop software, perhaps within a work station concept, that can truly integrate GIS, remote sensing data from several sensors, and the hydrologic models so that all the calibration, scale, format, and so on, problems become transparent to the scientist and he can concentrate on the hydrologic analysis.

REFERENCES

Chahine, M.T., 1992, The hydrologic cycle and Its influence on climate. Nature Vol 359, 373-380.

National Research Council, 1991, Opportunities in Hydrologic Sciences, National Academy Press, Washington, D.C. 348 pp.

Oh, Y., Sarabandi, K. and Ulaby, F.T., 1992, An empirical model and an inversion technique for radar scattering from bare surfaces. IEEE Trans. Geosci. Remote Sensing,Vol. 30(2), 370-381.

S/O-45
182850
8

DRIVING TERRESTRIAL ECOSYSTEM MODELS FROM SPACE

N94-15896

R.H. Waring
College of Forestry
Oregon State University
Corvallis, OR 97331

Introduction

Regional air pollution, land-use conversion and projected climate change all affect ecosystem processes at large scales. Changes in vegetation cover and growth dynamics can impact the functioning of ecosystems, carbon fluxes, and climate (NRC, 1988; IGBP, 1990). As a result, there is a need to assess and monitor vegetation structure and function comprehensively at regional to global scales.

To provide a test of our present understanding of how ecosystems operate at large scales we can compare model predictions of CO_2, O_2 and methane exchange with the atmosphere against regional measurements of interannual variation in the atmospheric concentration of these gases (Mattthews and Fung, 1987; Tans et al., 1990). Recent advances in remote sensing of the Earth's surface are beginning to provide methods for estimating important ecosystem variables at large scales. Ecologists attempting to generalize across landscapes have made extensive use of models and remote sensing technology (Tucker et al., 1986; Running et al., 1989). The success of such ventures is dependent on merging insights and expertise from two distinct fields. Ecologists must provide the understanding of how well models emulate important biological variables and their interactions; experts in remote sensing must provide the biophysical interpretation of complex optical reflectance and radar backscatter data.

Ecosystem models quantify the movement of carbon, water, and nutrients within and through terrestrial ecosystems and keep balance sheets on a daily, monthly, and annual basis. These models consider the source and fate of matter and energy that enter and leave ecosystems as a result of specified processes such as photosynthesis, respiration, decomposition, and the uptake and recycling of nutrients.

Through the process of photosynthesis, leaves of plants capture CO_2 to make simple sugars while producing O_2. Respiration returns CO_2 to the atmosphere using sugars in the growth process to construct complex organic compounds and to maintain living cells. Transpiration moves liquid water carrying dissolved nutrients from the soil through the vascular system of plants to the leaves where water evaporates into the atmosphere. Decomposition is performed by microbes that utilize organic substrates, recycling nutrients and releasing gaseous products such as methane and CO_2 to the atmosphere. To drive ecosystem models from space requires recognizing those structural features and environmental controls that affect the rates of key processes (the role of ecologists) and then finding ways of interpreting these variables remotely from space (the role of remote sensing experts).

Because this is a SAR workshop, I will mention some special contributions that synthetic aperture radar may make in improving the estimates of fluxes from global-scale ecosystem models. My main theme, however, is to emphasize the value gained by combining information from a number of sensors to obtain confidence through independent estimates of critical variables and to predict relationships impossible to obtain from single sensors alone.

Estimating Photosynthesis from Space

The upper limit on photosynthesis, given a specified atmospheric CO_2 level, is set by how much chlorophyll pigment can be packed into a landscape and by the amount of visible light intercepted by the chlorophyll. At any given latitude, on any given date, the solar radiation reaching the atmosphere is known. The challenge is to estimate the effects of clouds on attenuating the radiation through the atmosphere. Daily satellite-derived estimates of cloud cover can be made with a number of sensors. The TOMS (Total Ozone Mapping Spectrometer) satellite, which measures reflectance in ultraviolet waves lengths, provides monthly integrated estimate of visible radiation reaching the vegetation that correspondence directly with measurement recorded at ground stations (Eck and Dye, 1991).

The amount of chlorophyll available to intercept light can also be estimated at monthly intervals from observing seasonal changes in the greenness of vegetation using the NOAA AVHRR series of weather satellites. The Normalized Difference Vegetation Index (NDVI), estimated from near-infrared and red reflectance measurements, is closely related to the chlorophyll content and the photosynthetic capacity of the vegetation (Yoder, 1992 ; Goward and Huemmrich, 1992). Adverse conditions for plant growth reduce this "greenness index" whereas improved conditions favor increases in the index in response to added synthesis of chlorophyll.

Frequently, environmental conditions constrain photosynthesis below the potential established by the amount of visible light absorbed by chlorophyll. For example, stomatal pores close and halt all photosynthesis when leaves freeze at 0 to -2°C. Thermal sensors, coupled with measurements of NDVI, provide good estimates of ambient air temperatures on clear days when most extreme conditions occur (Fig. 1). Fundamental to predicting air temperature from satellites is the realization that (a) dense canopies of tall vegetation associated with maximum values of NDVI are within 2°C of ambient air and (b) that air temperatures can be estimated for less dense vegetation by linear extrapolation of the surface temperature/NDVI response to the maximum NDVI reference (Fig. 2). Because of a large change in dielectric constant when water freezes in the stems and branches of perennial plants, synthetic aperture radar provides an alternative means of evaluating freezing conditions (Way et al., 1990).

In the unfrozen state, plant tissue varies in turgor and in water content. This variation in water status affects growth, photosynthesis, and transpiration in different ways. When water moves rapidly through the vascular system of plants some of the water columns in capillaries may break. As an adaptation, plants have evolved to close their stomata when flow rates approach critical levels during the day (Tyree and Sperry, 1988).

Because CO_2 enters through stomata, closure of these pores reduces photosynthesis as well as transpiration.

The driving force on transpiration and the movement of water through plants is the humidity deficit established between the water-saturated cells within leaves and the air immediately surrounding. The absolute humidity of the air can be estimated using two different thermal bands, one sensitive to water vapor in the atmosphere and one insensitive (Justice et al. , 1991). NOAA weather satellites (Advanced Very High Resolution Radiometer) provide the required combination of red, near-infrared, and two thermal bands to derive simultaneous estimates of the absolute humidity of the atmosphere along with estimates of ambient air temperature near the ground (Goward et al., 1993). With these two values the humidity deficit of the air around the vegetation can be calculated on clear days and a judgement made as to the extent that transpiration and photosynthesis are constrained below potential rates.

Ecosystem models are particularly sensitive to the water status of vegetation at night when transpiration ceases and no (or very little) water uptake from the roots occurs. Under sustained drought, as progressively more water is extracted from the rooting zone, tension is placed on capillary water columns. Predawn measures of tensions on these water column allow prediction of how wide stomata can open the following day to permit photosynthesis and transpiration to proceed (Fig. 3).

It is extremely difficult to estimate the rooting depth of vegetation and even more difficult to define the amount of water available, yet both of these variables plus daily precipitation are required by most ecosystem models to calculate a water balance and derive estimates of predawn plant water tensions. As an alternative, Goward et al. (1993) has demonstrated a correlation between the steepness of the Temperature/NDVI relationship (Fig. 2) and measured predawn water tensions (see also Nemani and Running, 1989; Goward and Hope, 1989). The relationship proved useful in estimating predawn water stress in a Douglas-fir/oak woodland in Oregon during summer months (Fig. 4). The relationship is empirical, however, as illustrated by lack of correlation at times when small amounts of precipitation affected surface wetness but did not reach the roots.

Synthetic aperture radar, in principle, offers a more straight forward biophysical basis for estimating predawn tensions or a combined index that reflects major reductions in the hydraulic conductivity of branches and stems (Running and Waring, 1978). One would expect a reduction in the dielectric constant of the free water in conducting tissue, and accordingly, a reduced backscatter from L or P-Band radar (Narayanan and Vu, 1992). Diurnal variation in water tension is not nearly as useful in interpreting constraints of ecosystem processes (McDonald et al., 1992). On the other hand, if SAR can define progressive reduction in stem and branch water content during periods of high evaporative demand and restrictive soil water supply, it would provide a biophysically sound and more integrative basis for recognizing water stress on vegetation.

Ecosystem models that include just those variables that constrain photosynthesis predict measured forest growth across a steep

environmental gradient in Oregon rather well (Fig. 6). In the analysis, the effective or utilized visible radiation ranged from over 90% of all that intercepted by maritime coastal forests (Sites 1a & lh) to less than 25% of the radiation intercepted by juniper woodland (Site 6).

Estimating Plant and Soil Respiration from Space

Respiration associated with maintaining living cells increases with temperature and with the amount of protein in living biomass (Ryan, 1991). The leaves of plants contain the most active cells, the branches and stems contain progressively fewer live cells per unit weight. X-band (but not C-band) SAR shows potential for estimating the fresh weight of foliage, although seasonal and diurnal variation in leaf-water content may confound interpretations. Stem and branch biomass can be estimated with addition of L-band, but only up to levels of biomass in the range of 100-150 metric tons of dry weight per hectare (Ranson and Sun, 1992; Dobson et al., 1992). Other approaches using optical sensors offer a wider range of predictive abilities before saturating (See Fig. 5; Li and Strahler, 1986).

Soil respiration of CO_2 is also a function of temperature. Respiration from the surface litter decreases with drought; the drying of litter is related closely to the increased steepness of the Temperature/NDVI relationship described earlier. Energy balance equations can be applied to estimate soil temperatures and thermal sensors have been used to infer heat storage capacity (Luvall and Holbo, 1989).

Methane production from soils is a special kind of microbial respiration particularly important in the tundra region of the Northern Hemisphere where a combination of standing water and hollow sedges offer a uniquely active environment for the generation of methane (L.A. Morrissey, NASA Ames Research Center; S.L. Durden, J.P.L., personal communication). The ability of SAR (C-band, VV polarization) to distinguish standing water and the upright stems of sedges provides an accurate measure of where methane production in the tundra is concentrated. SAR should offer a similar ability to identify subtropical and temperate rice paddies and other vegetation types that are periodically inundated and under such conditions produces methane in some abundance.

Summary

Ecosystem models predict many variables that can not be easily sampled over broad areas in a timely manner that reflects inter- and intra-annual variation in the rates of important processes. The net exchange of CO_2 and other important trace gases, however, can be generated from ecosystem models. What is lacking is the means of initializing and driving these models at regional and global scale under continually changing conditions. To this end, satellites carrying a variety of remote sensing instruments appear the best means of testing the general reliability of regional-scale models. Some ecosystem variables require almost continuous monitoring such as cloud cover, as this affects the daily solar radiation reaching the Earth's surface. Other variables such as the "greenness" of the landscape may be recorded less frequently, dependent upon the degree of change seasonally.

There are advantages in synchronous coverage as shown in estimating vegetation greenness, ambient air temperature, surface wetness, and the humidity deficit of the atmosphere . By combining these series of remotely sensed observations limits on rates of photosynthesis, transpiration, respiration, nutrient uptake, and other ecosystem processes may be possible with present satellite technology. An evaluation of standing biomass and other structural characteristics of vegetation is required less frequently and therefore can be made at finer spatial resolution. Future satellites equipped with synthetic aperture radar (L and P bands) should be able to provide estimates of standing biomass below levels of about 150 metric tons/hectare. SAR appears ideal for recognizing some unique combinations of standing water and low stature vegetation associated with high rates of methane production in tundra and other landscapes. SAR also appears well suited to identify when vegetation is frozen. One of the most intriguing possibilities is that SAR technology may be able to provide a more direct biophysical measure of vegetation experiencing drought-stress than any other remote sensing system. This latter possibility warrants careful testing and documentation across a range of vegetation.

References

Eck, T., and D. Dye. 1991. Satellite estimation of photosynthetically active radiation at the Earth's surface. Rem. Sens. Envir. 38: 135-146.

Dobson, M.C., F.T. Ulaby, T. LeToan, A. Beaudoin, E.S. Kasischke, and N. Christensen. 1992. Dependence of radar backscatter on coniferous forest biomass. IEEE Transactions on Geoscience and Remote Sensing 30:412-415.

Goward, S.N., and A.S. Hope. 1989. Evapotranspiration from combined reflected solar and emitted terrestrial radiation: preliminary FIFE results from AVHRR data. Adv. Space Res. 9:239-249.

Goward, S.N., and K.F. Huemmrich. 1992. Vegetation canopy PAR absorptance and the normalized difference vegetation index: an assessment using the SAIL model. Rem. Sens. Envir. 39:119-140.

Goward, S.N., R.H. Waring, D.G.Dye, and J. Yang. 1993. Ecological remote sensing at OTTER: regional satellite observations. Ecol. Appl. (in review).

IGBP (International Geosphere Biosphere Programme). 1990. The International Geosphere Biosphere Programme: a study of global change. The Initial Core Project's Report, No. 12. The International Council of Scientific Unions. Stockholm, Sweden.

Justice, C.O., T. Eck, D. Tanre, and B.N. Holben. 1991. Effect of water vapor on the normalized difference vegetation index derived for the Sahelian Region from NOAA AVHRR data. Int. J. Rem. Sens. 12:1165-1188.

Li, X. and A.H. Strahler. 1986. Geometric-optical bidirectional reflectance modeling of a conifer forest canopy. IEEE Trasactions of Geoscience Remote Sensing 24:906-919.

Luvall, J.C. and H.R. Holbo. 1989. Measurements of short-term thermal responses of coniferous forest canopies using thermal scanner data. Rem. Sens. Envir. 27: 1-10.

Matthews, E., and I. Fung. 1987. Methane emissions from natural wetlands: global distribution, area and environmental characteristics of sources. Global Biogeochem. Cycles 1:61-86.

McCreight, R.W., R.H. Waring, and S.N. Goward. 1993. Ecological remote sensing at OTTER: ultralight aircraft site-scale observations. Ecol. Applic. (in review).

McDonald, K.C.., R. Zimmermann, J.B. Way, and R. Oren. 1992. An investigation of the relationship between tree water potential and dielectric constant. pages 523-525. In: Proceedings of the Int. Geoscience and Remote Sensing Symp., IGARSS'92, Houston, Texas, May 26-29.

Narayanan, R.M. and K.T. Vu. 1992. Microwave sensing of moisture content in selected fruits and vegetables. pages 1181-1182. In: Proceedings of the Int. Geoscience and Remote Sens. Symp., IGARSS' 92, Houston, Texas, May 26-29.

Nemani, R.R., and S.W. Running. 1989. Estimation of surface resistance to evapotranspiration from NDVI and thermal-IR AVHRR data. J. Climate and Appl. Meteorology 28:276-294.

NRC (National Research Council). 1988. Toward an understanding of global change: initial priorities for U.S. contributions to the International Geosphere Atmoposhere Program. National Academy Press, Washingtion, D.C.

Ranson, K.J. and G. Sun. 1992. Mapping biomass for a northern forest ecosystem using multi-frequency SAR data. Proceedings of the Int. Geoscience and Remote Sensing Symp. IGARSS' 92 II:1220-1222.

Tans, P.P., I.Y. Fung, and T. Takahashi. 1990. Observational constraints on the global atmospheric CO_2 budget. Science 247:1431-1438.

Tucker, C.J., I.Y. Fung, C.D. Keeling, and R.H. Gammon. 1986. Relationshipo between atmospheric CO_2 variations and a satellite-derived vegetation index. Nature 319:195-199.

Tyree, M.T., and J.S. Sperry. 1988. Do woody plants operate near the point of catastrophic xylem dysfunction caused by dynamic water stress? Plant Physiol. 88:574-580.

Running, S.W., R.R. Nemani, D.L. Peterson, L.E. Band, D.F. Potts, L.L. Pierce, and M.A. Spanner. 1989. Mapping regional forest evapotranspiration and photosynthesis by coupling satellite data with ecosystem simulation. Ecology 70:1090-1101.

Runyon, J., R.H. Waring, S.N. Goward, and J.M. Welles. 1993. Environmental limits on above-ground production: observations from the Oregon transect. Ecol. Applic. (in review).

Ryan, M.G. 1991. The effect of climate change on plant respiration. Ecol. Appl. 1:157-167.

Waring, R.H., and S.W. Running. 1978. Sapwood water storage: its contribution to transpiration and effect upon water and conductance through the stems of old-growth Douglas-fir. Plant, Cell and Environment 1:131-140.

Waring, R.H. and W.H. Schlesinger. 1985. Forest ecosystems: concepts and management. Academic Press, Orlando, Fla.

Way, J.B., J. Paris, E. Kasischke, C. Slaughter, L. Viereck, N. Christensen, M.C. Dobson, F. Ulaby, J. Richards, A. Milne, A. Sieber, F. Ahern, D. Simonett, R. Hoffer, M. Imhoff, and J. Weber. 1990. The effect of changing environmental condions on microwave signatures in forest ecosystems: preliminary results of the March 1988 Alaskan aircraft SAR experiment. Int. J. Remote Sens. 11:1119-1144.

Yoder, B. J. 1992. Photosynthesis of conifers: influential factors and potential for remote sensing. Ph.D. thesis, Oregon State University, Corvallis, OR.

Figure Captions

Fig. 1. Ambient air temperatures for twelve months were estimated from remotely sensed temperature measurements and vegetation "greenness obtained from NOAA AVHRR weather satellite for a series of sites ranging from temperate rainforest to juniper woodland (Goward et al. (1993).

Fig. 2. On a 9 X 9 km grid, AVHRR thermal sensors were used to estimate surface temperature (Ts) on a drought-prone ponderosa pine forest with variable stocking density. When the 81 separate estimates of surface temperature were analyzed in conjunction with paired estimates of vegetation greenness (NDVI), the ambient air temperature could be estimated by extrapolating the relationship to the maximum NDVI, representing a canopy intercepting more than 99% of all visible radiation (Goward et al., 1993).

Fig. 3. Under static conditions of no transpiration at night, tension measured on the water columns of twigs (predawn water potential) predicts the extent that stomatal will open during the day (Waring and Schlesinger, 1985).

Fig. 4. Seasonal comparison of predawn leaf water potential measurements and the NDVI/Ts slope were derived from near-infrared, red, and thermal channel measurements obtained from an ultralight aircraft flying at 300 m altitude. A steeping slope of the NDVI/Ts relationship correlates well with increasing drought stress measured on Douglas-fir trees, but some deviation occurs following small storms that only wet the surface litter (McCreight et al., 1993).

Fig.5. Classification of shadow in video images of forests correlate well with forestry estimates of above-ground foliage and woody biomass up to levels near 700 Mg/ha (McCreight et al., 1993).

Fig. 6.An ecosystem model that evaluates the light utilized by photosynthesis on an annual basis correlates well with observed above-ground growth of forests across a transect in Oregon. Only where forests have reached maximum height (Site 1, old-growth) was it necessary to take into account the increased respiration and reduced hydraulic conductivity of older trees to match observed growth (Runyon et al., 1993).

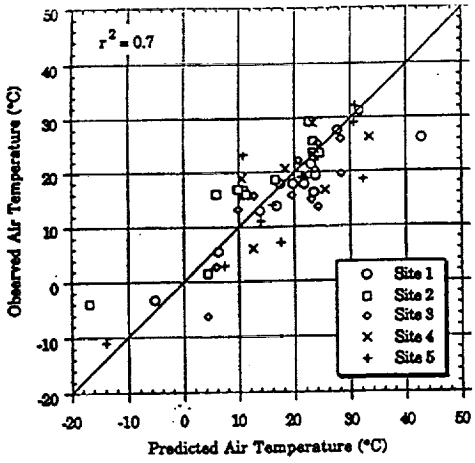

Figure 1

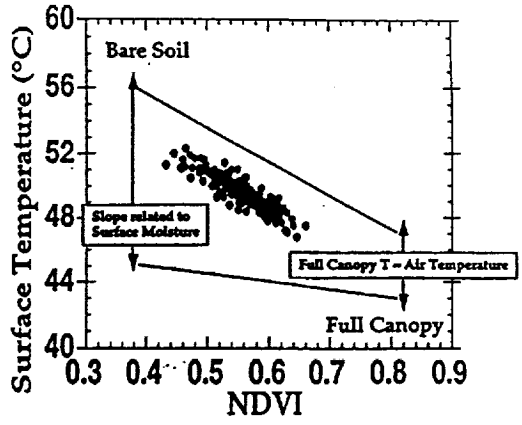

Figure 2

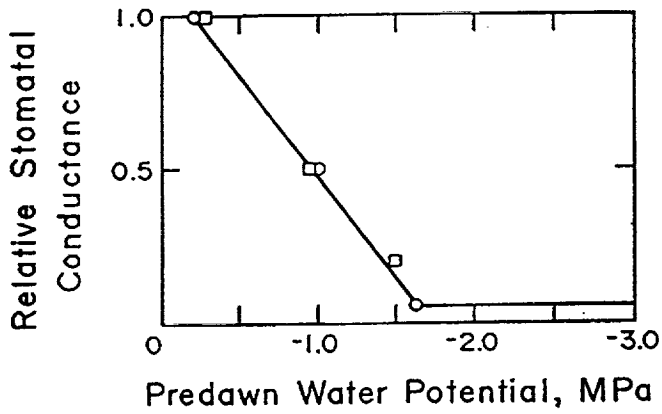

Figure 3

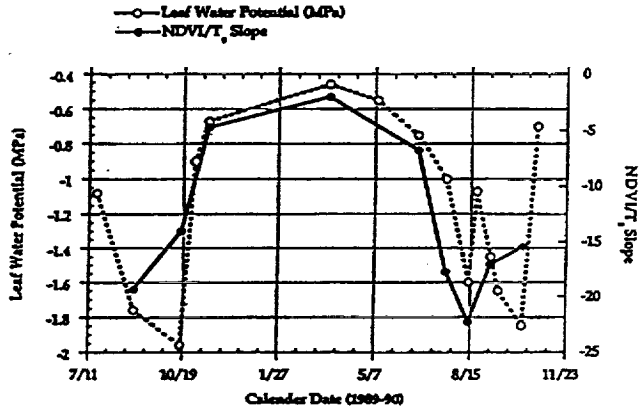

Figure 4

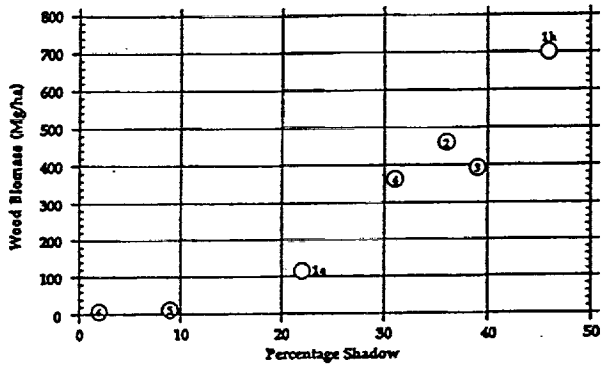

Figure 5

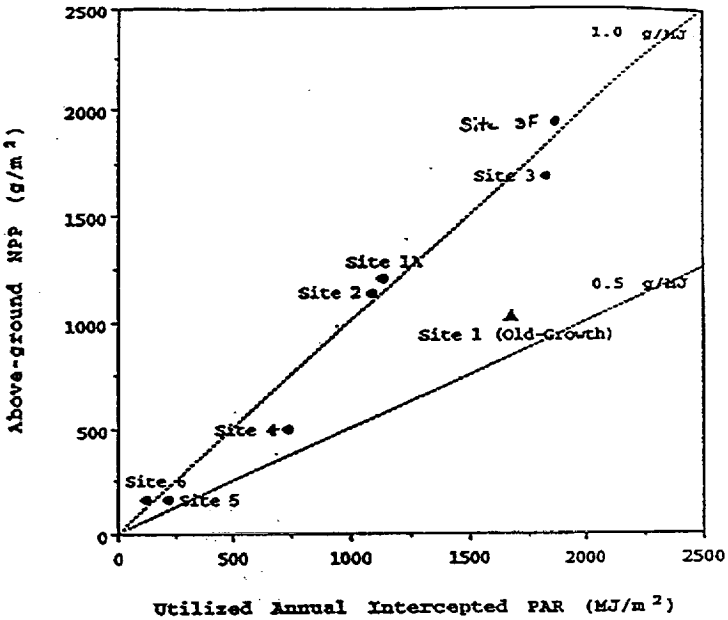

Figure 6

S11-43
18285
P 8

RECENT ADVANCES IN RADAR REMOTE SENSING OF FOREST

N94-15897

Thuy LE TOAN
Centre d'Etude Spatiale des Rayonnements
CNRS/Université Paul Sabatier
Toulouse - France

I - INTRODUCTION

On a global scale, forest represents most of the terrestrial standing biomass (80 to 90%). Thus, natural and anthropogenic change in forest covers can have major impacts not only on local ecosystems but also on global hydrologic, climatic and biogeochemical cycles that involve exchange of energy, water, carbon and other elements between the earth and atmosphere. Quantitative information on the state and dynamics of forest ecosystems and their interactions with the global cycles appear necessary to understand how the earth works as a natural system.

The information required include the lateral and vertical distribution of forest cover, the estimates of standing biomass (woody and foliar volume), the phenological and environmental variations and disturbances (clearcutting, fires, flood) and the longer term variations following to deforestation (regeneration, successional stages). To this end, seasonal, annual and decadal information is necessary in order to separate the long term effects in the global ecosystem from short term seasonal and interannual variations.

Optical remote sensing has been used until now to study the forest cover at local, regional to global scale. Radar remote sensing, which provides recently SAR data from space on a regular basis, represents an unique means of consistent monitoring with different time scales, at all latitudes and in any atmospheric conditions. Also, SAR data have shown potential to detect several forest parameters that cannot be inferred from optical data. The differences -and complementarity- lie in the penetration capabilities of SAR data and their sensitivity to dielectric and geometric properties of the canopy volume ; while optical data are sensitive to the chemical composition of the external foliar layer of the vegetation canopy.

Basically, the radar backscatter is sensitive to the quantity and state of water distributed in the complex vertical and horizontal structure of the canopy. Thus, it is expected that the radar measurement contains information on the forest type, tree architecture, tree biomass by parts (trunk, branches, leaves), canopy structure and also in certain conditions, the ground topography, soil moisture, soil surface roughness and understory vegetation. The physical relationships between radar backscatter and forest parameters depend on the radar frequency, polarization, incidence.

Past results using SEASAT, SIR-A, SIR-B and airborne data demonstrated the use of SAR data for mapping of forest extent, mapping of wetland extent in forested areas, detection of disturbances due to deforestation, fires or flood. Some research attempts have been made to relate the radar backscatter to forest height, age class and biomass but the approach used was almost empirical. Given the complexity of the interaction mechanisms, to develop and validate algorithms which will provide the biophysical product from SAR data require a quantitative approach evolving both experiments and theory.

II - RECENT ADVANCES

During the past three years, significant progress has been observed in radar remote sensing of forest. There has been an emerging international concensus on the need for worldwide studies on processes associated with climate change, in which forest covers play an important role. Also, research in radar remote sensing has been driven by the numerous spaceborne SAR missions scheduled in the 90's, starting with ERS-1 launched in 1991 and J-ERS-1 in 1992.

Technical advances in the development of SAR systems have provided in the past years multiparameter airborne SARs. Such systems, when calibrated, are optimum tools for algorithm development. Among those the current NASA/JPL system is an operational, three frequency polarimetric SAR which has taken part in many data acquisition campaigns in the world since 1988. Observation of forest covers is currently one of the most important research topics of such airborne missions. Experiments have been performed on a diversity of forest ecosystems in the US, Canada, Europe and in the tropics. Experimental procedures have been refined and more relevant ground data have been collected. Meanwhile, significant improvement in theoretical modeling of forest backscatter has been observed. This resulted from the availability and the relevance of experimental data and a better integration of the experimental and modeling approaches in the research projects.

Since 1991, ERS-1 has open a new era of SAR data that can be used on a regular basis. The radiometric and geometric quality of the data currently provided by ERS-1 makes possible the use of multitemporal observations either for terrain identification or for changes detection.

Recent results in remote sensing of forests concern several aspects including forest type classification, determination of phenological and environmental states of the forests (*Way et al. 1992)* or the extent of flooded forests. However, the emphasis has been put on two main subjects : deforestation monitoring and biomass determination.

II-1 DEFORESTATION

The conversion of forests to agriculture and pasture and the harvest of forest for timber and fuelwood cause a net release of C02 and also other trace gases such as methane and nitrous oxide. Uncertainties in the estimates of the amount of carbon released globally from vegetation and soils result from different assumptions concerning 1/ the rate of land use change, in particular the rate of deforestation and 2/ the biotic response to disturbances.

Even today although much progress has been made in recent years, estimates of the current rate of conversion of tropical forests to agricultural land vary from 70.000 to 100.000 km2 per year.

The SAR is expected to contribute significantly to determine accurately the perturbation characteristics including the rate and location of 1/ecosystem conversion to agriculture and pasture, 2/forests degraded for timber harvest of fuelwood and 3/afforestation and natural regrowth.

To measure the extent of deforestation has been well demonstrated with SEASAT, SIR-A, SIR-B and with airborne SARs operating at low frequencies (e.g. L and P bands). The contrast ratio between radar backscatter intensity of forests and other land uses including clearcut, agriculture, pasture is of the order of several dB in most cases.

At higher frequencies (e.g. C and X bands), the radar backscatter of deforested areas varies as a function of the terrain characteristics including soil surface roughness, soil moisture, crop, grass or regrowth vegetation parameters. Thus, deforested areas can have a large range of backscatter values. With ERS-1 (5.3 GHz, 23° of incidence, VV) the conversion of forest to wide spreading pasture can logically be detected as shown on ERS-1 images in the Amazone basin (ESA, 1993). On the other hand, small patches deforested for shifting cultivation, e.g. in Africa, might be difficult to identify on the basis of their radar backscatter intensity at a single date.

The availability of reliable multitemporal data by ERS-1 offers possibilities to develop classification methods based on their temporal changes. In general, forest covers exhibit minor temporal change compared to clear cut, agriculture and other land uses. Through several examples of overlaid multitemporal images of ERS-1, the use of temporal changes for forest and land use classification and monitoring appear obvious.

In the past few years, a new approach of classification methods based on scattering behaviour of different surface types instead of their backscattering intensity have been developed (*Kong et al 1988, Van Zyl 1989, Evans et al 1990, Freeman et al 1992*). The development and validation of such methods have been possible since reliable airborne, polarimetric SAR data have been collected). In general, the polarization state of the received wave is compared to that of the transmitted wave in order to deduce the properties of the scatterer. The classification can be unsupervised, based solely on comparing general properties of the Stokes parameters of the scattered wave to that of simple scattering models. As an example, results at L band (*Van Zyl 1989*) indicated that scattering from clear cut areas and agricultural fields is mostly similar to that predicted by the odd number of reflection class while the scattering from forest covers generally is classified as being a mixture of characteristics odd and even reflections and diffuse scattering.
For future spaceborne SARs, the use of polarimetric data may improve significantly the robustness of algorithms of forest/non forest delimitation.

II-2 FOREST BIOMASS

Besides the rate of deforestation, one of the greatest uncertainties concerning the global carbon budget arise from a lack of information on forest biomass. First the assessment of the biomass of existing forests is necessary to determine the amount of CO_2 released to the atmosphere by forest burning. Also, to determine whether forests are a source or a sink of carbon, accurate estimate of biomass and carbon storage is needed, especially that of regenerating forests which accumulate carbon quickly during the first 20-30 years after disturbance.

Optical remote sensing of forests is based on spectral reflectance data governed mainly by tree foliage properties including leaf internal structure, leaf chemical composition and leaf angle orientation. With longer wavelengths, radar waves can penetrate into the forest canopy and the radar backscatter can give information on the trunk, branches, which represents 90% of the total above ground biomass.

In the past years, it was observed that the intensity in a SAR image at low frequency (L-band) is proportional to several forest parameters including tree height, stand age and above ground biomass of the forest stands.

However, to develop a robust algorithm for inversion of SAR data into forest biomass requires a thorough understanding of the interaction mechanisms between microwave and forest canopy. This is necessary to define the validity domains of inversion algorithm regarding the SAR parameters, the forest characteristics and the environmental conditions.

The last few years have seen several experiments conducted on forest covers using multifrequency, polarimetric SARs together with an appropriate ground data collection plan (*Kasischke et al, 1991, Dobson et al. 1992 Ranson et al. 1992, Le Toan et al. 1992*). To reduce uncertainties in measurements of forest parameters most experiments have been performed on coniferous forests, which present a relatively simple structure at the tree and stand level.

The observations confirmed past results on the strong correlation between radar backscatter at low frequencies (P and L bands) and forest parameters. With well calibrated radars, quantitative comparison between frequencies and polarizations is now possible. P-band backscatter intensity yields the best correlation and the best sensitivity to forest biomass. Also cross polarization gives better results compared to like polarizations (*Le Toan et al. 1992, Dobson et al. 1992).* Polarimetric features, such as the polarization phase differences can be also related to forest age or biomass. However, their contribution compared to the backscatter intensity is not significant in terms of the retrieval of forest biomass. Nevertheless, polarimetric measurements have been very useful for the modeling of forest backscatter at different frequencies.

Theoretical modeling will constitute the foundation of inversion techniques. The requirement is that the models must include all the physical properties of the target involved in the interaction process so that they can cope with simultaneous observations of a large variety of active (and passive) systems using multiple frequencies and multiple polarizations.

In general, two main approaches have been used to solve the scattering problem : the field approach and the intensity approach. Also, approximations have been made to characterize the vegetation canopy either as a continuous medium or a discrete medium.

Most models developed to describe the backscatter of forest canopies use the radiative transfer theory with a discrete medium approach. The models consider vegetation as a collection of lossy scatterers representing vegetation components (leaves, stems, branches, trunks). The forest canopy is in general modeled as a multilayer medium, each with a specific distribution of dimension, orientation and dielectric constants of the scatterers of various shapes. Although the radiative transfer theory provides only the incoherent terms, with the vector formulation of the theory multiple scattering problems and polarimetric backscattering can be accounted for.

Recent improvements in modeling of forest canopies included :
a) the consideration of more complete structure of the trees instead of simplifications in the past assimilating the trees as leaves alone or branches and soil alone etc.
b) more accurate calculation of the scattering of vegetation elements assimilated to finite dielectric cylinders or dielectric discs,
c) the consideration of coherent interaction between elements of structured vegetation,
d) the addition of second order scattering and,
e) the consideration of the interaction between vegetation and rough soil surface.

However, the most important progress concerned the model validation which benefited from more concertation between experimenters and modelers. More appropriate vegetation data have been measured in view of their transformation into model input parameters. On the other hand, experimental observations on the polarization and frequency behaviour of the radar basckscatter have led to substantial improvements of the theoretical models.

Several results of model validation have been published recently (*Durden et al. 1989, Ulaby et al. 1990, Sun et al. 1991, Karam et al. 1992, Hsu et al. 1993*). Once validated, the models can be used to identify different scattering mechanisms at different frequencies and polarizations. It was found for example that at P-band, the most significant mechanism between radar wave and a pine forest is HH polarization from the interaction between trunk and ground and for HV and VV, the direct scattering from the branches (*Hsu et al. 1993*). Since there exists a strong correlation between different parts of the tree biomass, the correlation between radar backscattering coefficients and trunk biomass, branch biomass and total biomass as found experimentally are now understood (*Beaudoin et al. 1993*).

III - CURRENT AND FUTURE WORKS

More works are still needed to conduct experimental/theoretical studies on different forest ecosystems in order to generalize the results obtained on the retrieval of forest parameters. Also, the use of multifrequency, multipolarization data to retrieve different forest parameters including biomass by parts, canopy structure and ground information must be undertaken, at present with airborne SARs and in near future with SIR-C/X-SAR.

On the other hand, the use of data from current satellites (ERS-1, J-ERS-1) is presently assessed for forest observations.

One possible research direction concerns a reexamination of the types of forest parameters of interest retrievable from SAR data in relation with ecosystem modeling. The sensitivity of radar backscatter to tree water content, tree water status and tree structure can be taken into account to derive some condensed descriptors of forest ecosystems.

References

- *Beaudoin, A., T. Le Toan, S. Goze, E. Nezry, A. Lopes, E. Mougin, C.C. Hsu, C.C. Han, J.A. Kong.* "Retrieval of forest biomass from SAR data". To appear, Intern. Journal of Remote Sensing, Sept. 1993.
- *Dobson, M.C., F.T. Ulaby, T. Le Toan, A. Beaudoin, E.S. Kasischke and N. Christensen* (1992). "Dependence of radar backscatter on coniferous forest biomass", IEEE Trans. Geosci. Remote Sensing, 30, 412-415.
- *Durden, S.L., J.J. Van Zyl and H.A. Zebker* (1989). "Modeling and observation of the radar polarization signature of forested areas", IEEE Trans. Geosci Remote Sensing, 27, 290-301.
- *Evans, D.L., T.G. Farrs, J.J. Van Zyl and H.A. Zebker* (1988). "Polarimetry radar: Analysis tools and applications", IEEE Trans. Geosci and Remote Sensing, 26, N° 6, 774-789.
- *Freeman, A., S. Durden and R. Zimmerman.* "Mapping subtropical vegetation using multifrequency. Multipolarization SAR data". Proc. IGARSS 1992, Houston, Texas.
- *Hsu, C.C., H.C. Han, R.T. Shin, J.A. Kong., A. Beaudoin and T. Le Toan* "Radiative transfer theory for polarimetric remote sensing of pine forests", To appear, Intern. Journal of Remote Sensing, Sept. 1993.
- *Karam, M.A., A.K. Fung, R.H. Lang and N.S. Chauhan* (1992). "A microwave scattering model for layered vegetation", IEEE Trans Geosci. Remote Sensing, 30, 767-784.
- *Kasischke, E.S., L.L. Bourgeau-Chavez, N.L. Christensen and M.C. Dobson,* (1991). "The relationship between above ground biomass and radar backscatter as observed in airborne - SAR imagery", Proc. Aircraft Workshop, JPL, May 1991.
- *Kong, J.A., A.A. Swartz, H.A. Yuech, L.M. Novak and R.T. Shin.*(1988) "Identification of terrain cover using the optimum polarimetric classifer". J. Electromag. Waves Appl, 2, 171-194.
- *Le Toan, T., A. Beaudoin, J. Riom and D. Guyon* (1992). "Relating forest biomass to SAR data", IEEE Trans. Geosci Remote Sensing, 30, 403-411.
- *Ranson, K.J. and G. Sun* (1992). "Mapping biomass for a northern forest ecosystem using multifrequency SAR data", Proc. IGARSS 1992, 1220-1222, Houston, Texas.
- *Sun, G., D.S. Simonett and A.H. Strahler* (1991). "A radar backscatter model for discontinuous coniferous forests", IEEE Trans Geosci. Remote Sensing, 29, 639-650.

- *Ulaby, F.T., K. Sarabandi, K. MacDonald, M. Whitt and M.C. Dobson* (1990), "Michigan microwave canopy scattering model", Int. J. Remote Sensing, 11, 1223-1253.
- *Van Zyl J.J.*, (1989). "Unsupervised classification of scattering behavior using radar polarimetry data", IEEE, Trans. Geosci Remote Sensing, vol. 27, pp. 36-45, 1989.
- *Way J.B., E. Rignot, R. Oren, R. Kwok, K. McDonald, M.C. Dobson, G. Bohan, L. Viereck and J.E. Roth* (1992). "Monitoring temporal change and species in Alaskan forests using imaging radar data", IEEE Trans. on Geosci and Remote Sensing, in review.

RADAR RESPONSE OF VEGETATION: AN OVERVIEW

Fawwaz T. Ulaby and M. Craig Dobson
The University of Michigan

- Vegetation Classes
- Soil Scattering: (1) Backscatter
  (2) Forward Scattering
- Radar Response
  - Vegetation Biomass
  - Vegetation Structure
  - Temporal Variations: (1) Short Term (hours to days)
    (2) Long Term (Seasonal)
  - Effect of Rain
- Emergence of a User Community
- Concluding Remarks

The University of Michigan

STRUCUTRAL CLASSIFICATION OF VEGETATION FROM SAR

Growth Form	Herbaceous		Woody			
	Blade-like	Broadleaf	Shrubs	Trees		
				Excurrent	Decurrent	Columnar
		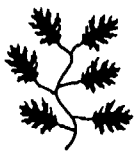	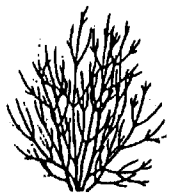		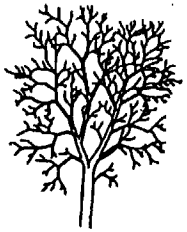	
	(i.e., grass, corn)	(i.e., soybeans)	(i.e., alder)	(i.e., pine and spruce) Gymnosperms	(i.e., oak and maple) Angiosperms dicotyledons	(i.e., palm) Angiosperms Monocotyledons
Structural Characteristics Trunks	none	none	Many small trunks with characteristic orientation distributions	conical layered dielectric	cylindrical, forked layered dielectric	cylindrical homogeneous dielectric
Branches	some non-woody stalks or stems	some non-woody stems	many small branches & stems	branch size and orientation varies with height •large branches- planophile •many small stems- erectophile branches tend to be long and thin	many forked with few horizontal elements branches tend to be short and thick	none
Foliage	blade-like erectophile	broad leaves	blade-like or broadleaves	needles	broadleaves	blade-like in clump at top of trunk
General Scattering Properties f < 5 GHz	low to moderate σ^0 dominated by surface scattering $\sigma^0_{VV} \geq \sigma^0_{HH} >> \sigma^0_{HV}$ zero mean $\Delta\phi$		moderate σ^0 $\sigma^0(f,P,\theta)$ dependent upon trunks & branches uniform $\Delta\phi$	very high like-polarized σ^0 moderate σ^0_{HV}, dominated by ground-trunk and few large branches $\sigma^0_{HH} \geq \sigma^0_{VV}$, $\sigma^0_{HH} / \sigma^0_{VV}$=f (trunk biomass) broad distributions of $\Delta\phi$	high σ^0 dominated by large branches, $\sigma^0_{HH} \geq \sigma^0_{VV}$ σ^0_{HV} = f (branch biomass) broad distributions of $\Delta\phi$	moderate σ^0 large crown structures may dominate σ^0 low transmissivity through crown non-zero mean $\Delta\phi$
f > 5 GHz	moderate to high σ^0 dominated by vegetation $\sigma^0_{VV} \approx \sigma^0_{HH} > \sigma^0_{HV}$		mod. to high σ^0 stem orientation and leaf size very important	high σ^0 dominated by branches and stems	mod. to very high σ^0, can vary seasonally with foliage and stem properties	high σ^0 determined by crown

RADAR SCATTERING MECHANISMS

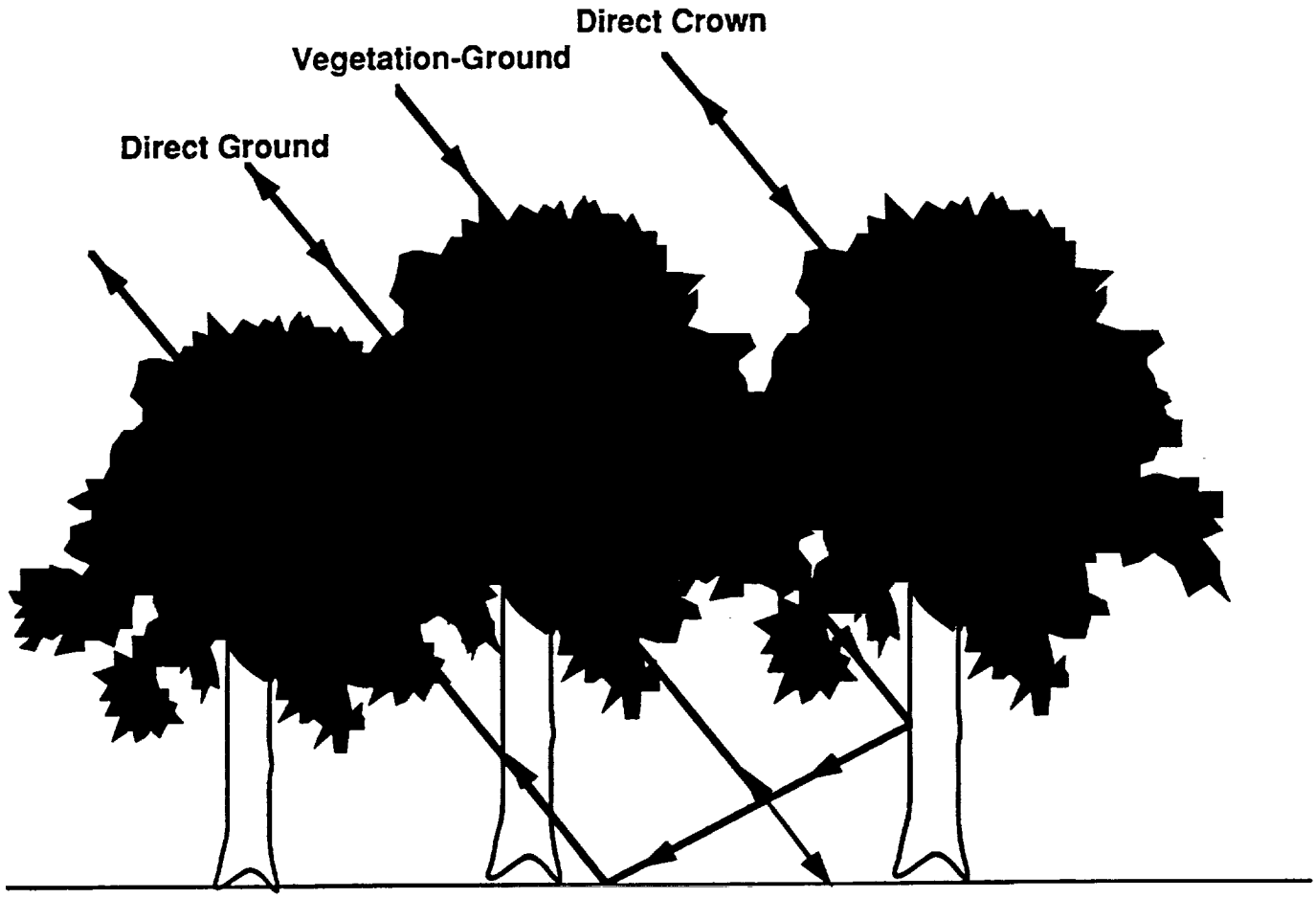

- Direct Ground Backscatter
- Vegetation-Ground Bistatic Scattering
  - Trunks
  - Leaves (needles)
  - Branches
- Direct Crown Backscatter

SOIL BACKSCATTERING

A. Theoretical Models

- Small Perturbation Model
- Physical Optics Model
- Geometric Optics Model
- Phase Perturbation Method
- Full Wave Model
- Integral Equation Model

Models agree with experimental observations only under certain conditions. Overall, models not useful.

B. Michigan Empirical Model

- Frequency Range : 1-10 GHz
- Angular Range : 20° - 70°
- Roughness range : s = 0.32 cm to s = 4.0 cm (expected validity for any s >0.3 cm)
- Moisture range : 0.05 g/cm^3 to 0.31 g/cm^3

Moisture Sampling Depth

L-Band (1.25 GHz) : Average Moisture of Top 10 cm layer

C-Band (5.3 GHz) : Average Moisture of Top 3 cm layer

X-Band (9.5 GHz) : Average Moisture of Top 1 cm layer

$$\text{Sampling Depth} \simeq \lambda / 3$$

- Model Verification For A smooth Surface (s=0.4 cm)

1.5 GHz

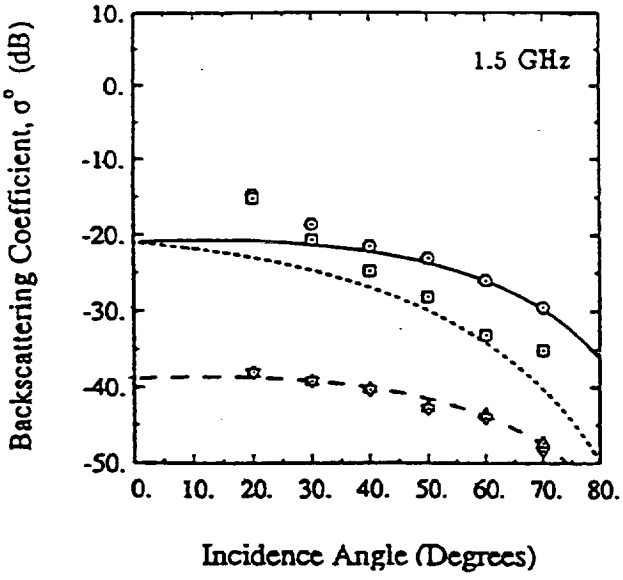

s = 0.4 cm
m_v = 0.29

- σ°_{vv}, Model
- σ°_{hh}, Model
- σ°_{vh}, Model
- σ°_{vv}, Measured
- σ°_{hh}, Measured
- σ°_{vh}, Measured
- σ°_{hv}, Measured

4.75 GHz

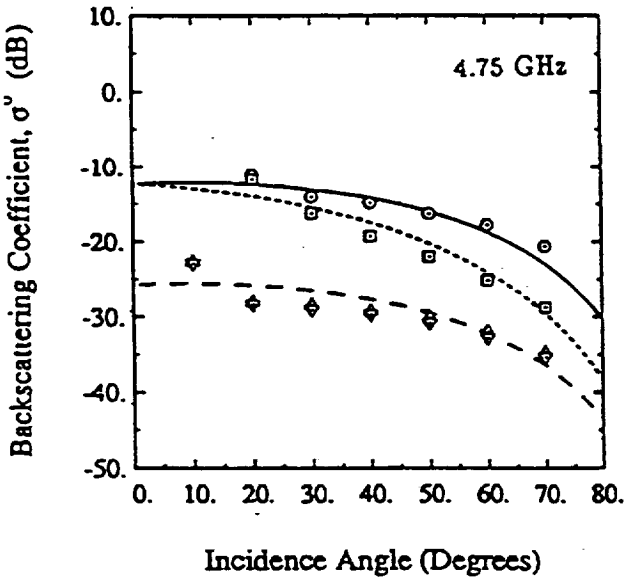

9.5 GHz

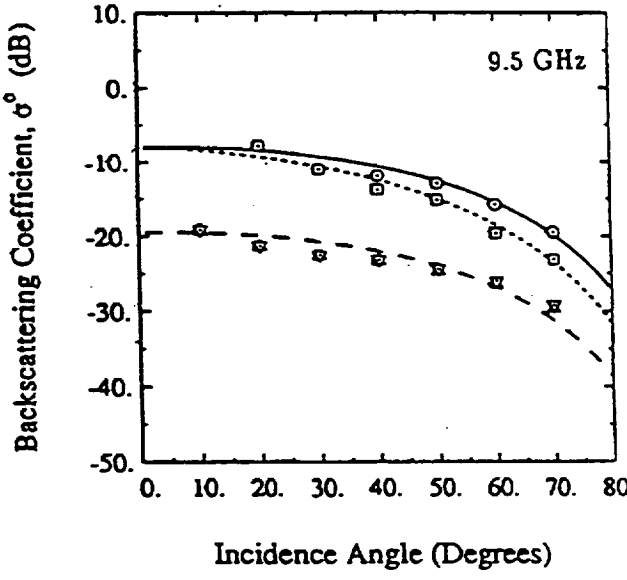

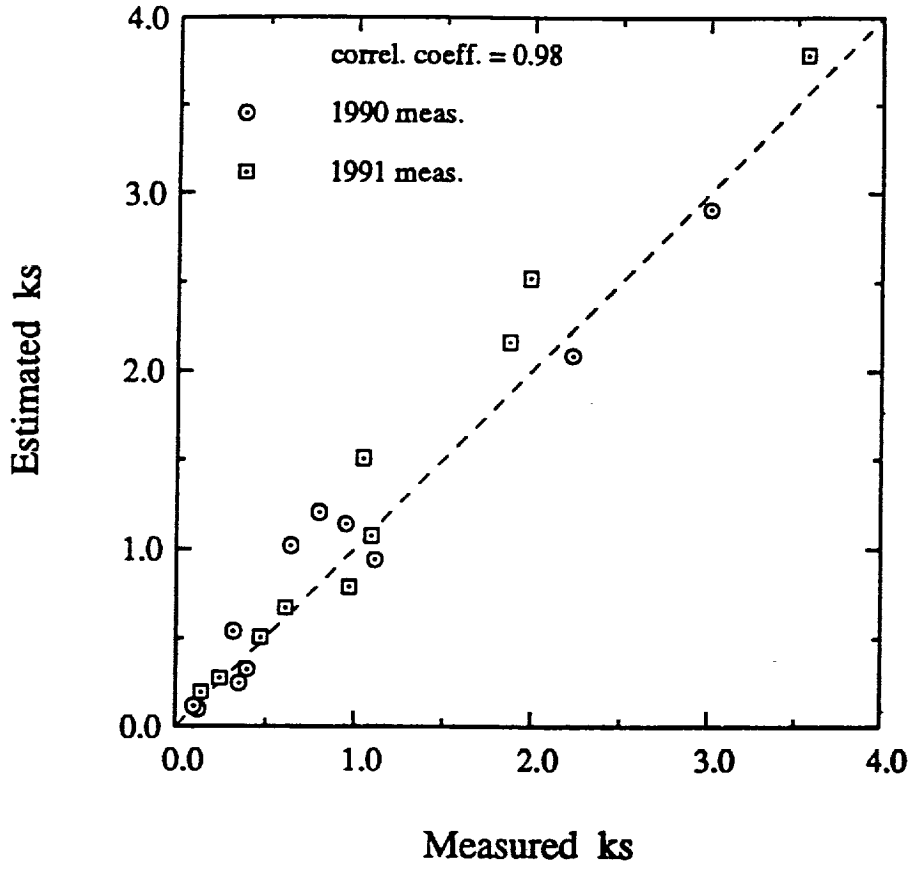

rms height

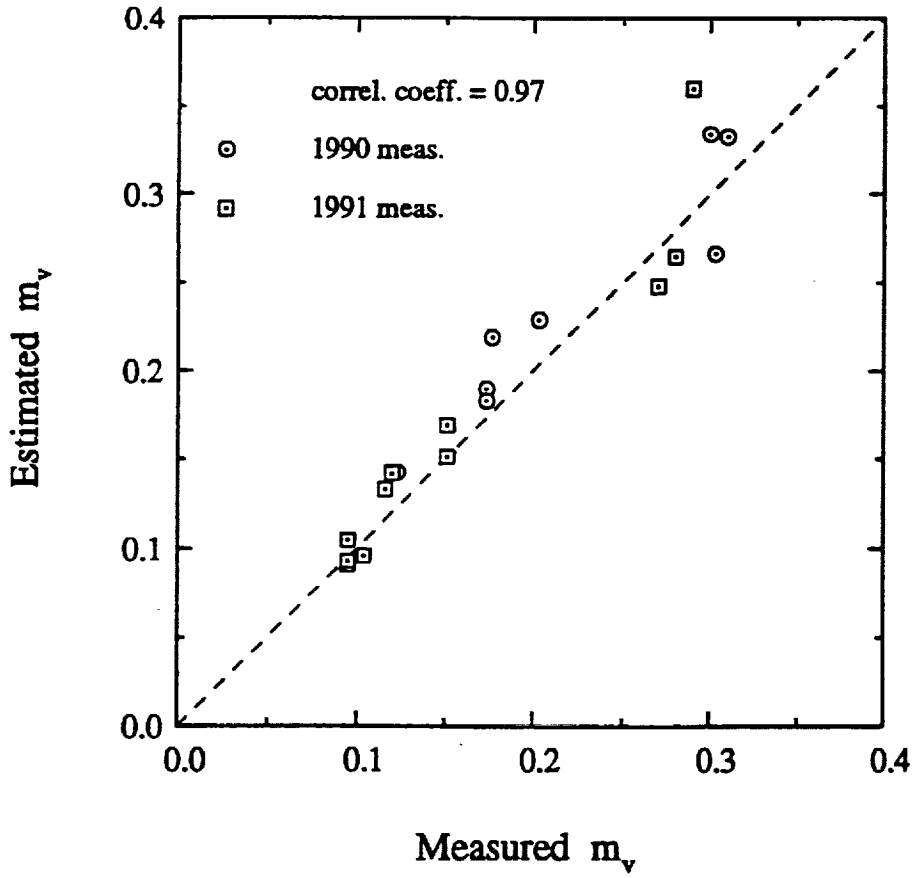

soil moisture

Inversion Algorithm

If radar measures σ^0_{vv}, σ^0_{hh}, and σ^0_{hv} at a given frequency and angle, both s and m_v can be determined from the ratios:

$$p = \sigma^0_{hh} / \sigma^0_{vv}$$
$$q = \sigma^0_{hv} / \sigma^0_{vv}$$

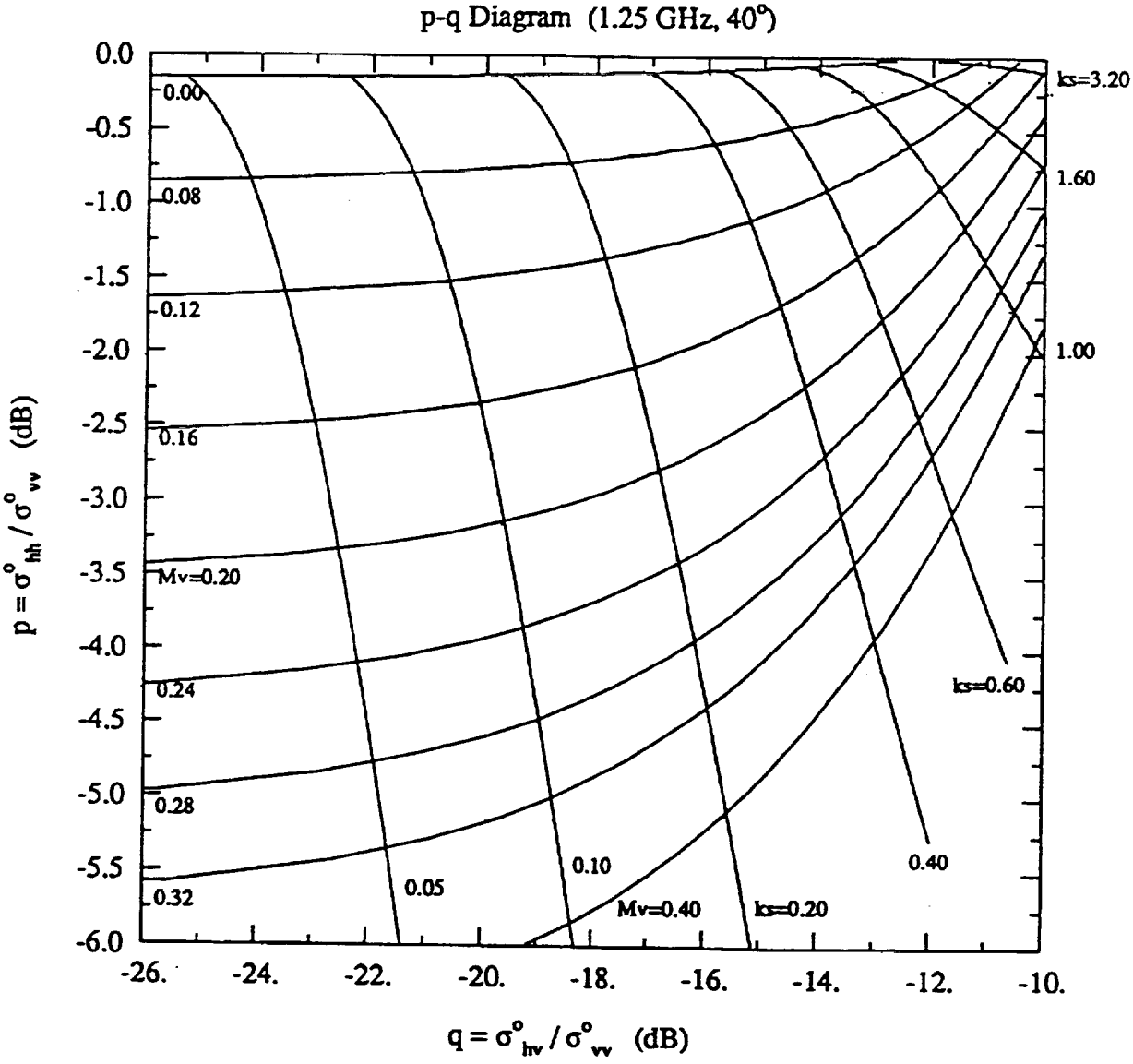

Note: $p(\text{dB}) = 10\log\left(\sigma^0_{hh} / \sigma^0_{vv}\right) = \sigma^0_{hh}(\text{dB}) - \sigma^0_{vv}(\text{dB})$

$q(\text{dB}) = \sigma^0_{hv}(\text{dB}) - \sigma^0_{vv}(\text{dB}).$

ERS-1 SAR Response

$\theta = 23°$
vv Polarization

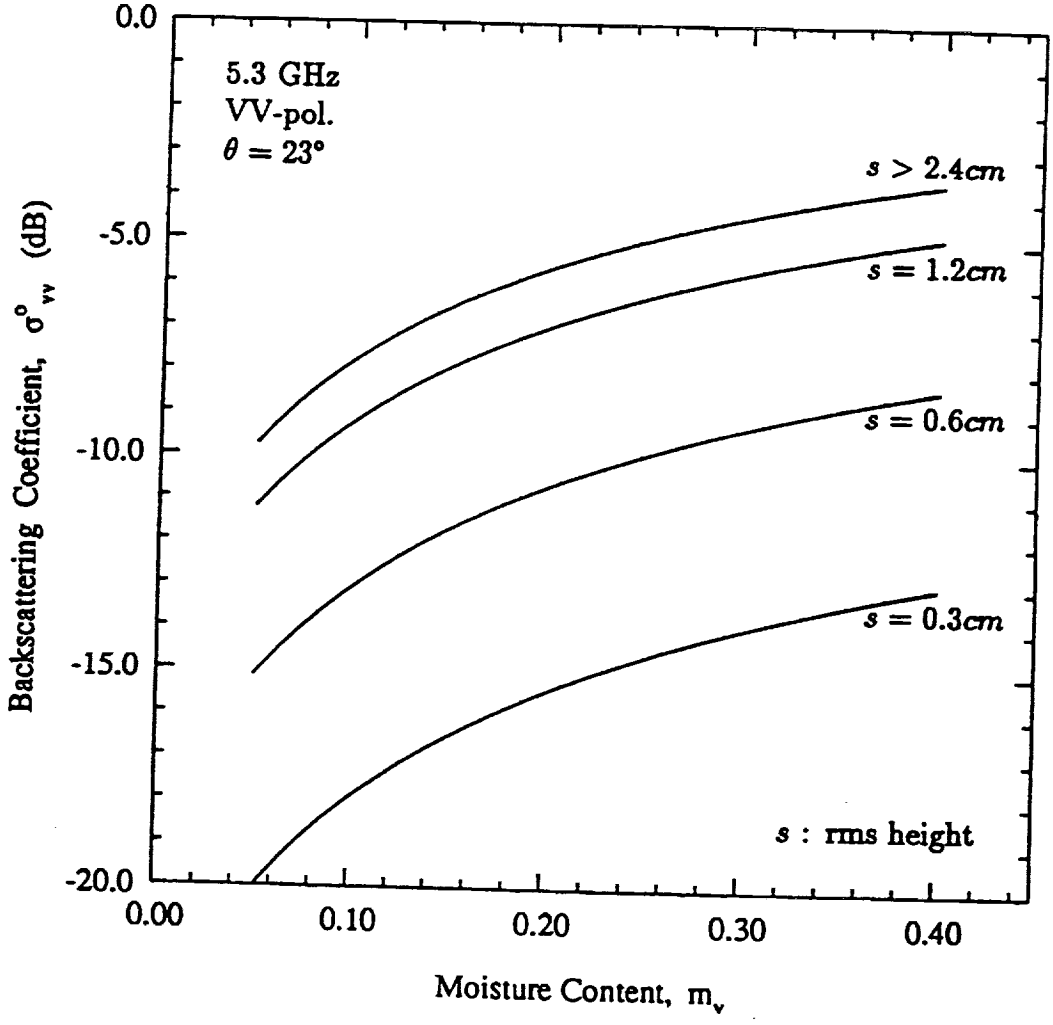

RADIATION LABORATORY

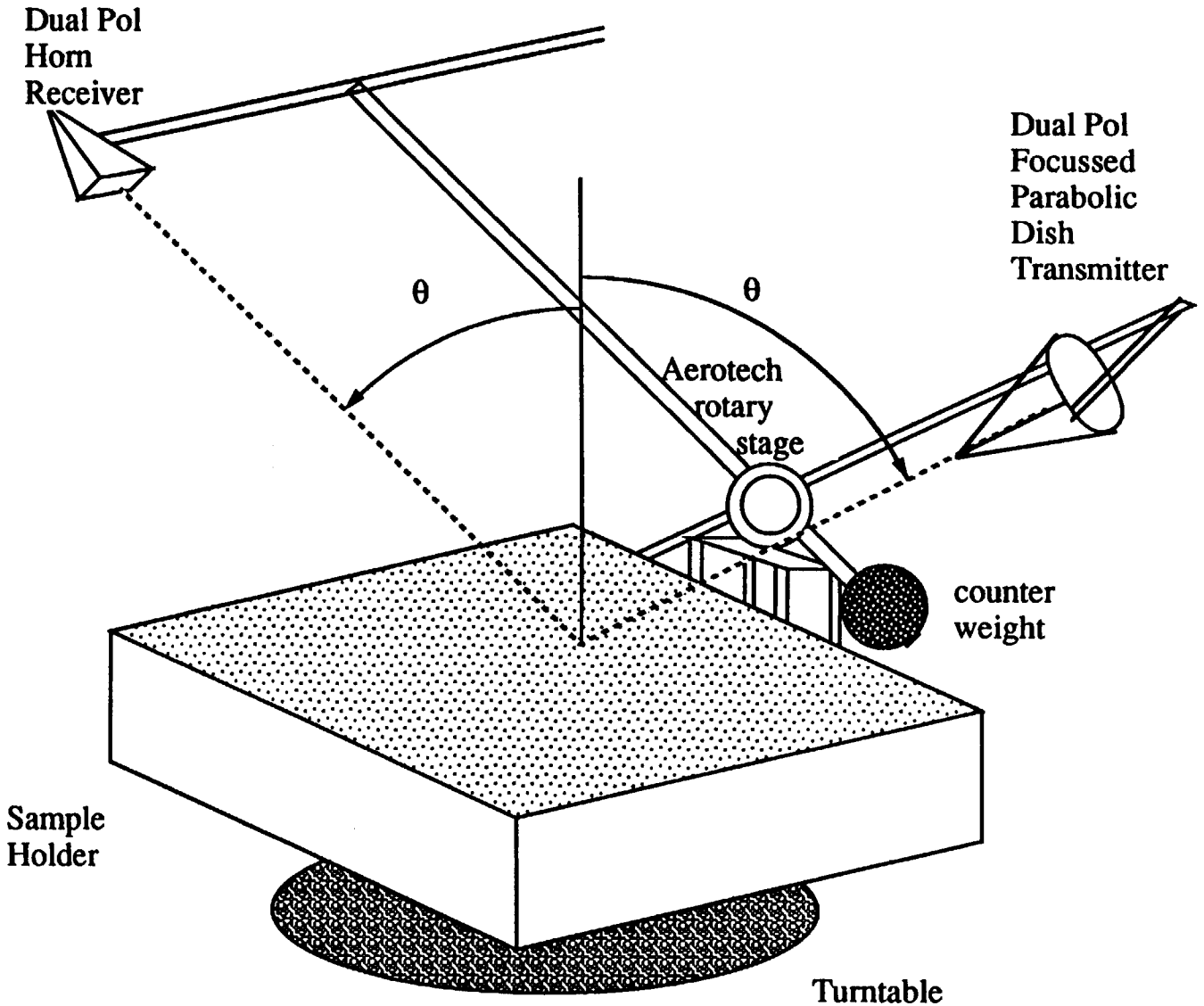

Bistatic Facility

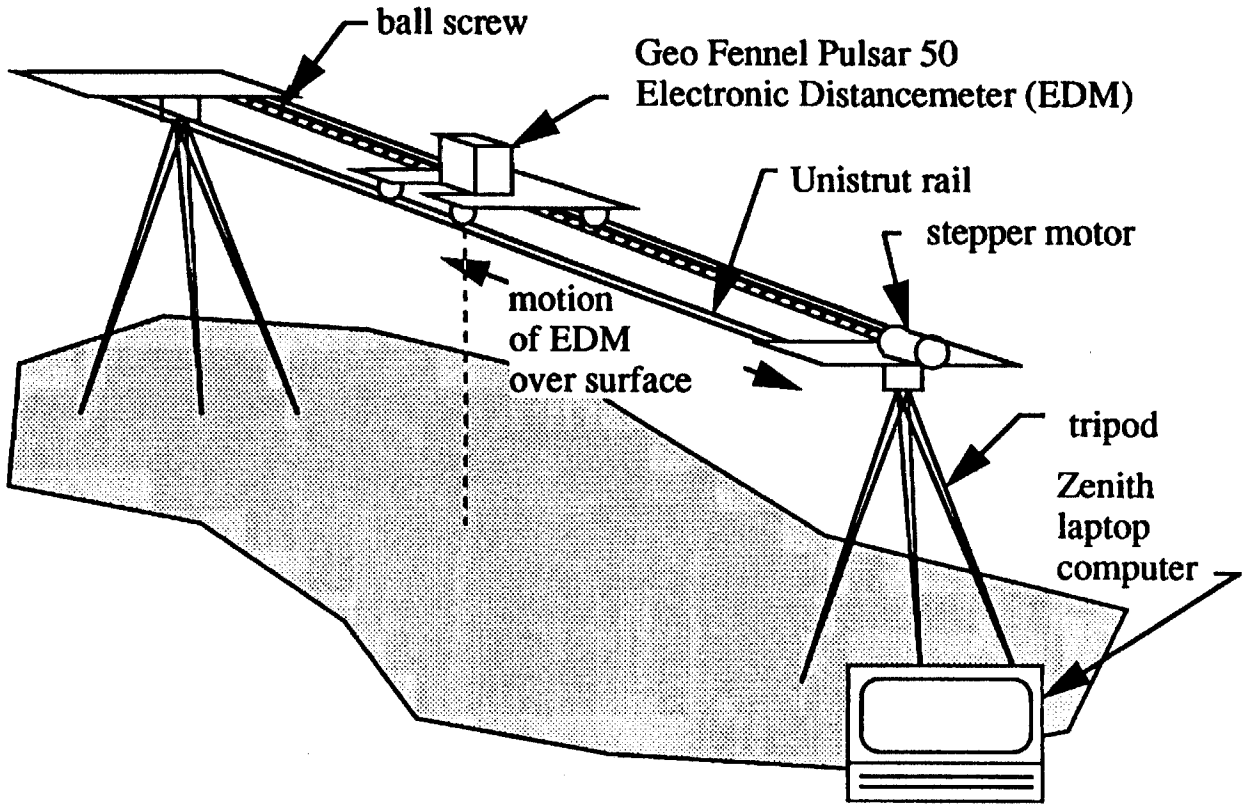

Laser Profiler

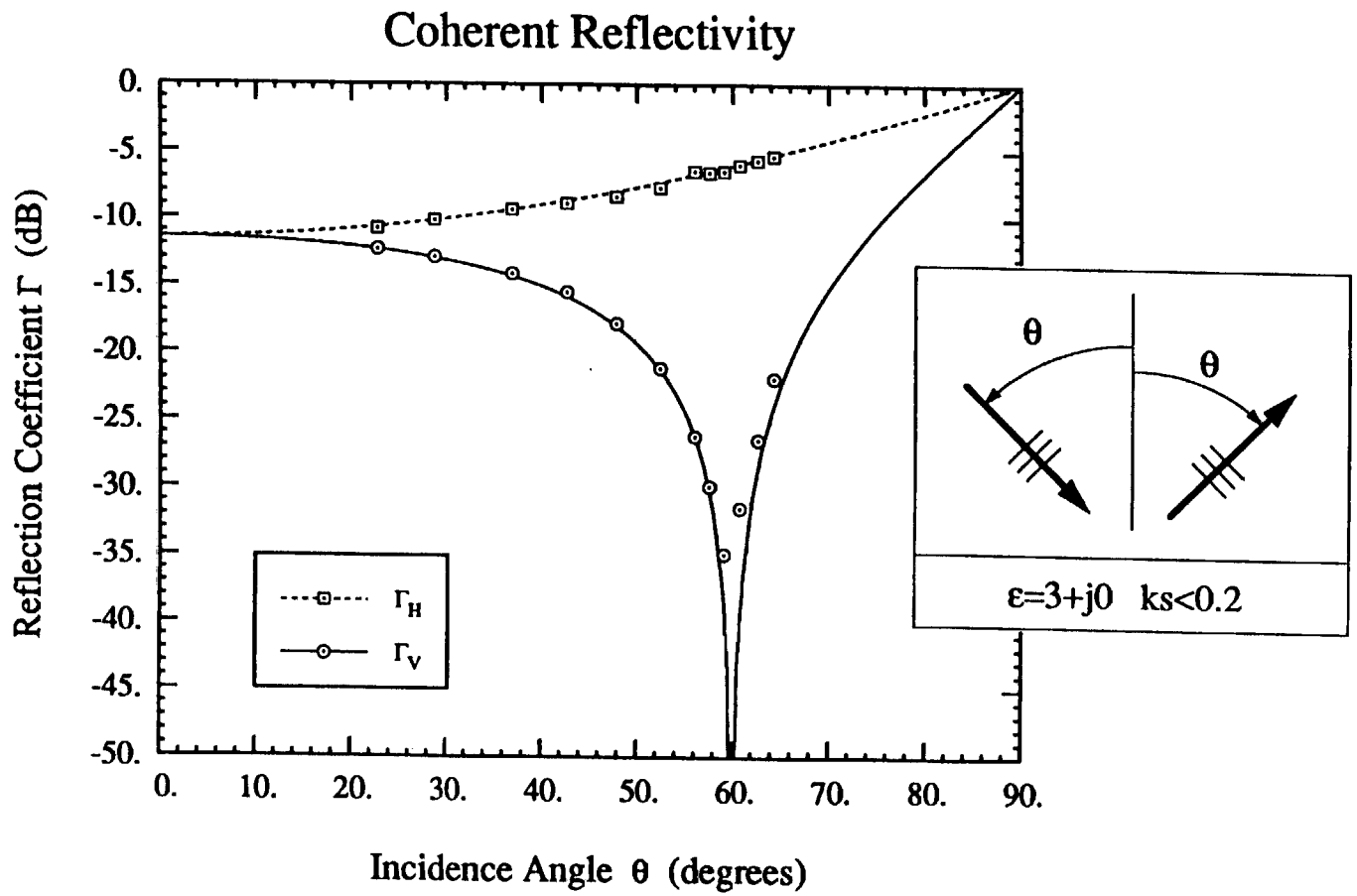
Coherent Reflectivity
Reflection Coefficient Γ (dB)
0.
-5.
-10.
-15.
-20.
-25.
-30.
-35.
-40.
-45.
-50.
0.
10.
20.
30.
40.
50.
60.
70.
80.
90.
Incidence Angle θ (degrees)
Γ_H
Γ_V
θ
θ
ε=3+j0 ks<0.2

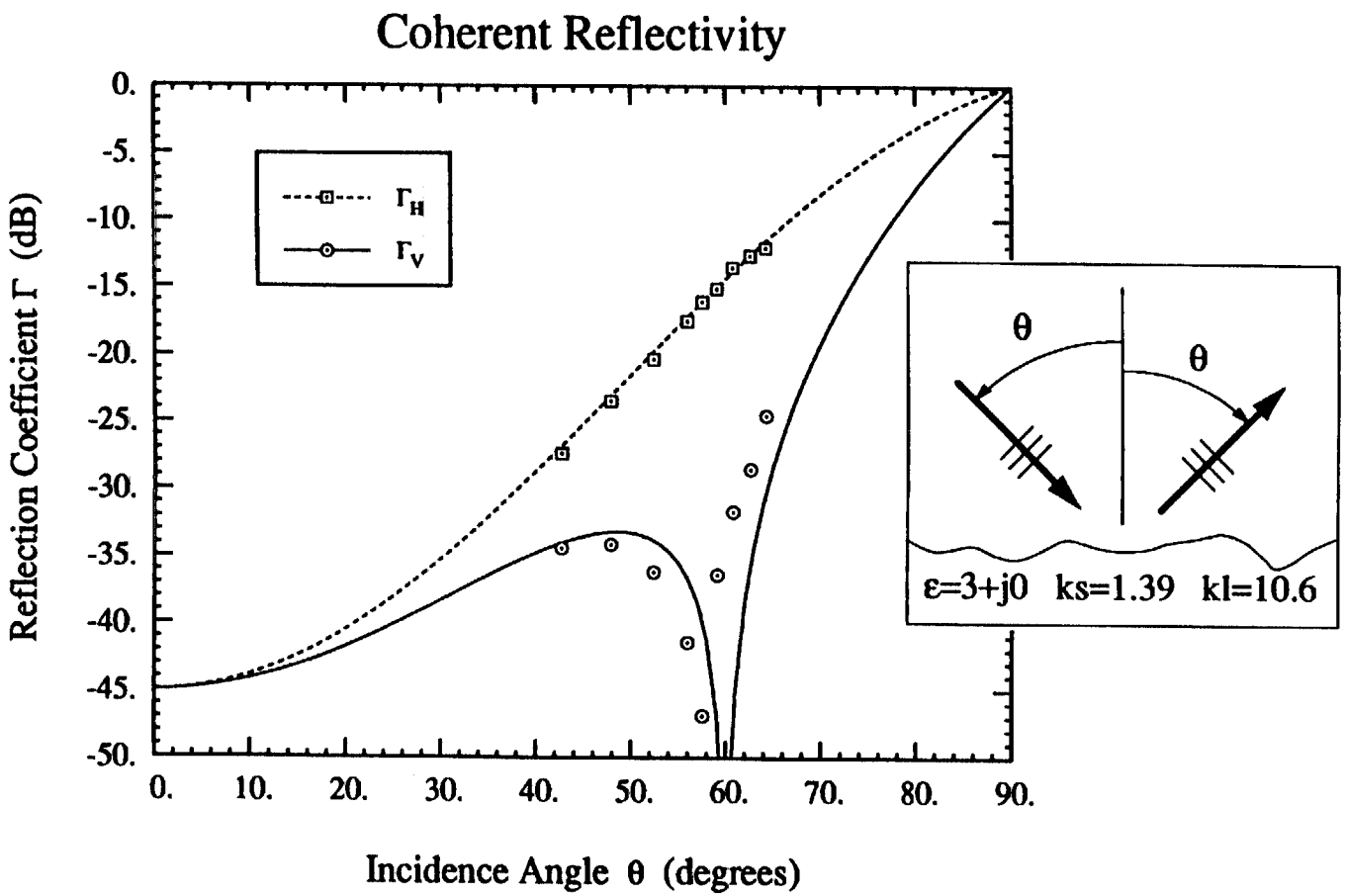
Coherent Reflectivity
Reflection Coefficient Γ (dB)
0.
-5.
-10.
-15.
-20.
-25.
-30.
-35.
-40.
-45.
-50.
0.
10.
20.
30.
40.
50.
60.
70.
80.
90.
Incidence Angle θ (degrees)
Γ_H
Γ_V
θ
θ
ε=3+j0 ks=1.39 kl=10.6

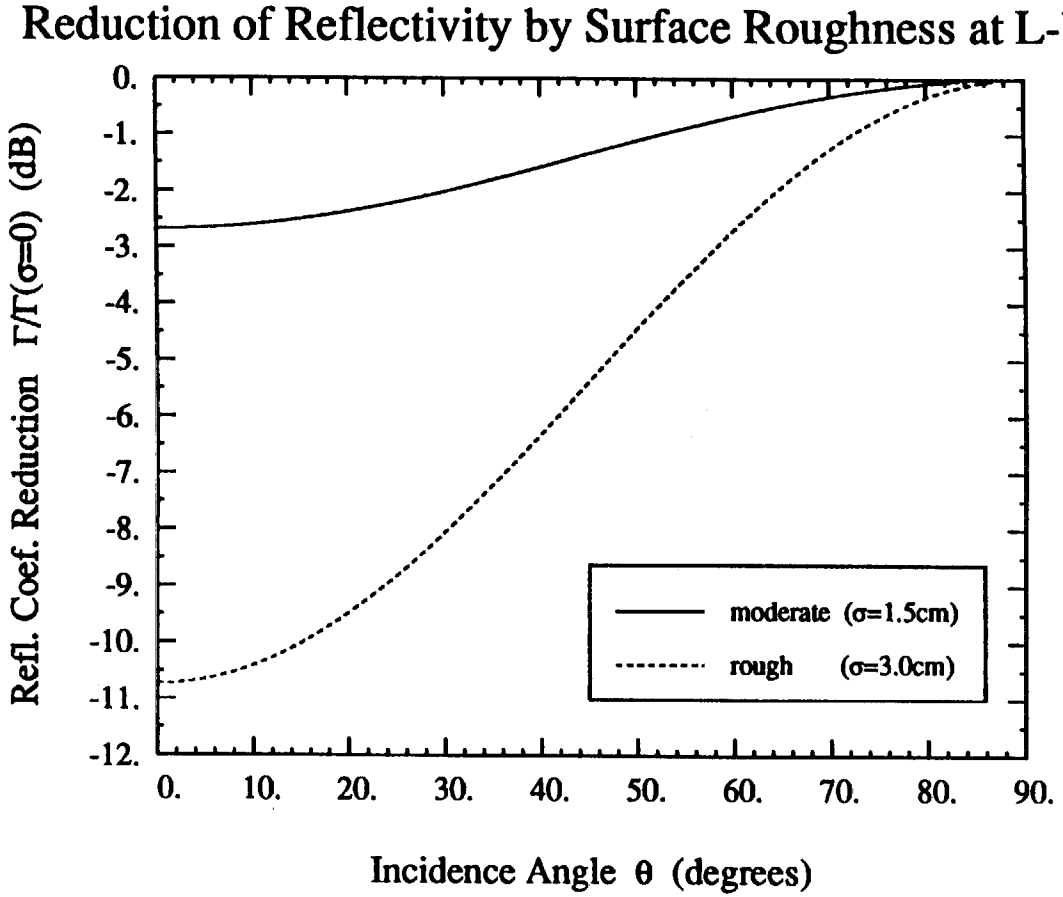
Reduction of Reflectivity by Surface Roughness at L-band
Refl. Coef. Reduction Γ/Γ(σ=0) (dB)
0.
-1.
-2.
-3.
-4.
-5.
-6.
-7.
-8.
-9.
-10.
-11.
-12.
0.
10.
20.
30.
40.
50.
60.
70.
80.
90.
moderate (σ=1.5cm)
rough (σ=3.0cm)
Incidence Angle θ (degrees)

RADAR RESPONSE TO VEGETATION

- OBJECTIVES
  - To Discriminate/Classify Vegetation Classes
  - To Estimate Biomass
  - To Estimate LAI
  - To Estimate Soil Moisture
  - To Monitor Changes (deforestation, growth, stress, etc.)
  - Other

- VEGETATION CANOPY
  - Structure: (1) Macro (tree or plant scale): Tree height, density, ground cover
    (2) Micro (wavelength scale): Leaves, branches
  - Dielectric Properties
  - Ground Cover (soil, debris, undergrowth, etc.)

- TOOLS
  - Wavelength
  - Polarizations
  - Phase Statistics
  - Incidence Angle
  - Time

- APPROACH
  - Theory
  - Observations
    - Lab
    - Field
    - Air SAR
    - Satellite

DIURNAL VARIATION IN σ^0

Humid Temperate Forest Loblolly Pines at Duke Forest

While ε^* of trunks are found to vary by 30%,

σ^0 varies by only $\approx$ 1dB

Calibration accuracy is 1dB

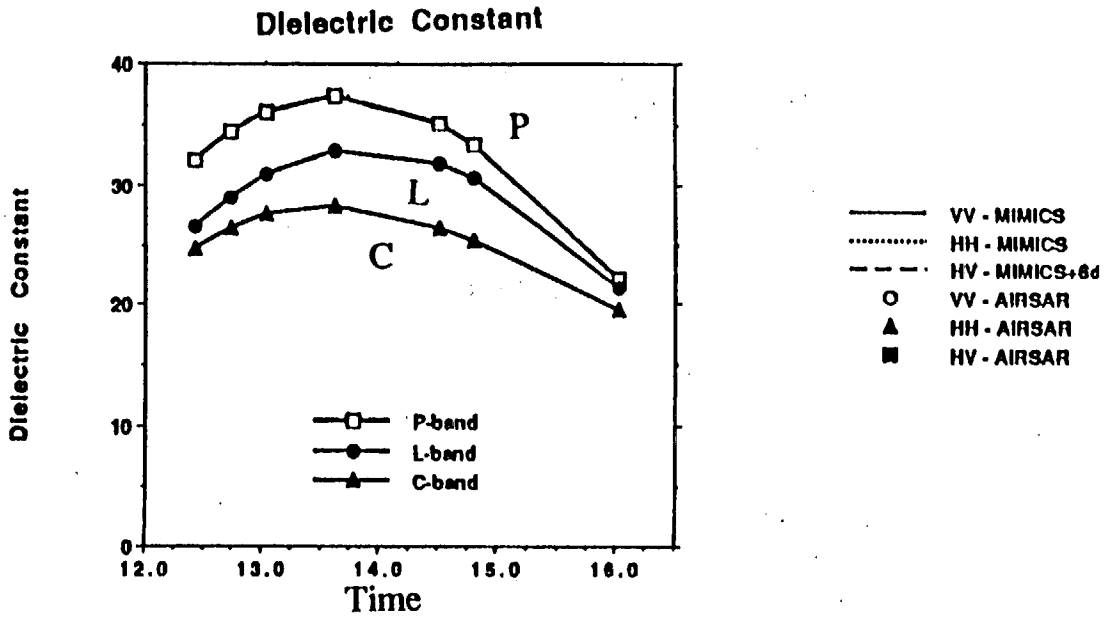

P-Band

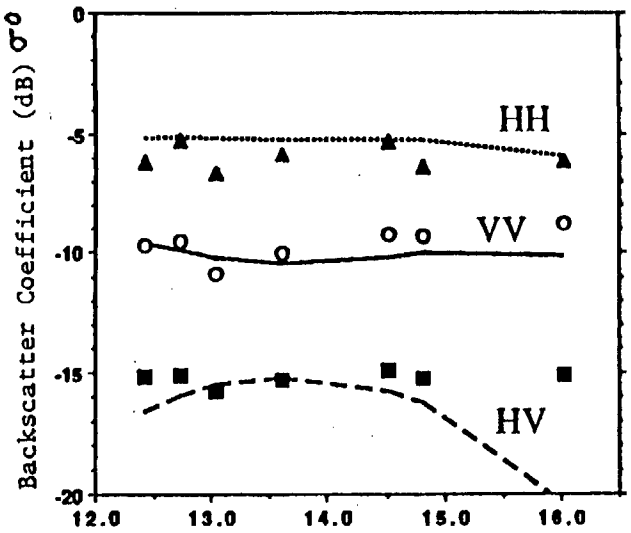

L-Band

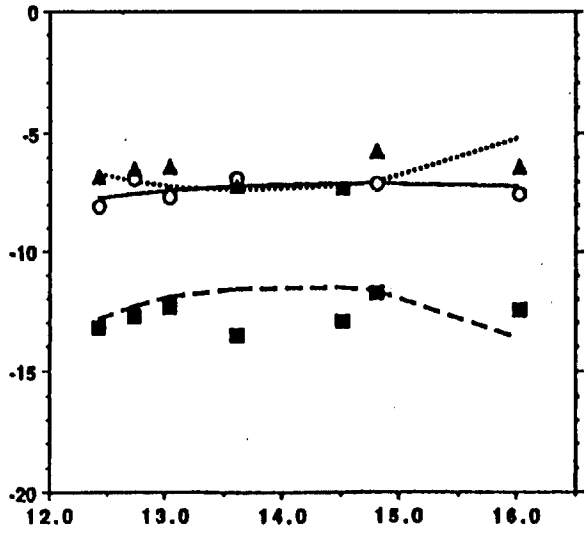

C-Band

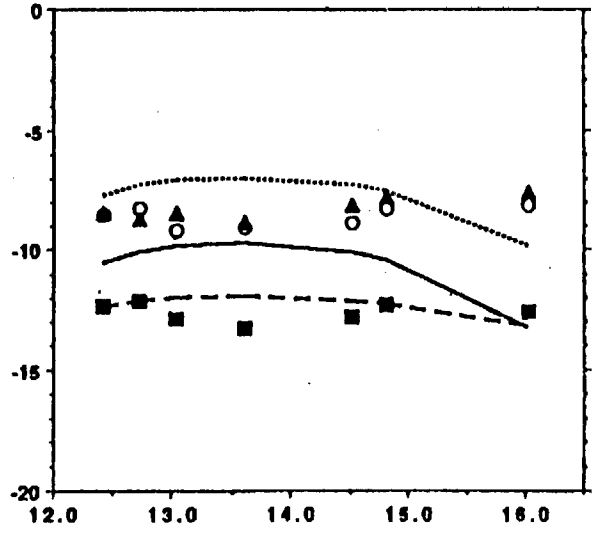

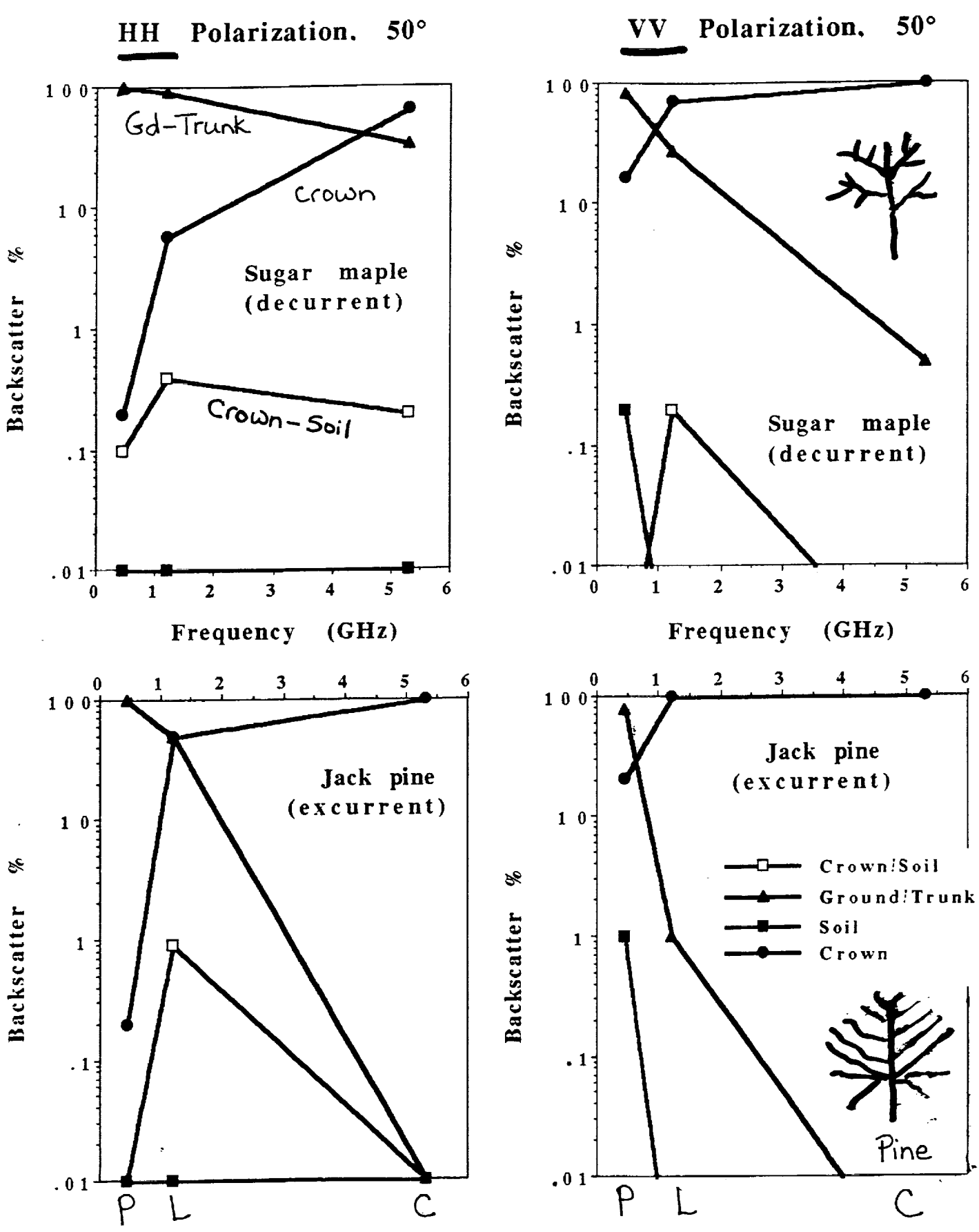
HH Polarization. 50°
VV Polarization. 50°
Backscatter %
100
10
1
.1
.01
Gd-Trunk
Crown
Sugar maple
(decurrent)
Crown-Soil
0 1 2 3 4 5 6
Frequency (GHz)
Jack pine
(excurrent)
Crown/Soil
Ground/Trunk
Soil
Crown
Pine
P L C

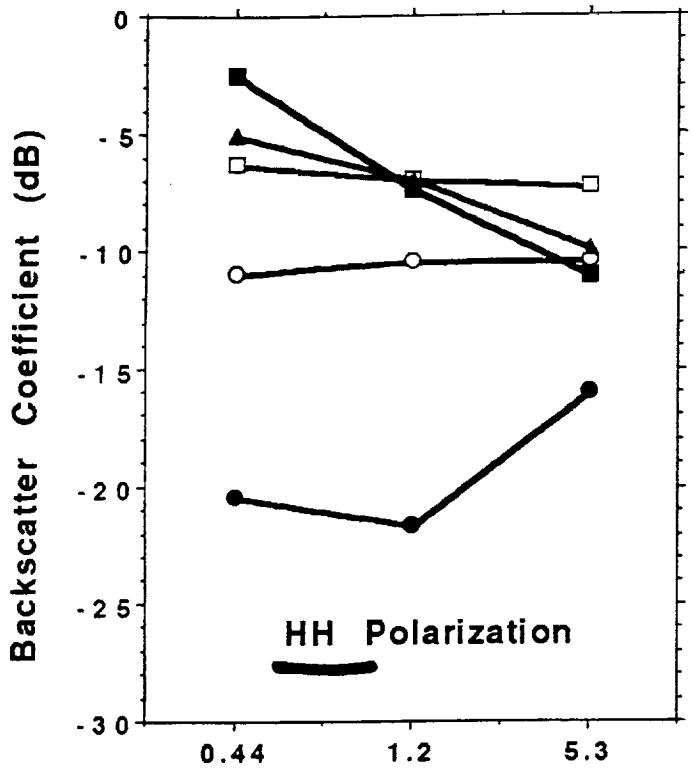
Backscatter Coefficient (dB)
0
-5
-10
-15
-20
-25
-30
HH Polarization
0.44
1.2
5.3
Frequency (GHz)

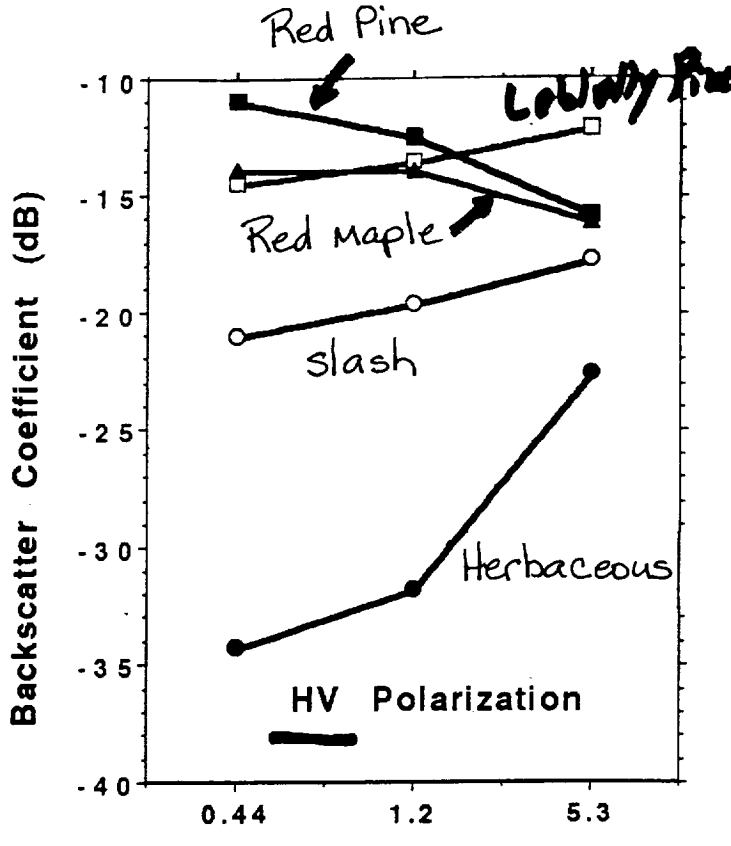
Red Pine
Red Maple
slash
Herbaceous
Backscatter Coefficient (dB)
-10
-15
-20
-25
-30
-35
-40
HV Polarization
0.44
1.2
5.3
Frequency (GHz)

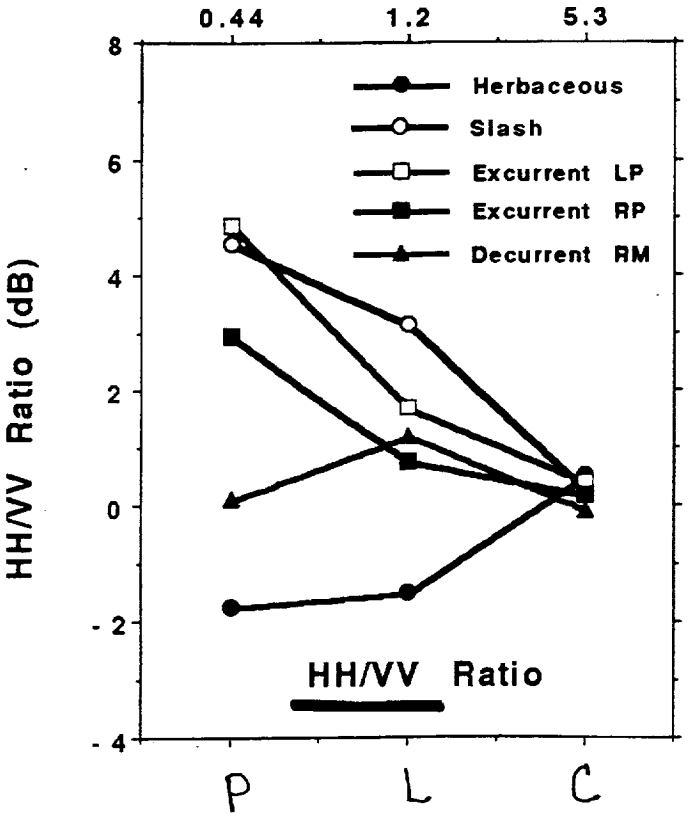
0.44
1.2
5.3
Herbaceous
Slash
Excurrent LP
Excurrent RP
Decurrent RM
HH/VV Ratio (dB)
8
6
4
2
0
-2
-4
HH/VV Ratio
P
L
C

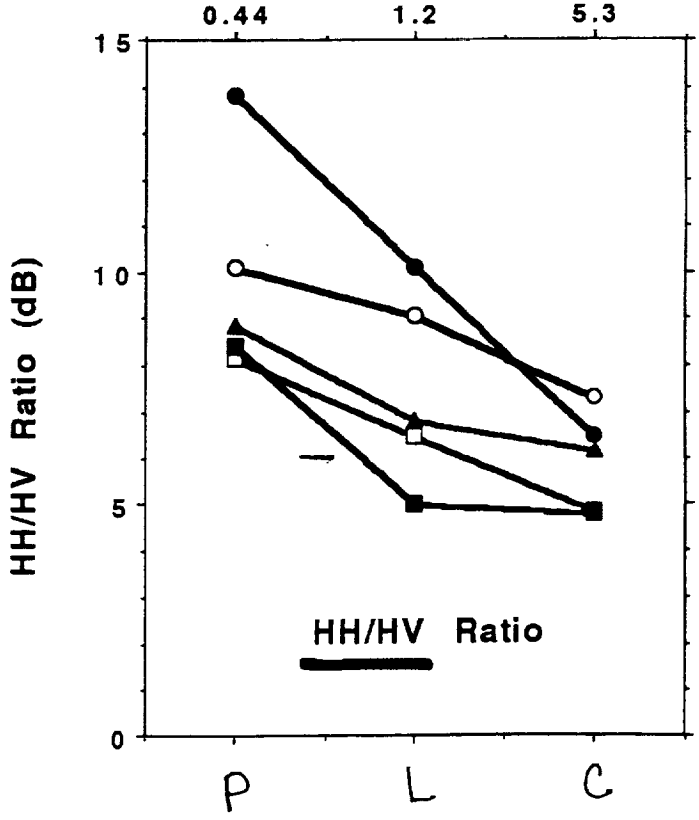
0.44
1.2
5.3
HH/HV Ratio (dB)
15
10
5
0
HH/HV Ratio
P
L
C

Calibrated AIRSAR Response at L-Band to Standing Forest Biomass

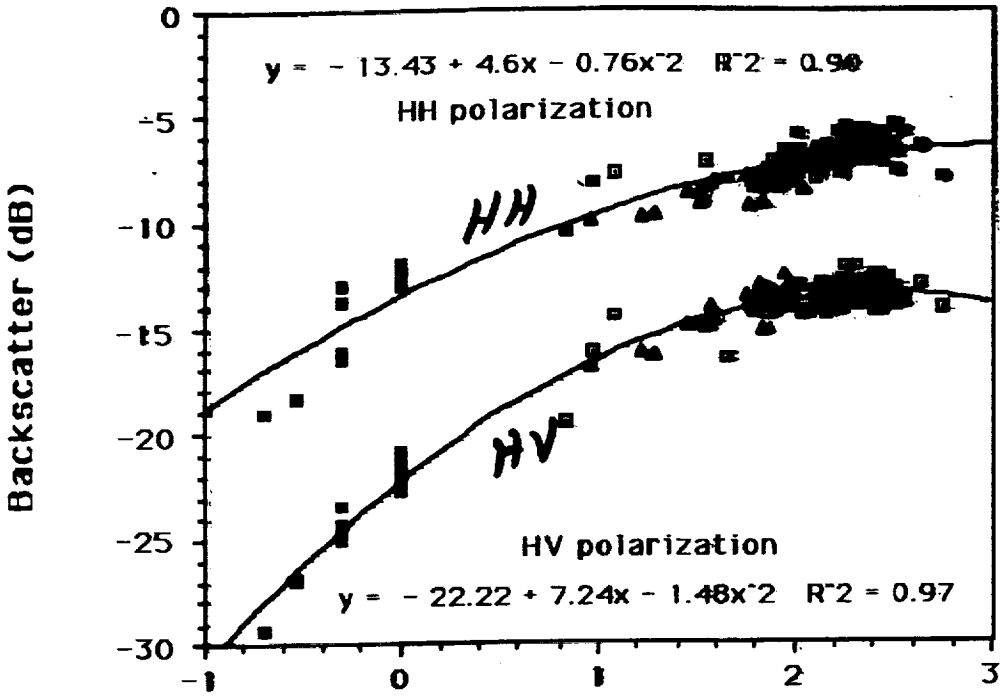

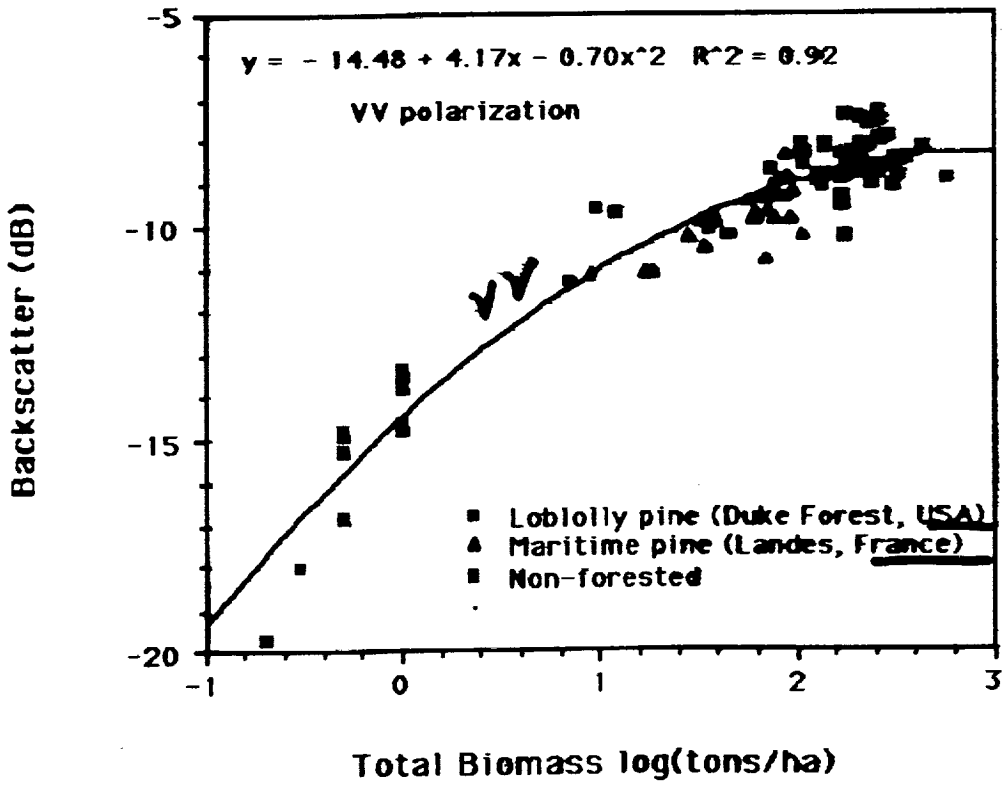

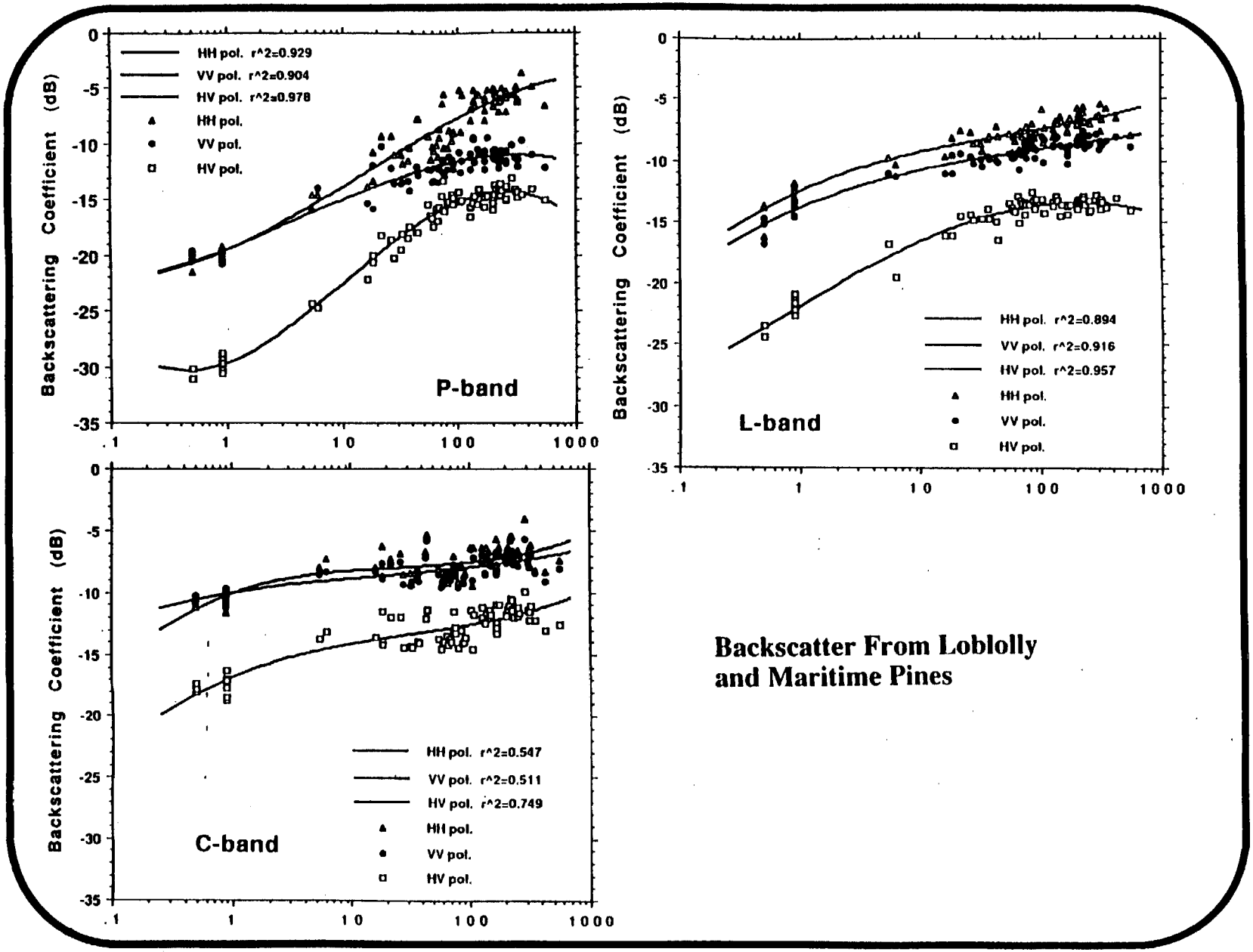

Backscatter From Loblolly and Maritime Pines

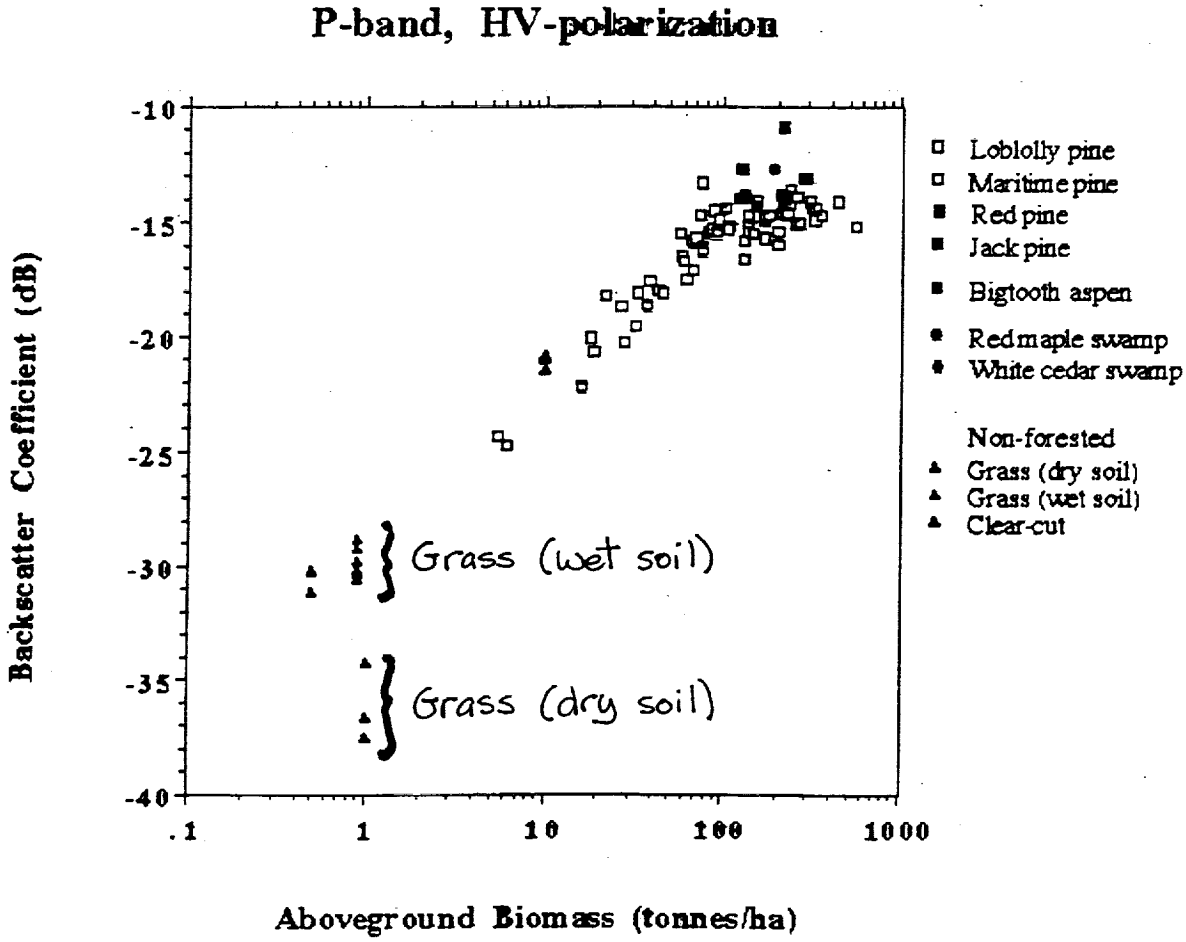

Duke Forest
Michigan Forests
Landes "

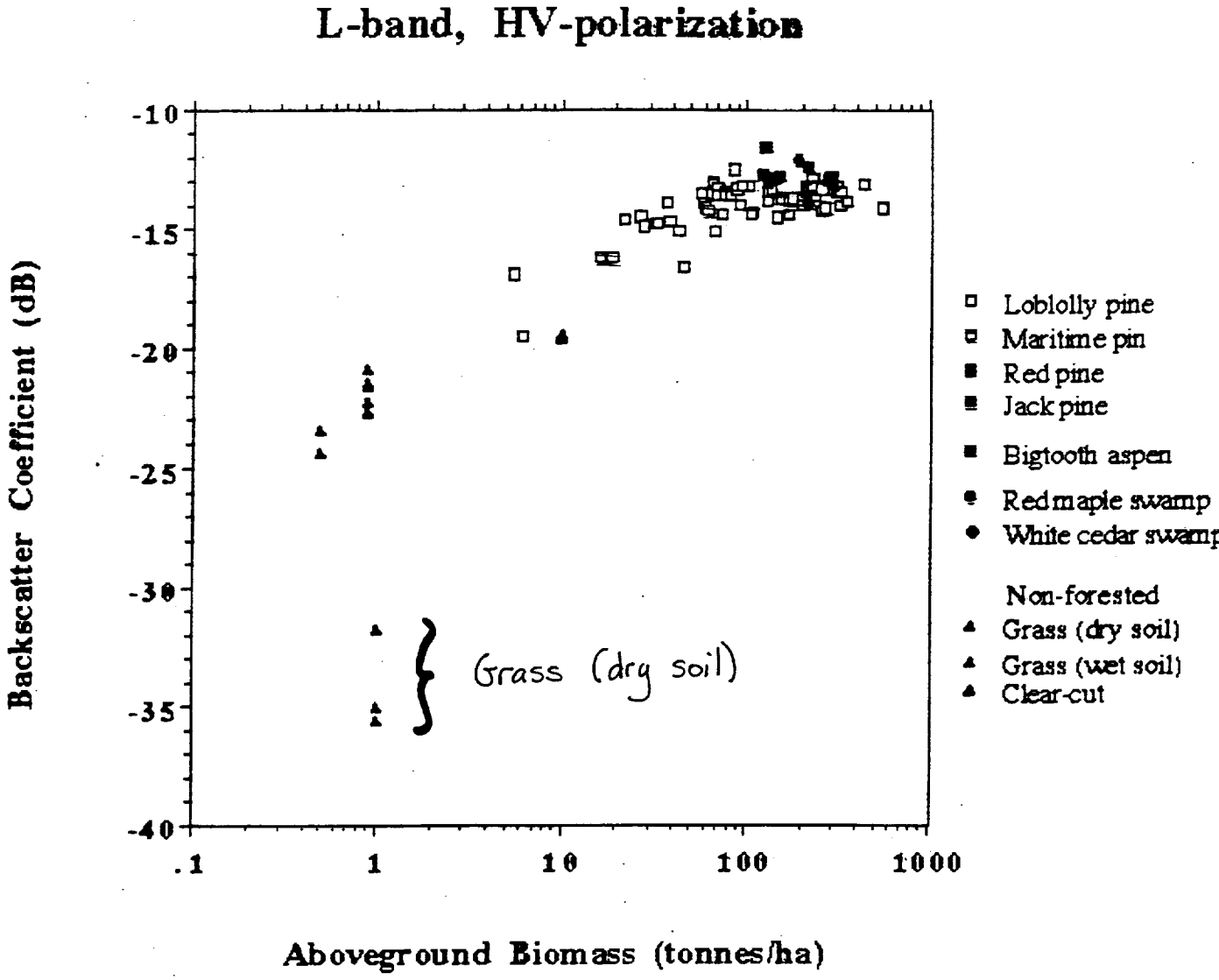
L-band, HV-polarization
Backscatter Coefficient (dB)
-10
-15
-20
-25
-30
-35
-40
.1
1
10
100
1000
Aboveground Biomass (tonnes/ha)
Grass (dry soil)
Loblolly pine
Maritime pin
Red pine
Jack pine
Bigtooth aspen
Red maple swamp
White cedar swamp
Non-forested
Grass (dry soil)
Grass (wet soil)
Clear-cut

6. L-BAND SAR OBSERVATIONS IN ALASKA

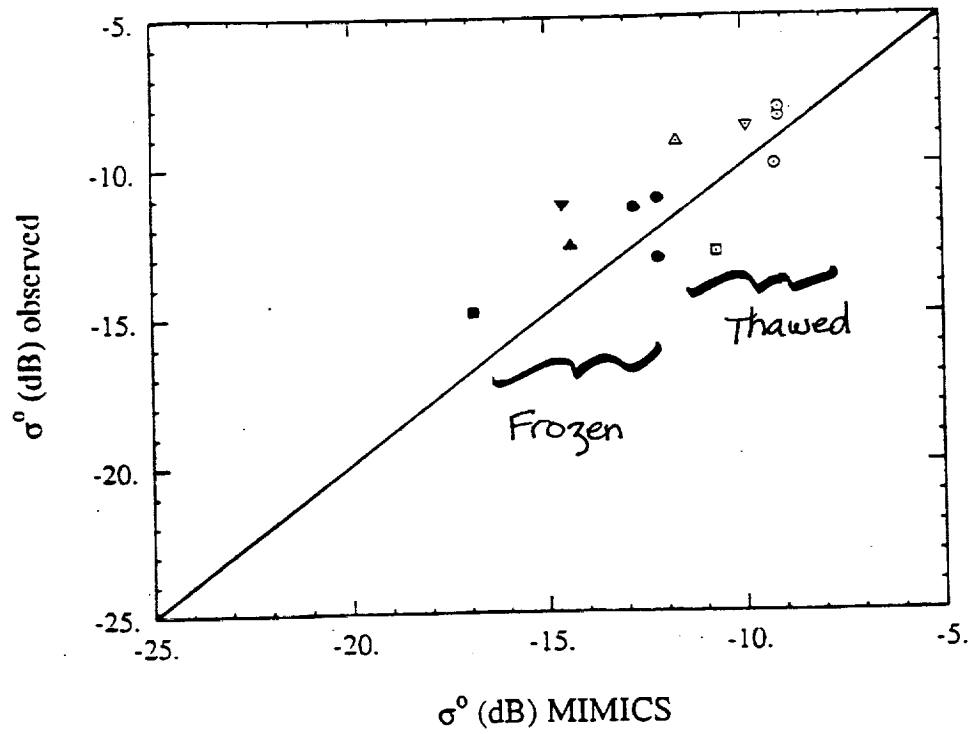

⊙	White Spruce -- Thawed
●	White Spruce -- Frozen
⊡	Black Spruce -- Thawed
■	Black Spruce -- Frozen
△	Balsam Poplar -- Thawed
▲	Balsam Poplar -- Frozen
▽	Alder -- Thawed
▼	Alder -- Frozen

Pellston $\Delta\sigma^0$, July 8 – July 10, HH-polarization

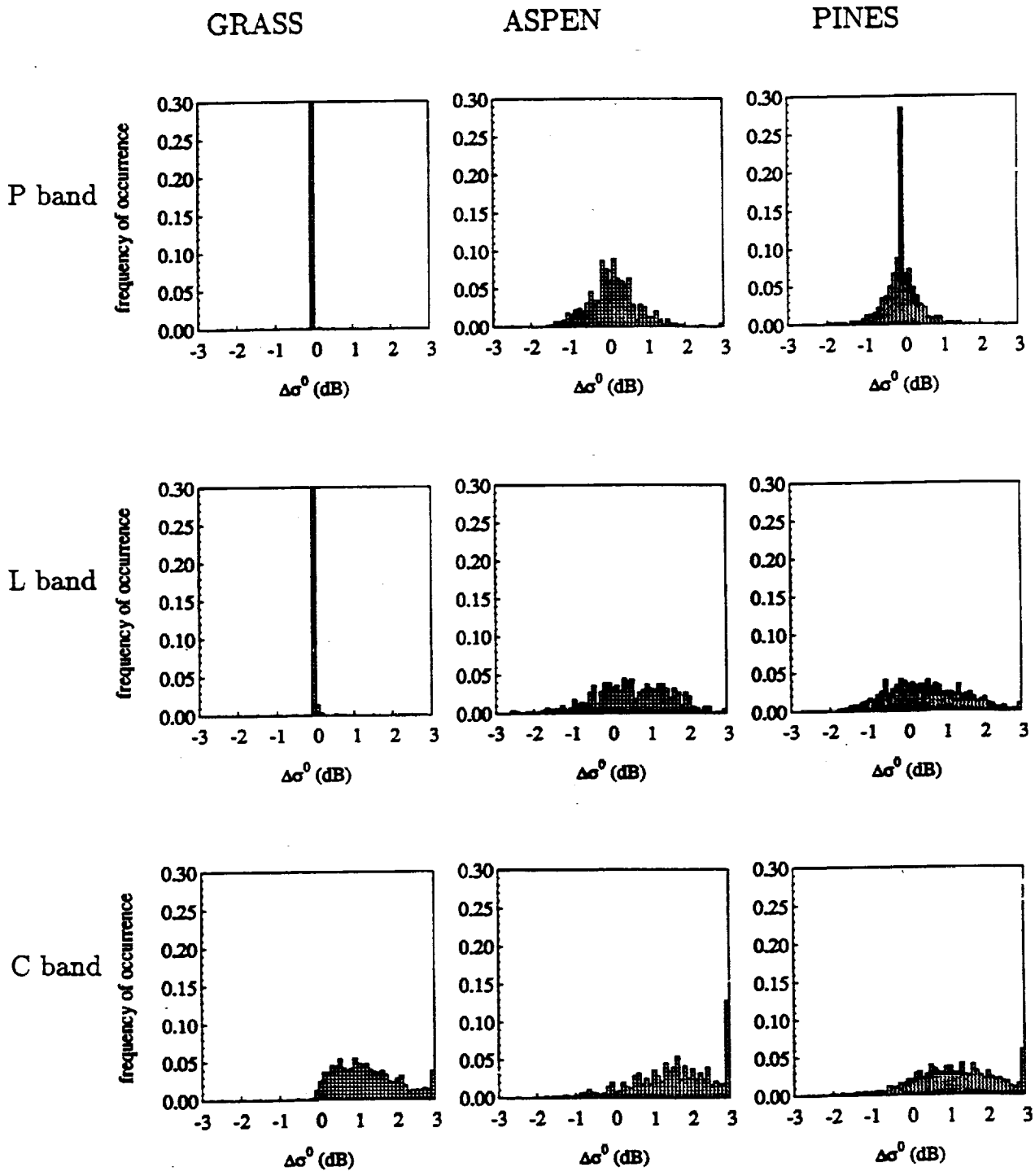

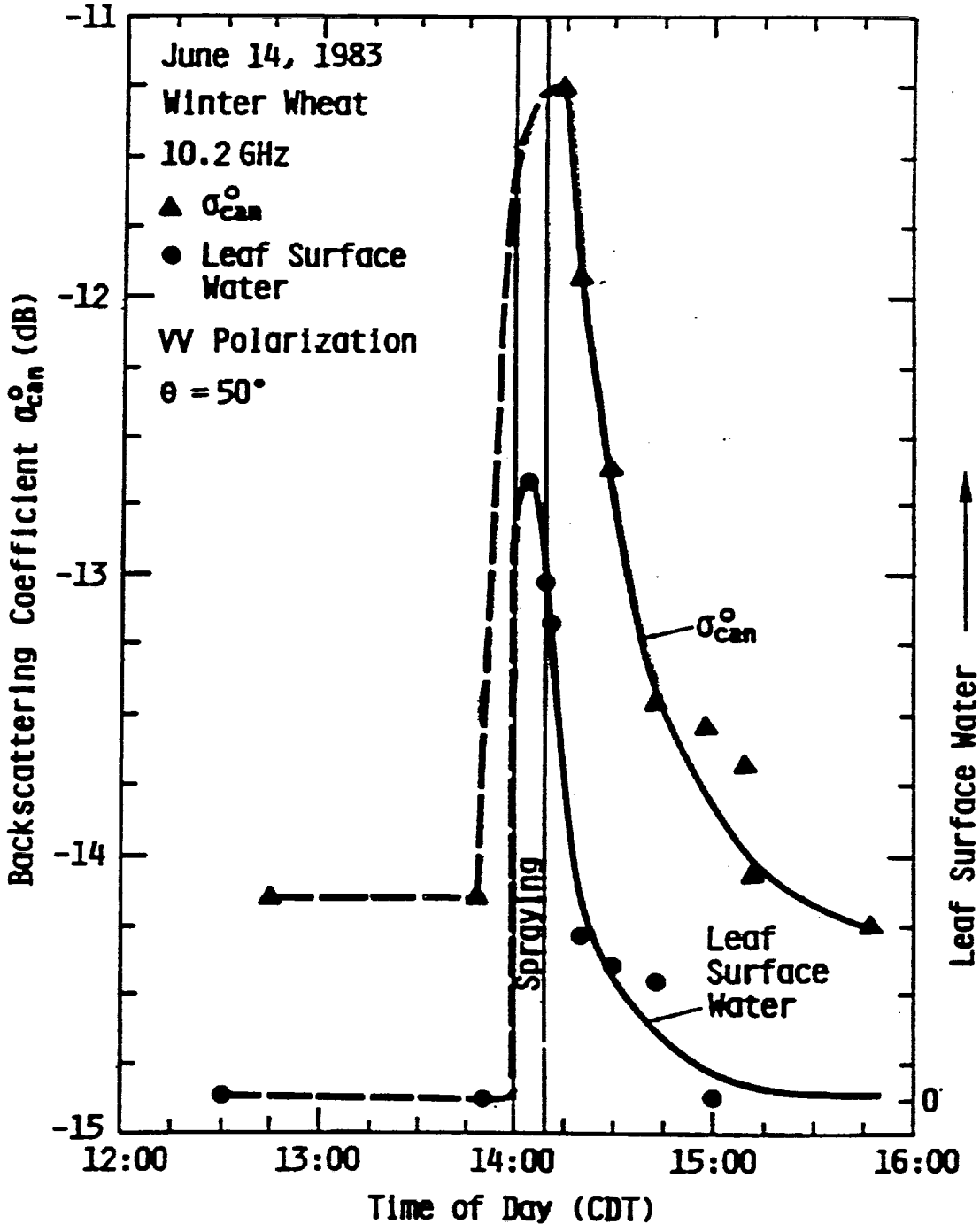
June 14, 1983
Winter Wheat
10.2 GHz
▲ σ^{o}_{can}
● Leaf Surface Water
VV Polarization
θ = 50°
Backscattering Coefficient σ^{o}_{can} (dB)
-11
-12
-13
-14
-15
12:00
13:00
14:00
15:00
16:00
Time of Day (CDT)
Spraying
σ^{o}_{can}
Leaf Surface Water
Leaf Surface Water
0

ERS-1 RESULTS

- Class Statistics
- Observation *versus* Theory (MIMICS)
- Biomass Response (Deciduous and Coniferous)
- Seasonal Variation (LAI)
  - Deciduous
  - Coniferous

ERS-1 Class Statistics for 3x3 Pixel Averages

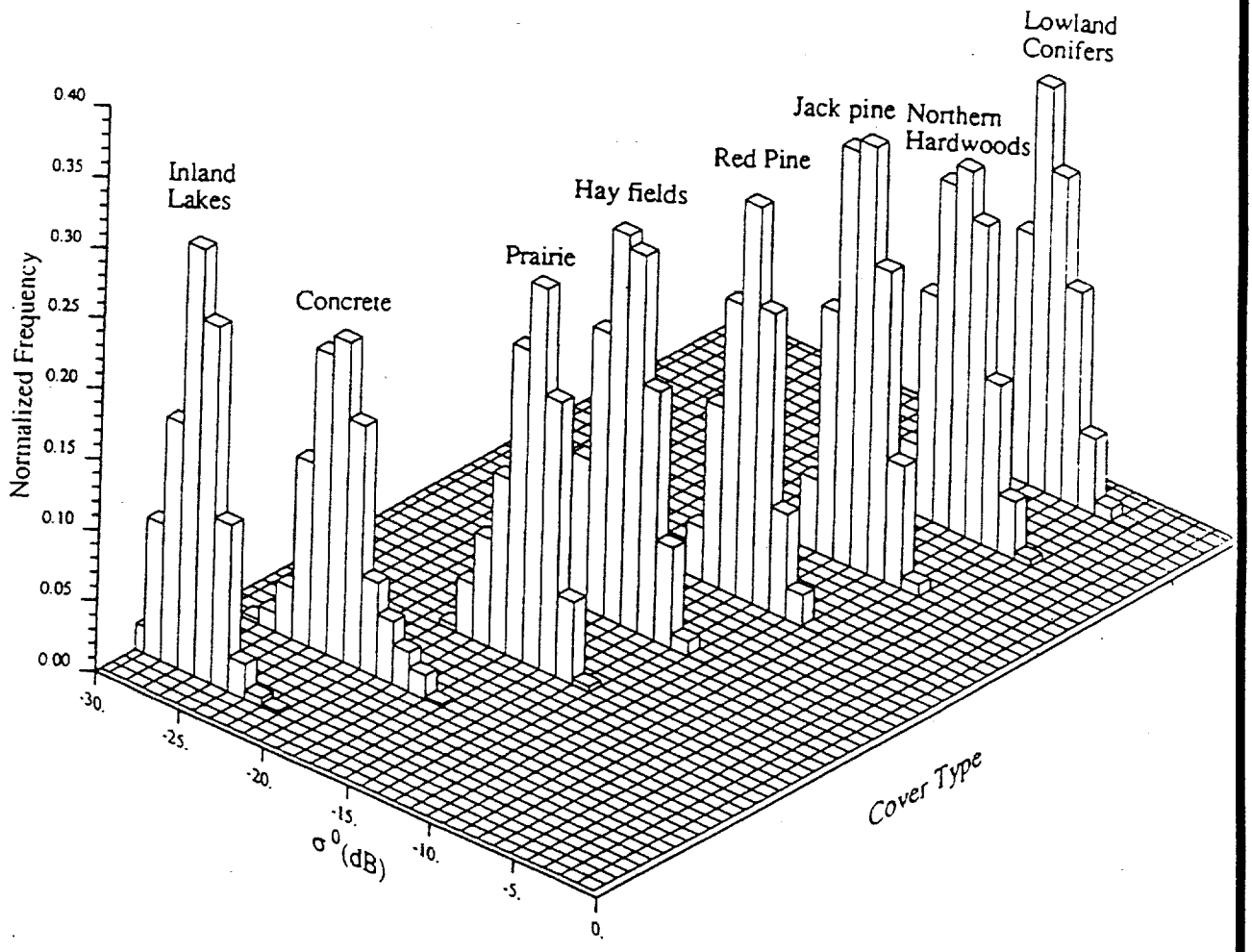

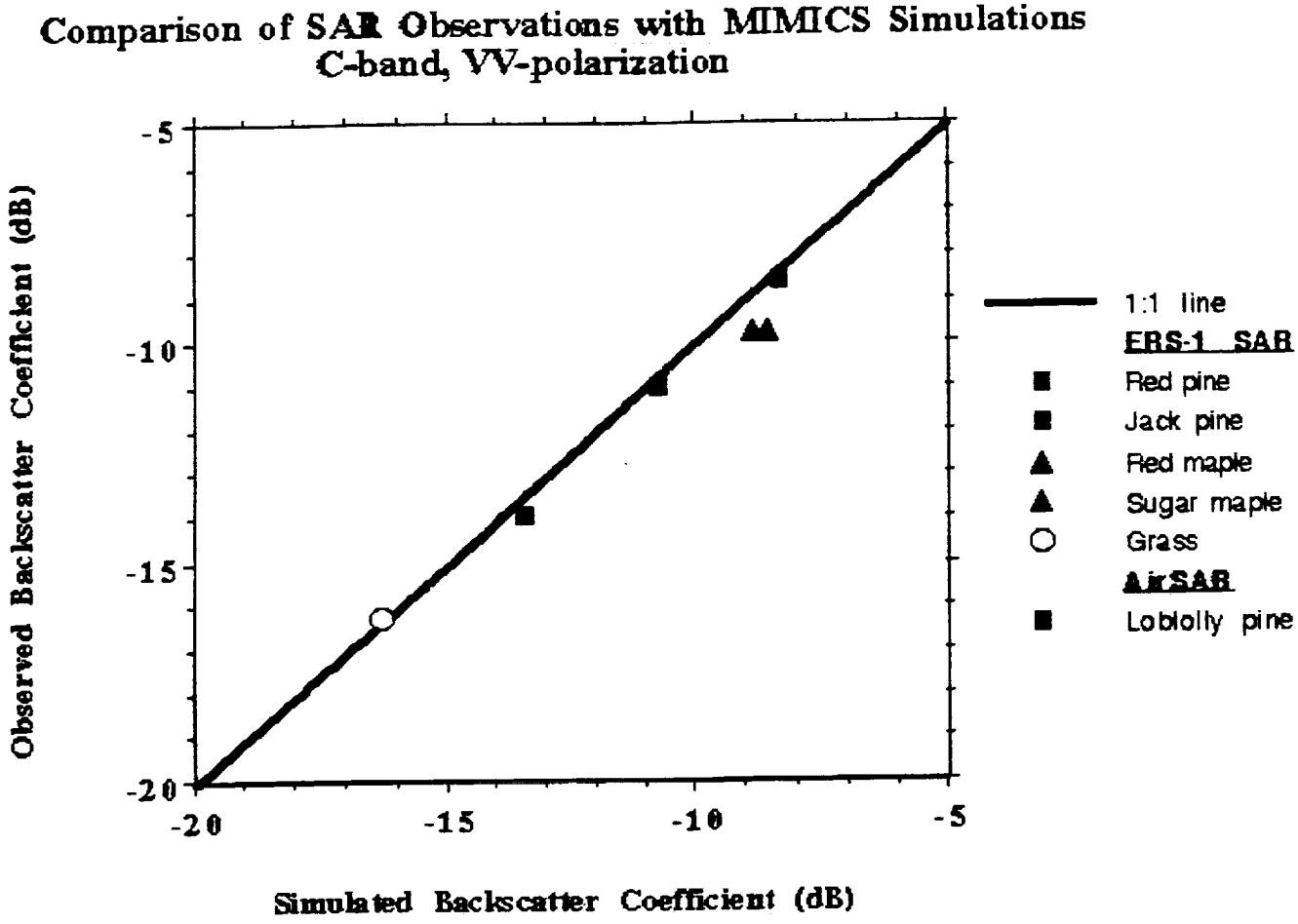
Comparison of SAR Observations with MIMICS Simulations
C-band, VV-polarization
Observed Backscatter Coefficient (dB)
-5
-10
-15
-20
-20
-15
-10
-5
Simulated Backscatter Coefficient (dB)
1:1 line
ERS-1 SAR
Red pine
Jack pine
Red maple
Sugar maple
Grass
AirSAR
Loblolly pine

ERS-1 Backscatter Modeled by MIMICS for Northern Michigan Forests in August 1991

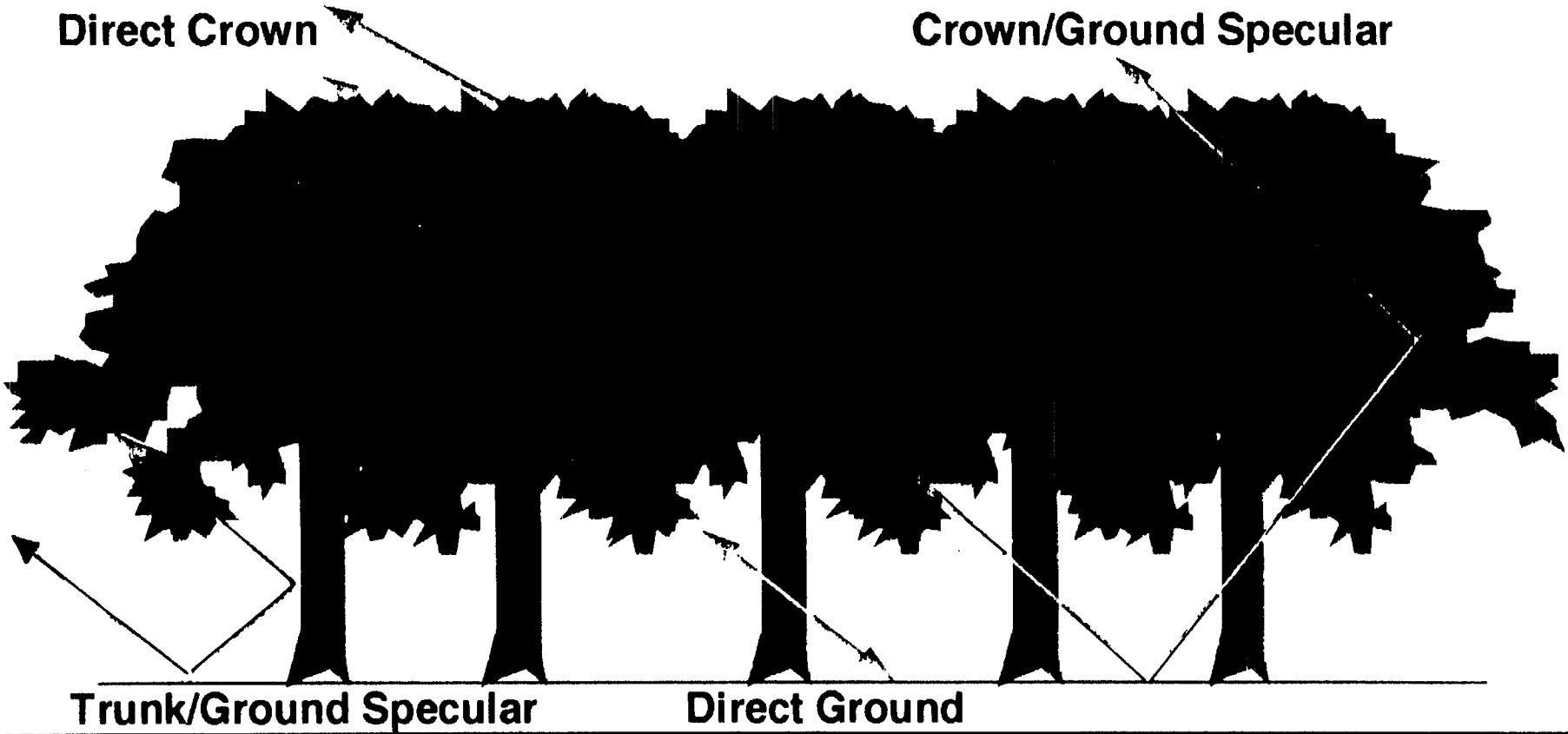

Dominant Specie	Percent of Total Return				
	Crown	Crown/Ground	Trunk/Ground	Ground	σ° (dB)
Red maple	95.5	0.3	4.3	-	-8.6
Sugar maple	96.4	0.4	3.2	-	-8.9
Jack pine	100	-	-	-	-10.7
Red Pine	41.3	10.4	48.1	.2	-13.4
grass	0.03	0.2	-	99.8	-14.4

ERS-1

Dependence Upon Above Ground Forest Biomass

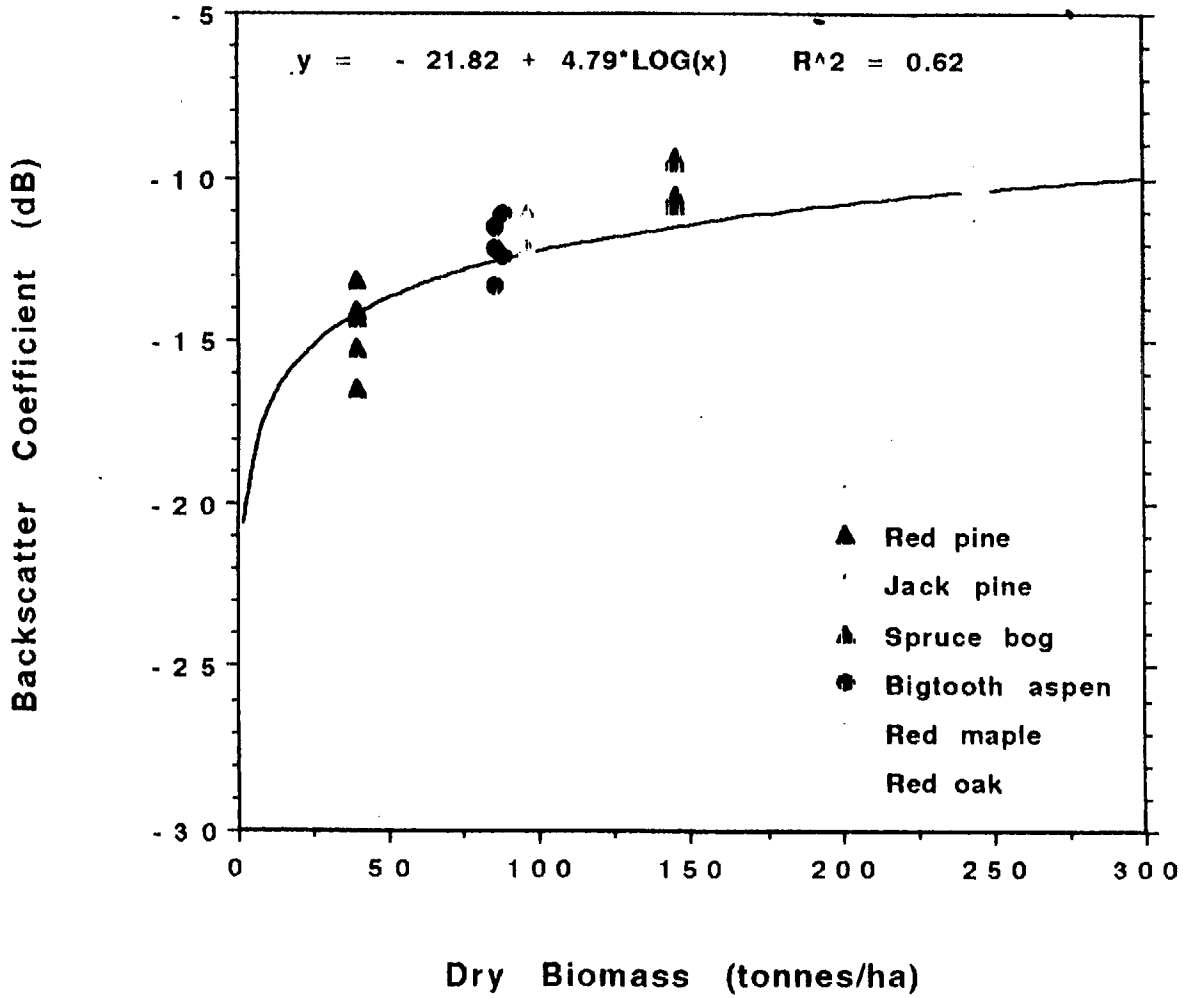

ERS-1

Backscatter vs. LAI for Deciduous Forests

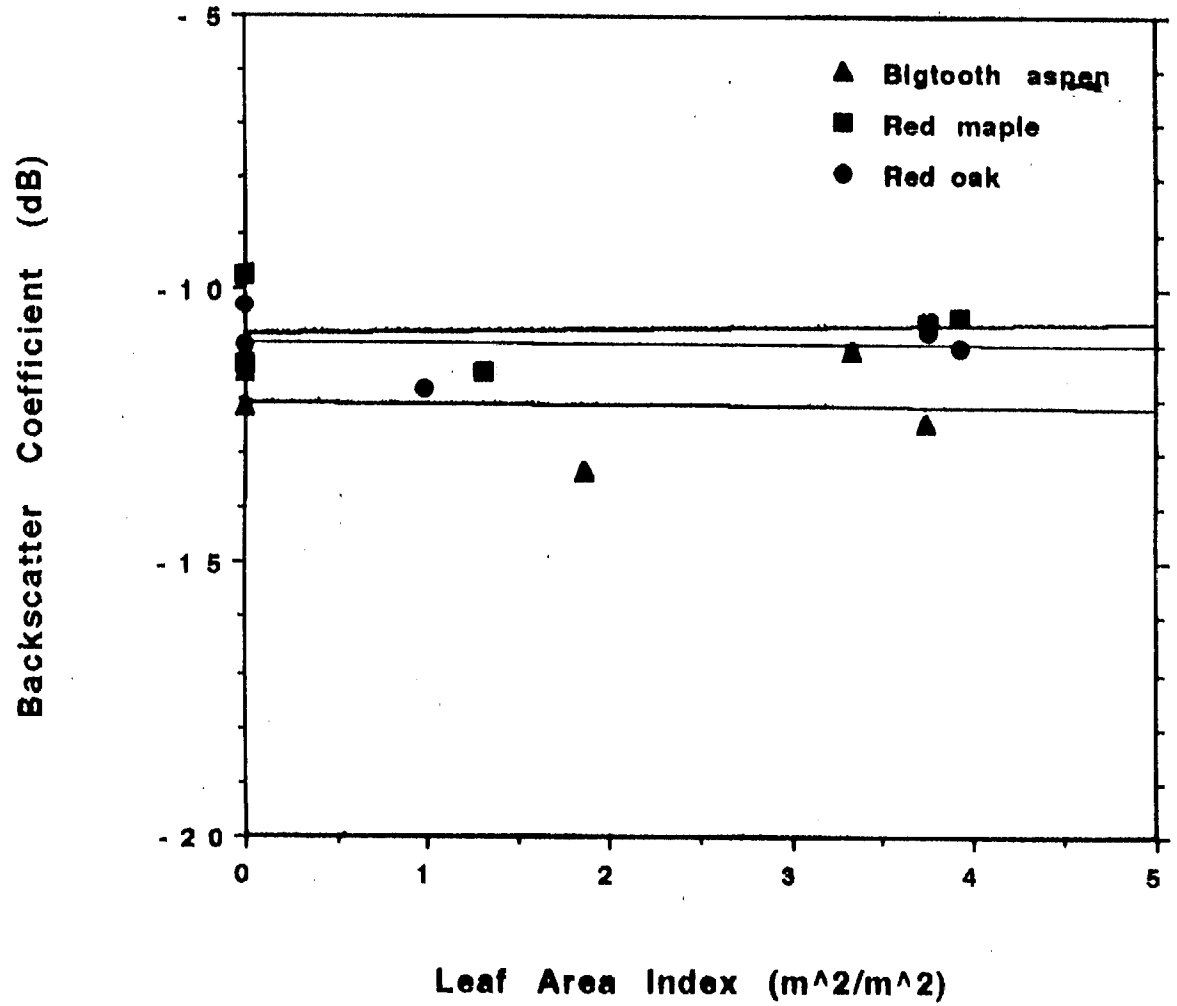

ERS-1

Backscatter vs. LAI for Closed-Canopy Conifer Forests

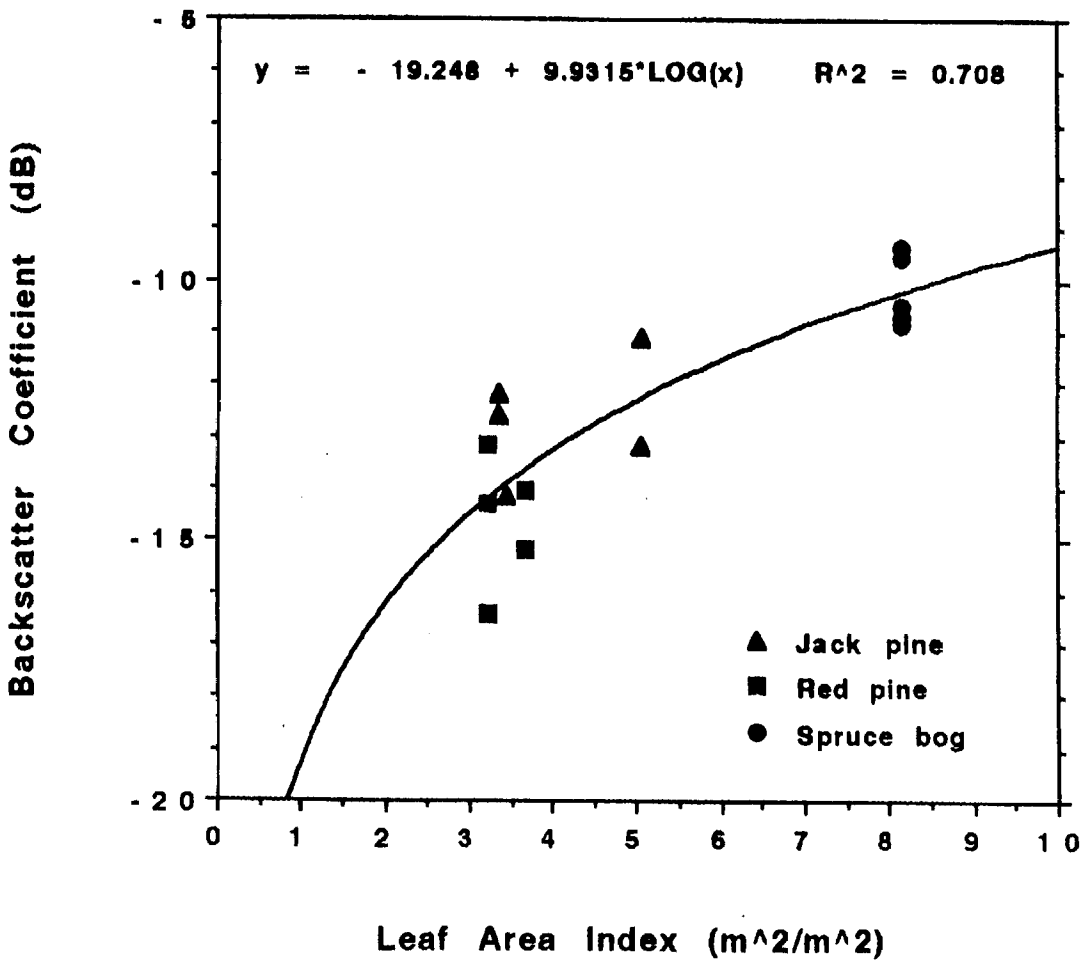

CONCLUSIONS & RECOMMENDATIONS

I. SURFACE SCATTERING

Status

1. Retrieval of Soil Moisture and Surface Roughness

   Field tested, Some AirSAR Verification

   - L-Band Quad-Pol for bare soil
   - P-Band Quad-Pol: extends to agricultural crops

2. Effects of Organic Debris

   Demonstrated in lab

   - Extinction depends on size / λ

     At P and L-Bands, only trunks and large branches are significant

II. VEGETATION SCATTERING

MIMICS, AirSar, ERS-1

1. In general σ° = f (biomass, structure)
2. Extinction by crown layer increases with frequency
3. Scattering by foliage and small branches:
   - negligible at P and L Bands
   - dominates at C and X Bands
4. Scattering by trunks and large branches:
   - dominates at P and L Bands

The University of Michigan

CONCLUSIONS & RECOMMENDATIONS

- Even P-Band is insensitive to high biomass forests (Pacific NW ≅ 500 tons/ha)

6. Innundation under Forest Cover — SIR-B, AirSAR Verified

   L-Band HH

7. Effects of Intercepted Precipitation

   - negligible at P Band
   - ≅ 1 dB increase or decrease at L-Band — AirSAR, Scattering Verified
   - ≅ 2 dB increase at C-Band

8. Freezing of Vegetation Leads to — AirSAR, MIMICS Verified

   Significant changes in σ° at all Bands

9. Deforestation Readily Detectable at — SIR-B, AirSAR

   P and L-Band

10. LAI Foliar Biomass Estimation — MIMICS, Field, AirSAR

    C-Band Quad or X-Band

11. Multi-Date Observations: Very Powerful Tool

    - Requires good Relative Calibration (Stability) ≅ ± 1 dB
    - Requires good Absolute Calibration ≅ ± 1 dB

The University of Michigan

IMAGING RADAR STUDIES OF POLAR ICE

Frank Carsey
Jet Propulsion Laboratory
California Institute of Technology

Topics

- Scientific Overview
- Radar Data Opportunities
- Sea Ice Investigations
- Ice Sheet Investigations
- Conclusions

- - - - - - - - - - - - - - - - - - - -

Scientific Overview

Sea Ice Scientific Objectives:

- To estimate globally the surface brine generation, heat flux, and fresh water advection (as ice).

- To monitor phasing of seasonal melt and freeze events and accurately estimate melt and growth rates.

- To develop improved treatment of momentum transfer and ice mechanics in coupled air-sea-ice models.

Key Radar Observations: Ice Type and Velocity

STUDY PHILOSOPHY, UNDERSTANDING THE ROLE OF SEA ICE IN CLIMATE

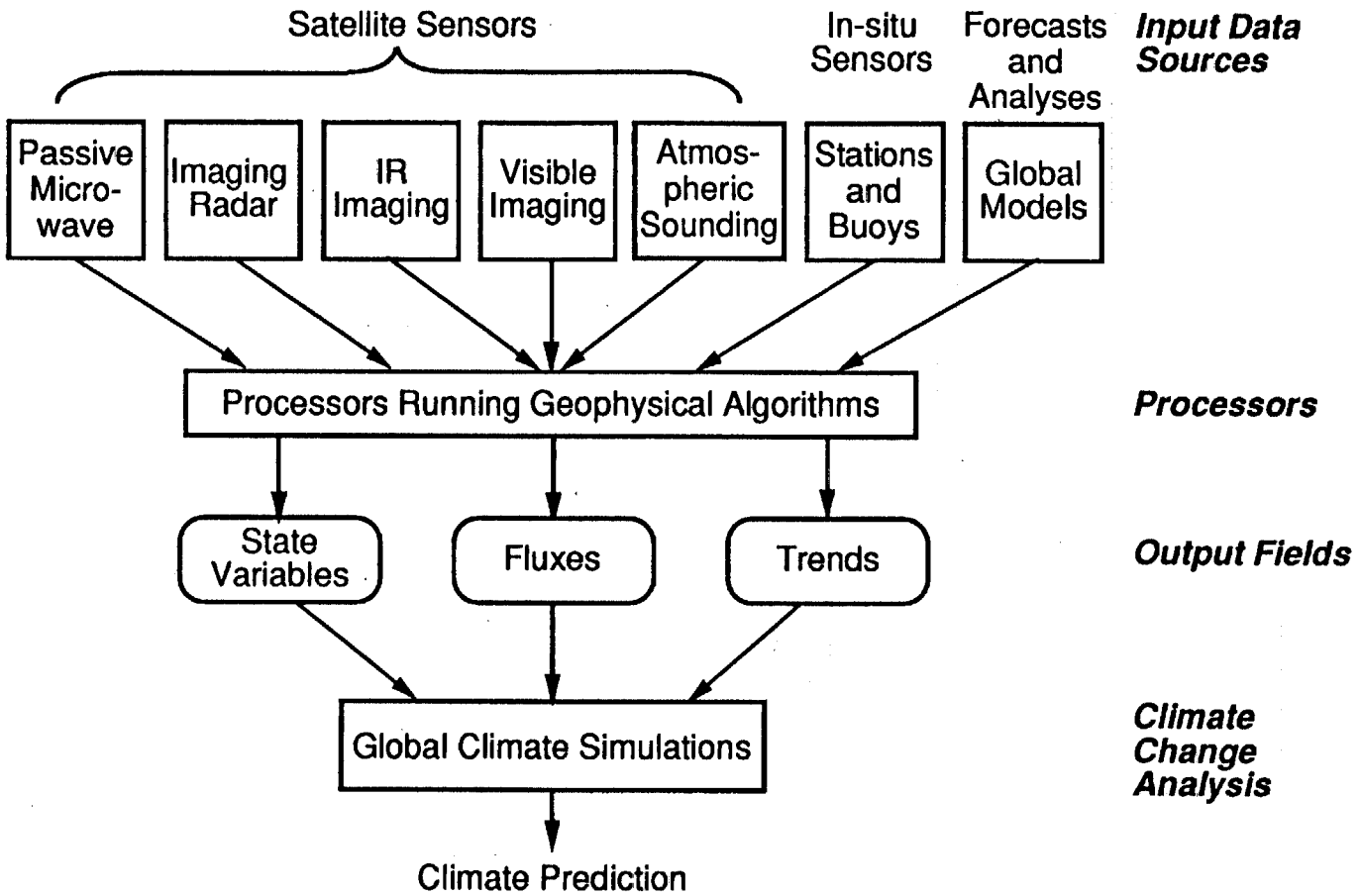

RADARSAT Data Coverage (500Km Swath): Days: 1 (Bold) and 3 (Dotted)
McMurdo, Bernardo O'Higgins, Syowa Station Masks at 3 Deg. Elev.
Ascending Data Only: 15 Sec. time steps

September 1975 ESMR Maximum Ice Edge
Day 1 Total Time: 58 minutes
Day 3 Total Time: 59 minutes

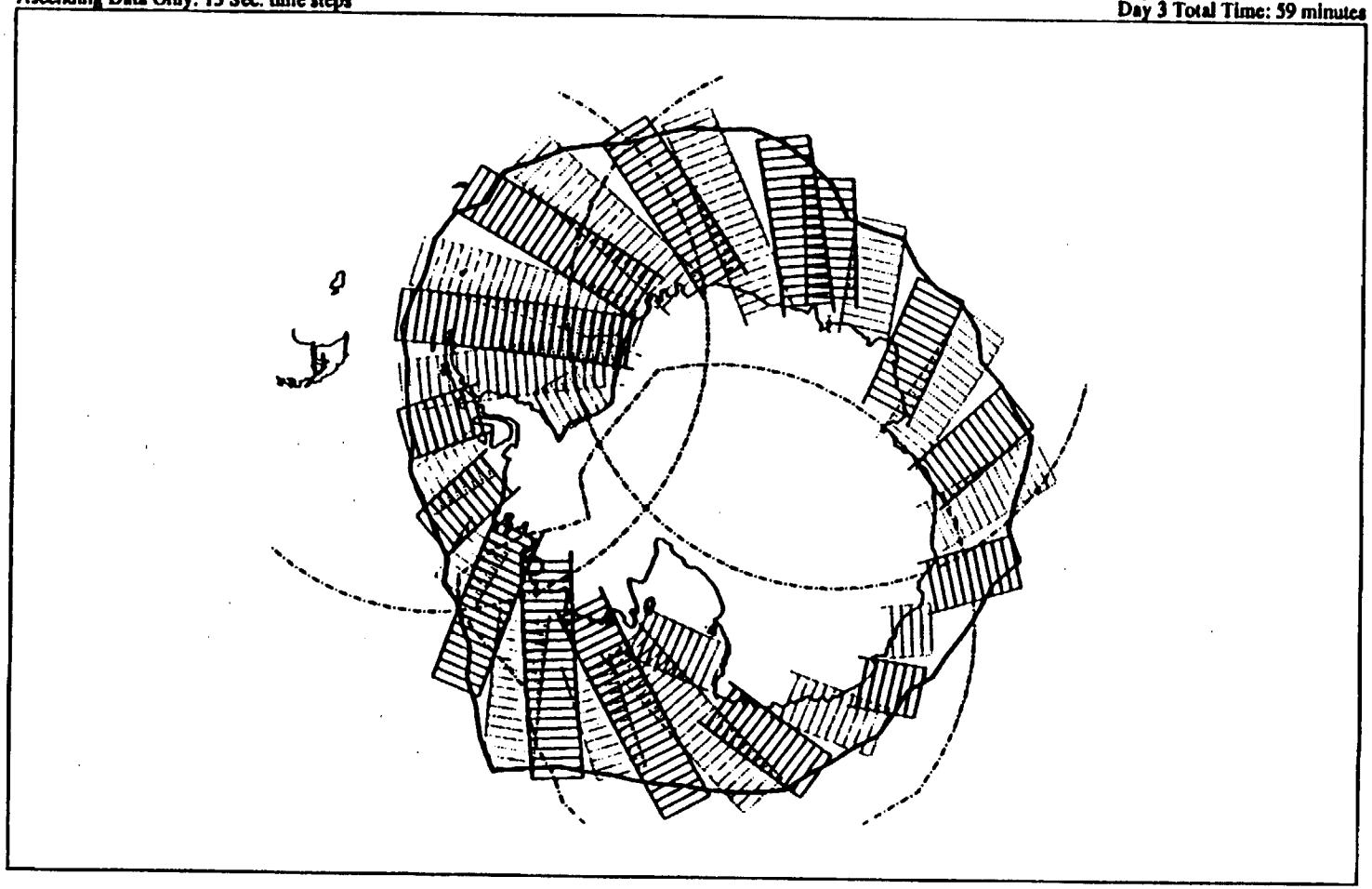

C-3

SATELLITE DATA SETS FOR SEA ICE OBSERVATIONS

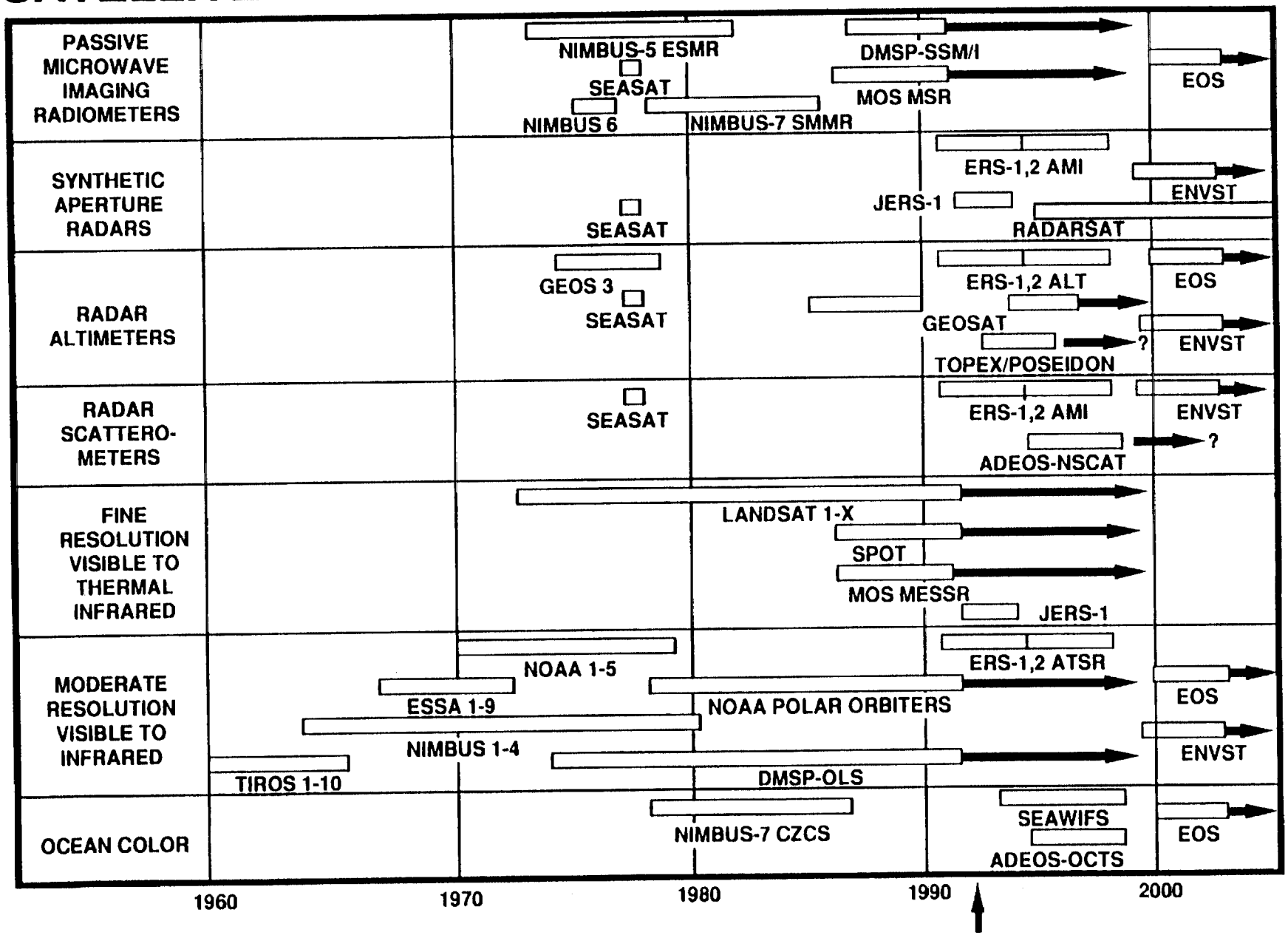

Statistics of Ice Deformation

Average over SAR Scenes

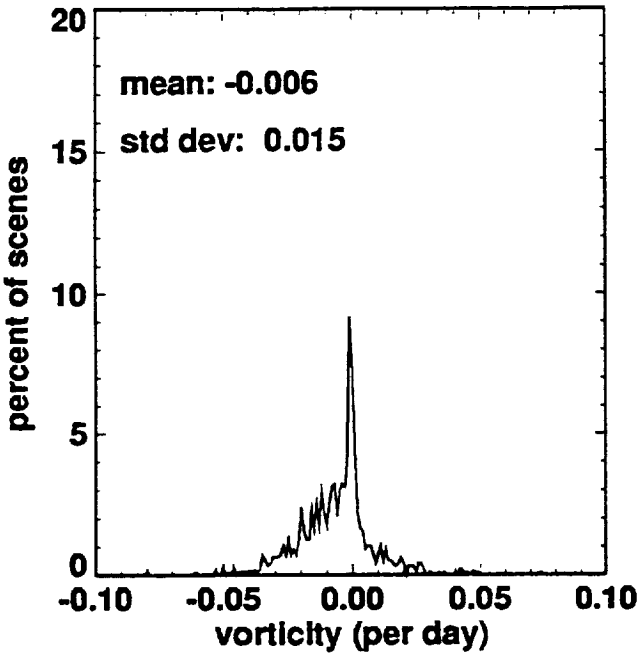

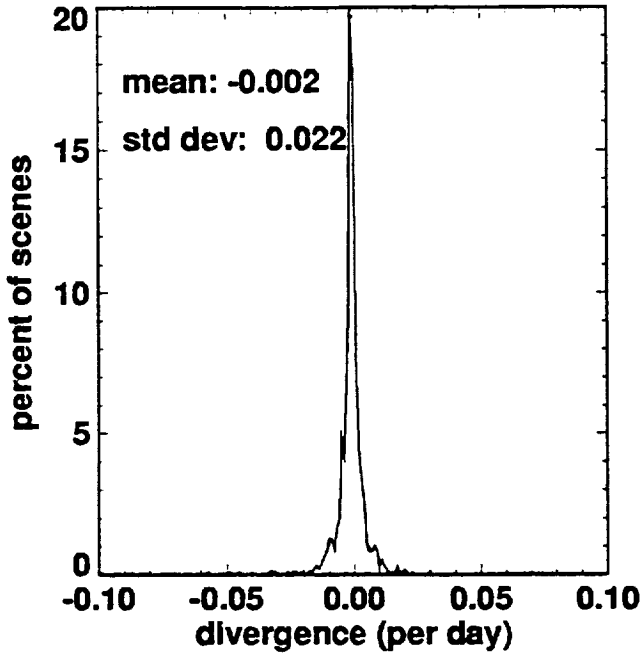

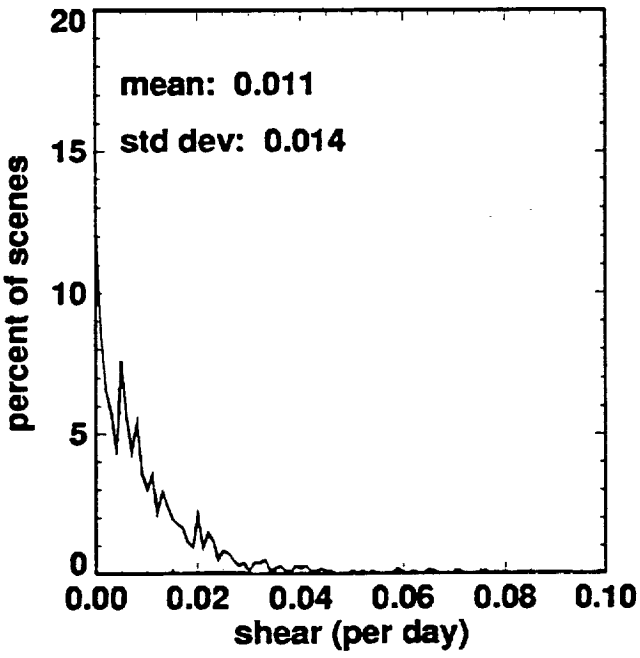

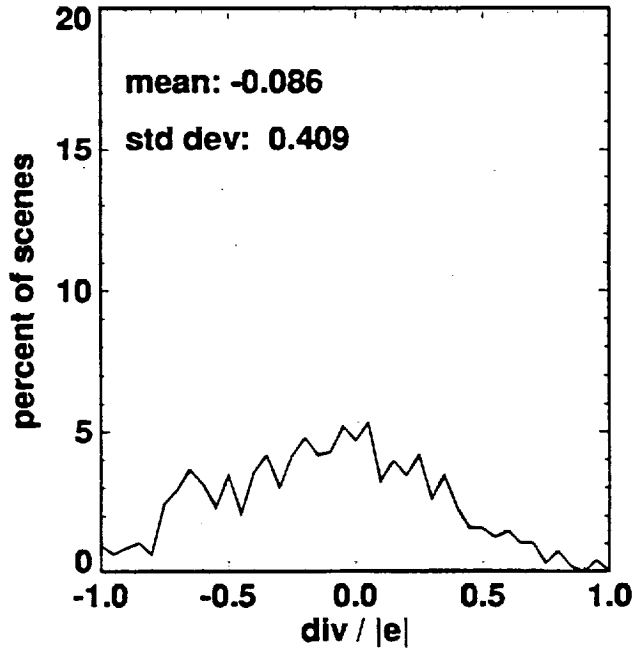

ERS-1 SAR / Beaufort Sea / LEADEX'92

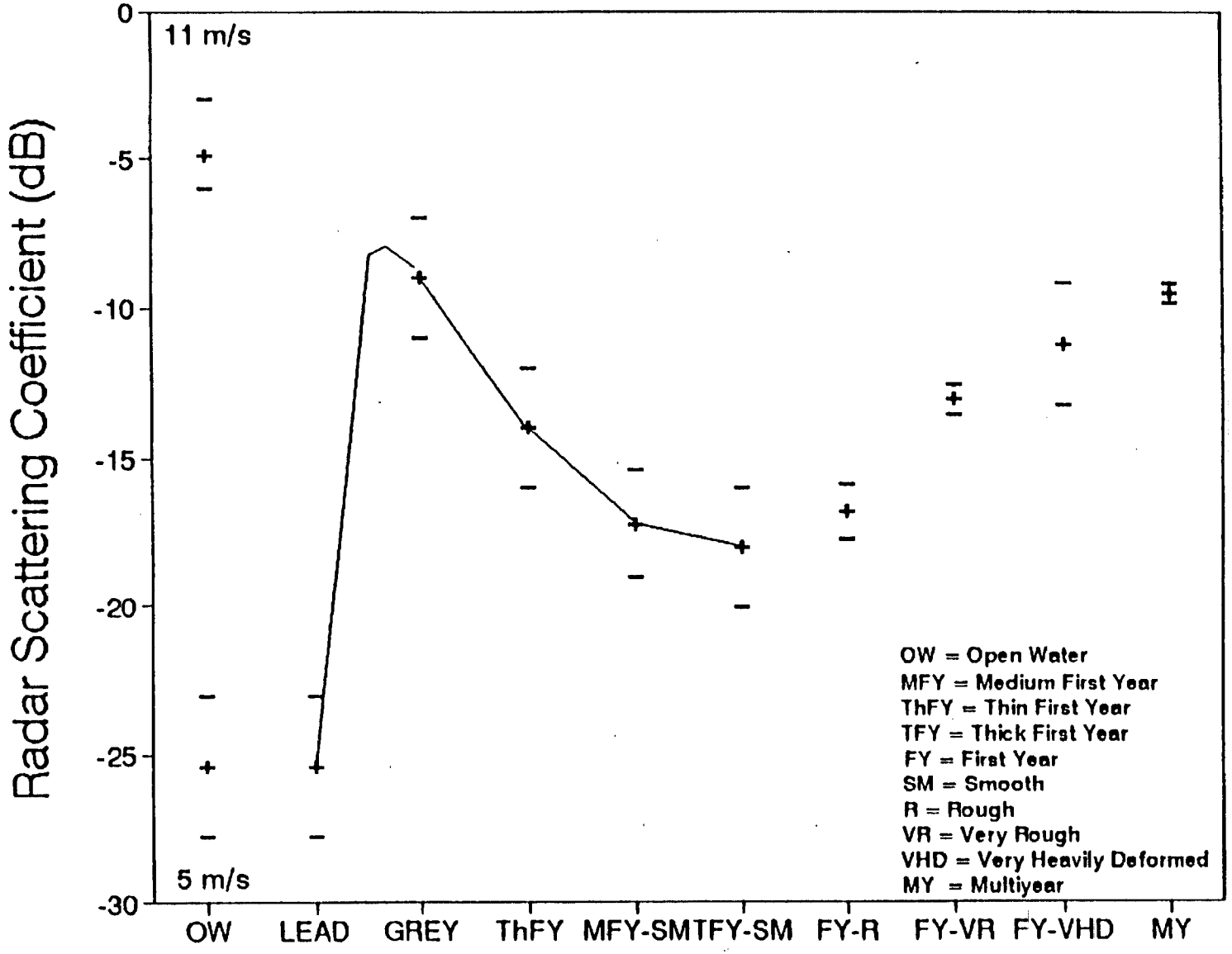

ERIM

SEASONAL CHANGE IN ERS-1 BACKSCATTER

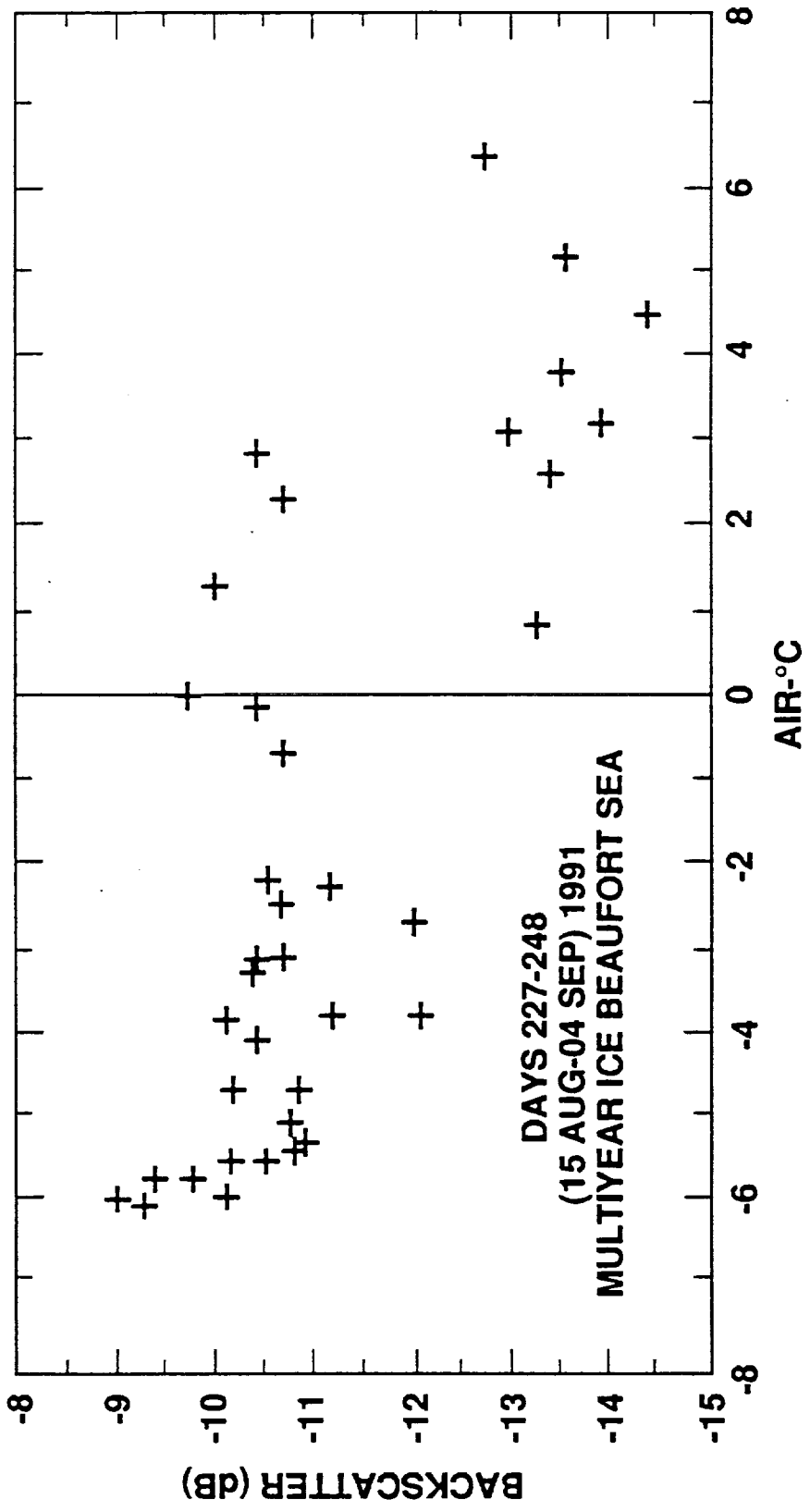

Radar Opportunities

- Systems Now Deployed in Space:
  ERS-1, JERS-1
- Ground Station SAR Processors, Geophysical Processors
  International Collaboration--Could Improve
- Systems Approved for the Near Term, Far Term
  RADARSAT (Coverage)
- Proposed Systems for the Far Term
- Airborne Systems, Polarimetric Data
- In-Situ and Laboratory Scatterometers
- Historical Data

In Summary: Data Opportunities are Excellent, Will Funded Research Opportunities Keep Up?

- - - - - - - - - - - - - - - - - - - -

Scientific Overview

Ice Sheet Scientific Objectives

- To Map and Classify the Ice Sheets According to Dominant Processes in the Mass budget
- To Monitor the Calving Ice Flux From Greenland and Antarctica

Key Radar Observations: Surface Conditions, Ice Velocity

RADAR INVESTIGATIONS OF GREENLAND ICE SHEET ZONATION

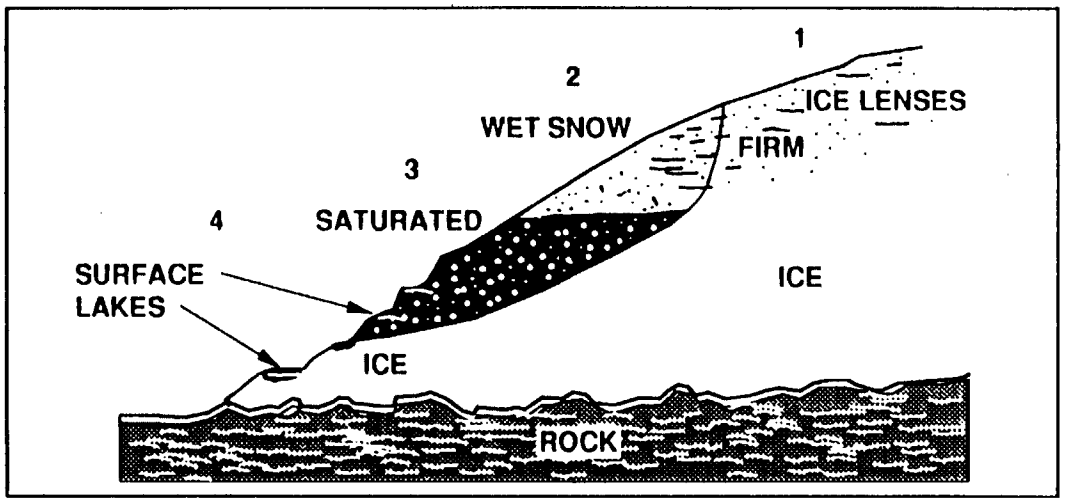

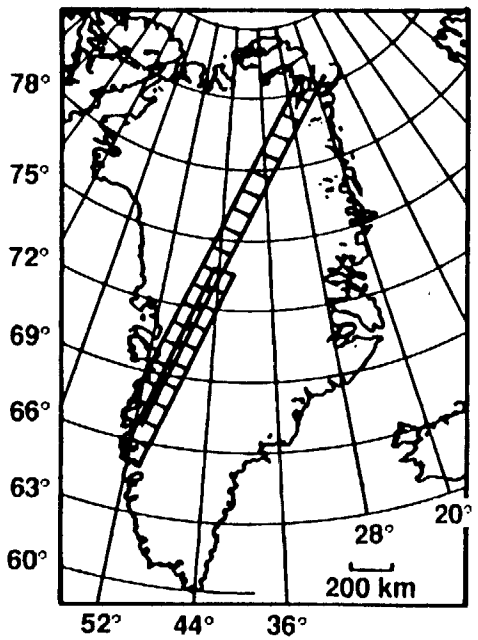

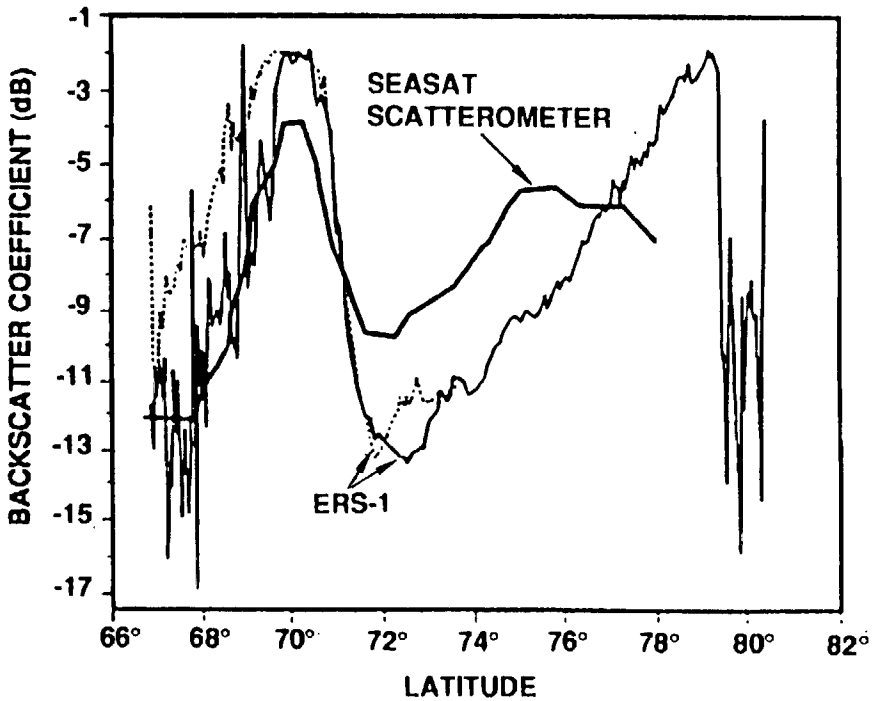

GEOLOGIC REMOTE SENSING WITH RADAR

Thomas G. Farr

Jet Propulsion Laboratory
California Institute of Technology
Pasadena, California

GEOLOGIC REMOTE SENSING WITH RADAR

ONGOING STUDIES CONCENTRATE ON:

- **WEATHERING PROCESSES:** EOLIAN TRANSPORT AND DEPOSITION, DESERT PAVEMENT DEVELOPMENT
- **VOLCANIC PROCESSES:** ERUPTION HISTORY, SIZE, AND TYPE; ATMOSPHERIC EFFECTS, OTHER PLANETS
- **LAND DEGRADATION:** HUMAN EFFECTS ON VEGETATION, SOIL ARABILITY
- **TECTONIC PROCESSES:** HISTORY OF FAULTING, FAULT LOCATION
- **SURFACE AND SUBSURFACE MAPPING:** LANDFORMS, PALEODRAINAGES

LAND SURFACE AND COVER PROPERTIES
(HIGH RESOLUTION OBSERVATIONS)

IMAGING RADARS

PHYSICAL/
ELECTRICAL
PROPERTIES

VISIBLE/NEAR IR
IMAGING SPECTROMETERS

CHEMICAL
COMPOSITION

TOPOGRAPHY

RADAR INTERFEROMETRY/
LASER ALTIMETERS/STEREO

CHEMICAL
COMPOSITION/
THERMAL
PROPERTIES

THERMAL IR
IMAGING SPECTROMETERS

RADAR-AERODYNAMIC ROUGHNESS PROJECT (RARP)

Goal

To derive a technique to assess potential sand and dust movement over large areas

Rationale

- Eolian activity (e.g., "threshold" and flux) is governed partly by surface roughness
- Aerodynamic roughness (z_0) is the relevant parameter, but is derived from *in situ* field measurements of limited areas
- Radar backscatter (σ°) is also governed partly by surface roughness
- If z_0 and σ° correlate, then there is potential to predict eolian activity using airborne or orbital radar data

Approach

Develop and test the correlation via field experiments by analyzing wind data (z_0), radar data (σ°), and roughness data

TOPSAR: HEKLA LAVA FLOW

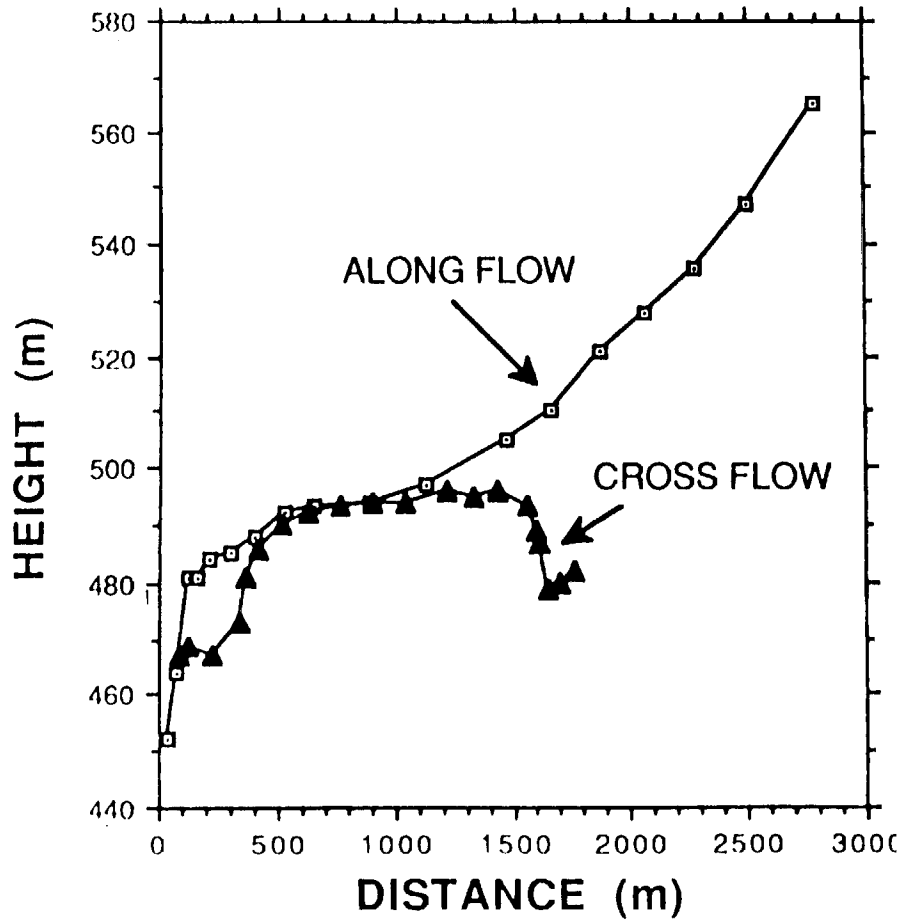

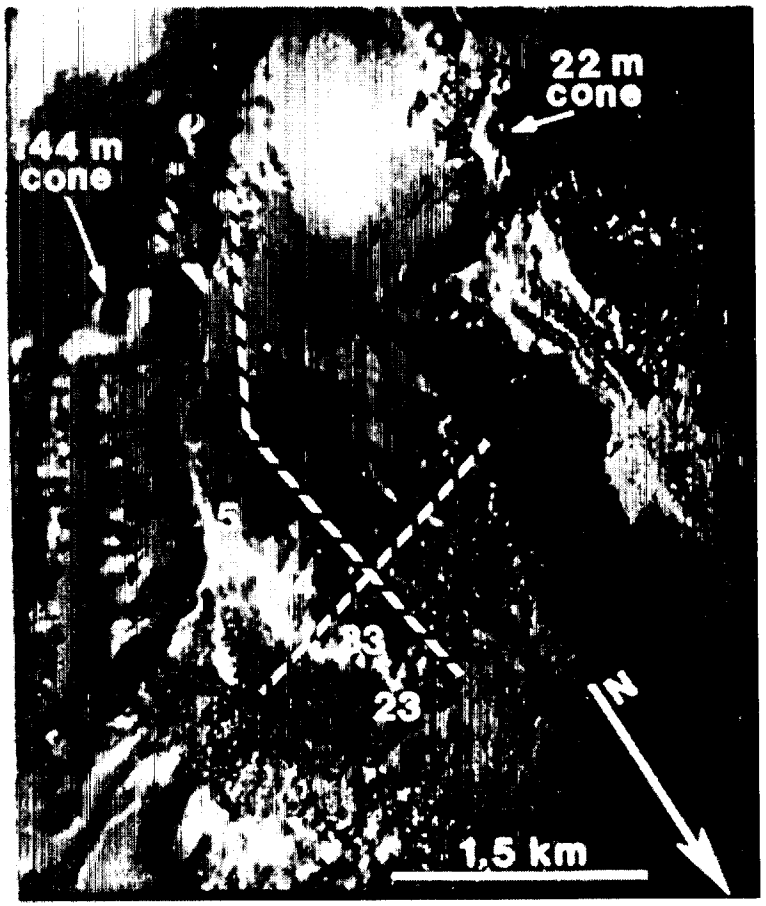

TOPSAR topographic data of the west side of Death Valley, CA. A shaded-relief image has been generated from the data and contours overlain. Image is oriented with north approximately up and is about 10 km wide.

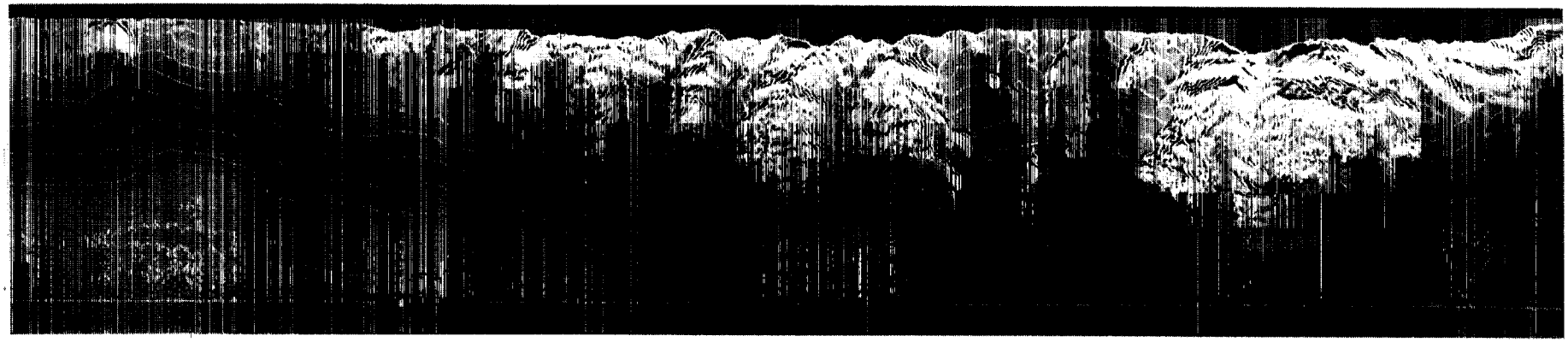

ERS-1 image of eastern Libya showing ancient drainages, some of which may be buried, as evidenced by the bright linear sand dunes trending NW-SE over the dark drainages. North is approximately up and the image is about 100 km wide.

THE CLIMATE RECORD: HOW GLOBAL CHANGES IN CLIMATE ARE MANIFESTED LOCALLY

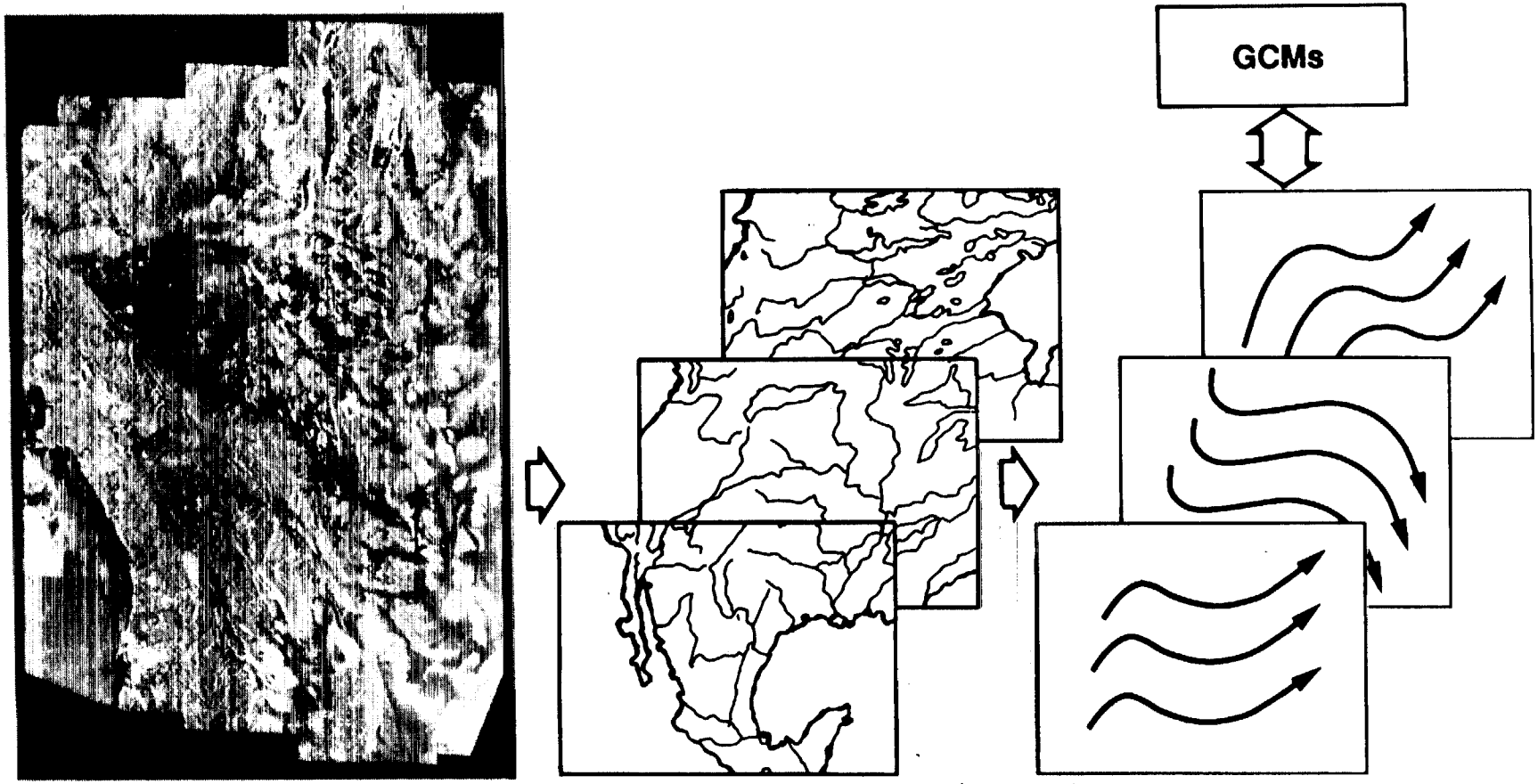

REGIONAL CORRELATIONS

CHANGES IN THE LAND SURFACE THROUGH TIME

REGIONAL ATMOSPHERIC CIRCULATION THROUGH TIME

GEOLOGIC REMOTE SENSING WITH RADAR

SUMMARY OF REQUIREMENTS

- **WEATHERING PROCESSES**: MULTIFREQUENCY DUAL-POL. TOPOGRAPHY
- **VOLCANIC PROCESSES**: MULTIFREQUENCY POLARIMETRY TOPOGRAPHY
- **LAND DEGRADATION**: MULTIFREQUENCY POLARIMETRY
- **TECTONIC PROCESSES**: MULTIFREQUENCY DUAL-POL. TOPOGRAPHY
- **SURFACE AND SUBSURFACE MAPPING**:

  MULTIFREQUENCY DUAL-POL. TOPOGRAPHY COVERAGE

RECENT

TECHNIQUES ADVANCES

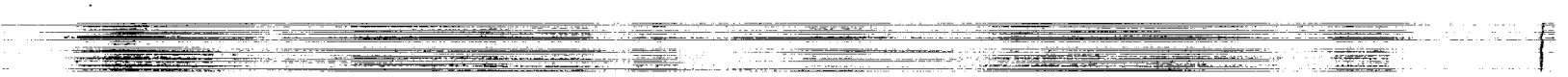

Application of Cloude's target decomposition theorem to polarimetric imaging radar data

Jakob J. van Zyl

Jet Propulsion Laboratory
California Institute of Technology
4800 Oak Grove Drive, Pasadena, CA 91109

ABSTRACT

In this paper we applied Cloude's decomposition to imaging radar polarimetry. We show in detail how the decomposition results can guide the interpretation of scattering from vegetated areas. For multifrequency polarimetric radar measurements of a clear-cut area, the decomposition leads us to conclude that the vegetation is probably thin compared to even the C-band radar wavelength of 6 cm. For a forested area, we notice an increased amount of even number of reflection scattering at P-band and L-band, probably the result of penetration through the coniferous canopy resulting in trunk-ground double reflection scattering. The scattering for the forested area is still dominated by scattering from randomly oriented cylinders, however. It is found that these cylinders are thicker than in the case of clear-cut areas, leading us to conclude that scattering from the branches probably dominates in this case.

1. INTRODUCTION

In the analysis of polarimetric imaging radar data, one is often faced with the situation where some geophysical parameters must be inferred from an area that exhibits significant natural variability in the scattering properties. In such cases, the resulting average Stokes or covariance matrix differs significantly from that of a single scatterer. It has long been speculated that if a unique way could be found to decompose such an average Stokes or covariance matrix into a sum of matrices representing single scatterers, one would not only be able to more accurately interpret the scattering processes, but the problem of inferring geophysical parameters from the measured radar data would also be significantly simplified.

One of the first examples of such a target decomposition technique was provided by Chandrasekhar [1] in his book on radiative transfer. Considering the case of lateral scattering of light by small anisotropic particles, he decomposed the total average phase matrix into the sum of a phase matrix that represents dipole scattering and a phase matrix that represents pure random scattering, or noise. As such, his target decomposition followed the same principle that breaks the Stokes vector of a partially polarized wave into the sum of a Stokes vector representing a fully polarized wave, and a Stokes vector representing a completely unpolarized wave (see Papas [2] for example).

Huynen [3], in his thesis published in 1970, also introduced a target decomposition theorem in which he decomposed an average Mueller matrix into the sum of a Mueller matrix for single a scatterer and a "noise" or N-target Mueller matrix. However, unlike Chandrasekhar's decomposition, Huynen's N-target is not polarization independent, and has been shown to be just one of an infinite set of such residue matrices, meaning that Huynen's decomposition is not unique.

In 1988 Cloude [4] introduced a target decomposition based on an eigenvector decomposition of the target covariance matrix. This decomposition was shown to be unique and, in the monostatic case, breaks the average covariance matrix up into the weighted sum of three covariance matrices representing three different single scatterers, analogous to the decomposition of a Stokes vector of a partially polarized wave into the sum of the Stokes vectors of two full polarized waves that are orthogonally polarized [2].

In this paper we examine the application of Cloude's decomposition to the analysis of polarimetric synthetic aperture radar (SAR) data.

2. CLOUDE'S DECOMPOSITION

Cloude showed that a general covariance matrix **[T]** can be decomposed as follows:

$$[\mathbf{T}] = \sum_{t=1}^{4} \lambda_t \quad \mathbf{k}_t \cdot \mathbf{k}_t^{\dagger} \tag{1}$$

In (1), $\lambda_t \; ; t = 1,2,3,4$ are the eigenvalues of the covariance matrix, $\mathbf{k}_t \; ; t = 1,2,3,4$ are the eigenvectors of **[T]**, and $\mathbf{k}_t^{\dagger}$ means the *adjoint* (complex conjugate transposed) of $\mathbf{k}_t$. In the monostatic case, for reciprocal media, the covariance matrix has one zero eigenvalue and the decomposition results in at most three covariance matrices on the right-hand side of (1).

In (1) the elements of the eigenvectors are the elements of an equivalent scattering matrix in the basis in which the decomposition is performed. For example, if the covariance matrix elements are expressed in the normal HV basis, then the four elements of the eigenvectors are simply the four scattering matrix elements in the linear basis. Also, since the covariance matrix is, by definition, a hermitian matrix, it follows that the eigenvalues are all real, and the eigenvectors are orthogonal. Therefore, one can interpret (1) to mean that this decomposition breaks the covariance matrix into the weighted sum of covariance matrices from "orthogonal" scattering matrices.

Cloude did his decomposition in the basis formed by the Pauli spin matrices, but pointed out that the decomposition can be done using any four complex matrices that satisfy the constraint of completeness and normalization. Here, we shall interpret our results in the natural linear basis in which the radar measurements are performed.

Also useful in our discussions later is Cloude's definition of target entropy,

$$H_T = -\sum_{i=1}^{4} P_i \log_4 P_i \tag{2}$$

where

$$P_i = \frac{\lambda_i}{\lambda_1 + \lambda_2 + \lambda_3 + \lambda_4} \tag{3}$$

As pointed out by Cloude, the target entropy is a measure of target disorder, with $H_T = 1$ for random targets and $H_T = 0$ for simple (single) targets.

3. DECOMPOSITION OF SCATTERING FROM AZIMUTHALLY SYMMETRIC NATURAL TERRAIN

Before getting into the radar data analysis, let us illustrate the decomposition using a general description of the covariance matrix for azimuthally symmetrical natural terrain in the monostatic case. Borgeaud *et al.* [5] showed using a random medium model, that the average covariance matrix for azimuthally symmetrical terrain in the monostatic case has the general form

$$[\mathbf{T}] = C\begin{pmatrix} 1 & 0 & \rho \\ 0 & \eta & 0 \\ \rho^* & 0 & \zeta \end{pmatrix} \tag{4}$$

where

$$C = \langle S_{hh} S_{hh}^* \rangle \tag{5}$$

$$\rho = \frac{\langle S_{hh} S_{vv}^* \rangle}{\langle S_{hh} S_{hh}^* \rangle} \tag{6}$$

$$\eta = 2\frac{\langle S_{hv} S_{hv}^* \rangle}{\langle S_{hh} S_{hh}^* \rangle} \tag{7}$$

$$\zeta = \frac{\langle S_{vv} S_{vv}^* \rangle}{\langle S_{hh} S_{hh}^* \rangle} \tag{8}$$

The superscript * means complex conjugate, and all quantities are ensemble averages. The parameters C, η, ζ and ρ all depend on the size, shape and electrical properties of the scatterers, as well as their statistical angular distribution. It is easily shown that the eigenvalues of [T] are

$$\lambda_1 = \frac{C}{2}\left\{\zeta + 1 + \sqrt{(\zeta-1)^2 + 4|\rho|^2}\right\} \tag{9}$$

$$\lambda_2 = \frac{C}{2}\left\{\zeta + 1 - \sqrt{(\zeta-1)^2 + 4|\rho|^2}\right\} \tag{10}$$

$$\lambda_3 = C\,\eta \tag{11}$$

The corresponding three eigenvectors are

$$\mathbf{k}_1 = \sqrt{\frac{\left[\zeta - 1 + \sqrt{\Delta}\right]^2}{\left[\zeta - 1 + \sqrt{\Delta}\right]^2 + 4|\rho|^2}} \begin{pmatrix} 2\rho \,/\, \left[\zeta - 1 + \sqrt{\Delta}\right] \\ 0 \\ 1 \end{pmatrix} \tag{12}$$

$$\mathbf{k}_2 = \sqrt{\frac{\left[\zeta - 1 - \sqrt{\Delta}\right]^2}{\left[\zeta - 1 - \sqrt{\Delta}\right]^2 + 4|\rho|^2}} \begin{pmatrix} 2\rho \,/\, \left[\zeta - 1 - \sqrt{\Delta}\right] \\ 0 \\ 1 \end{pmatrix} \tag{13}$$

$$\mathbf{k}_3 = \begin{pmatrix} 0 \\ 1 \\ 0 \end{pmatrix} \tag{14}$$

In these expressions, we used the shorthand notation

$$\Delta = [\zeta - 1]^2 + 4|\rho|^2 \tag{15}$$

We note that Δ is always positive. Also note that we can write the ratio of the first elements of the first two eigenvectors as

$$\frac{k_{11}}{k_{21}} = -\sqrt{\frac{\left[\zeta - 1 + \sqrt{\Delta}\right]^2 \left(\left[\zeta - 1 - \sqrt{\Delta}\right]^2 + 4|\rho|^2\right)}{\left[\zeta - 1 - \sqrt{\Delta}\right]^2 \left(\left[\zeta - 1 + \sqrt{\Delta}\right]^2 + 4|\rho|^2\right)}} \; \frac{\left[\zeta - 1 - \sqrt{\Delta}\right]^2}{4|\rho|^2} \tag{16}$$

which is always negative. This means that the first two eigenvectors represent scattering matrices that can be interpreted in terms of odd and even numbers of reflections. In the rest of this paper, we shall examine decompositions of the form shown above for different types of terrain using measured polarimetric radar data.

4. EXAMPLES OF CLOUDE DECOMPOSITION)

4.1 Randomly oriented dielectric cylinders.

Before analyzing measured data, let us examine a special theoretical case of uniformly randomly oriented dielectric cylinders. In general, the scattering matrix of a single dielectric cylinder oriented horizontally can be written as

$$[\mathbf{S}] = \begin{pmatrix} a & 0 \\ 0 & b \end{pmatrix} \tag{17}$$

where a and b are complex numbers whose magnitudes and phases are functions of cylinder dielectric constant, diameter and length [6]. Generally, when the cylinder is thin compared to the wavelength, $|a| > |b|$. To calculate the average covariance matrix for randomly oriented cylinders, one has to apply a rotation operator to **[S]** and average the results over all angles of orientation. Assuming a uniform distribution in angles about the line of sight, one can easily show that the resulting average covariance matrix for the monostatic case is of the form given in (4) with

$$C = \left[3|a|^2 + 3|b|^2 + 2\Re\left(a^* b\right)\right] / 8 \tag{18}$$

$$\rho = \frac{\left[|a|^2 + |b|^2 + 6\Re\left(a^* b\right)\right]}{\left[3|a|^2 + 3|b|^2 + 2\Re\left(a^* b\right)\right]} \tag{19}$$

$$\eta = \frac{2|a-b|^2}{\left[3|a|^2 + 3|b|^2 + 2\Re\left(a^* b\right)\right]} \tag{20}$$

$$\zeta = 1 \tag{21}$$

It is easily shown using (9) -- (14) that

$$\lambda_1 = C(1+|\rho|) \tag{22}$$

$$\lambda_2 = C(1-|\rho|) \tag{23}$$

$$\lambda_3 = C\,\eta \tag{24}$$

The corresponding three eigenvectors are

$$\mathbf{k}_1 = \frac{1}{\sqrt{2}} \begin{pmatrix} \rho / |\rho| \\ 0 \\ 1 \end{pmatrix} \tag{25}$$

$$\mathbf{k}_2 = \frac{1}{\sqrt{2}}\begin{pmatrix} -\rho/|\rho| \\ 0 \\ 1 \end{pmatrix} \tag{26}$$

$$\mathbf{k}_3 = \begin{pmatrix} 0 \\ 1 \\ 0 \end{pmatrix} \tag{27}$$

From (19) and (20), it is easily shown that

$$1-|\rho| = \eta \tag{28}$$

This means that for the case of randomly oriented cylinders, the second and third eigenvalues are the same.

In the thin cylinder limit, $|b|$ approaches zero, and we find that

$$\rho_{thin} = 1/3 \tag{29}$$

$$\eta_{thin} = 2/3 \tag{30}$$

$$[\mathbf{T}] = C\left\{\frac{2}{3}\begin{pmatrix} 1 & 0 & 1 \\ 0 & 0 & 0 \\ 1 & 0 & 1 \end{pmatrix} + \frac{1}{3}\begin{pmatrix} 1 & 0 & -1 \\ 0 & 0 & 0 \\ -1 & 0 & 1 \end{pmatrix} + \frac{2}{3}\begin{pmatrix} 0 & 0 & 0 \\ 0 & 1 & 0 \\ 0 & 0 & 0 \end{pmatrix}\right\} \tag{31}$$

In this case, equal amounts of scattering are contributed by the matrix that resembles scattering by a sphere (or a trihedral corner reflector) and by the cross-polarized return, although a significant fraction of the total energy is also contained in the third matrix resembling scattering by a dihedral corner reflector. The entropy in this case is 0.95 indicating a high degree of target disorder or randomness.

On the other hand, in the thick cylinder limit, $|b|$ approaches $|a|$ and we find that

$$\rho_{thick} = 1 \tag{32}$$

$$\eta_{thick} = 0 \tag{33}$$

In this case, only one eigenvalue is non-zero, and the average covariance matrix is identical to that of a sphere (pr a trihedral corner reflector). The entropy is 0, indicating no target randomness, even though we have calculated the average covariance matrix for *randomly oriented* thick cylinders! The explanation for this result lies in the fact that when the cylinders are thick, the single cylinder scattering matrix becomes the identity matrix, which is insensitive to rotations. Therefore, even after rotations, we still added up only identity matrices, and no apparent target randomness is introduced.

For cylinders that are neither thick compared to the wavelength, nor thin compared to the wavelength, $0 \leq |b/a| \leq 1$. Figure 1 shows the behavior of the normalized the eigenvalues as predicted by (22)-(24). We notice, as mentioned before, that the

second and third eigenvalues are always the same magnitude, but they get smaller relative to the first eigenvalue as the ratio of the two scattering matrix elements approaches 1.

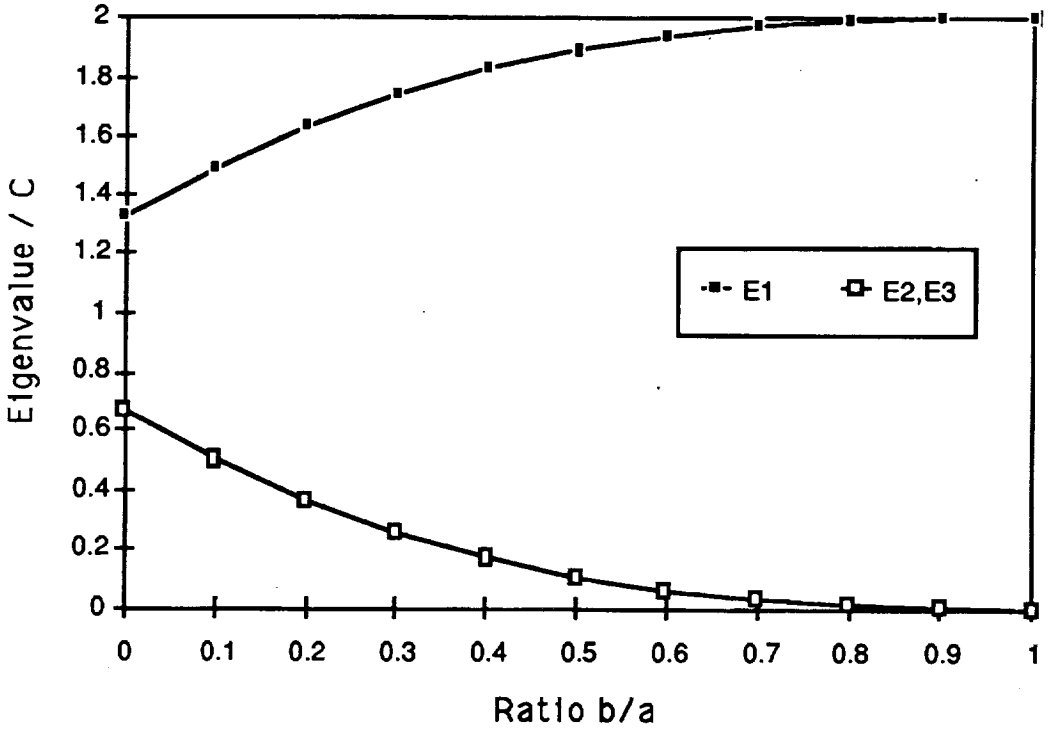

Figure 1. *Ratio of eigenvalues as a function of the ratio of b to a. The ratio of b to a depends on the cylinder dielectric constant and cylinder size compared to the wavelength.*

4.2 Measured scattering from clear-cut area.

Using the NASA/JPL AIRSAR system [7], the complete Stokes matrix [8] can be measured for each pixel in a scene. The actual measurements in general compare well with the general form of the covariance matrix assumed in (8), except that the four terms assumed to be zero are not exactly equal to zero. However, these four terms are typically much smaller than the other terms, so that to a good approximation, the assumption in (8) is valid. Here, we shall set those four terms to zero. Table 1 below shows the measured parameters at P-band, L-band and C-band for a clear-cut area in the Shasta Trinity National Forest in California.

The clear-cut area is covered with short shrub-like vegetation. We note that at all three frequencies the scattering is dominated by an odd number of reflections. At P-band the

even number of reflections and the cross-polarized returns are almost the same strength, and about half that of the odd numbers of reflections. This is very similar to the thin randomly oriented cylinder case discussed earlier. As the frequency increases, the even number of reflections and the cross-polarized returns become more different, and also become a smaller fraction of the total scattering. This is consistent with the randomly oriented cylinder case where the radius of the cylinder increases. The same conclusion is reached when considering the entropy. The highest value (most randomness) is observed at P-band, and the randomness decreases with increasing frequency. As pointed out before, as the cylinder radius increases, the entropy decreases. Therefore, from the decomposition results we conclude that the vegetation in the clear-cut is randomly oriented, and that most of the scattering comes from vegetation that has branches that are thin compared to the three radar wavelengths.

Table 1. *Measured values for a clear-cut in the Shasta Trinity National Forest. Also shown are the results of the Cloude decomposition.*

Parameter	P-band	L-band	C-band
η	0.5261	0.5308	0.4083
ζ	0.5642	0.7580	0.7159
ρ	0.0928+i0.0582	0.2324+i0.1057	0.3558+i0.0440
λ_1	1.0260	1.1615	1.2437
λ_2	0.5382	0.5964	0.4722
λ_3	0.5261	0.5308	0.4083
Entropy	0.95	0.94	0.88

4.3 Measured scattering from a forested area.

Table 2 below shows the measured parameters at P-band, L-band and C-band for a forested area in the Shasta Trinity National Forest in California. We note that at all three frequencies the scattering from this coniferous forest is dominated by an odd number of reflections. At P-band the even number of reflections contribution is stronger relative to the cross-polarized returns when compared to the case of scattering by randomly oriented cylinders. This is likely a result of the P-band signals penetrating through the canopy and then suffering a double reflection when scattering from the ground and then from the tree trunks before returning to the radar. We notice that the imbalance of the even numbers of reflections and the cross-polarized returns decrease as the frequency increases, and also become a smaller fraction of the total scattering. A possible interpretation of this is that as the frequency increases, the penetration

through the canopy decreases and the scattering from the randomly oriented branches becomes more important. The highest value of the entropy (most randomness) is

Table 2. *Measured values for a forested area in the Shasta Trinity National Forest. Also shown are the results of the Cloude decomposition.*

Parameter	P-band	L-band	C-band
η	0.3301	0.3485	0.2416
ζ	0.6529	0.7122	0.4685
ρ	0.2803+i0.0167	0.3950+i0.0582	0.3669+i0.0016
λ_1	1.1566	1.2805	1.1873
λ_2	0.4963	0.4316	0.2812
λ_3	0.3301	0.3485	0.2416
Entropy	0.87	0.84	0.75

observed at P-band, and the randomness decreases with increasing frequency. From the decomposition results we conclude that the penetration through this coniferous canopy cannot be neglected. Most of the scattering can still be contributed to the randomly oriented branches, however. The relative strengths of the different mechanisms, as well as the lower values of the entropy, suggest that the branches are thicker than those of the vegetation in the clear-cut area.

5. DISCUSSION

In this paper we applied Cloude's decomposition to imaging radar polarimetry. The decompositions illustrated here have been implemented on a pixel-by-pixel basis to analyze polarimetric radar images. Space does not permit the inclusion of more examples, however.

We have shown how the decomposition results can guide the interpretation of scattering from vegetated areas. For clear-cut areas, we concluded that the vegetation is probably thin compared to even the C-band radar wavelength of 6 cm. For forested areas, we noticed an increased amount of even number of reflection scattering at P-band and L-band, probably the result of penetration through the coniferous canopy resulting in trunk-ground double reflection scattering. The scattering for the forested area is still dominated by scattering from randomly oriented cylinders. It is found that these cylinders are thicker than in the case of clear-cut areas, leading us to conclude that scattering from the branches probably dominates in this case.

The quantitative analysis of scattering requires detailed analysis of the decompositions that will result from model predictions. Future work will concentrate on analyzing the decompositions of model predicted covariance matrices. The results can then be used to analyze polarimetric radar images.

6. ACKNOWLEDGMENT

This work was performed at the Jet Propulsion Laboratory, California Institute of Technology with a grant from the Director's Discretionary Fund.

7. REFERENCES

[1] S. Chandrasekhar, *Radiative Transfer*, Dover Publications, New York, p. 50, 1960.

[2] C. H. Papas, *Theory of Electromagnetic Wave Propagation*, Dover Publications, New York, pp. 118-134, 1988.

[3] J. R. Huynen, *Phenomenological Theory of Radar Targets*, Ph.D. dissertation, Drukkerij Bronder-Offset, N.V., Rotterdam, Netherlands, 1970.

[4] S. R. Cloude, "Uniqueness of target decomposition theorems in radar polarimetry," *Direct and Inverse Methods in Radar Polarimetry: Part 1*, W.M. Boerner (Ed.), Kluwer Academic Publishers, Dordrecht, Germany, pp. 267-296, 1992.

[5] M. Borgeaud, R. T. Shin and J. A. Kong, "Theoretical models for polarimetric radar clutter," *Journal of EM Waves and Applications*, 1, pp. 73-91, 1987.

[6] C. F. Bohren and D. R. Huffman, *Absorption and Scattering of Light by Small Particles*, Wiley and Sons, New York, 1983.

[7] J. van Zyl, R. Carande, Y. Lou, T. Miller, and K. Wheeler, "The NASA/JPL three-frequency polarimetric AIRSAR system," *Proceedings of IGARSS'92*, Volume I, pp. 649-651, 1992.

[8] J. J. van Zyl, H.A. Zebker and C. Elachi, "Imaging radar polarization signatures: Theory and observation," *Radio Science*, 22, pp. 529-543 , 1987.

MULTIFREQUENCY OBSERVATIONS

R. Glitz, F. Heel, H. Kietzmann, H. Öttl, and C. Schmullius

1. Introduction

Analyses of SAR image data were performed at DLR to classify various kinds of vegetation and different terrain types. The data were collected both with the DLR experimental synthetic aperture radar (E-SAR) in X-band, C-band and L-band and with the NASA/JPL DC-8 SAR in C-band, L-band and P-band.

E-SAR is a single frequency and single polarization system (both parameters can be selected) but several flights were used to collect multifrequency/multipolarization data which were geometrically matched after processing. Classification of different crop types was based on comparison of the backscatter coefficients of calibrated SAR data in different frequency bands and polarizations.

The DC-8 SAR collects polarimetric data in different bands simultaneously. Data acquired with the NASA/JPL DC-8 SAR are qualified for scientific investigations by reducing the cross-talk and channel imbalance to a tolerable extent. The data are absolutely calibrated by using reference targets with known backscattering cross-sections. The signatures and polarimetric features of terrain types, such as grassland, concrete, sea, forest (coniferous; deciduous) and urban areas, are extracted and discussed with respect to frequency and incidence angle dependence. A multifrequency polarimetric feature vector was applied for classification. The results of this new approach for separating and classifying different object classes are presented here.

2. Crop Classification Based on E-SAR Data

During the Multi-Sensor Airborne Campaign (MAC) Europe '91 on July 12th, the test site Oberpfaffenhofen was covered by E-SAR flights in order to collect X-HH, X-VV and C-VV SAR data.

The latest capabilities of the DLR E-SAR are described in [1], and the results of the MAC '91 agricultural classification in [2]. The high spatial resolution of E-SAR (2 to 3 m) allowed even the analysis of small fields with very good results. An unsupervised migrating means classification (k-distribution) resulted in a rejection of only about 5 % of the observed area.

On May 20th, 1992, another airborne campaign was performed with the E-SAR, after it had been modified to provide an additional L-band capability. L-HH, C-VV, X-VV, and X-HH data were collected. A selected agricultural test site is shown in Fig.1 corresponding to these four data sets.

It should be mentioned that the spatial resolution of the L-HH image is lower than in C-band and X-band images. The approximately equally spaced white spots in the images represent electric pylons. Test site statistics of the six main crop types are illustrated as scatter grains in Fig. 2 for C-VV and X-VV and in Fig. 3 for L-VV and C-VV. The ellipses include ± 1 standard deviation around the mean.

The plots in Fig. 2 permit a proper discrimination of the various crop types, while Fig. 3 only shows small differences in L-band for a number of crops. This observation is valid for the vegetation in late May.

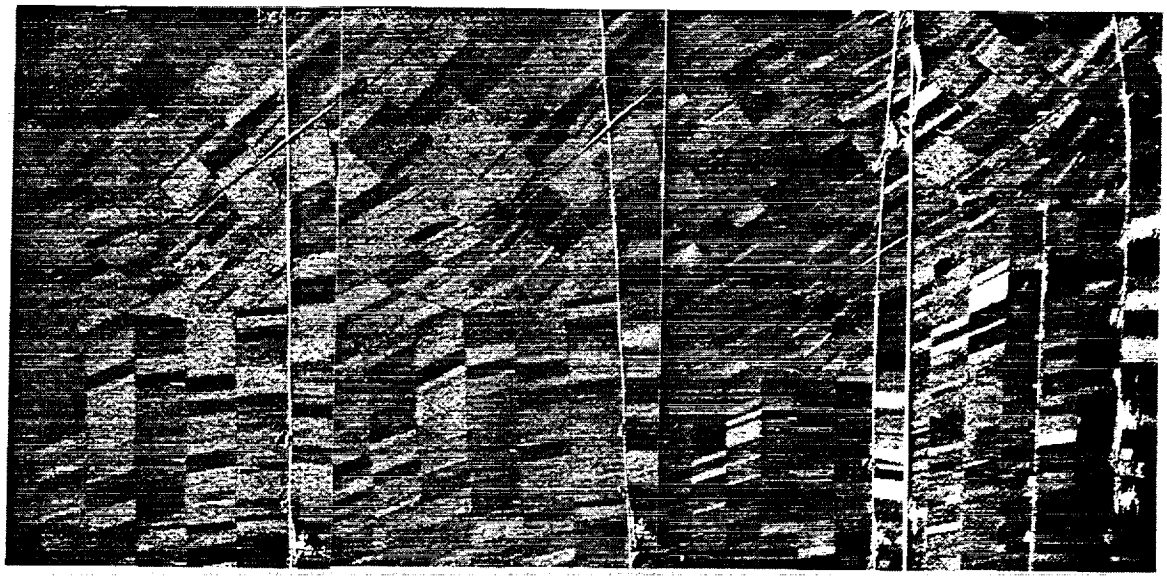

Fig. 1: Top: The SAR images based on X-HH, X-VV, C-VV and L-HH data.
Bottom: Color composite image consisting of the following co-registered channels: L-HH (red), X-VV (green), and C-VV (blue).

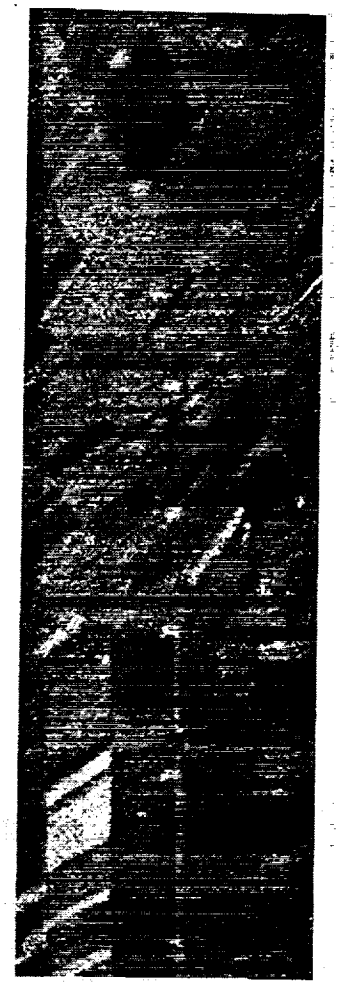

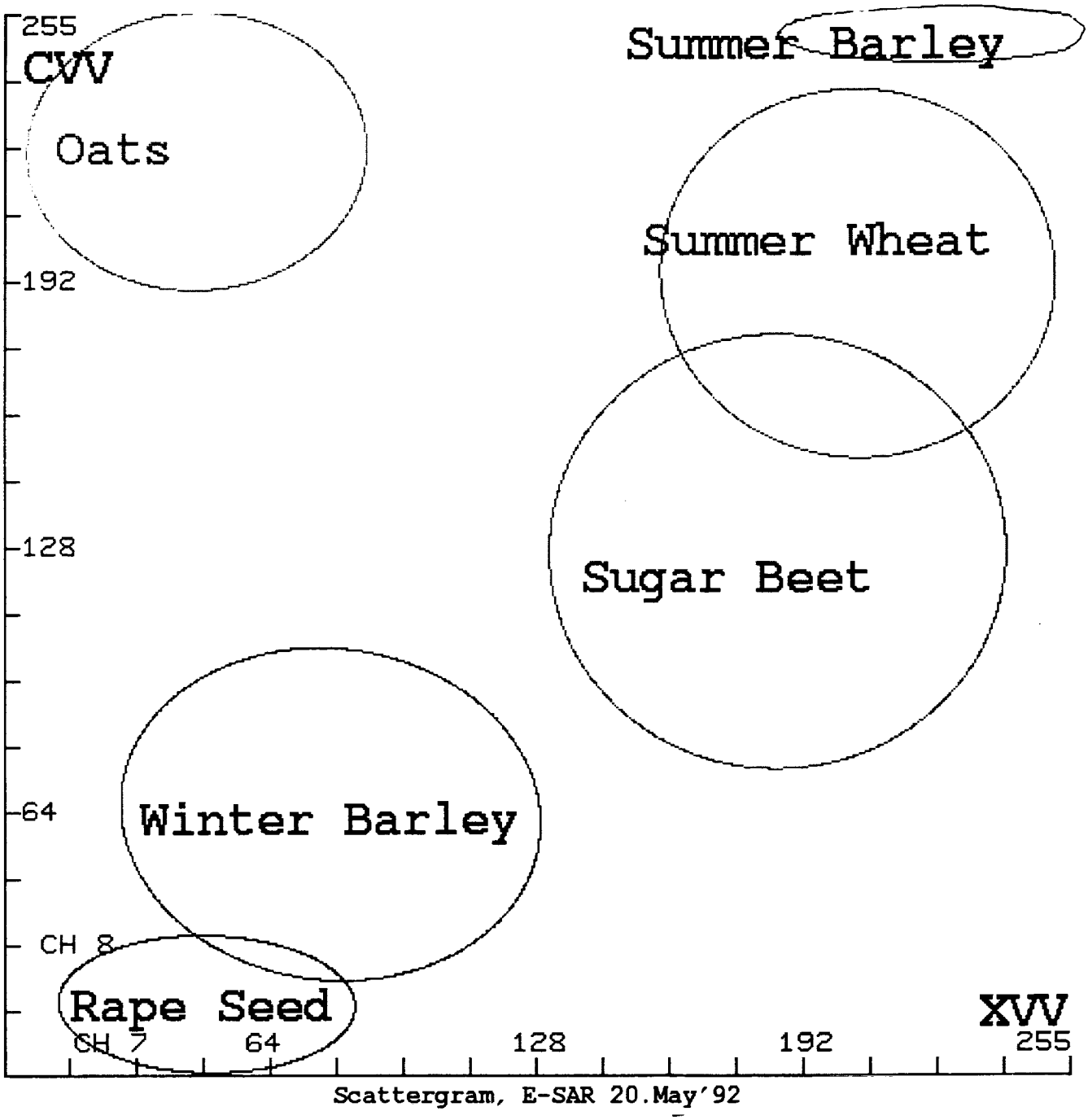

Fig. 2: Scattergram of C-VV versus X-VV bands showing proper crop type discrimination.

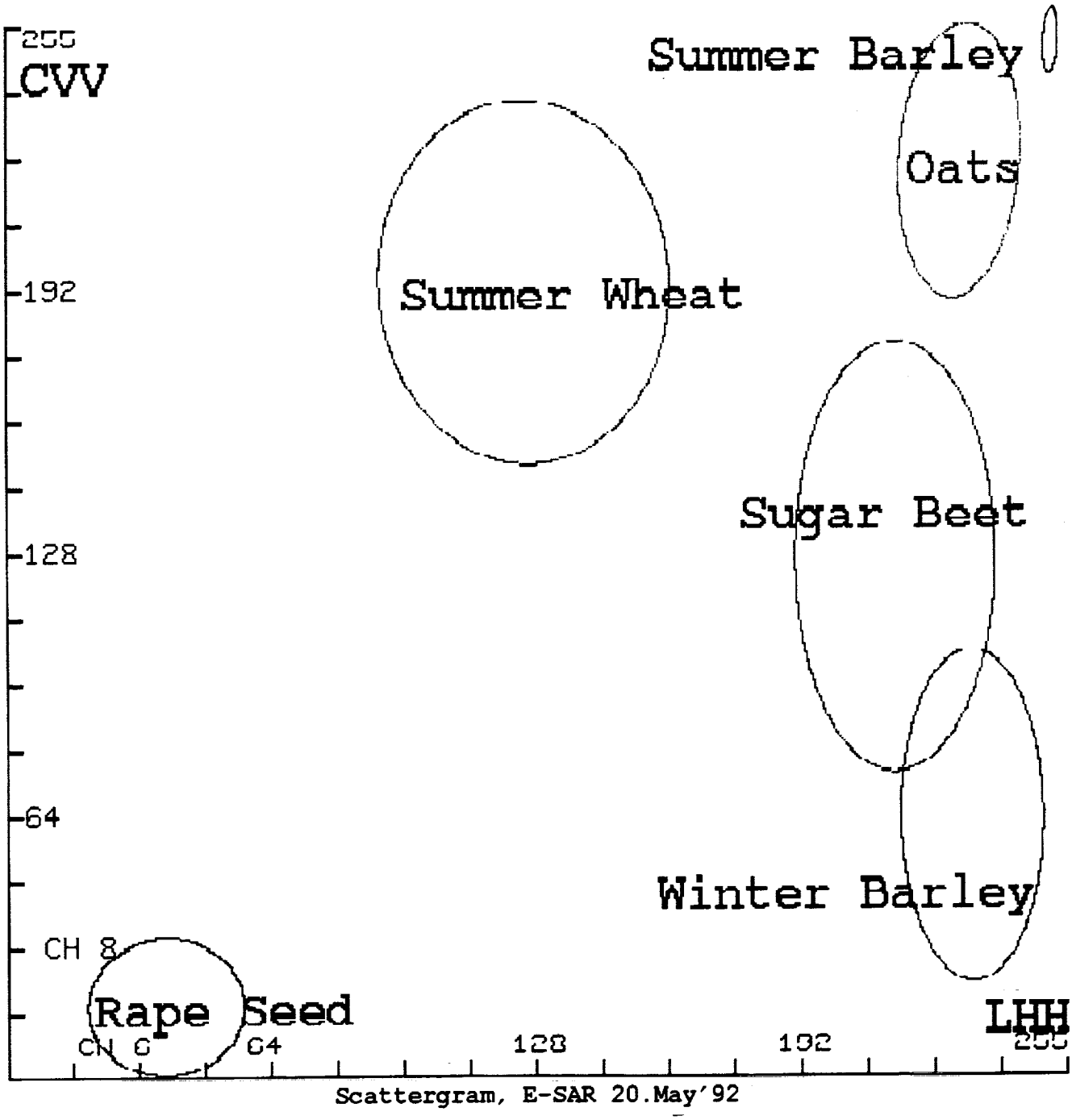

Fig. 3: Scattergram of C-VVversus L-HH bands showing overlapping crop type statistics in the L-band.

3. Airborne Campaign with the NASA/JPL DC-8 SAR

In August 1989, an airborne SAR measurement campaign took place at the Oberpfaffenhofen (OP) test site area. The NASA/JPL DC-8 SAR system is equipped with three simultaneously operating SAR sensors, comprising C-, L- and P-band with wavelengths of 5.6 cm, 24 cm and 68 cm [3]. This system permits fully polarimetric measurements [4] which means acquiring the scattering matrix elements HH, HV, VH and VV. Three parallel tracks were flown to cover scenes of the same area under different incidence angles of 35°, 45°, and 55°.

In order to qualify these multifrequency data products for comprehensive signature analysis, the appropriate preprocessing had to be carried out [5]. The data prepared in this way, with their diversity in frequency, incidence angle and polarization states, form a good basis for signature and classification studies.

4. Data Preparation and Terrain Type Selection

JPL delivered single look complex SAR image data. These fully polarimetric data covered the P-, L- and C-frequency bands and had been radiometrically corrected.

As a first step to qualify all the data products for signature analysis, polarimetric calibration (cross-talk, channel imbalance) was performed at the Institute for Radiofrequency Technology followed by absolute calibration [6], [7]. Finally, the data were transformed to a 4-look image format.

After adequate image data preparation, a total power C-band image (Fig.4) representing the central part of the Oberpfaffenhofen test site area (12.5 km x 5 km) was selected for terrain type investigations. This image includes the contours of the specific terrain types to be analysed, such as grassland (W1, W2), concrete (B1, B2), lake water surface (S1, S2), coniferous forest (N1, N2), deciduous forest (L1, L2) and urban areas (A1, A2). The terrain type sizes vary from about 10 000 m^2 to 30 000 m^2 depending on the availability of the corresponding terrain types.

5. Multifrequency Terrain Type Signatures and Classification

The simultaneous P-, L- and C-band measurements of each selected terrain type enabled the study of their backscattering behaviour. Fig. 5 shows the comparison of their copolarized backscattering coefficients σ°_{hh}. It is generally seen that urban areas and forests give rise to considerably higher returns than grass, concrete or lake targets. This can be explained by an increased roughness and reflection-like interactions. As expected for surface targets, especially in the case of grassland, a σ°_{hh} decrease could be found in the C-L-P sequence. An inversion of this sequence can be recognized for all forest areas. C-band signals mainly interact with needles or leaves in the upper forest region. Medium sized twigs and branches predominantly scatter the L-band signals, and the P-band signals couple essentially with the larger branches and trunks. This demonstrates that the size of the scattering elements considerably influences the target return. The urban area data show no significant wavelength dependence because of similar scattering mechanisms for the aforementioned frequencies.

The corresponding copolar phase differences are shown in Fig. 6. We recog-

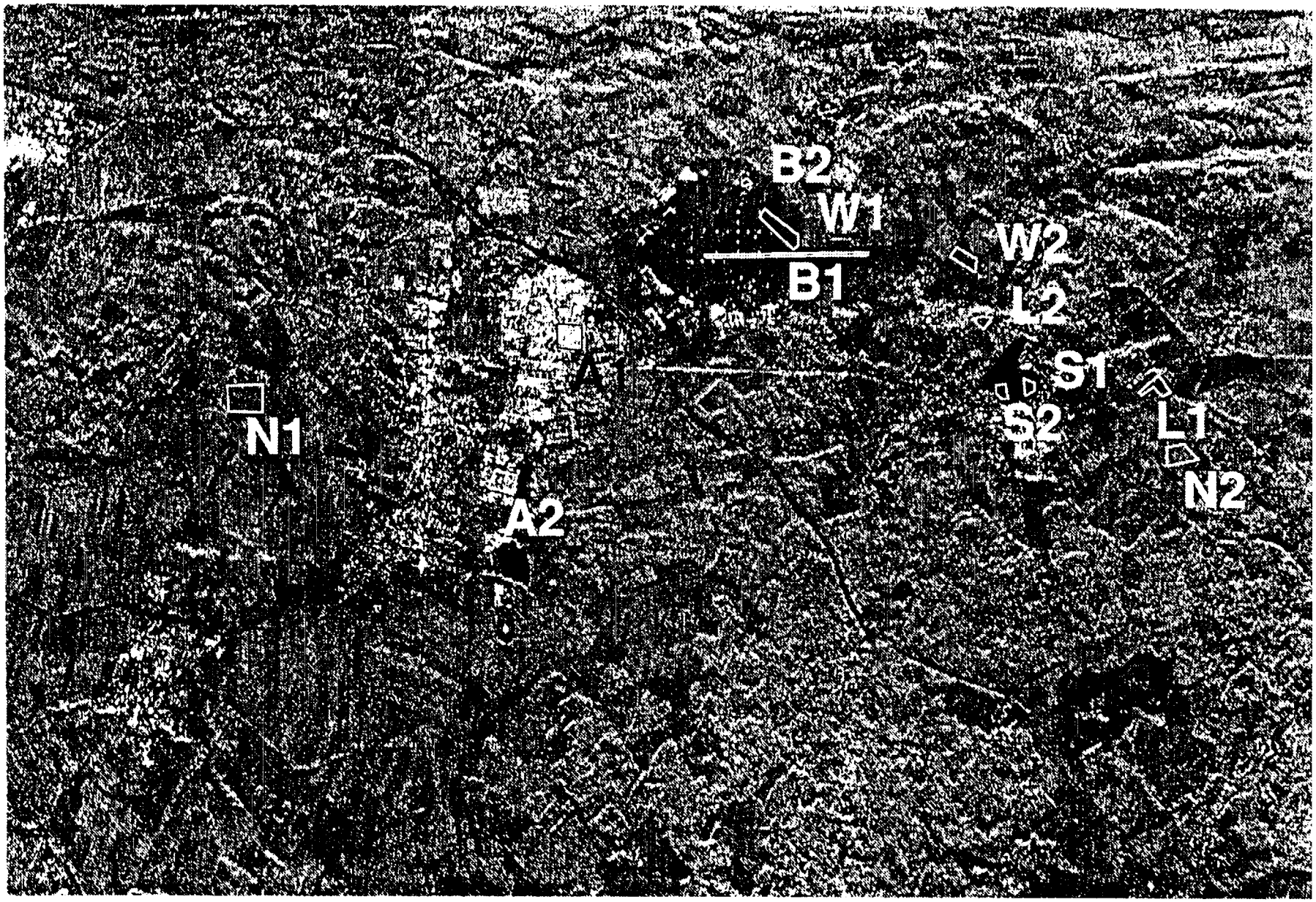

Figure 4: Total power C-band image with selected terrain types

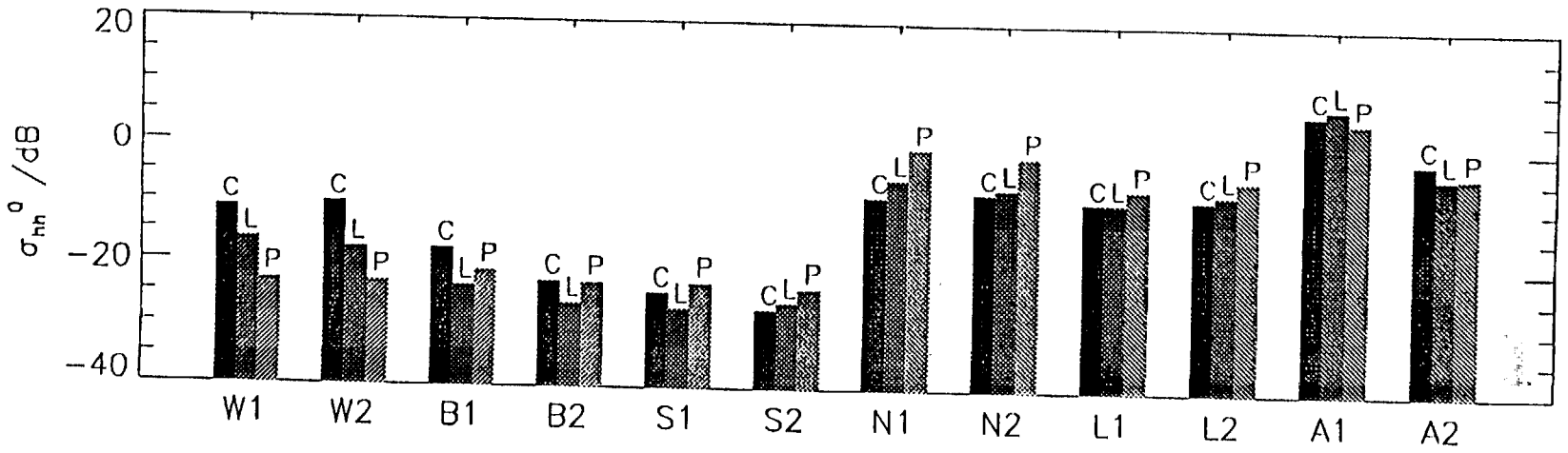

Figure 5: Backscattering coefficient σ^o_{hh} for P-,L- and C-Band.

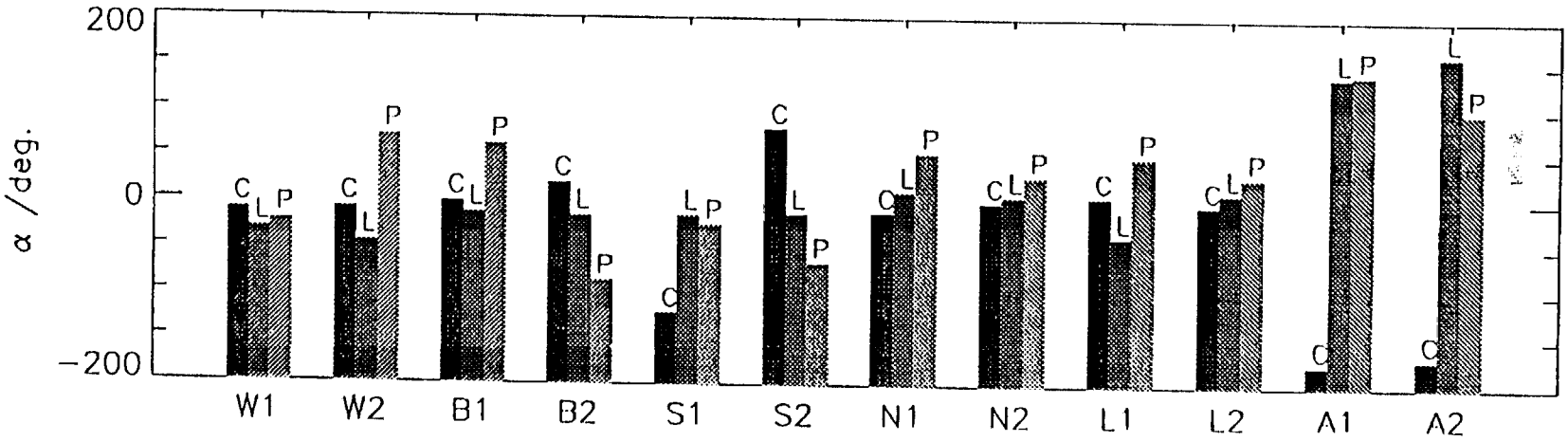

Figure 6: Copolar phase difference α for P-,L- and C-Band.

nize a phase difference for urban areas of approximately ±180°, indicating a relatively clear double bounce scattering in contrast to all analysed surface type targets. In the case of concrete and lake areas, there are some phase anomalies due to interferences from stronger targets. Regarding forests, the phase increases with increasing wavelength due to scattering mechanisms, as shown in Fig. 6.

Further investigations deal with the influence of the incidence angle on the backscattering coefficient σ°_{hh} of coniferous and deciduous (Fig. 7) forests. For coniferous forest, a clear decrease in σ°_{hh} is observed in the incidence angle range from 40° to 50° for all concerned wavelengths, whereas deciduous forest shows this dependence only for C-band. This latter target type reveals no obvious incidence angle variation of σ°_{hh} for P- and L-band which could be explained by the orientation of branches and twigs in this angle range. The σ°_{hh} behaves like that of a rough surface consisting of a layer of needles or leaves. The bars in Fig. 7 indicate the standard deviation around the mean values.

A statistical procedure [5] has been developed, based on the maximum-likelihood method, to take into account the ramdomness of distributed targets.

Analyses of a variety of polarimetric quantities allow the extraction of the most significant components to establish a multifrequency polarimetric feature vector. This feature vector consists of the scattering amplitudes HH,

VV, HV and the HH/VV phase difference for the applied P-, L- and C-band frequencies resulting in a total of twelve dimensions. In order to meet the statistical nature of each terrain class of interest, the mean and the covariance have to be determined for the single features and the overall feature vector. Adequate processing of this feature representation permits a separation of different terrain classes depending on their specific scattering properties. Thus, a procedure is established for classifying different terrain types. Fig. 8 illustrates a classification result extracted from the scene in Fig. 4 concerning coniferous forests. The black areas in the scene are classified as coniferous forest. The corresponding test areas N1 and N2 are correctly assigned whereas negligible misclassification occurs in all other test areas. Results with similar quality have also been obtained for other terrain classes.

6. Conclusions

The comparison with ground truth observations shows that terrain classification from calibrated radar image data in different frequency bands exhibits a high degree of reliability. The amplitude relationship of backscattered signals in X-band and C-band contains sufficient information for crop classification.

In general, for the classification of different terrain types, the use of a multifrequency polarimetric feature vector showed promising results. The large number of degrees of freedom associated with this vector allows an increased variety of signature investigations.

Therefore, to enhance the potential of remote sensing, such methods should be further investigated and applied in the future.

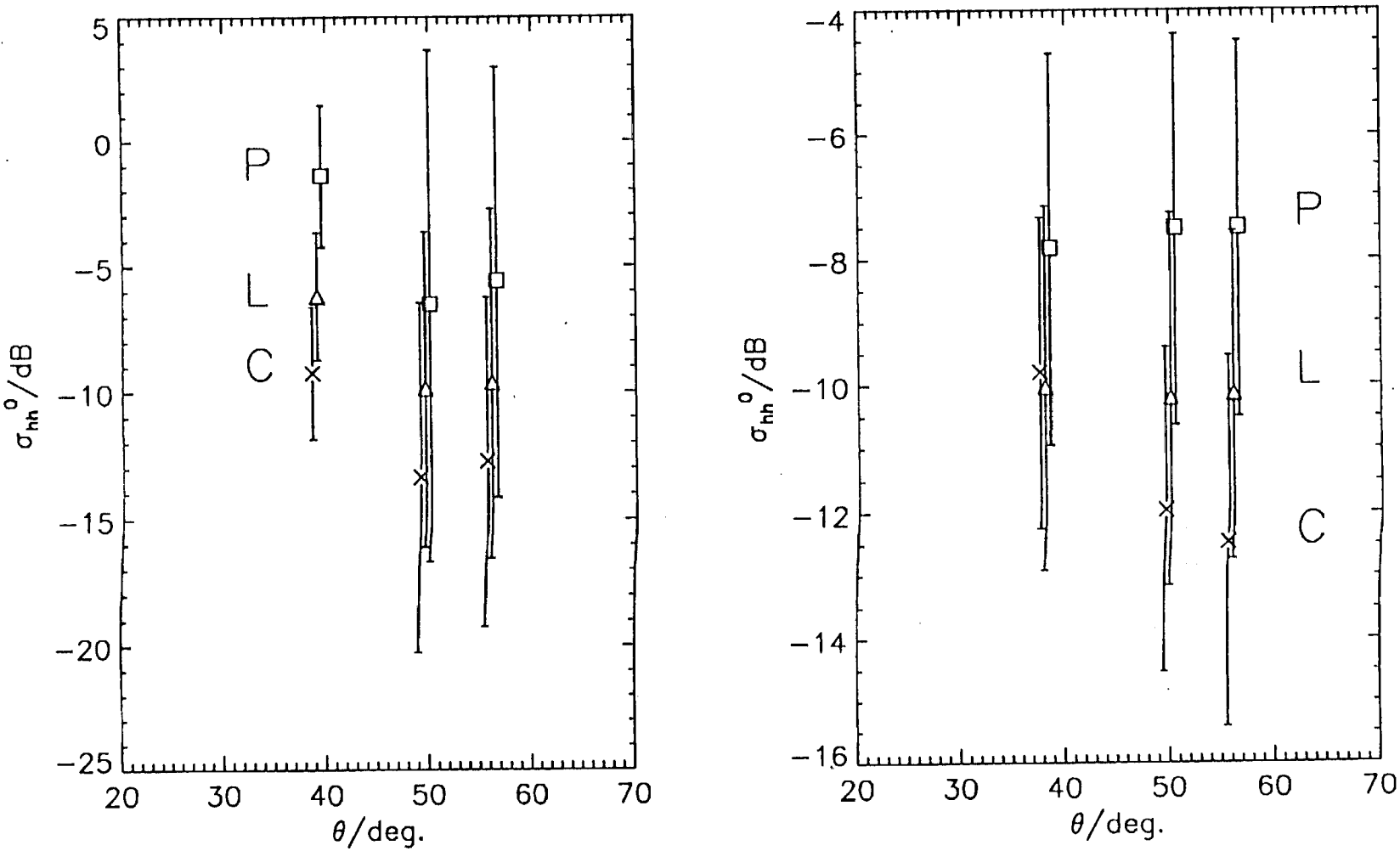

a. coniferous forest N1

b. deciduous forest L1

Figure 7: Backscattering coefficient σ_{hh}^{o} versus incidence angle Θ.

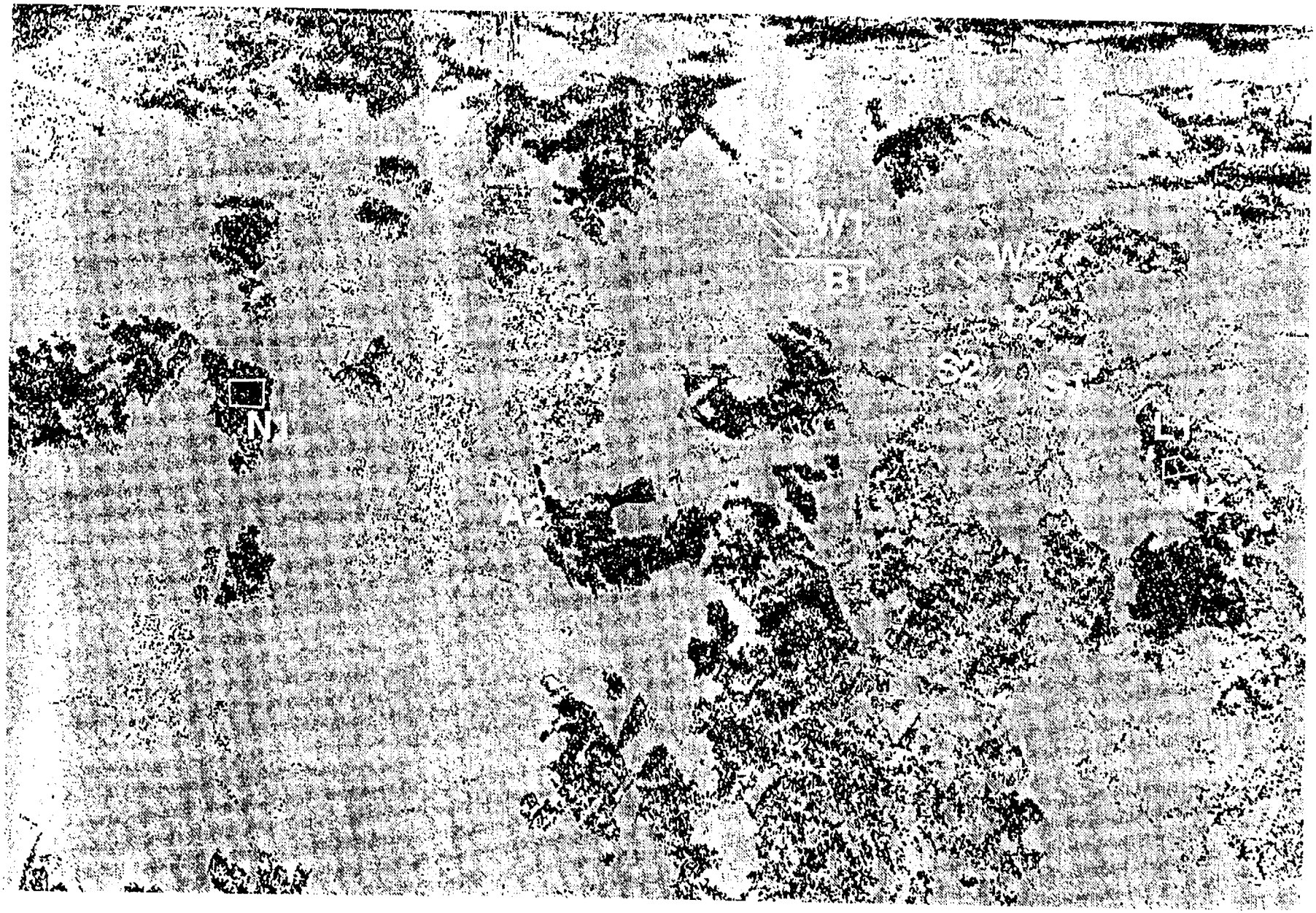

Figure 8: Coniferous forest classification image.

5. References

[1] Horn, R. et al. — A Refined Procedure to Generate Calibrated Imagery from Airborne Synthetic Aperture Radar Data.

Will be published 1993 in IEEE Trans. on Geosc. and Rem. Sens.

[2] Schmullius, C., Nithack, J. — High-Resolution SAR Frequency and Polarization Dependent Backscatter Variations from Agricultural Fields,

Proc. IGARSS '92, 26-29 May, Houston, pp. 930-932.

[3] Held, D.N. et al. — The NASA/JPL Multifrequency, Multipolarization Airborne SAR System.

Proc. IGARSS '88, pp. 345-350, Edinburgh, Scotland, Sept. 1988.

[4] Evans, D.L. et al. — Radar Polarimetry: Analysis Tools and Applications.

IEEE Trans. on Geoscience and Remote Sensing, Vol. 26, pp. 774-789,(1988).

[5] Glitz, R. — The Use of Polarimetric Multifrequency SAR for Characterizing Terrain Classes.

Proc. of the Central Symposium of the 'International Space Year' Conf., Vol. II, pp. 411-418, Munich, Germany, March 30 - April 4, 1992.

[6] Van Zyl, J.J. — Calibration of Polarimetric Radar Images Using only Image Parameters and Trihedral Corner Reflector Responses.

IEEE Trans. on Geoscience and Remote Sensing.

[7] Zink, M., Heel, F. Kietzmann, H. — The Oberpfaffenhofen SAR Calibration Experiment of 1989.

Journal of Electromagnetic Waves and Application, Vol. 5, No. 9, pp 935-951, 1991.

Submit

THE NEED FOR RADAR SIGNATURE MEASUREMENTS

Alois J. Sieber, Carlo Lavalle
Institute for Remote Sensing Applications
Joint Research Centre
I–21020 Ispra – Italy

Parameters which are characteristic for selected objects are known as signatures for these objects. As an example one may think about the handwriting as being such a characteristic signature for the individual writer. One important task in working with radar data is to search for information about targets of interest which are unique for these objects. However, previous work with air– and spaceborne radar images demonstrated that the resulting object information does not only depend on the prime measurement parameters like the frequency, the polarization and the illumination geometry adopted in the measurement. Further important effects are due to the illumination technique, the length of the synthetic aperture or the changing illumination angle throughout the synthetic aperture, the bandwidth and,as a consequence, it seems that each system, air or space–borne, shows different object features.

The upcoming two years will provide for the first time unique opportunities to compare target information collected almost simultaneously over the identical sites by SAR systems on the successfully working ERS–1 of ESA, the Japanese ERS–1, the unique multi–temporal Shuttle Imaging Radar (SIR) programme, the NASA/JPL multiparameter AIRSAR, the Canadian multi parameter SAR sensor of the CCRS and INTERA, the European multi–parameters SAR sensor EARSEC as well as many ground based radar systems in different parts of the covered part of the earth. All these data collection efforts will be complemented by a device dedicated to radar signature measurements under fully controlled environmental conditions, the European Microwave Signature Laboratory (EMSL).

The paper will present a systematic approach to investigate the signatures of selected objects using controlled experiments and translating them into the real world by physically sound models.

While in–field experiments are locally fixed, while air–borne measurements are regionally bound and while space–borne systems are often discussed in the frame of global issues, the multi–parameters Shuttle Imaging Radar programme is a perfect tool for the data collection of geophysically calibrated radar signature on a large scale – if the interpretation of its data is physically based and supported by controlled signature measurements. The paper will demonstrate that the Shuttle Imaging Radar (SIR) programme and the work in the European Microwave Signature Laboratory (EMSL) are complementing each other and are linked by the North American and the European airborne SAR systems.

FUTURE PROGRAMS

SIR-C/X-SAR FREE FLYER CONCEPT

R. Monson

NASA Headquarters, Code SE
Washington, D. C.

SPACEBORNE IMAGING RADAR - C

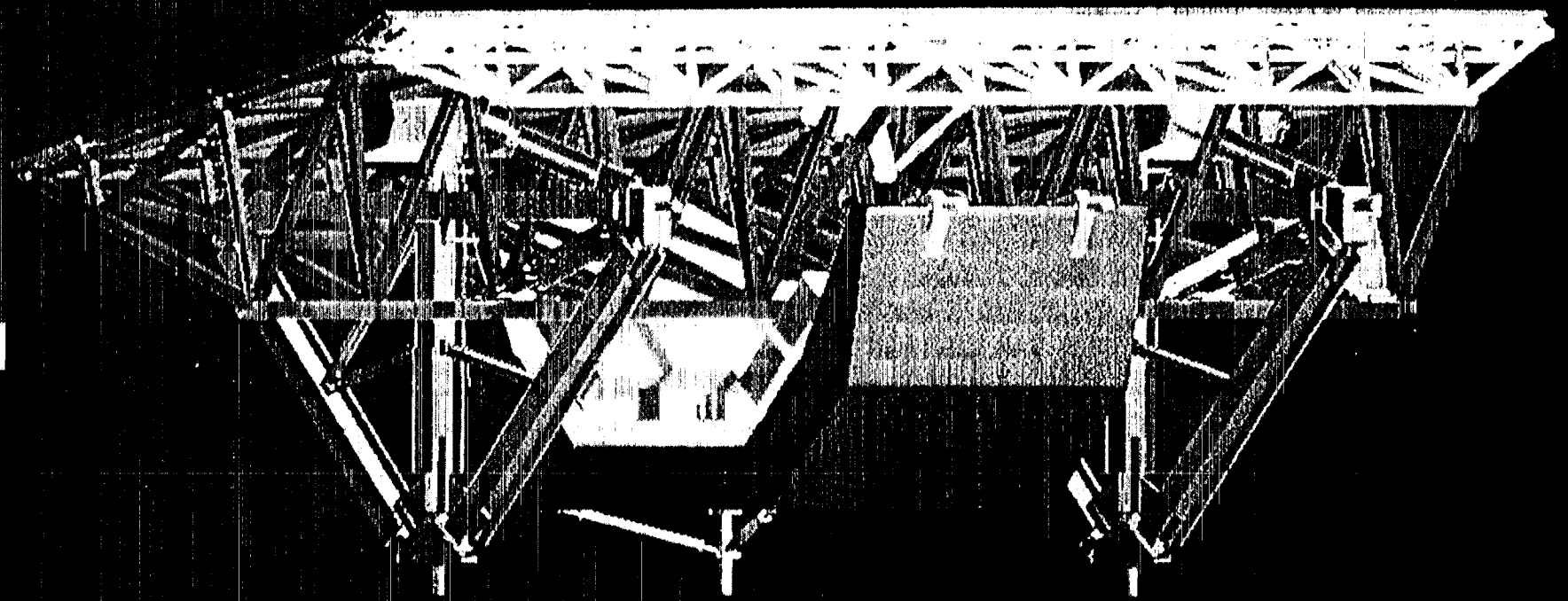

234

- X-SAR PANELS
- L-BAND PANELS
- C-BAND PANELS
- PALLET
- ANTENNA CORE STRUCTURE (ACS)
- ANTENNA TRUNNION STRUCTURE (ATS)
- X-SAR SUPPORT STRUCTURE (XSS) & TRI-DRIVE

SIR-C/X-SAR FREE FLYER CONCEPT - OVERVIEW

- WHAT IS IT?
  - THE ADDITION OF SPACECRAFT SUBSYSTEMS TO EXISTING SIR-C/X-SAR SUBSYSTEMS TO PRODUCE A FREE FLYING, NEAR-TERM MULTIPARAMETER SPACEBORNE SAR
  - INTERIM CAPABILITY LEADING TO EOS SAR/MULTISAR ERA
- WHY?
  - PROVIDES OPPORTUNITY FOR A ONE (PLUS) YEAR DATA SET AT A MODEST COST
  - PROVIDES A SCIENCE DATA SET NOT POSSIBLE WITH AN ATTACHED PAYLOAD
  - PROVIDES SCIENCE COMMUNITY WITH LONGER TERM MULTIPARAMETER SAR DATA SOON.
  - PROVIDES OPPORTUNITY TO DEMONSTRATE A RAPID TURNAROUND ENGINEERING PROJECT IN ADDITION TO PLACING A VERY HIGH PERFORMANCE SET OF INSTRUMENTS IN ORBIT
- WHEN?
  - WHEN SCIENCE RESULTS DEMONSTRATE NEED FOR MULTIPARAMETER SAR

SCIENCE OBJECTIVES

1. EXTEND SIR-C/X-SAR MULTIFREQUENCY, MULTIPOLARIMETRIC, MULTIINCIDENCE ANGLE OBSERVATIONS TO PRODUCE DATA SETS OVER MULTIPLE SEASONS AND OVER MORE SITES

2. EXTEND SIR-C/X-SAR ALGORITHM VALIDATION OVER A MULTISEASONAL PERIOD

3. COLLECT A GLOBAL* MULTIPARAMETER SAR DATA SET AS AN EOS SAR PRECURSOR

4. BEGIN THE GLOBAL SCALE GEOPHYSICAL PRODUCT SET CONSISTENT WITH THOSE PLANNED FOR EOS SAR/MULTISAR
   - CALIBRATED
   - VALIDATED AGAINST GROUND TRUTH

*TO 57° LATITUDE

SCIENCE RATIONALE

GLOBAL GEOPHYSICAL PRODUCTS:

- ALGORITHMS VALIDATED LOCALLY WITH AIRCRAFT SARs, ERS-1, JERS-1, RADARSAT, AND SHUTTLE-BASED SIR-C/X-SAR
- GLOBAL PRODUCTS ARE HIGH PRIORITY FOR CLIMATE MODELS (E.G., VEGETATION TYPE, AERODYNAMIC SURFACE ROUGHNESS)

REGIONAL ALGORITHM VALIDATION:

- IMPORTANCE OF MULTITEMPORAL OBSERVATIONS SHOWN BY AIRCRAFT SARs AND ERS-1
- SIR-C/X-SAR SHUTTLE MISSIONS PROVIDE MAXIMUM OF THREE SHORT PERIODS IN TIME
- EXTENDED MULTITEMPORAL DATA WILL ALLOW:
  - MONITORING
  - PROVIDE ADDITIONAL DIMENSION TO ENHANCE CLASSIFICATION
  - MUST BE UNDERSTOOD AS IT AFFECTS ANY OPERATIONAL ALGORITHM
- MEANS OF ASSESSING TRADEOFFS BETWEEN SEASONAL MULTITEMPORAL OBSERVATIONS AND FREQUENCY/POLARIZATION DIVERSITY

GEOPHYSICAL PARAMETERS FROM SAR

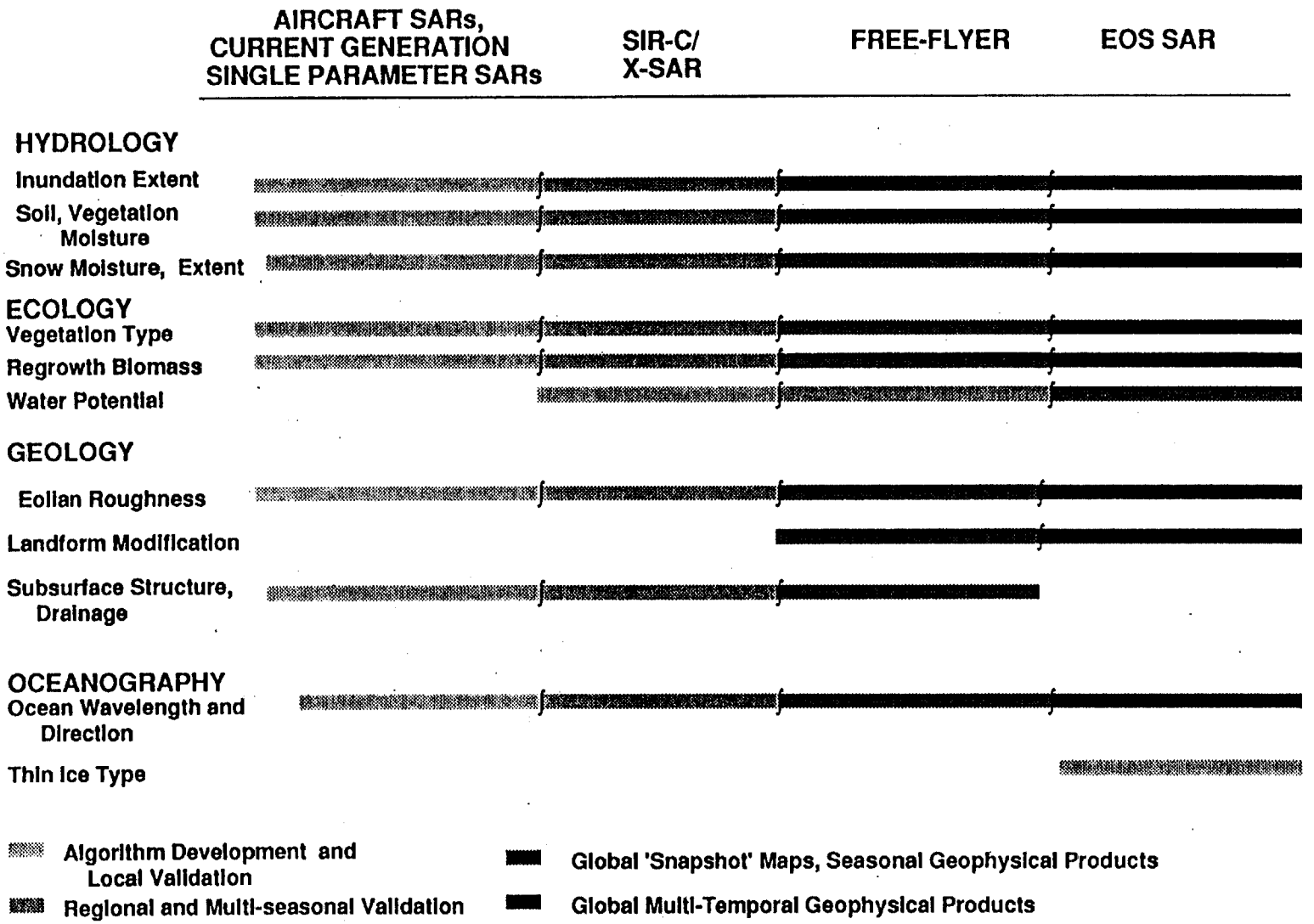

PROGRAMMATIC GOALS

- PROVIDE A NEAR-TERM, INTERIM, HIGH-PERFORMANCE MULTIPARAMETER FREE FLYER SAR
- DEMONSTRATE LONG-TERM STABILITY OF NEW TECHNOLOGY SARs
- PROVIDE A HIGH-CAPABILITY SYSTEM AT MODEST COST
- MAXIMIZE SCIENCE RETURN FOR INVESTMENT TO DATE
- EARLY START FOR EOS SAR DATA SET INCLUDING PROCESSING DISTRIBUTION AND ARCHIVING
- DEMONSTRATE A FAST TRACK IMPLEMENTATION

CONCEPT DESCRIPTION

- COMPLETE SIR-C/X-SAR SHUTTLE MISSIONS
- UTILIZE A SHUTTLE FLIGHT OPPORTUNITY TO PLACE AN AUGMENTED SIR-C/X-SAR SYSTEM IN ORBIT
- AUGMENTATION CONSISTS OF ADDING SPACECRAFT SUBSYSTEMS TO EXISTING STRUCTURE
- SUBSYSTEMS ARE LARGELY EXISTING DESIGNS TO PROVIDE ELEMENTS NOW SUPPLIED BY STS
  - POWER
  - THERMAL CONTROL
  - DATA STORAGE/COMMUNICATIONS
  - COMMAND AND CONTROL
  - ATTITUDE CONTROL
  - PROPULSION

} POSSIBLE USE OF MARS OBSERVER SPARES

SIR-C/X-SAR FREE FLYER CONSTRAINTS AND ASSUMPTIONS

- COOPERATIVE PROGRAM WITH GERMANY AND ITALY (X-SAR)
- NO CHANGES (OTHER THAN REPAIR, IF NEEDED) TO EXPERIMENT HARDWARE
  - SAME BOXES, INTERFACES
- AUGMENT EXISTING STRUCTURE TO PROVIDE STRUCTURAL FUNCTIONS OF SPACELAB PALLET
- LAUNCH FROM STS. USE SPACECRAFT PROPULSION TO RAISE ORBIT
- WILL REQUIRE A CONTROLLED REENTRY
- INITIALLY PROCESS DATA THROUGH SYSTEMS BASED ON EXISTING SIR-C AND X-SAR DATA SYSTEMS AUGMENTED BY ALASKA SAR FACILITY
- EVENTUALLY UTILIZE EOS DIS FOR DATA STORAGE / CATALOGING / DISTRIBUTION
- LAUNCH DATE DRIVEN BY IMPLEMENTATION LEAD TIME, SIR-C/X-SAR RESULTS, AND SPACE STATION UTILIZATION OF STS
- COST IS THE PRINCIPAL DETERMINANT OF FEASIBILITY

A CONFIGURATION CONCEPT

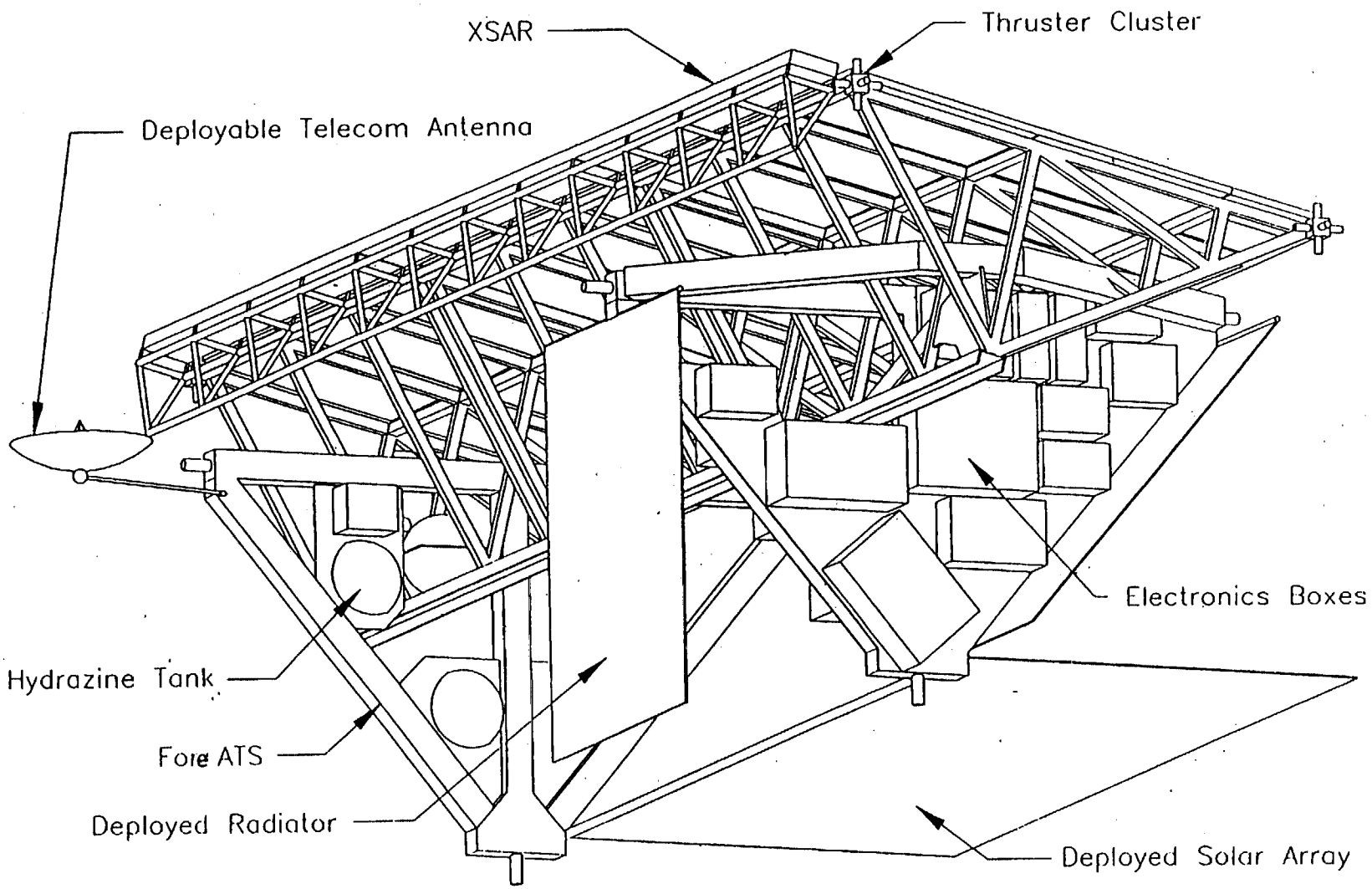

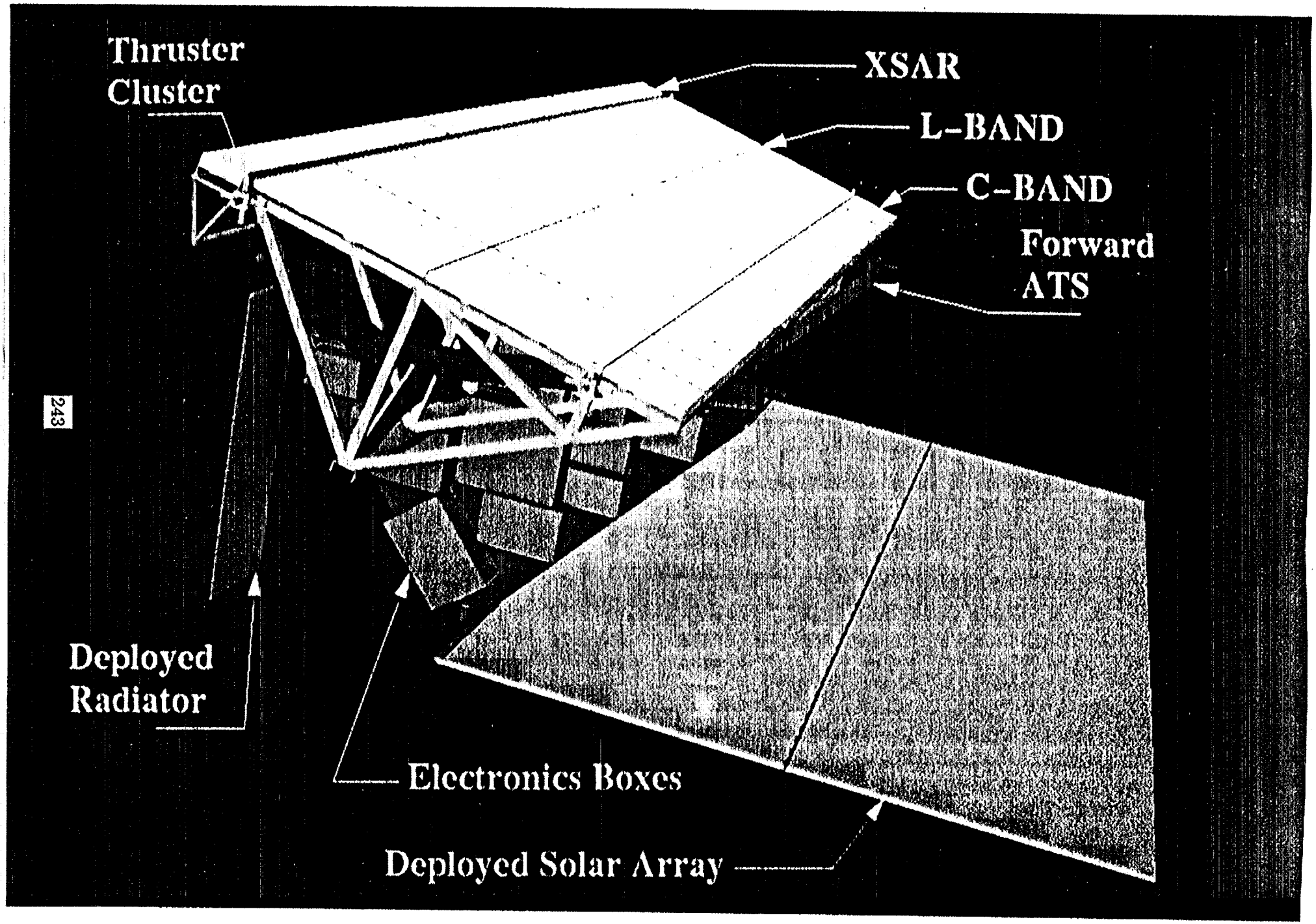
Thruster Cluster
XSAR
L-BAND
C-BAND
Forward ATS
Deployed Radiator
Electronics Boxes
Deployed Solar Array

A CONFIGURATION CONCEPT

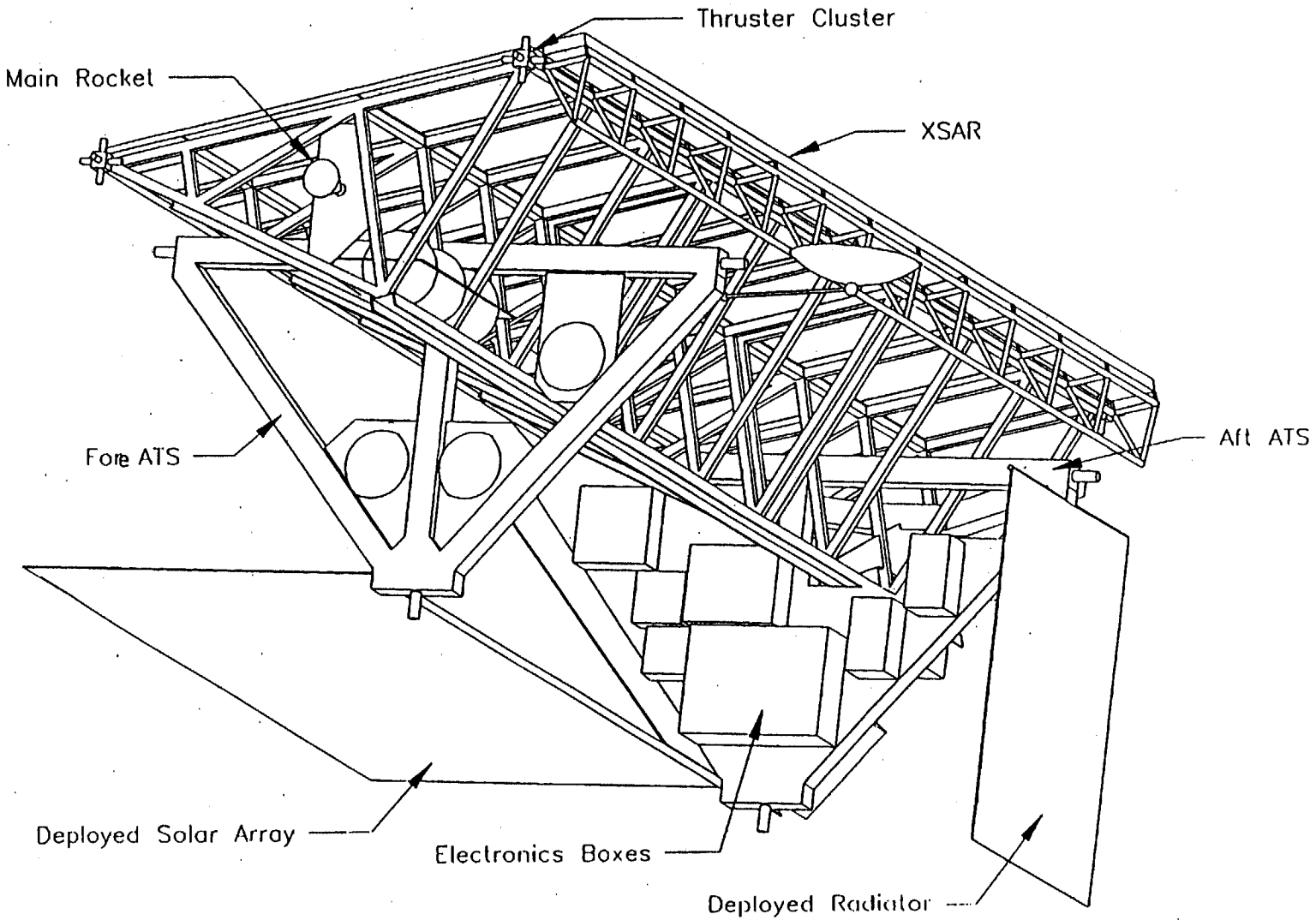

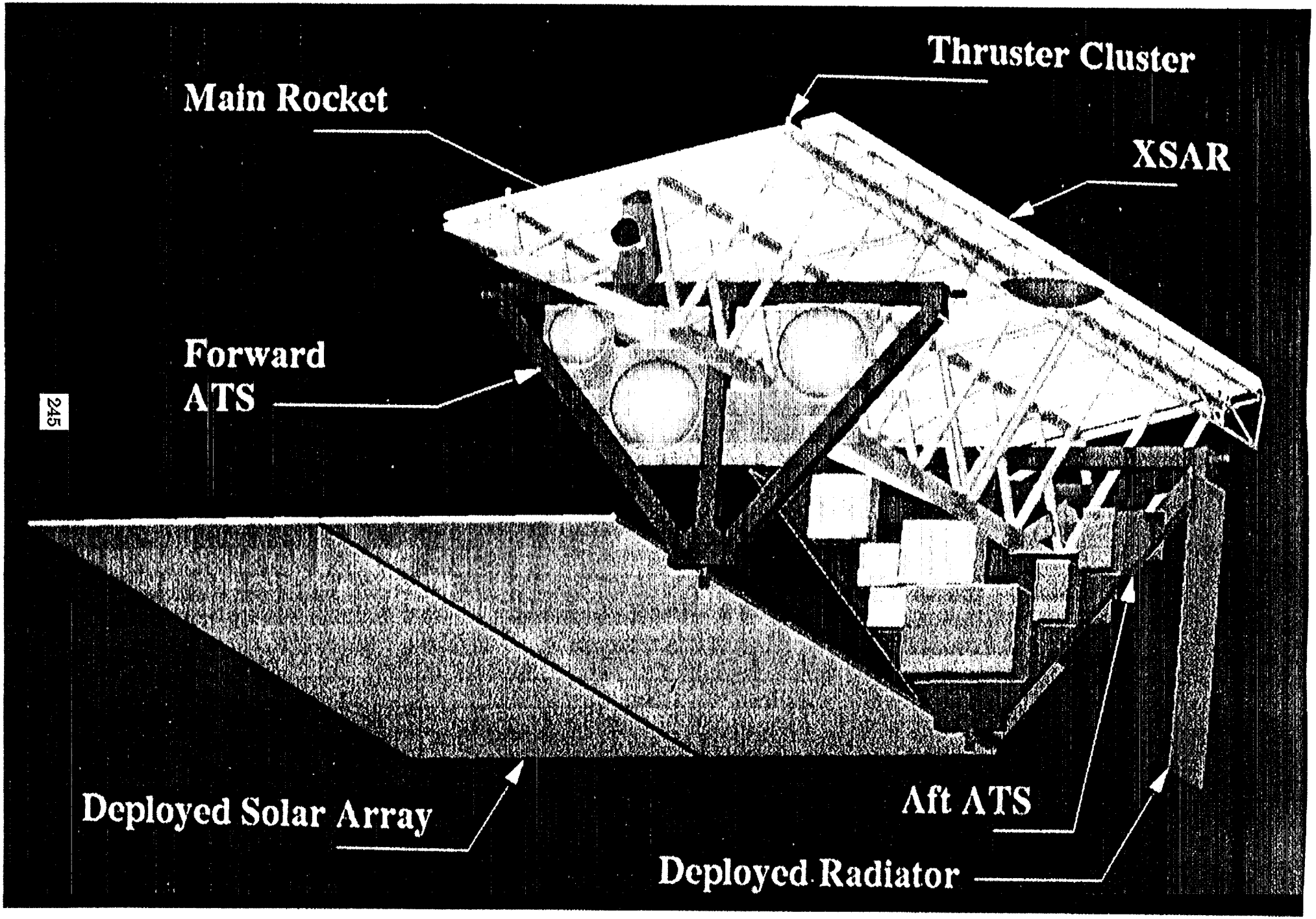
Thruster Cluster
Main Rocket
XSAR
Forward
ATS
Deployed Solar Array
Aft ATS
Deployed Radiator

A CANDIDATE MISSION DESCRIPTION

- LAUNCH ON STS AT 57° INCLINATION TO MAXIMUM ATTAINABLE ALTITUDE
- RAISE ORBIT WITH ON-BOARD PROPULSION UP TO HIGHER ALTITUDE
  - GREATER THAN OR EQUAL TO 50 KM WIDE SWATH
  - ALLOWS GLOBAL COVERAGE (±57° LATITUDE)
- ORBIT MANEUVERS ON 7-DAY INTERVALS ALLOWS GROUND TRACK CONTROL ±1 KM
- MISSION LIFE OF ONE YEAR REQUIREMENT, EXTENDED PAST THAT AS A GOAL
- DATA ACQUISITION - 200 MBPS FOR APPROXIMATELY 10 PERCENT DUTY CYCLE
- TARGETED REENTRY WILL BE REQUIRED (APPROXIMATELY 100 M/SEC DELTA V)

SIR-C Freeflyer - 450 km altitude
40° incidence angle, left-looking, 70 km swath
Days 1-6 (descending tracks), 2 min ticks

Orbit: J2
Map: Ortho (40N,100W - 3.5 Zoom)
Daren Casey - 8 Jan 1993

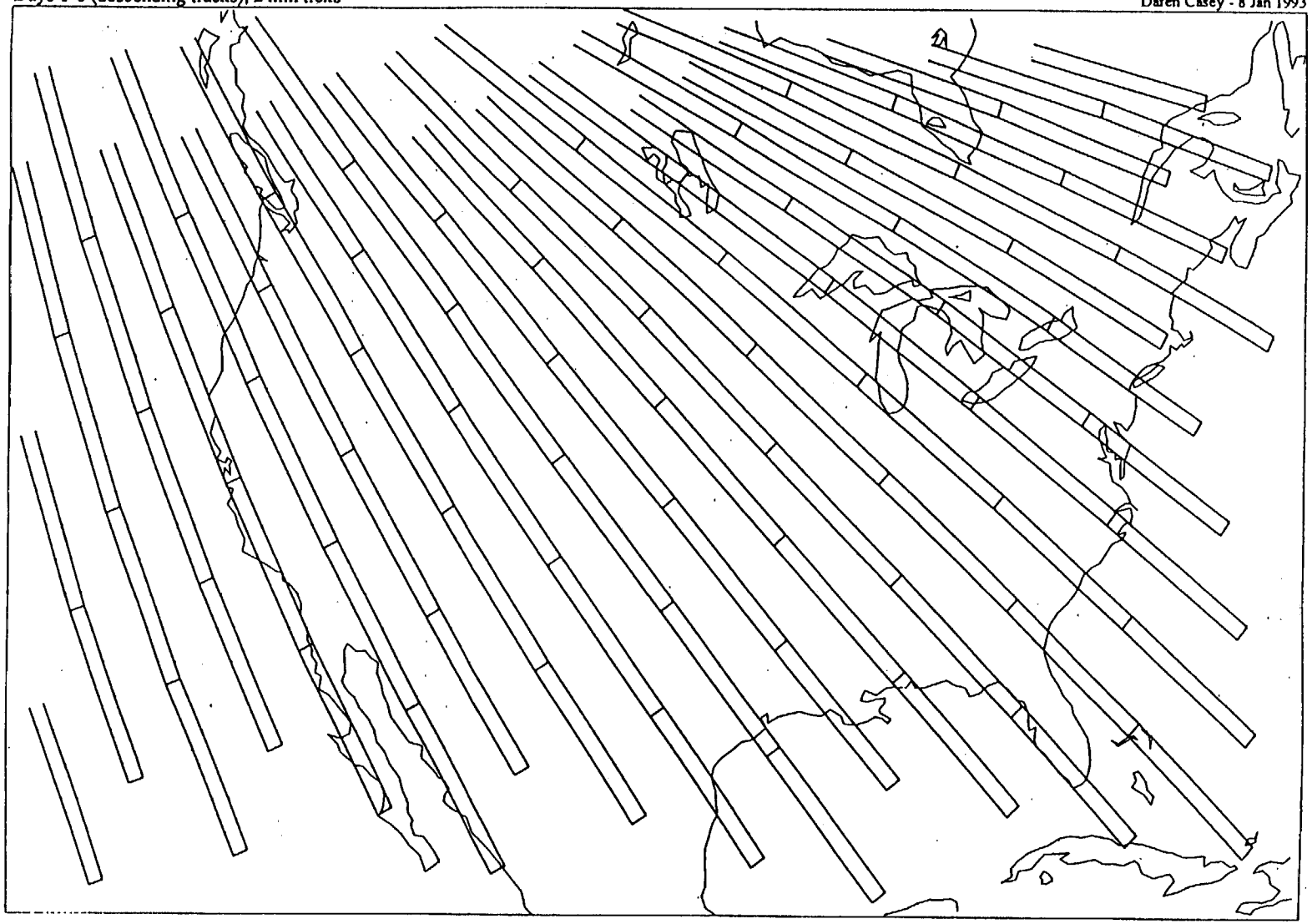

AN IMPLEMENTATION SCENARIO

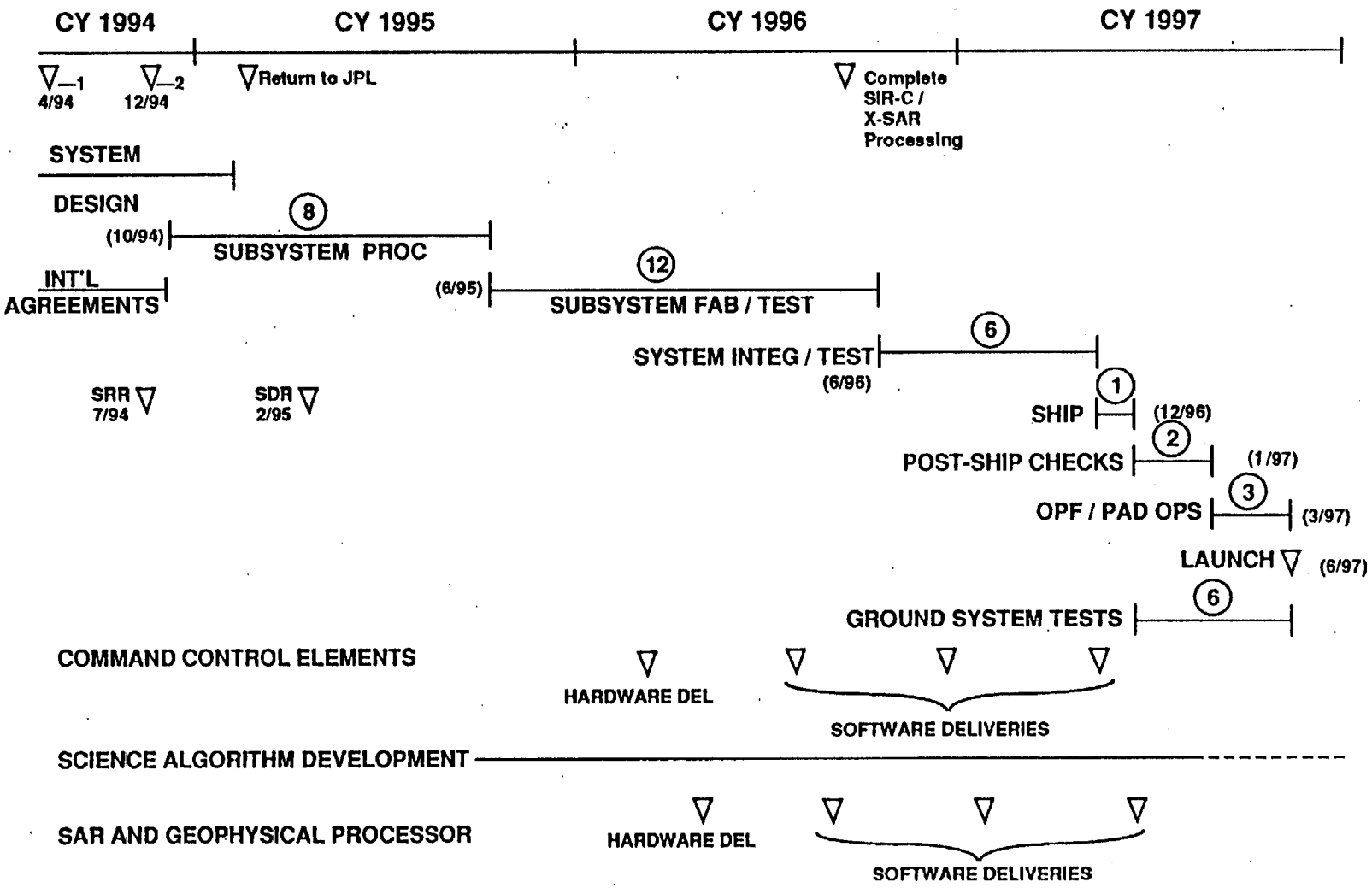

SUMMARY

- RECENT LOOK AT PLACING THE EXISTING SIR-C/X-SAR INSTRUMENTS IN LOW EARTH ORBIT SUGGESTS NO MAJOR TECHNICAL OBSTACLES EXIST
- CONTINUING INTERNATIONAL COOPERATION
- COST APPEARS TO BE MODEST AND AMOUNT WILL BE CRITICAL TO PROGRAM INITIATION
- SHUTTLE LAUNCH MANIFEST IS A SCHEDULE DRIVER
- MISSION COULD BE LOW COST IF EXECUTED QUICKLY USING EXISTING SUBSYSTEM DESIGNS
- SIGNIFICANT SCIENCE VALUE. BEGINS EOS SAR GLOBAL DATA SET EARLY

S/8-32
182858
N94-15964

EOS SAR: A New Approach

JoBea Way
Jet Propulsion Laboratory
California Institute of Technology

The Mission

Earth Observing System Goals:

Develop the modeling and observational capabilities to predict and/or monitor atmospheric, terrestrial and oceanic processes that are either causing global change or resulting from global change

EOS SAR Goals:

To provide important geophysical products to the EOS data set to improve our understanding of the state and functioning of the Earth system

EOS SAR Strategy:

Define the instrument requirements based on required input to geophysical algorithms

Provide the processing capability and algorithms to generate such products on the required spatial (global) and temporal (3-5 days) scales

Provide the spaceborne instrumentation with international partnerships

- initially with Germany
- currently exploring broader international partnerships

Geophysical Properties

Ecology:
Vegetation type
Water status
Biomass
Seasonal state
Fire extent

Hydrology:
Soil moisture
Snow moisture and extent
Inundation extent
Glacier zonation

Oceanography:
Sea ice type and motion
Wavelength and direction
Currents and eddies

Geology:
Landform distribution
Surface roughness
Subsurface structure and drainage

Progress in 1992

ERS-1 Polar Ice Results

- ERS-1/2 -> RADARSAT provide excellent data for polar ice community
- Polarimetric capabilities still required for thin ice type

Waring's SAR Vegetation Working Group *(Ecological Applications)*

- *Current understanding of vegetation products from SAR*
- *Value in ecosystem models*
- Freeze/thaw
- Biomass (<150 tons/ha)
- Inundation extent
- Water status

Engman's Hydrology Working Group and ISLSCP Workshop

- Soil moisture in root zone is the requirement
- Surface moisture measured by SAR may be related to soil moisture
- Algorithm independent of surface roughness developed (Ulaby)
- Shorter wavelength improves snow discrimination (Rott)

References

Operational Geophysical Products from SAR

Product	Band Reqmt's	Temporal Reqmt's
Current ASF for ERS-1:		
Sea ice motion	C-VV or C-HH	3-days
Sea ice type	C-VV or C-HH	3-days
Ocean wavelength and direction	C-VV or C-HH	weekly
JERS-1:		
Landform distribution	L-HH	once
Deforestation extent	L-HH	yearly
ASF Upgrade for RADARSAT/ERS-2:		
Glacier zonation	C-VV or C-HH	yearly
Freeze-thaw state	C-VV	< weekly
Fire extent	C-VV or C-HH	monthly
Inundation extent (tundra)	C-VV or C-HH	weekly
SIR-C/X-SAR Free Flyer:		
Vegetation type	L-quad, C-quad, X-VV	winter and summer
Regrowth biomass	L-quad	yearly
Surface roughness	L-quad, C-quad, X-VV	yearly
Subsurface structure/drainage	L-HH, high angle	once
EOS SAR:		
Soil moisture (and roughness)	L-quad	3 days, constant time of day
Snow moisture and extent	L-quad, C-quad, X	weekly, day-time
Vegetation water potential/moisture	L-quad, C-quad, X	diurnal
Thin ice type	L-quad	3 days
Inundation extent (forests)	L-HH	weekly

EOS SAR Mission Strategy: MultiSAR

Previous Strategy:

EOS SAR for all geophysical products:
- L- and C-band from U.S.
- X-band from Germany
- Single platform
- Mission start with EOS SAR launch

Potential International MultiSAR Strategy:

Obtain "baseline" global classification with SIR-C/X-SAR Free Flyer
- Geology products
- Vegetation type
- Regrowth biomass

Continue products started with ERS-1/2, JERS and RADARSAT
- Ice and ocean
- Glaciers
- Freeze/thaw, fire extent, inundation (tundra)

Design multiple spacecraft/SAR international mission series
- "hydrologic" properties
- change in "classification" properties

Split Concept for Global Data Products

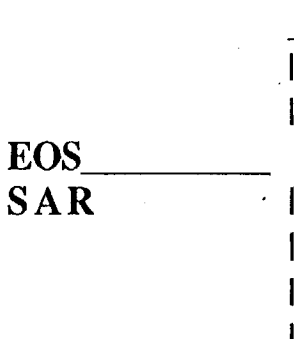

SIR-C/X-SAR Free Flyer

- Begin Long-Term Properties:
  - Geometry
  - High resolution
  - Multiple channels
  - Limited temporal coverage

MultiSAR

- Begin Temporally Varying Properties:
  - Dielectrics
  - Frequent temporal coverage
    - Select channels
    - Low resolution
- Continue Long-Term Properties

Outstanding MultiSAR Requirements

- *Outstanding relative to current international program and SIR-C/X-SAR Free Flyer*

Data Products:

Product	Band Reqm't	Temporal Reqm't
Soil moisture (and roughness)	L-quad	3 days, constant time of day
Snow moisture and extent	L-quad, C-quad, X	weekly, day-time
Vegetation water potential/moisture	L-quad, C-quad, X	diurnal
Thin ice type	L-quad	3 days
Inundation extent (forests)	L-quad	weekly

New Requirements:

Frequency/polarization:	L-quad, C-quad, X
Resolution:	250 - 500 m (L, C), 30 m (X)
Swath width:	500 km (including quad)
Calibration:	<1dB relative lifetime
Repeat coverage:	3-5 days
Equator crossing time:	1:30 p.m., 1:30 a.m.; dawn, dusk
Duty cycle:	20-50%

Potential Synergism of International MultiSAR Mission

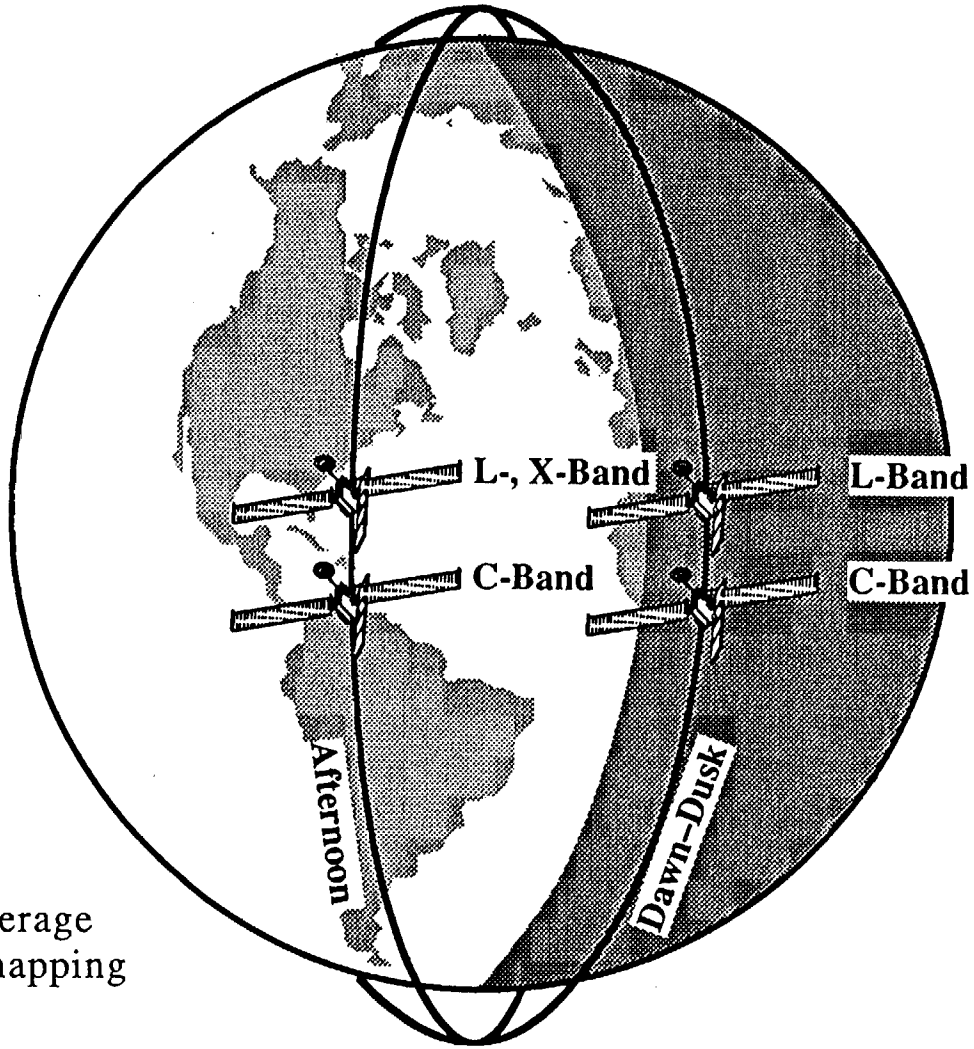

- diurnal coverage
- increased mapping

Evolution of Geophysical Products Through Long-Term International Program

ERS-1/2, RADARSAT, JERS-1 → SIR-C/ X-SAR Free Flyer → MultiSAR

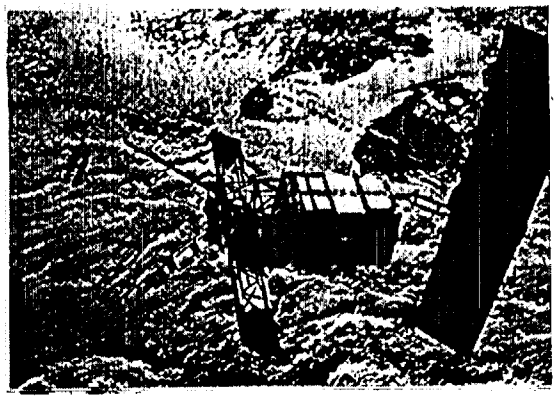

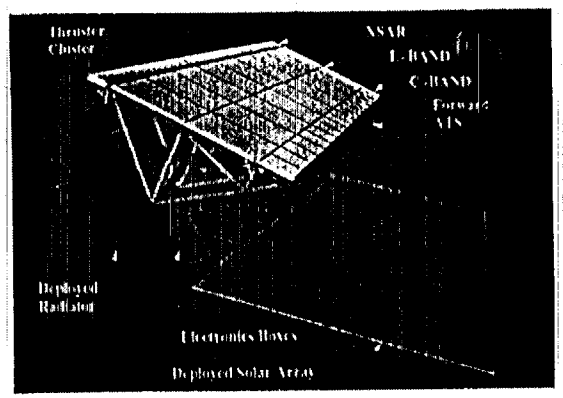

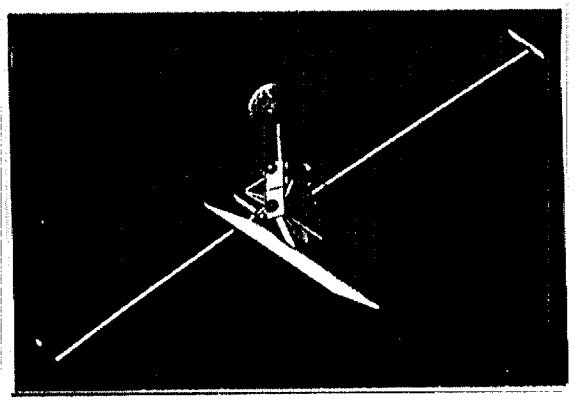

Sea Ice Type/Motion
Currents, Eddies, Internal Waves
Glacier Zonation
Freeze/Thaw State
Fire Extent
Inundation Extent (Tundra)
Landform Distribution
Deforestation Extent

Vegetation Type
Regrowth Biomass
Surface Roughness
Subsurface Structure/Drainage
Ocean Wavelength/Direction

Soil/Vegetation Moisture
Snow Moisture/Extent
Water Potential
Thin Ice Type
Inundation Extent (Forests)

Energy Flux → *Carbon Flux* → *Water Flux*

Conclusions

- Current international capabilities provide some temporally varying data products
- Multifrequency and multipolarization required for many products
- SIR-C/X-SAR Free Flyer provides initial look at long-term geophysical products
- Additional EOS SAR task is to add temporally varying water-related properties
  - must also continue long-term products
- International MultiSAR approach provides opportunity to optimize temporal multifrequency/pol. coverage of the globe

Next Steps

International agreement on science requirements

Series of discipline-oriented workshops and field campaigns

Mission scenario options for study

International approach to operational data product generation

519-43

182859

N94-15905

TOPSAT
GLOBAL SPACE TOPOGRAPHIC MISSION

Sergio Vetrella
University of Naples, Italy

Third Spaceborne Imaging
Radar Symposium

Figure 2. Percentages of total world area covered in each scale category, 1968-1974-1980-1987

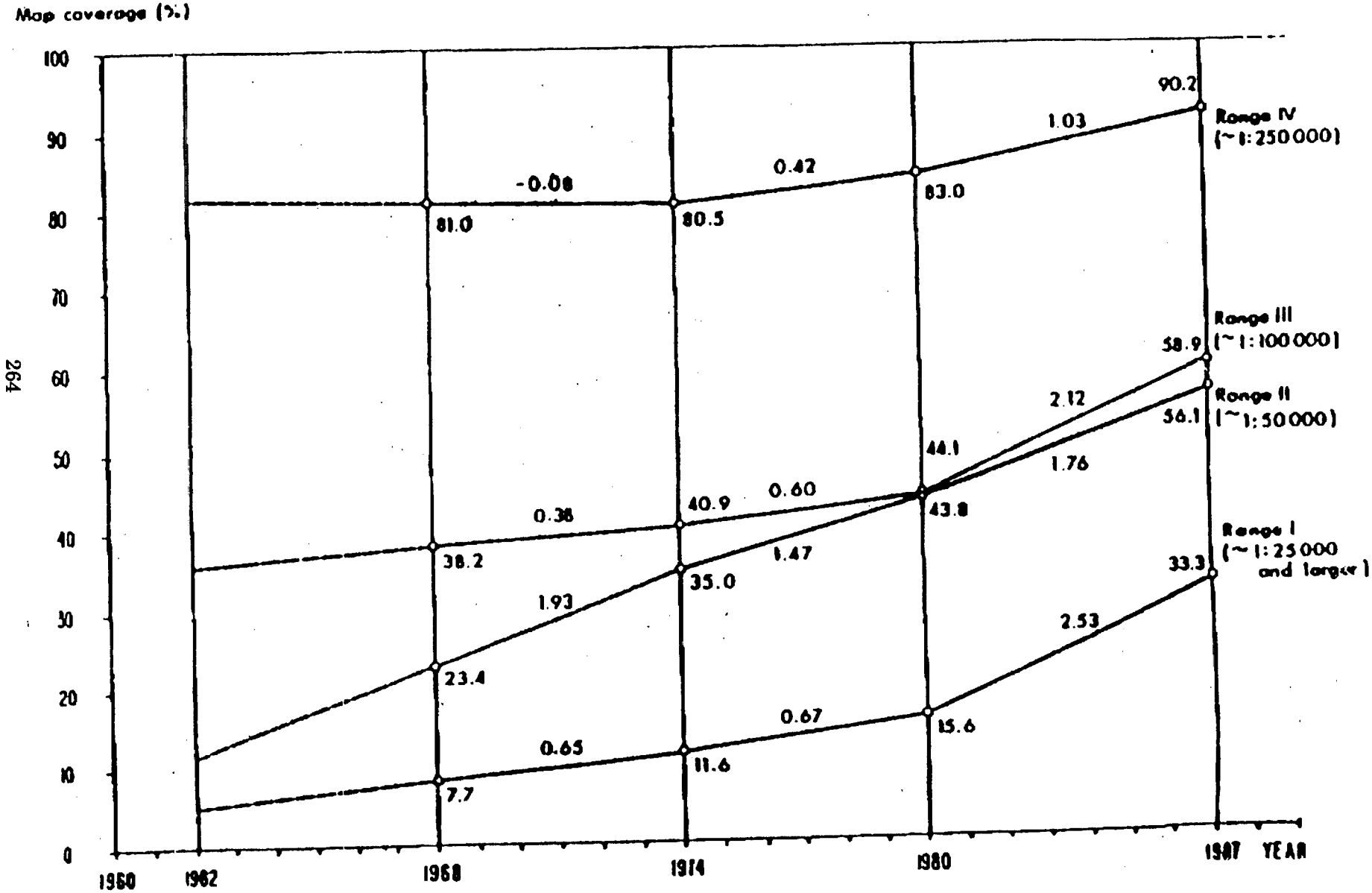

I	**HYDROLOGY**
I.1	Global water balance
I.2	Lumped catchment rfg.
I.3	Funct. rel. model
I.4	Snow accumulation
I.5	Fin. elem. / diff. mod.
I.6	Westland Circulation
II	**ECOLOGY**
II.1	Life Zones
II.2	Hillslope position
II.3	Wetland dynamics
III	**GEOMORPHOLOGY**
III.1	Tectonic provences
III.2	Mountain ranges
III.3	Large valley Systems
III.4	Hillslopes streams
III.5	Dunes
III.6	Coastal Changes
III.7	Large landslides and landslides fields in seismically active areas
III.8	Worldwide landslide mapping
III.9	Study of specific landslides
IV	**GLACIOLOGY**
IV.1	Glacial Moraines
IV.2	Alpine glaciers
IV.3	Ice sheets
V	**GEOLOGY/GEOPHYSICS**
V.1	Gravity/Magnetics
V.2	Plate boundaries
V.3	Marine geology
V.4	Structural geology
V.5	Fault Zone Tectonics
V.6	Flow and ash volumes
V.7	Volcanic swelling
V.8	Volcano morphology
V.9	Global long term monitoring in regional tectonic movements
V.10	Subsiding area
VI	**DISASTER MANAGEMENT**
VI.1	Earthquakes
VI.2	Volcanic Eruptions
VI.3	Avalanches
VI.4	Landslides
VI.5	Floods
VI.6	Wildfire
VII	CARTOGRAPHY
VII.1	1:1.000.000
VII.2	1: 500.000
VII.3	1: 250.000
VII.4	1: 100.000

CONTINENTAL TOPOGRAPHY

JPL

POLAR REGION APPLICATIONS

WHY STUDY THE POLAR REGIONS?

- POLAR ICE SHEETS HOLD 80-90% OF WORLD's FRESH WATER
- CHANGES IN ICE SHEET VOLUME COULD HAVE MAJOR EFFECTS ON GLOBAL SEA LEVEL AND CLIMATE
- ICE SHEET STABILITY IS NOT KNOWN
- ATMOSPHERIC CO_2 IS INCREASING; GREENHOUSE EFFECT?

WHY IS ELEVATION DATA IMPORTANT IN THE POLAR REGIONS?

1) BASIC LANDFORM INVENTORY

- UNDULATIONS
- RIFTS
- FLOW LINES

} GIVE INFORMATION ON DETAILED FLOW DYNAMICS

2) MASS BALANCE AND DYNAMICS

- ICE FLOW IS RELATED TO SURFACE HEIGHT AND THICKNESS
- REPEAT, HIGH RESOLUTION ELEVATION DATA WOULD ALLOW MONITORING OF ICE TRANSPORT AND ABLATION

CONTINENTAL TOPOGRAPHY

TERRESTRIAL ECOSYSTEM APPLICATIONS

- ABSOLUTE ELEVATION, LOCAL SLOPE AND SLOPE ASPECT (e.g., N OR S-FACING) EXERT FUNDAMENTAL INFLUENCE ON THE TERRESTRIAL ECOSYSTEM

  EXAMPLES INCLUDE:

  1) TEMPERATURE, INFLUENCED BY
     a) ABSOLUTE ELEVATION
     b) SLOPE ASPECT

  2) MOISTURE AVAILABILITY, INFLUENCED BY
     a) OROGRAPHIC EFFECTS
     b) REGIONAL DRAINAGE NETWORKS
     c) LOCAL RUNOFF CONDITIONS
        i) LOCAL SLOPE
        ii) SLOPE ASPECT (AFFECTS EVAPO-TRANSPIRATION)
     d) SOIL TYPE, AFFECTED BY
        i) ABSOLUTE ELEVATION
        ii) LOCAL SLOPE
        iii) SLOPE ASPECT

- MOST OF THESE APPLICATIONS REQUIRE

  1) HIGH SPATIAL RESOLUTION TOPOGRAPHIC DATA, ≅ 30 m (TO MATCH) RESOLUTION OF IMAGING SENSORS SUCH AS LANDSAT TM)

  2) GOOD VERTICAL ACCURACY (5 m OR BETTER) FOR ACCURATE SLOPE CALIBRATION

- EXISTING DATA ARE INADEQUATE; BEST QUALITY DEM DATA MAY HAVE 30 m HORIZONTAL RESOLUTION. BUT VERTICAL ACCURACY 10-50 m DEPENDING ON RELIEF

Table 1 - List of requirements for each of the applications

Application	Planimetric Resolution min-max	Planimetric Error A/P min max	Altimetric error A/P min-max	Extent G/R/L	Site E/A/SS	Repetitevity	Vegetation V/G	Sensor I(m)/N	Mission Lifetime
HYDROLOGY									
Global water balance	1000-100	500-100	10-5	G	E	0.5	G	I(2)	>10
Lumped catchment rtg.	500-50		$5\text{-}1^{A}$	R	A	∞	V		
Funct. rel. model	100-50		$1\text{-}0.5^{P}$	R	A	∞	V		
Snow accumulation	80-10	50-20	$1^{A}\text{-}02$	R/L	E	0.3	G	I(2)	>10
Fin. elem./ diff. mod.	20-8		$0.6\text{-}0.1^{P}$	L	SS	∞	G		
Westland circulation	700-100		$0.2\text{-}0.1^{A}$	R	A/SS	∞	G		
ECOLOGY									
Life zones	5000-1000		$10\text{-}5^{A}$	R	A	∞	V	I(>6)	
Hillslope position	60-10		1-0.5	L	E	∞	G		
Wetland dynamics	700-100		$0.1\text{-}0.05^{A}$	R	A	5	G	I(2)	
GEOMORPHOLOGY									
Tectonic provences	10.000-2000		$100\text{-}40^{A}$	G	A	∞	G	I	
Mountain ranges	5000-200		$50\text{-}8^{A}$	G	A	∞	G		
Large valley systems	500-100		$10^{A}\text{-}1$	R	A	∞	G	I	

Application	Planimetreic resolution min	max	Planimetric erorr min	max A/P	Altimetric error min	max A/P	Extent G/R/L	Site Select E/A/SS	Frequency repetitivity period	Vegetation V/G	Class numeric value I/N	Mission lifetime	Note
Cartografy (scale)													
1:1.000.000	57	95	100 300	(A)	30 (A)	60	G	E	10	G/V	8	~~more~~ > 10	
1:500.000	29	48	50 150	(A)	15 (A)	30	G/R	E	10	G/V	8	~~more~~ > 10	
1:250.000	14	25	25 (A)	75	8 (A(	16	R	E/SS	7	G/V	8	~~more~~ > 7	
1:100.000	6	10	10 (A)	30	6 (A)	12	R/L	SS	5	G/V	20	> 3	
1:50.000	3	5	5 (A)	15	3 (A)	6	L	SS	5	G/V	20	> 3	
1:25.000	1,5	2,5	2,5 (A)	7,5	1,5 (A)	3	L	SS	5	G/V	20	> 3	

GLOBAL TOPOGRAPHY MISSION

SCIENCE REQUIREMENTS

Obtain global, contiguous Earth center-of-mass referenced surface elevation measurements with horizontal resolution of 30 m, horizontal accuracy of 10 m, and vertical accuracy of 1 - 3 m over $\geq$ 95% of the Earth's land surfaces and ice sheets.

Obtain regional, contiguous Earth center-of-mass referenced surface elevation, roughness, and vegetation height measurements with horizontal resolution of 30 m, horizontal accuracy of 10 m, and vertical accuracy of 20 cm - 1 m over selected areas of the Earth's land surfaces and ice sheets.

Obtain complete global coverage in less than 6 months and continue measurement capability for at least 12 months in order to monitor seasonal and shorter period changes of ice, vegetation, wetlands, and time-varying landforms.

Stereo electro-optical sensors

- Along-track stereoscopic observation (e.g. Large Format Camera, Stereo MOMS)
  - allows simultaneous acquisition of a stereoscopic pair
  - requires a complex attitude control system to ensure automatic correlation along epipolar planes

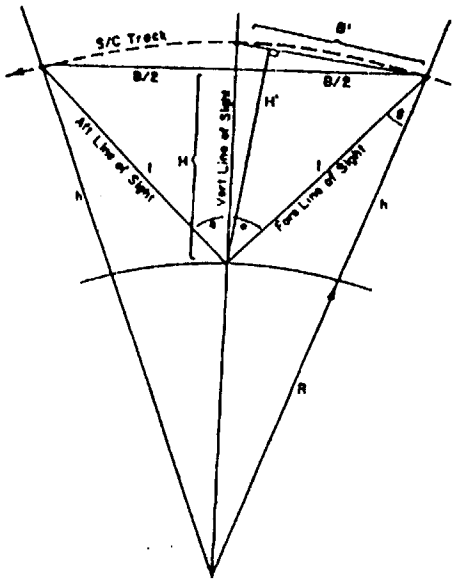

- Cross-track stereoscopic observation (e.g. HRV SPOT)
  - stereoscopic pair obtained from two different orbits under different illumination conditions

LATERAL STEREOSCOPY PRINCIPLE

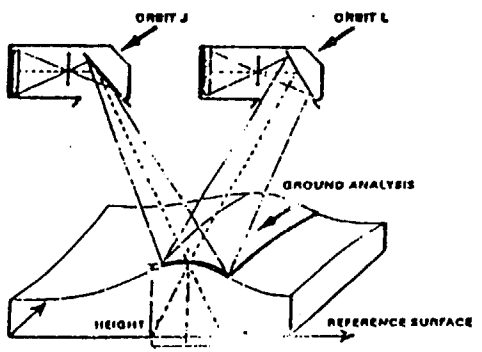

SPACE-BASED STEREOSCOPIC * MISSIONS

INSTRUMENT/ MISSION	AGENCY/ YEAR	RESOLUTION OR GROUND PIXEL SIZE (m)	BASE/ HEIGHT	RMS-ACCURACY (m) HEIGHT†	RMS-ACCURACY (m) PLANIM.	TOTAL GROUND COVER‡ 10^6 km^2	SWATH WIDTH km
METRIC CAMERA SPACELAB-1/STS-9	ESA/DFVLR 1983	~13	1:3-1.6	15	15	12	190
LARGE FORMAT CAM. STS-41C	NASA 1984	~8	1:1.6-1:0.8	10	10	8	190
HRV SPOT-1	CNES 1986	10	1:2-1:1	10	10	?	60
MEOSS SROSS-II	DFVLR/ISRO 1988	80	1:1	~50	~30	INDIA, SOUTHERN EUROPE	255
HRV SPOT-2	CNES 1988/89	10	1:2-1:1	10	10	NOT DEFINED	60
METRIC CAMERA ATLAS-1	DFVLR/NASA 1991	5	1:3-1:1.6	~10	~10	10	190
STEREO-MOMS SPACELAB-D2	DFVLR/NASA 1991/92	5-10	1:1	~10	~10	0.25	32
SPOT 3	CNES 1991/92	10	1:2-1:1	10	10	NOT DEFINED	60
ADVANCED LANDSAT (LANDSAT-7)	EOSAT 1992	10	TBD	TBD	TBD	NOT DEFINED	41

* SOURCE: NASA TOPOGRAPHIC SCIENCE WORKING GROUP REPORT; M. SCHROEDER, DFVLR, 1987

† NOTE THAT VERTICAL ACCURACY DOES NOT MEET MAJORITY OF SCIENCE REQUIREMENTS

‡ PROBLEMS ASSOCIATED WITH CLOUD COVER DATA , REDUCTION COSTS, AND COSTS DUE TO NEED FOR EXTENSIVE GROUND CONTROL PRECLUDE FULL GLOBAL COVERAGE ($\simeq 2 \times 10^8$ km ^{2}LAND PLUS ICE SURFACE AREA) WITH OPTICAL STEREO

GLOBAL TOPOGRAPHY MISSION

OPTICAL STEREO APPROACH

ADVANTAGES

- EXISTING TOPOGRAPHIC DATA BASED ON OPTICAL STEREO (MAINLY AIRCRAFT); STRONG TECHNICAL HERITAGE
- SPACE-BASED STEREO (e.g., SPOT) IS FEASIBLE NOW FOR SELECTED AREAS; NO ADDITIONAL SPACE SEGMENT COSTS
- SPATIAL RESOLUTION 10-30 m

DISADVANTAGES

- VERTICAL PRECISION 5-10 m; VERTICAL ACCURACY >10 m, EXACT AMOUNT DEPENDING ON NUMBER OF GCP's
- GLOBAL COVERAGE UNLIKELY (LIMITED BY CLOUDS, ORBITAL CONSTRAINTS, IMAGING GEOMETRY)
- POLAR COVERAGE RESTRICTED DUE TO NEED FOR TERRAIN MATCHING AND TIE POINTS
- COVERAGE ACQUIRED PIECEMEAL (5-10 years) PRECLUDING CONTIGUOUS, UNIFORM QUALITY DATA SET, AND COMPLICATING CHANGE DETECTION
- COST
    - ACQUISITION COSTS AT CURRENT PRICES > $400 M
    - DATA REDUCTION
    - GROUND CONTROL POINTS

CONCLUSIONS

- "MISSION" COSTS > $500 M
- VERTICAL ACCURACY DOES NOT MEET SCIENCE REQUIREMENTS
- COVERAGE NOT GLOBAL
- DIFFICULT TO ENSURE UNIFORM QUALITY, CONTIGNUOUS DATA SET

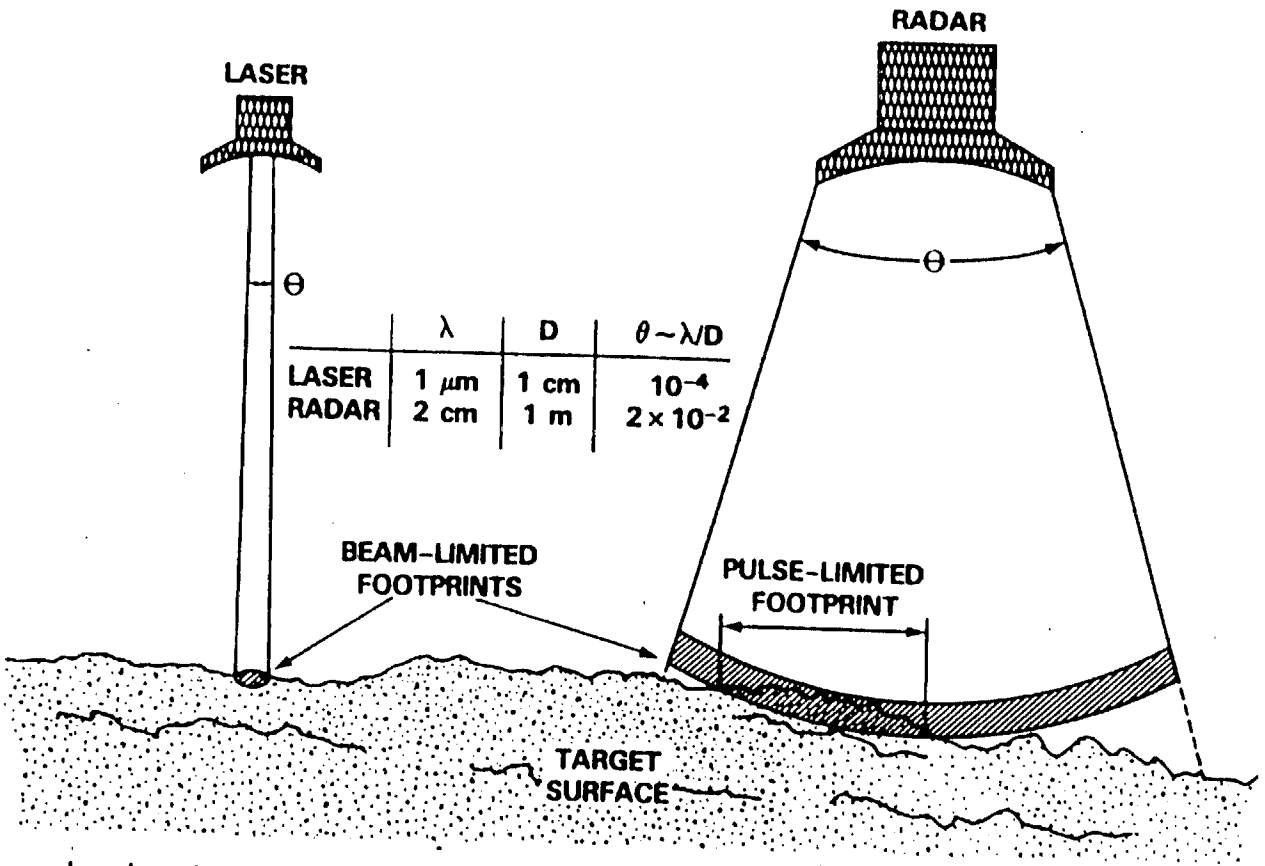

Comparison of laser and radar altimetry.

RADAR INTERFEROMETRY

THEORY

DEFINING GEOMETRY AND PARAMETERS:

SURFACE TOPOGRAPHY	z(x)
AIRCRAFT ALTITUDE	h
BASELINE DISTANCE	B
SLANT RANGE	ρ
LOOK ANGLE	θ
BASELINE ANGLE	α
PATH LENGTH DIFFERENCE	δ

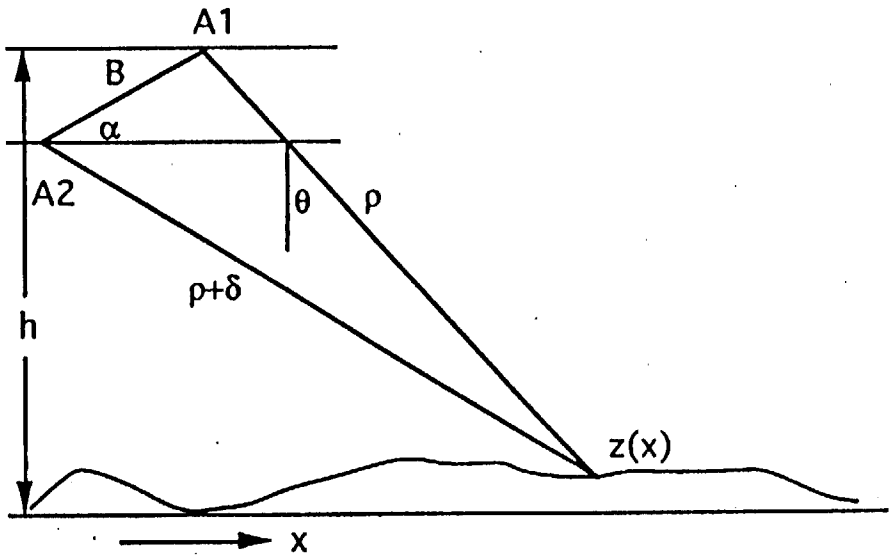

RESULTING EQUATIONS FOR MEASURED PHASE ϕ, WAVELENGTH λ

$$\delta = \phi\lambda/2\pi \qquad (1)$$

$$\sin(\theta-\alpha) = ((\rho+\delta)**2 - \rho**2 - B**2)/(2*\rho*B) \qquad (2)$$

$$z(x) = h - \rho\cos(\theta) \qquad (3)$$

TOPSAT SATELLITE IMPLEMENTATIONS

REPEAT PASS / SINGLE / TWIN SATELLITES

REPEAT PASS, 1 GHz

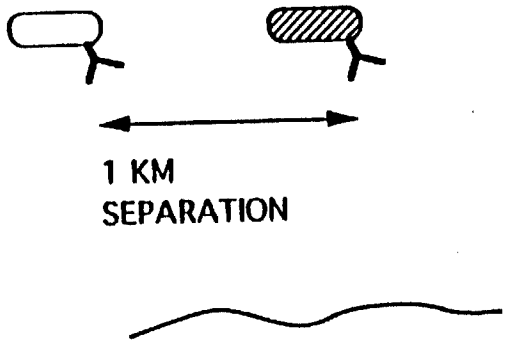

SINGLE SATELLITE, 35 GHz

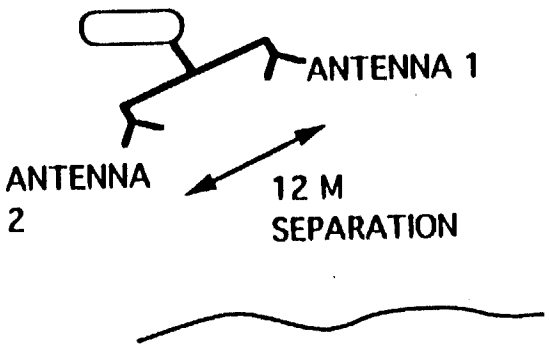

TWIN SATELLITES, 1 GHz

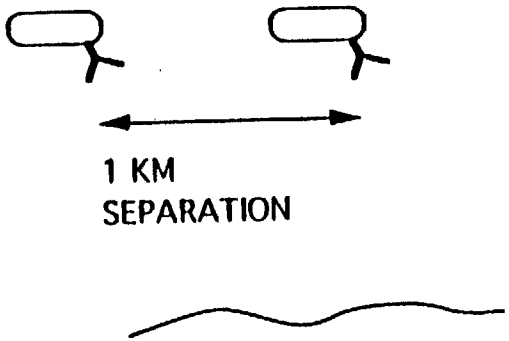

ALONG TRACK INTERFEROMETRY

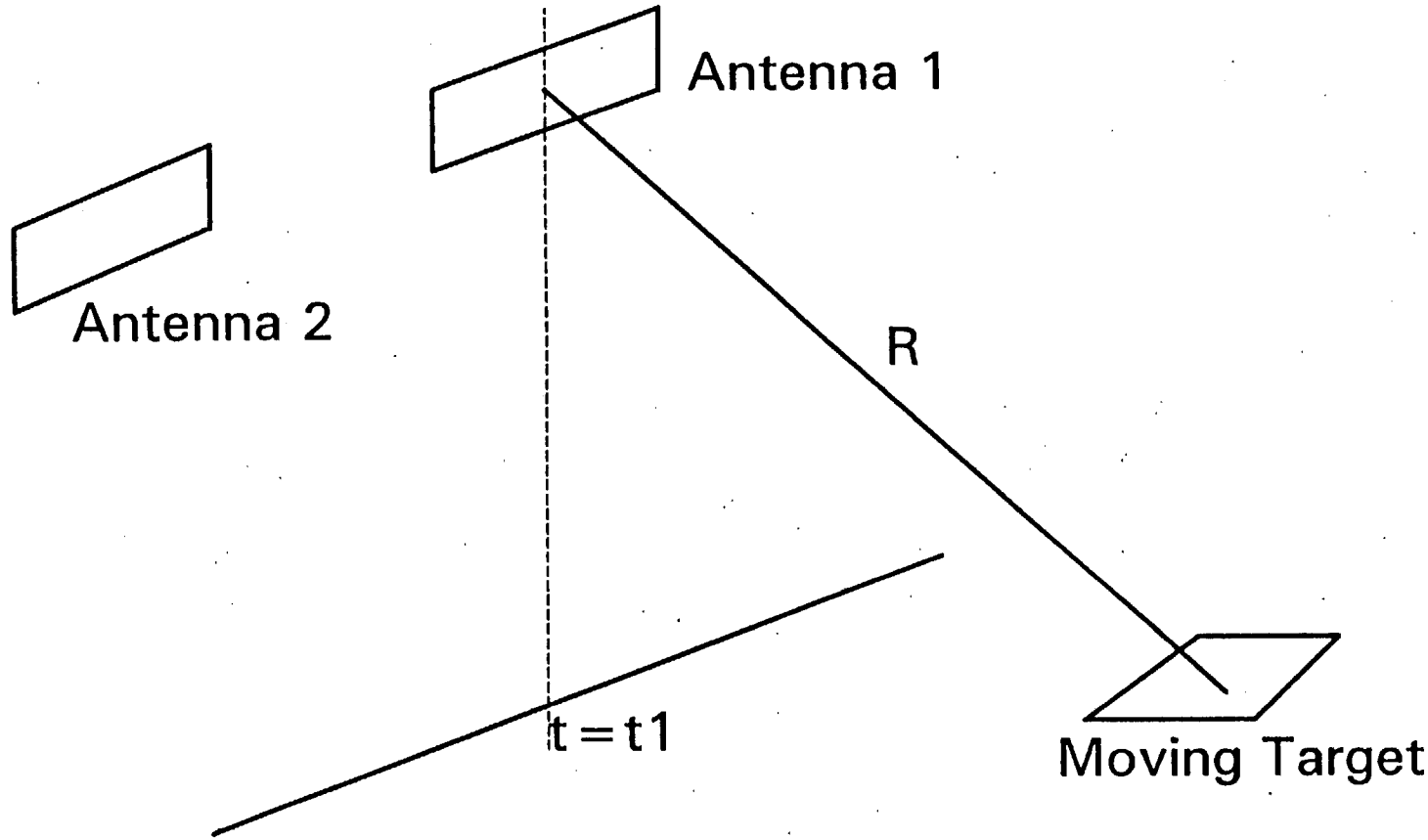

In the case of along-track interferometry, only the line of site velocity can be measured and therefore the along track velocity component is unknown.

VISTA

ON-ORBIT CONFIGURATION

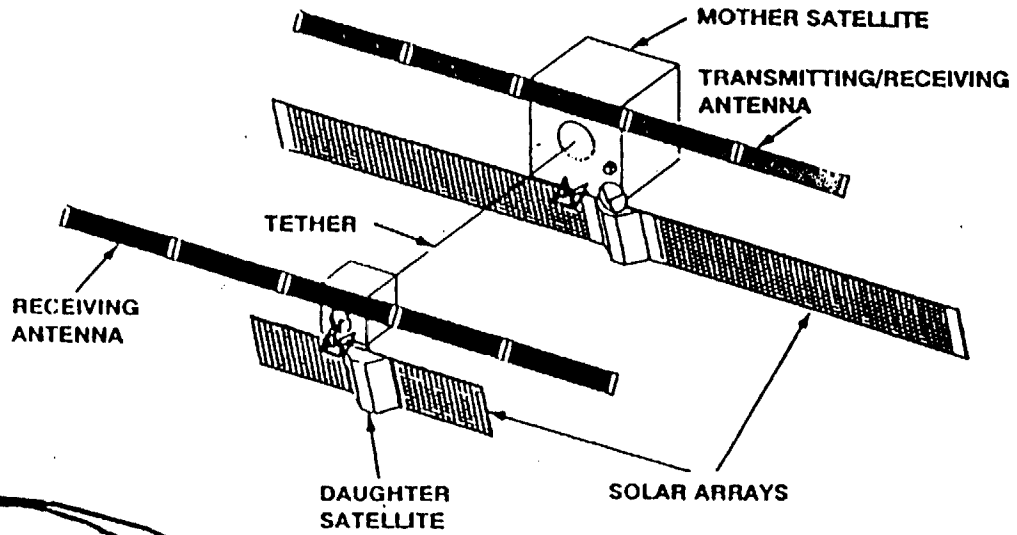

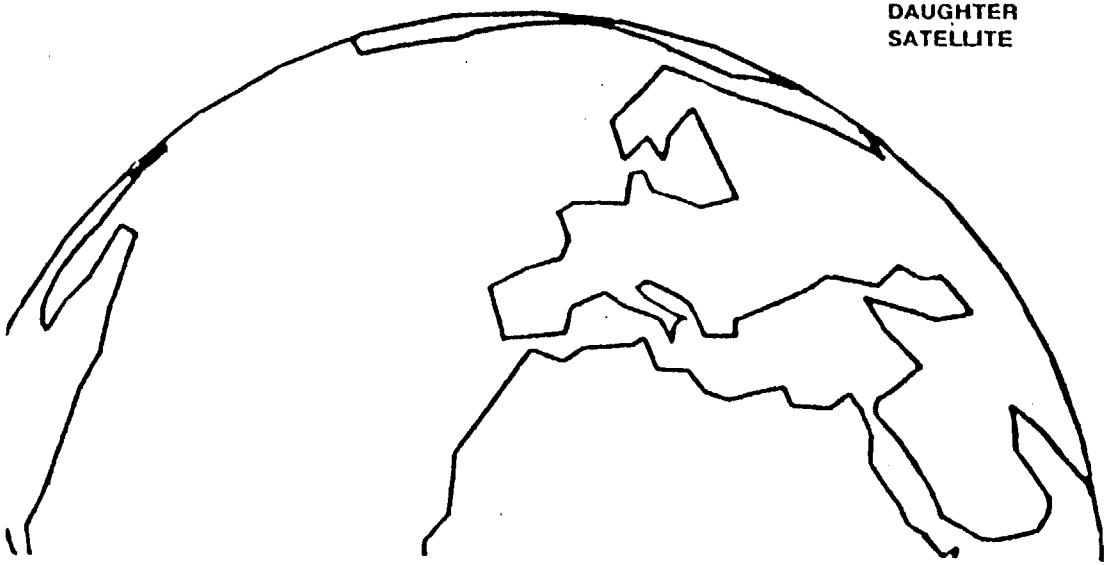

TOPSAT - VISTA

System Approach

- Sun-synchronous orbit, 6 pm local time ascending node, 450 Km altitude
- Frequency: 1.25 GHz
- Cross-track resolution by bandwidth projection
- Along-track resolution by focused SAR
- Spatial resolution 30 m x 30 m
- 50 Km (S_R) cross-track swath achieved by side-looking at 25 deg (α_0)
- Two 8.7 m (L) x 2.6 m (W) antennas
- Antenna separation (B): 500 to 1000 m
- Antennas bound by flexible tether
- Two satellites needed
- Global land coverage in six months: 95%
- SNR19.5 dB (at 25 deg surface incidence and for -20 dB σ_0)
- Antenna elevation beamwidth (θ_E) (-3 dB): 5.29 deg
- Antenna azimuth beamwidth (θ_A) (-3 dB): 1.58 deg
- Number of looks: 8 azimuth / 1 range
- Height accuracy: ~3 m

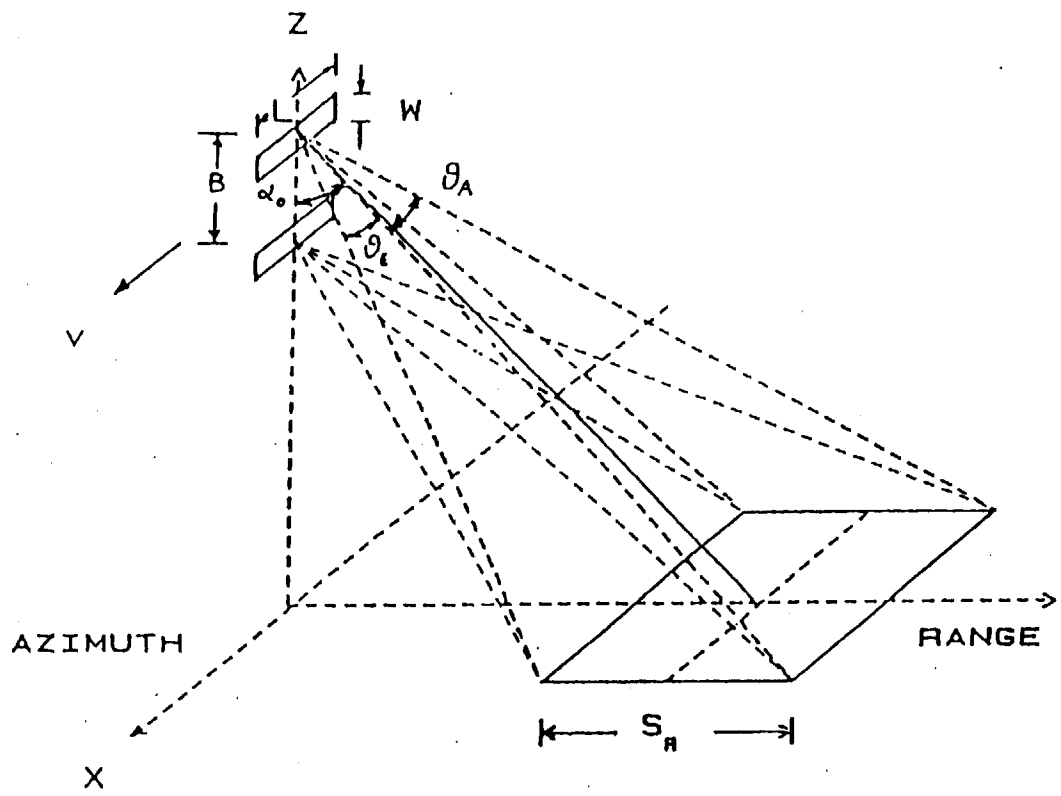

VISTA Advantages

- Meets all science requirements, including vertical and horizontal resolution;
- Uses existing SAR technology with proven history of use;
- Exploits existing investments by NASA and ASI in tether technology;
- Configuration is stabilized by the gravity gradient force;
- A long variable baseline is offered for new experiments.

VISTA Disadvantages

- Tether technology is new
- Antenna attitude uncertainty may be a major source of error
- Tether lifetime may be a problem
- Two platforms are required
- Attitude control of each platform
- Larger antennas are more difficult to stow and deploy

JPL

ISARA

System Approach

- Frequency : 35 GHz
- Cross-track resolution by bandwidth projection
- Along-track resolution by unfocused SAR
  - Spatial resolution: 33 m × 33 m
- 10-km cross-track swath achieved by side-looking at 25°
  - Two 8 m × 0.3 m antennas
  - Antenna separation : 10 m
  - Complete global coverage in 1 year
- Single pulse SNR ≥ 17 dB (at 30° surface incidence and for -10 dB σ°)
- Number of looks = 8
- Height accuracy: ~4 m

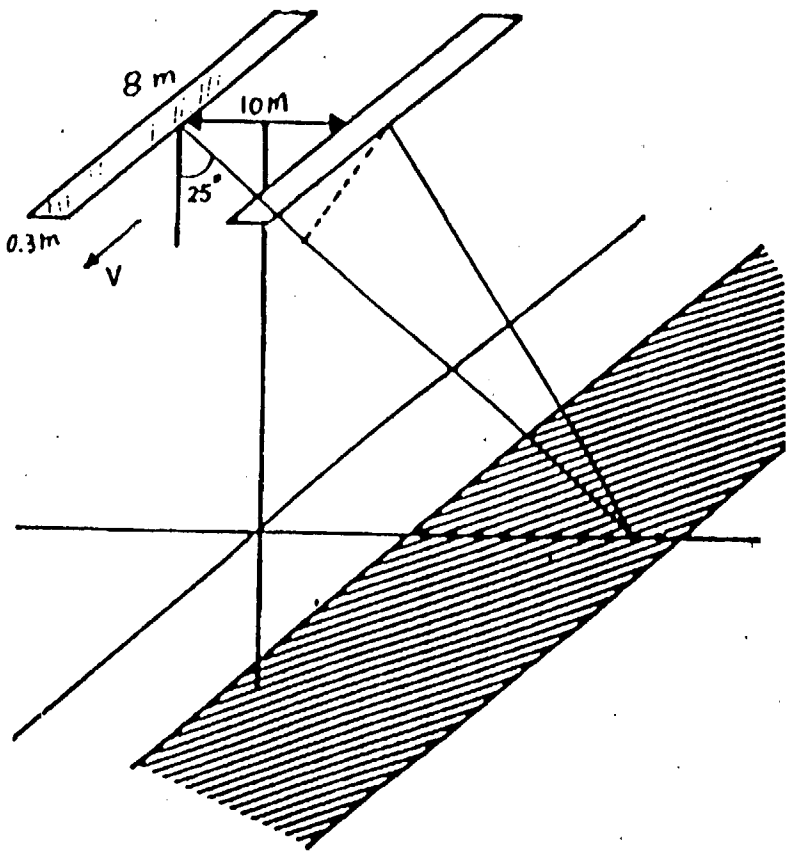

DUAL SPACECRAFT CONCEPT

VIEW FROM BEHIND VELOCITY VECTOR

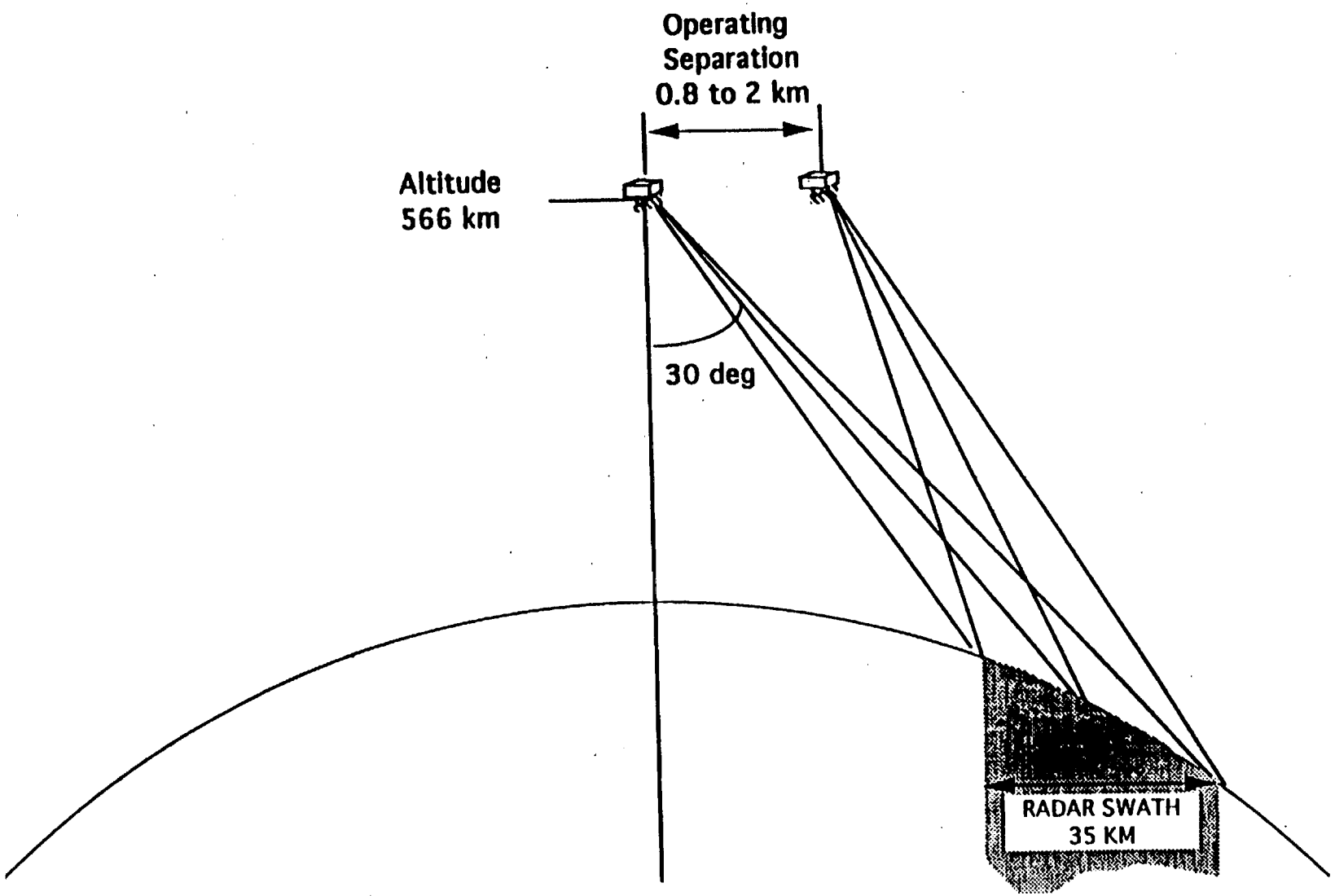

GEOMETRY NEEDED TO OBTAIN NEAR POLAR COVERAGE
65° TO 79° LATITUDE

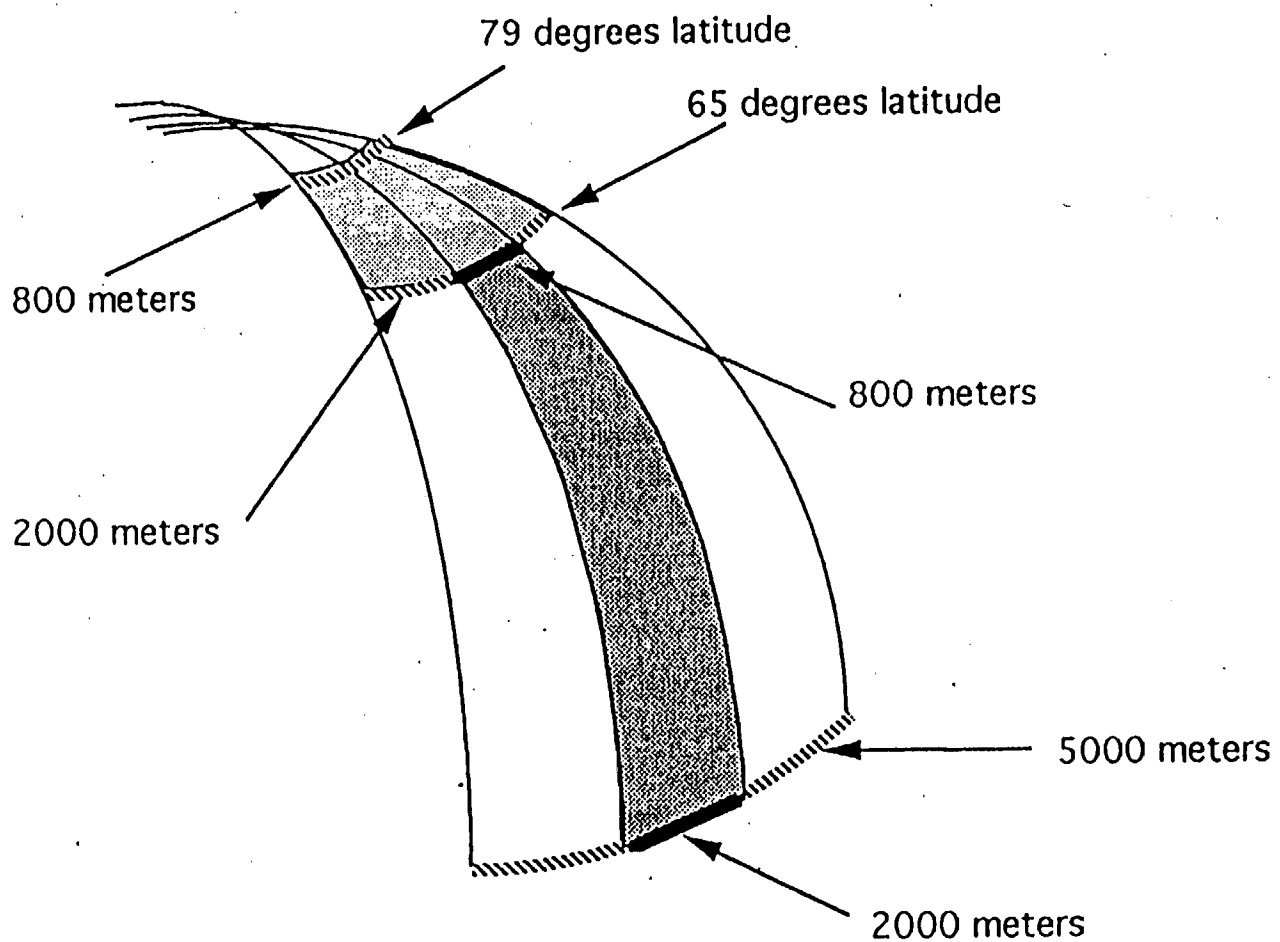

L-band Technology Assessment Summary

Subsystem	Technology	Performance	Availability/Heritage	Risk
Antennas				
	Microstrip array	3.5 x 9.0 m	SEASAT	Low
Transmitter				
	Solid state	8 x 200 w	SEASAT/Magellan	Low
Waveform gen/ ref. frequency generation				
	Digital chirp	20 MHz variable 50 us	SIR-C	Low
Stalo				
	Quartz oscillator	$<10^{-11}$	SEASAT/Voyager	Low
Receiver				
	HEMT/GAs Fet	3-4 dB (<450K)	SEASAT/SIR-C	Low
Range processor				
	SAW		SEASAT	Low
A/D system				
	Offset video	20MHz	SIR-B / SIR-C	Low
Digital data system				
	CMOS FPGA	45MHz clock	SIR-B	Low
Calibration Subsystem				

TOPSAT TWO S/C / DELTA II
FLIGHT CONFIGURATION

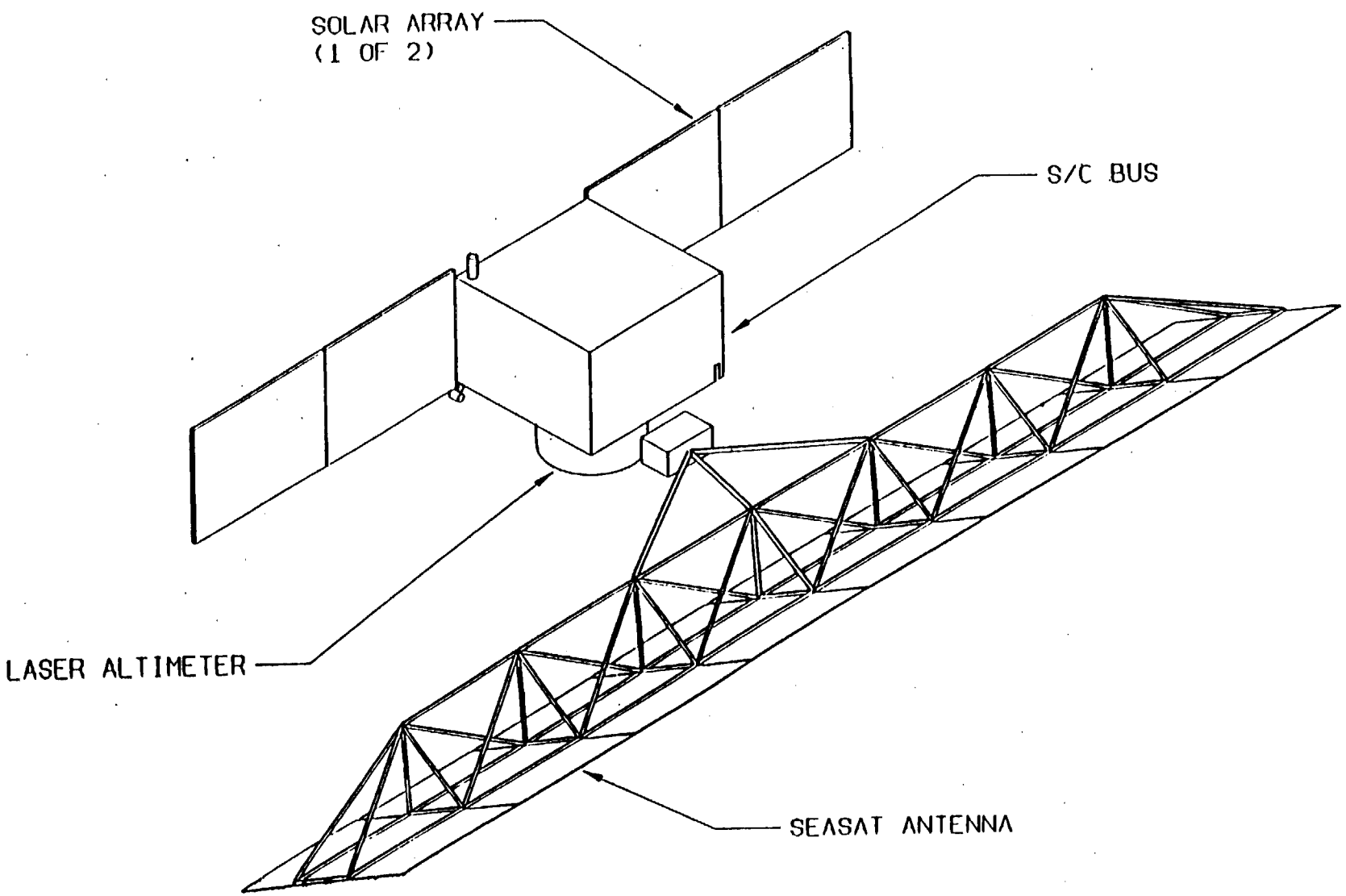

C-4

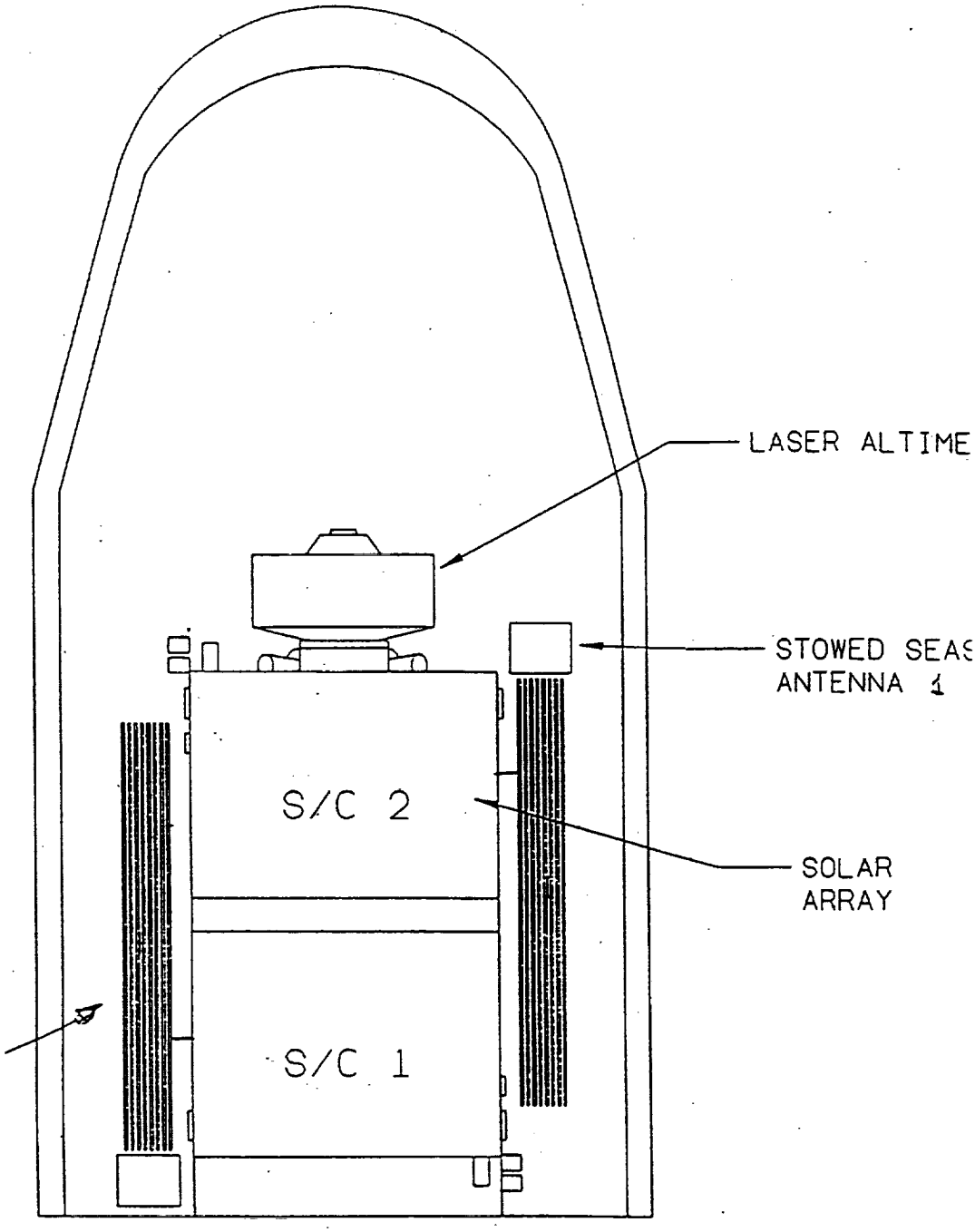

TWO S/C / DELTA II
LAUNCH CONFIGURATION

RISK SUMMARY

Issue	L-band Dual Spacecraft	K-band Single Spacecraft
Sensor development	Low	Moderate/Hi-amplifier &antenna
Spacecraft development	Low	Moderate-12m boom cont'l&know
Orbit/Operations	Moderate-navigation	Moderate-Frequent reboost
Science	Degraded performance near poles	Loss of data in severe weather
Mission duration	6 months	2 years
S/C failure scenario	Repeat-pass viable	None

TOPOGRAPHIC MAPPING LASER ALTIMETER

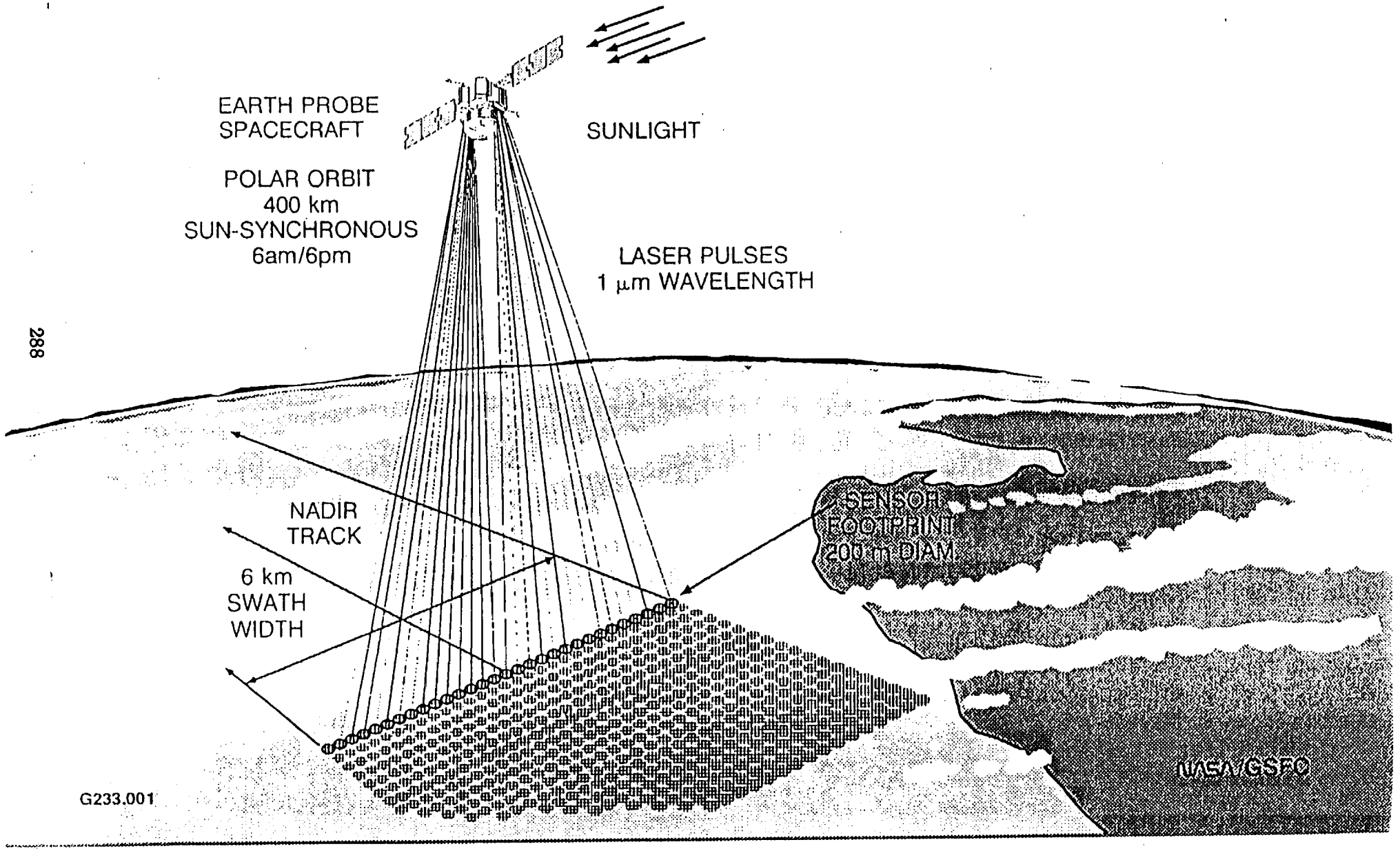

GLOBAL TOPOGRAPHY MISSION

ROLE OF MULTI-BEAM LASER ALTIMETER

* **ABSOLUTE MEASUREMENT OF SURFACE ELEVATION**
  - UNAMBIGUOUS, DIRECT MEASUREMENT BY PULSE TIME-OF-FLIGHT
  - SUB-METER VERTICAL CONTROL FOR INSAR AND STEREO-PHOTOGRAMMETRY
  - SUB-PIXEL (~ 10 m) HORIZONTAL CONTROL
  - REFERENCE TO A SINGLE, EARTH CENTER-OF-MASS COORDINATE SYSTEM
  - GLOBAL COVERAGE AT 200 m SPATIAL RESOLUTION OR PARTIAL COVERAGE AT HIGH RESOLUTION (30 m)

* **GROUND TOPOGRAPHY AND VEGETATION HEIGHT**
  - LASER PENETRATION OF VEGETATION CANOPY
  - RETURN-PULSE WAVEFORM MEASUREMENTS OF GROUND AND CANOPY

* **SURFACE SLOPE MEASUREMENT**
  - SLOPE MEASUREMENT ACCURACY at the 1° LEVEL
  - ALONG-TRACK AND ACROSS-TRACK SLOPES

ROLE OF MULTI-BEAM LASER ALTIMETER

(CONTINUED)

* **HIGH-ACCURACY ICE SHEET TOPOGRAPHY**
  - SINGLE PULSE MEASUREMENT ACCURACY: ~ 20 cm
  - ICE SHEET MAPPING - HIGH DENSITY OF DATA POINTS, TRACK CROSSINGS

* **METER-LEVEL DATA QUALITY IN HIGH-RELIEF TERRAIN**
  - < 3 m VERTICAL ACCURACY AT 20° SURFACE SLOPE
  - DATA ACQUISITION FOR ALL SLOPES (NO SHADOWING OR LAYOVER)

* **SUB-PIXEL MEASUREMENT OF SURFACE VERTICAL STRUCTURE (i.e. roughness)**
  - RETURN-PULSE WAVEFORM SPREADING

* **HIGH-ACCURACY CONNECTION OF LAND AND OCEAN TOPOGRAPHY**
  - ≤ 20 cm SURFACE HEIGHT ERRORS IN COASTAL REGIONS
  - < 10 cm WITH MULTI-PULSE AVERAGING

SOME THOUGHTS ON FUTURE RAIN MAPPING MISSIONS (TRMM FOLLOW-ON)

John S. Theon
National Aeronautics and Space Administration
Washington, D.C. 20546

INTRODUCTION

The release of latent heat of condensation is the largest internal energy source of the atmosphere. Latent heating is most significant during the precipitation process. Our knowledge of the distribution of precipitation is poor. It is only well observed within limited areas of the globe. Over the oceans, for example, it is known only to within a factor of two. Thus, there are strong scientific requirements for observations of precipitation from instruments on board a satellite. The Tropical Rainfall Measuring Mission (TRMM) will be the first satellite to measure rainfall with adequate accuracy and provide information about the vertical distribution of precipitation, not in only in a tropics and sub tropics, but to plus or minus 35 degrees of latitude. There is a need for the continuity of rain observations for climate modeling purposes and to expand observations to cover more of the globe than simply plus or minus 35 degrees latitude.

TRMM FOLLOW-ON MISSION REQUIREMENTS

One of the requirements that can be met by a TRMM follow-on mission is the need for five additional years of tropical rainfall measurements for short term climate studies. A three year data set simply may not include both normal and El Niño Southern Oscillation (ENSO) conditions. ENSO occurs about twice in a decade, maybe three times, but we need to extend the data set to include El Niño; La Niña which is a cold eastern pacific oscillation; and normal conditions. A total of eight years should achieve this goal. Shukla from the University of Maryland has shown that the results of large scale climate models are immensely sensitive to the amount and vertical profiles of latent heating in the tropics. The only way to obtain adequate quantitative values for latent heating is from TRMM and its hydrometeor profiling. Shukla also showed that the impacts of tropical circulations on mid latitude weather and climate requires a much better knowledge of tropical latent heat release than we have at present.

We also have a need to extend measurements to middle and high latitudes both for analysis of the global hydrological cycle and to understand precipitation and its impact on the environment. Measurements are urgently needed for the Global Energy and Water Cycles Experiment

(GEWEX). We need to begin the measurement of frozen precipitation from space. Over land, only radar can make these measurements. Even radar will have problems detecting light snow fall. The GEWEX Continental Scale Experiment (GCIP) will greatly help testing and validating snow retrievals over land. By the year 2000 we need rainfall measurements in the tropics and mid latitudes on a near real-time basis to assimilate in large scale forecast models. This means rain and latent heat data simulations will have been developed during TRMM-1. This could lead to significant increases in accuracy for one to five day weather forecasts and greatly improved assessment and prediction of global change, particularly global warming, by improving the climate models. We need better models which couple the land surface hydrology with precipitation. Most hydrological studies are on mid latitude sites. (Personal communication from J. Simpson, GSFC, January 1993

Shown in Figure 1 are the satellite data requirements from the World Climate Research Program. The third entry is liquid water. For measuring liquid water, microwave imaging radiometers are needed such as on SSM/I; Eos, which is the MIMR; and TRMM microwave imager TMI. For the liquid water profile, only a rain radar can make that measurement, and of course, the only precipitation radar available will be on TRMM. Therefore, since TRMM is only a three year mission, we need a follow-on in order to fully extend the coverage of GEWEX.

Measurements	Instrument type	Candidate sensor	Mission
Wind profile	Doppler lidar	LAWS	(undetermined)
Temperature & humidity profile	IR & microwave sounder	AIRS, IASI, MSU, AMSU, MHS (1)	EOS, NOAA, POEM, GEWEX (2)
Liquid water (total)	Microwave imaging radiometer	SSM/I, MIMR, TRMM microwave imager (TMI)	DMSP, EOS, TRMM, GEWEX (2)
Liquid water (profile)	Rain radar	Precipitation radar (PR)	TRMM, GEWEX(2)
Cloud amount and cloud top temperature	Imaging radiometer (vis & RI)	AVHRR (3), MODIS	NOAA, EOS, POEM, GEWEX (2)
Cloud particle properties	Polarimeter	POLDER, EOSP	ADEOS, POEM, EOS
Cloud particle profiles	Millimeter wave radar altimeter	(undetermined)	(undermined)
Atmospheric chemistry: minor constituents including ozone	Spectrometer	TOMS, GOME, GOMOS, SCIAMACHY, MOPITT, IMG, ILAS, HIRDLS, TES	NOAA, ERS-2, ADEOS, POEM, EOS
Aerosol: stratospheric	Limb-scanning spectrometer	SAGE, SCIAMACHY, ILAS	EOS, POEM, ADEOS
Aerosol: tropospheric	Multi-directional imager	MISR	EOS
Solar radiation	Solar radiometer	ACRIM	EOS
Earth radiation (top of the atmosphere)	Wide-band scanning radiometer	ScaRaB, CERES	Meteor; TRMM, EOS, POEM, GEWEX(2)
Earth surface/ cloud multi-directional reflectance	Multi-directional imager	ATSR, MISR	ERS, EOS, POEM
Earth surface reflectance and colour	Imaging radiometer (vis & near IR)	AVHRR(3), AVNIR, MODIS	NOAA, ADEOS, EOS, POEM

Figure 1. World Climate Research Program (WCRP) Satellite Data Requirements (From a presentation by P. Morel, Director, WCRP, Hamilton, Bermuda, January 1991).

Ocean surface colour	Imaging radiometer (vis)	SeaWIFS, OCTS, MODIS	SeaWIFS, ADEOS, EOS, POEM
Sea surface temperature	Imaging radiometer or sounder (IR)	AVHRR$_{(3)}$, ATSR, OCTS, MODIS, AIRS, IASI	NOAA, ERS, ADEOS, EOS, POEM
Ocean surface wind vector	Microwave scatterometer	AMI, NSCATT, STIKSCAT	ERS, ADEOS, EOS, POEM
Ocean wave height	Radar altimeter	RA	ERS, EOS, POEM
Ocean surface topography	Precision radar altimeter and orbitometry	Single or 2-frequency altimeter; GPS + water vapour radiometer or DORIS	TOPEX-POSEIDON, ALT$_{(4)}$
Sea ice cover	Microwave imaging radiometer	SSM/I, MIMR	DMSP, EOS, POEM
Sea ice texture, edge and motion	Imaging radar	AMI, SAR	ERS, RadarSat, JERS-1
Snow cover	Imaging radiometer (vis and microwave)	AVHRR, MODIS, SSM/I, MIMR	NOAA, EOS, POEM, DMSP
Snow water equivalent and soil moisture	(undetermined)	(undetermined)	(undetermined)
Glacial and iceberg discharge	High-resolution imager (vis) and radar altimeter	TM, HRV, ASTER AND RA	LANDSAT, SPOT, EOS and ERS, EOS, POEM

Figure 1 (Continued)

Footnotes: (1) The accuracy and vertical resolution of HIRS in the troposphere are insufficient for climate studies

(2) GEWEX dedicated non-sunsynchronous earth observing mission on a 55-60 degree inclined orbit (undetermined).

(3) AVHRR calibration only marginally adequate for cloud classification, vegetation mapping and sea surface temperature measurements.

(4) TOPEX follow-on high precision ocean altimetry mission (undetermined)

GLOBAL HYDROLOGICAL CYCLE

PROBLEM IS TO COMPLEMENT THE SURFACE-BASED NETWORK FOR DETERMINING GLOBAL PRECIPITATION AND SOIL WETNESS

- GLOBAL PRECIPITATION ESTIMATES EXIST, BASED ON IR CLOUD IMAGES OR PASSIVE μ-WAVE RADIOMETRY AND EMPIRICAL CLIMATIC CORRELATIONS
- VERTICAL DISTRIBUTION OF RAIN DROPS NEEDED FOR DIRECT QUANTITATIVE ESTIMATION
- RESOLVING THE DIURNAL CYCLE IS ESSENTIAL
- TRMM IS ESSENTIAL FIRST STEP. TECHNIQUE TO BE FURTHER DEVELOPED IN FOLLOW-ON "EARTH-SCANNING" MISSION

Figure 2. Global Hydrological Cycle Problem

Figure 2 presents the global hydrological cycle problem. We see that the problem is to compliment the surface based network for determining global precipitation and soil moisture. Global precipitation measurements estimates exist based on infrared cloud images or passive microwave radiometry and empirical climatic correlations. The vertical distribution of raindrops is needed for the direct quantitative estimation of precipitation. Resolving the diurnal cycle is essential which TRMM certainly can do. We need a non-sun-synchronous orbit in order to measure the diurnal cycle. TRMM is the essential first step, but the technique can be further developed in follow-on Earth scanning missions.

TRMM FOLLOW-ON PLANNING

Planning for tropical rainfall measurements to follow TRMM has been a part of the French Space Agency (CNES) planning since Bilan Enegetique du Systeme Tropical (BEST), which means the tropical energy budget, was first proposed in 1989 as a candidate to meet GEWEX space observing system requirements and for an operational mission to begin at the turn of the century. The proposers invited international cooperation, but the mission has never really been approved. In Hamilton, Bermuda where the GEWEX Joint Scientific Steering Group met in January of 1991, the scientific need for continued precipitation measurements from space after the TRMM mission was presented by Professor Pierre Morel, Director of the World Climate Research Program. About that same time the Japanese discussed a plan to begin a TRMM follow-on mission. At the fourth session of Joint Scientific Steering Group for GEWEX, which was held January 1992 in Tokyo, Japan, a resolution was agreed upon that said, "TRMM follow-on missions, that could continue the cooperation between USA and Japan, include discussions of a satellite launched after the year 2000 in a 55 degree inclined orbit with an advanced multi-beam, multi-frequency precipitation radar, and an advanced passive microwave imager." (From presentation by Thomas La Vigna, GSFC, January 1993).

A TRMM follow-on was also discussed at the International Workshop on the Processing and Utilization of the Rainfall Data Measured from Space which was held March 1992 in Tokyo, Japan. At that time it had been established that precipitation is an important component of the Earth system which influences global weather and the climate. Moreover, there now exists strong evidence that rain rates can be measured from space platforms to within the scientific requirements for improving weather forecasting and for improving the models used in the prediction of climate change. Continuation of the measurements is crucial for detecting and monitoring global change of precipitation. In view of these considerations, the workshop participants strongly endorsed the concept of a follow-on mission to TRMM. They urged that

the necessary steps be taken by NASA, NASDA, ESA, and CNES to begin pre-phase A studies immediately for such a cooperative mission. A candidate configuration for a 55 degree inclination orbit, which allows sampling over the diurnal cycle and full coverage of the mid-latitude weather, was put forward. The payload was suggested to be similar to that of TRMM except for upgrades in the instruments, such as the dual frequency radar, multi-channel microwave radiometer, and visible and infrared radiometers.

At the International Symposium on Active Sensors and Non-Synchronous Missions Dedicated to GEWEX, held June 1992 in Jouy en Josas, France, strong science recommendations came for the continued measurement of precipitation from space after TRMM. The meeting proposed a non-sun-synchronous mission to extend the results of TRMM beyond the tropics in order to realize the global objectives of GEWEX. The various space agencies were encouraged to define the scope and specification of a TRMM follow-on mission and sensors for appropriate interactions with the scientific community, to coordinate and conduct the corresponding feasibility studies and development, with a view to creating the conditions for a program decision, and accomplish studies and trade-off assessments of several options for the rain radar, for example, dual beam, two-frequency, and dual polarization.

At the Asia-Pacific International Space Year Conference, "The Earth in Space", held November 1992 in Tokyo, Japan, the opening key lecture by Professor P. Morel discussed a follow-on TRMM for continued measurements from space of rainfall and importance to climate models. The opening day lecture by S. Tilford entitled "U. S. Earth Observation Satellite Program" discussed future potential space missions including a TRMM follow-on, TRMM-2.

In the GEWEX Dedicated Space Mission Study Workshop, held November 1992 in Tokyo, Japan, the focus was on a TRMM follow-on mission. The workshop recommendations included unique and essential scientific requirements for GEWEX and global climate science as being the observations of radiation, clouds, and rain which show diurnal variations, and for the latter two parameters, vertical resolutions are indispensable for characterizing relationship among these quantities. In order to meet these requirements, a TRMM follow-on mission is required to provide data continuity over the tropics and to extend coverage to higher latitudes. In view of these considerations NASDA's proposal for a TRMM follow-on mission aiming at a launch in the year 2000 was endorsed as a basis for development. In addition to the original TRMM instruments, inclusion of a cloud profiling radar was recommended to be considered for monitoring the global 3-dimensional distributions of clouds.

At the 6th Standing Senior Liaison Group (SSLG) Meeting, held December 1992 in Washington, D.C., the NASDA presentation entitled "Study on TRMM Follow-On" also recommended that the TRMM follow-on mission to meet GEWEX requirements be started. There are a number of improvements which could be made to the basic TRMM in the TRMM follow-on. However, in order to meet the schedule laid out for continuing the observations, which would mean a launch in the year 2000, it appears that changes for the TRMM follow-on will be minimal. They will include only the increase in the inclination angle to 50 to 60 degrees of latitude, in order to cover the globe more geographically, and an increase in the altitude of the orbit so that the space craft will be able to have a five year lifetime. This basically means that the radar might have to be increased in power and antenna size. The passive microwave imager might also have to be increased in antenna size in order to keep the resolution of the footprint small enough to observe rainfall accurately, especially in convective situations.

Other improvements, such as the inclusion of a radar with multiple frequencies, or a push-broom type scan pattern, or polarization, or all of these, will have to wait until a successor mission to the TRMM follow-on. Likewise, a cloud radar whose feasibility has not been demonstrated yet will also have to await development at the laboratory and aircraft levels to prove the concept. Then, possibly, it can be implemented on a mission sometime after the year 2000.

SUMMARY REMARKS

If we are to maintain data continuity, we need to initiate a TRMM follow-on mission very soon. NASA is considering this action and may fund a study on the subject during this fiscal year. The resources to fund the phase C/D portions of the mission remain to be identified. They will have to compete with all the other ideas that have been proposed for specialized Earth Probe Missions in the years following the turn of the century. The measurement of rainfall from space is and ought to be a high priority in studying the Earth system and global change. It remains to be seen whether we can improve upon the very fundamental measurements that TRMM will make. How we go about this should be the subject of continuing research in the years between now and the end of the decade.

Acknowledgments: The author wishes to acknowledge the able assistance of Dr. William W. Vaughan in reviewing and editing the manuscript and Ms. Jean Taylor for typing the manuscript.

TECHNOLOGICAL ADVANCES

Dr. Jacques Louet
ESA
The Netherlands

CALIBRATION

PRACTICAL EXPERIENCE WITH ERS-1

- Introduction
- Radiometric Calibration
- Geometric Calibration
- Phase Calibration
- Polarimetric Calibration

Introduction

Basic SAR measurement parameters are :

- Radar backscattering
- Target position
- Target speed
- Polarisation

SAR calibration facilitates ***quantative*** measurements needed to derive geophysical parameters of the area under observation from basic SAR measurements (e.g. soil moisture, biomass,ocean wave energy,ocean currents, ice type, ice flow,.....)

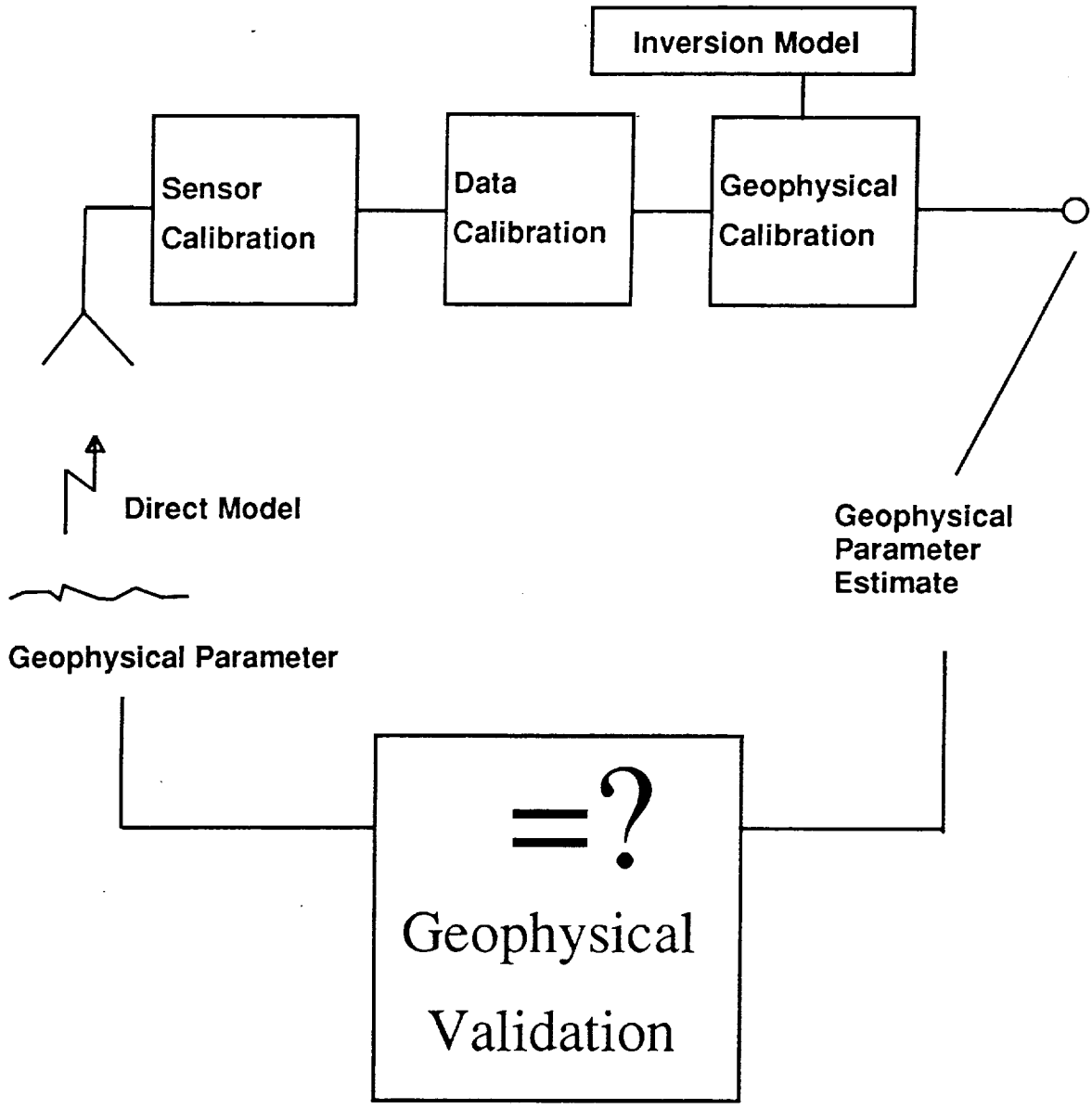
Inversion Model
Sensor Calibration
Data Calibration
Geophysical Calibration
Direct Model
Geophysical Parameter Estimate
Geophysical Parameter
=?
Geophysical Validation

Radiometric Calibration

Radiometric calibration is relating the SAR output in terms of digital number to σ^o.

- Design for stability
- Sensor calibration
  - — pre-flight characterisation
  - — internal calibration
  - — external calibration
- Data calibration

Characterisation parameters for ERS-1

- Transmitter Parameters
  - — Frequency
  - — Pulse power
  - — Pulse duration
  - — Chirp bandwidth
- Antenna Parameters
  - — Relative azimuth pattern
  - — Absolute elevation pattern
- Receiver Parameters
  - — Sensitivity
  - — Bandwidth
  - — Power transfer function
- Calibration Parameters
  - — Internal calibration stability

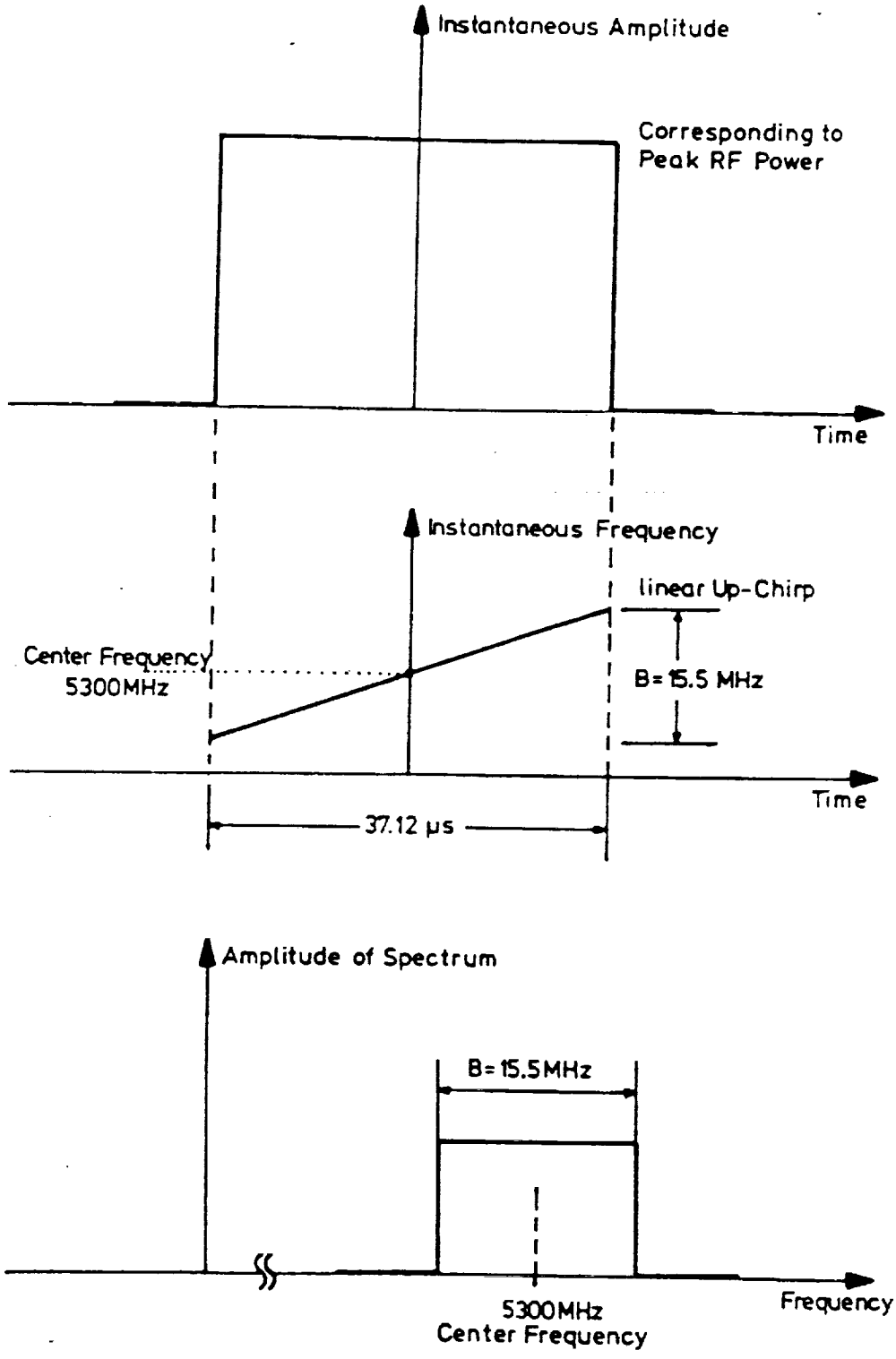
Instantaneous Amplitude
Corresponding to
Peak RF Power
Time
Instantaneous Frequency
linear Up-Chirp
Center Frequency
5300MHz
B=15.5 MHz
Time
37.12 µs
Amplitude of Spectrum
B=15.5MHz
5300MHz
Center Frequency
Frequency

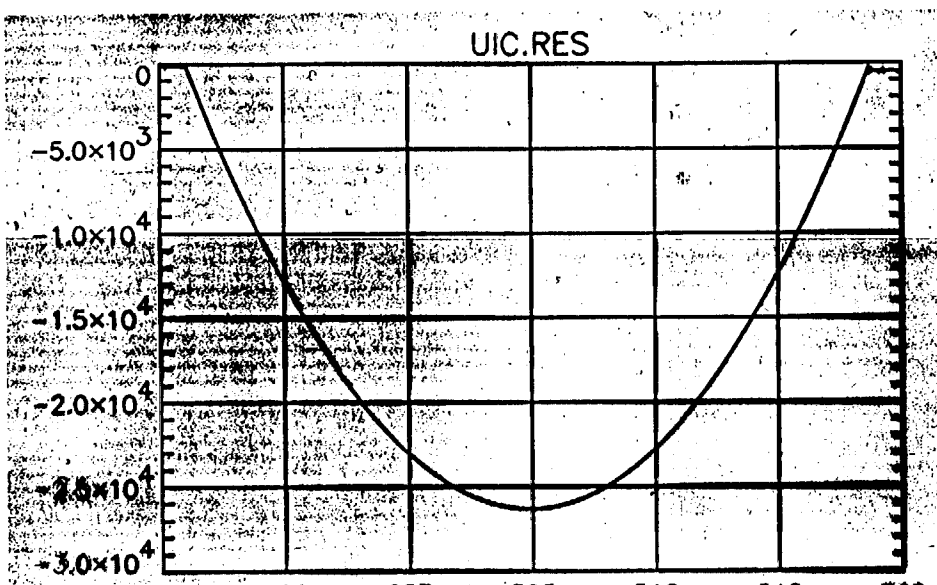

jpg plotting : 12-Nov-1992 10:30:48.00_local fig 1

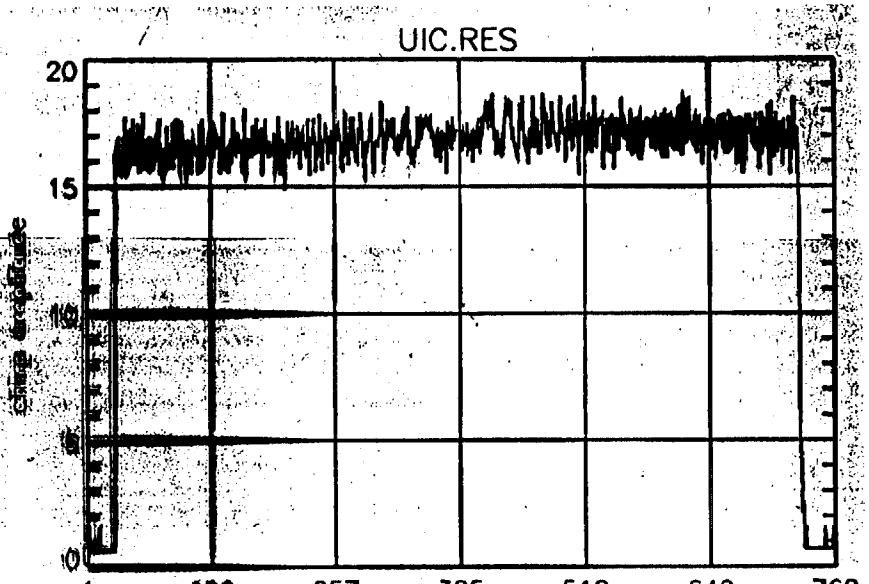

file : uic$:uic__921102kscf9928.e1;1 fig 2

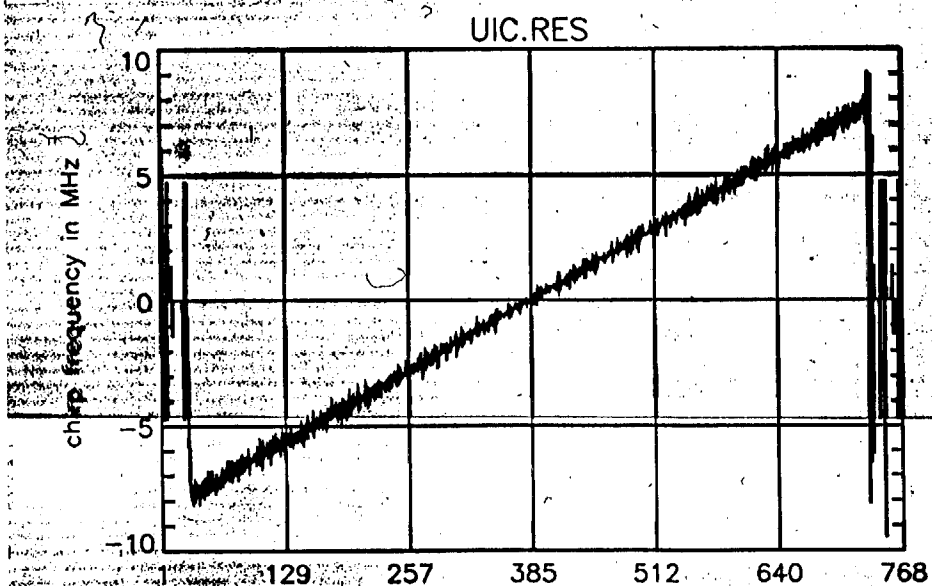

start : 2-NOV-1992 14:19: 8.096_utc fig 3

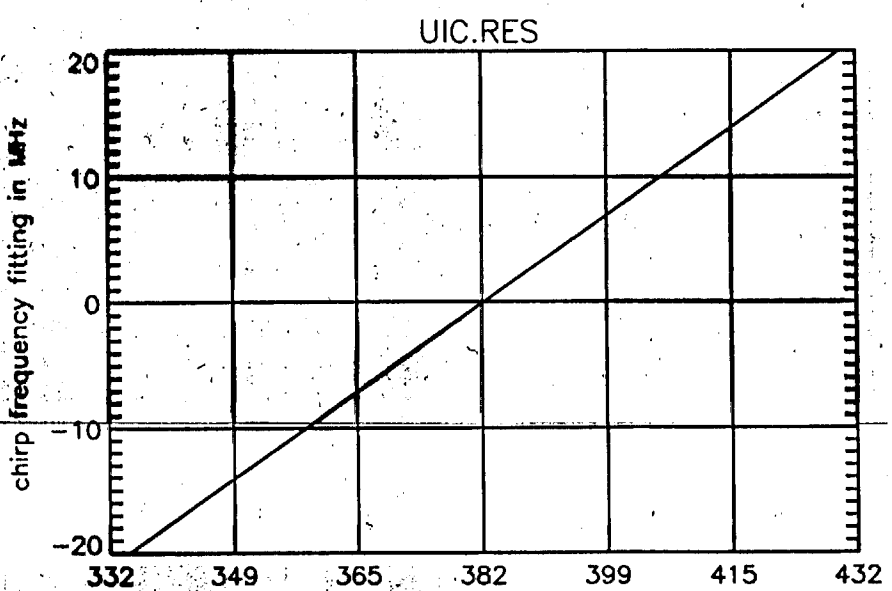

id : [87929 17 1] index = 30 fig 4

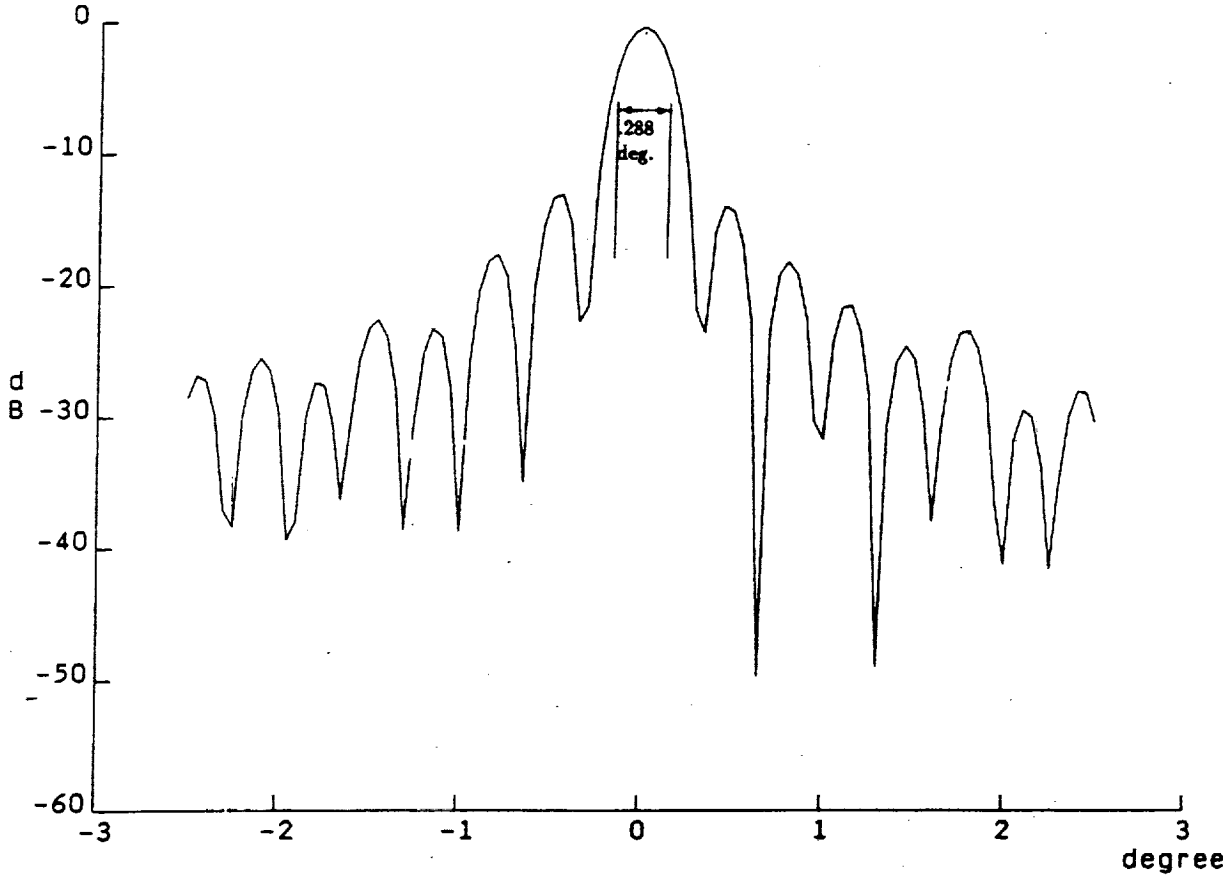
0
-10
-20
d
B -30
-40
-50
-60
-3
-2
-1
0
1
2
3
degree
.288
deg.

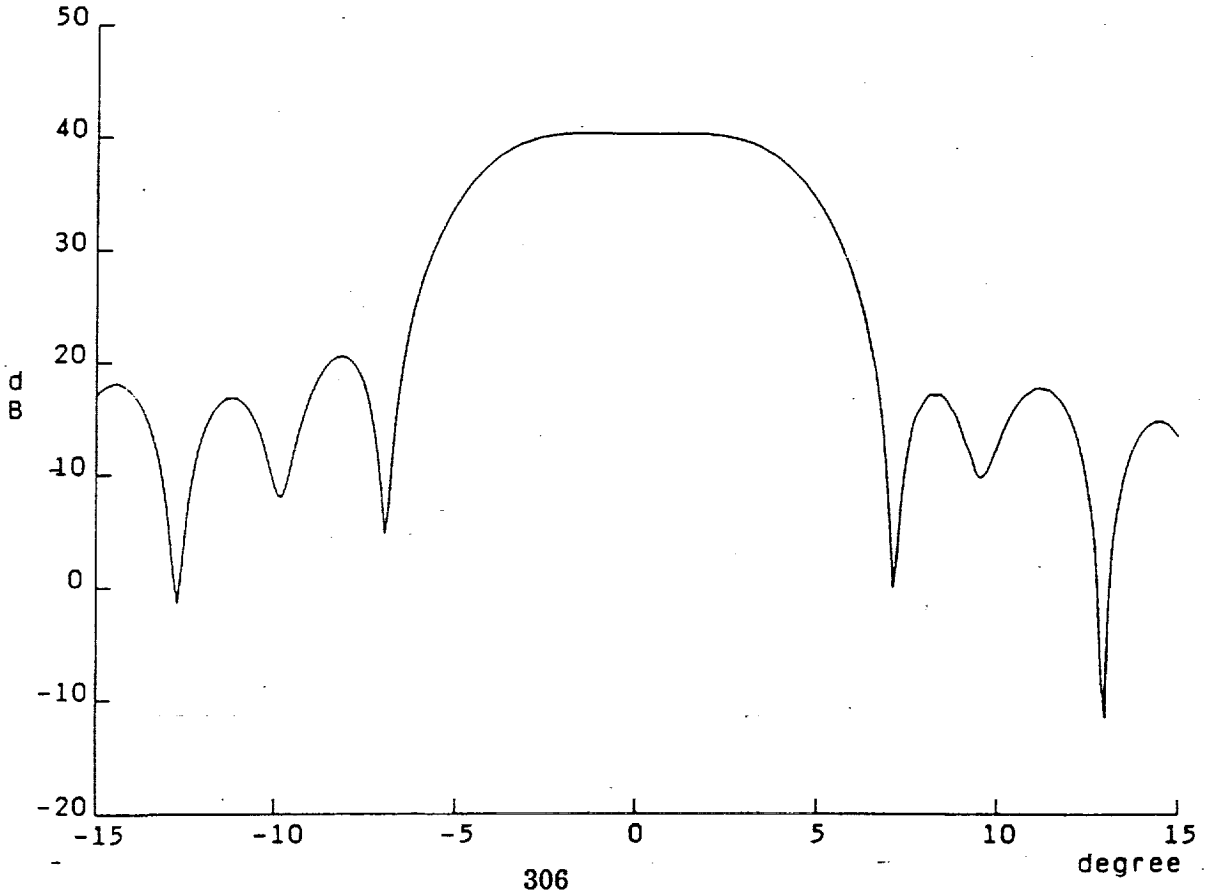
50
40
30
20
d
B
10
0
-10
-20
-15
-10
-5
0
5
10
15
degree

EXAMPLE OF 2-BIT CODE

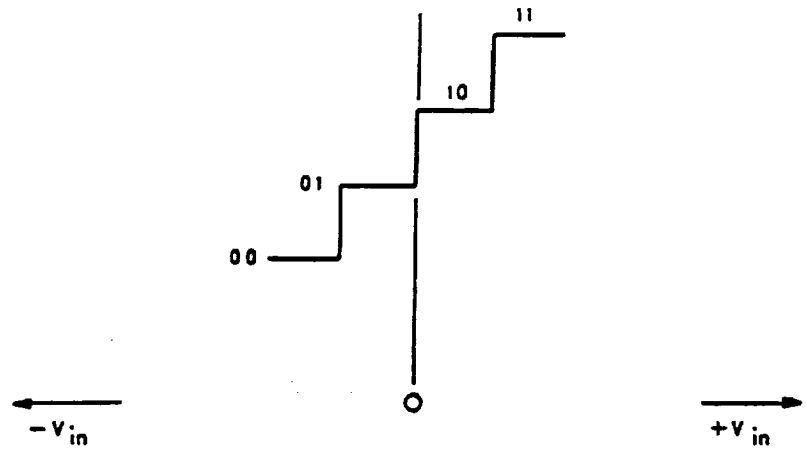

EXAMPLE OF 5-BIT CODE

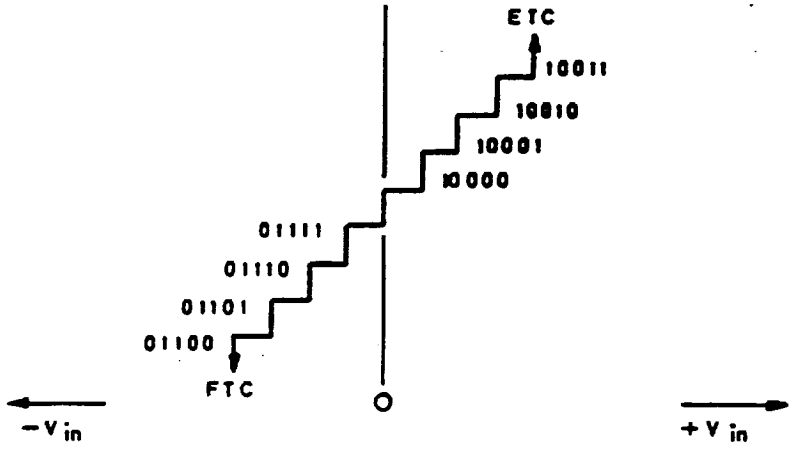

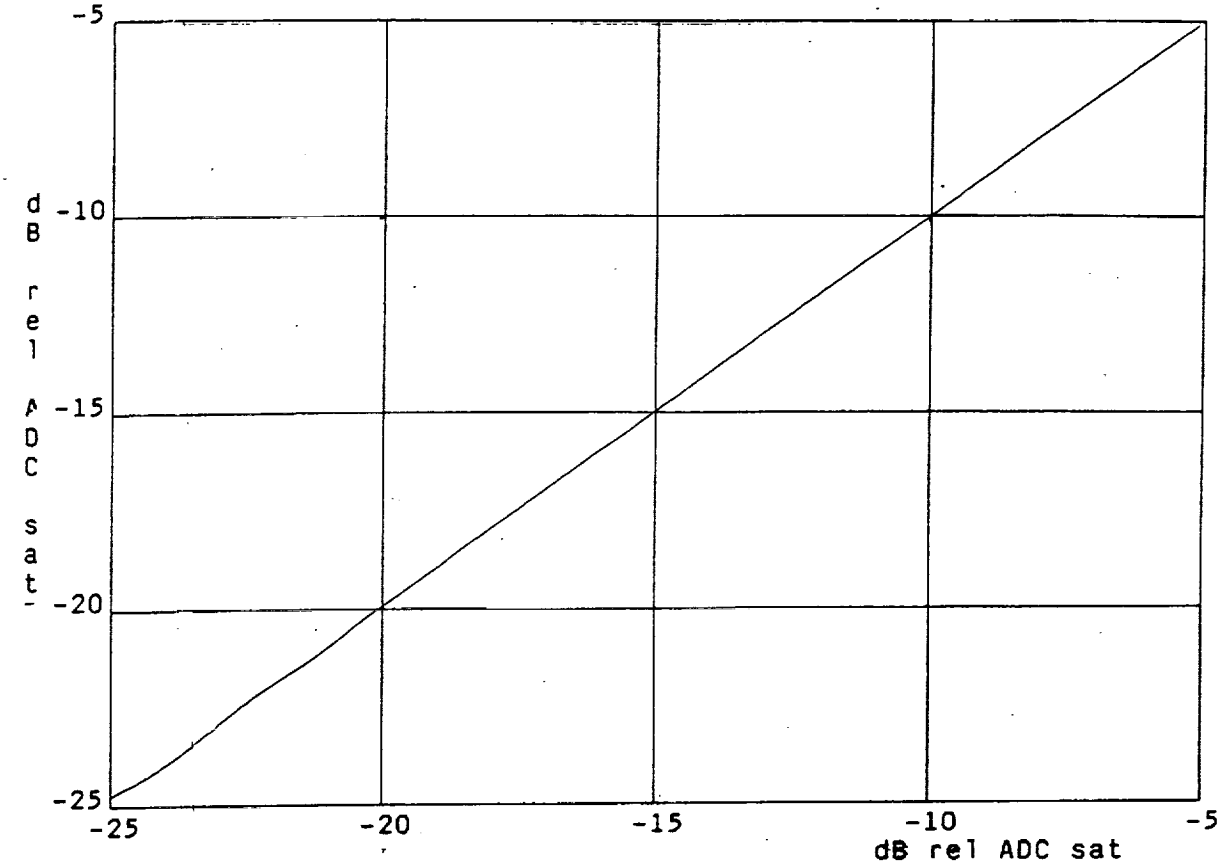
-5
-10
-15
-20
-25
dB rel ADC sat
-25
-20
-15
-10
-5
dB rel ADC sat

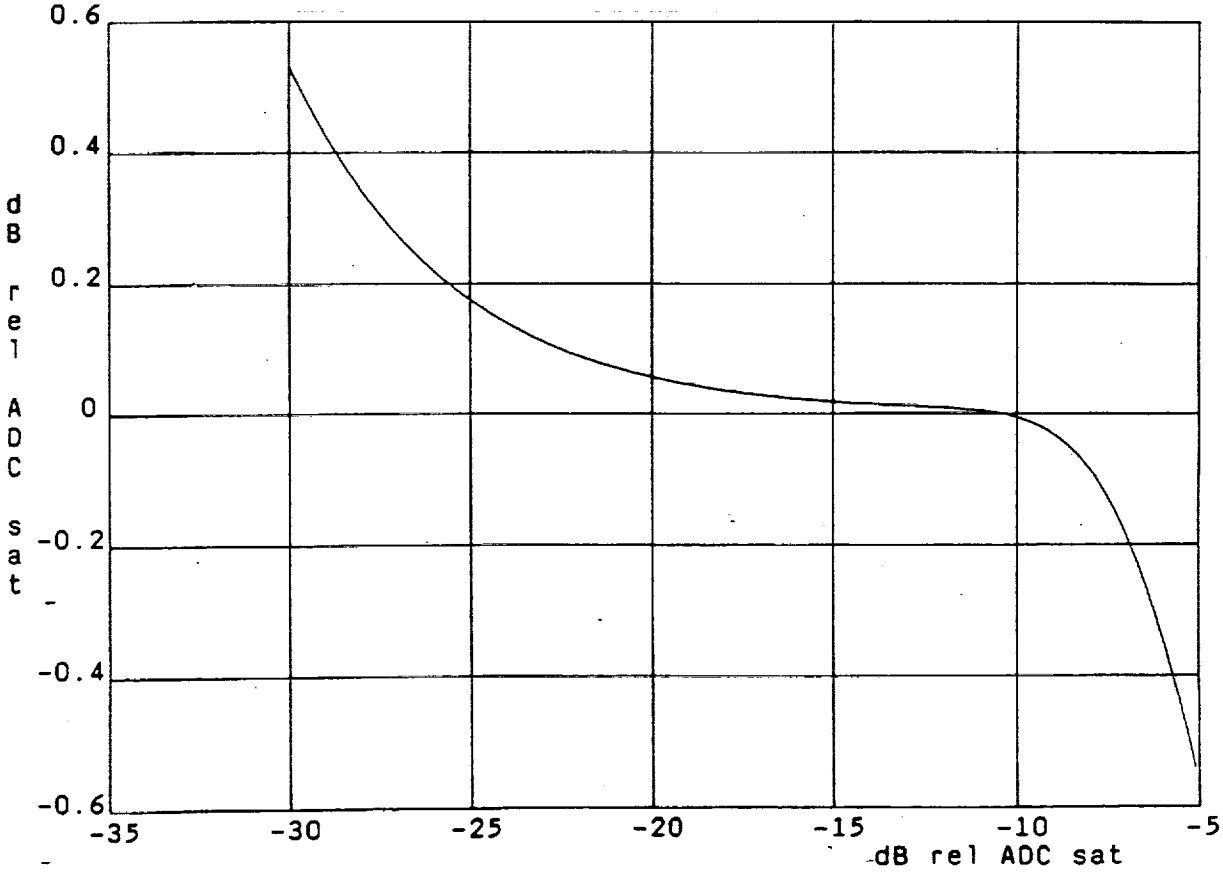
0.6
0.4
0.2
0
-0.2
-0.4
-0.6
dB rel ADC sat
-35
-30
-25
-20
-15
-10
-5
dB rel ADC sat

Internal Calibration

The objective of internal calibration is monitoring system parameter changes with time, such as

- Output power
- Receiver gain
- Linear distortion (amplitude & phase)
- Non-linear distortion (amplitude & phase)
- Noise level
- Level of spurious signals

Internal calibration methods include

- Calibration using transmit pulse sample (ERS-1 method)
- Reference signals : noise, cw
- Transmit power measurements

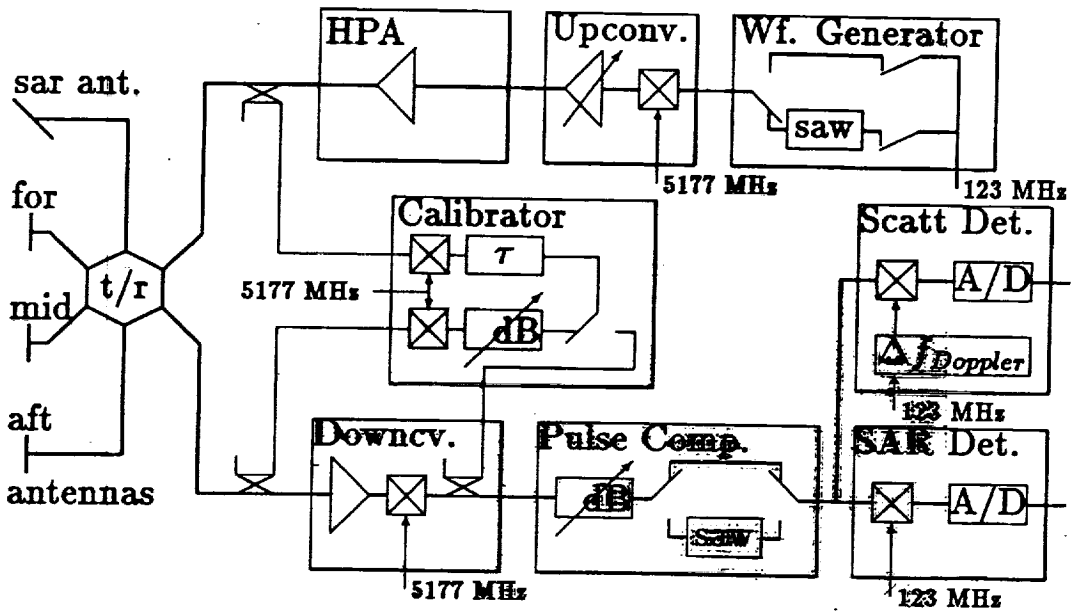
sar ant.
for
mid
aft
antennas
t/r
HPA
Upconv.
Wf. Generator
saw
5177 MHz
123 MHz
Calibrator
τ
dB
5177 MHz
Scatt Det.
A/D
Doppler
123 MHz
Downcv.
Pulse Comp.
dB
Saw
SAR Det.
A/D
5177 MHz
123 MHz

ERS-1

CALIBRATION PULSE POWER SEQUENCE

COMMISSIONNING PHASE (from 7-SEP-1991 to 6-DEC-1991)

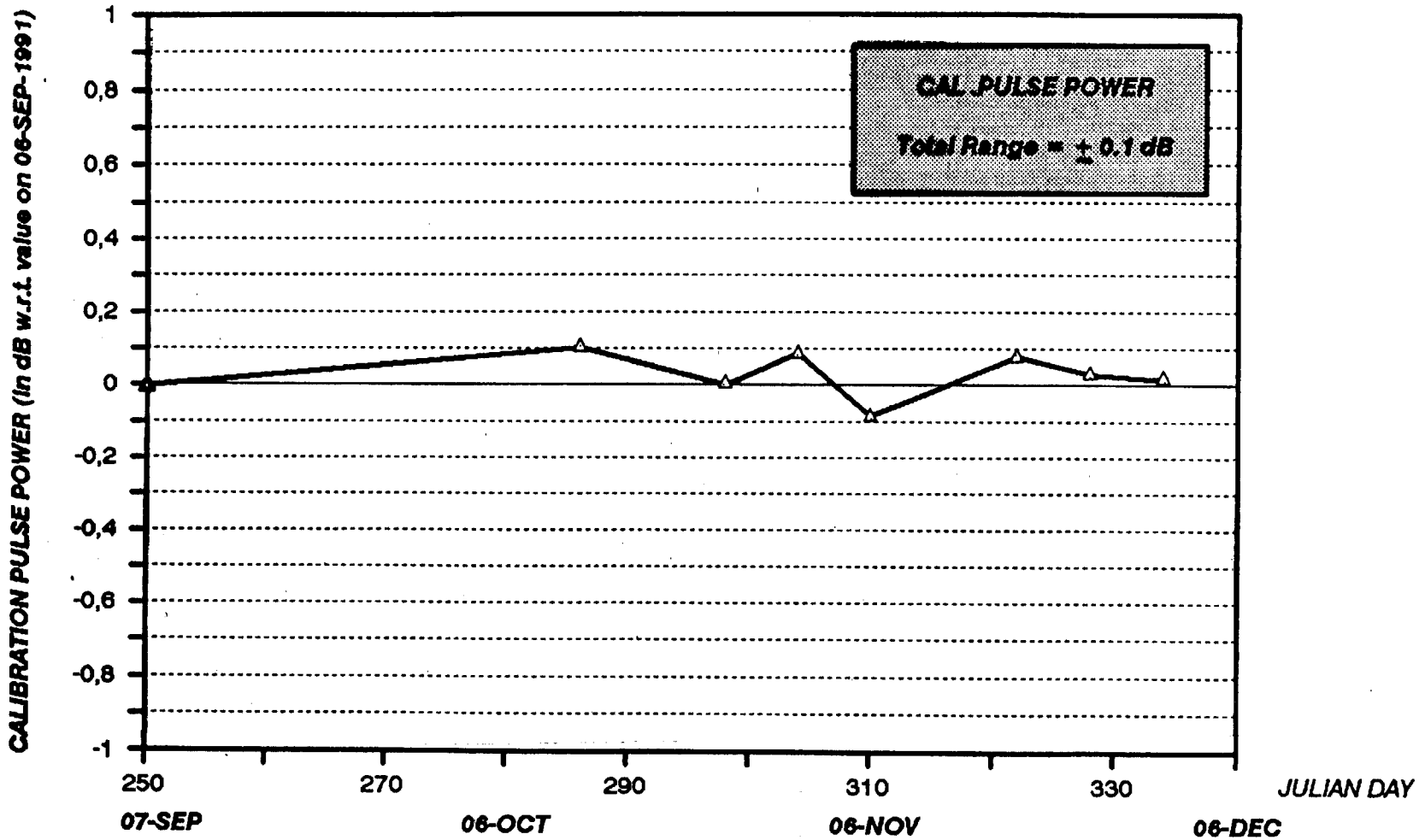

esa

ESRIN / ERS-1 PRODUCT CONTROL SERVICE

External Calibration

The objective of external calibration is to measure and monitor system components outside the internal calibration loop.

External calibration uses made-made or natural targets.

External calibration can be used to determine the radar image calibration factor either in combination or without reference to internal calibration.

AMI Transponder Specifications

Parameter	Wind Mode	Image/Wave
Radar Cross Section	$87.5dBm^2$	$65.0dBm^2$
Adjustment Range	$+0, -5dB$	$+0, -5dB$
Calibration Accuracy	$\pm.5dB$	$\pm.5dB$
Cross-calibration Accuracy	$\pm.2dB$	$\pm.2dB$
Stability(Over 3 Years)	$\pm.1dB$	$\pm.1dB$

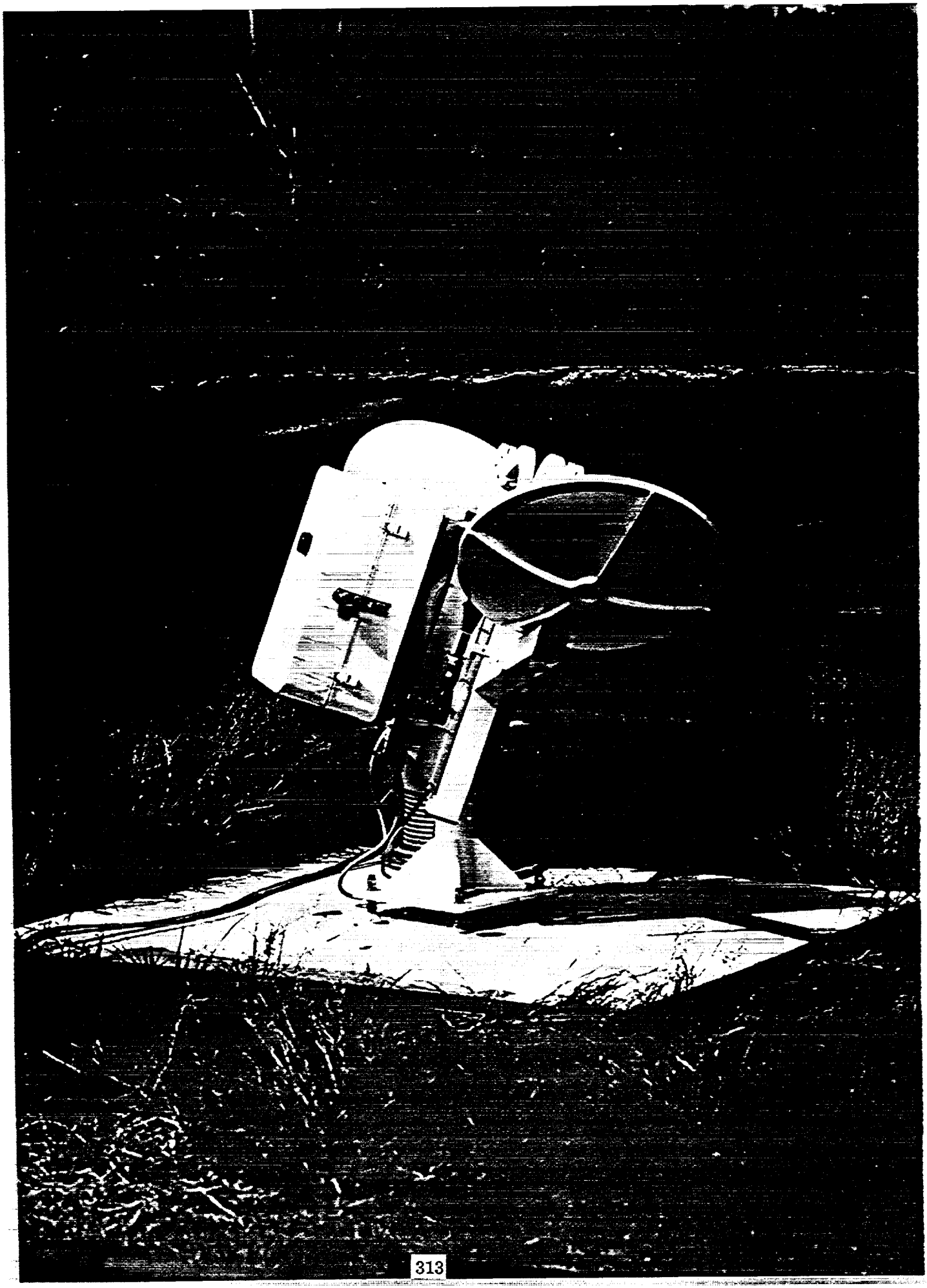

esa

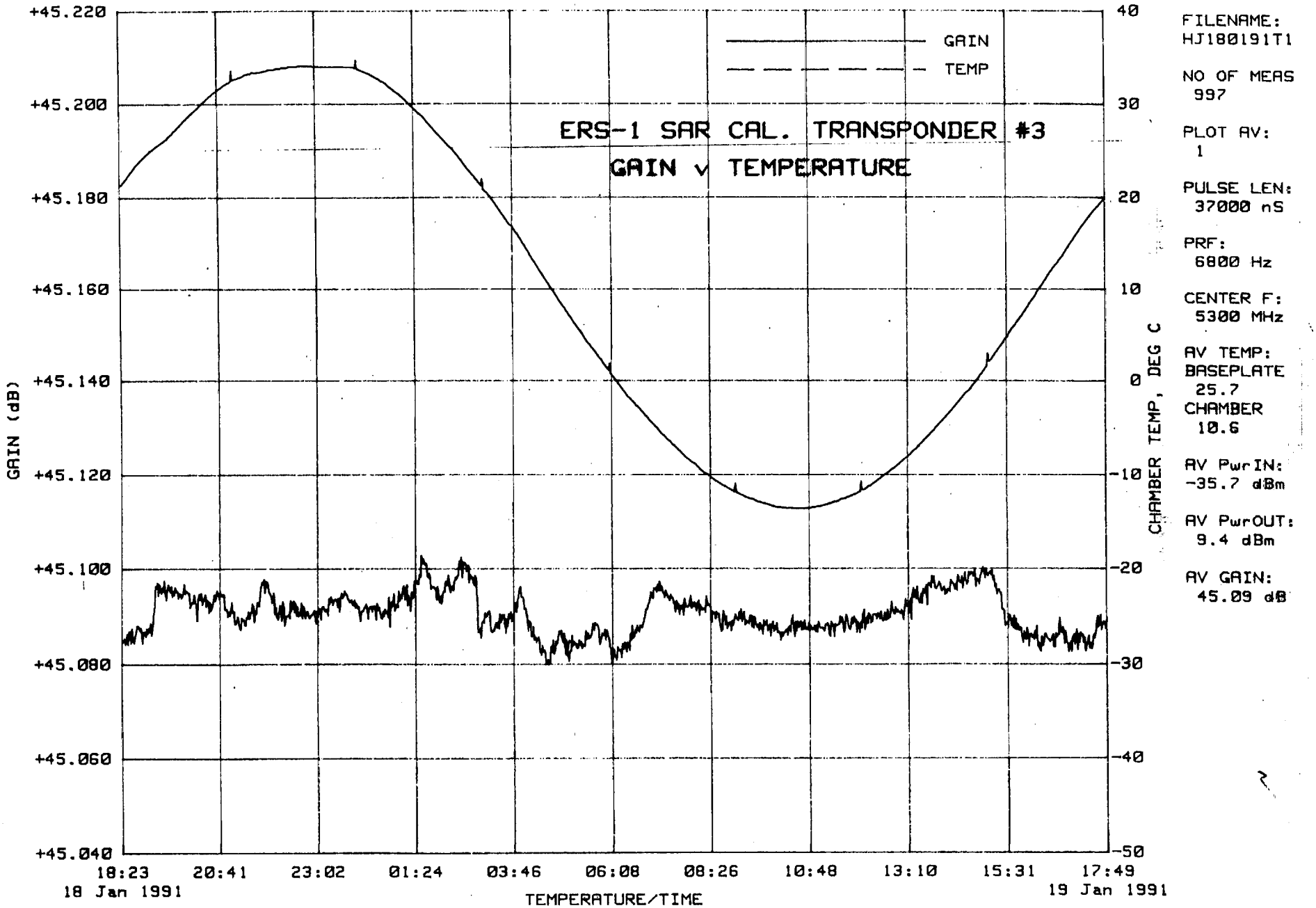

XRI Laboratory ESTEC ESA

ERS-1 Transponder Antennas

Gain Values for 12 Antennas

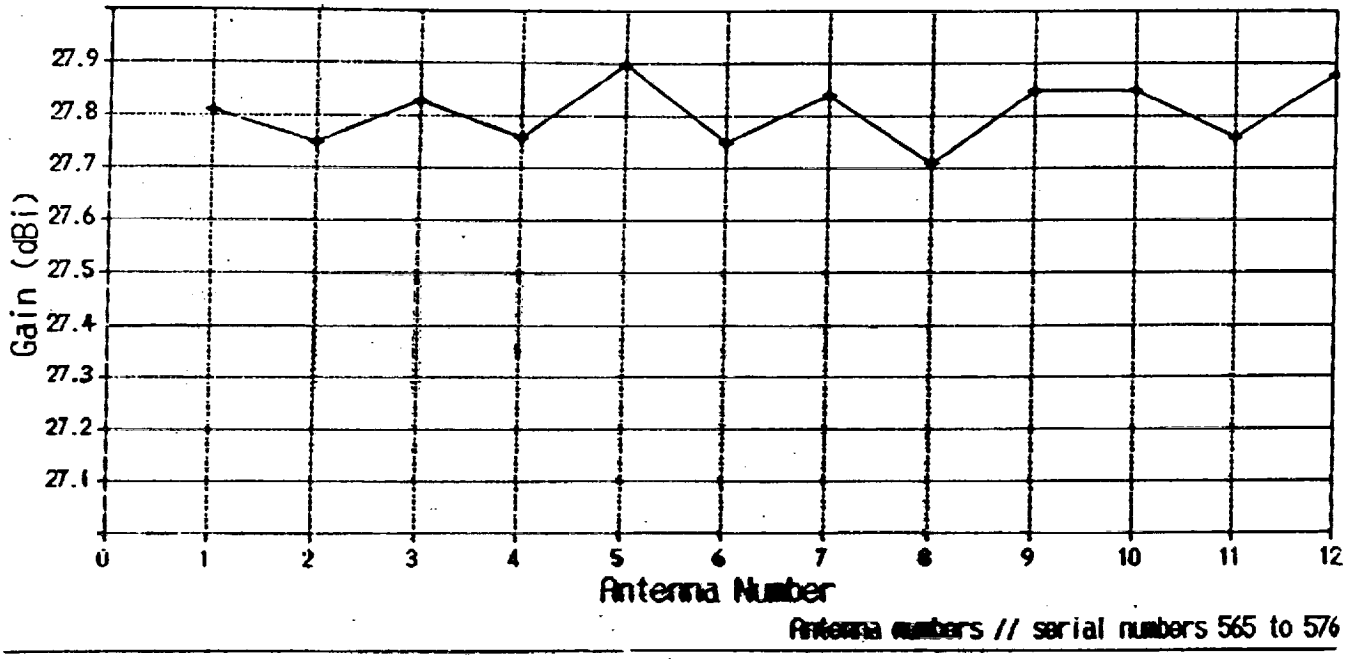

Average Gain = 27.81 dB

Standard Deviation = 0.06 dB

Transponder Error Model

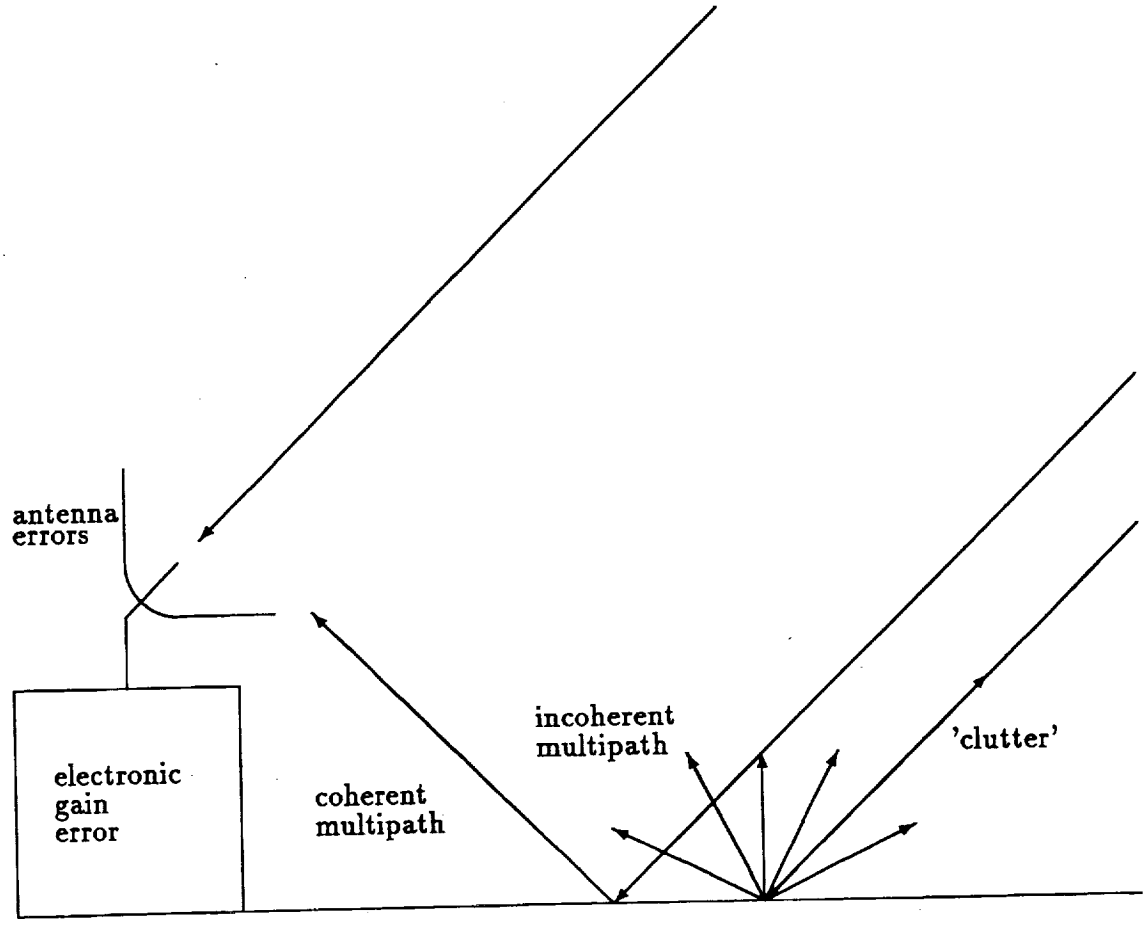

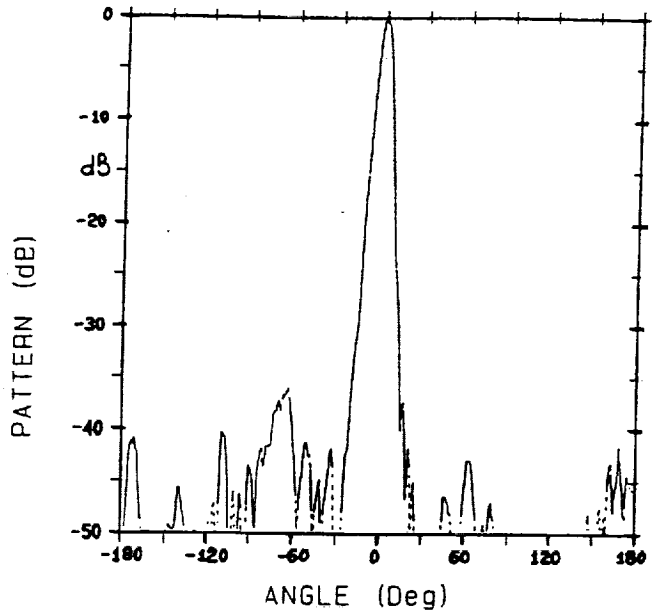

Sidelobe structure in H-plane pattern (plane of offset).

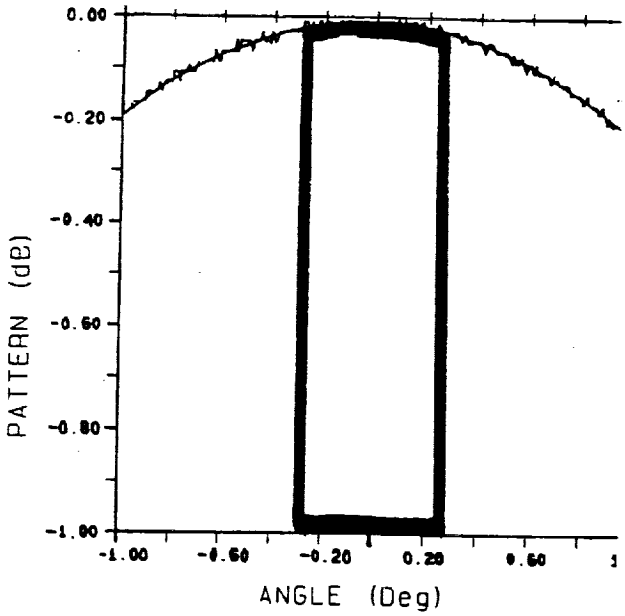

Pointing evaluation E-plane, based on LMS curve fi

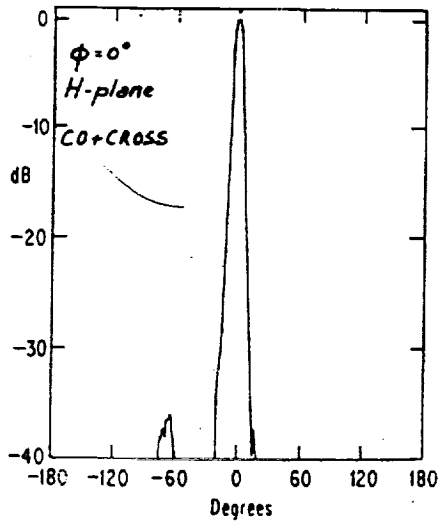

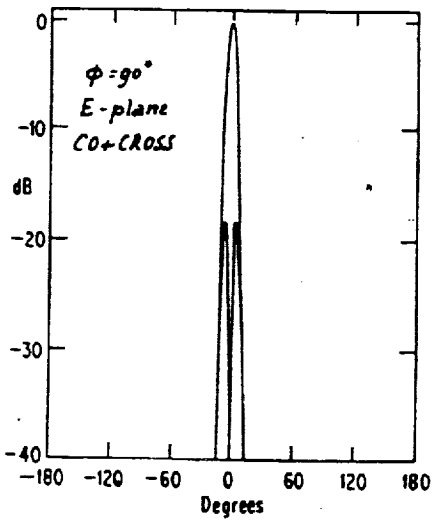

E and H plane patterns, co and cross-polarisation.

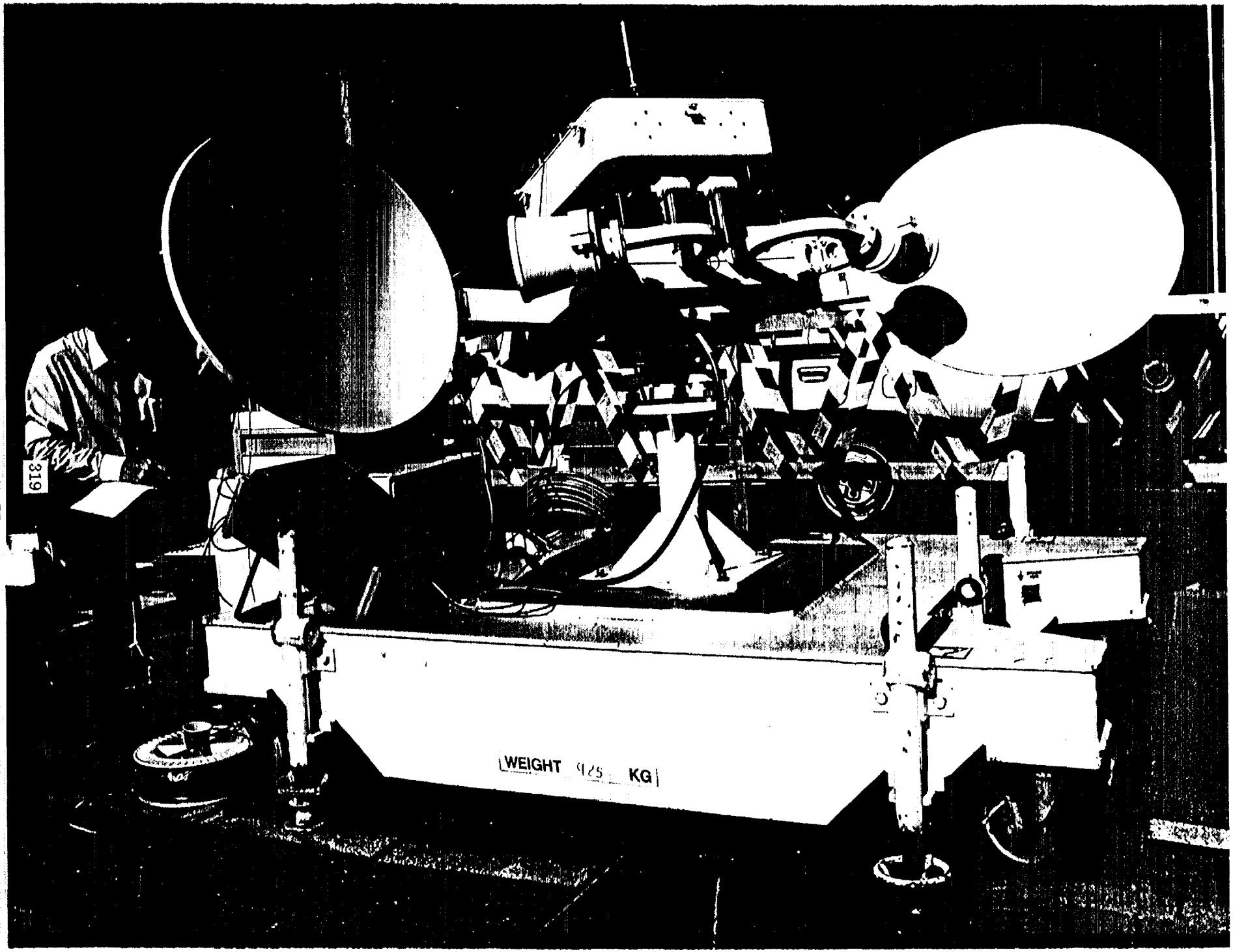
WEIGHT 125 KG

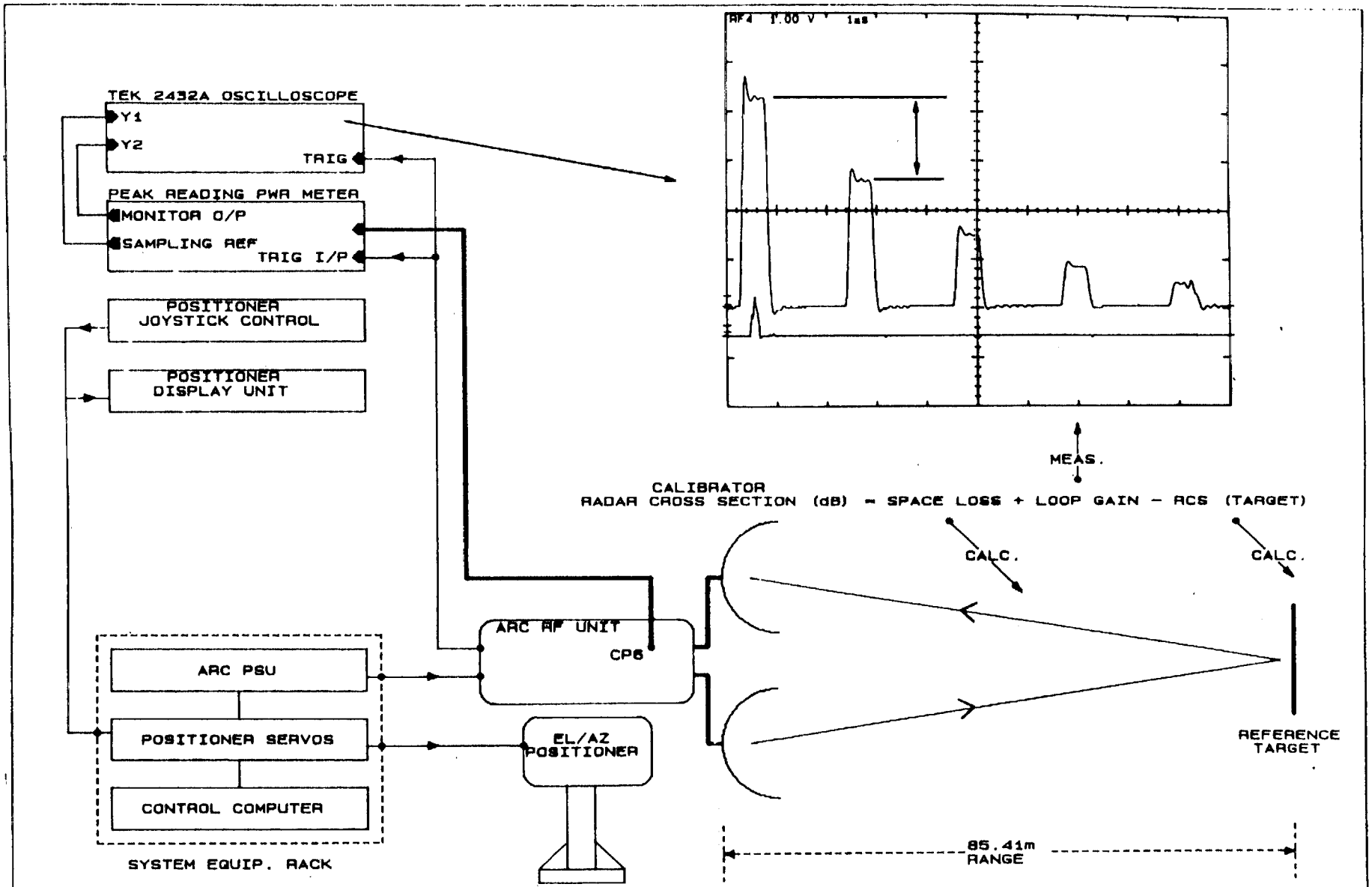

FIGURE 2. RADAR CROSS SECTION CALIBRATION

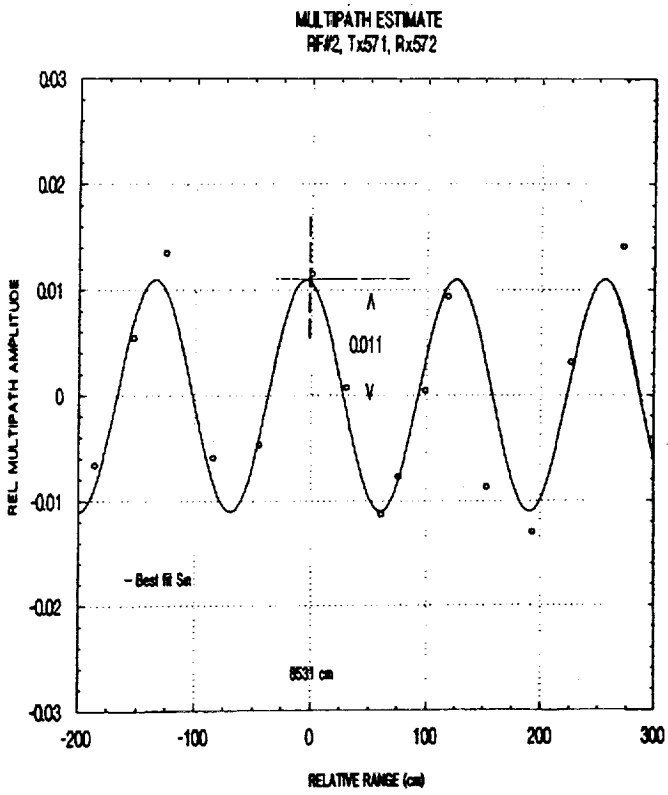
MULTIPATH ESTIMATE
RF#2, Tx571, Rx572
REL. MULTIPATH AMPLITUDE
0.03
0.02
0.01
0
-0.01
-0.02
-0.03
A
0.011
V
Best fit Sin
8531 cm
-200
-100
0
100
200
300
RELATIVE RANGE (cm)

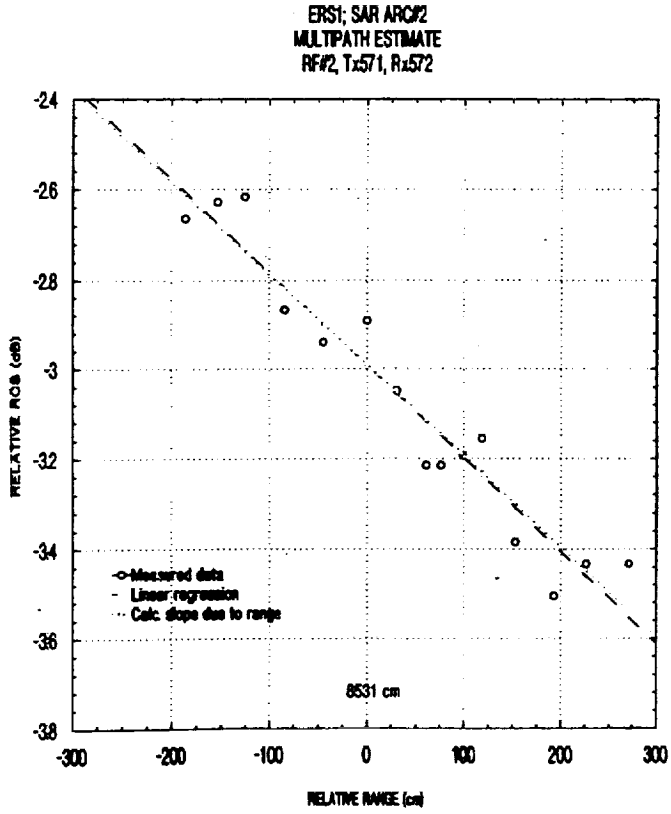
ERS1; SAR ARC#2
MULTIPATH ESTIMATE
RF#2, Tx571, Rx572
RELATIVE RCS (dB)
-24
-26
-28
-30
-32
-34
-36
-38
Measured data
Linear regression
Calc. slope due to range
8531 cm
-300
-200
-100
0
100
200
300
RELATIVE RANGE (cm)

Transponder Calibration Accuracy

		SAR	SCATT	
		full range	full range	
A	Antenna Gain Error	0.028	0.032	dB
	Pointing Error	0.53	0.56	deg
B	Electronic Gain Error	0.05	0.056	dB
C	Antenna Coupling Error	0.002	-	dB
	Transponder Stability A+B+C	.08	0.088	dB
		$1\ \sigma$	$1\ \sigma$	
D	Transponder Stability $1\ \sigma$ = (A+B+C)/3	0.027	0.029	dB
E	Clutter & Noise against $\sigma^0 = 0$ background	0.0495	0.0217	dB
F	Coherent Multipath	0.0207	0.0388	dB
G	Incoherent Multipath	0.0410	0.0767	dB
	Single Transponder Observation Error $\sqrt{D^2 + E^2 + F^2 + G^2}$	0.07	0.093	dB
H	Atmospheric Loss Uncertainty	0.07	0.07	dB
	Combined Error = $\sqrt{D^2 + E^2 + F^2 + G^2 + H^2}$	0.1	0.117	dB
I	Transponder Calibration Accuracy	0.2	0.2	dB

Representative SAR Calibration Budgets

SAR Radiometric Accuracy

			$1\ \sigma$	
A	Absolute Calibration Error	a	0.14	dB
B	Cross Swath Calibration Error	b	0.08	dB
C	Radiometric Stability Drift	b	0.25	dB
	Nominal Calibration Accuracy		0.3	dB
D	Radiometric Stability Drift Nominal - Observation	c	0.25	dB
E	Across Swath Characterisation Error	c	0.1	dB
F	Across Dynamic Range Characterisation	c	0.1	dB
G	Atmospheric Loss Uncertainty	c	0.07	dB
	Total Radiometric Error = $\sqrt{A^2+B^2+C^2}+\sqrt{D^2+E^2+F^2+G^2}$		0.6	dB

(a) Dominated by transponder calibration

(b) Single sample error, reduced by in-flight monitoring

(c) Random error per observation

Absolute Calibration Error

		Number of Samples	Single Sample Error($1\ \sigma$)	
H	Transponder Calibration Accuracy	3	0.2	dB
I	Antenna Gain Characterisation	3	0.1	dB
J	Single Transponder Observation Error	3	0.07	dB
K	Atmospheric Loss Uncertainty	3	0.07	dB
	Combined Error = $\sqrt{H^2/3+I^2/3+J^2/3+K^2/3}$		0.14	dB

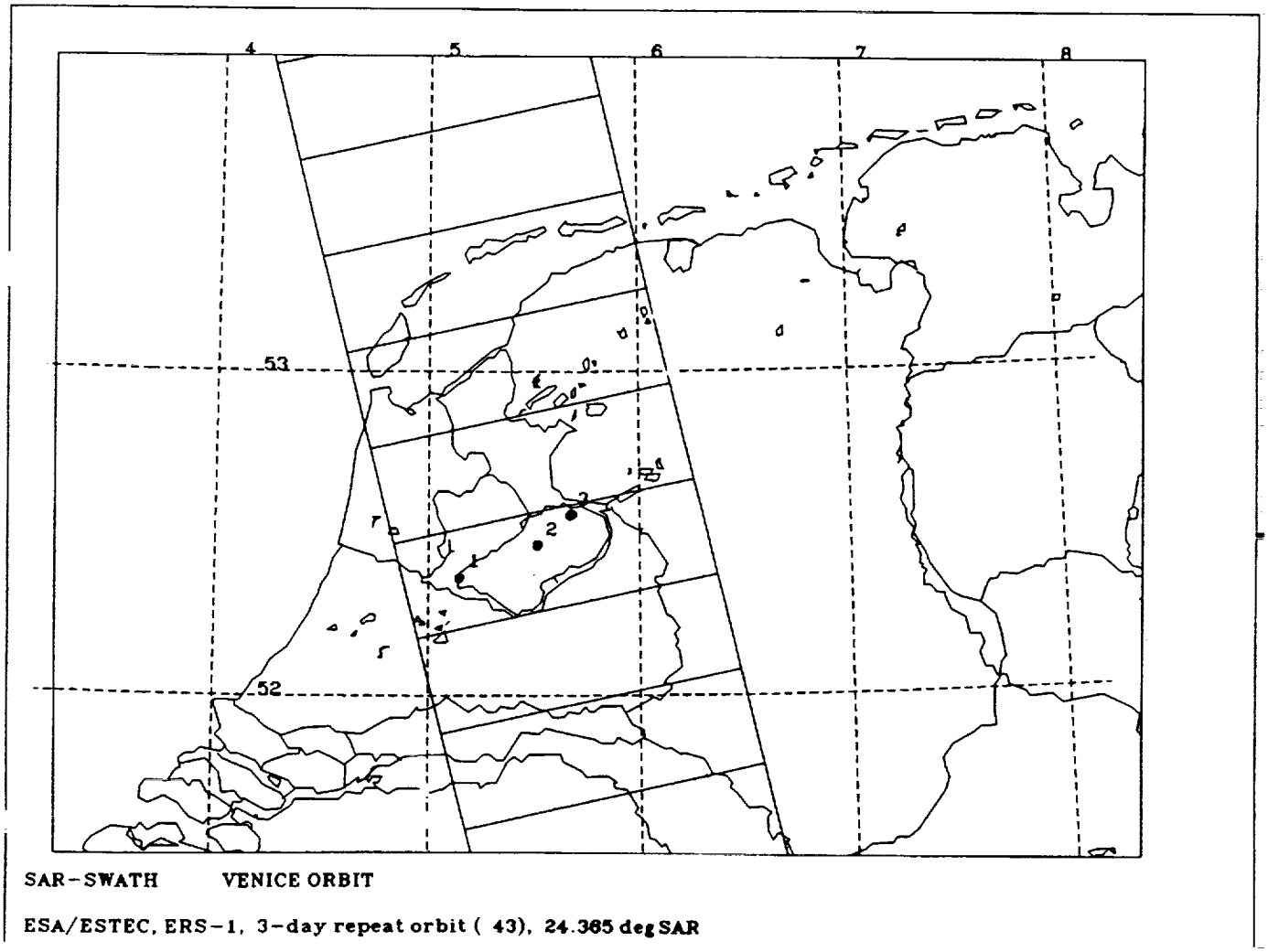

Figure 7: Transponder Sites Flevoland, Commissioning Phase Coverage

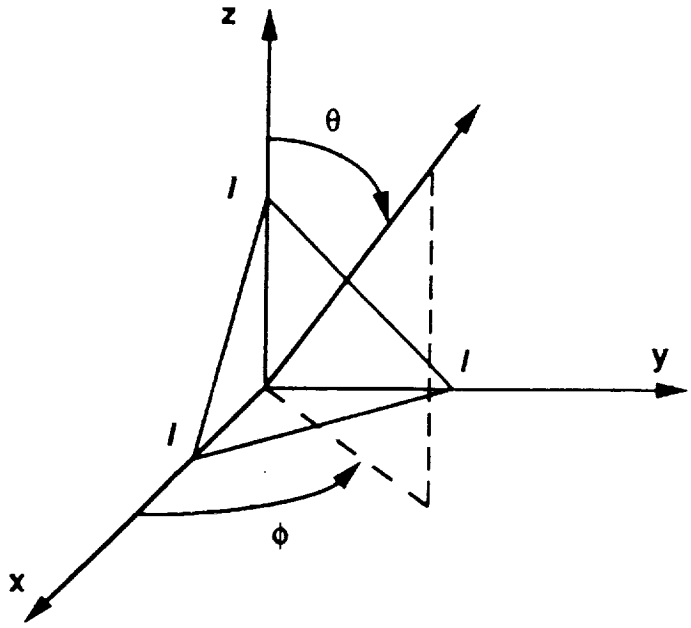
z
θ
l
l
y
l
x
ϕ

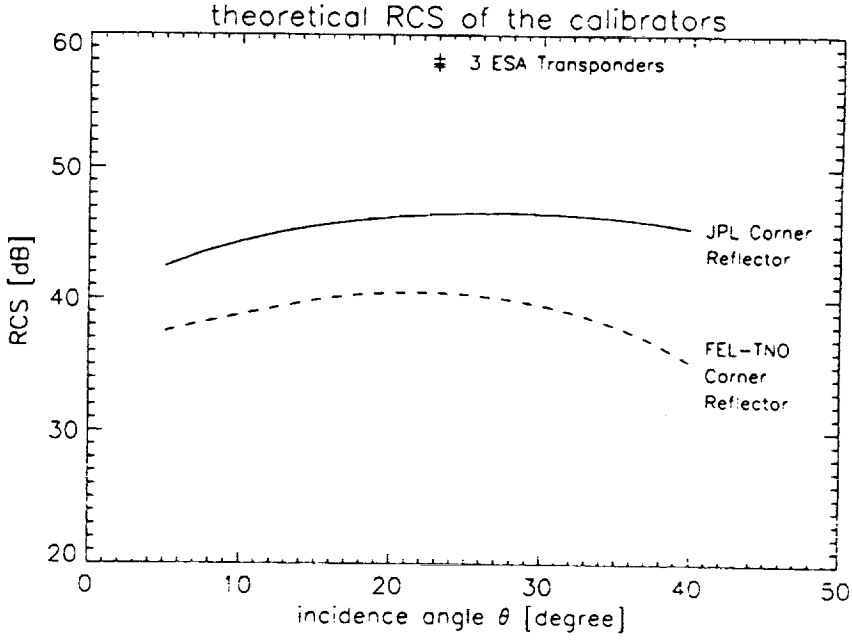
theoretical RCS of the calibrators
3 ESA Transponders
JPL Corner Reflector
FEL-TNO Corner Reflector
RCS [dB]
60
50
40
30
20
0
10
20
30
40
50
incidence angle θ [degree]

ERS-1

TRANSPONDER & CORNER REFLECTORS ABSOLUTE R.C.S.

COMMISSIONNING PHASE (from 25-OCT-1991 to 6-DEC-1991)

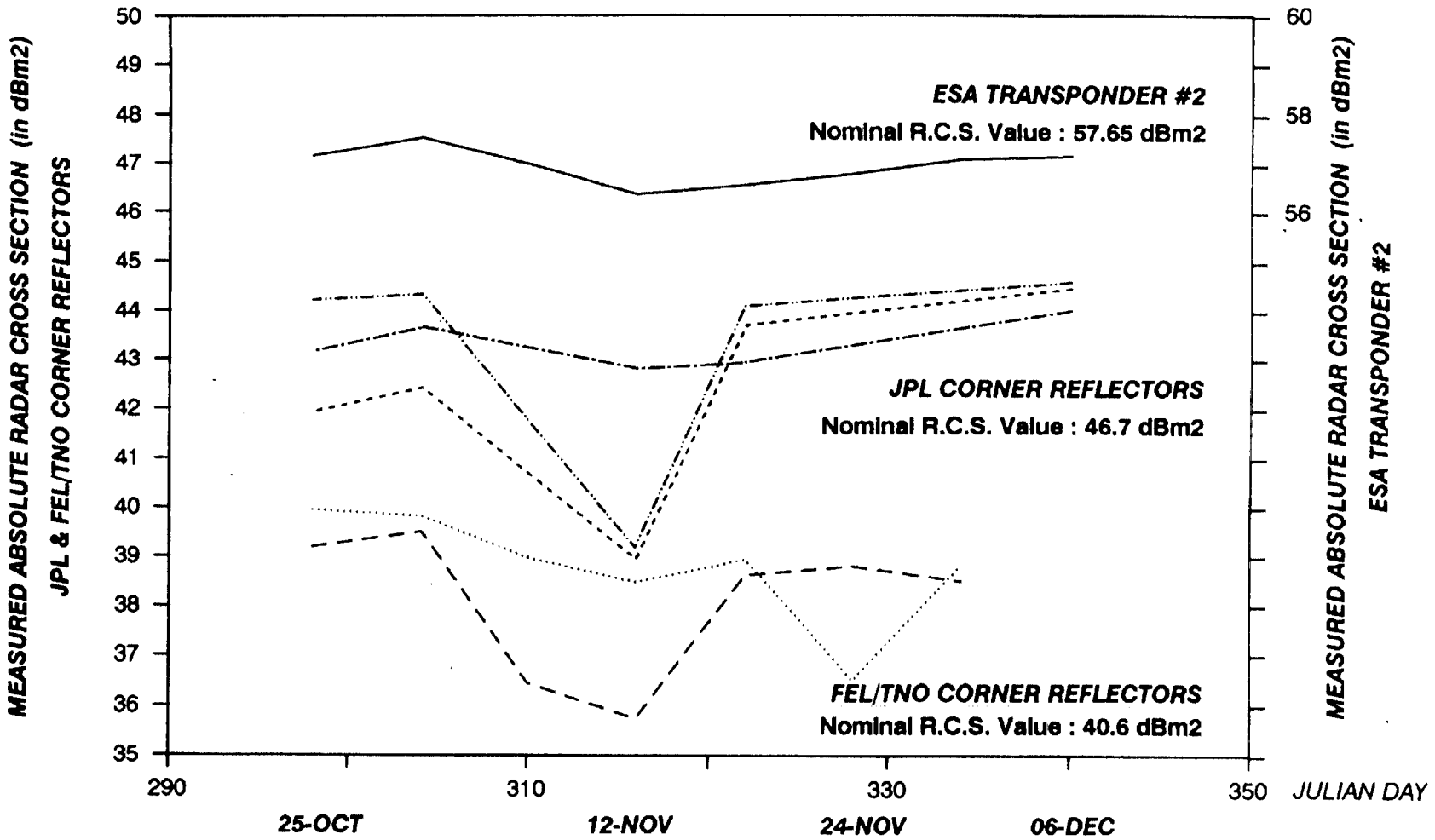

SAME CALIBRATION CONSTANT USED *Reference : 13-OCT-1991 Transponder #2*

esa

ESRIN / ERS-1 PRODUCT CONTROL SERVICE

ERS-1

SAR CALIBRATION HISTORY

COMMISSIONNING PHASE & ICE PHASE (from 7-SEP-1991 to 11-MAR-1992)

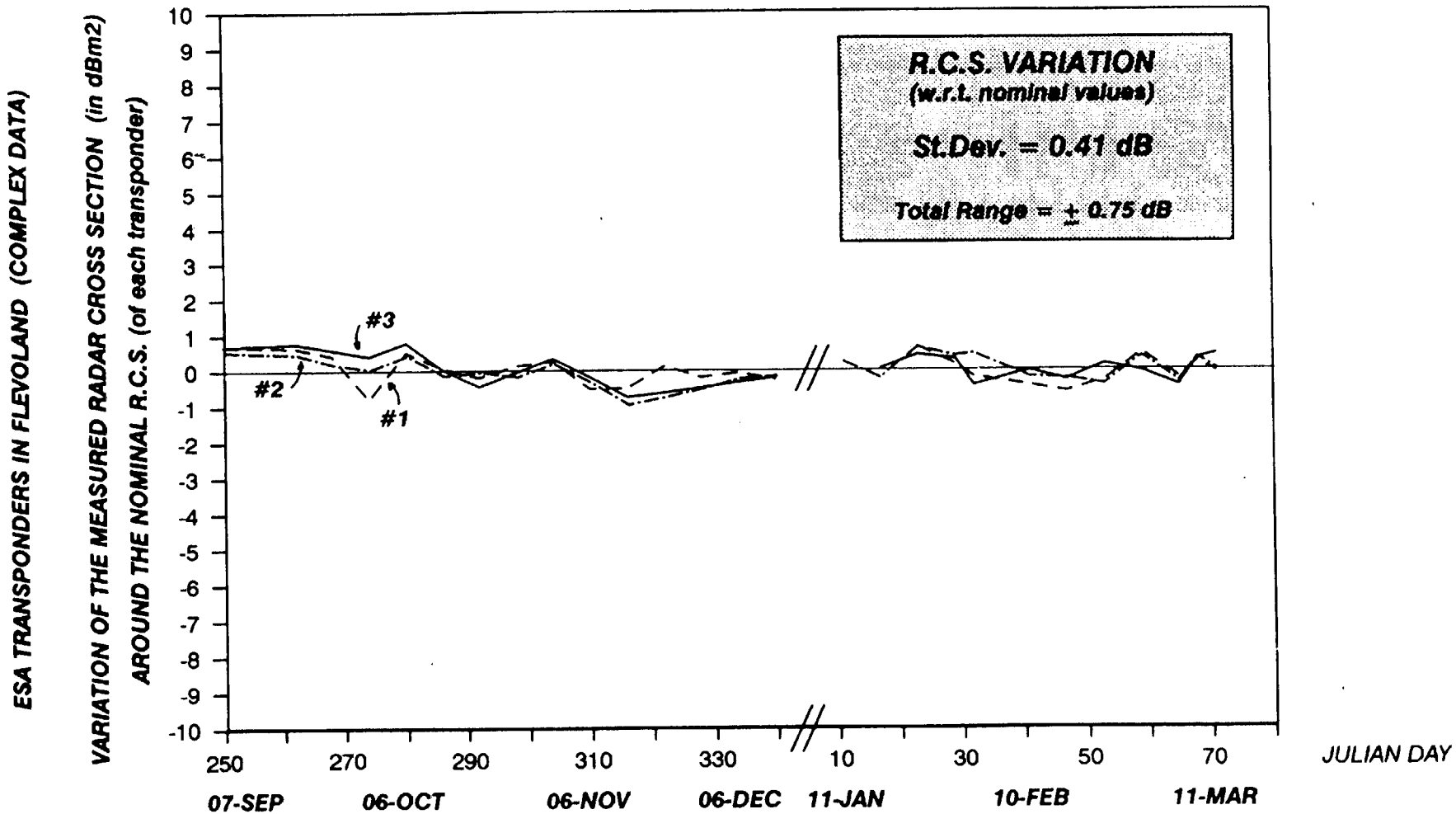

SAME CALIBRATION CONSTANT USED *Reference : 13-OCT-1991 Transponder #2*

Calibration of other areas

The application of the calibration factor to other areas requires knowledge of geometry (range & antenna angle) and stability over time.

High resolution information about the antenna diagram can be obtained from imagery of extended uniform targets such as the tropical forest or ice shelves.

No absolute information is required for these 'targets of opportunity'. Stability over time and a smooth dependence of σ^0 on incidence angle is necessary.

ERS-1 Wind Scatterometer Fore Beam Sigma 0 Cycle 37
Sigma 0 (dB)
4
5
6
7
8
9
Latitude
15
10
5
0
-5
-10
-15
-20
Longitude
-50
-55
-60
-65
-70
-75
-80

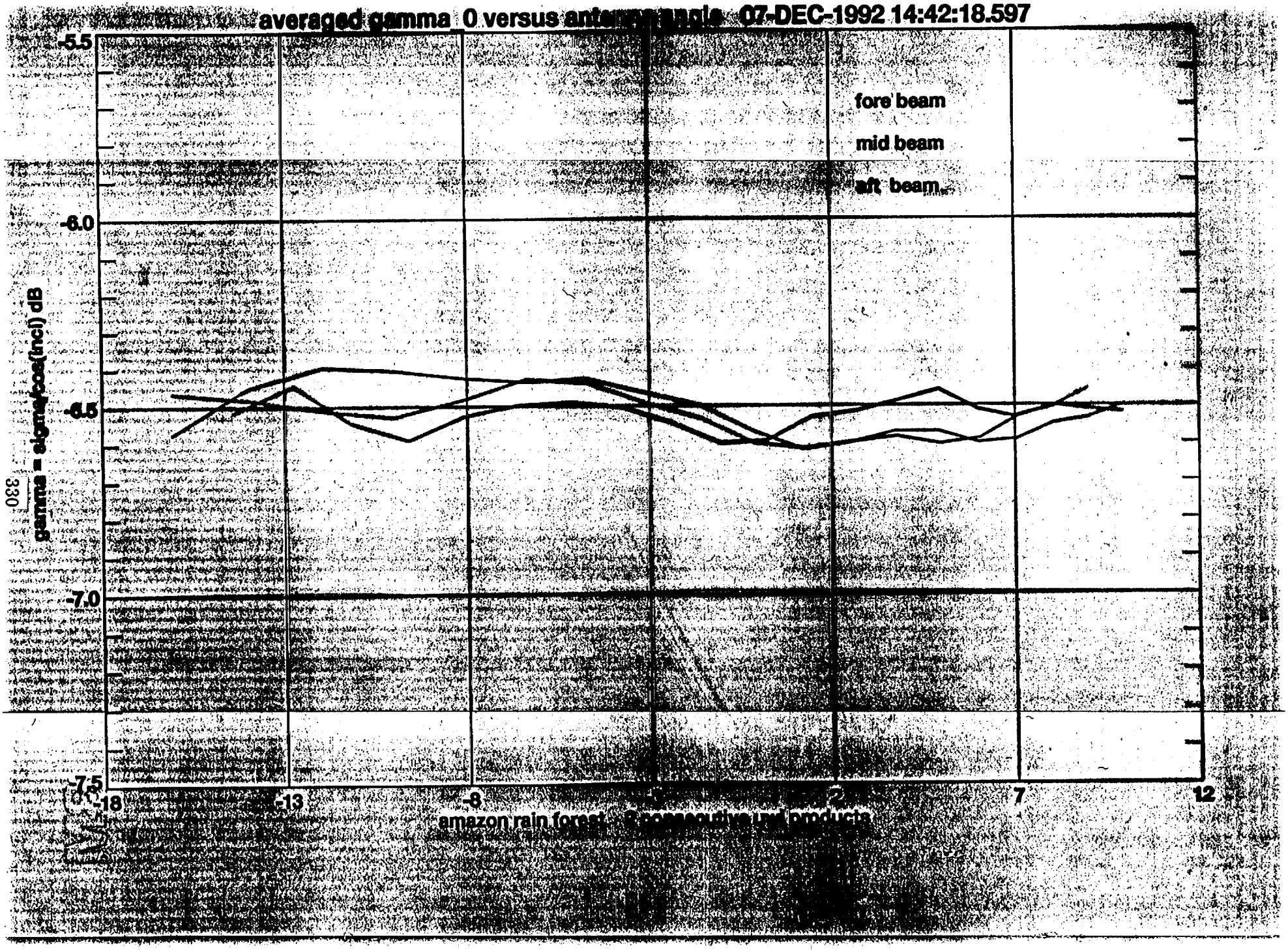
averaged gamma_0 versus antenna angle 07-DEC-1992 14:42:18.597
fore beam
mid beam
aft beam
-5.5
-6.0
-6.5
-7.0
-7.5
gamma = sigma/cos(incl) dB
330
-18
-13
-8
-2
7
12
amazon rain forest - 3 consecutive rev products

Data calibration

Data calibration include the following steps

- Correct raw data for a number of system parameters
  - — Linear distortion (amplitude & phase)
  - — Non-linear distortion
  - — Detector imperfections (DC-biases, amplitude & phase imbalance)
  - — time variations as measured by internal calibration
  - — noise bias
- Application of calibration factor to the entire image, taking into account geometry and antenna angle.

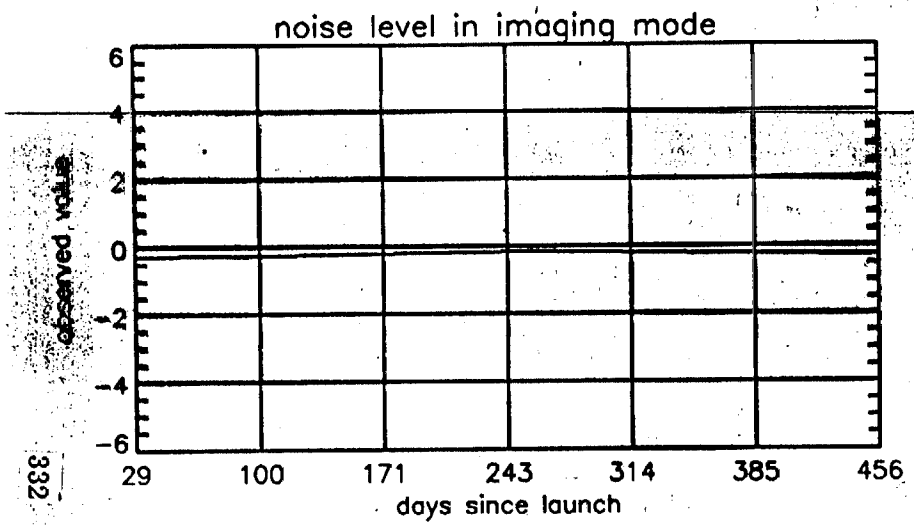
noise level in imaging mode
observed value
6
4
2
0
-2
-4
-6
29
100
171
243
314
385
456
days since launch

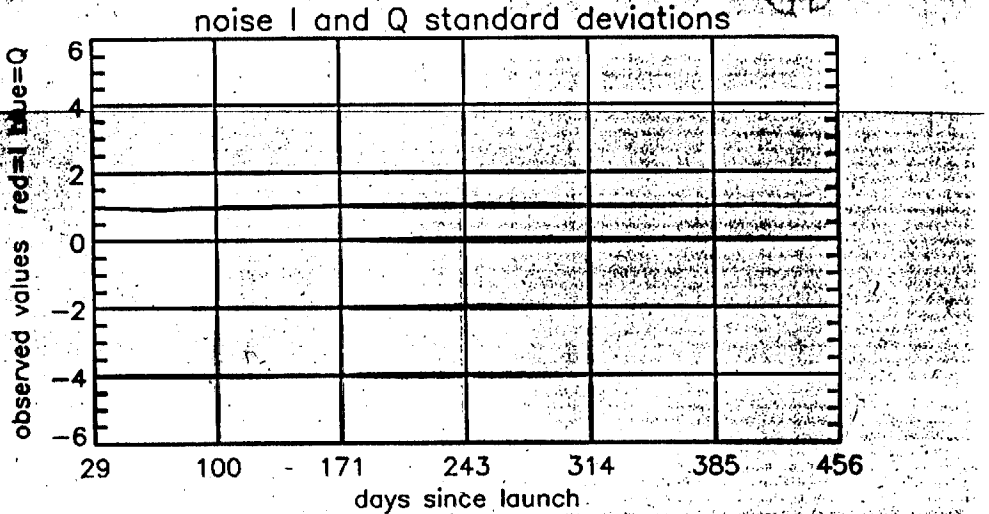
noise I and Q standard deviations
observed values red=I blue=Q
6
4
2
0
-2
-4
-6
29
100
171
243
314
385
456
days since launch

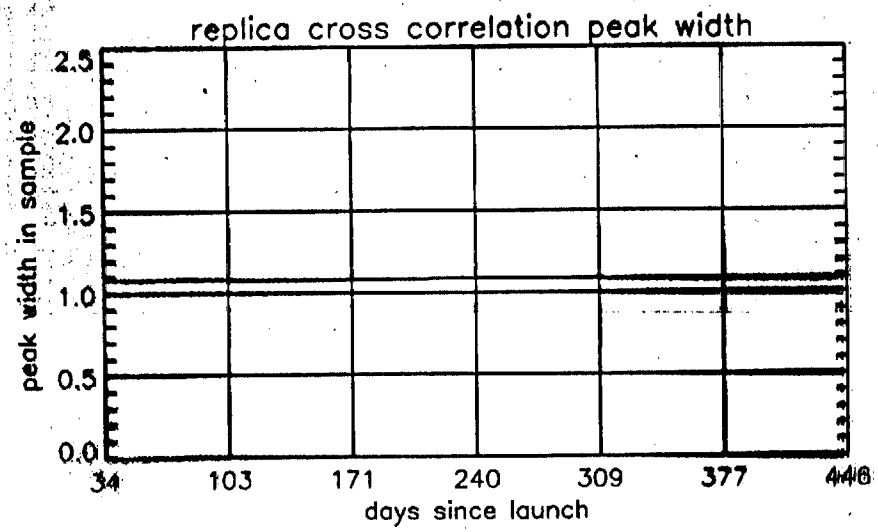
replica cross correlation peak width
peak width in sample
2.5
2.0
1.5
1.0
0.5
0.0
34
103
171
240
309
377
446
days since launch

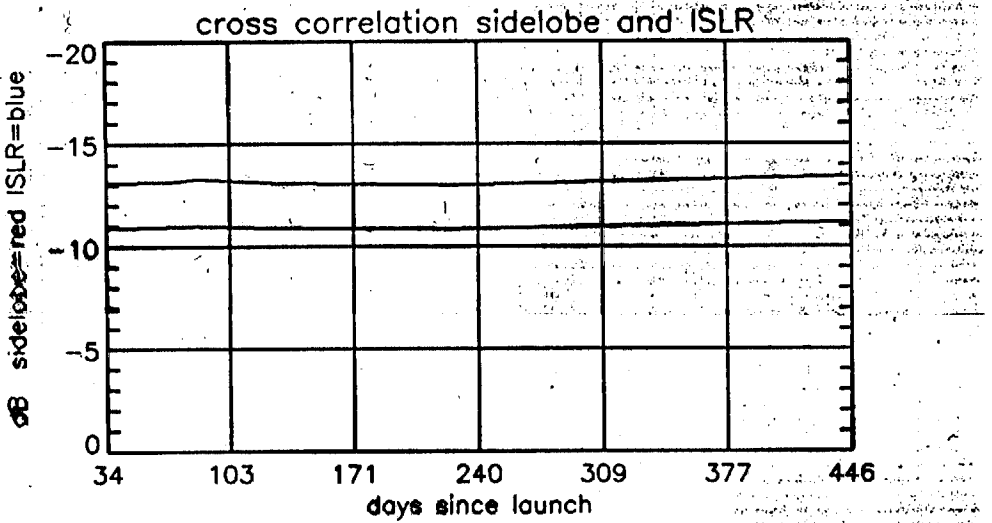
cross correlation sidelobe and ISLR
dB sidelobe=red ISLR=blue
-20
-15
-10
-5
0
34
103
171
240
309
377
446
days since launch

Geometric calibration

Geometric calibration can be achieved following the same principles as for radiometric calibration.

- Design for stability
- Characterise SAR system in terms of delay, phase error and frequency offset
- Calibrate using point target with accurately known position

Geometric image calibration is carried out in the data calibration stage by correction for known system biases and applying geometry information (platform position & attitude and terrain models).

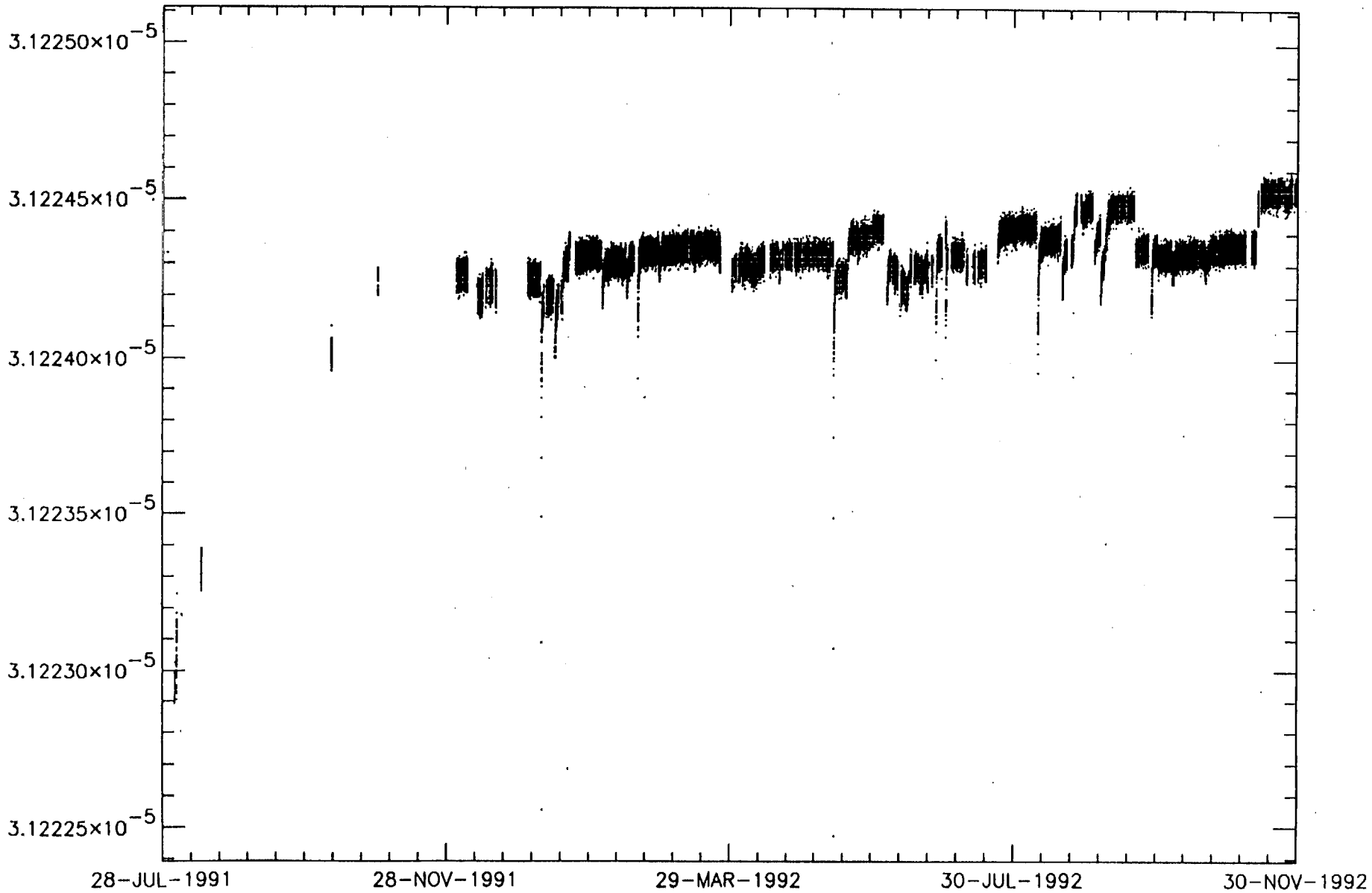
3.12250×10^-5
3.12245×10^-5
3.12240×10^-5
3.12235×10^-5
3.12230×10^-5
3.12225×10^-5
28-JUL-1991
28-NOV-1991
29-MAR-1992
30-JUL-1992
30-NOV-1992

Phase calibration

During the formation of an intensity image the phase information in the radar data is lost. For applications in interferometry and polarimetry complex images are formed which provide two data points per pixel, amplitude & phase or real & imaginary parts of the complex signal.

Careful and elaborate phase characterisation of both the SAR sensor and the SAR processor are required. Time stability is critical for the above applications.

Polarimetric calibration

Polarimetric calibration can be treated essentially as a multi-channel extension of the methods discussed above. Polarimetric SAR differ from single channel SAR in the following ways.

- There are two orthogonal transmit channels to consider and four receive channels.
- Radiometric calibration can be separated into absolute calibration and relative between channel calibration
- Geometric calibration can be separated into absolute calibration and relative between channel calibration
- Phase calibration between channels is essential
- Crosstalk has to be taken into account

SYNTHETIC APERTURE RADAR SIGNAL PROCESSING: TRENDS AND TECHNOLOGIES

VEXCEL
CORPORATION

JOHN C. CURLANDER

presented at the
3rd SPACEBORNE IMAGING RADAR SYMPOSIUM

JET PROPULSION LABORATORY
PASADENA, CA
JANUARY 20, 1993

OVERVIEW OF SAR PROCESSING

SAR DATA SYSTEM OVERVIEW

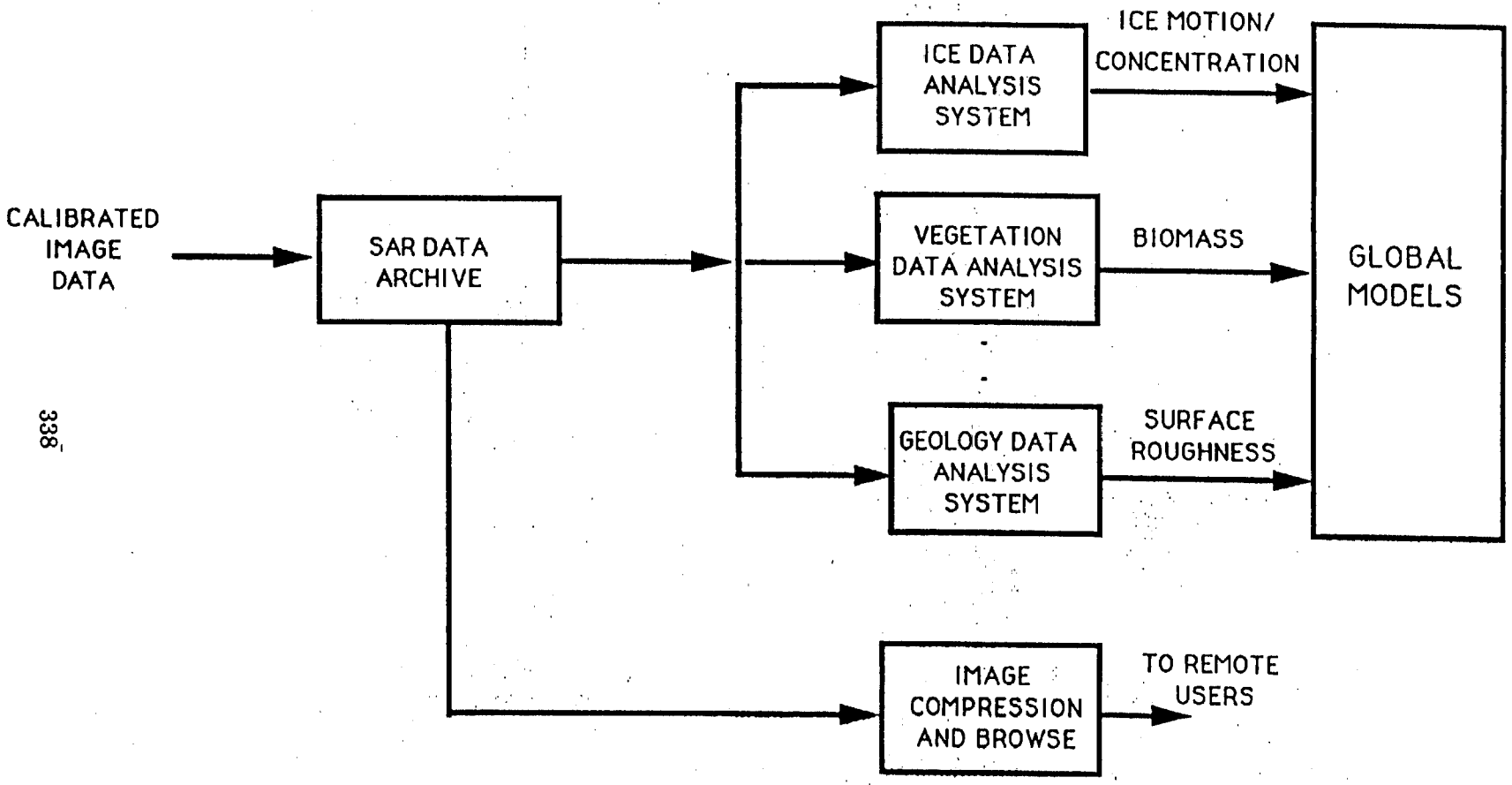

DATA UTILIZATION AND INFORMATION EXTRACTION SYSTEM

SAR CORRELATOR: TRENDS AND TECHNOLOGIES

OUTLINE

- OVERVIEW
  - SAR GROUND DATA SYSTEM
  - SAR SIGNAL PROCESSING ALGORITHMS
  - SAR CORRELATOR ARCHITECTURES
- CURRENT OPERATIONAL SYSTEM IMPLEMENTATIONS
  - ARCHITECTURES
  - ALGORITHMS
- SUMMARY
  - CURRENT, FUTURE TRENDS

OVERVIEW OF SAR PROCESSING

SAR DATA SYSTEM OVERVIEW

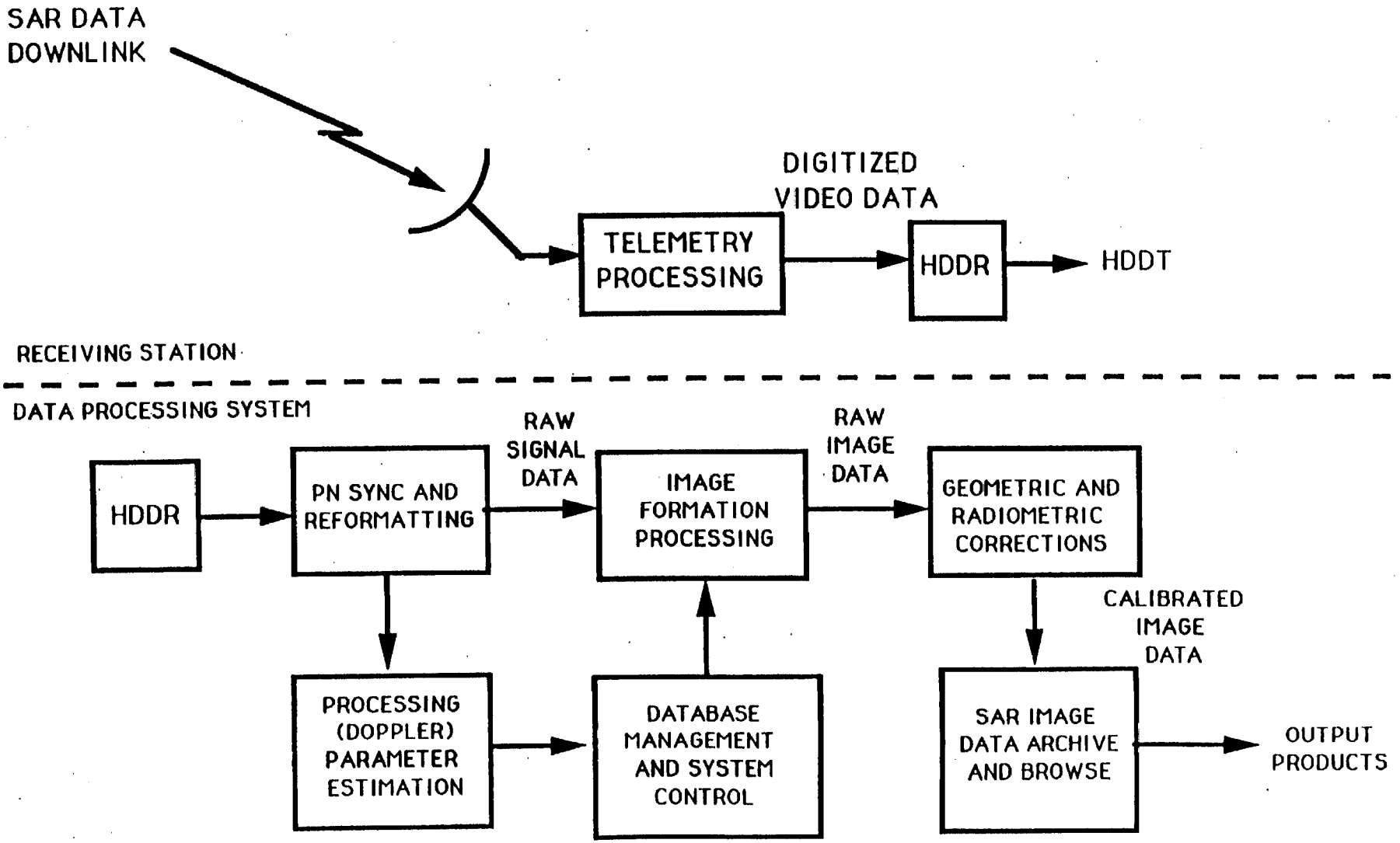

SAR CORRELATOR: TRENDS AND TECHNOLOGY

SAR PROCESSOR ALGORITHM OVERVIEW

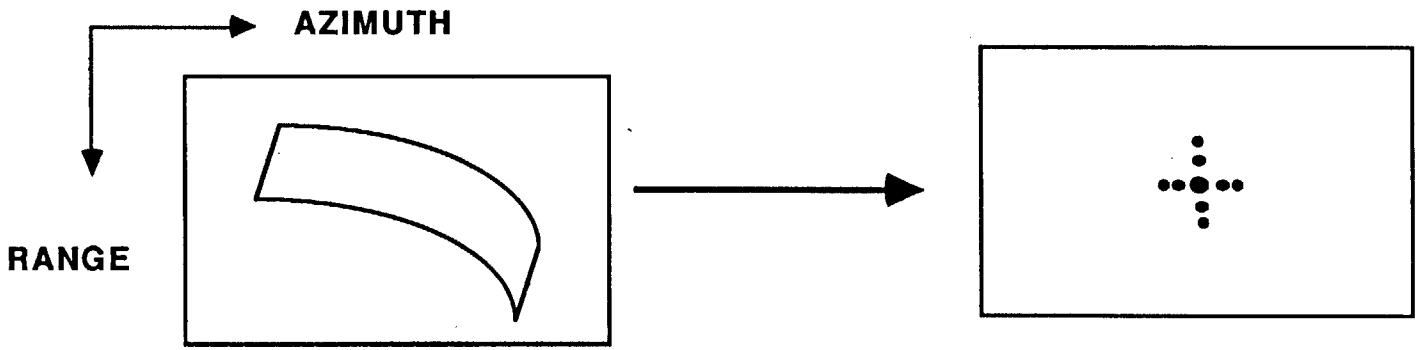

APPROACH 1: APPPLY 2-D FILTER TO COMPENSATE FOR PHASE DISPERSION

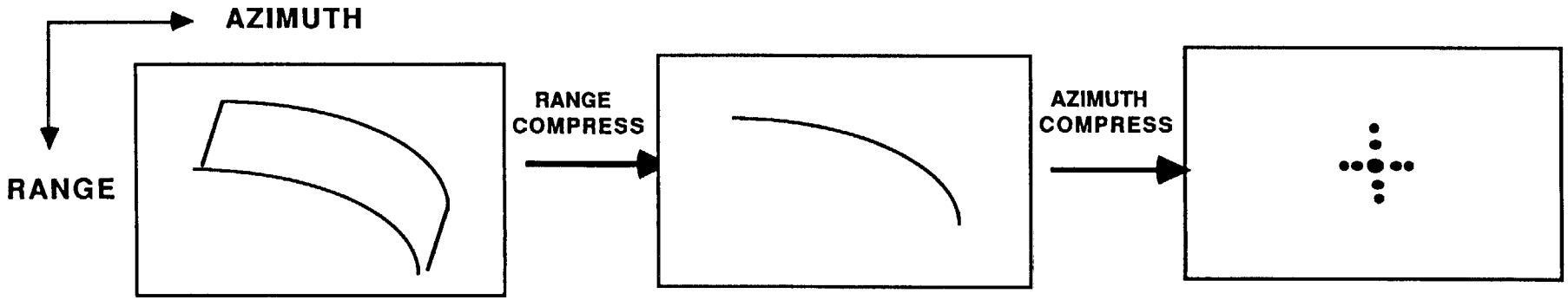

APPROACH 2: APPLY TWO 1-D FILTERS FORMING A RANGE COMPRESSED IMAGE

SAR CORRELATOR: TRENDS AND TECHNOLOGIES

ALGORITHM OVERVIEW

- SPECTRAL ANALYSIS ALGORITHMS
  - COMPUTATIONALLY EFFICIENT, GOOD IMAGE QUALITY FOR SMALL TIME-BANDWIDTH PRODUCTS, CANNOT ACHIEVE FULL AZIMUTH RESOLUTION, VARIABLE SNR ACROSS IMAGE BLOCK
  - SPECAN (DERAMP/FFT): SCANSAR, BURST MODE RADARS
  - POLAR ALGORITHM: MILITARY APPLICATIONS, HIGH SQUINT, SMALL PATCH

- RANGE/DOPPLER ALGORITHMS
  - FULL AZIMUTH RESOLUTION, GOOD IMAGE QUALITY FOR MODERATE SQUINT, PROVEN ALGORITHM FOR SPACEBORNE SAR, EASY PREPROC AND MOCOMP, POOR PERFORMANCE ON HIGH SQUINT AND HIGH RESOLUTION SAR
  - SECONDARY RAGE COMPRESSION (SRC): BROADSIDE, STRIP IMAGERS
  - SQUINT IMAGING MODE (SIM): STRIP IMAGERS SQUINT UP TO 20 DEGREES

- 2D TRANSFORM (WAVE DOMAIN) ALGORITHMS
  - BEST APPROX, EXCELLENT PHASE FIDELITY, LITTLE OR NO INTERPOLATION, UNPROVED IN OPERATIONAL SYSTEMS, DIFFICULT PREPROC AND MOCOMP, APPLICATION IN INTERFEROMETRY AND POLARIMETRY
  - WAVE EQUATION: HIGH SQUINT (75 DEGREES), PHASE PRESERVING
  - CHIRP SCALING: REQUIRES LINEAR FM CHIRP, NO INTERPOLATION

SPECAN ALGORITHM FLOWCHART

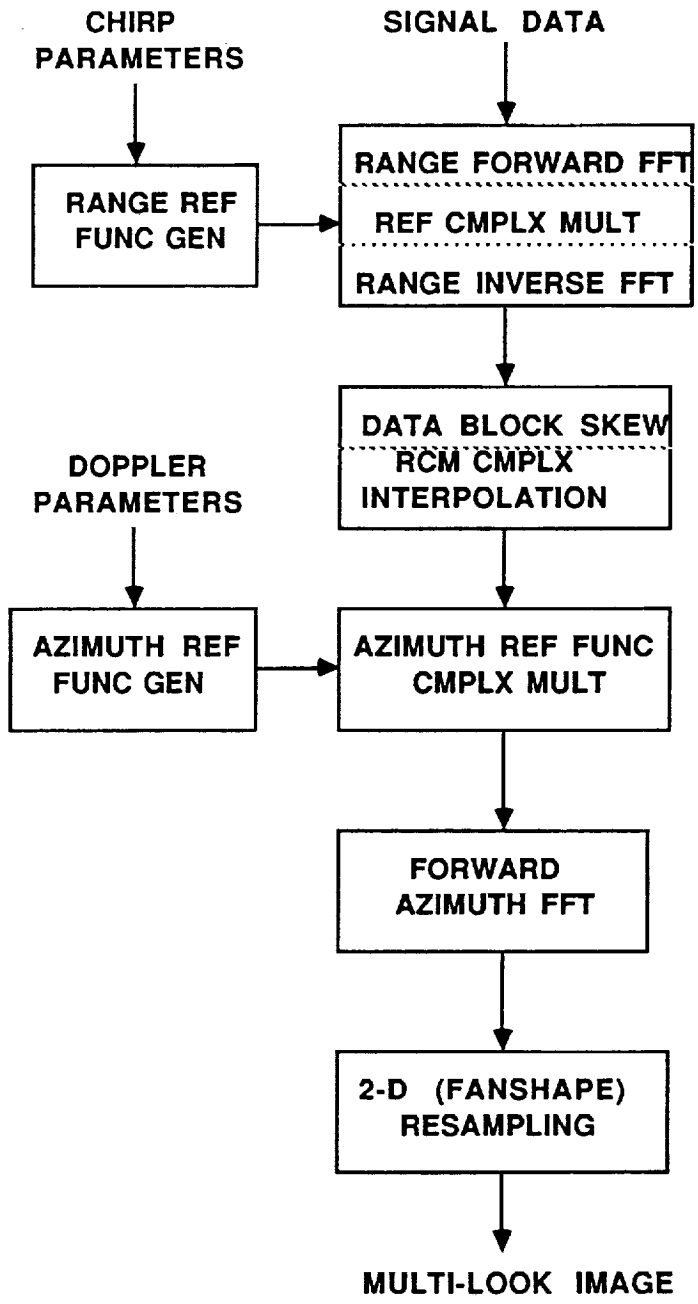

RANGE/DOPPLER ALGORITHM FLOWCHART
WITH SECONDARY RANGE COMPRESSION (SRC)

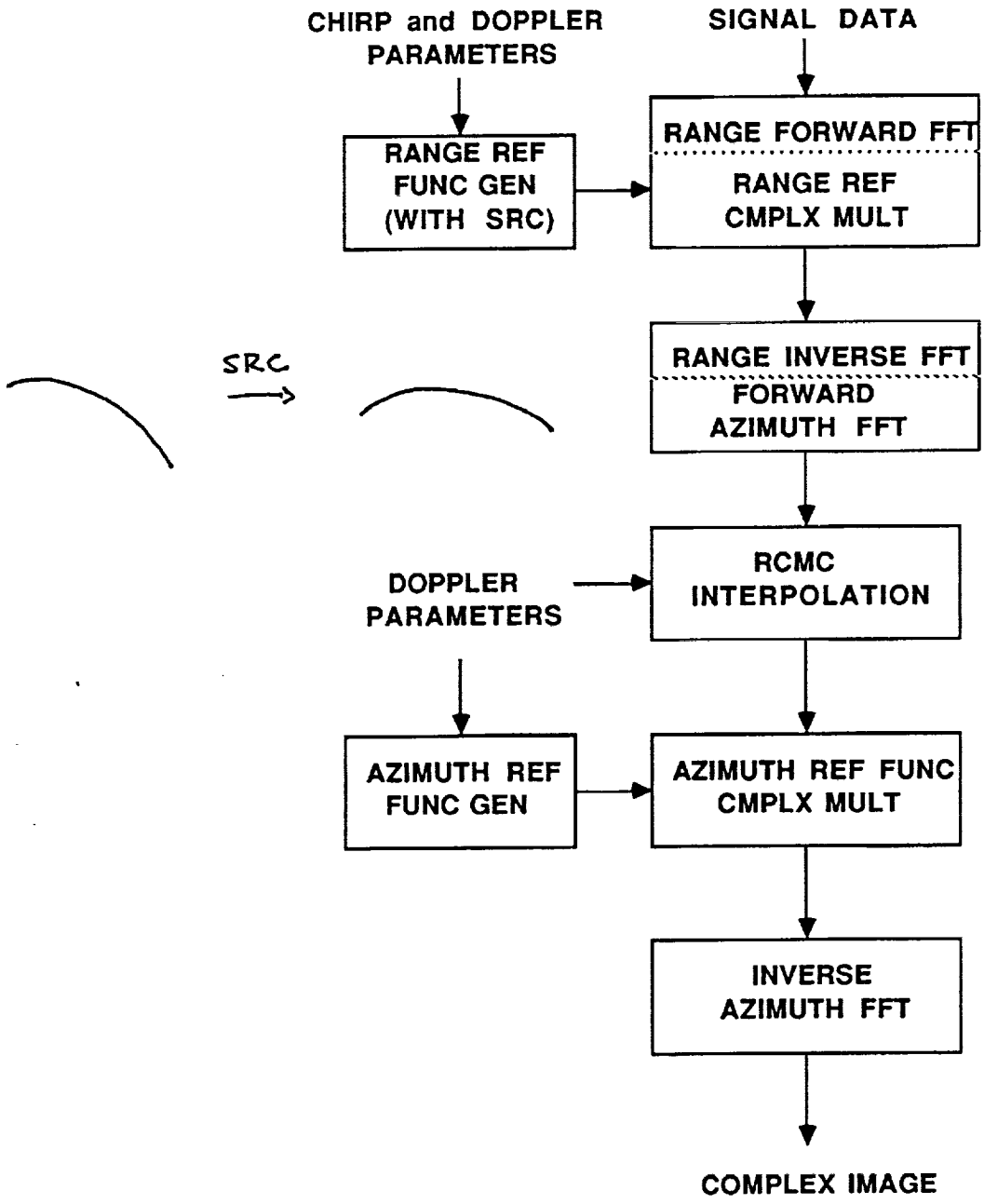

SAR CORRELATOR: TRENDS AND TECHNOLOGIES

RANGE DOPPLER ALGORITHM PERFORMANCE

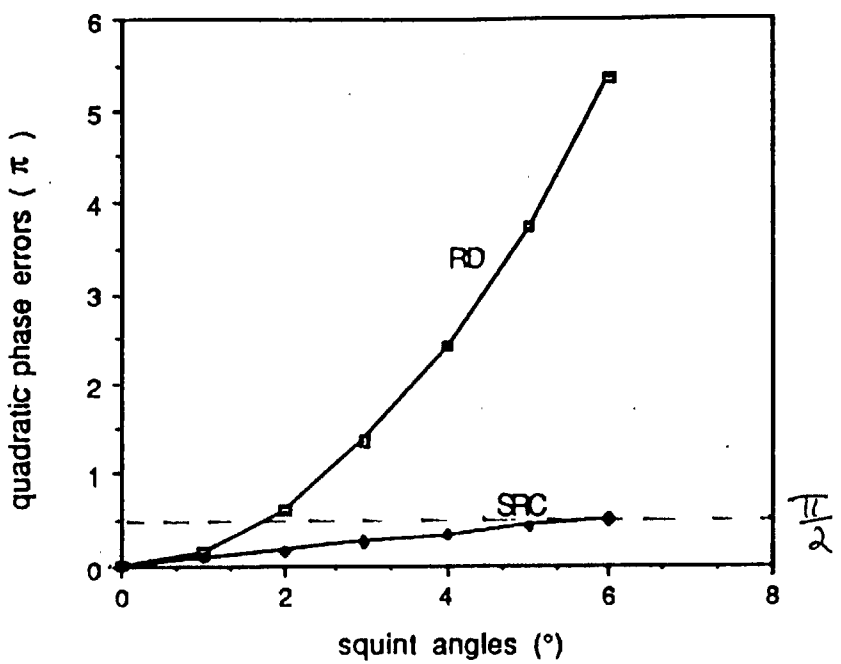

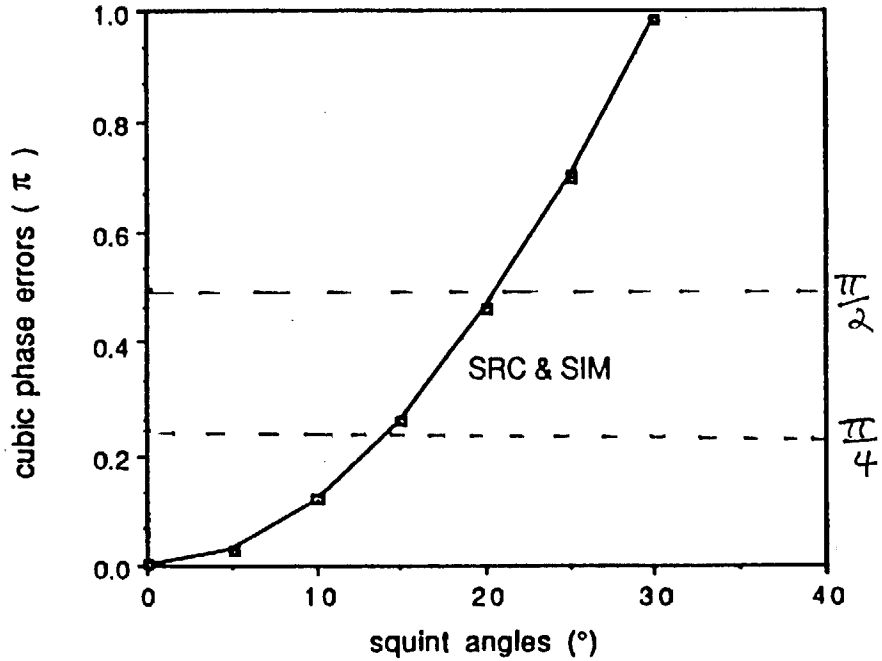

- RESIDUAL PHASE ERRORS FOR THE SECONDARY RANGE COMPRESSION (SRC) AND THE SQUINT IMAGING MODE (SIM) ALGORITHMS (CHANG, ET AL, 1992)

2-D TRANSFORM (WAVE EQUATION) ALGORITHM FLOWCHART

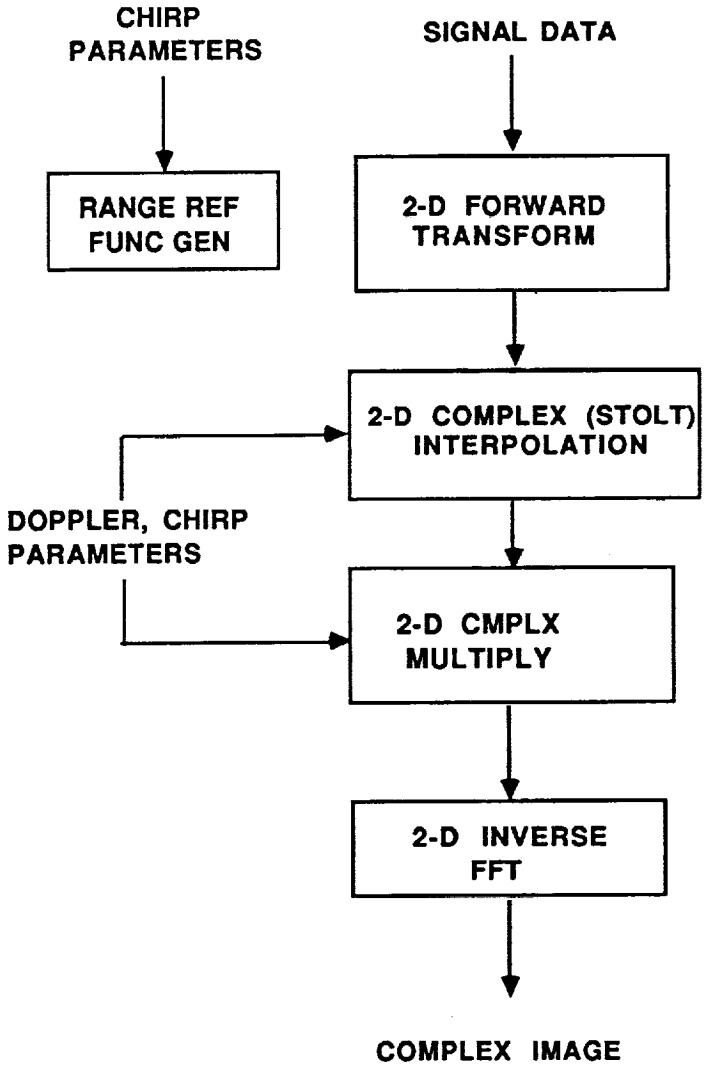

ROCCA, 1987; CAFFORIO, 1991

2-D TRANSFORM (CHIRP SCALING) ALGORITHM FLOWCHART

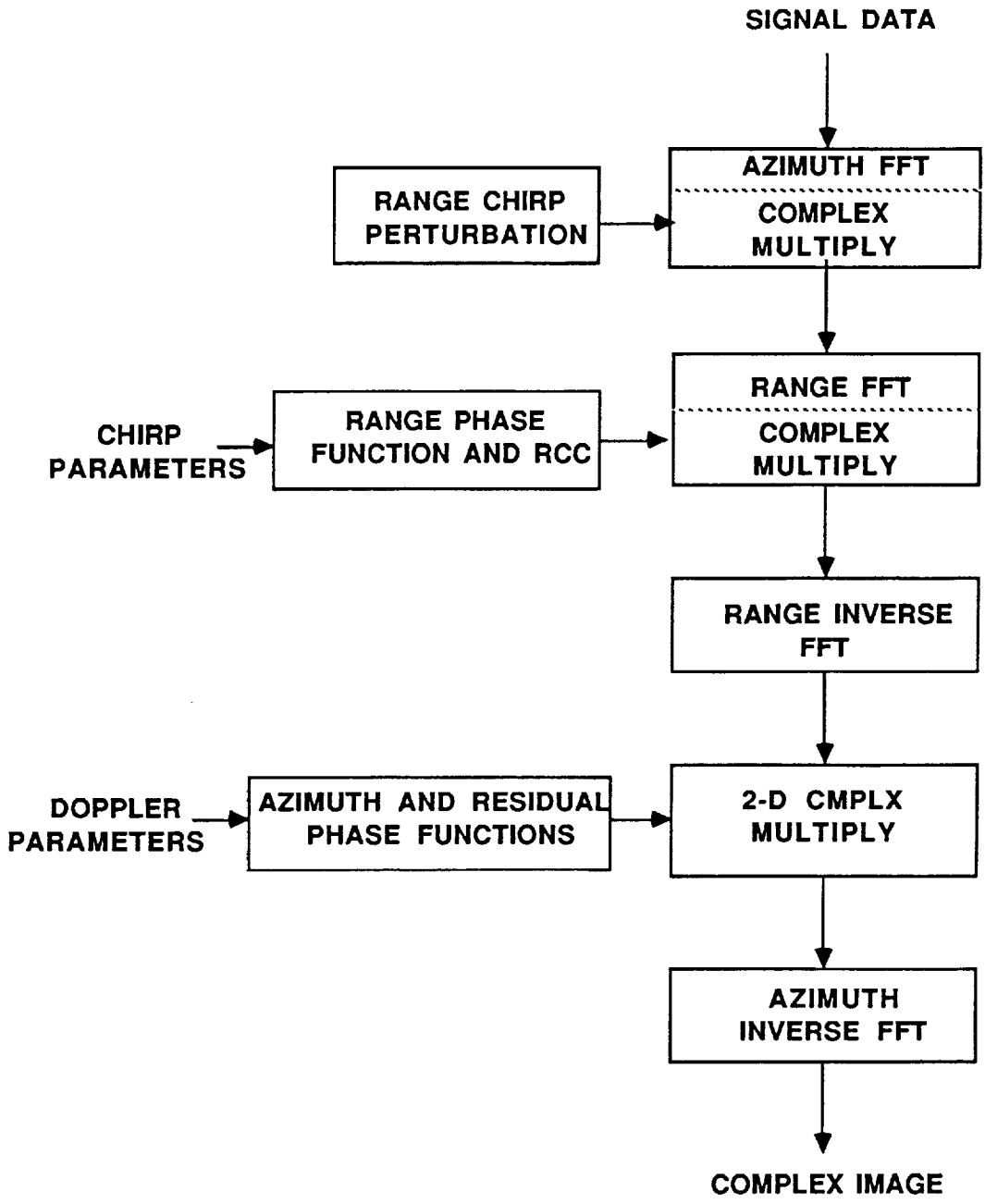

RANEY, 1991

SAR CORRELATOR: TRENDS AND TECHNOLOGIES

ARCHITECTURE OVERVIEW

- COMMON NODE
  - USED IN MOST OPERATIONAL SAR PROCESSORS, SHARED MAIN MEMORY, LOW COST, PORTABLE S/W, CONSTRAINED BY NODE (BUS, SWITCH) BANDWIDTH
  - GENERAL PURPOSE COMPUTERS (WITH ACCELERATORS): WORKSTATIONS
  - CUSTOM ARCHITECTURES: COMMON SIGNAL PROCESSOR

- PIPELINE
  - LIMITED APPLICATION PROCESSOR (ONE PRODUCT), BEST ARCHITECTURE FOR REAL-TIME PROCESSING, NOT EASILY ADAPTABLE TO NEW PRODUCTS OR SENSORS, SINGLE FAILURE SHUTDOWN
  - ADVANCED DIGITAL SAR PROCESSOR (ADSP): JPL BUILT FOR SEASAT, MGN
  - AIRBORNE SAR PROCESSORS: QUICK-LOOK ON-BOARD, KRAS, LORAL

- MASSIVELY PARALLEL
  - UNLIMITED COMPUTATIONAL CAPACITY, GRACEFUL DEGRADATION, LOW COST PER PROCESSOR, DIFFICULT I/O, COMPLEX SOFTWARE DEVELOPMENT, FUTURE FOR ALL LARGE COMPUTATION TASKS
  - MIMD (DUAL PARALLELISM): THINKING MACHINES CM-5, INTEL I-WARP
  - SIMD MACHINES: DEC MASSPAR

SAR CORRELATOR ARCHITECTURES

I) GENERAL PURPOSE COMPUTERS WITH (OR WITHOUT) SPECIAL PROCESSORS

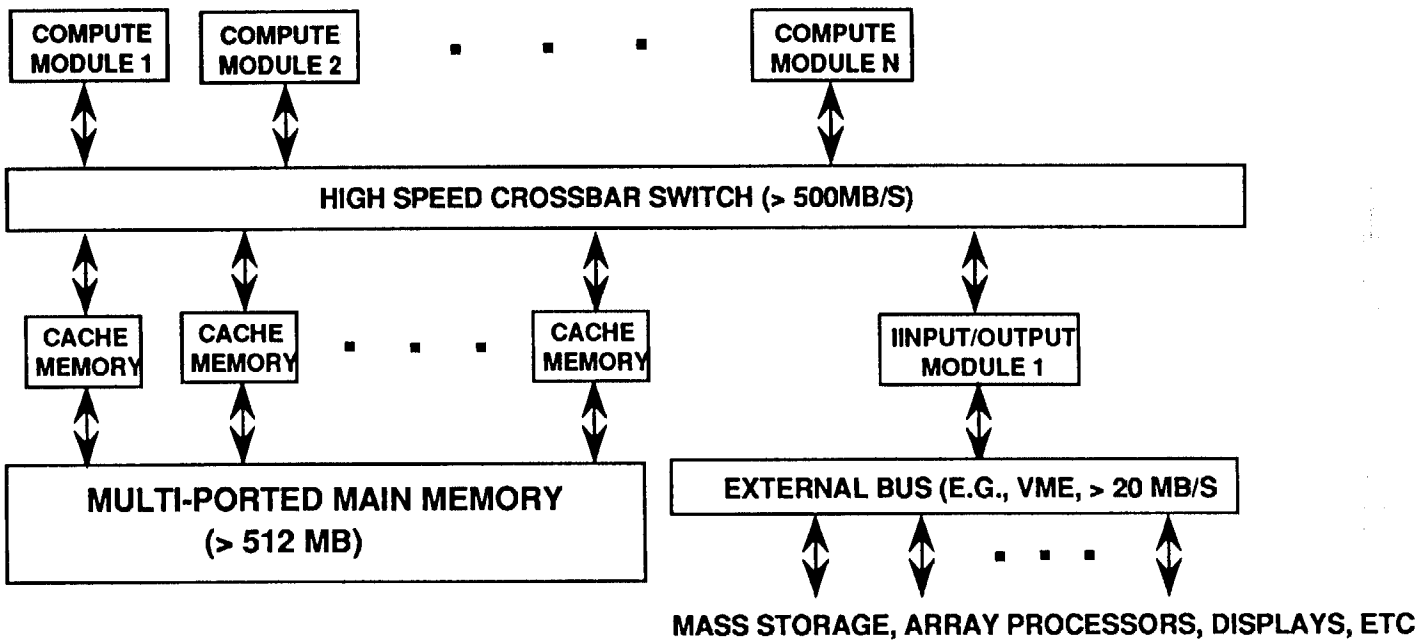

- ADVANTAGES
  - HIGH LEVEL OPERATING SYSTEM (SIMPLE TO PROGRAM), SOFTWARE STANDARDS/PORTABILITY
- DISADVANTAGES
  - HIGH COST PER MFLOP, PERFORMANCE LIMITED BY CENTRAL BUS DATA RATE

ADVANCED SAR CORRELATOR ARCHITECTURE
BRITISH AEROSPACE ERS-1 PROC

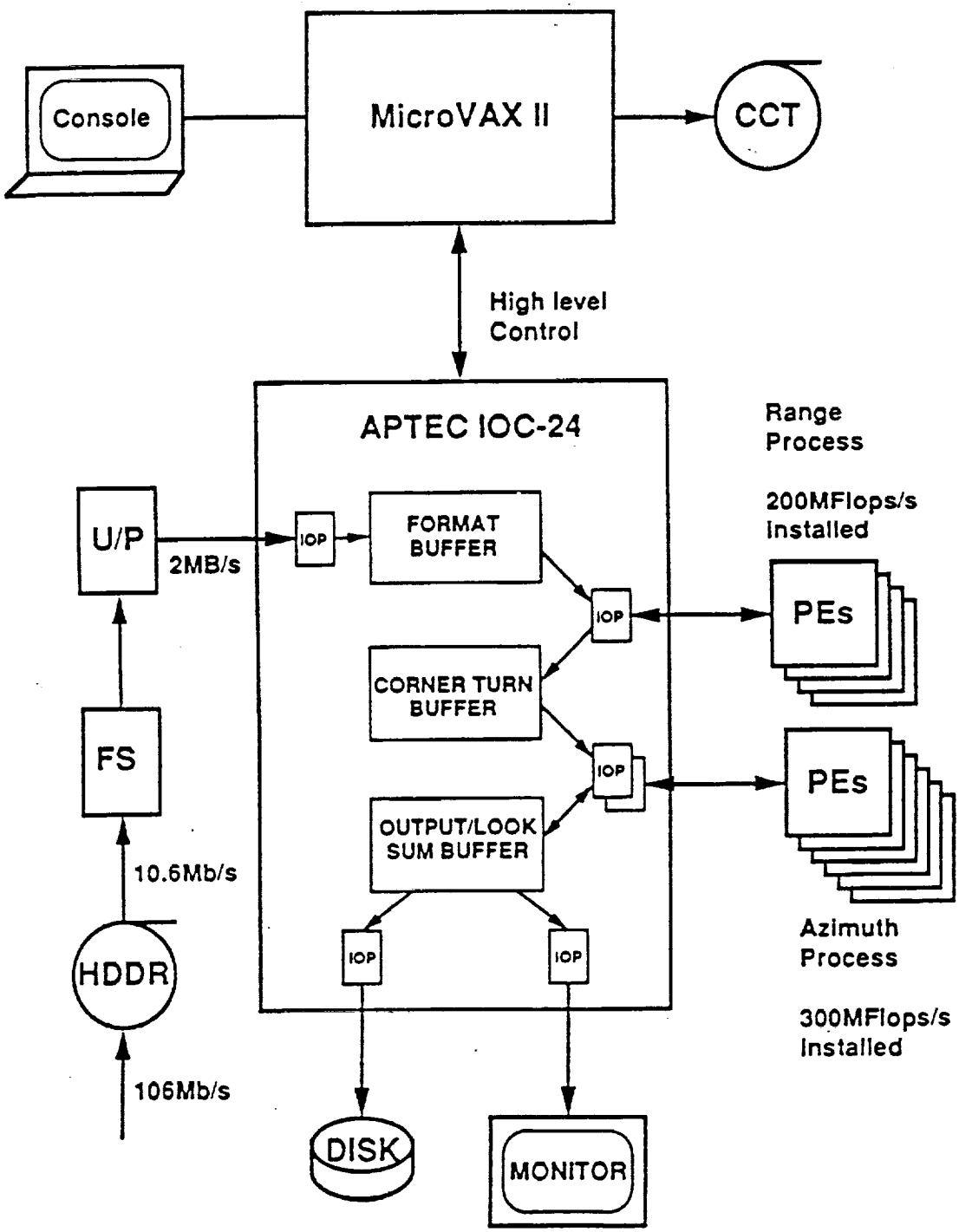

SAR CORRELATOR: TRENDS AND TECHNOLOGY

SAR CORRELATOR ARCHITECTURES

II) CUSTOM PIPELINE PROCESSORS

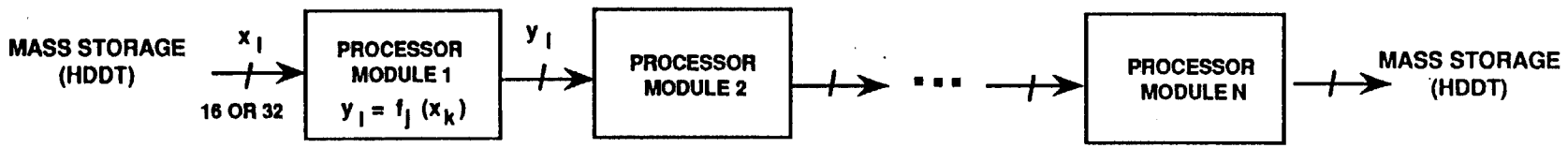

- ADVANTAGES
  - OPTIMUM ARCHITECTURE FOR SAR IN TERMS OF THROUGHPUT, LOW COST/MFLOP
- DISADVANTAGES
  - INFLEXIBLE ARCHITECTURE, NO GRACEFUL DEGRADATION, TYPICALLY REQUIRES ALGORITHM APPROXIMATIONS

SAR CORRELATOR: TRENDS AND TECHNOLOGY

SAR CORRELATOR ARCHITECTURES

III) MASSIVELY PARALLEL PROCESSORS

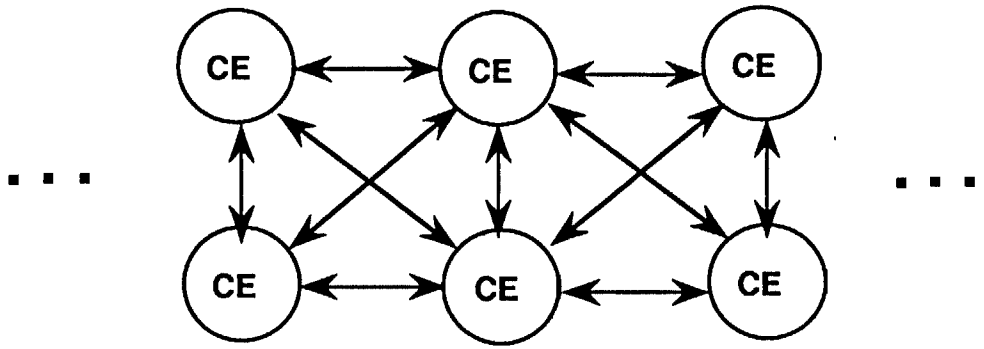

- ADVANTAGES - LOW COST/MFLOP, UNLIMITED SYSTEM EXPANDABILITY, HIGH RELIABILITY
- DISADVANTAGES - PRIMITIVE OPERATING SYSTEMS, REQUIRES SPECIAL ALGORITHMS FOR EFFICIENCY, POOR I/O TO EACH PROCESSOR

SAR CORRELATOR DESIGN

EMMA MIMD CONCURRENT ARCHITECTURE

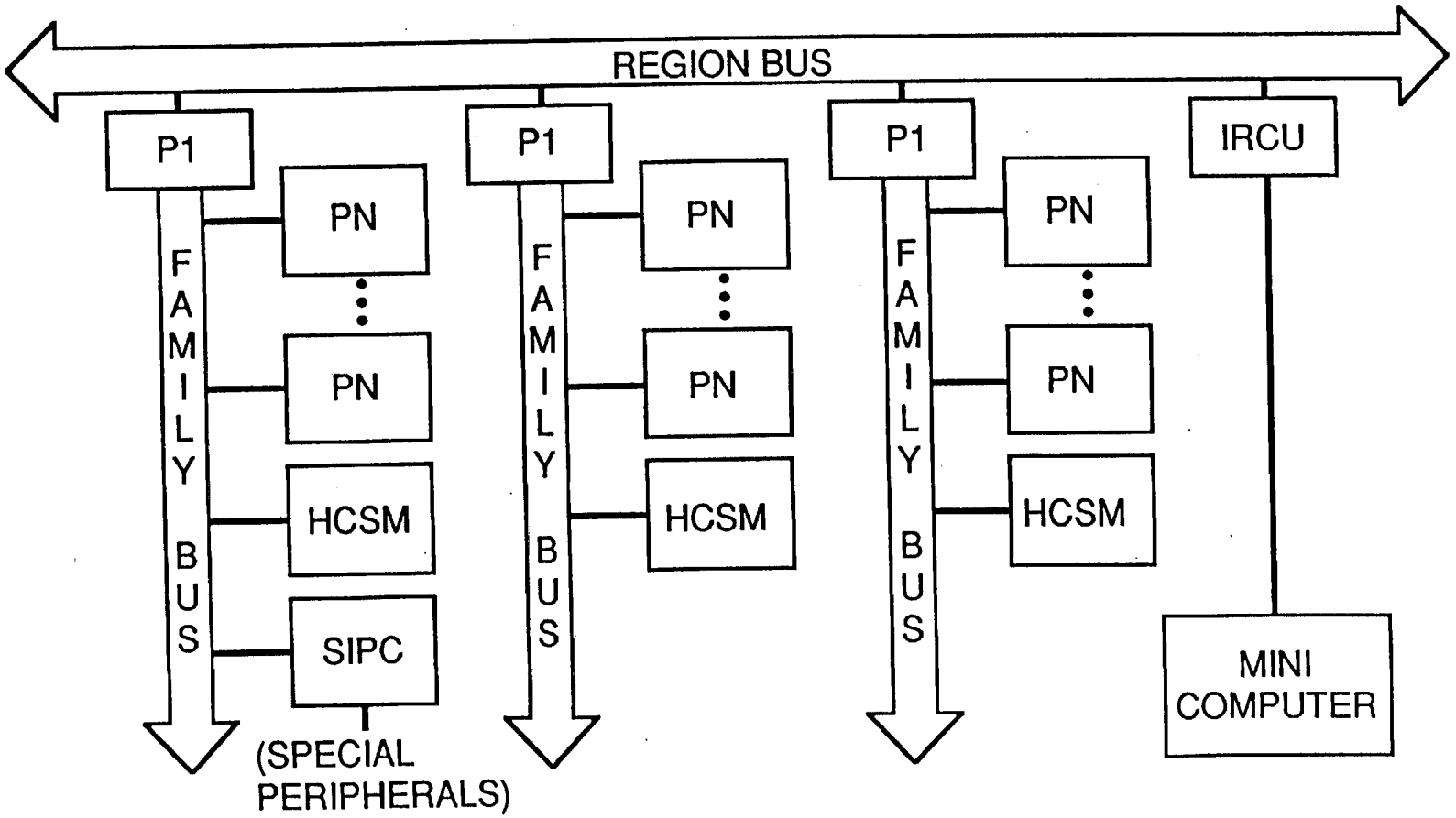

SAR CORRELATOR: TRENDS AND TECHNOLOGIES

OPERATIONAL SAR PROCESSING SYSTEMS

ARCHITECTURES

- COMMON NODE
  - ERS-1 FAST DELIVERY PROCESSORS, AUSTRALIA PAF, CANADA PAF, GERMANY PAF AND X-SAR
- PIPELINE
  - ERS-1/JERS-1 ALASKA SAR FACILITY, MAGELLAN
- MASSIVELY PARALLEL
  - ITALY PAF, NASA/JPL SIR-C

ALGORITHMS

- SPECAN
  - NASA/JPL MAGELLAN, RADARSAT SCANSAR, NASA/JPL SIR-C SURVEY PROCESSOR
- RANGE/DOPPLER
  - ERS-1 PAF AND FAST DELIVERY PROCESSORS
  - NASA/JPL SEASAT, SIR-B AND SIR-C PRECISION PROC
  - DLR XSAR, ASF ERS-1 AND JERS-1, NASDA JERS-1
- 2-D TRANSFORM
  - RESEARCH PROCESSORS: ESA, CCRS, JPL, DLR

SAR CORRELATOR: TRENDS AND TECHNOLOGY

PROJECTED HARDWARE NEEDS/PERFORMANCE

JPL PROCESSOR HARDWARE REQUIREMENTS*

	INPUT DATA RATE (MBps)	DATA VOLUMES (Gsamples/DAY)	COMPUTATIONAL CAPACITY (GFLOPS)	MAIN MEMORY (MB)
AIRSAR	0.5	5	0.2	400
SIR-C	0.8	10	0.3	500
RADARSAT	1.2	57	0.8	750
EOS SAR	6.0	173	3.3	900

* ASSUME 10 SHIFT PER WEEK OPERATIONS WITH 50% REPROCESSING

MICROPROCESSOR PERFORMANCE AND MEMORY CHIP CAPACITY EVOLUTION

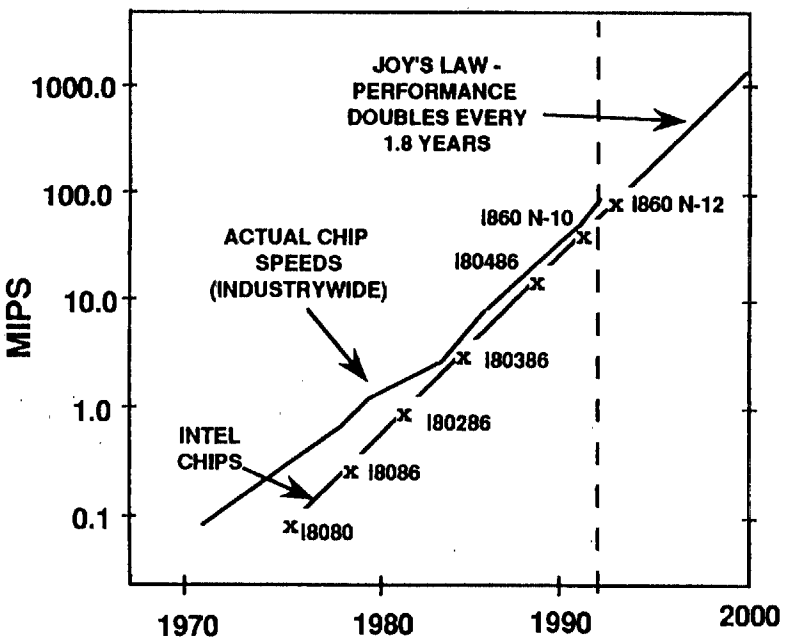

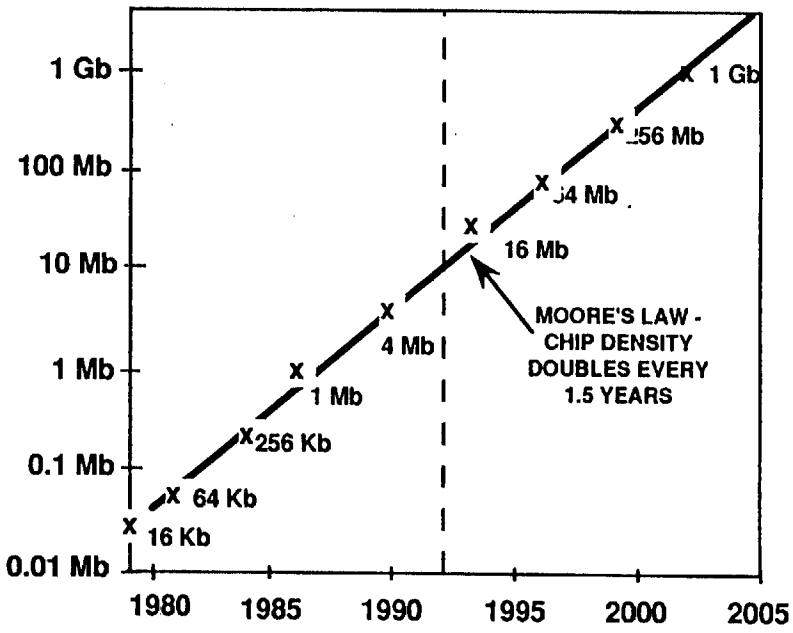

SAR CORRELATOR: TRENDS AND TECHNOLOGIES

SUMMARY

- CURRENT OPERATIONAL SYSTEMS (PAST 5 YEARS TO PRESENT)
  - ALGORITHMS: RANGE/DOPPLER
  - ARCHITECTURES: COMMON NODE
- FUTURE OPERATIONAL SYSTEMS (PRESENT TO NEXT 5 YEARS)
  - ALGORITHMS: 2D TRANSFORM
  - ARCHITECTURES: MASSIVELY PARALLEL
- DATA SYSTEM SUCCESSES (PAST 5 YEARS)
  - RADIOMETRIC/POLARIMETRIC CALIBRATION
  - DATA FORMATS (CEOS)
  - RELIABLE CORRELATOR DESIGNS
- DATA SYSTEM CHALLENGES (NEXT 5 YEARS)
  - END-TO-END OPERATIONS, INCLUDING DATA DISTRIBUTION
  - GEOPHYSICAL PROCESSORS, OPERATIONAL REDUCTION OF DATA TO HIGH LEVEL PRODUCTS
  - USER INTERACTION IN MISSION OPERATIONS, TELESCIENCE

Recent Advances and Plans in Processing and Geocoding of SAR Data at the DFD

W. Noack

German Aerospace Research Establishment (DLR)

German Remote Sensing Data Center, DFD

W–8031 Oberpfaffenhofen, Germany

1. Introduction

Because of the needs of the future projects like ENVISAT and the experiences made with the current operational ERS–1 facilities a radical change in the SAR processing scenarios can be predicted for the next years. At the German PAF several new developments have been initialized which are driven mainly either by user needs or by system and operational constraints ("lessons learned").

At the end there will be a major simplification and uniformation of all used computer systems. Especially the following changes are likely to be implemented at the German PAF:

transcription before archiving, processing of all standard products with high throughput directly at the receiving stations, processing of special "high–valued" products at the PAF, usage of a single type of processor hardware, implementation of a large and fast on–line data archive and improved and unified fast data network between the processing and archiving facilities.

In the following a short description of the current operational SAR facilities as well as the future implementations will be given.

2. Archiving and Catalogue System

At present, archiving of SAR products from ERS–1 and later on also from X–SAR is done using Archival Optical Disks (WORMS) with a capacity of 2 GByte per disk. The disk drives are installed at each processing system and the disks are carried by hand to the facility where they are needed. The main disadvantages are the slow throughput, the limited storage capacity, the susceptibility to operator errors and the high maintenance requirements of the drives.

An improvement of this situation is represented by the Epoch–1 system, which consists of a mixture of non–erasable and erasable disks with a total on–line capacity of 400 GByte. The system is used for many projects, among them are the storage of AVHRR data and the background storage for the image processing laboratories. But there are still the disadvantages of relatively slow throughput and the limited storage capacity. Also, this system would not be able to guarantee the on–line access of one year ERS–1 PAF production of SAR and Geocoding which is actually more than 400 GByte.

Therefore, in view of ERS−2 and ENVISAT the next generation archiving system is being studied. During a first analysis of the market two systems have been selected for a detailed investigation, of which the one system allows a total on−line capacity of up to 10.000 TByte. The study is carried out in 1993 with the goal of having the first unit installed and operational end 1994.

Due to historic reasons there are a variety of catalogues for the different kind of sensors. The biggest catalogue is the one for ERS−1. In near future these catalogues will be accessible by a recently developed common user interface. This interface is also considered to be available for external SIR−C/X−SAR users and shall be implemented before the second SIR−C/X−SAR mission, depending on availability of funding.

3. Processing

With respect to processing two major milestones have been achieved within the last year: first the Multisensor SAR Processor MSAR has become operational for ERS−1 beginning '92 and second the precision processor of the X−SAR PAF has been accepted in December '92. The following two figures are showing the hardware and the software block diagram of the XPS system. A SUN UNIX computer enhanced by an array processor of STAR Technologies with direct access to the solid state Corner Turn Memory are the major hardware units of the processor. The X−SAR data will be read in from a SONY recorder using a real time capable Frame Synchronizer and Formatter.

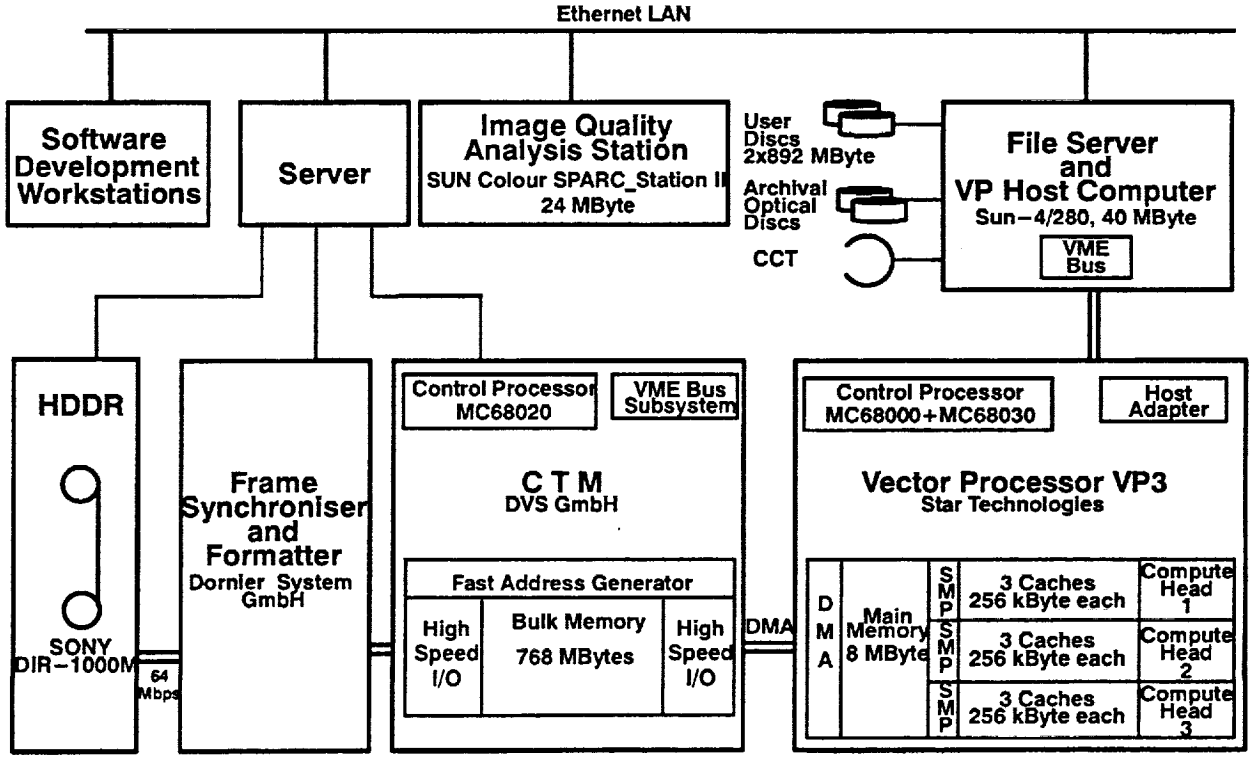

figure 1: XPS hardware block diagram

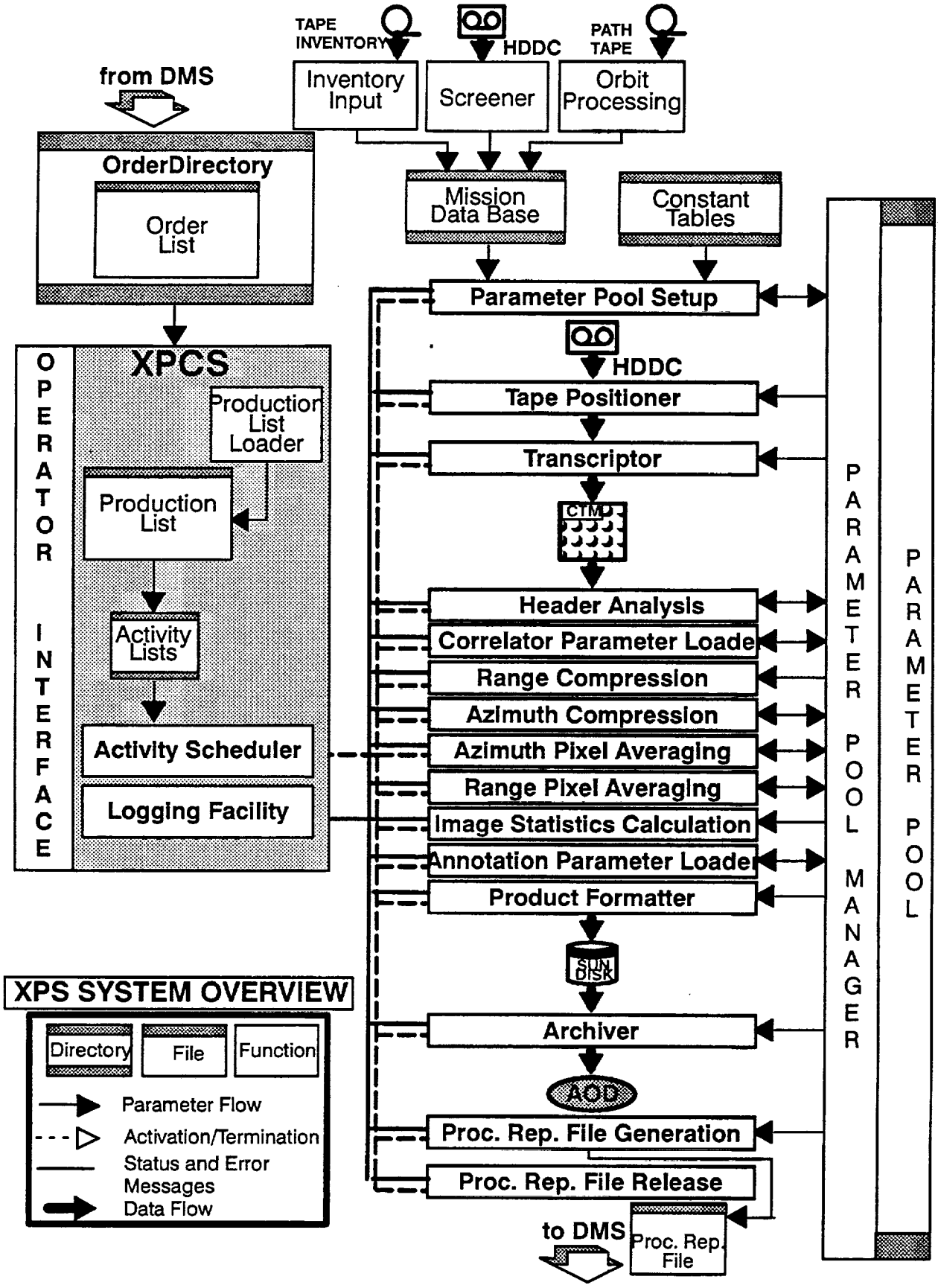

figure 2: XPS software block diagram

The software structure of the XPS is shown in figure 2 above. The Control System allows among many other options especially automatic and parallel processing of three different orders which are divided in the steps Transcription, Processing, and Archiving. The Control System has been accepted already and is since then in operational use. The Correlator has been accepted also and is in the integration phase. It uses the slightly modified and supplemented Range–Doppler algorithm. The other subsystems are either in the final acceptance phase (Formatter, Archiver) or in the design and development phase (Screener, Transcriptor).

In opposition to ERS–1, where the MSAR Screener is mainly used for archiving and quality estimation of raw data, the Screener of the XPS system is designed as a preprocessor of the Correlator and covers many different tasks. Among these are the Doppler Screening, the Doppler Ambiguity Resolving, the calculation of the internal calibration parameters, the extraction of header data, the inventarisation of the tape contents, the analysis of the mission data base and the geolocation of the raw data.

Control System, Screener, Processor, Formatter, and Archiver have been written in Ada except the modules running on the array processor. This will allow for a reuse of components in a different environment in future projects.

Beginning this year a new project has been started with the goal of the development of a high precision SAR processor making use of a powerful workstation only without external devices like an array processor or a Corner Turn Memory. The system will be quite flexible with "open" interfaces between the modules allowing the easy exchange of components. It shall mainly support the development of new, higher–valued products and shall be used as a prototype processor for future sensors like ENVISAT. The programming language will again be Ada and existing software shall be reused. Especially the Control System of the XPS shall be used for the parametrisation and monitoring of processes as well as other components. Because of the foreseeable increase in compute power of workstations throughput requirements will be investigated during the first phase with low priority only. This project is in a preparatory phase. The development will be done inhouse with possible cooperation with universities or institutes.

4. Geocoding

The present Geocoding System GEOS which is in operational use for ERS–1 and which will be adapted to X–SAR runs on SUN workstations (SPARC2) and will be implemented on the new generation (SPARC10) in early 1993. The system generates mainly ellipsoid or terrain corrected products with a throughput of several products per day. Currently no batch processing facility is implemented and therefore, each product has to be generated individually.

In future it is foreseen to include the generation of the ellipsoid corrected product directly in the SAR processor and additionally direct at the receiving stations. At present the throughput of the terrain geocoded products is one item per day. The limiting factors are the time consum-

ing determination of tiepoints, the quality control and the compute power. To improve the situation the tiepoint interface will be upgraded and the quality control will be automised.

Additionally, the list of geocoded products shall be extended by a radar mosaic, a geocoded map quadrant and coregistered data sets. Each extension requires software upgrades and will be performed in part with the support of industry and universities.

S24-82

182864

N94-15910

Data Distribution

J. E. Hilland

Jet Propulsion Laboratory
California Institute of Technology
Pasadena, California

364

This presentation:

1. Presents data distribution from the perspective of Earth observations and the end user
2. Reviews problems associated with SAR data distribution
3. Discusses future data distribution techniques

JPL

Third Spaceborne Imaging Radar Symposium

Representative Requirements

Typical End User Requirements which drive distribution technology

	Timeliness	Resolution	Data transfer rate
Near real time	< 6hr	>200m	20 images/day
Scientific research	Weeks to Months	100m	200 images/day

Data Distribution Problems

- Raw Signal Data
  - Huge data volume- Terabytes per year
  - Significant expense copying High Density Digital Tapes ($250,000/yr)
  - Different tape formats (recorders) between many data distributors
- Images
  - Large data volume for global studies
  - Nonstandard format
  - High demand, large volume precludes data networks
  - Prior to ERS-1, JERS-1, Magellan user base was small compared to Landsat/SPOT
- Geophysical Products
  - Tend to be restricted to expert users

JPL

Third Spaceborne Imaging Radar Symposium

Multimission SAR Processing System Architecture

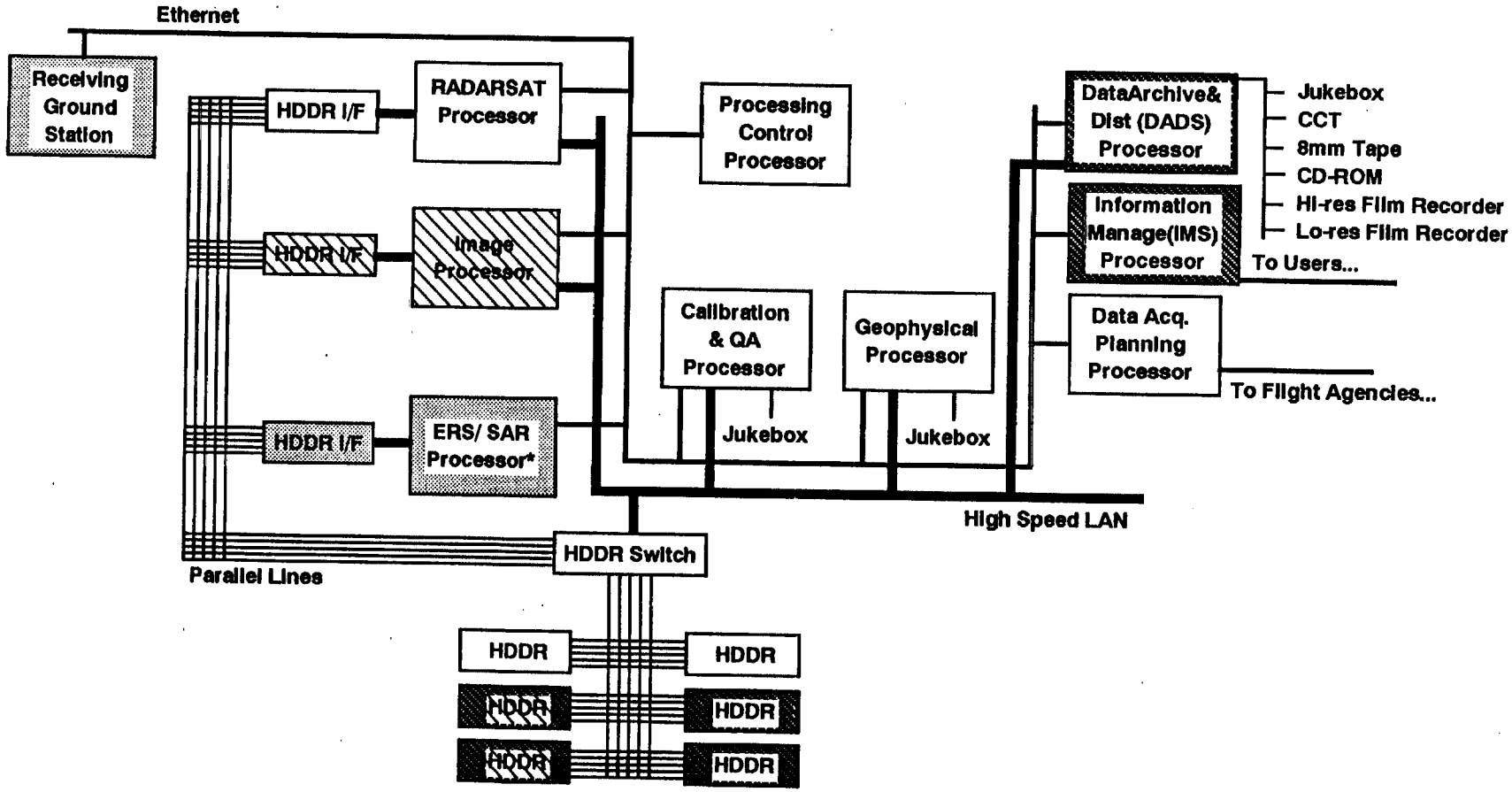

HDDR-High Density Digital Recorder

JPL

Third Spaceborne Imaging Radar Symposium

Data Product Formats

- A standard data format improves data product usability by:
  1. Standardizing image annotation structures
  2. Providing an international standard
  3. Promoting data usability with standard software data packages

- For Earth Observing Satellites:
- CEOS SAR computer compatible tape is the output product format standard for:
  - The Alaska SAR Facility
  - SIR-C
  - National flight agencies, e.g., for ERS-1, JERS-1 distribution

- CEOS structure is designed for computer compatible tapes (based on LandSat tapes)

- Hierarchical Data Format (HDF) For SAR
  - Improves SAR usability through compatibility
    - Large Earth science user community for data in HDF structure
    - Facilitates intersensor comparison, global model comparison
  - Preferred format for the Earth Observing System Data and Information System Version 0 (and probably for versions in the late 1990's)
  - HDF is supported by a large software tool base for science data visualization
  - Translator developed by the Alaska SAR Facility for converting CEOS to HDF

JPL

Third Spaceborne Imaging Radar Symposium
CEOS Format

- VOLUME DIRECTORY FILE

  Volume Descriptor Record
  File Pointer Records
  Text Records

- SAR LEADER FILE

Data Set Summary Record	mission, data acquisition, sensor, processing parameters
Map Projection Record	geometric characteristics of image data
Platform Position Data Record	orbit parameters, spacecraft position and velocity vectors
Attitude Data Record	attitude and attitude rate
Radiometric Data Record	tables relating data numbers to backscatter coefficients
Radiometric Compensation Record	radiometric correction vectors
Data Quality Summary Record	data quality analysis results summary
Data Histogram Record	data histograms
Range Spectra Record	range spectra
Radar Parameter Update Record	radar parameters (gain, DWP) change
Detailed Processing Parameters	mission specific processing parameters

- SAR IMAGERY OPTION FILE

  File Descriptor Record
  SAR Data Record (Image or Signal Data) with line ID (prefix, suffix not used)

- NULL VOLUME DIRECTORY FILE

  Null Volume Descriptor Record

HDF Format

- HDF was developed by the National Center for Supercomputer Applications (NCSA)
- HDF provides:
  - A format for the exchange of data in distributed computing environments
  - Support for scientific data; large data sets, data descriptions, sharable data
  - Public domain software; data analysis, visualization, computer communications
- Approximately 100,000 users

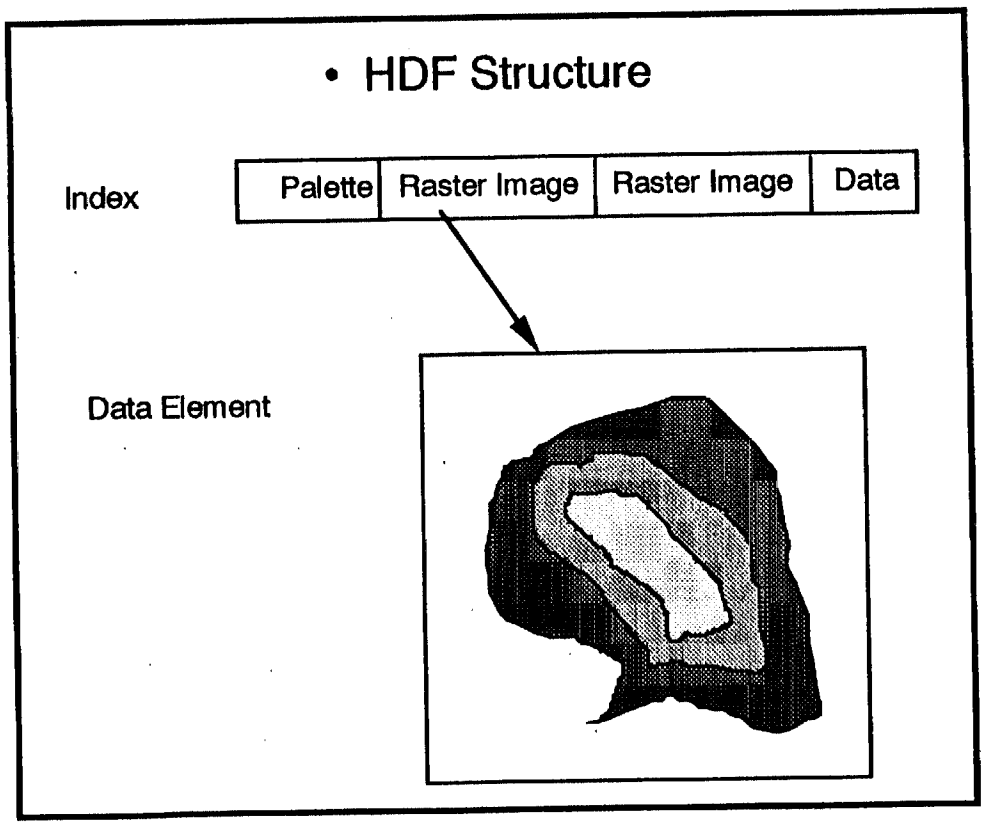

Information Objects	
Raster image -	8-bit, 24-bit
Palette-	Look-up table
Data-	Arrays
Annotation-	Text (metadata)
Vsets-	Grouped data

JPL

Third Spaceborne Imaging Radar Symposium

High Density Media Comparison

- High density media for the distribution of raw signal data

Media Format	Drive	Read/Write	Data Capacity (Bytes)	Access Time (ms)	Search Time (s)	Transfer Rate MBps	Drive Cost ($K)	Media Cost	Availability
Optical paper, 35mm paper, length: 880 m, 12 in diam. reel	New design reel-to-reel	Write Once Read Many (WORM) Laser, non-contact	$1x10^{12}$	28	60	3	225	$5K/reel $0.005/MB	In operation
Optical paper, 0.5 in tape, length: 255, IBM 3480 cartridge	Modified IBM 3480	Write Once Read Many (WORM) Laser, non-contact	$50 x10^{9}$ plus 50 cart. jukebox	600 (to 200 MB)	15	3	20	$250/cartridge $0.005/MB	1992
HDDT, cartridge	Rotary scan	Read/Write	$45x10^{9}$	1	300	1-12	200	$500/cartridge $0.01/MB	In operation
CCT, 0.5 in reel		Read/Write	$120x10^{6}$	10	150	0.4	30	$12/tape $0.1/MB	In operation
Dig. Opt Disk, 12 in		WORM	$6x10^{9}$	60	0.060	0.2	25	$300/platter $0.15/MB	In operation
Magnetic disk		Read/Write	$1x10^{9}$	15	0.030	1	5	$5k/drive $5/MB	In operation

JPL

Third Spaceborne Imaging Radar Symposium

Distribution Media

- Distribution media for multilook detected and geophysical data products

1978 (Seasat)	1993	
Black/white Strips 50 μm resolution	Black/white prints Frames (scene) 8k x 8k pixels 25 μm resolution	Color Prints 1.5 x 2k pixels 80 μm resolution
Computer Compatible Tape 50 MB/tape 200 KBps transfer rate	8mm magnetic tape 2 or 5 GB capacity 250 KBps transfer rate CD-ROM 600 MB capacity 200 KBps transfer rate	Computer Compatible Tape 100 MB/tape 400 KBps transfer rate Data networks 300 KBps transfer rate

Data Communications Networks

Current Networks Utilized For SAR Data Transfer

- NASA Science Network
- Earth Observing System Data and Information System Version 0 Network

- Performance
  - T1 56 Kbps
  - T3 1.5 Mbps

- Key to network utilization
  - Distribute products derived from SAR images, e.g., ice motion fields, vegetation index
    - Reduces data volume,
    - Increases SAR data usability and user base
  - Data compression for browse image transfer

- Near real-time applications
  - DOMSAT with image data compression (1 Mbps data channel)

JPL

Third Spaceborne Imaging Radar Symposium

EARTH OBSERVING SYSTEM DATA AND INFORMATION SYSTEM (EOSDIS)

DISTRIBUTED ACTIVE ARCHIVE CENTERS (DAACs)

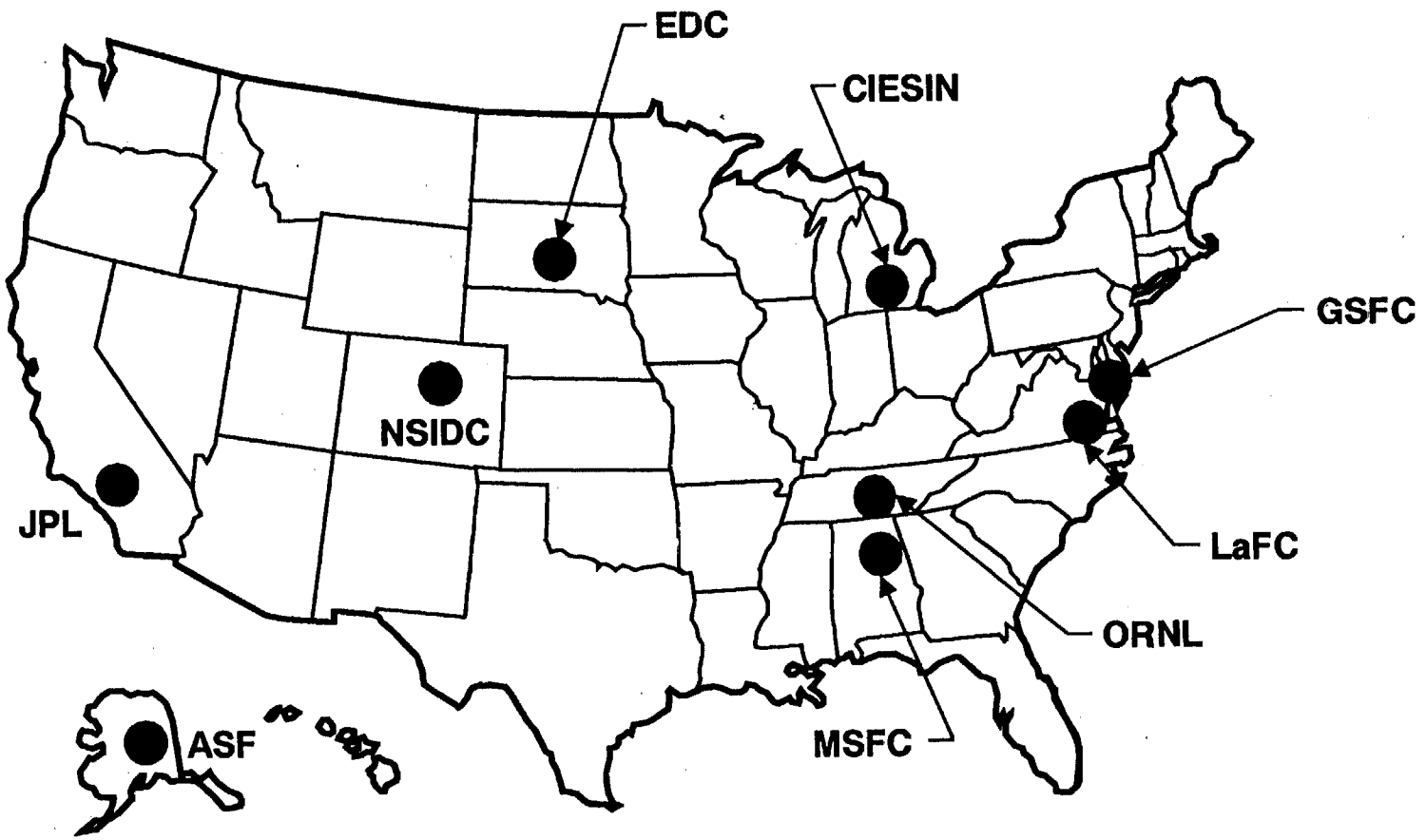

JPL

Third Spaceborne Imaging Radar Symposium

EOSDIS ARCHITECTURE

EOSDIS-SPONSORED DATA CENTERS*

EARTH SCIENCE DAACs

CENTER	INITIAL SYSTEMS	AREAS OF INTEREST	EOS AND OTHER MISSIONS/INSTRUMENTS
GSFC GODDARD SPACE FLIGHT CENTER	NCDS, PLDS, CDDIS	CLIMATE, METEOROLOGY, STRATOSPHERE, OCEAN BIOLOGY, AND GEOPHYSICS; AVHRR AND TOVS PATHFINDER DATA SETS	MODIS-N, AIRS, MHS, AMSU, SeaWIFS, GLRS-A, HIRDLS, TOMS, AND TMI
LaRC LANGLEY RESEARCH CENTER	ERBE PROCESSING	CLOUDS, RADIATION, AEROSOLS, AND TROPOSPHERIC CHEMISTRY	CERES, ERBE, MOPITT, MISR, EOSP, SAGE, AND TES
EDC EROS DATA CENTER	GLIS, LANDSAT PROCESSING	LAND PROCESSES	ASTER, HIRIS, SAR (LAND), LANDSAT (MSS AND TM), AND AVHRR
UAF UNIVERSITY OF ALASKA-FAIRBANKS	ASF SYSTEM	SAR IMAGERY OF ICE, SNOW, AND SEA SURFACE	ERS-1, JERS-1, ERS-2, RADARSAT; AND ONGOING ROLE AS GROUND STATION

* EOSDIS Handbook, 1992

EOSDIS ARCHITECTURE (Cont'd)

EOSDIS-SPONSORED DATA CENTERS*

CU UNIVERSITY OF COLORADO	CDMS	POLAR OCEANS AND ICE	SMMR, SSM/I, AND OLS
JPL JET PROPULSION LABORATORY	NODS	PHYSICAL OCEANOGRAPHY	TOPEX/POSEIDON, NSCAT, STIKSCAT, AND ALT
MSFC MARSHALL SPACE FLIGHT CENTER	WetNet	HYDROLOGIC CYCLE; SSM/I PATHFINDER DATA SETS	MIMR, TMI, TRMM PR, LIS, AND SSM/I
ORNL OAK RIDGE NATIONAL LABORATORY	TGDDIS	TRACE GAS FLUXES	GROUND-BASED DATA RELATING TO FLUXES OF TRACE GASES (e.g., CO_2, CH_4)
SOCIO-ECONOMIC DATA AND APPLICATIONS CENTER			
CDRC CIESIN DATA AND RESEARCH CENTER	—	HUMAN DIMENSIONS OF GLOBAL CHANGE AND POLICYMAKING APPLICATIONS	SOCIO-ECONOMIC DATA

*EOSDIS Handbook, 1992

JPL

Third Spaceborne Imaging Radar Symposium

EOSDIS ARCHITECTURE

NETWORK STRATEGY*

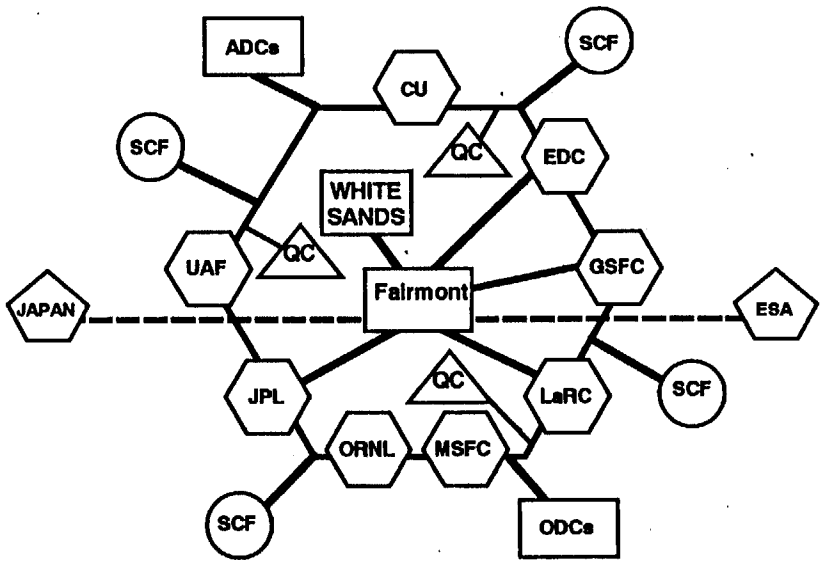

ODCs = OTHER DATA CENTERS NON-INTEROPERABLE WITH DAACs

ADCs = AFFILIATED DATA CENTERS INTEROPERABLE WITH DAACs (NOAA/NESDIS, NOAA/UNIVERSITY OF WISCONSIN.....)

SCF = USERS SUPPORTED BY GENERAL SCIENCE NETWORKS (NSF INTERNET, NSN, NREN...)

DAAC = DISTRIBUTED ACTIVE ARCHIVE CENTER

QC = QUALITY CONTROL SCIENCE COMPUTING FACILITIES

Complex = FACILITIES FOR LEVEL 0 AND 1 DATA HANDLING

EOSDIS INTERNAL NETWORKS

INTERNAL NETWORKS LEVEL OF SERVICE

EOSDIS EXTERNAL NETWORKS

EXTERNAL NETWORKS LEVEL OF SERVICE

*from EOSDIS Handbook, 1992

EOSDIS SCIENCE USER INTERFACE

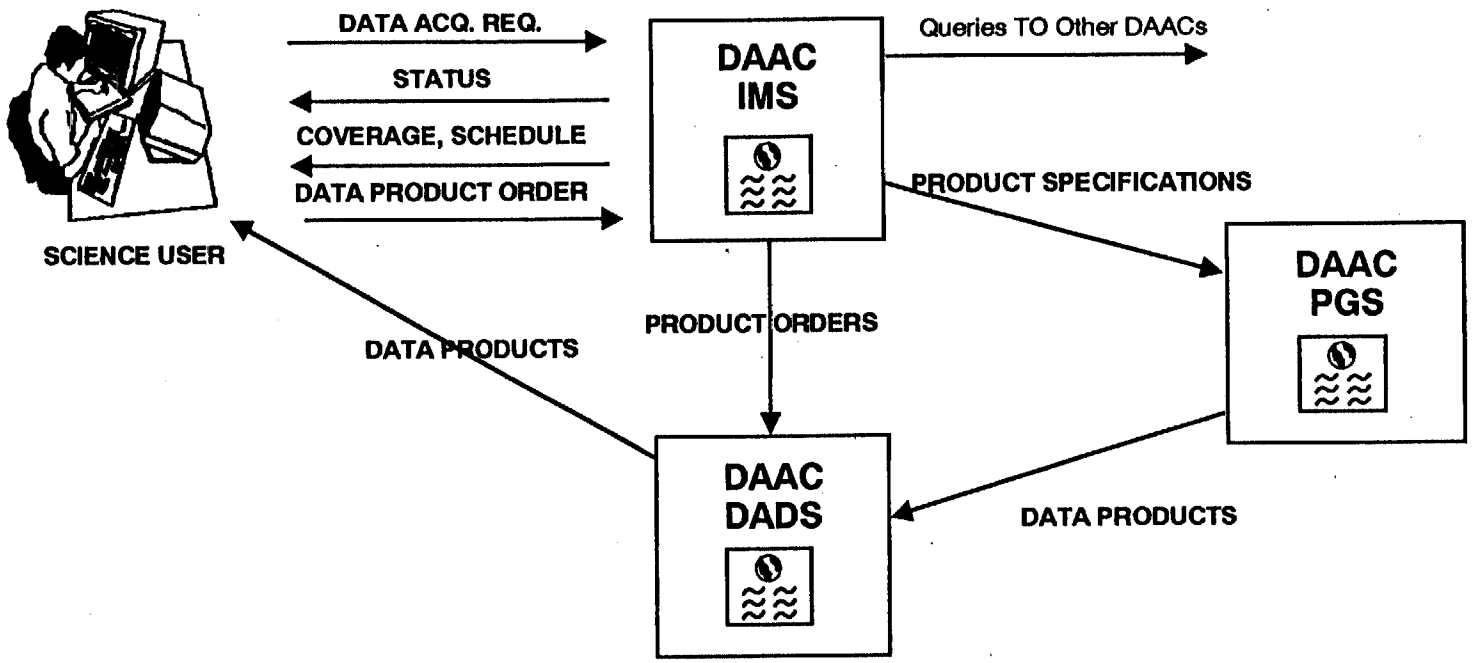

EOSDIS - Earth Observing System Data and Information System
DAAC - Distributed Active Archive Center
IMS - Information Management System
PGS - Product Generation System
DADS - Data Archive and Distribution System

SAR SENSOR ELECTRONICS

T/R MODULES

Dr. MOH'D A. HASAN

Dr. ALBERT E. PREYSS

Acknowledgement

- **JPL** — Mr. Mike Sander, Dr. Bob Ferber
- **Texas Instruments** — Mr. Gene Harrell
- **Westinghouse** — Mr. Charles Corson, Mr. Michael Doty
- **GE** — Dr. Leonard Yorinks, Mr. Joe Tedeschi, Dr. Doug Reep

Outline

- INTRODUCTION
  - Opening Remarks
  - Module Architecture
  - T/R Module in SAR System
- MODULE REQUIREMENTS
  - Requirements Traceability
  - Antenna Configuration
  - Typical Module Specifications/Requirements
- MODULE TECHNOLOGY DEVELOPMENT
  - L-Band
  - C-Band
  - X-Band
- CONCLUDING REMARKS

T/R Module Photo

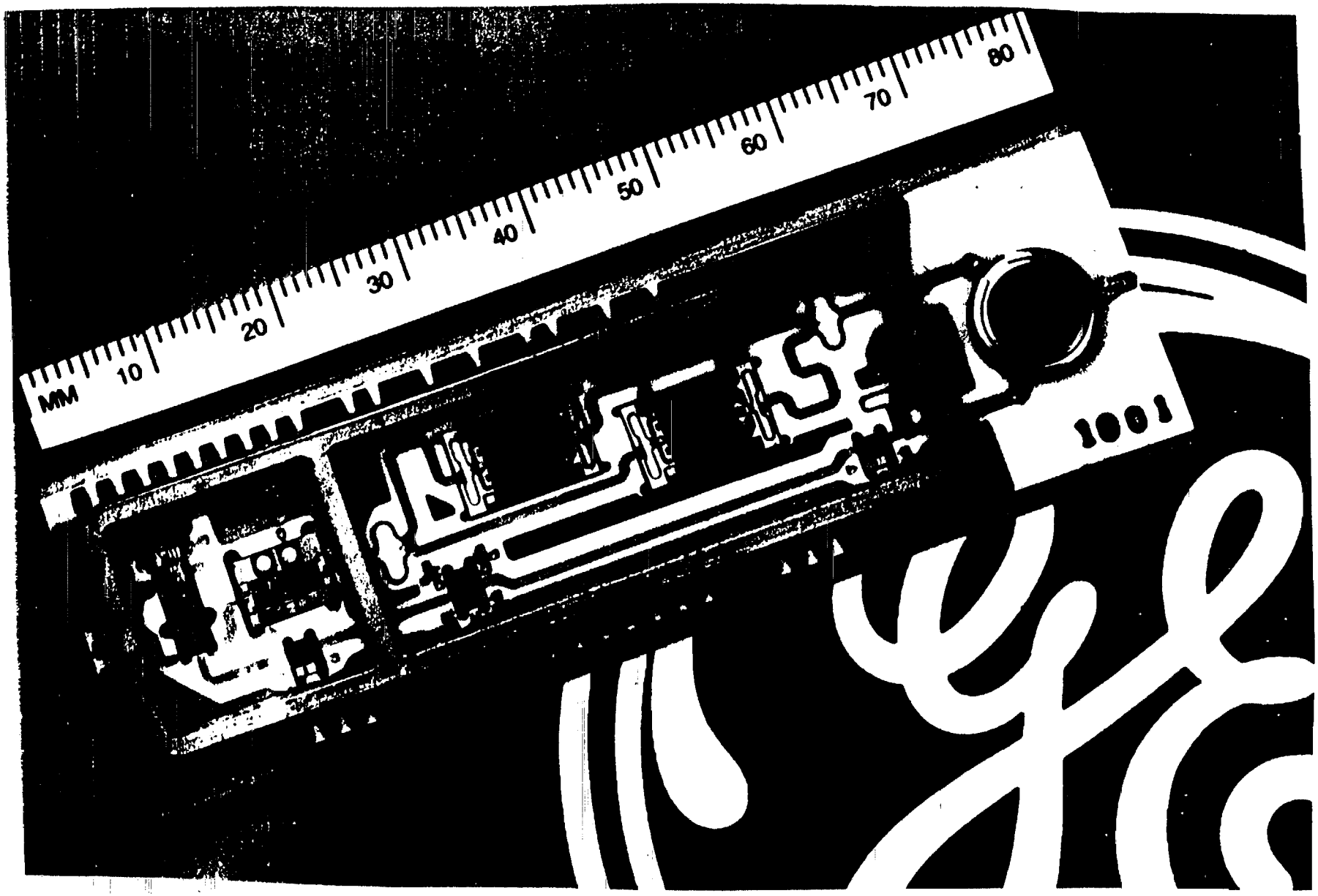

SAR T/R Module Architecture

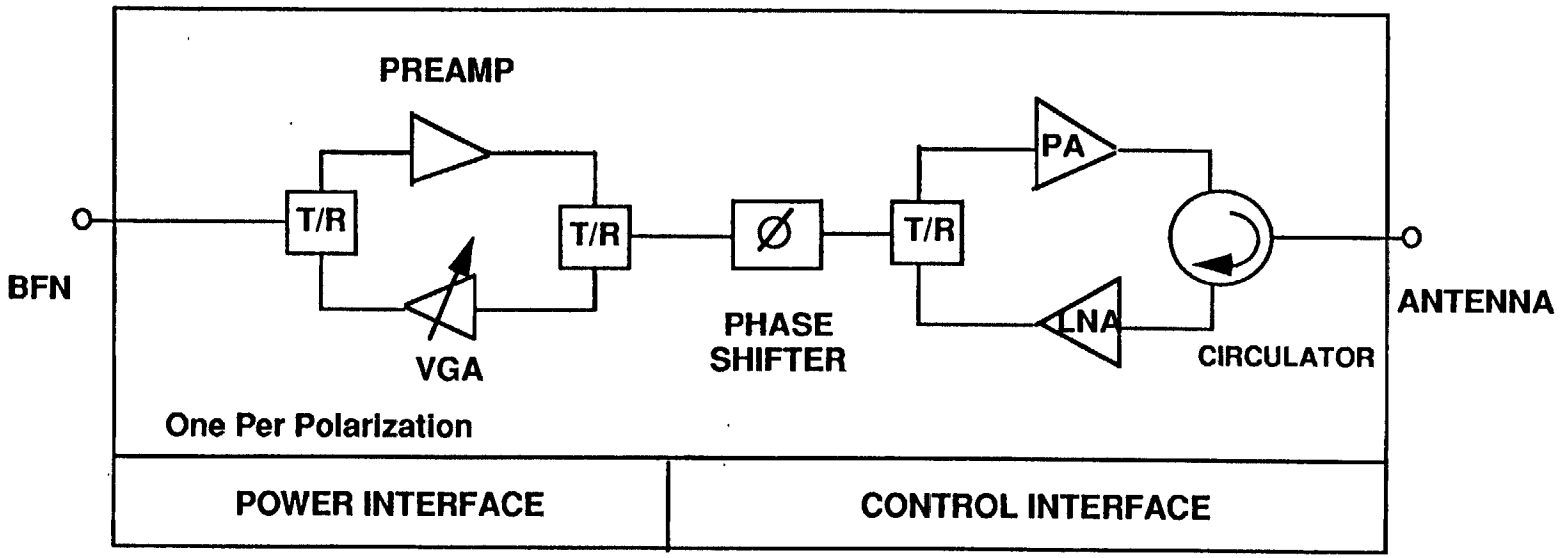

T/R Module is a Unique Assembly of the SAR Functional RF Components

Simplified Block Diagram of SAR System

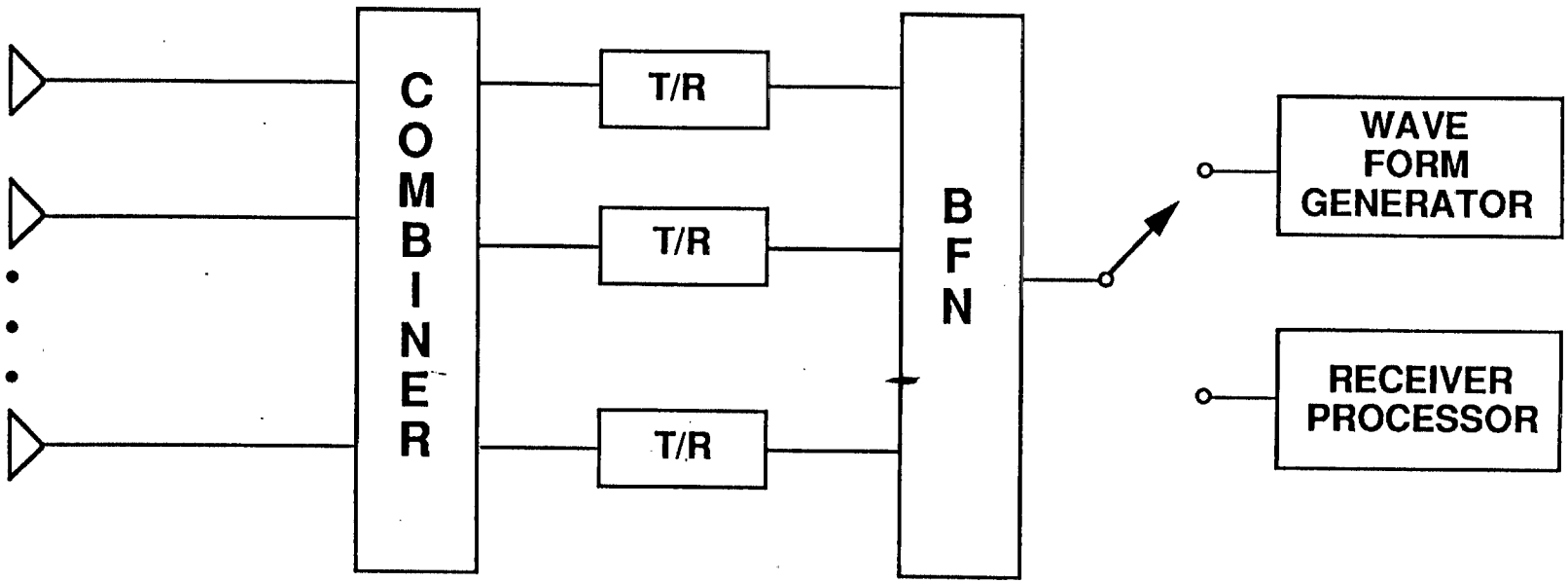

Antenna Elements

Element Combiner

Transmit/Receive (T/R) Modules

Beam Forming Network

Wave Form Gen/ Receiver Processor

T/R Module is a Key Element in the Overall SAR system

Requirements Traceability

- SCIENCE MISSION
  - Biomass Assessment
  - Soil and Snow Moisture Measurements
  - Ice Type and Ice/Water Boundary Identification
  - ...

- SAR CAPABILITIES
  - Spectral Coverage
  - Polarimetric Coverage
  - Global Coverage and Nested High Resolution
  - ...

- SAR PERFORMANCE REQUIREMENTS
  - Sensitivity, Resolution
  - Dynamic Range, Data Rate
  - System ISLR, Ambiguities
  - Life
  - ...

Requirements Traceability (cont'd)

SAR ANTENNA SUBSYSTEM

- RF
  - Frequency/Bandwidth/Polarization
  - Input/Output Power
  - Beam Steering/Boresight Accuracy/Beamwidth Control
  - Gain(Aperture, Directivity, Receive)/ Sidelobes
  - Receive Noise Temperature
- ELECTRICAL
  - Dwell Time/ Beam Switching/ Waveform
  - DC Input Power
- THERMAL, MECHANICAL AND STRUCTURAL
  - Antenna Flatness and Stiffness
  - Antenna Size and Weight
  - Deployment and Stowage

Typical SAR Antenna Configuration

Astro Space Division

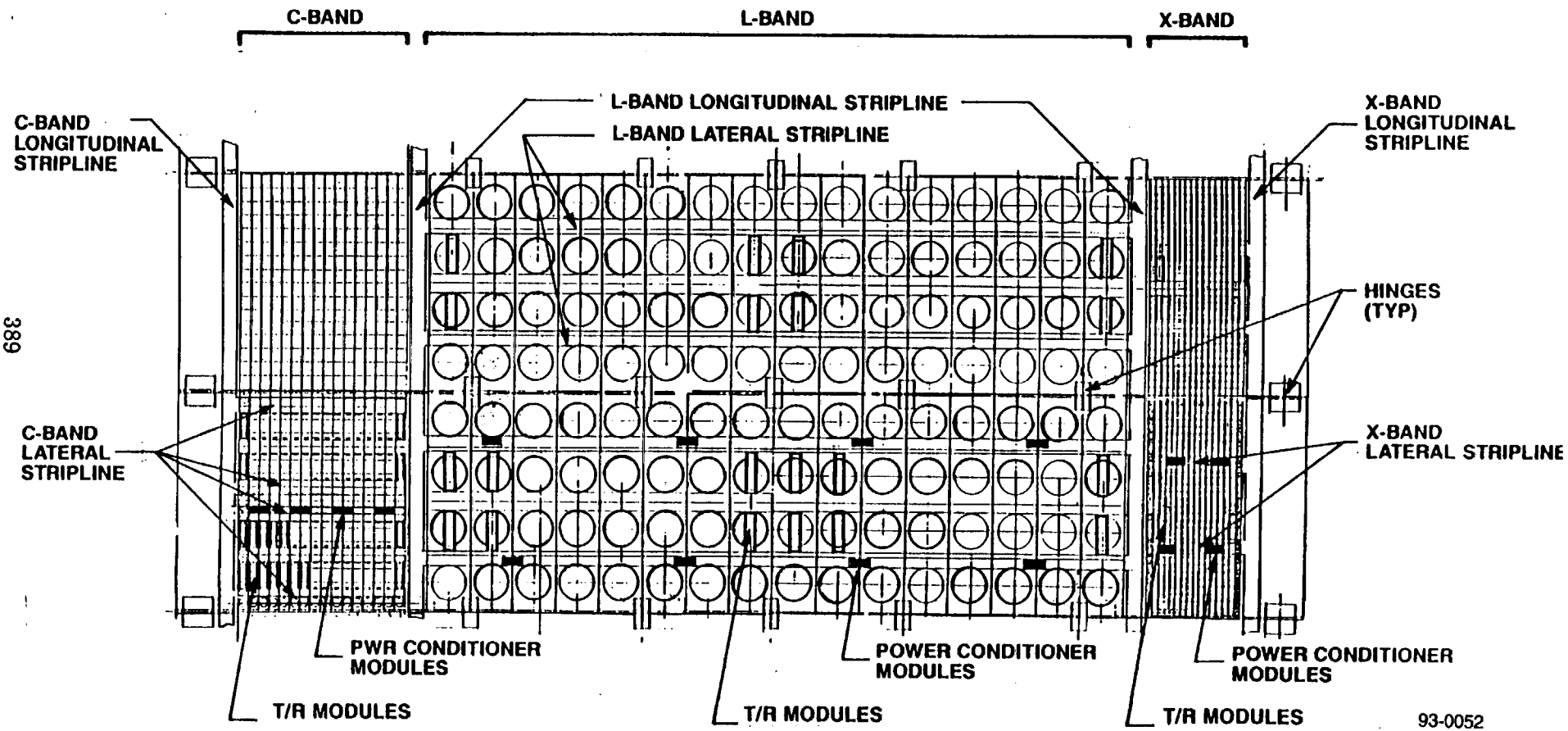

389

T/R Module is an Integral Part of Antenna Design

Typical SAR Antenna Panel Cross Section

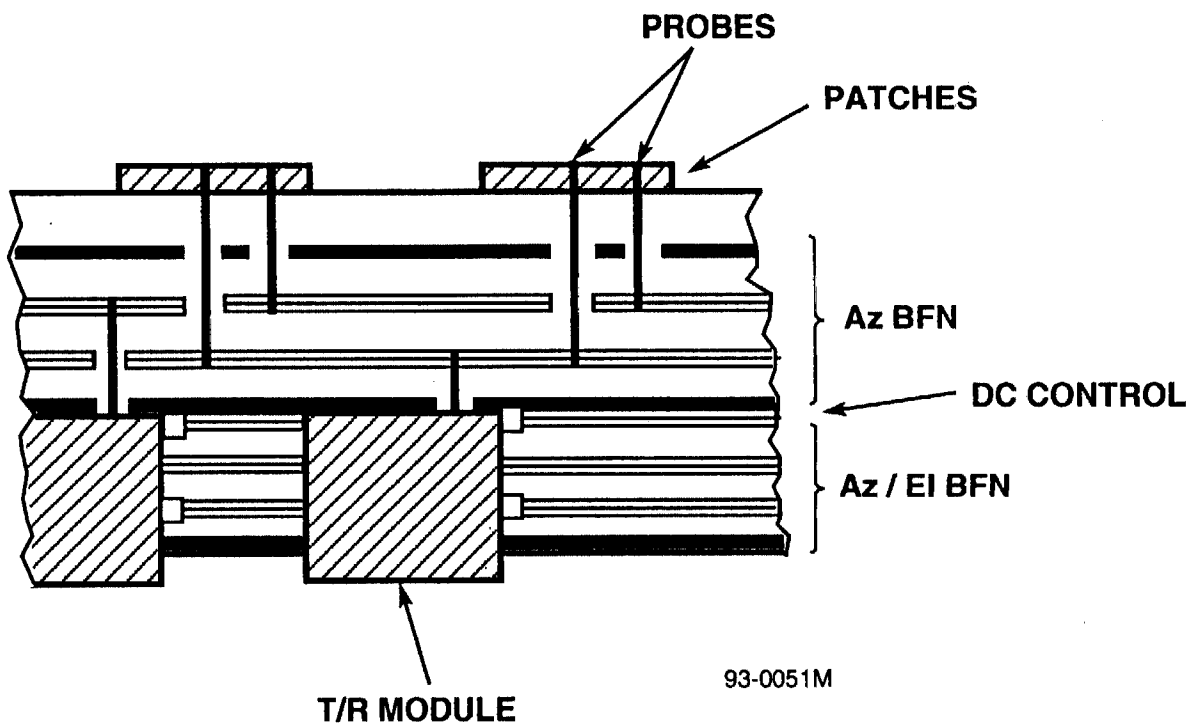

T/R Module Characteristics Are Key Drivers of Electrical, Mechanical and Thermal Designs of Antenna and SAR System

Desired Module Characteristics

- Electrical
  - High Power Added Efficiency
  - Low Losses
  - Low Receiver Noise Figure
- Mechanical
  - Small Size
  - Low Weight
- Thermal
  - Low Power Dissipation
  - Good Thermal Conduction

The Better the Module, the Better the Antenna and Overall SAR System

Typical T/R Module Specifications/Requirements

Parameter	L-Band	C-Band	X-Band
Frequency (GHz)	1.25	5.3	9.6
Bandwidth (MHz)	30	30	30
Phase Control (bits)	6	6	6
Gain (dB)			
Receive	≥25	≥27	≥32
Transmit	≥35	≥34	≥34
Amplitude Tracking (dB)	<0.5	<0.5	<0.5
Phase Tracking (deg)	<3	<3	< 3
Noise Figure (dB)	≤2.5	≤3.0	≤3.5
Peak Power (W)	≥4.5	≥3.5	≥2.5
Efficiency (%)		>25	>15
Size (inches)	5x1.4x.25	3.3x1x.25	2x1x.25
Weight (grams)	<50	<40	<30

* Application: EOS SAR

T/R Module Specifications are a Combination of Derived, Self-Imposed, and Direct Flow Down Requirements

L- Band T/R Module Development

SEASAT

- Solid State Power Amplifier

SHUTTLE IMAGING RADAR - C

- T/R Module With Less Emphasis on Size and Weight

SPACE BASED RADAR

- Industry Built High Performance, Advanced Light Weight Modules
- Primarily DoD Sponsored Development
- Technical Data is Export Restricted by the Arms Export Control Act

L-Band T/R Module is Ready For Insertion into SAR Applications With Little or no Modifications

SEASAT L-Band 500 W SSPA

Astro Space Division

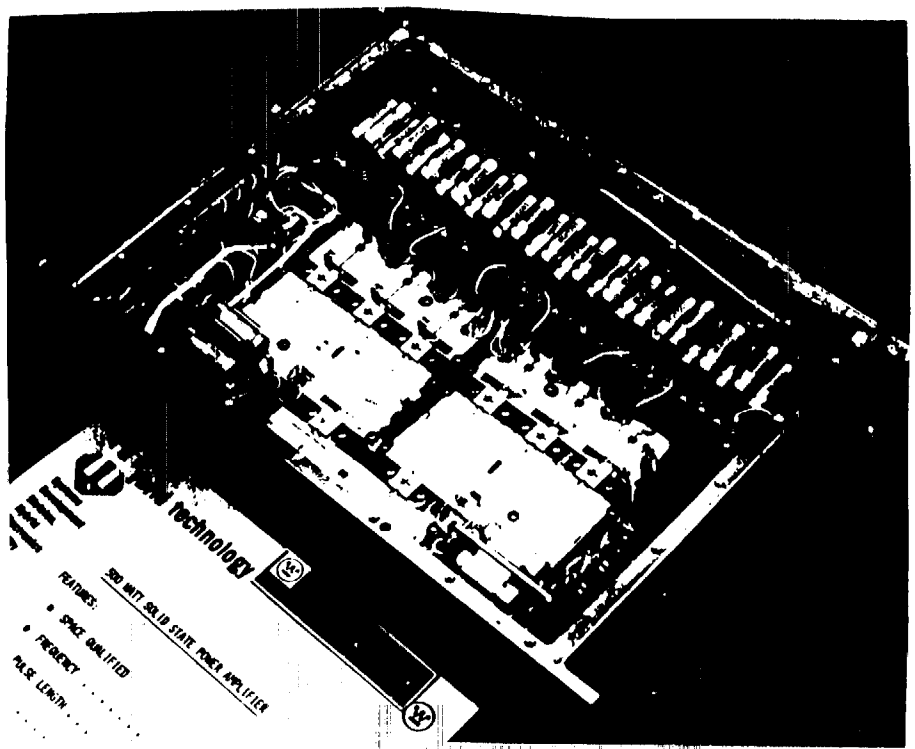

Solid State Power Amplifier Features :

- Frequency	1.225-1.325 GHz
- Pulse Length	34 usec
- Duty	6%
- Efficiency	31 %
- Size	2x7x9 in

3 Combined :

- Power	1200 W
- Size	9x16x31 in
- Weight	90 lbs

SIR-C L-Band T/R Module

Module Specifications

- **Transmit**
  - Output Power — 28 W
  - Duty Cycle — 4-7 %
- **Receive**
  - Noise Figure — 2.5 dB
  - Gain — 25.5 dB
- **Mechanical**
  - Size — 5.5x4x in
  - Weight — 454 grams

SBR L- Band T/R Module

Parameter	Phase A	Phase B	Phase C
Bandwidth (MHz)	100	200	>200
Noise Figure (dB)	X	X-0.5	X-1.0
Peak Power (W)	X	X	X(var.)
Efficiency (%)	X	X+5	X+10
Size (inches)	5x1.4x.5	smaller	smaller
Weight (grams)	227	142	56-112*

* Radar System Configuration Dependent

D. Temme, Space Radar Technology Program Review, MIT Lincoln Laboratory, June 1987.

Current SBR T/R Module Performance Meets or Exceeds SAR Requirements and Improvements are Possible

GBR C-Band T/R Module

Parameter	1987 Tech	MMIC - Phase I
Bandwidth (MHz)	700	700
Noise Figure (dB)	3.0	2.5
Peak Power (W)	10	10
Efficiency (%)	20	25
Size (inches)	1.08x.87x.11	1.08x.87x.11
Weight (grams)	4.22	4.22

Hughes/GE - Ground Based Radar
F. Brand, IEEE MTT-S Int'l Microwave Symp Keynote Address, IEEE Trans MTT,Vol 36, No 12, Dec 1988

C-Band Module Can Be Made Even Lighter and Space Qualified

SIR-C C-Band T/R Module

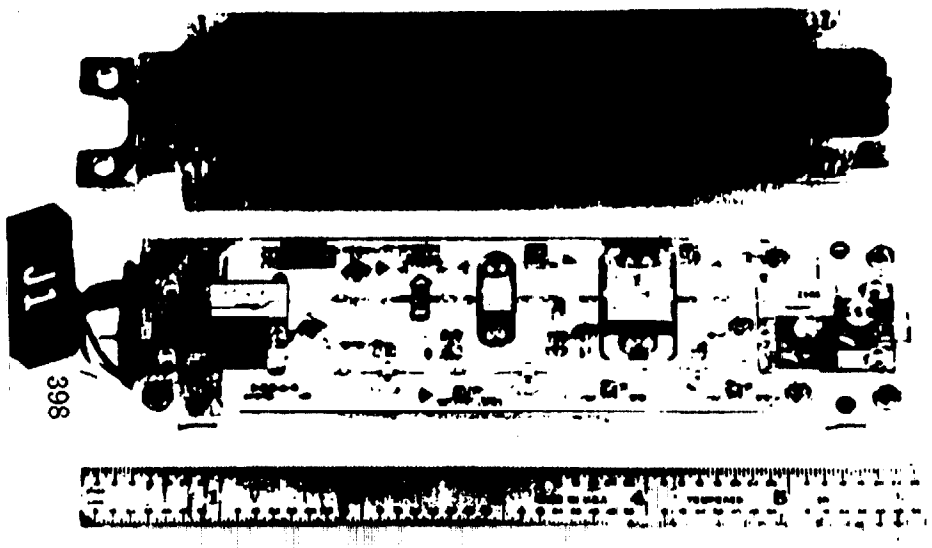

Module Specifications

- **Transmit**
  - Output Power 7.8 W
  - Duty Cycle 4-7 %
- **Receive**
  - Noise Figure 2.8 dB
  - Gain 32.5 dB
- **Mechanical**
  - Size 5.5x1.5x0.56 in
  - Weight 159 grams

COBRA C-Band T/R Module

Astro Space Division

Module Characteristics :

- Output Power <10 W
- Noise Figure <4.0 dB

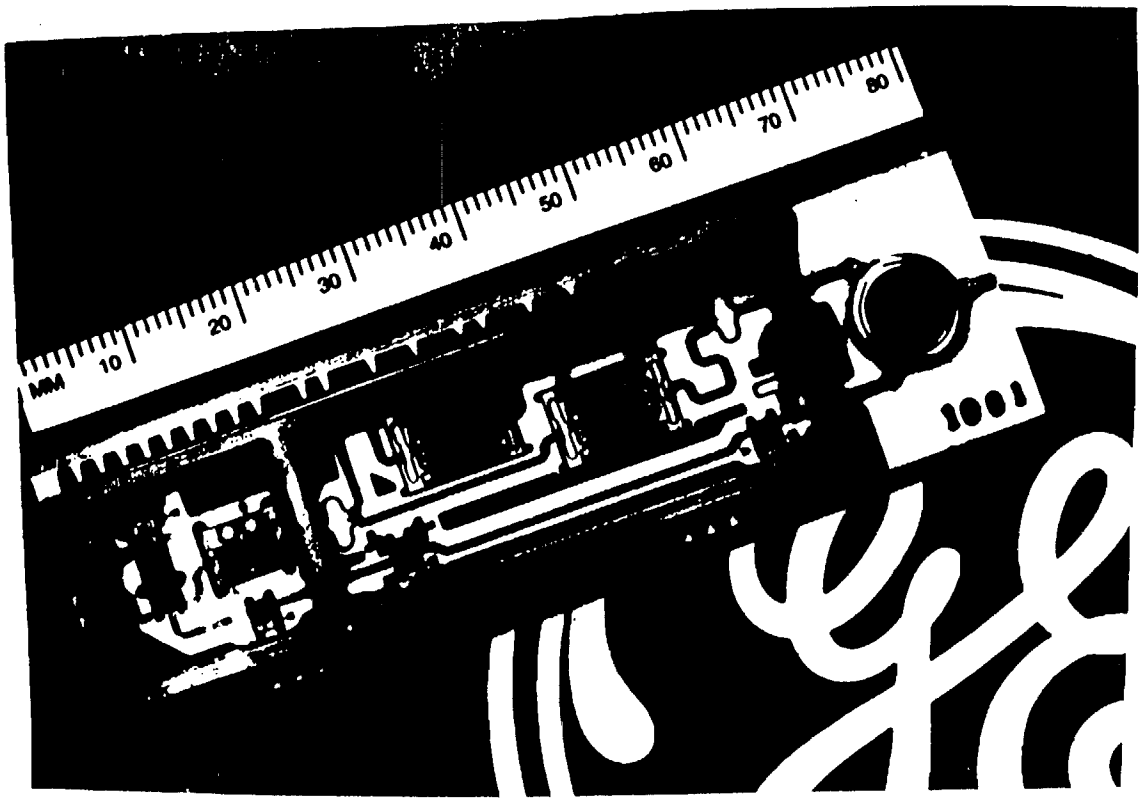

Airborne X-Band T/R Module

Parameter	1987 Tech	MMIC - Phase I
Bandwidth (MHz)	2000	2000
Noise Figure (dB)	3.0	2.0
Peak Power (W)	2	2.5
Efficiency (%)	15	25
Size (inches)	1.34x.48x.11	1.34x.3x.11
Weight (grams)	2.57	1.8

Hughes/GE - Airborne Radar
F. Brand, IEEE MTT-S Int'l Microwave Symposium Keynote Address, IEEE Trans. MTT, Vol 36, No 12, Dec 1988

X-Band Module is Ready and Can Be Made Space Qualified

X-Band T/R Module

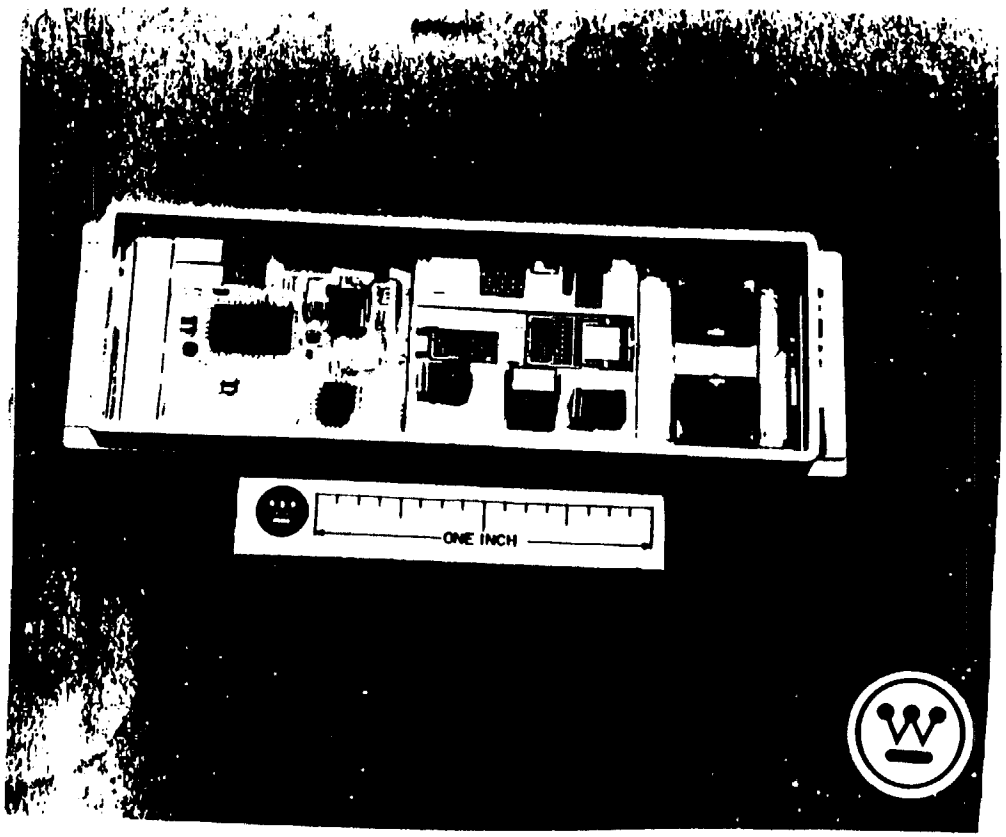

Functional Module :

Transmit :

Freq/Bandwidth	X-Band/20%
Power/Duty	5-10 W/>30%
Efficiency	25-30%

Receive :

Noise Figure	3 dB
Size	2.5x0.6x0.2 in
Weight	30 gm

Concluding Remarks

- GaAs MMIC Technology Has Been Demonstrated and Complete T/R Modules have been Developed in L, C, and X Frequency Bands

- Technology is at Hand to Produce Light, Small, Efficient T/R Modules that Meet the Spaceborne Imaging Radar Requirements

- SAR is an Opportunity to Leverage the Huge DoD and Industry Investment in MMIC and T/R Module Development

S26-32
182866
P.

Advanced Antennas for SAR Spacecraft

N94-15912

William B. Gail
Ball Communication Systems Division
P. O. Box 1235
Broomfield, CO 80038-1235

Abstract

Single and multi-frequency antenna concepts have been developed to evaluate the feasibility of building large aperture polarimetric SAR systems to be launched in low cost launch vehicles such as the Delta II. The antennas are 18.9 m long by 2.6 m wide (L-band) and achieve single polarization imaging to an incidence angle of 55^{o} and dual/quad imaging to 42^{o}. When combined with strawman spacecraft designs, both concepts meet the mass and volume constraints imposed by a Delta II launch.

Introduction

Advanced spaceborne SAR missions generally require large aperture antennas to meet the needs of the user community. SAR antenna concepts presented to date, however, have not fully realized the potential of available antenna technologies. The two EOS SAR industry briefing studies, for example, indicated that the largest L/C/X SAR that could be launched in a Delta II has an antenna aperture of only 2.6x10.9 m. The performance of this antenna, particularly with regard to maximum incidence angle ranges, is considerably less than that desired by the science community.

To evaluate the limiting performance of a mass, volume, and cost constrained SAR, an antenna feasibility study was performed. Four constraints were placed on this study:

1) Satisfy known science requirements so as to place the user community ahead of the technology
2) Base the design on the proven SIR-C heritage, minimizing design changes but incorporating new technologies where most useful
3) Design to a Delta 7920 launch to limit launch cost
4) Generate a design which minimizes the number of parts and processes to reduce cost

Alternate design approaches were then examined, based on these constraints, to identify feasible (not necessarily optimal) designs.

Requirements

The science requirements specified by the user community for EOS SAR were used to drive the design. Mission/system requirements were derived from the science requirements. An orbit at 700 km was selected to minimize atomic oxygen exposure and drag and thus extend the spacecraft lifetime. Requirements imposed by selection of the Delta 7920 as a launch vehicle are strong drivers for the spacecraft and antenna designs. While other launch options could be more effective, designing to the Delta option effectively identifies the key technology and cost drivers for the antenna. Both single and multiple frequency design options were considered.

L-band Advanced SAR (LASAR)

The single frequency quad-polarization L-band Advanced SAR (LASAR) concept developed during this study is shown in Figure 1. Characteristics of this antenna are summarized in Table 1. The LASAR antenna is 18.9 m long and consists of seven leaves that fold for launch. Bus and payload subsystems are contained on the backside of the square vertical structure in this figure.

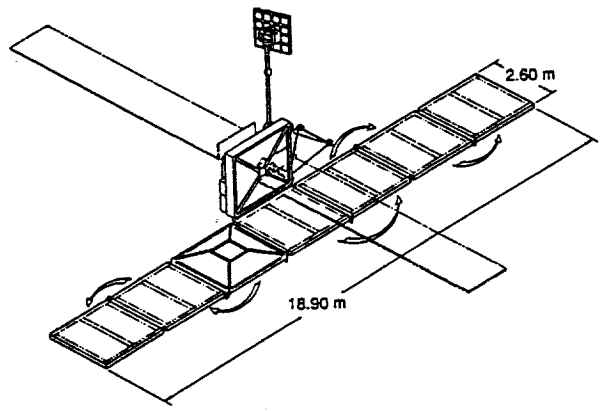

Figure 1 Conceptual illustration of the LASAR spacecraft showing the deployed 18.9 m antenna.

Table 1 Characteristics of the LASAR antenna.

CHARACTERISTIC	VALUE
Array size (m)	18.9 x 2.6
Antenna mass (kg)	511
Peak radiated power (W)	4900
Number of T/R modules	224
Peak output power per T/R circuit (W)	11
Number of leaves	7
Leaf size (m)	2.68 x 2.6
Leaf thickness (cm)	6.4
Panels per leaf	2
Polarization	quad
Elements per stick	6
Sticks per panel	16

The aperture uses the same six-element-per-stick microstrip patch architecture used on SIR-C, as illustrated in Figure 2. This approach maximizes SIR-C heritage in manufacturability as well as performance. The peak radiated power of 4900 W requires a module peak power of only 28 W, well within the capability of current devices. Because the antenna support structure is integral to the panels, total panel thickness is only 6.4 cm.

The use of thin panels allows the 18.9 meter antenna to be folded and stowed within the tight launch shroud of the Delta, as shown in Figure 3 Panels are connected by simple hinges and deployed with reliable motorized actuators. Figure 4 illustrates the first step of this deployment sequence.

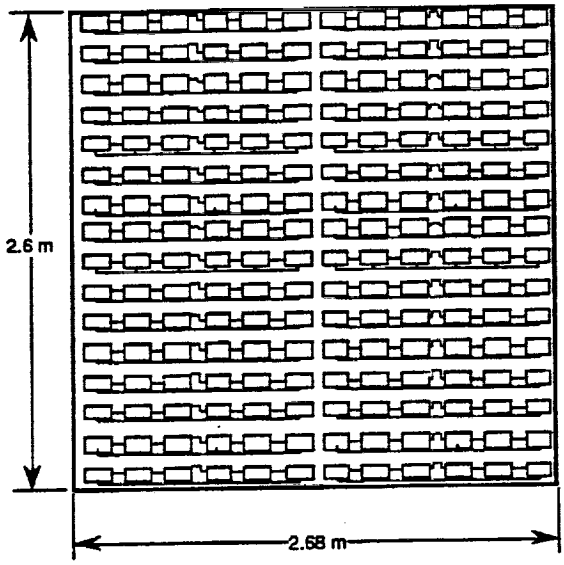

Figure 2 Layout of a leaf showing the microstrip patch elements.

The pattern characteristics of the LASAR antenna are very similar to those of the SIR-C antenna, the most obvious difference being that the azimuth beamwidth is considerably smaller. Figure 5 shows the H-polarization transmit pattern when the beam is scanned 15^{o} off boresight.

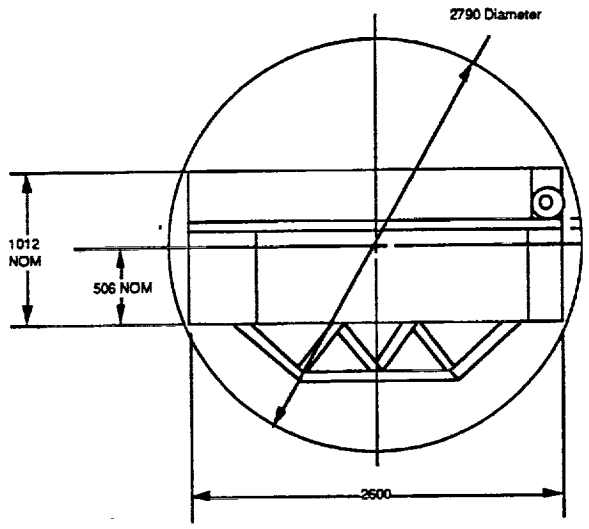

Figure 3 Stowed configuration of the LASAR spacecraft within a Delta 7920 shroud.

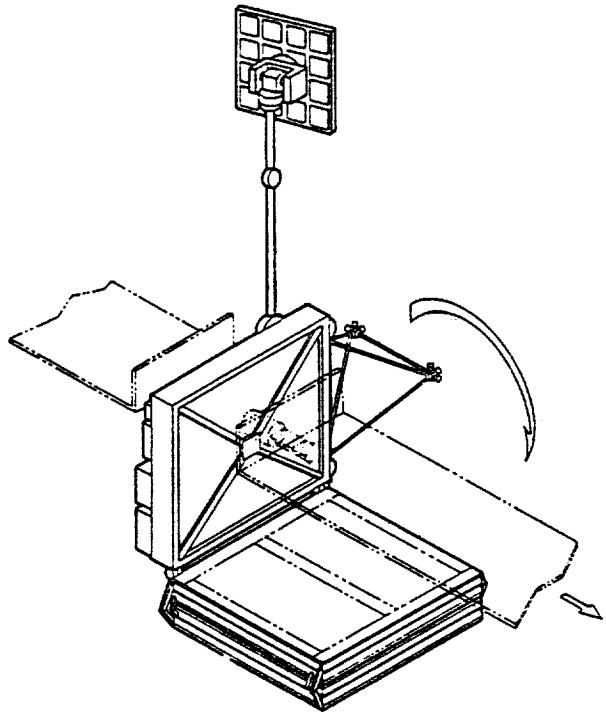

Figure 4 Initial deployment sequence for the LASAR antenna.

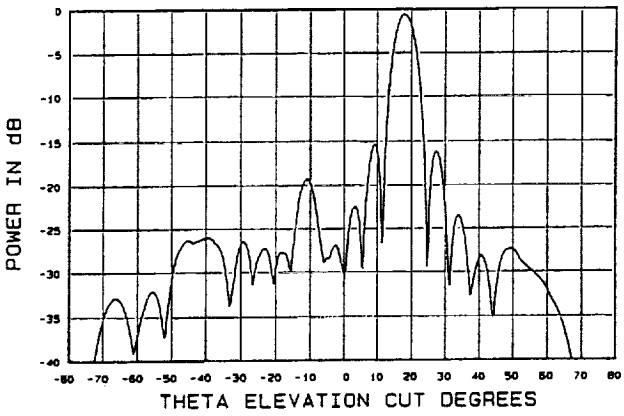

Figure 5 Sample antenna pattern for the LASAR antenna showing the H-polarization transmit beam scanned at 15°.

Antenna flatness is maintained through the structural integrity of the panels, which are designed with sufficient stiffness to withstand the launch load using materials carefully selected to minimize bending when the antenna is subject to thermal gradients. A thermo-mechanical analysis showed that the antenna maintains the required $\lambda/20$ flatness with a 20% margin.

SAR performance of the LASAR design meets or exceeds all of the known science requirements for EOS SAR. Figure 6 demonstrates both incidence angle and sensitivity performance. The 18.9 m aperture supports imaging to incidence angles of 55° for single polarization and 42° for dual/quad polarization. This satisfies the EOS SAR science requirements of 50° and 40° respectively and is well beyond the 40°/30° performance of the 10.9 m aperture presented in the EOS SAR industry briefing. Thermal noise equivalent σ^0 of this antenna is -41 dB at 45°. The maximum SCANSAR swath is 670 km for single polarization and 400 km for dual polarization.

Using mass estimates developed during this study and the EOS SAR industry studies, a mass budget was derived for the LASAR design. This budget is shown in Table 2. Mass savings are obtained primarily from the antenna mass reduction and use of a single-frequency instrument. Additional mass reductions from the industry study values, particularly in the instrument, are expected with further analysis. The LASAR approach meets the Delta launch requirement with considerable margin including design contingency.

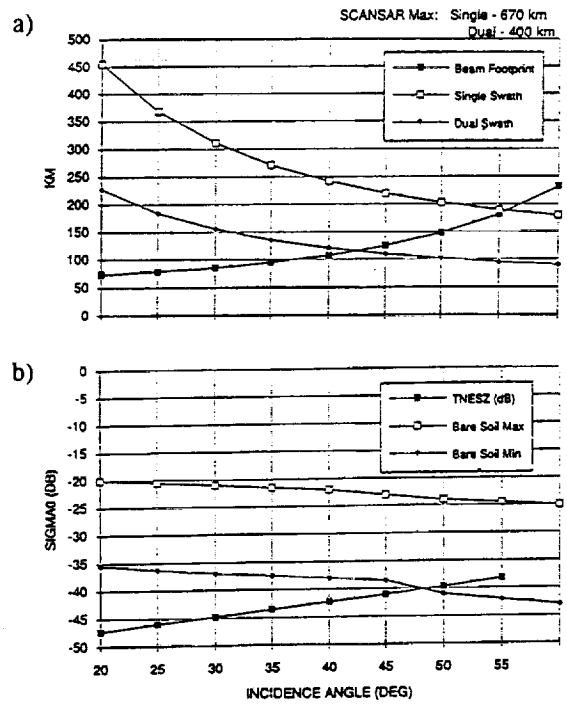

Figure 6 LASAR performance versus incidence angle: a) ambiguity and beamwidth limited swath for single and dual/quad modes. b) thermal noise equivalent σ^0.

Table 2 Mass budget for the LASAR spacecraft.

ITEM	MASS (kg)
Antenna	**511.39**
Flight Electronics	**263.00**
RF electronics	50.00
DDHA	60.00
CTTA	75.00
PCDA	20.00
DDRE	20.00
Harness	30.00
Adapter plate	8.00
Bus System (dry)	**1268.00**
Structure	298.00
AACS	102.00
Cabling	15.00
Propulsion	62.00
Thermal control	30.00
Power	358.00
Command and data	152.00
Mechanisms	148.00
Communications	103.00
Miscellaneous	**698.48**
Launch adapter/misc	100.00
Propellant	90.00
Project reserve	100.00
Contingency	408.48
TOTAL (kg)	**2740.87**
MARGIN (kg)	559.13

Multiband Advanced SAR (MASAR)

The performance advantages obtained through the LASAR design were extended to a multi-frequency system in the MASAR design. The design employs the same general seven-leaf configuration used shown in Figure 1 to obtain an 18.9 meter L/C/X aperture. The characteristics of the MASAR antenna are summarized in Table 3. Peak transmitted power levels were selected to satisfy the science requirements while maintaining a feasible spacecraft DC power budget. Module peak powers are 11 W at L-band, 4 W at C-band, and 4 W at X-band. Panel thickness is the same as for LASAR, providing for the same stowage and deployment procedures.

Table 3 Characteristics of the MASAR antenna.

CHARACTERISTIC	VALUE		
Array size (m)	18.9 x 2.6		
Antenna mass (kg)	711		
Number of leaves	7		
Leaf size (m)	2.68 x 2.6		
Leaf thickness (cm)	6.4		
Panels per leaf	2		
	L	C	X
Polarization	quad	quad	dual
Peak radiated power (W)	1900	1400	1200
Number of T/R modules	224	224	224
Peak power per T/R circuit (W)	11	4	4
Sticks per panel	32	64	64

To obtain the largest possible aperture size for each frequency within the 18.9 x 2.6 m area constraint, a shared aperture approach was used. As shown in Figure 7, the L-band array uses the full area to achieve an aperture size that is the same as that for LASAR. The C-band and X-band apertures *share* the space occupied by the L-band aperture. This approach is known to be feasible at the element level; further work is in progress to understand the impact on performance at the array level.

Antenna flatness is maintained through 1) the structural integrity of the panels, which are designed to be individually flat to the required X-band $\lambda/20$ flatness, and 2) use of active hinges between panels. A thermo-mechanical analysis showed that, with the inclusion of active hinges, the antenna maintains the X-band $\lambda/20$ flatness across the entire array.

Table 4 provides a mass budget for the MASAR concept, showing that a MASAR spacecraft meets the Delta launch mass requirement, although with only a small margin.

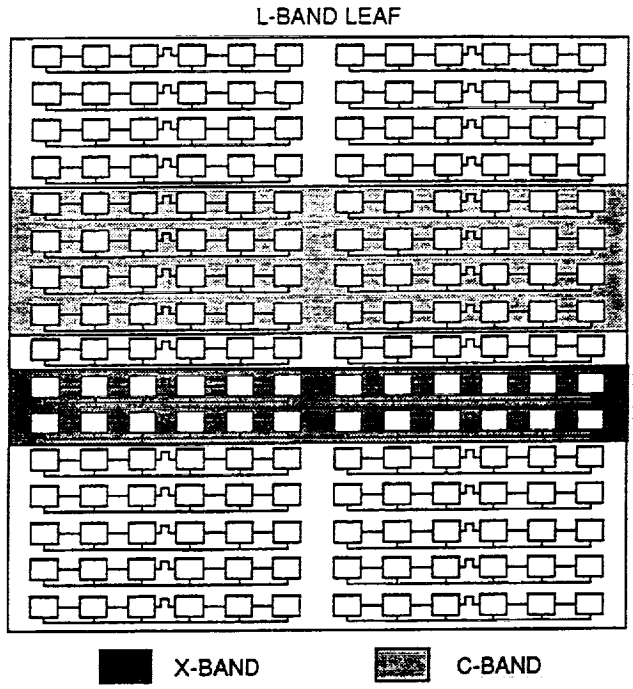

Figure 7 Layout of a shared aperture leaf showing L-band elements and regions of C- and X-band elements.

Table 4 Mass budget for the MASAR spacecraft.

ITEM	MASS (kg)
Antenna	**711.08**
Flight Electronics	**383.00**
RF electronics	91.00
DDHA	75.00
CTTA	114.00
PCDA	27.00
DDRE	23.00
Harness	45.00
Adapter plate	8.00
Bus System (dry)	**1314.00**
Structure	298.00
AACS	102.00
Cabling	15.00
Propulsion	62.00
Thermal control	30.00
Power	404.00
Command and data	152.00
Mechanisms	148.00
Communications	103.00
Miscellaneous	**771.62**
Launch adapter/misc	100.00
Propellant	90.00
Project reserve	100.00
Contingency	481.62
TOTAL (kg)	**3179.70**
MARGIN (kg)	120.30

The importance of the shared aperture approach is shown in Figure 8, which illustrates the incidence angle performance of comparable shared and separate aperture antennas. Both antennas are assumed to have a fixed 18.6 x 2.6 m area available for the aperture. In the shared aperture approach, the L-band aperture uses the full 2.6 m width. In the separate aperture approach, the 2.6 m width is apportioned between the L, C, and X-band apertures so that the L-band aperture has a width of only 1.9 m. As a result, the maximum incidence angle decreases from 55° to 47° for single polarization and from 42° to 33° for dual/quad polarization.

Conclusion

The LASAR/MASAR feasibility study shows that SAR antennas large enough to satisfy the needs of the science user community can indeed be built using non-exotic SIR-C heritage technology and launched with the low-cost launch vehicles.

Acknowledgment

The work described in this paper was performed by the staff of Ball Communication Systems Division.

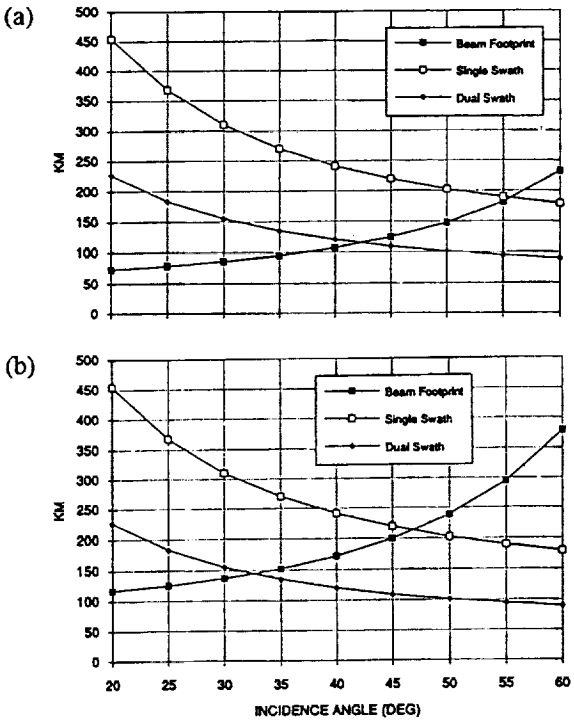

Figure 8 Comparison of ambiguity and beamwidth limited swath versus incidence angle for a) shared aperture, and b) non-shared aperture.

Table 4 Science requirements and compliance of the MASAR spacecraft.

REQUIREMENT	VALUE	DESIGN VALUE
Frequency	L, (C, X)	L, (C, X)
Polarization	quad, (quad, dual)	quad, (quad, dual)
Resolution		
- Local mode	20-30 m	30 m (3 looks)
- Regional mode	50-100 m	50-100 m
- Global mode	250 m	250 m
Incidence angle range		
- Single polarization	15-50 deg	TBD-55 deg
- Quad polarization	15-40 deg	TBD-42 deg
Thermal noise equiv σ^o @ 45°	-36 dB, (-27 dB, -22 dB)	-37 dB, (-28 dB, -23 dB)
Max single swath width		
- Single polarization	30-50 km	within ambiguity limits
- Quad polarization	30-50 km	within ambiguity limits
Max SCANSAR swath	600 km	>600 km
Calibration		
- Relative amplitude	+/- 1.0 dB	+/- 1.0 dB
- Absolute amplitude	+/- 1.0 dB	+/- 1.0 dB
- Relatvie phase	TBD	TBD
- Geometric	+/- 0.5 pixel	+/- 0.5 pixel
Ambiguity level	<-20 dB	<-23 dB
Sidelobe level		
- Elevation	<-14 dB	<-15 dB
- Azimuth	<-12 dB	<-13 dB
Polarization isolation	<-25 dB	<-30 dB
Orbit exact repeat interval	<5 days	2 days
Orbit near repeat interval	16 days	16 days

J27-32
182867
N94-15913

High resolution SAR applications and instrument design

C. Dionisio, A. Torre

Alenia Spazio

via Saccomuro, 24
00131 Rome, ITALY

ABSTRACT

The Synthetic Aperture Radar (SAR) has viewed, in the last years, a huge increment of interest from many preset and potential users.
The good spatial resolution associated to the all weather capability lead to consider SAR not only a scientific instrument but a tool for verifying and controlling the human daily relationships with the Earth Environment. New missions have been identified for SAR as spatial resolution became lower than three meters : disasters , pollution , ships traffic ,volcanic eruptions, earthquake effect are only few of possible objects which can be effectively detected, controlled and monitored by SAR mounted on satellites. This paper deals with high resolution radar design constraints and dimensioning .

INTRODUCTION

The recent years have been characterized by a increasing of interest on remote sensing by SARs both for civil and not civil applications. The technology development can now assure new features to SAR sensors and spacecraft missions can be better tailored to the specific user requirement.
The two key parameters for new missions are: revisit time and resolution.
The first parameter deals with the mission definition, coverage, orbits selection and the number of satellites which can be allocated in orbit at the same time. The high resolution permits the analysis of manmade or natural objects with the capability of their detection and in same case their identification. Furthermore high resolution leads to better radiometric resolution for the conventional applications where pixel dimensions requirement are less stringent. A resolution better than three meters is generally requested for these Surveliance Missions but the target is to reach the one meter resolution within next decade. Civil applications could be identified in the controlling and monitoring of environment areas and phenomena like:

- Pollution
- Fires
- Volcanic activity
- Ships traffic control
- Land traffic control
- Environmental disasters
- Crisis monitoring
- Urbanization control
- coast erosion

The high resolution is generally attractive in countries like Europe where we find high population density and limited land extension so the number of objects to be discriminated is very large.

Alenia Spazio has been involved , in the last few years, in a number of studies for high resolution SAR sensor and their potential applications. In this note only few considerations will be provided identifying the most significative aspects of high resolution SAR design.

REQUIREMENT OVERVIEW

The main requirement of an high resolution SAR sensor are here below identified:

parameter	**unit**	**high resolution mode**	**survey mode**
range resolution	meters	1 to 3	5 to 100
azimuth resolution	meters	1 to 3	5 to 100
swath extension	Kmeters	5 to 10	50 to 400
sensitivity	dB	-20	-20
number of looks	-	1	1 to 16
azimuth ambiguities ratio	dB	-22	-22
range ambiguity ratio	dB	-22	-22
radiometric accuracy	dB	< 2	< 1
access area	degree	30 t0 60+	20 to 60+
polarization	-	HH or VV	HH or VV/ HH and VV
altitude	Kmeters	550 to 800	550 to 800

The high resolution is obtained in the range direction by wide bandwidth (BW) chirp transmission. The figure 1. shows the bandwidth needs as function of angle of incidence for a defined resolution. The minimum BW for one meter resolution is 300 MHz if 30 Deg incidence angle is requested. Now if we look to the International Regulation about frequency allocation for RADAR applications (S: 200 MHz, C: 100 MHz, X: 300 MHz ,Ku: 600 MHz), then we discover that only X and Ku bands can be used for the scope.
The azimuth resolution can be obtained by a conventional stripmap mode with two meters antenna length or the most promising spotlight mode which consists of increasing the conventional synthetic aperture by tracking with the antenna beam the ground swath. This implies azimuth steering capability in the antenna. Figure 2. gives the frequency dependence of resolution in case only the quadratic term of the SAR echo is compensated into the processing. The present compression algorithms should be improved for high resolution processing looking in particular to the depth of focus and to the combination of the discrete synthetic sub apertures produced by the antenna steering.
The Swath dimensions for high resolution SAR is limited mainly by the data rate but should be pointed out that in case of spotlight mode the antenna dimensions are heavily affected because the azimuth beam width should fit with swath dimension in the along track direction. Then the antenna height is dictated by ambiguities (minimum antenna area) and link budget considerations. The result of dimensioning appears in an antenna with 15 / 20 square meters area, narrow in the along track direction. Therefore in same cases, when it is requested to combine high resolution with a survey-medium resolution / medium swath mode, it becomes difficult to find swath coverage solution without using the complex Scansar technique . Alternatively antenna beam forming by TR modules weighting or switching-off a certain number of TR modules, so reducing the antenna height , are techniques to be attempted. The drawbacks of spotlight mode are the need of an active antenna with azimuth steering and the gaps on ground between an images and the next one (fig 4 .). The gap for an X band sensor is in the order of one/ two times ,depending on satellite altitude and incidence angle, the Swath dimension in the azimuth direction. The access area (fig 3.) is important in determining the revisit time of the sensor and the incidence angle at which a "spotswath" could be viewed. The access area lower limit comes from resolution/ BW requirement while the upper limit from link budget/ antenna dimension constraints.

The multipolarization doesn't seem essential to surveillance mission SAR adding complexity to the system without dramatically improving detection capability. The spacecraft altitude is defined from mission requirement and impacts specifically high resolution in antenna dimension and data rate. The data rate of an instrument like we are outlining in this notes has a data rate in the order of one Gigabit/sec. This high amount of data can be transmitted to ground directly or by a Data Relay Satellites which are under study for the next future.

CONCLUSIONS

ALS has studied the high resolution implementation on SAR sensor . The result shows that the design is feasible in X band where resolution can be achieved and technology is available. The selected solution is based on spotlight mode: active antenna is requested with azimuth steering capability (1/2 Deg) for azimuth resolution and elevation steering capability (20/ 30 Deg) for imaging within the access area.

Range resolution

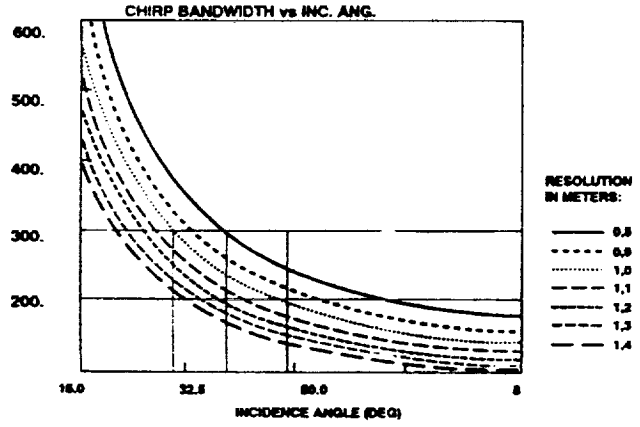

fig.1.

Max achievable resolution (azimuth)
Frequency dependence

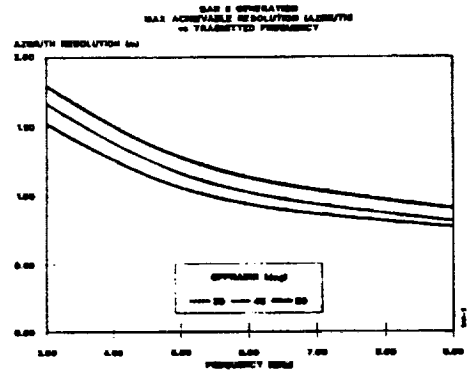

fig.2.

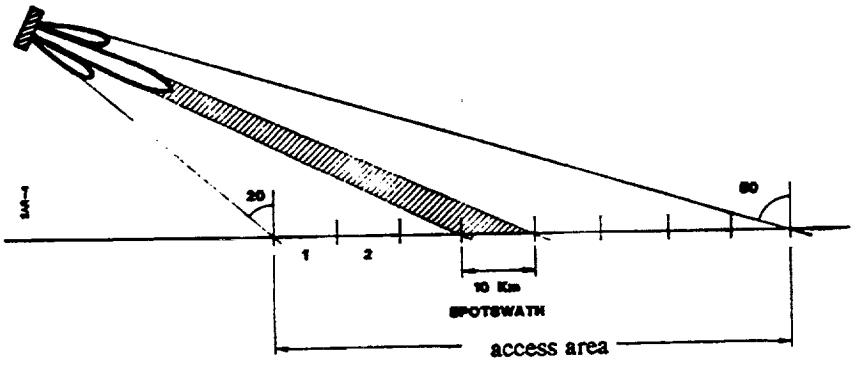

fig.3.

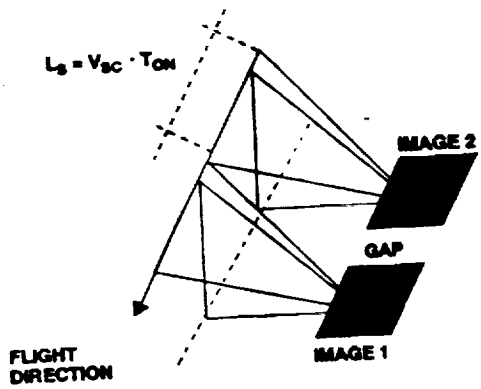

fig.4.

ADDITIONAL PAPERS

A Summary of Microwave Remote Sensing Investigations Planned for BOREAS

Kyle C. McDonald
Jet Propulsion Laboratory
California Institute of Technology
4800 Oak Grove Drive
Pasadena, CA 91109, U.S.A.

Summary

The Boreal Ecosystem - Atmosphere Study (BOREAS) is a multidisciplinary field and remote sensing study that will be implemented jointly by the United States and Canada. The goal of BOREAS is to obtain an improved understanding of the interactions between the boreal forest biome and the atmosphere in order to clarify their roles in global change. Specific objectives are to improve the understanding of the processes that govern the exchanges of water, energy, heat, carbon, and trace gases between boreal ecosystems and the atmosphere, and to develop and validate remote sensing algorithms for transferring the understanding of these processes from local to regional scales.

Two principal field sites, both within Canada, have been selected for this study. The northern site is located near Thompson, Manitoba, and the southern site encompasses Prince Albert National Park in Saskatchewan. The growing season in the northern site tends to be limited by growing-degree days while the southern site is limited by soil moisture and fire frequency. Most of the field work will occur at these two sites during 1993 and 1994 as part of six field campaigns. The first of these campaigns is scheduled for August 1993 and will involve instrument installation and an operational shakedown. Three large scale Intensive Field Campaigns (IFCs) are scheduled for 1994, along with two smaller scale Focused Field Campaigns (FFCs). The first 1994 campaign will be an FFC designed to capture the biome under completely frozen conditions during the winter. The second FFC and the first IFC are scheduled to capture the spring thaw period. Another IFC will take place in the summer during a period of maximum water stress. Finally, the third FFC will be scheduled to capture the collapse into senescence during the fall.

The BOREAS science team has been organized into six disciplines, one of which centers on remote sensing science investigations. The five microwave investigations have been included in this group. These activities consist of four radar studies and one passive microwave investigation. Titles of these studies are listed below together with the principal investigators and a brief statement of their primary objectives:

(1) Microwave scatterometer observations of boreal forest species.
M. C. Dobson, The University of Michigan

Objective: Obtain c- and x-band scatterometer measurements of 2-3 tree species within the two test sites. Backscatter from each species will be observed for 4-5 days continuously during each of the three IFCs. These measurements will then be used to verify linkages between biophysical controls and SAR observations.

(2) Distribution and structure of biomass in boreal forest ecosystems.
K. J. Ranson, NASA Goddard Space Flight Center
R. H. Lang, George Washington University

Objective: Determine the amount and spatial distribution of above-ground biomass. The planned activity includes development of algorithms for determining the amount standing biomass and its apportionment from SAR backscatter, development of model inversion techniques, and determination of the optimum radar parameters for use in estimating canopy biomass.

(3) Estimation of hydrological parameters in boreal forest using SAR.
S. Saatchi, Jet Propulsion Laboratory, California Institute of Technology

Objective: Estimate hydrologic parameters of the forest and underlying ground surface. The water content of the vegetation and ground surface and surface cover will be examined with SAR. Hydrologic parameters of soil, snow, moss and permafrost will be studied.

(4) Monitoring environmental and phenologic state and duration of state with SAR as input to improved CO_2 flux models.
J. B. Way, Jet Propulsion Laboratory, California Institute of Technology
K. C. McDonald, Jet Propulsion Laboratory, California Institute of Technology

Objective: Classify boreal forest by functional group and determine the environmental and phenologic state and water status within each functional group. In so doing, SAR will be used to determine the photosynthetically active period of these functional groups. This information will be provided as new input for estimating the CO_2 flux of the biome.

(5) The diurnal and annual radiobrightness of boreal forest.
A. W. England, The University of Michigan

Objective: Monitor and model diurnal and seasonal radiobrightness signature of boreal forest. This information will be used to update existing cold region radiobrightness models to account for seasonal and diurnal signatures of the boreal forest.

These studies have been designed to investigate both the static and temporally varying microwave signatures of the boreal forest biome. Multifrequency polarimetric SAR imagery will be collected by aircraft-borne systems during the field campaigns. This will allow detailed analysis of the static and temporally varying aspects of backscatter. During the intervals between these campaigns, imagery from the ERS-1 satellite will provide more of a continuous monitoring capability.

This article was prepared at the Jet Propulsion Laboratory, California Institute of Technology, under contract to the National Aeronautics and Space Administration. The research described in this article is co-sponsored by the National Aeronautics and Space Administration and Energy, Mines and Resources, Canada.

SPACEBORNE RADAR FOR GEOSCIENTIFIC APPLICATIONS IN NORTH CHINA

Guo Huadong
Institute of Remote Sensing Applications, Academia Sinica

Wu Guoxiang
National Remote Sensing Center of China

Wang Zhen-song
Institute of Electronics, Academia Sinica

The Shuttle Imaging Radar-A and -B (SIR-A and SIR-B) carried on the Space Shuttle Columbia in November 1981 and the Challenger in October 1984 acquired images of test sites of North China. The Russian ALMAZ SAR also acquired imagery of part of this test site in September, 1992. In November of 1990, the airborne SAR developed by the Chinese Academy of Sciences (CAS/SAR) covered this area for the purpose of Chinese spaceborne radar development. By studying and analyzing these SAR data we have achieved positive results in geoscientific applications.

Penetration. It is discovered that SIR-A has penetrated through the thin dry sand sheet at the Altengaobao area in Inner Mongolia. A triangular geologic body, which has a strong radar return, is clearly shown on the SIR-A image (Fig. 2a). The central part of the triangular geological body is totally covered by dry sand which is shown on the Landsat MSS image (Fig. 2b). Digging a shallow hole at the central part, the bedrock is exposed at about 1 meter of sand in the field verification. The geological map of this region shows that the upper part of the triangular body is Precambrian metamorphic rock, the lower part is comprised of Mesozoic granites, and the central part, covered by dry sand, is gneisses. The theoretical study indicates that the penetrating ability of radar should at least meet three conditions: 1) fine grain size; 2) less thickness; 3) extremely dry. The surface conditions of the test site are content with the former two conditions. The meteorological records of the test site show that the annual mean rainfall is less 150 mm, some places even less 10 mm, dryness is 4 - 12 (the dryness of adjacent desert is 7 - 12), and evapotranspiration is 31.5 times as rainfall, which means that the test site is content with the third condition.

Rock Type and Fault Recognition. The distribution and range of Caledonian plagioclase-granite at Wang Yang area in Gansu Province has been detected by using SIR-B data. Due to adverse natural circumstances and poor traffic, the test site is geologically under-studied, with only a few plagioclase granite bodies being displayed on the geological map. The large Bayinnorgong strike slip fault, 80 km long, was recognized on CAS/SAR and SIR-A images at the Bayinnorgon area of inner Mongolia, and the field work proved its existence. Several bunches of faults were interpreted from the SIR-A image of the Keping area in Xinjiang Province. The longest one is 50 km. Many secondary faults are well developed along the two sides of the major fault which cuts through all of the strata in the test site. The strata on the two sides are strongly distorted, deformed, and displaced, and the displacement is over 5 km.

Mineral Exploration. SAR is useful for detecting ore-controlling structures. A gold-bearing structure belt was directly discovered by the interpretation of SIR-A images in Honguyulin area. The belt is about 650 km long and composed of Sinian sandstone, limestone and quartz-diorite. Sampling along the belt, the chemical analysis results show that the gold tenor of most samples reaches 1 ppm and the highest sample is 7.94 ppm. The discovery of the gold-bearing structure belt has two leading factors: 1) The linear strong return anomaly. On one hand the strong return comes from the rough surface of the belt. On the other hand, it is caused by the high dielectric constant of altered rocks. The dielectric constant of the country rock is less than 7, but the mineralized rock is over 20. 2) The relevant analysis result. The gold-bearing structure belt is a fractured structure belt, distributing along and contacting with the granite body, which is an ideal location for metal mineral deposit.

Multi-parameter SAR Data Comparison. Jilantai area of Inner Mongolia is our spaceborne radar science test site. SIR-A, SIR-B, ALMAZ SAR and CAS/SAR data of the test site have been acquired so far (Fig. 1). Their parameters are as follows: Operation Bands: L, L, S and X; Spatial Resolution: 40mx40m, 32mx28m, 10-15m and 10mx10m; Look Angle: 47°, 26°, 45°, and 19°; Flight Direction: NW 80°, NE 20°, NW 20°, and NE 90°. All four SAR systems operate in HH polarization. With the diverse imaging parameters, they have different imaging effects.

The high-resolution imagery is more suitable for rock type discrimination. The detecting ability is better for desert areas when the radar illuminating direction is perpendicular to the slipface or sand dunes. The small depression angle will bring a lot of shadow and reduce the information.

We would like to acknowledge Dr. Charles Elachi and Dr. Tom Farr of JPL. Also NPO and ALMAZ Corporation, who kindly provided SIR-A, SIR-B and ALMAZ SAR data to our study.

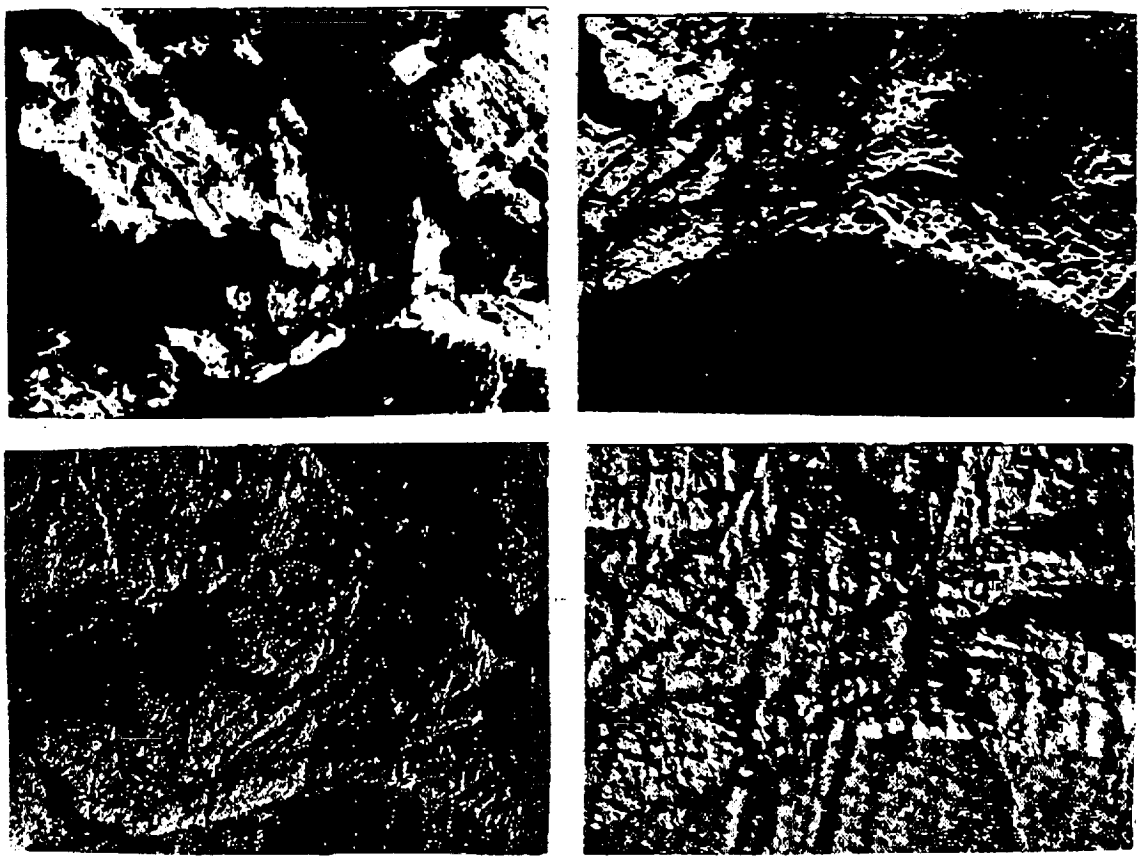

Figure 1. Jilantai test site of North China

SIR-A Image (upper left)
ALMAZ SAR Image (lower left)
SIR-B Image (upper right)
CAS/SAR Image (lower right)

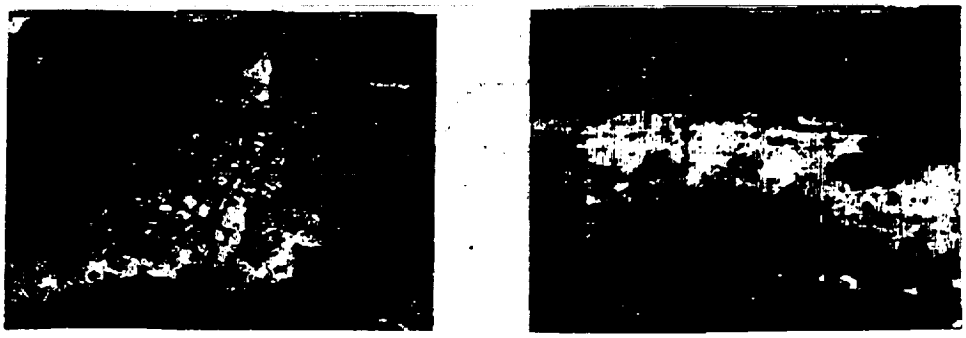

Figure 2. Altengaobao area of Inner Mongolia, North China

SIR-A image showing penetration phenomena (left).
Landsat MSS image (right).

PRIMARY STUDIES OF CHINESE SPACEBORNE SAR

Wang Zhensong, Wu Guoxiang, Guo Huadong, Wei Zhongquan, Zhu Minhui

ABSTRACT

This paper deals with the primary studies on spaceborne synthetic aperture radar (SAR) in China. The SAR will be launched aboard a Chinese satellite and operated at L-band with HH polarization. The purpose of the mission in consideration is dedicated to resources and environment uses, especially to natural disaster monitoring. The ground resolution is designed as 25 m x 25 m for detailed mode and 100 m x 100 m for wide scan-SAR mode. The off-nadir angle can be varied from 20 to 40 degrees. The key system concepts are introduced here.

I. INTRODUCTION

It is well known that SAR can map the Earth surface under poor optical conditions. Spaceborne SAR data can be widely used for natural resources exploration and environment monitoring. SAR is also suggested as the most important payload for a natural disaster reduction satellite system, which has been considered by many countries and international organizations. To meet the requirement for all-weather Earth observation of remote sensing users both from China and around the world, China is considering the development of a Chinese spaceborne SAR system. The primary studies on related techniques are conducted in the framework of the National High-Tech Research and Development Plan of China, which is to develop techniques to be industrialized and practically applied by the end of this century. The primary studies on spaceborne SAR show that the SAR operated at L-band in a sun-synchronized circular orbit can partly fulfill the tasks suggested by Chinese users for flood disaster monitoring and other resources and environment related fields.

The SAR will use horizontally polarized L-band (wavelength 23.5 cm) for both transmitting and receiving of the SAR signal. Two operating modes, detailed mode and wide scan-SAR mode, can be chosen by ground instructions according to different working tasks. The satellite will also have a limited orbit change capability to meet the need of flood monitoring in the eastern part of China, where flood disasters every summer are common. This capability means that the satellite can be changed to a lower orbit which is frozen to over East China.

In past years, China has used airborne SAR to monitor flooding areas during the flood season. An airborne SAR system developed in China played an important role in this kind of monitoring. This system, working in X-band with four polarizations, has a resolution of 10 m x 10 m, a swath width of 35 km, and an acting range of 150 km. This experience contributed greatly to the studies on spaceborne SAR in China.

The primary results presented here are based on the mission study, on domestic experience with airborne SAR systems, and on SAR data processing.

II. MISSION

The Chinese spaceborne SAR mission will no doubt meet many requirements for SAR data in resources and environment uses. Applications of importance to China also includes flood and drought monitoring. The SAR system will be onboard a Chinese satellite with a circular sun-synchronized orbit. The orbit parameters are shown as Table 1.

Table 1. Parameters of Chinese SAR Satellite

Orbit height	608 km
Orbit inclination	97.8°
Orbit period	96.83 min.
Repetitive period	31 day
Number of revolutions per day	14+27/31
Total number of revolutions	461
Local time of descending node	10:30
Orbit regression	24.2° westward
Space between neighbor orbits	81.7 km (equator)
	75.5 km (20°)

The planned satellite will be a 3-axis stabilized one. The orbit is chosen according to the consideration of Earth coverage and better S/N ratio in the SAR operation under the power allocated to the SAR system.

The SAR system is designed according to user requirements that demand a variety of incidence angles from 20 to 40 degrees. A microstrip array antenna measuring 12.5 m x 2.5 m is considered with electronic beam steering capability. Selected radar characteristics are listed as Table 2.

Table 2. Chinese Spaceborne SAR Characteristics

Frequency	1.275 GHz
Wavelength	23.5 cm
Polarization	HH
Off-nadir angle	20-40°
Spatial resolution	25 m / 100 m
Swath width	100 km / 400 km
Pulse bandwidth	20 MHz
Pulse length	33 micro sec.
Pulse repeat frequency	Selectable
Noise equivalent	< -20 dB
Quantization bit number	3 or 5
Down link data rate	100 Mb/s

The SAR system will transmit a linear frequency modulated signal, which is generated by the use of a surface acoustic device. A solid state high-power amplifier will be used for transmitting high-peak power probing signals. The SAR electronics for use onboard the satellite are being developed. The primary studies on the spaceborne SAR show the possibility that the requirements of spaceborne SAR to the space platform can be realized.

Techniques for spaceborne SAR image processing are developed in the primary studies and SAR images have been reconstructed. Studies on the applications of spaceborne SAR data are also being carried out in geology, hydrology, agriculture, forestry, oceanology, and surveying and mapping. We believe that a mature user group will be the key to the successful realization of the future Chinese spaceborne SAR project.

For peaceful uses of space remote sensing technology, we are looking forward to having international collaboration with other countries in the field of spaceborne imaging radar development.

Dr. Wang Zhensong and Prof. Zhu Minhui, Institute of Electronics, Academia Sinica; Mr. Wu Guoxiang, National Remote Sensing Center, State Science and Technology Commission of China; Prof. Guo Huadong, Institute of Remote Sensing Applications, Academia Sinica; Prof. Wai Shongquan, Shanghai Institute of Satellite Engineering.

A GROUP DISCUSSION AT THE
3rd SPACEBORNE IMAGING RADAR SYMPOSIUM

INTERNATIONAL COLLABORATION IN SAR GROUND DATA SYSTEMS

LED BY

JOHN C. CURLANDER
VEXCEL CORPORATION

JET PROPULSION LABORATORY
PASADENA, CA
JANUARY 21, 1993

VEXCEL

SAR GROUND DATA SYSTEMS

INTERNATIONAL COLLABORATION

CONSIDERATIONS

- SUCCESS OF FUTURE SPACEBORNE SAR MISSIONS WILL REQUIRE MULTI-AGENCY AND/OR MULTI-NATIONAL COLLABORATION
  - JOINT DEVELOPMENT AND OPERATIONS FUNDING
  - SHARED TECHNOLOGY DEVELOPMENT

- GROUND PROCESSING IS TYPICALLY PERFORMED BY EACH AGENCY FOR THEIR USER BASE
  - LOCAL CONTROL OF DATA PROCESSING QUEUE AND PRODUCT QUALITY
  - COMMERCIAL UTILIZATION, REAL-TIME APPLICATIONS
  - APPLICATION SPECIFIC PROCESSING, GEOPHYSICAL PRODUCTS

- INTERNATIONAL STANDARDS ARE REQUIRED TO ACHIEVE A UNIFORM DATA PRODUCT INDEPENDENT OF THE PROCESSING CENTER
  - COMMON FORMATS: DATA STRUCTURES, COMMON READERS
  - COMMON PRESENTATION: PRODUCT DEFINITION
  - DATA PRODUCT QUALITY STANDARDS: CALIBRATION, ALGORITHMS

VEXCEL

SAR GROUND DATA SYSTEMS

INTERNATIONAL COLLABORATION

CONSIDERATIONS - 2

- TO REDUCE THE AGGREGATE COST OF THE GROUND DATA SYSTEMS, COLLABORATION IS REQUIRED IN DESIGN AND DEVELOPMENT

- EFFECTIVE UTILIZATION OF THE DATA BY AN INTERNATIONAL USER COMMUNITY
  - INTERNATIONAL HIGH RATE DATA NETWORKS FOR ELECTRONIC DATA ACCESS: INTERFACES, PROTOCOLS, DATA RATES
  - JOINT MISSION PLANNING SYSTEMS
  - DISTRIBUTED DATABASES

- COMMERCIALIZATION OF DATA PRODUCTS
  - COORDINATION OF POLICIES BY VARIOUS AGENCIES
  - RATE STRUCTURE FOR DATA PRODUCTS

- SECURITY OF DATA SYSTEMS
  - CONTROL OF UNAUTHORIZED DISTRIBUTION
  - CONTROL OF UNAUTHORIZED ACCESS

VEXCEL

SAR GROUND DATA SYSTEMS

INTERNATIONAL COLLABORATION

SOLUTIONS

- COMMITTEES
  - LESS ADMINISTRATIVE, MORE TECHNICAL
  - INVOLVEMENT OF PROJECT ENGINEERS TO ASSURE IMPLEMENTATION OF RESULTS
  - FUNDING FOR REQUIRED WORK, MEMBERS HELD ACCOUNTABLE TO MEET GOALS

- ONGOING COMMITTEE WORK
  - DATA FORMATS: CEOS SAR WG ON DATA IS INACTIVE, FORMAT MUST BE MAINTAINED
  - DATA POLICY: NEW US/CANADA RADARSAT GROUP, EXPAND ROLE
  - CALIBRATION/ VALIDATION: ACTIVE GROUP, CEOS, NO FUNDING

VEXCEL

SAR GROUND DATA SYSTEMS

INTERNATIONAL COLLABORATION

SOLUTIONS - 2

- JOINT DEVELOPMENT OF GROUND PROCESSORS
  - ERS-1 BETWEEN > 8 INDEPENDENT DEVELOPMENTS OF SAME OPERATIONAL PROCESSOR: MINIMAL COLLABORATION WITHIN ESA PAFs, NONE OUTSIDE OF ESA
  - US AND CANADA: BOTH EMBARKING ON UNDERFUNDED COLLATERAL EFFORTS TO DEVELOP SAME GROUND PROCESSING SYSTEM, NO INTERACTION
- SHARED TECHNOLOGY
  - WORKING COOPERATIVELY IS ONLY METHOD TO ENSURE UNIFORM QUALITY DATA PRODUCTS FROM NATIONAL PROCESSING CENTERS
  - SHARED DEVELOPMENT IS MAJOR COST SAVINGS
  - RESEARCH COLLABORATION WILL MORE QUICKLY ADVANCE STATE OF ART IN PROCESSING TECHNOLOGY AND ALGORITHMS: BETTER SCIENCE
  - RESIDENT ENGINEER EXCHANGE PROGRAM

VEXCEL

SAR GROUND DATA SYSTEMS

INTERNATIONAL COLLABORATION

SOLUTIONS - 3

- GEOPHYSICAL PROCESSING/PRODUCTS
  - INCORPORATION OF SCIENTIST'S ALGORITHMS INTO OPERATIONAL DATA SYSTEM: ALGORITHM VALIDATION, PRODUCT QUALITY ASSURANCE, MAINTENANCE
  - ASF GEOPHYSICAL PROCESSOR: EXPERIMENTAL SYSTEM TO GENERATE ICE MOTION, CONCENTRATION AND WAVE PRODUCTS
  - US JOINT ICE CENTER AND CANADIAN ICE CENTER HAVE BEGUN INITIAL EXCHANGE OF PRODUCTS

GLOBAL ENERGY AND WATER CYCLE EXPERIMENT (GEWEX) AND THE CONTINENTAL-SCALE INT'L PROJECT (GCIP)

DEBORAH VANE

Jet Propulsion Laboratory
California Institute of Technology
Pasadena, California

The Complex Role of Water in Climate Processes

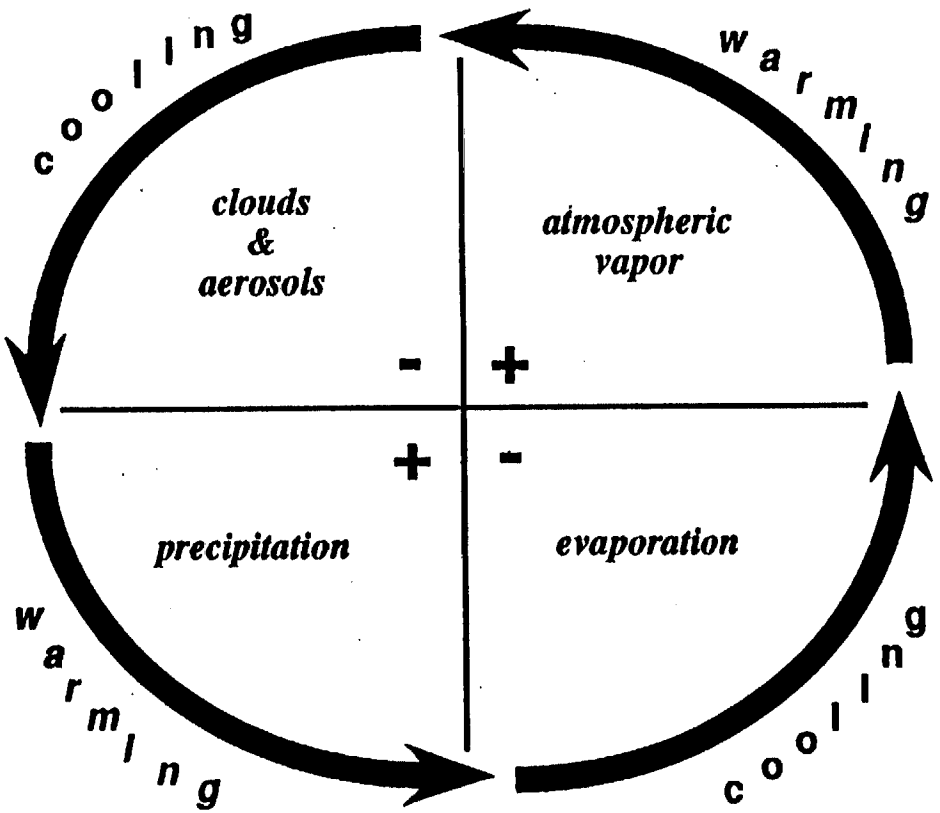

GEWEX OBJECTIVES

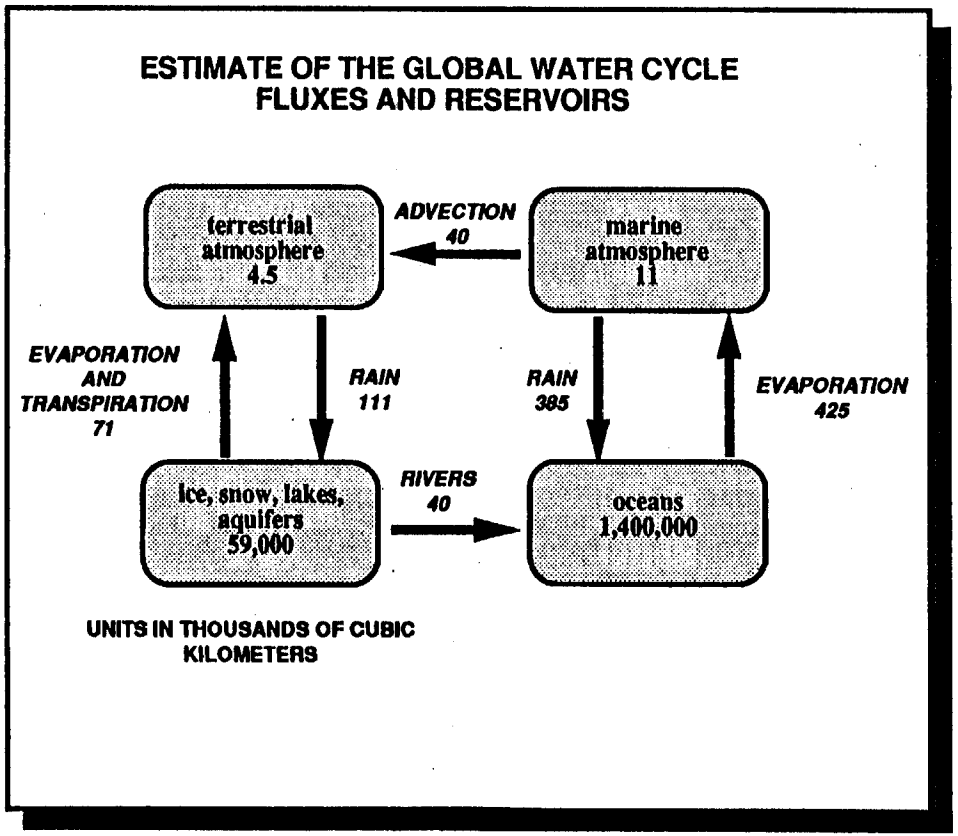

- DETERMINE THE HYDROLOGICAL CYCLE BY GLOBAL MEASUREMENTS
- MODEL THE GLOBAL HYDROLOGICAL CYCLE
- IMPROVE OBSERVATIONS AND DATA ASSIMILATION
- PREDICT RESPONSE TO ENVIRONMENTAL CHANGE

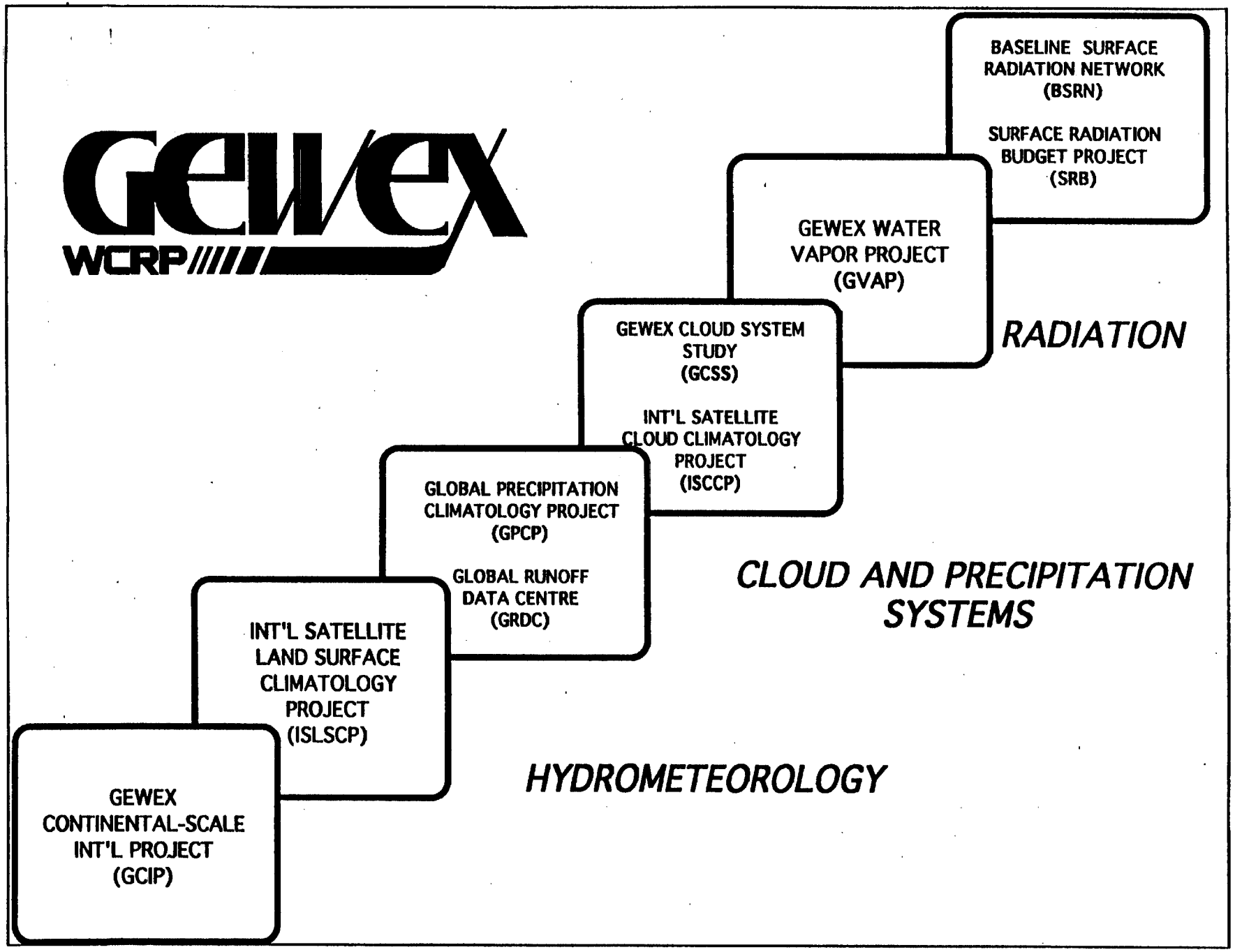
GEWEX
WCRP
BASELINE SURFACE RADIATION NETWORK (BSRN)
SURFACE RADIATION BUDGET PROJECT (SRB)
GEWEX WATER VAPOR PROJECT (GVAP)
GEWEX CLOUD SYSTEM STUDY (GCSS)
INT'L SATELLITE CLOUD CLIMATOLOGY PROJECT (ISCCP)
GLOBAL PRECIPITATION CLIMATOLOGY PROJECT (GPCP)
GLOBAL RUNOFF DATA CENTRE (GRDC)
INT'L SATELLITE LAND SURFACE CLIMATOLOGY PROJECT (ISLSCP)
GEWEX CONTINENTAL-SCALE INT'L PROJECT (GCIP)
RADIATION
CLOUD AND PRECIPITATION SYSTEMS
HYDROMETEOROLOGY

GCIP OBJECTIVES

GEWEX

- DETERMINE TIME/SPACE VARIABILITY OF HYDROLOGICAL CYCLE OVER A CONTINENTAL-SCALE REGION
- DEVELOP MACRO-SCALE HYDROLOGIC MODELS, COUPLED TO ATMOSPHERIC MODELS
- DEVELOP INFORMATION RETRIEVAL SCHEMES
- SUPPORT REGIONAL CLIMATE CHANGE IMPACT ASSESSMENT

GCIP STRATEGY: DEVELOPING COUPLED LAND-SURFACE/ATMOSPHERE MODELS

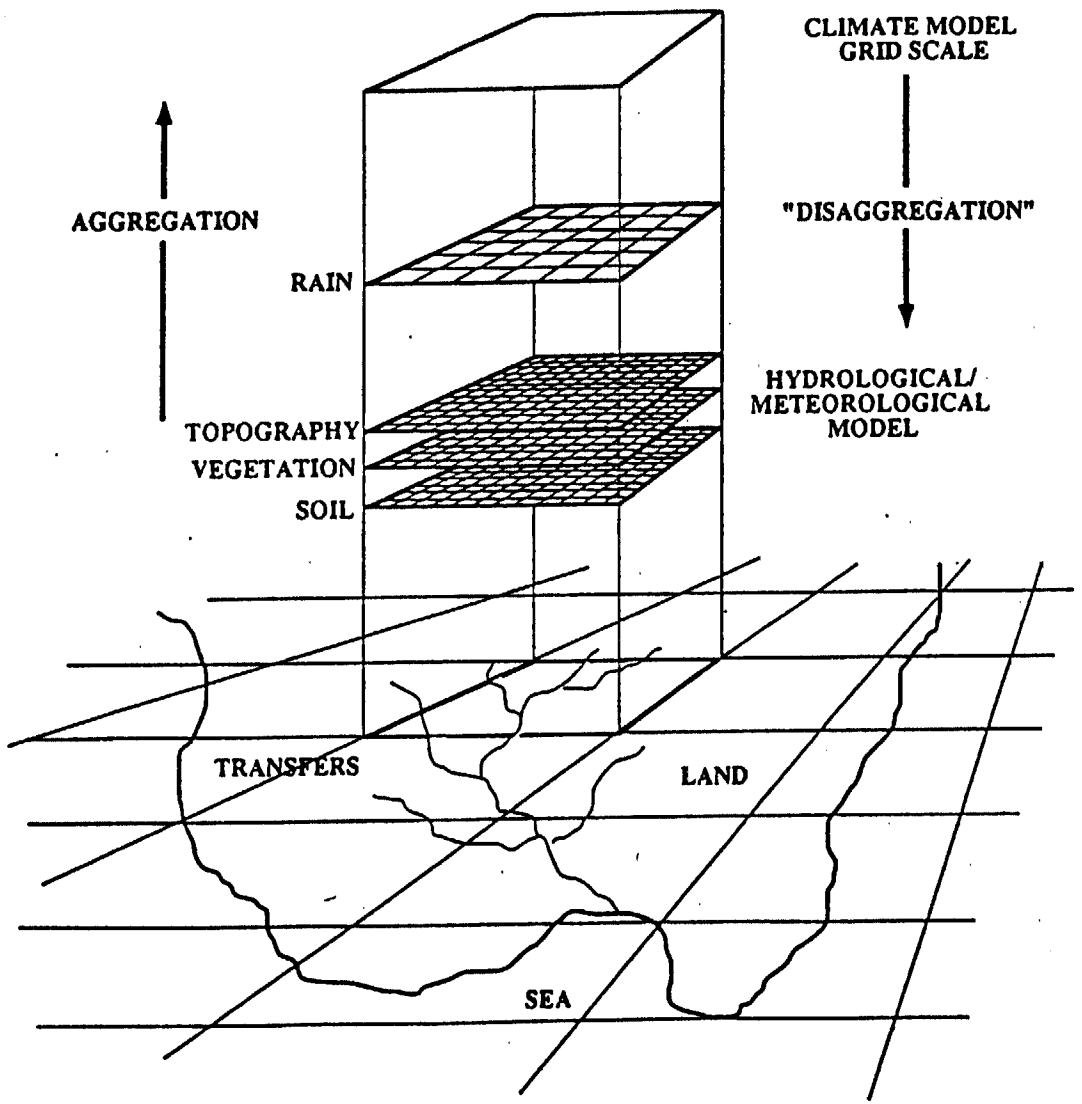

GCIP, GCSS, AMIP AND SCALE-INTERACTIVE MOIST PROCESSES

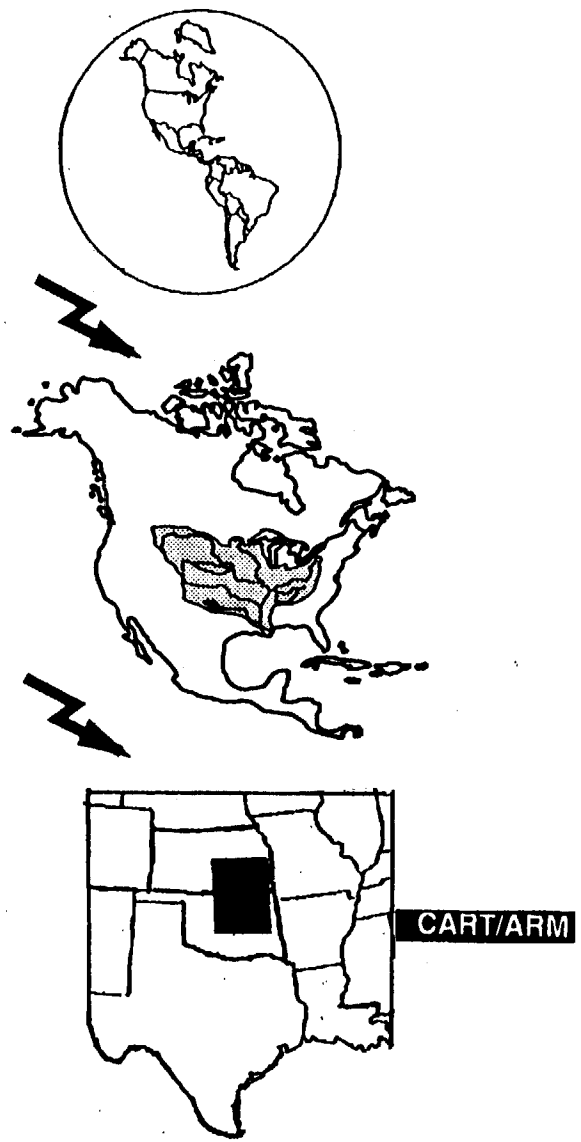

ATMOSPHERIC MODEL INTERCOMPARISON PROJECT (AMIP)

- CLIMATE/GCM INTERCOMPARISONS
- REGIONAL DISTRIBUTION AND NATURE OF CLIMATOLOGY ERRORS
- FOCUS ON "FAST" COMPONENT OF CLIMATE

GEWEX CONTINENTAL-SCALE INTERNATIONAL PROJECT (GCIP)

- COORDINATE WITH AMIP:
  REGIONAL SKILL OF GCMs vs MESO MODELS
- COORINATE WITH GCSS:
  TEST GCSS-DEVELOPED MOIST PARAMETERS ON REGIONAL SCALE

GEWEX CLOUD SYSTEM STUDY (GCSS)

- MULTI-SCALE INVESTIGATIONS OF CLOUD PROCESSES JOINS OBSERVATIONS AND MODELS
- DEVELOP NEW CLOUD, CONVECTION PARAMETERS
- USE TRAILFINDER/ARM SITES AS MAJOR DATA SOURCE

GCIP DATABASE

GEWEX

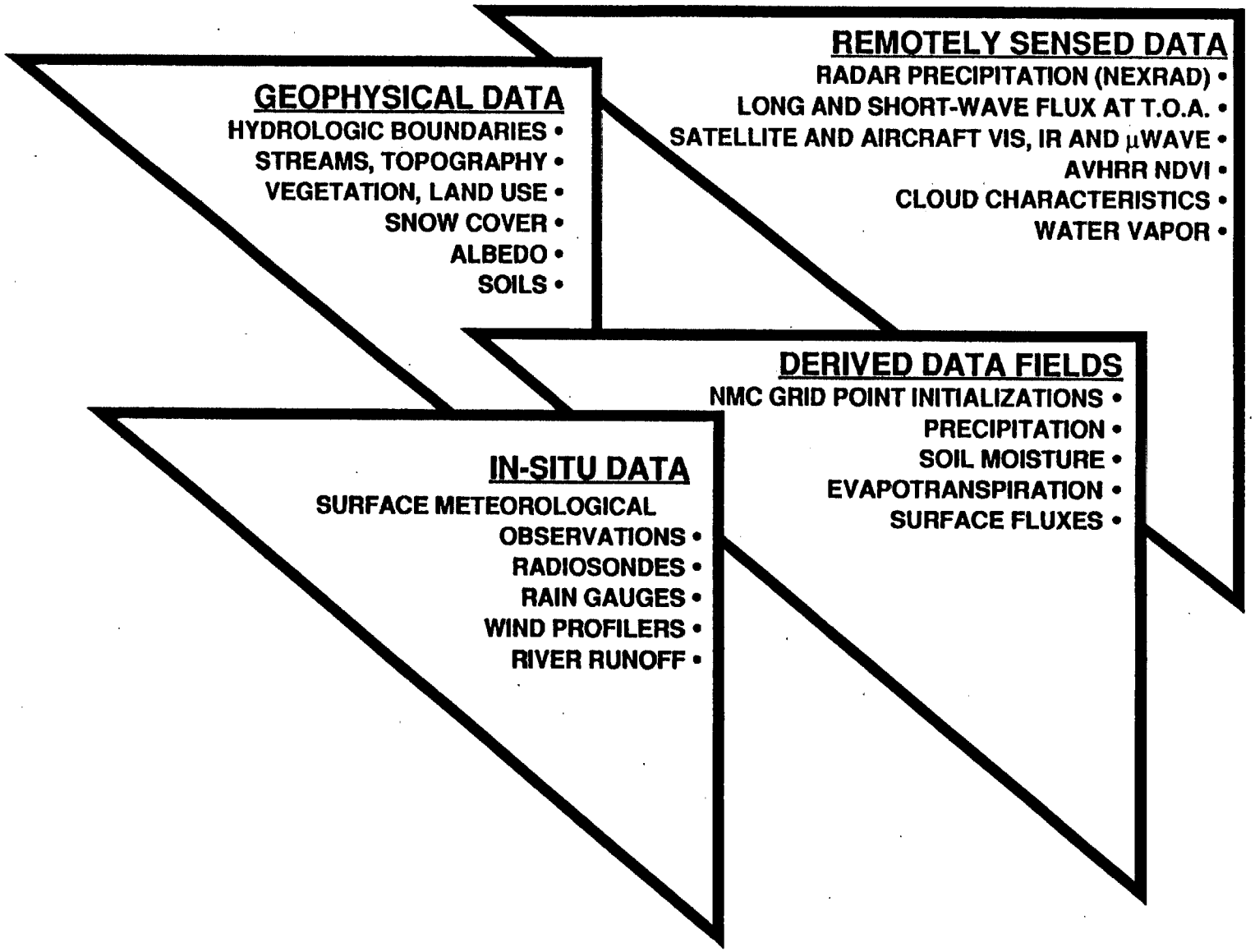

GCIP FIELD CAMPAIGNS

- FEW, FOCUSED

  -- TEST MODELS
  -- VALIDATE REMOTE SENSING DATA

- COOPERATIVE MULTISCALE EXPERIMENT SPRING/SUMMER '95 (CMESS)

  -- STUDY MESOSCALE CONVECTIVE SYSTEMS IN CENTRAL U.S.
  -- USWRP, DOE/ARM, FAA, GVAP, GCSS, GCIP

- 1996/97 (?)

  -- VALIDATE FLUX MODELS FORCED BY REMOTE SENSING AND IN-SITU DATA

AIRSAR South American Deployment

M. Kobrick

Jet Propulsion Laboratory
California Institute of Technology
Pasadena, California

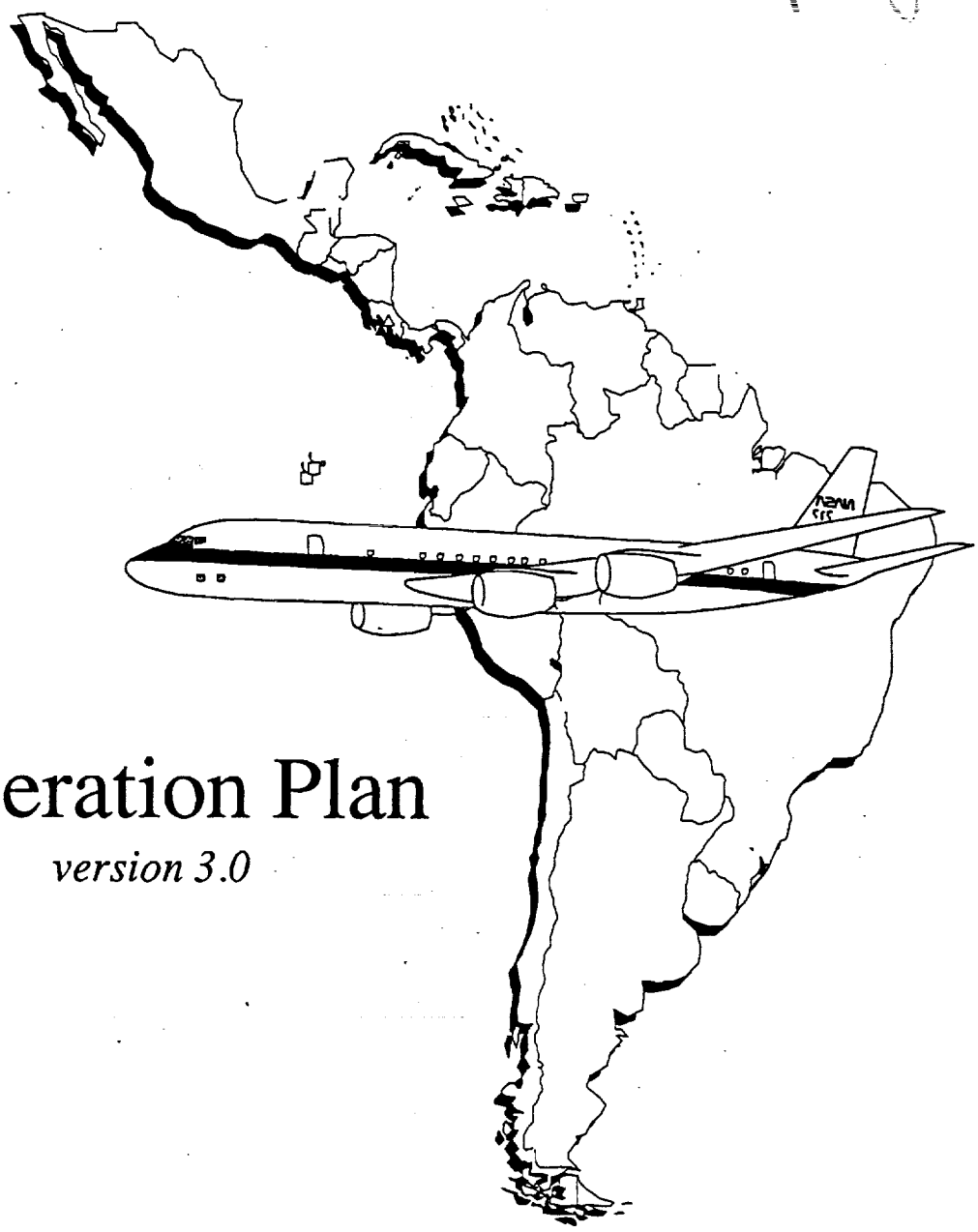

Operation Plan

version 3.0

AIRSAR South American Deployment

The United States National Aeronautics and Space Administration (NASA) and the Brazilian Commission for Space Activities (COBAE) are undertaking a joint experiment involving NASA's DC-8 research aircraft and the Airborne Synthetic Aperture Radar (AIRSAR) system during late May and June 1993. The research areas motivating these activities are: (1) fundamental research in the role of soils, vegetation, and hydrology in the global carbon cycle, and (2) in cooperation with South American scientists, airborne remote sensing research for the upcoming NASA Spaceborne Imaging Radar (SIR)-C/X-SAR flights on the Space Shuttle.

The following pages show a flight schedule and plans for the deployment that were developed at the Ames Research Center and the Jet Propulsion Laboratory (JPL) by using the flight requests received and approved by NASA Headquarters in response to a Dear Colleague letter dated May 29, 1992. The approved Principal Investigators (PIs), investigation titles, and approximate site locations are also listed.

The plan development included an attempt to accommodate all data requirements in the approved requests within the resources available, with the primary limitations being the length of the deployment (37 days) and the total number of DC-8 flight hours available within that time frame. The only major restriction imposed by those limits was the deletion of the sites south of about 24°S latitude. Most of the other approved data requests are accommodated by this plan, subject to some caveats listed below.

Included in the following pages are maps of the site locations and schematic indications of flight routes and dates, plots showing swath locations derived from the flight requests and generated by flight planning software and, most importantly, a calendar showing which sites will be imaged each day. Although the scheduling may not follow any obvious logical pattern, it is the result of incorporating a large number of disparate and sometimes conflicting requirements such as the desire to acquire multitemporal data at sites, coordination with satellite overflights, and so on. It should also be understood that the schedule is not set in concrete and will continue to evolve in response to changing PI experiment plans, changes imposed by the acquisition of international flight clearances, and any anomalies experienced during the deployment itself. Every attempt will be made to coordinate any and all such changes with the PIs involved, and the establishment and maintenance of good lines of communication both during the planning and operations phases will be of utmost importance.

The schedule has been developed based upon the following assumptions:

1. Both the DC-8 and the AIRSAR systems will function normally and any hardware problems will be minimal. A small amount of margin has been built into each day's flight plan, but since the deployment cannot be extended beyond the planned number of days, any major hardware anomalies will necessarily result in the loss of data. Although historically the reliability of both systems has been exceptionally high, and in fact the AIRSAR has not failed to acquire planned data due to hardware or system problems in its five years of operation, it must be remembered that the deployment is done on a best-effort basis and aircraft or radar problems could result in schedule changes or, in the worst case, the deletion of some sites.

2. Clearance will be obtained through the NASA International Affairs Office to overfly and acquire radar imaging data from each of the countries involved. At this writing, this has not yet been completed and historically it has been difficult to obtain flight clearance for some countries.

3. There will be no significant problems with Air Traffic Control (ATC) or with flying into military or other restricted flight zones. The DC-8 flies at the same altitudes as commercial air traffic and each day's flight plan must be cleared and approved by the proper ATC authorities. In the past, this has occasionally resulted in changes to flight plans or take-off times to minimize interference with other air traffic, particularly in foreign countries. Work so far indicates that no sites violate any military or restricted flight zones, but a final determination will have to wait for the development of more detailed flight plans by the DC-8 navigators.

4. Unless otherwise requested by the PI, all AIRSAR data will be acquired in the standard three-frequency quad-polarization mode. Where TOPSAR mode data have been requested, C-band polarimetric data will not be acquired but, instead, a CVV image will be produced along with a digital topographic map registered to the C-band image and L- and P-band polarimetric data sets. Note that although JPL has developed operational TOPSAR processor software, hardware for the systematic processing of TOPSAR data is not yet available. Thus processing of all TOPSAR mode data will be done by arrangement as special products outside the normal AIRSAR processing system.

In addition to AIRSAR, two other interesting and important experiments will also be installed on the DC-8 and will acquire data during this deployment: the lightning detection and lidar experiments, which will utilize upward-looking optical sensors and will prefer to have data acquired during dark conditions, i.e., during early evening or night and with no moon. Since AIRSAR flights generally have morning takeoffs so that during the daylight the video and film cameras may operate and the PIs collecting surface truth data at ground sites may work, some adjustments will be made.

The plan for the deployment will be to have afternoon takeoffs whenever weather forecasts indicate that a thunderstorm imaging opportunity will occur. This will allow the acquisition of: SAR data during daylight, and lightning and lidar data during the latter part of the flight in the early evening. These opportunities are most likely to occur during mid June 1993, and in the central and western portions of Brazil, Bolivia, and Peru. Unfortunately this means that exact take-off times cannot yet be determined for each flight, but every attempt will be made to coordinate take-off and overflight times with the PIs in the field during the deployment itself.

PI Affiliation	Title	Site	approx Lon, Lat	
John R. Baker British National Space Centre	AIRSAR Estimation of Tropical Forest Biomass for Carbon Cycle Studies	Manaus-Reserva Du. Sena Maduriera Rio Tapajos	-59.57 -68.67 -55.00	-2.57 -9.25 -3.50
Paolo Canuti Univ. of Florence	Contribution of SAR for Estimating Soil Erosion	Bermejo Basin Homahuaca	-63.00 -65.50	-23.50 -23.75
Luciano Dutra INPE	Rain Forest Type Discrimination, Flood Plain Mapping, Calibration Studies, and SAR Model Assessment Using AIRSAR Data: Tapajos Region	Rio Tapajos Cachoeira Porteira	-54.80 -57.05	-3.05 -0.65
Tony Freeman Jet Propulsion Lab	JERS-1 Calibration Underflight (Amazon)	Manaus Rio Tapajos	-60.10 -55.20	-3.20 -3.70
Ron Greeley Arizona State Univ.	The Relationship Between Radar Backscatter and Aerodynamic Roughness	Cerro Quisharo, Alti	-68.75	-18.75
Dirk H. Hoekman Wageningen Agricultural Univ.	Remote Sensing of Tropical Rain Forests	Araracuara, Columbia Mabura Hill, N, Guyana Mabura Hill, S, Guyana San Jose del Guaviare	-72.07 -57.90 -58.64 -72.61	0.65 6.70 5.08 2.47
Bryan Isacks Cornell University	SIR-C Analysis of Topography and Climate in the Central Andes	Cordillera Blanca, Peru Cordillera Real, Bolivia Quelccaya Ice Cap Potosi	-77.53 -68.29 -70.42 -65.63	-9.25 -16.19 -13.96 -19.69
Hermann Kux INPE	Forestry and Land Use in Western Amazonia, Acre State Brazil	Sena Maduriera	-68.45	-9.00
John Kwiatkowski Michigan Technological Univ.	Applications of Polarimetric Radar in Coherent Imaging of Earth and Remote Sensing of Precipitation	Ocean sites en route		
Thuy Le Toan Centre d'Etude Spatiale des Rayonnements	Study of Tropical Rain Forest by SAR Data in French Guiana	Kaw St Elie Paracou St Laurent	-52.10 -53.03 -53.97	4.72 5.28 5.48
John M. Melack Univ. of California, Santa Barbara	Determining the Extent of Inundation on Subtropical Floodplains Beneath Vegetation of Varying Types	Anavilhanas Cabaliana Pantanal	-60.78 -60.90 -57.42	-2.64 -3.40 -19.67
Peter J. Mouginis-Mark Univ. of Hawaii	Radar-Derived Topography of Volcanoes in the Western Galapagos Islands	Galapagos	-91.00	-1.00

PI Affiliation	Title	Site	approx Lon, Lat	
Waldir Paradella INPE	Geobotanical Investigation and Lithological Discrimination by AIRSAR Data in the NE of Brazil	Curaca Valley	-39.83	-9.21
Jack Paris Calstate Fresno	Global Biodiversity: Assessment of Habitat Change and Species Extinctions with Multinanometer SAR	Manaus area	-59.75	-2.50
Kevin O. Pope GeoEcoArc Research	SIR-C Tropical Wetlands Project	Merida Rio Bravo Rio Hondo	-90.25 -89.03 -88.55	20.75 17.52 18.27
Jeffrey E. Richey Univ. of Washington	Land Use, Forest Type and Biomass Assessment Using Polarimetric SAR	Manaus-Fazenda Di. Manaus-Reserva Du.	-59.97 -60.10	-2.43 -2.93
Davis D. Sentman University of Alaska Fairbanks	Optical Imaging of Cloud-to-Ionosphere Electrical Discharges in Brazil	Thundercloud sites		
David Sheres Stennis Space Center	SAR Measurements of Rain, Waves, Fronts and Eddies	Gulf of Mexico	-89.00	27.00
David Skole University of New Hampshire	Assessing Secondary Growth and Carbon Accumulation in Disturbed Tropical Forests Using Airborne Synthetic Aperture Radar	Nova Vida Paradise	-62.79 -63.31	-10.19 -9.58
Joao Vianei Soares INPE	Surface Hydrology of Semiarid Floodplains (Varzeas) in Northeast Brazil (SIR-C/X-SAR)	Bebedouro	-40.28	-9.08
Vincente Paulo Soares Federal Univ. of Vicosa	Relationship between Radar Image Backscatter and Eucalyptus Stand Characteristics	Minas Gerais	-42.63	-19.80
John W. Terborgh Duke University	Vegetation Mapping of a Headwater Catchment in the Amazon Basin: Manu National Park, Peru	Manu National Park	-12.05	-70.35
Jakob J. vanZyl Jet Propulsion Lab	Use of SAR Imagery in Monitoring the Hydrology of Semi-Arid Floodplain Areas in Brazil	Bebedouro	-40.28	-9.08
Howard A. Zebker Jet Propulsion Lab	Topsar Topographic Mapping Research and Support for the South American DC-8 Deployment	Manaus area Galapagos Islands	-59.75 -91.00	-2.50 -1.00

The Schedule

The following calendars for May and June 1993 show each flight day for the DC-8, indicated by an aircraft icon. The notation *Data Flight* indicates flights where the DC-8 takes off from and returns to the same base, and *Transit to...* indicates takeoff from one base and landing at another, generally with data being acquired en route.

May 25: The DC-8 will depart from its home base at Moffett Field, California and will acquire oceanographic data over the Gulf of Mexico before landing at Houston International Airport.

May 27: After one day in Houston the aircraft will transit to San Jose, Costa Rica with data acquired en route over the Gulf of Mexico and ecology sites near Merida, Mexico and Rio Hondo and Rio Bravo, Belize.

May 29: After one day in San Jose the next flight will be a transit to Guayaquil, Ecuador via the Galapagos Islands. The objective will be to map all of Isla Fernandina and Isla Isabela in TOPSAR mode, as indicated on the attached map, but as currently planned this flight is near the duration limit for a one day DC-8 flight and a slightly smaller data set may be acquired.

May 31: During this flight from Guayaquil the sites at Aracuara and San Jose del Guaviare in Colombia will be imaged, as well as the set of lines called the"volcano transect." Not yet planned in detail, these lines will image a number of Andean volcanoes along a track intended to cover as many individual sites as possible.

June 2: During the transit to Santa Cruz, Bolivia TOPSAR mode data will be acquired at Cordillera Blanca and the Quelccaya Ice Cap in the Peruvian Andes, and the site at Manu National Park will also be imaged.

June 4: Data sites for this flight from Santa Cruz include Cordillera Real and Potosi, which will be imaged in TOPSAR mode, and Cerro Quisharo near the Chilean border.

June 6: Flying south into Argentina, AIRSAR will collect data at the hydrology sites at Bermejo Basin and Homahuaca, then the rest of the flight will be dedicated to Dave Sentman's lightning imaging experiment. Since the lightning experiment is weather dependent, the scheduling for this flight may be modified in real time to match the opportunities that arise.

June 8: This transit flight to Recife, Brazil will cover the Pantanal site in Brazil and the SIR-C/X-SAR "super site" at Bebedouro.

June 11: This flight will be second of four to overfly Bebedouro, the intent being to acquire data under different ground conditions, primarily soil moisture. For that reason the date of this and the following flight may be adjusted slightly according to weather conditions. Also covered on this day will be the site at Minas Gerais.

June 12: During this flight data will be acquired at the Curaca Valley site as well as Bebedouro.

June 15: This transit flight into Manaus provides one last opportunity to image Bebedouro, and in transit the site at Rio Tapajos will be covered in both SAR and TOPSAR modes.

June 17: This will be the first of two flights over the Manaus area, with the plan being to acquire data along tracks matching the ground swaths of both the JERS-1 and Shuttle Imaging Radar experiments. The dates of this and the following flight may be adjusted to accommodate the lightning imaging experiment.

June 19: This flight will be divided between the acquisition of data along certain specific tracks in the Manaus area for Howard Zebker's forest investigation, and at targets of opportunity for the lightning imaging experiment. Due to the weather-dependent nature of the lightning experiment, the flight may occur on a different day or be swapped with the preceding flight.

June 21: During this flight data will be acquired at the SIR-C/X-SAR site at Sena Madureira as well as at Paradise and Nova Vida. Finally, data lines will be flown at the Rio Tapajos site to match an overflight of the JERS-1 satellite which will be imaging the region on that day.

June 24: The transit to San Juan, Puerto Rico will provide coverage at the Cachoreira Porteira site northeast of Manaus, Kaw, Paracou and St. Laurent along the coast of French Guiana, and Mabura Hill in Guyana.

June 26: This last flight of the deployment will be a transit back to Moffett and no AIRSAR data will be acquired.

May 1993

Sunday	Monday	Tuesday	Wednesday	Thursday	Friday	Saturday
						1
2	3	4	5	6  Engineering flight	7	8
9	10  Engineering flight	11	12	13	14	15
16	17	18  Calibration flight Rosamond Fort Irwin Crystal Spring	19  Data flight Jornada Sevilleta	20	21	22
23	24	25  Transit to Houston Gulf of Mexico	26	27  Transit to San Jose Gulf of Mexico Merida Rio Hondo Rio Bravo	28	29  Transit to Guayaquil Galapagos
30	31  Data Flight Colombian volcanics San Jose del Guaviare Araracuara					

June 1993

Sunday	Monday	Tuesday	Wednesday	Thursday	Friday	Saturday
		1	2 <u>Transit to Santa Cruz</u> Cordillera Blanca Manu National Park Quelccaya Ice Cap	3	4 <u>Data Flight</u> Cordillera Real Cerro Quisharo Potosi	5
6 <u>Data Flight</u> Bermejo Basin Homahuaca thunderstorm oppty	7	8 <u>Transit to Recife</u> Pantanal Bebedouro	9	10	11 <u>Data Flight</u> Minas Gerais Bebedouro	12 <u>Data Flight</u> Curaca Valley Bebedouro
13	14	15 <u>Transit to Manaus</u> Bebedouro Rio Tapajos	16	17 <u>Data Flight</u> Manaus sites	18	19 <u>Data flight</u> Manaus sites thunderstorm oppty
20	21 <u>Data flight</u> Sena Madureira Paradise Nova Vida Rio Tapajos (JERS)	22	23	24 <u>Transit to San Juan</u> Cachoeira Porteira Kaw Paracou St. Laurent Mabura Hill	25	26 <u>Transit to Moffett</u>
27	28	29	30			

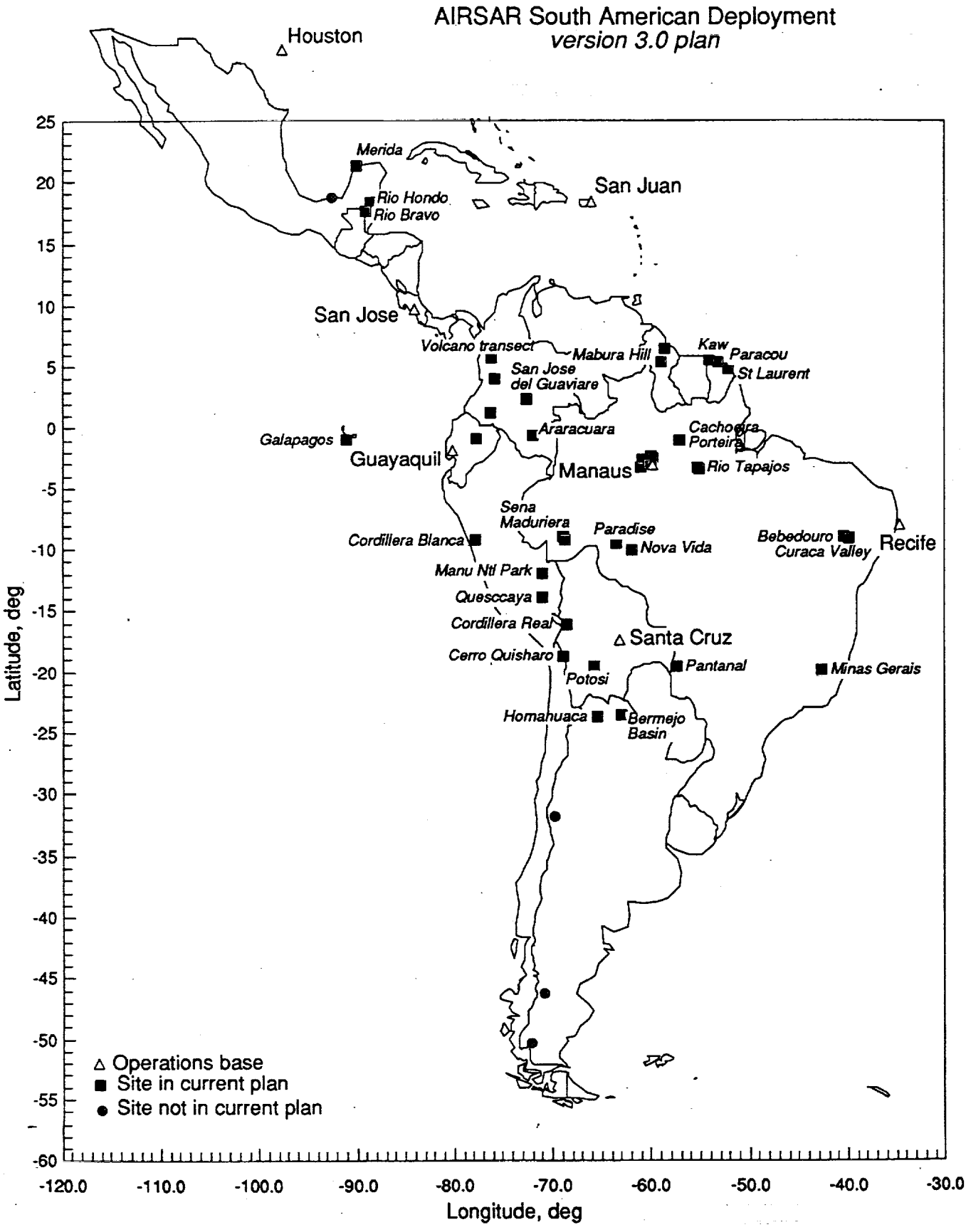
AIRSAR South American Deployment
version 3.0 plan
Houston
Merida
Rio Hondo
Rio Bravo
San Juan
San Jose
Volcano transect
Mabura Hill
Kaw
Paracou
St Laurent
San Jose del Guaviare
Galapagos
Guayaquil
Araracuara
Cachoeira Porteira
Manaus
Rio Tapajos
Sena Maduriera
Paradise
Nova Vida
Cordillera Blanca
Bebedouro
Curaca Valley
Recife
Manu Ntl Park
Quesccaya
Cordillera Real
Santa Cruz
Cerro Quisharo
Potosi
Pantanal
Minas Gerais
Homahuaca
Bermejo Basin
Operations base
Site in current plan
Site not in current plan
Latitude, deg
Longitude, deg
25
20
15
10
5
0
-5
-10
-15
-20
-25
-30
-35
-40
-45
-50
-55
-60
-120.0
-110.0
-100.0
-90.0
-80.0
-70.0
-60.0
-50.0
-40.0
-30.0

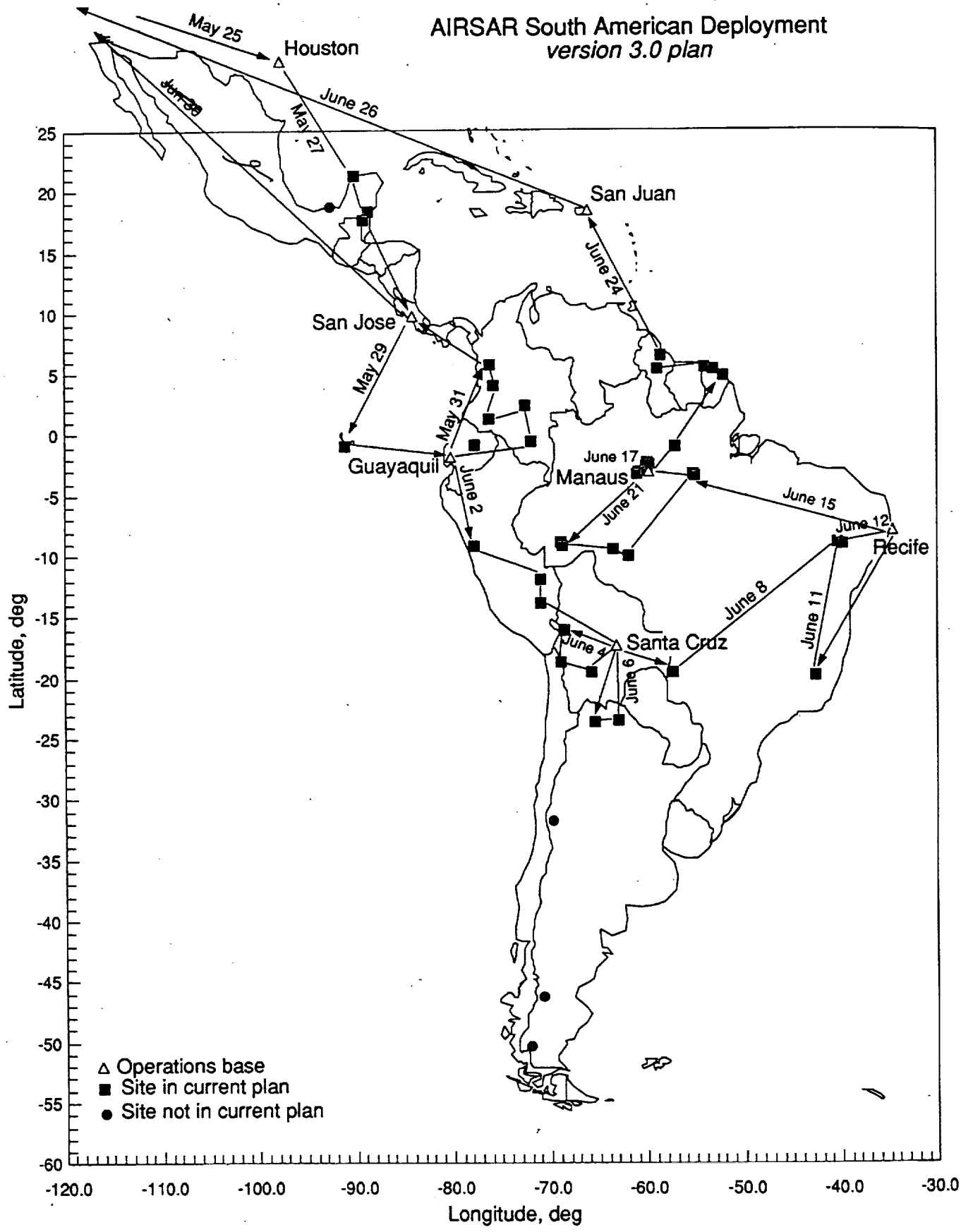
AIRSAR South American Deployment
version 3.0 plan
Houston
May 25
May 27
June 26
San Juan
June 24
San Jose
May 29
May 31
Guayaquil
June 2
June 17
Manaus
June 21
June 15
June 12
Recife
June 8
June 11
June 4
June 6
Santa Cruz
Operations base
Site in current plan
Site not in current plan
Latitude, deg
Longitude, deg
25
20
15
10
5
0
-5
-10
-15
-20
-25
-30
-35
-40
-45
-50
-55
-60
-120.0
-110.0
-100.0
-90.0
-80.0
-70.0
-60.0
-50.0
-40.0
-30.0

South America '93

version 3.0

Date	450 kt Latitude d	m	0.02 Longitude d	m		Transit to	Data	Total
25-May	37	24.9	-122	2.8	Moffett			
	27	55.0	-93	35.0	Gulf of Mexico	3.4	2.0	
	29	27.0	-95	12.6	Houston	0.3		
					Block time	0.8		6.45
27-May	29	27.0	-95	12.6	Houston			
	27	55.0	-93	35.0	Gulf of Mexico	0.3	1.0	
	20	45.0	-90	15.0	Merida	1.0	0.8	
	18	16.2	-88	33.0	Rio Hondo	0.4	0.5	
	17	31.2	-89	1.8	Rio Bravo	0.1	0.5	
	9	33.6	-84	3.0	San Jose	1.2		
					Block time	0.8		6.57
29-May	9	33.6	-84	3.0	San Jose			
	-1	0.0	-91	0.0	Galapagos	1.7	4.0	
	-2	6.0	-79	30.0	Guayaquil	1.5		
					Block time	0.8		7.97
31-May	-2	6.0	-79	30.0	Guayaquil			
	0	58.8	-77	54.9	Mayasquer volcano	0.5	0.3	
	1	1.8	-77	48.3	Cumbal volcano	0.0	0.3	
	1	9.0	-77	30.9	Azurfal volcano	0.0	0.3	
	1	22.2	-77	6.9	Galeras volcano	0.1	0.3	
	1	56.7	-76	39.3	Dona Juana vol.	0.1	0.3	
	2	41.1	-76	10.8	Huila volcano	0.1	0.3	
	3	49.5	-75	40.5	Tolima volcano	0.2	0.3	
	4	45.9	-75	22.2	Ruiz volcano	0.1	0.3	
	5	6.9	-75	34.6	Herveo volcano	0.1	0.3	
	2	28.2	-72	36.6	San Jose del Gu.	0.5	0.5	
	0	39.0	-72	4.2	Araracuara	0.3	0.5	
	-2	6.0	-79	30.0	Guyaquil	1.1		
					Block time	0.8		6.99
2-Jun	-2	6.0	-79	30.0	Guayaquil			
	-9	15.0	-77	32.0	Cordillera Blanca	1.0	1.3	
	-12	2.0	-71	12.0	Manu Ntl Park	0.9	1.2	
	-13	57.5	-70	47.5	Quelccaya Ice Cap	0.3	1.2	
	-17	28.8	-63	6.0	Santa Cruz	1.1		
					Block time	0.8		7.59
4-Jun	-17	28.8	-63	6.0	Santa Cruz			
	-16	11.5	-68	16.5	Cordillera Real	0.7	1.5	
	-18	45.0	-68	45.0	Cerro Quisharo	0.3	1.0	
	-19	41.5	-65	38.0	Potosi	0.4	0.5	
	-17	28.8	-63	6.0	Santa Cruz	0.4		
					Block time	0.8		5.63
6-Jun	-17	28.8	-63	6.0	Santa Cruz			
	-23	30.0	-63	0.0	Bermejo Basin	0.8	0.5	
	-23	45.0	-65	30.0	Hornahuaca	0.3	0.5	
	-17	28.8	-63	6.0	Thunderstorms/Li.	0.9	4.0	
	-17	28.8	-63	6.0	Santa Cruz	0.0		
					Block time	0.8		7.75
8-Jun	-17	28.8	-63	6.0	Santa Cruz			
	-19	40.2	-57	15.0	Pantanal	0.8	0.0	
	-19	40.2	-57	15.0	Pantanal	0.0	2.0	
	-9	4.8	-40	16.8	Bebedouro	2.6	1.0	
	-8	1.8	-34	32.0	Recife	0.8		
					Block time	0.8		7.92

11-Jun	-8	1.8	-34	32.0	Recife			
	-9	4.8	-40	16.8	Bebedouro	0.8	1.0	
	-19	48.0	-42	37.8	Minas Gerais	1.5	1.3	
	-8	1.8	-34	32.0	Recife	1.9		
					Block time	0.8		7.12
12-Jun	-8	1.8	-34	32.0	Recife			
	-9	4.8	-40	16.8	Bebedouro	0.8	1.0	
	-9	4.8	-40	16.8	Curaca Valley	0.0	1.0	
	-8	1.8	-34	32.0	Recife	0.8		
					Block time	0.8		4.29
15-Jun	-8	1.8	-34	32.0	Recife			
	-9	4.8	-40	16.8	Bebedouro	0.8	1.0	
	-3	48.0	-60	0.6	Tapajos	2.7	4.0	
	-3	48.0	-60	0.6	Manaus	0.0		
					Block time	0.8		7.46
17-Jun	-3	48.0	-60	0.6	Manaus			
	-3	48.0	-60	0.6	dummy	0.0		
	-2	56.0	-60	6.0	Manaus sites	0.1	6.5	
	-3	48.0	-60	0.6	Manaus	0.1		
					Block time	0.8		7.48
19-Jun	-3	48.0	-60	0.6	Manaus			
	-2	56.0	-60	6.0	Manaus sites	0.1	4.0	
	-2	56.0	-60	6.0	Thunderstorms	0.0	3.0	
	-3	48.0	-60	0.6	Manaus	0.1		
					Block time	0.8		7.98
21-Jun	-3	48.0	-60	0.6	Manaus			
	-9	0.0	-68	45.0	Sena Maduriera	1.3	1.5	
	-9	34.8	-63	26.4	Paradise	0.7	0.8	
	-10	11.4	-62	47.4	Nova Vida	0.1	0.8	
	-3	48.0	-60	0.6	Manaus	0.9		
					Block time	0.8		6.85
24-Jun	-3	48.0	-60	0.6	Manaus			
	0	-57.0	-57	3.0	Cachoeira Porteira	0.5	0.5	
	4	43.0	-52	7.0	Kaw	1.0	0.5	
	5	17.0	-53	2.0	Paracou	0.1	0.5	
	5	29.0	-53	58.0	St Laurent	0.1	0.5	
	5	50.0	-58	38.5	Mabura Hill S	0.6	0.5	
	6	41.8	-57	53.9	Mabura Hill N	0.2	0.5	
	18	16.8	-66	4.2	San Juan	1.9		
					Block time	0.8		5.67
26-Jun	18	16.8	-66	4.2	San Juan			
	37	24.9	-122	2.8	Moffett	7.0		
					Block time	0.8		7.71

Totals 111.42

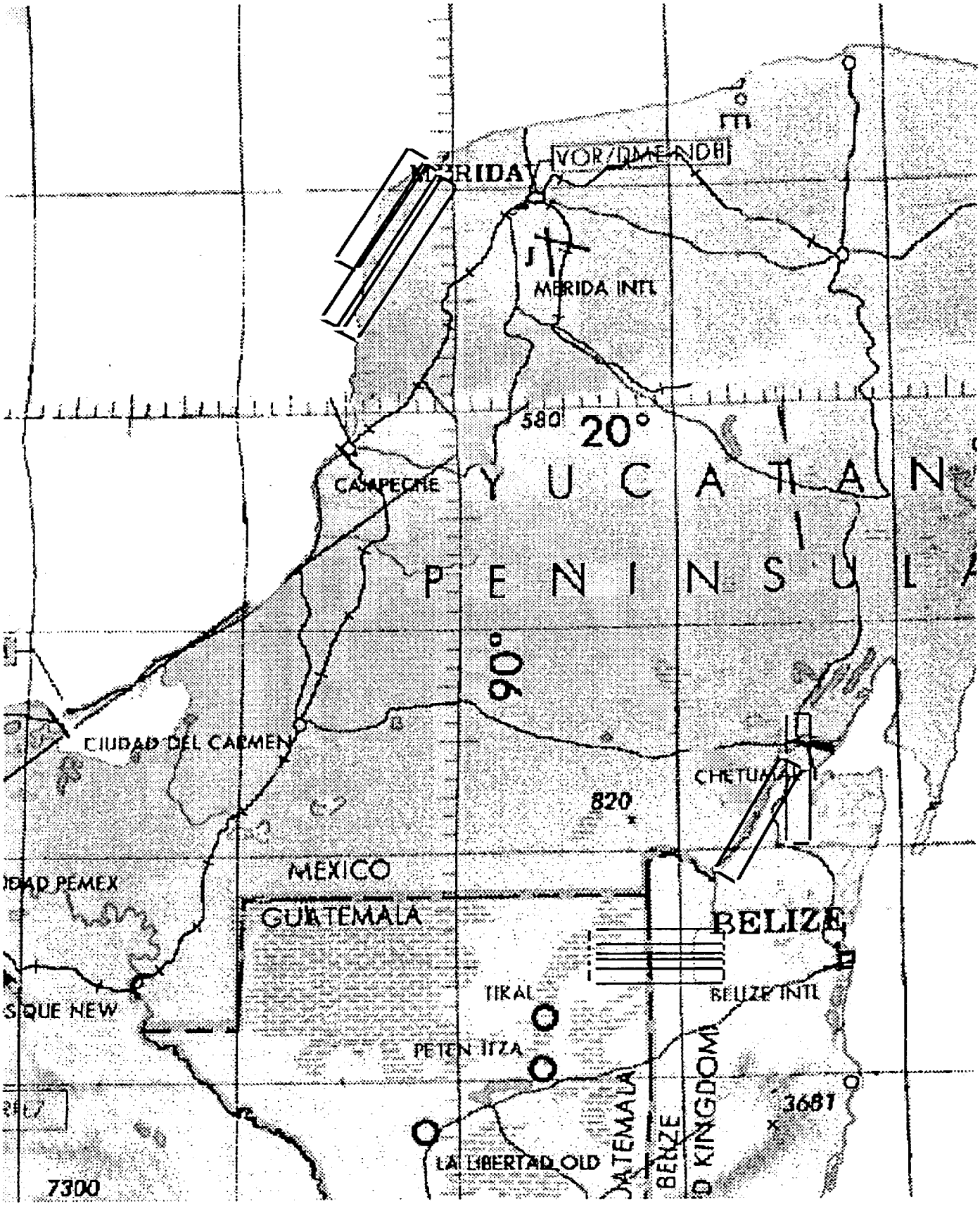
MERIDA
VOR/DME-N/DH
MERIDA INTL
580
20°
CAMPECHE
YUCATAN
PENINSULA
90°
CIUDAD DEL CARMEN
CHETUMAL
820
MEXICO
GUATEMALA
BELIZE
TIKAL
BELIZE INTL
PETEN ITZA
LA LIBERTAD OLD
3681
7300

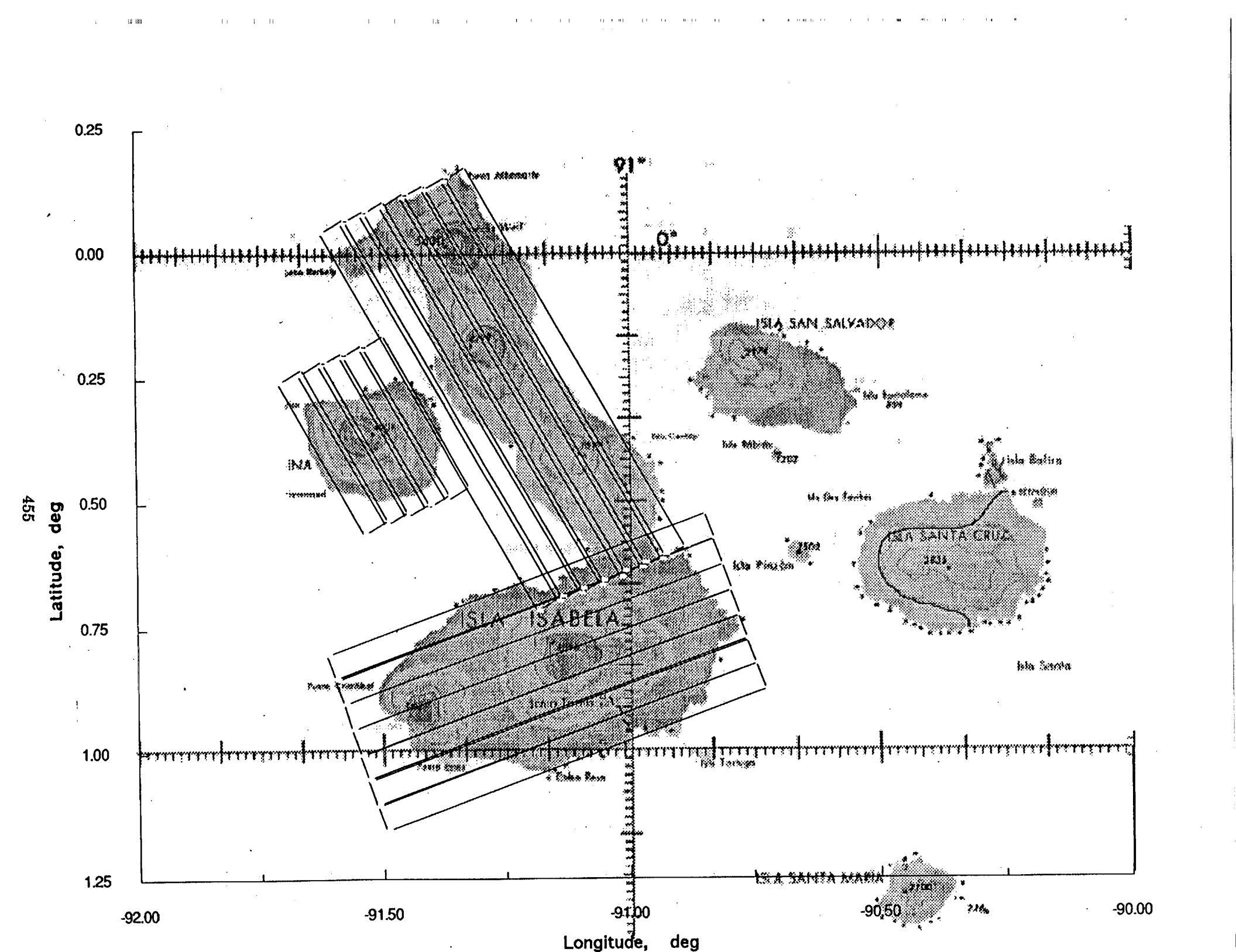
0.25
0.00
0.25
0.50
0.75
1.00
1.25
Latitude, deg
91°
0°
ISLA SAN SALVADOR
ISLA SANTA CRUZ
ISLA ISABELA
ISLA SANTA MARIA
-92.00
-91.50
-91.00
-90.50
-90.00
Longitude, deg

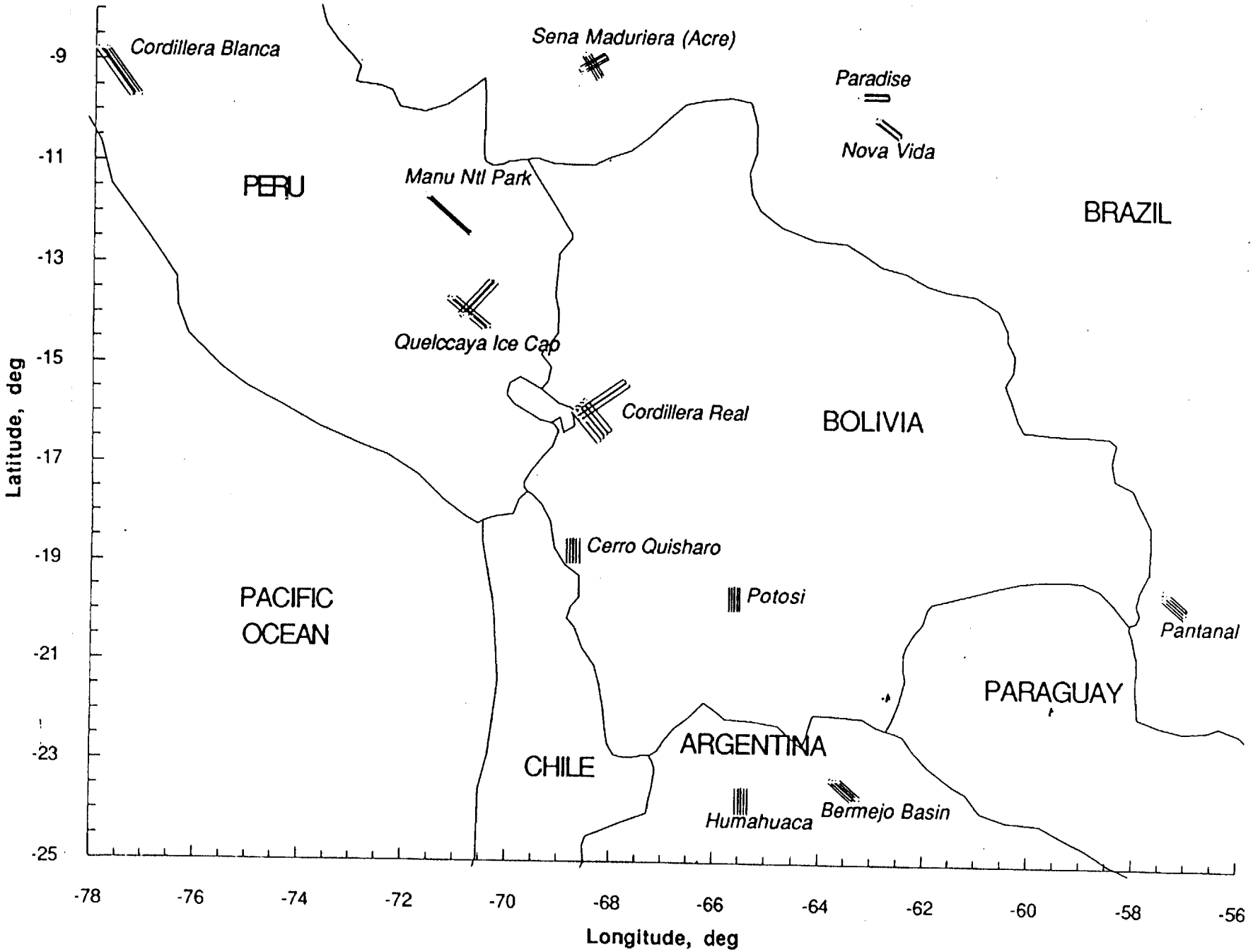
Cordillera Blanca
Sena Maduriera (Acre)
Paradise
Nova Vida
PERU
Manu Ntl Park
BRAZIL
Quelccaya Ice Cap
Cordillera Real
BOLIVIA
Cerro Quisharo
Potosi
PACIFIC
OCEAN
Pantanal
PARAGUAY
ARGENTINA
CHILE
Humahuaca
Bermejo Basin
-9
-11
-13
-15
-17
-19
-21
-23
-25
Latitude, deg
-78
-76
-74
-72
-70
-68
-66
-64
-62
-60
-58
-56
Longitude, deg

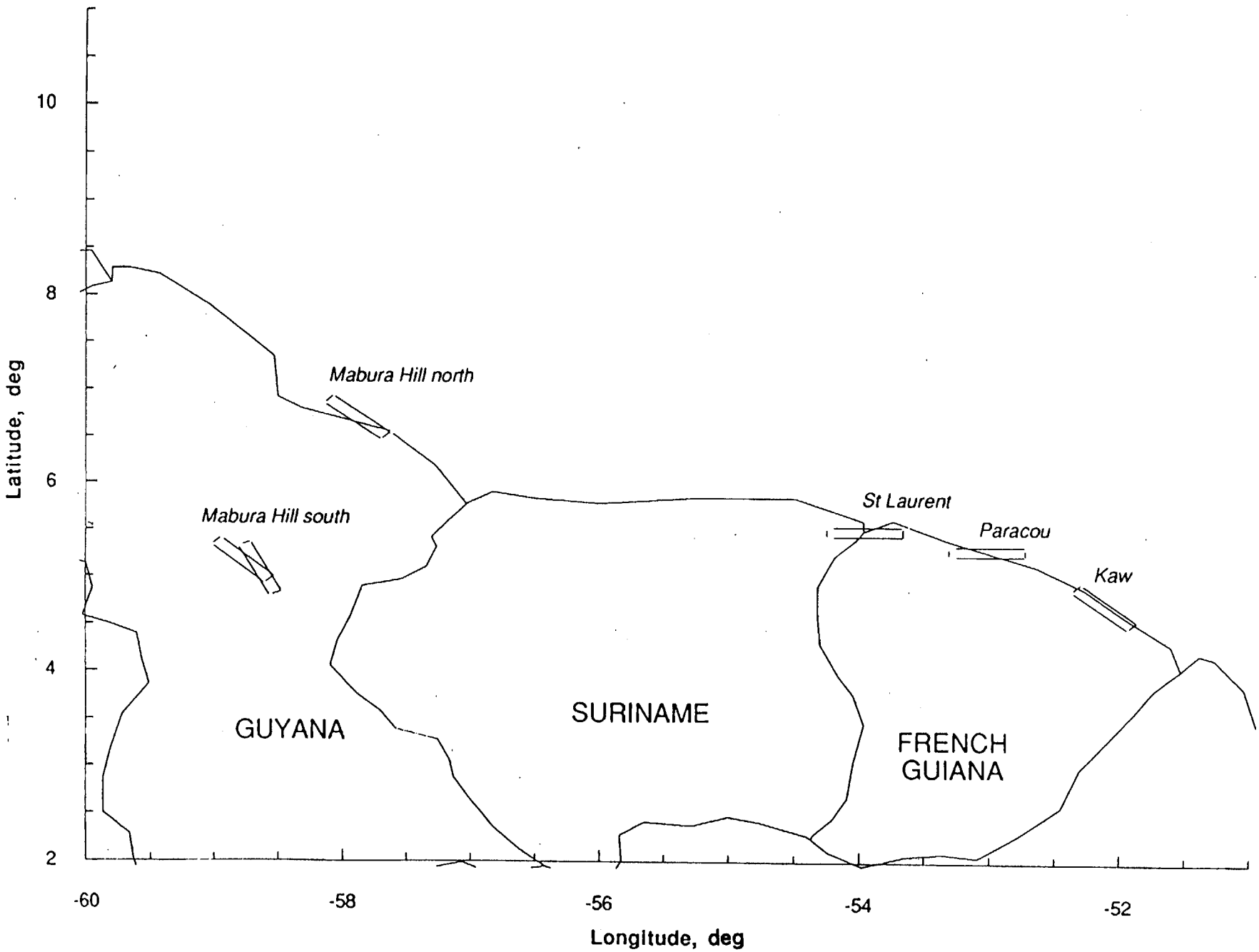
Mabura Hill north
Mabura Hill south
St Laurent
Paracou
Kaw
GUYANA
SURINAME
FRENCH
GUIANA
10
8
6
4
2
Latitude, deg
-60
-58
-56
-54
-52
Longitude, deg

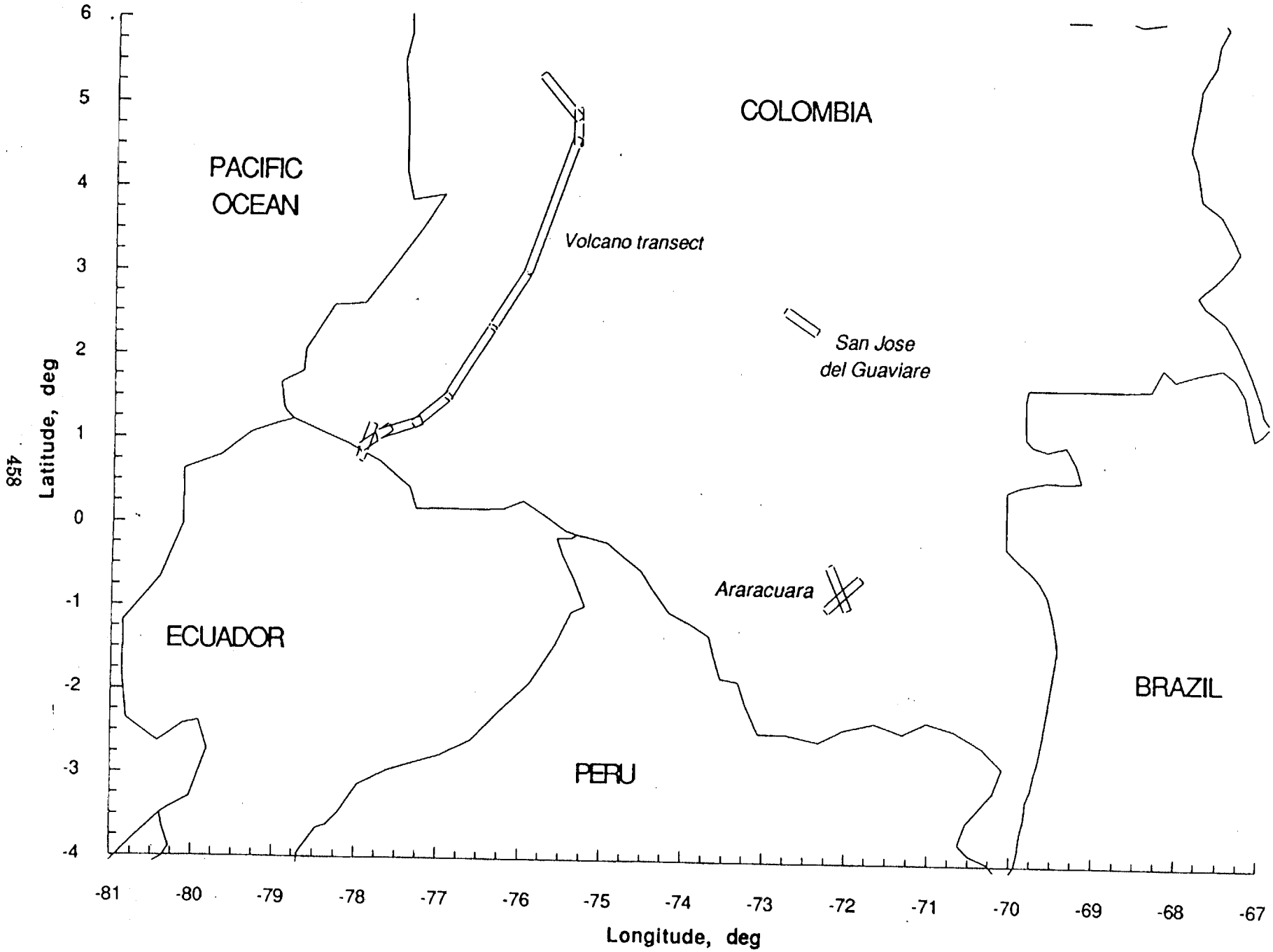
COLOMBIA
PACIFIC
OCEAN
Volcano transect
San Jose
del Guaviare
Araracuara
ECUADOR
PERU
BRAZIL
Latitude, deg
Longitude, deg
6
5
4
3
2
1
0
-1
-2
-3
-4
-81
-80
-79
-78
-77
-76
-75
-74
-73
-72
-71
-70
-69
-68
-67

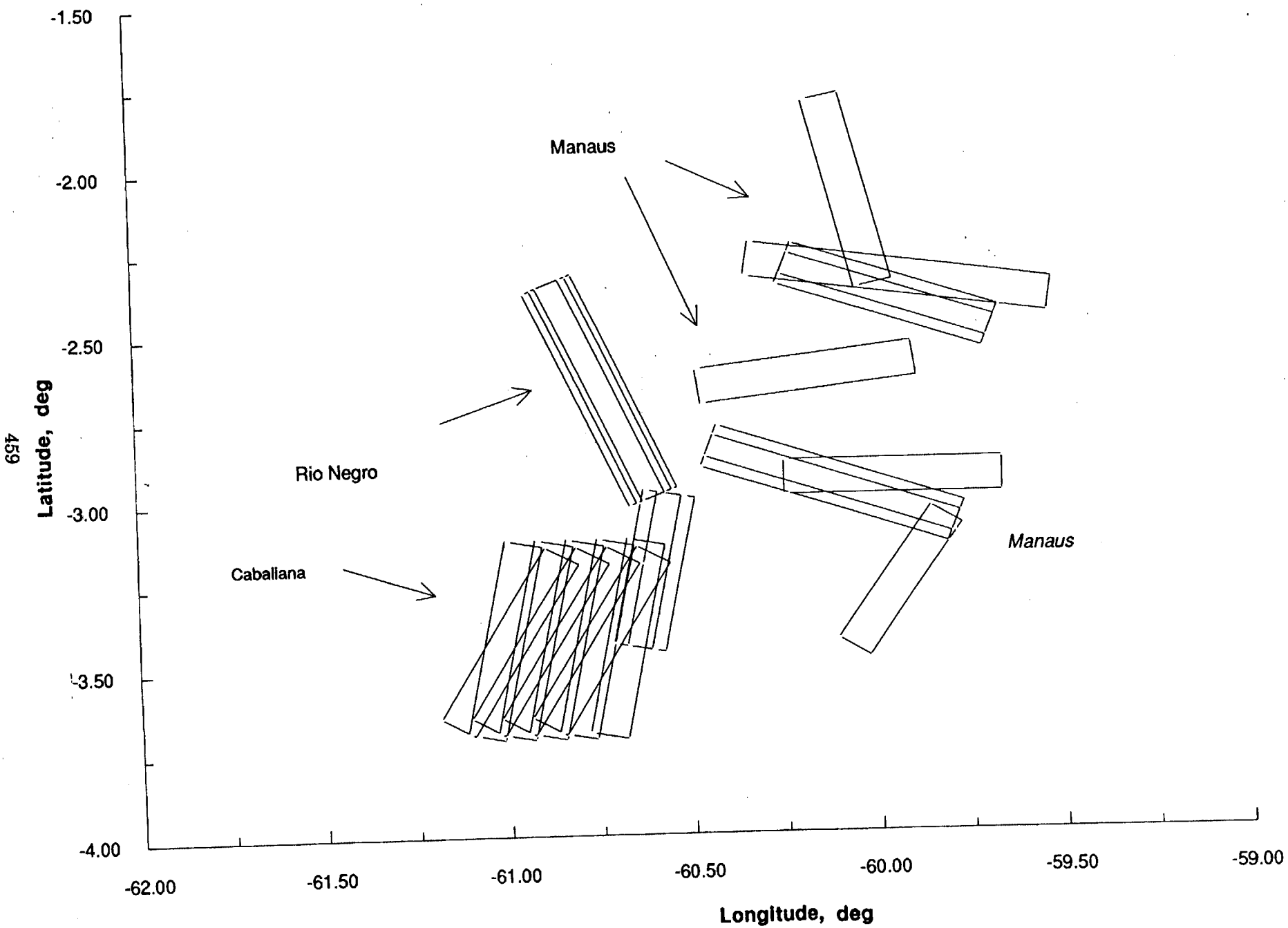
-1.50
-2.00
-2.50
-3.00
-3.50
-4.00
Latitude, deg
-62.00
-61.50
-61.00
-60.50
-60.00
-59.50
-59.00
Longitude, deg
Manaus
Rio Negro
Caballana
Manaus

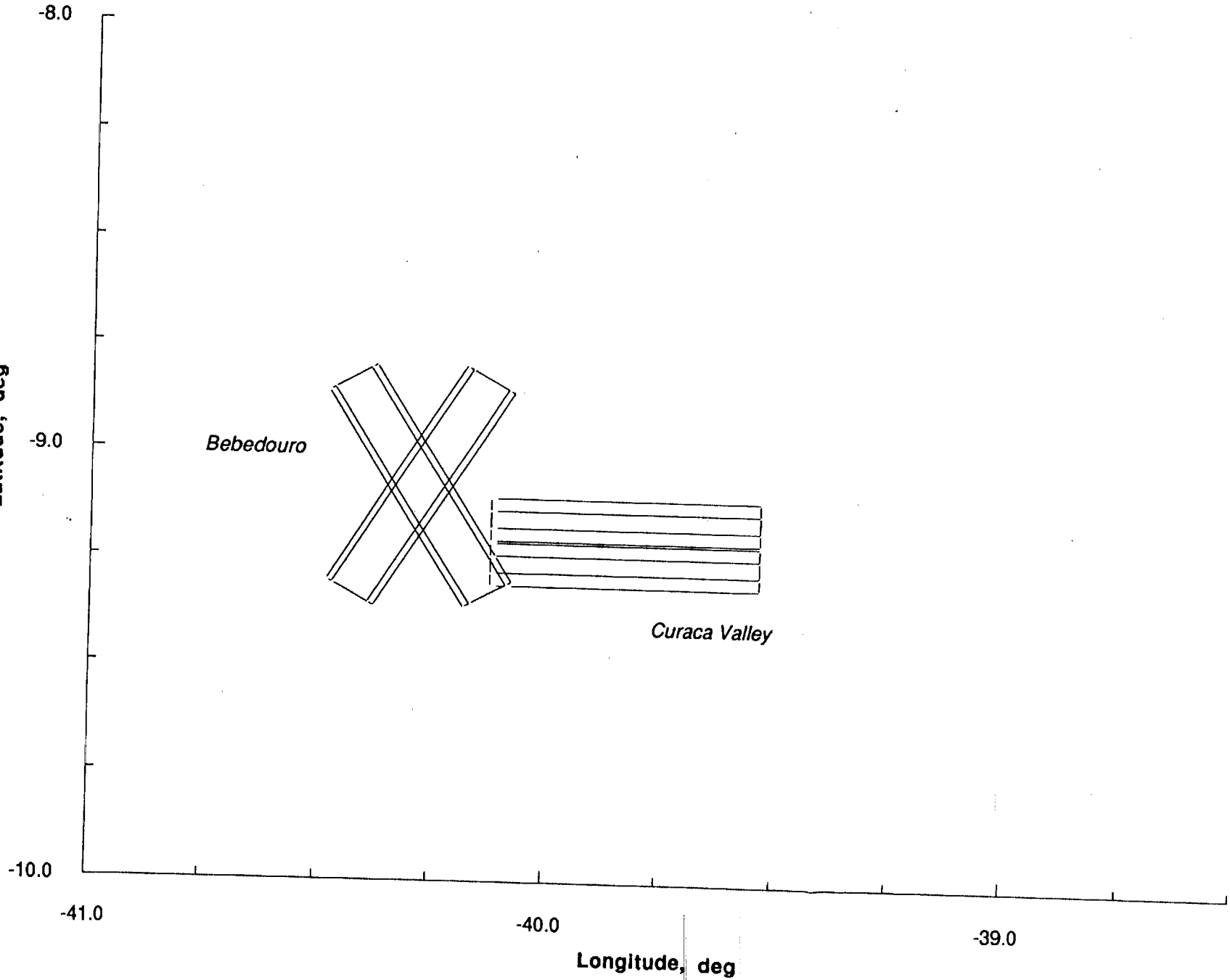
-8.0
-9.0
-10.0
Latitude, deg
Bebedouro
Curaca Valley
-41.0
-40.0
-39.0
Longitude, deg

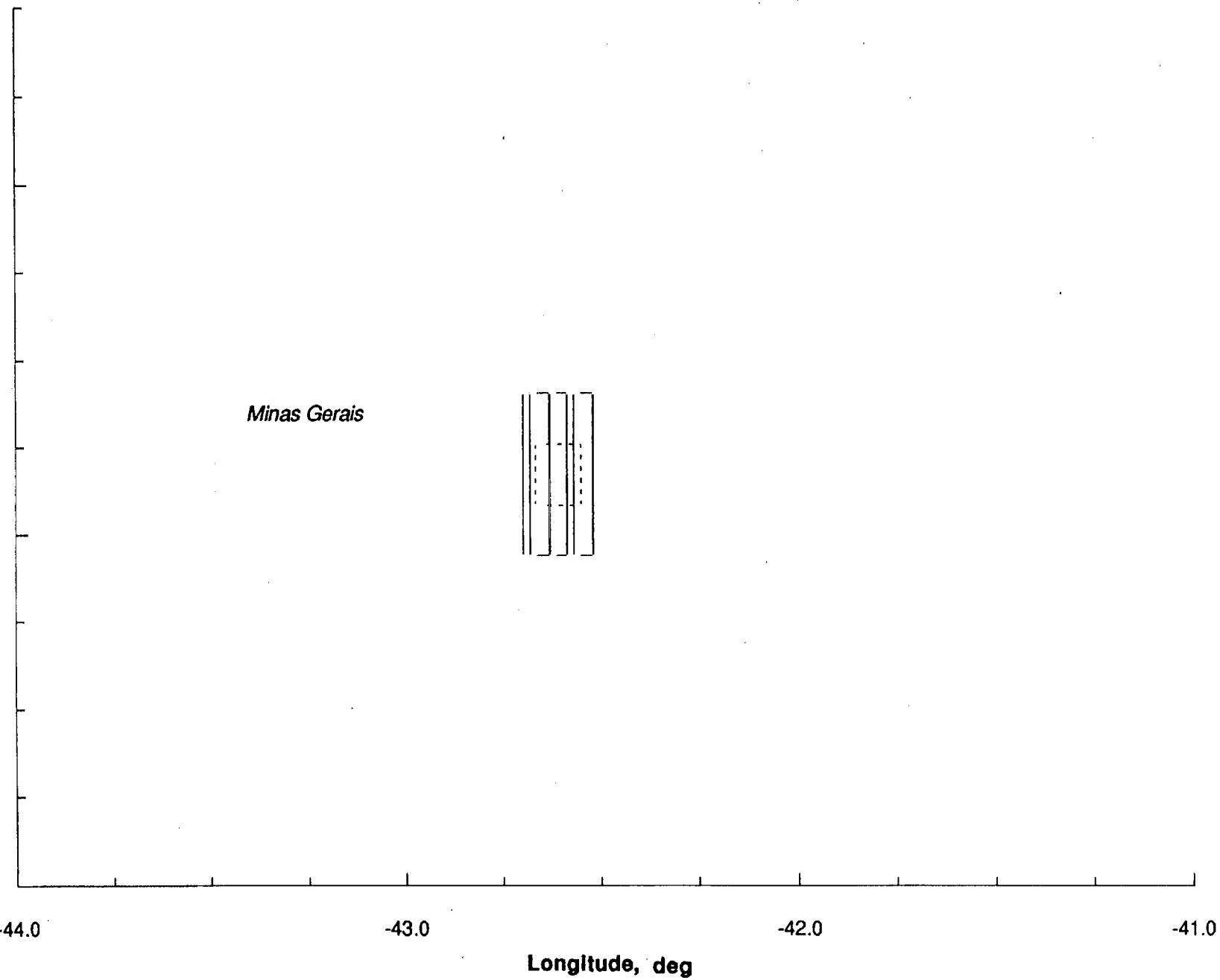
-19.0
-20.0
-21.0
Latitude, deg
Minas Gerais
-44.0
-43.0
-42.0
-41.0
Longitude, deg

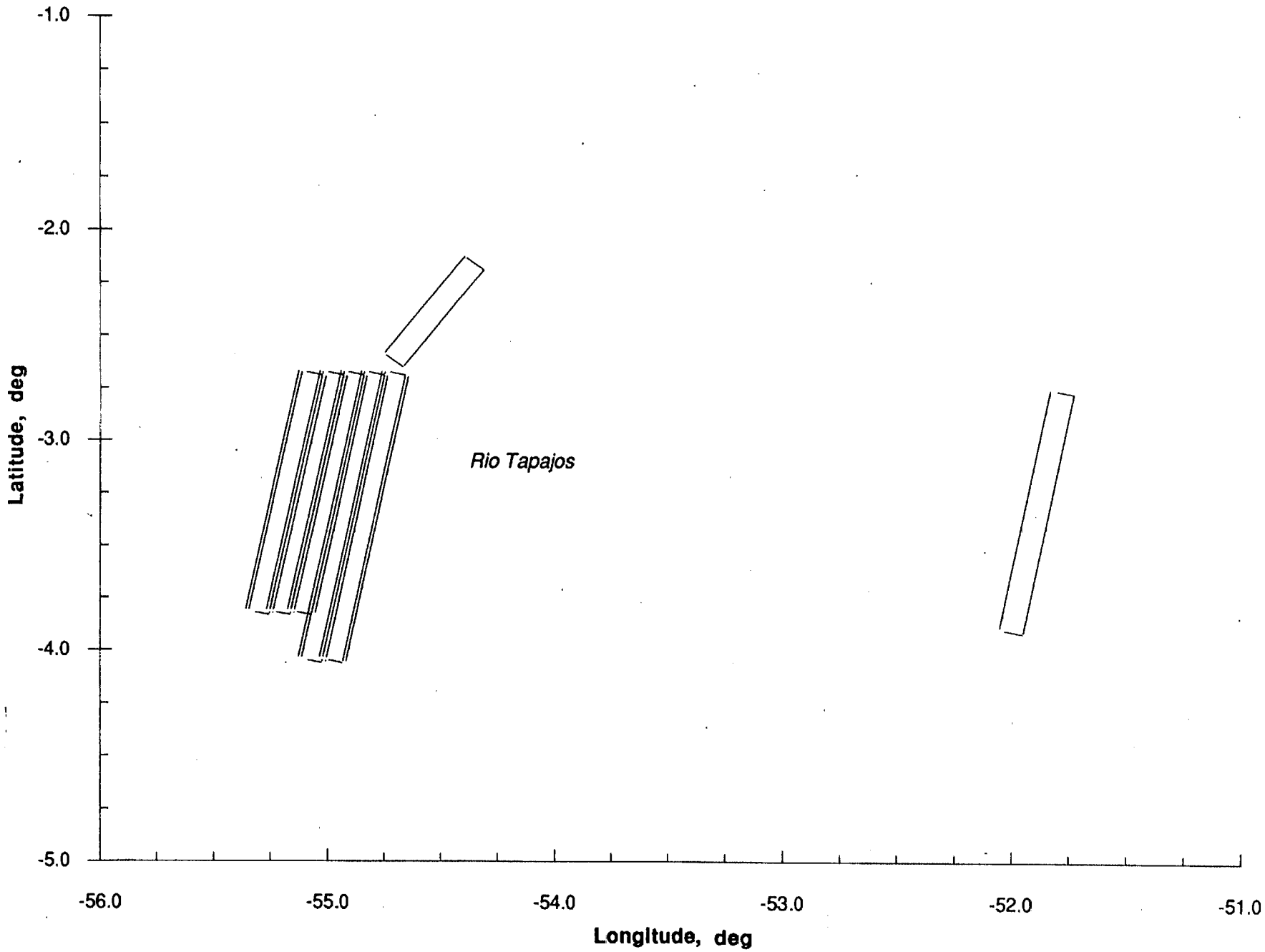
-1.0
-2.0
-3.0
-4.0
-5.0
Latitude, deg
Rio Tapajos
-56.0
-55.0
-54.0
-53.0
-52.0
-51.0
Longitude, deg

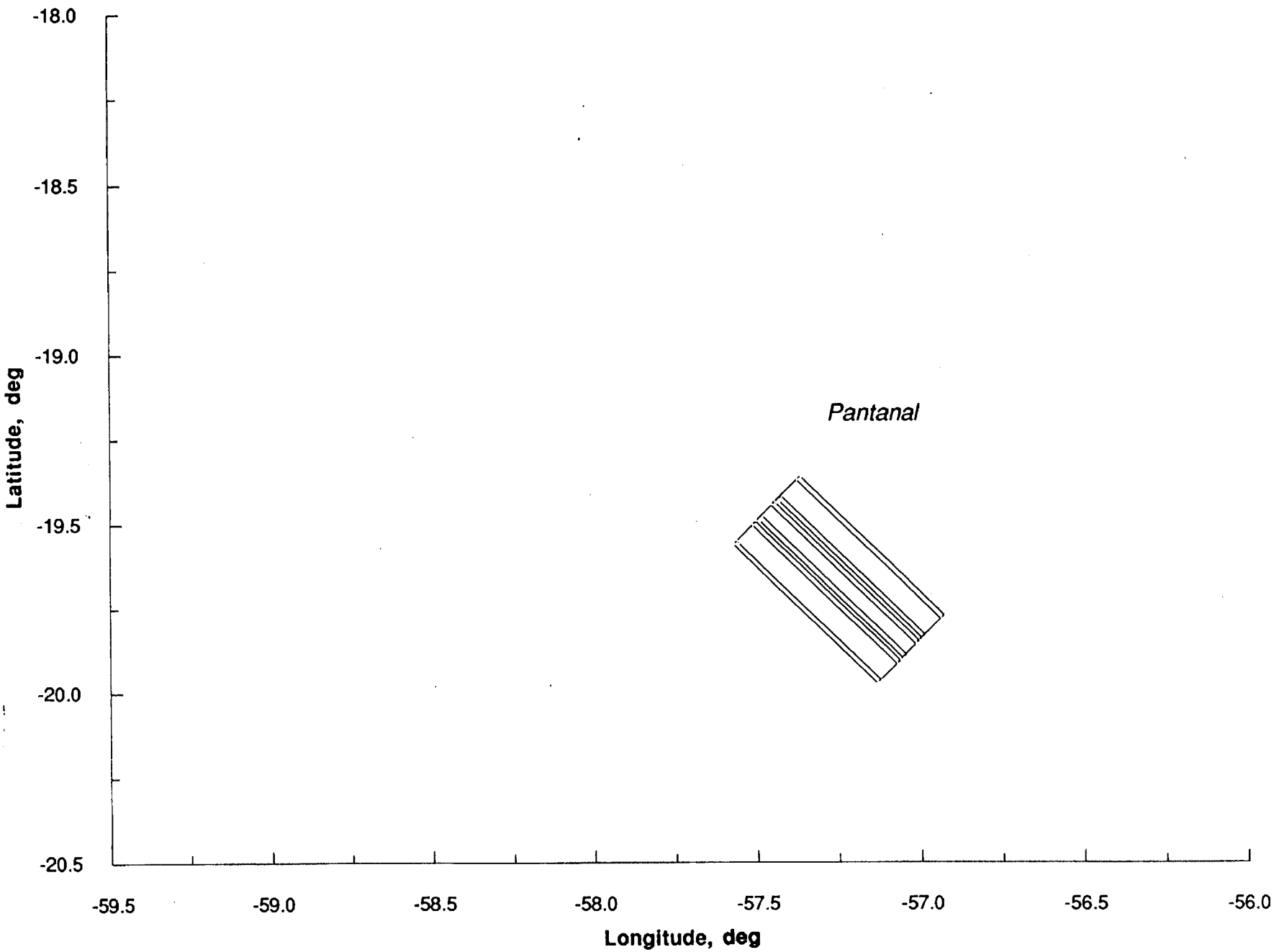
-18.0
-18.5
-19.0
-19.5
-20.0
-20.5
Latitude, deg
Pantanal
-59.5
-59.0
-58.5
-58.0
-57.5
-57.0
-56.5
-56.0
Longitude, deg

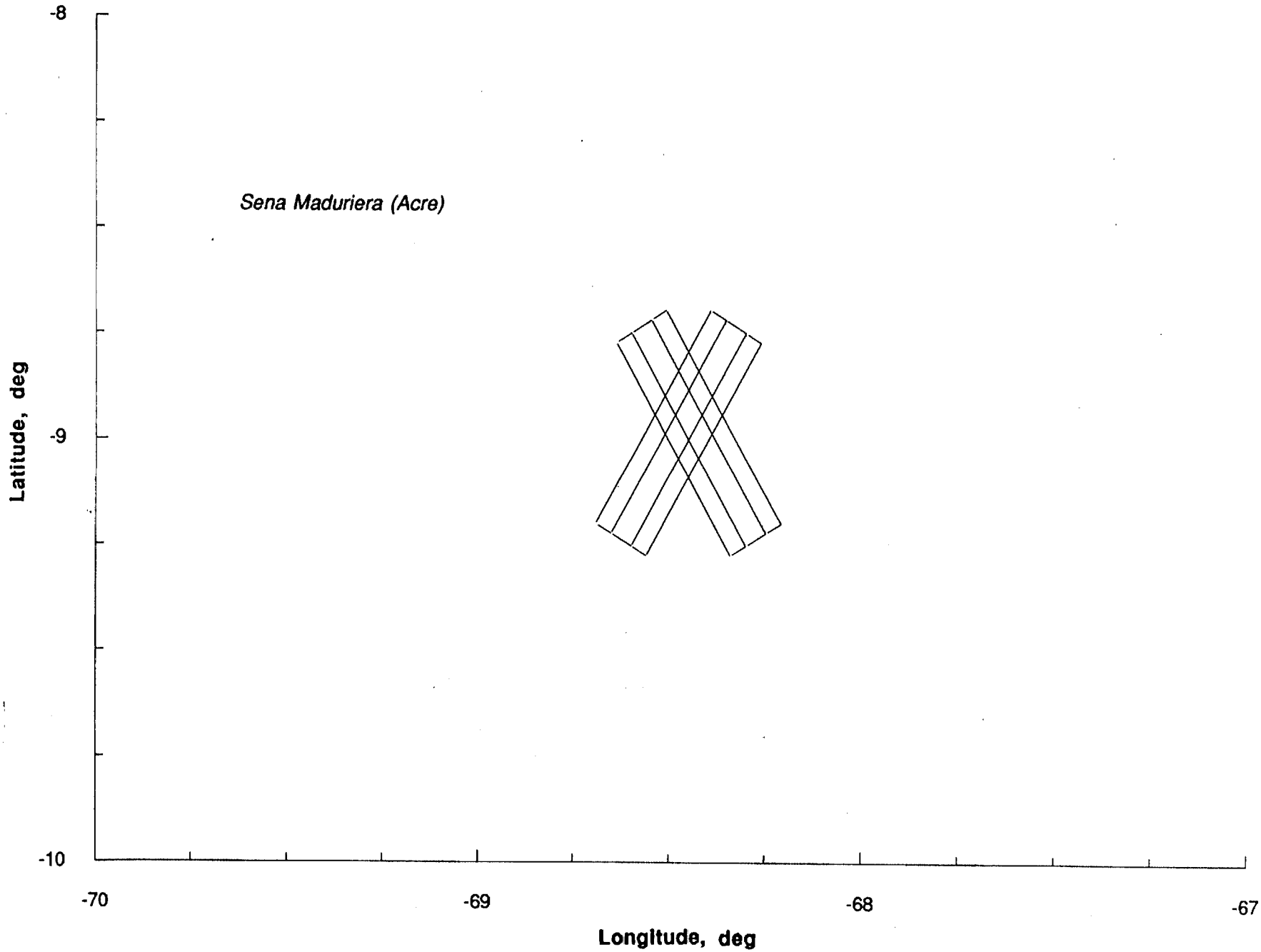
Sena Maduriera (Acre)
-8
-9
-10
Latitude, deg
-70
-69
-68
-67
Longitude, deg

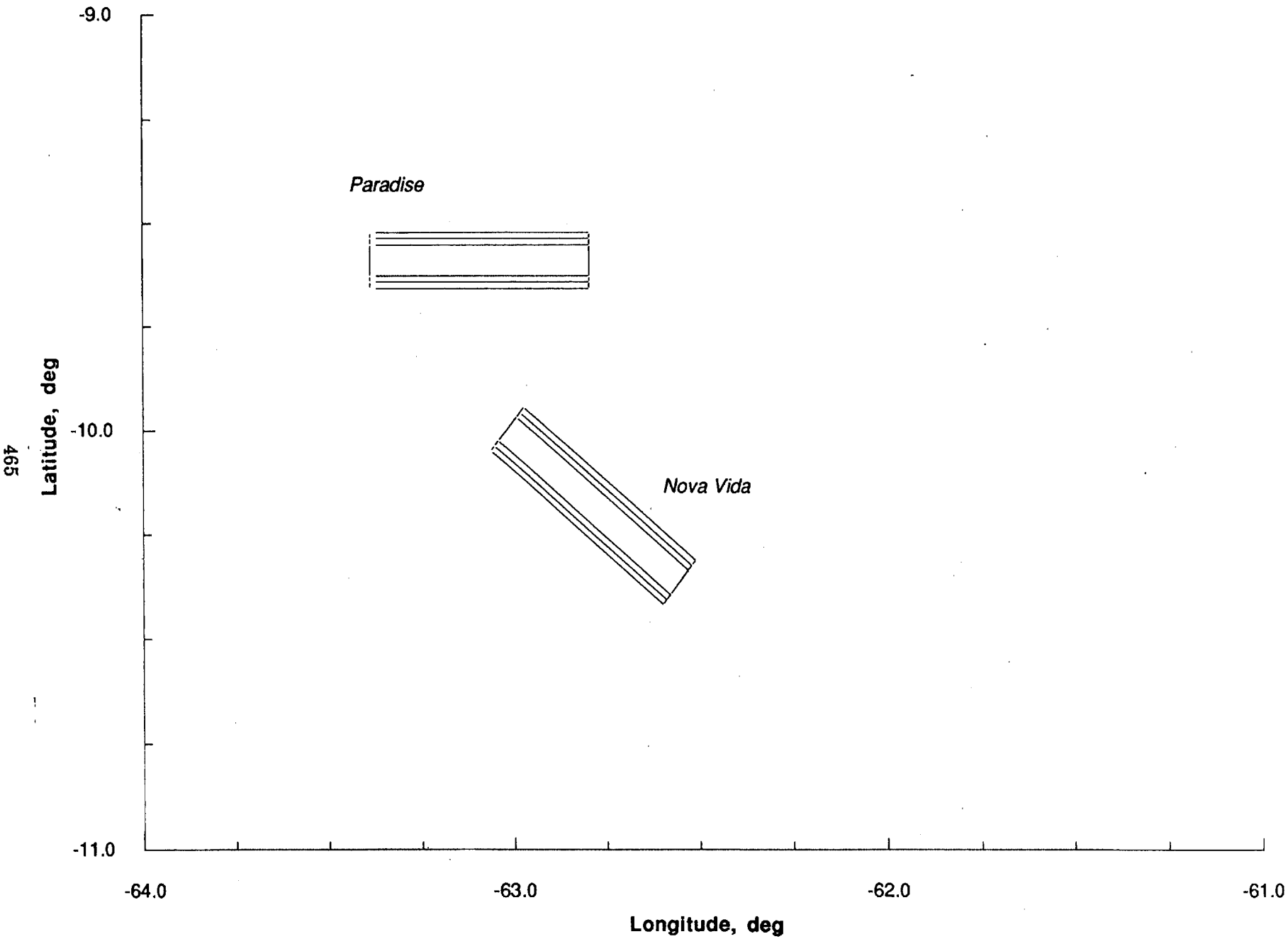
-9.0
-10.0
-11.0
Latitude, deg
Paradise
Nova Vida
-64.0
-63.0
-62.0
-61.0
Longitude, deg

TECHNICAL REPORT STANDARD TITLE PAGE

1. Report No. 93-16	2. Government Accession No.	3. Recipient's Catalog No.
4. Title and Subtitle PROCEEDINGS OF THE THIRD SPACEBORNE IMAGING RADAR SYMPOSIUM		5. Report Date May 28, 1993 6. Performing Organization Code
7. Author(s)		8. Performing Organization Report No.
9. Performing Organization Name and Address JET PROPULSION LABORATORY California Institute of Technology 4800 Oak Grove Drive Pasadena, California 91109		10. Work Unit No. 11. Contract or Grant No. NAS7-918 13. Type of Report and Period Covered JPL External Publication
12. Sponsoring Agency Name and Address NATIONAL AERONAUTICS AND SPACE ADMINISTRATION Washington, D.C. 20546		14. Sponsoring Agency Code

15. Supplementary Notes

16. Abstract

This publication contains summaries of the papers presented at the Third Spaceborne Imaging Radar Symposium held at the Jet Propulsion Laboratory (JPL), California Institute of Technology, in Pasadena, California, on January 18–21, 1993. The purpose of the symposium was to present an overview of recent developments in the different scientific and technological fields related to spaceborne imaging radars and to present future international plans.

This symposium is the third in a series of "Spaceborne Imaging Radar" symposia held at JPL. The first symposium was held in January 1983 and the second in 1986.

17. Key Words (Selected by Author(s))	18. Distribution Statement
211.Geosciences & Oceanography (general); 326.Physics (general); radar; data processing; ecosystem; and remote sensing.	Unclassified; unlimited

19. Security Classif. (of this report)	20. Security Classif. (of this page)	21. No. of Pages	22. Price
unclassified	unclassified	465	